SHEAR BEHAVIOUR OF ROCK DISCONTINUITIES AND SOIL-ROCK INTERFACES

by

T. T. Papaliangas

Dipl. Civ. Eng., Dipl. Mech. Eng., M.Sc.(Eng. Geol.)

Submitted in accordance with the requirements for the degree of
Doctor of Philosophy

The University of Leeds
Department of Earth Sciences

August 1996

The candidate confirms that the work submitted is his own and that appropriate credit
has been given where reference has been made to the work of others

ABSTRACT

Basic aspects of the shear behaviour of rock-rock and rock-soil interfaces are investigated by physical modelling.

Shear characteristics of rock discontinuities are studied by conducting direct shear tests on identical models of various natural rough surfaces. A strong synthetic rock is developed and used to cast several sets of identical samples by using a rubber moulding material. All samples are subjected to direct shear testing in the same relative direction of shearing and under various normal stresses, over the full range of dilatant behaviour. The effect of scale on peak shear strength is studied by testing models of natural rock surfaces in full and divided into sub-samples of various sizes. Identical samples are reproduced by using two different casting materials of different mechanical properties and are tested under various normal stresses.

The test results indicate that independent of rock material, roughness, scale and normal stress level, the peak shear strength can be interpreted as comprising two components, one purely frictional and one geometrical. The controlling parameter of peak shear strength is the dilation angle, which for a particular joint type, reduces logarithmically with normal stress over four orders of magnitude and becomes zero at a normal stress which in most cases is about one order of magnitude lower than the unconfined compressive strength. Beyond this normal stress, the shear behaviour of the sample becomes purely frictional.

A simple, theoretical but readily applicable criterion is proposed, for a realistic mechanism of shearing and based on the suggestion that peak shear strength comprises one frictional and one geometrical component. Changes in peak friction angle due to normal stress, sample size or roughness are interpreted in terms of change in the geometrical component only. The magnitude of the frictional component is determined from the shear strength of the rock wall material, whereas the magnitude of the geometrical component is predicted from consideration of surface roughness and normal contact theory. The results of a compilation of data concerning the friction angle of various types of fresh rock are provided. The advantage of the new criterion is its simplicity, the use of physically meaningful parameters and the ability to explain the observed behaviour of natural rock discontinuities. Verification of the new criterion is established by testing against published data.

The behaviour of soil-rock interfaces is studied by direct shear tests on interfaces between granular materials and modelled rock surfaces of various roughness. Two

different granular materials of various sizes and a diversity of surfaces with different roughness, are used to model the soil-rock interface. It is found that for a particular type of rock and soil material, the shear behaviour of the interface depends upon the rock surface roughness, the grain size and shape of the soil particles and the normal stress. Some aspects of double soil-rock interfaces are presented.

Recommendations are made concerning the suitability of casting materials in reproducing natural rock surfaces, the expected friction angle for various types of fresh rock and the determination of in-situ shear strength both for rock-rock and rock-soil interfaces.

TABLE OF CONTENTS

CHAPTER 1
INTRODUCTION

PART I: DEVELOPMENT OF A SYNTHETIC ROCK

CHAPTER 2
DEVELOPMENT OF A SYNTHETIC ROCK

CHAPTER 5

A NEW COMPREHENSIVE CRITERION FOR PEAK SHEAR
STRENGTH OF ROCK DISCONTINUITIES

CHAPTER 6

APPLICATION OF THE NEW CRITERION ON PUBLISHED
EXPERIMENTAL RESULTS

PART III
SHEAR BEHAVIOUR OF SOIL-ROCK INTERFACES

CHAPTER 7
SINGLE SOIL-ROCK INTERFACES

CHAPTER 8
DOUBLE SOIL-ROCK INTERFACES

PART IV: SUMMARY AND CONCLUSIONS

CHAPTER 9
SUMMARY AND CONCLUSIONS

LIST OF FIGURES

CHAPTER 7

CHAPTER 8

LIST OF TABLES

LIST OF PLATES

LIST OF SYMBOLS

a 1) mean roughness amplitude of joint surface

       2) empirical constant used in shear strength criteria of power law form

A 1) constant in the relation between normal closure and normal stress

       (after Greenwood & Williamson, 1966)

       2) apparent area of contact

       3) weight of aggregate

A_a actual area of contact between two rough joints (after Jaeger, 1971)

A_r real area of contact between surfaces

$A.B.(\%)$ asperity base length as a percentage of the sample length

       (after Barton, 1971 a & b)

b empirical constant used in shear strength criteria of power law form

B constant in the relation between normal closure and normal stress

       (after Greenwood & Williamson, 1966)

c 1) cohesion of intact rock

       2) apparent cohesion of rock joints (after Patton, 1966 a & b)

       3) weight of cement

C intercept in the relation between peak friction angle and dilation angle

       (after Barton, 1971 a & b)

C_o unconfined compressive strength

d distance between reference plane and smooth surface under stress

       (after Greenwood & Williamson, 1966)

d_o distance between reference plane and smooth surface without stress

       (after Greenwood & Williamson, 1966)

D pore diameter

D_{10} 10% finer particle size

D_{50} mean particle diameter

D_{60} 60% finer particle size

d_n peak dilation angle (after Barton, 1971a,b)

dh incremental shear displacement (after Hencher & Richards, 1989)

$dh_{\psi max}$ shear displacement at maximum dilation angle

dv incremental normal displacement (after Hencher & Richards, 1989)

E' composite modulus of elasticity (after Greenwood & Williamson, 1966)

E_1, E_2	modulus of elasticity of materials 1,2
h	standarised separation between a rough and a flat surface
H	shear load along a horizontal plane
f	thickness of soil layer
f_{crit}	critical thickness of soil layer
i	1) average angle of deviation of particle displacements from the direction of applied shear stress (after Newland & Allely, 1957)
	2) asperity inclination angle (after Patton, 1966a & b)
	3) instantaneous dilation angle (Hencher & Richards, 1989)
i_o	asperity inclination angle (after Ladanyi & Archambault, 1970)
JCS	Joint Compressive Strength (after Barton & Choubey, 1977)
JCS_n	Joint Compressive Strength at field scale (after Barton & Bandis 1982)
JCS_o	Joint Compressive Strength at laboratory scale (after Barton & Bandis, 1982)
JRC	Joint Roughness Coefficient (after Barton & Choubey, 1977)
JRC_n	Joint Roughness Coefficient at field scale (after Barton & Bandis 1982)
JRC_o	Joint Roughness Coefficient at laboratory scale (after Barton & Bandis, 1982)
k	mean value of tangential stress correction factor (after Brown & Scolz, 1985)
K	empirical constant relating the variation with normal stress of dilation rate (after Ladanyi & Archambault, 1970)
L	1) empirical constant relating the variation with normal stress of the ratio of area of asperities sheared off to total area (after Ladanyi & Archambault, 1970)
	2) length of sample
	3) asperity half base length
L_{cr}	critical scale-free block length
L_n	length of joint at field scale (after Barton & Bandis 1982)
L_o	length of joint at laboratory scale (after Barton & Bandis 1982)
m	intact rock parameter (after Hoek & Brown, 1980 a&b)
M	1) gradient in the relation between peak friction angle and dilation angle (after Barton, 1971 a & b)
	2) damage coefficient (after Barton & Choubey, 1977)
n	1) compressive/tensile strength
	2) constant relating the area of contact to normal load (after Archard,1957)
	3) number of contact spots (after Greenwood & Williamson,1966)

N	1) total normal load
	2) normal load on an inclined plane
p	1) hardness of weaker rock material in contact
	2) total mercury pressure
q	constant relating principal stresses
r	Schmidt rebound value on weathered rock (after Barton & Choubey, 1977)
R	1) Schmidt rebound value on unweathered rock
	(after Barton & Choubey, 1977)
	2) surface roughness
R_{max}	maximum peak to valley height of profile
$R_{max(L=D)}$	R_{max} with gauge length L=D (after Kishida & Uesugi, 1987)
R_n	normalised roughness of a surface
R_R	relative interface roughnes (after Kulhawy & Peterson, 1979)
$R_{Rstructure}$	roughness of structural face (after Kulhawy & Peterson, 1979)
R_{soil}	roughness of soil (after Kulhawy & Peterson, 1979)
R_t	maximum peak to valley height of profile
s	1) rock mass parameter (after Hoek & Brown, 1980 a & b)
	2) shear strength of welded junctions
	3) standard deviation
S	frictional force
$S.D.(i)$	standard deviation of angle of asperities (after Barton, 1971 a & b)
s_n	asperity failure component (after Barton & Choubey, 1977)
s_t	shear strength of weaker material in contact (after Terzaghi, 1925)
t	thickness of shear band
T	shear force along an inclined plane
T_o	tensile strength of intact rock material
V	normal load on an a horizontal plane
$\dot{v}$	dilation rate (after Ladanyi & Archambault, 1970)
x	tangential distance along a surface profile
y	amplitude of a surface point about the centerline of the roughness profile
z	distance of a surface peak to its reference plane
	(after Greenwood & Williamson, 1966)
Z_2	root mean square slope gradient

α	angle of a plane with the specimen axis
α_s	ratio of area of aperities sheared off to total area
	(after Ladanyi & Archambault, 1970)
β	radius of asperity summits (after Greenwood & Williamson, 1966)
γ	mercury surface tension
δ	1) normal closure between a rough and a flat surface under stress
	(after Greenwood & Williamson, 1966)
	2) angle of friction of a soil-rock interface
ε	axial strain
η	1) number of asperities per unit area (after Greenwood & Williamson, 1966)
	2) degree of interlocking (after Ladanyi & archambault, 1970)
μ	measured peak stress ratio
μ_k	kinetic stress ratio
μ_m	non-dilational stress ratio
ν_1, ν_2	Poisson's ratio of materials 1, 2
σ	1) normal stress
	2) standard deviation
$\sigma_{1, 2, 3}$	principal stresses
σ_c	unconfined compressive strength
σ_i	normal stress on the plane of shearing (after Hencher & Richards, 1989)
σ_n	normal stress
σ_{no}	normal stress causing negligible deformation
σ_{nT}	critical normal stress able to suppress all dilation
σ_T	normal stress at brittle-plastic transition
τ	shear strength
τ_a	shear stress on a plane inclined at an angle a to the specimen axis
τ_i	shear stress on the plane of shearing (after Hencher & Richards, 1989)
τ_p	peak shear strength.
τ_r	shear strength of irregularities in the joint wall
	(after Ladanyi & Archambault, 1970)
ϕ	angle of internal friction
ϕ_b	basic friction angle (after Barton, 1971a & b)
ϕ_{cv}	constant volume friction angle
ϕ_m	friction angle of the rock material adjacent to a joint
ϕ_μ	angle of frictional sliding between sand grains (after Newland & Allely, 1957)

ϕ_p peak friction angle

ϕ_r 1) angle of frictional sliding resistance along a plane surface or residual

            frictional angle (after Patton, 1966 a & b)

            2) Residual friction angle (after Barton, 1971a & b)

ϕ_{true} true friction angle (after Ripley & Lee, 1961)

ψ dilation angle at peak shear stress

ψ_f dilation angle at failure

ψ_{max} maximum dilation angle

ψ_o maximum asperity angle of a rock surface

ACKNOWLEDGEMENTS

CHAPTER 1

INTRODUCTION

1.1 General Introduction

Many problems in geotechnical engineering practice involve dealing with the shear behaviour of geotechnical interfaces, which generally form weak elements within the geotechnical environment. Interfaces are boundaries between geomaterials of the same or similar strength, for example rock-rock, concrete-rock and soil-soil, or between two different lithological units of which one is classified as rock and the other as soil Such interfaces weaken the mechanical properties of the geomaterials and introduce interaction mechanisms with engineering structures, which may be critical for stability.

The general term *discontinuities* is used to describe mechanical breaks or fractures of negligible tensile strength regardless of their geological origin (faults, joints, bedding planes etc.). The term *joints* tends also to be used generally in rock mechanics to cover all types of structural weakness despite their particular geological origin. Both terms are used in this thesis with the same meaning. The overall behaviour of a rock mass is largely dependent on the geometrical (number of sets, orientations, apertures, persistence, roughness etc.) and mechanical properties (cohesion, friction angle, stiffness etc.) of rock discontinuities. Rock-concrete interfaces like those formed between a concrete dam and the foundation rock or a concrete pier and the walls of a rock socket behave in a similar way with rock-rock interfaces, except that they may have a small cohesion due to bond between concrete and rock. In some geotechnical problems instead of two rocks separated by a discontinuity, the case of a soil layer adjacent to a rock stratum is encountered. In this case the properties of the *soil-rock interface* are important. When the soil layer is contained between two rock strata a *double soil-rock interface* is formed and the type of soil, its thickness and mechanical properties govern the overall behaviour.

Some typical examples illustrating the importance of rock-rock or rock-concrete interfaces in rock engineering problems are shown in Figure 1.1, where several interaction mechanisms may occur. For example, low friction angle of a critically oriented rock discontinuity may cause sliding of the rock mass above it (Figure 1.1a); open joints in the rock mass beneath the foundation of a bridge may cause considerable settlement upon the application of load (Figure 1.1b); key blocks may slide following the excavation of a tunnel (Figure 1.1c); stress concentrations may develop in the corners of a deep excavation and/or swelling may occur as a result of the unloading caused by the excavation, especially in the case of joints filled with clayey material as shown in Figure 1.1d; the existence of a main discontinuity and a system of
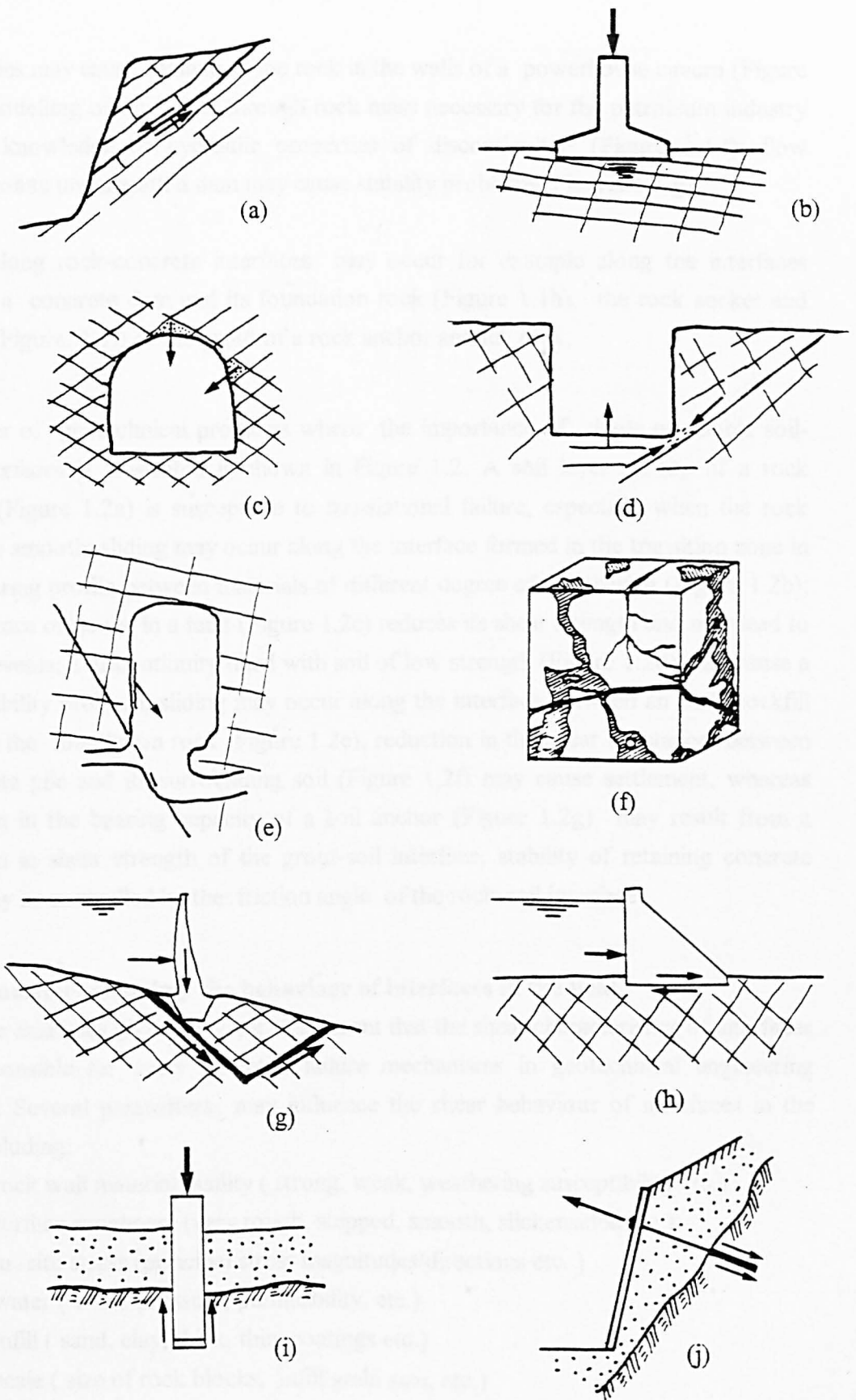
Figure 1.1: Typical examples illustrating the influence of rock-rock and rock-concrete interfaces on rock engineering projects: (a) slope stability; (b) foundation on rock; (c) underground excavation; (d) surface excavation; (e) hydroelectric power cavern; (f)-(g) fluid flow through joints; (h)-(j) concrete - rock interfaces

secondaries may cause spalling of the rock in the walls of a powerhouse cavern (Figure 1.1.e) modelling of fluid flow through rock mass necessary for the petroleum industry requires knowledge of hydraulic properties of discontinuities (Figure 1.1.f); flow through joints underneath a dam may cause stability problems (Figure. 1.1.g).

Failure along rock-concrete interfaces may occur for example along the interfaces between a concrete dam and its foundation rock (Figure 1.1h), the rock socket and the pier (Figure. 1.1i) or the grout of a rock anchor and its rock.

A number of geotechnical problems where the importance of single or double soil-rock interfaces is illustrated is shown in Figure 1.2. A soil layer on top of a rock stratum (Figure 1.2a) is susceptible to translational failure, especially when the rock surface is smooth; sliding may occur along the interface formed in the transition zone in a weathering profile between materials of different degree of weathering (Figure 1.2b); the presence of gouge in a fault (Figure 1.2c) reduces its shear strength and may lead to seismic events; a discontinuity filled with soil of low strength (Figure 1.2d) may cause a slope stability problem; sliding may occur along the interface between an earth/rockfill dam and the foundation rock (Figure 1.2e); reduction in the shear resistance between a concrete pile and its surrounding soil (Figure 1.2f) may cause settlement, whereas reduction in the bearing capacity of a soil anchor (Figure 1.2g) may result from a reduction in shear strength of the grout-soil interface: stability of retaining concrete walls may be controlled by the friction angle of the rock-soil interface.

1.2 Parameters affecting the behaviour of interfaces in the field

From the examples given above, it is apparent that the shear characteristics of interfaces are responsible for many potential failure mechanisms in geotechnical engineering projects. Several parameters may influence the shear behaviour of interfaces in the field, including:

1) rock wall material quality (strong, weak, weathering susceptibility etc.)
2) surface roughness (very rough, stepped, smooth, slickensided etc.)
3) in -situ stress (principal stress magnitudes/directions etc.)
4) water (water pressure, permeability, etc.)
5) infill (sand, clay, thick, thin, coatings etc.)
6) scale (size of rock blocks, infill grain size, etc.)
7) time (creep, relaxation, cycling loading, strain rate etc.)
8) stiffness
9) weathering
10) engineering (stress redistribution, change in hydraulic conditions, construction method, etc.).
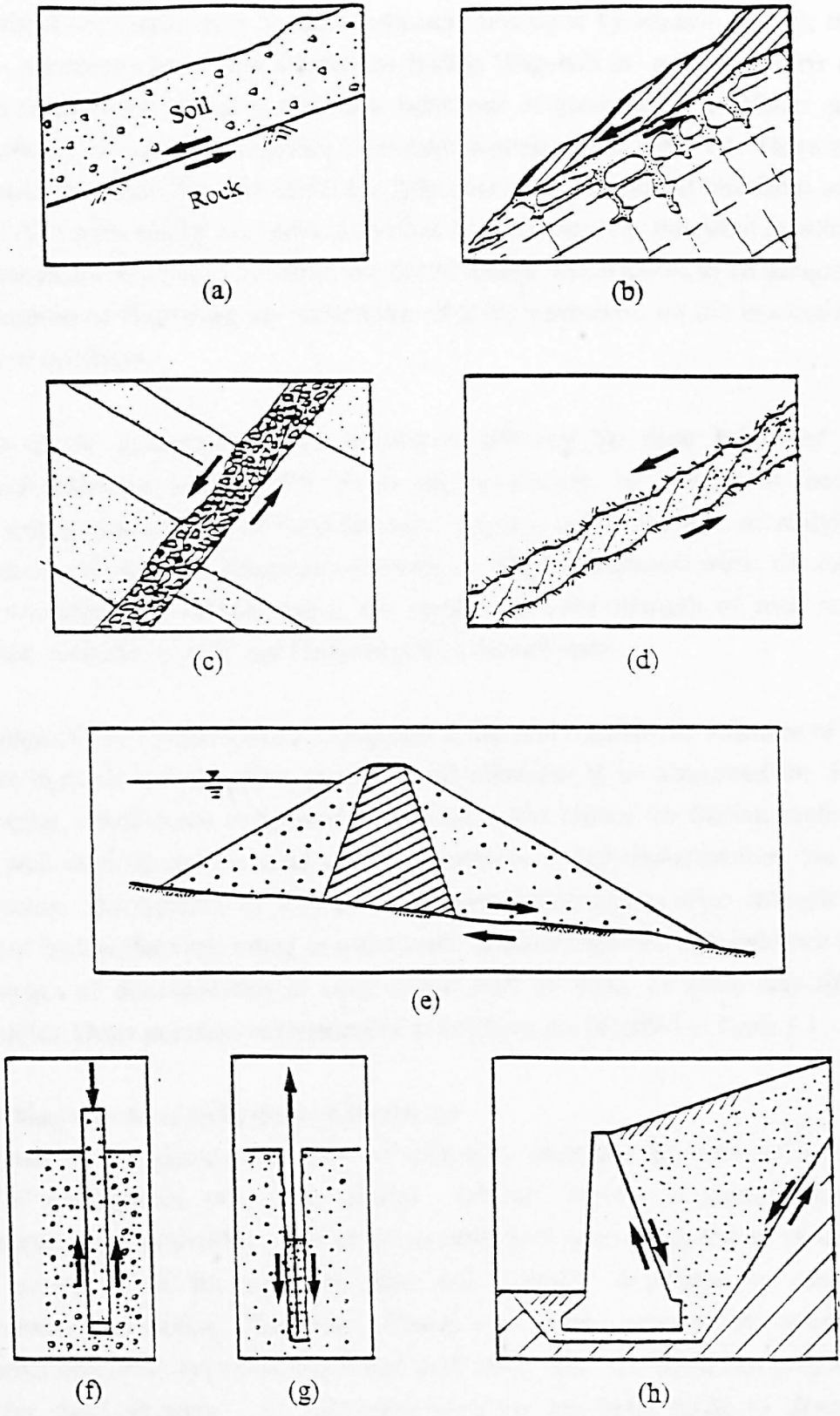
Figure 1.2: Typical examples illustrating the influence of soil-rock and soil-concrete interfaces on rock engineering projects: (a) soil layer on rock; (b) transition zone in weathering profile;c) gouge in fault; (d) filled joint; (e) foundation of earth/ rockfill dam; (f) pile in soil; (g) soil anchor; (h) retaining wall

Applying the Rock Engineering Systems approach developed by Hudson (1992), the above ten parameters have been selected as leading diagonals in a 10x10 matrix of interaction mechanisms related to the shear behaviour of geotechnical interfaces and more specifically to rock discontinuities. The result is presented in Table 1.1. There are other parameters which may also affect the behaviour of geotechnical interfaces and the size of the matrix can be increased, as well as its resolution, i.e. the detail to which the interactions are described. However, the 10x10 matrix is considered to be adequate for the purpose of illustrating the importance of some parameters on the mechanical behaviour of interfaces.

The study of the influenceof all the parameters affecting the shear behaviour of geotechnical interfaces is impossible within the framework of a doctoral thesis, therefore only a small number of them has been selected, for the purpose of studying specific aspects of the shear behaviour of interfaces. These parameters were: the rock surface roughness, the normal stress, the sample size, the strength of rock wall material, the thickness of infill and the grain size of the soil layer.

Extrapolation of the results of this investigation in the field requires the influence of all parameters likely to have an effect on the overall behaviour to be accounted for. For example water, which is not considered in this study, may reduce the friction angle of the rock wall material and the total shearing resistance of the discontinuities due to water pressure; the presence of clay infill may considerably reduce shear strength by masking the rock surface and acting as a lubricant; displacement rate may influence the shear strength of discontinuities in some rocks such as shale, or some clay filled discontinuities. Other possible mechanisms of interactions are included in Table 1.1.

1.3 Modelling the shear behaviour of interfaces

Over the past few decades the behaviour of rock-rock interfaces has attracted a great number of investigators, who have studied several aspects of shearing along discontinuities. A considerable number of models have been proposed to describe specific parameters or the complete shear and normal behaviour or coupled hydromechanical response. However, despite the huge amount of available experimental data from both laboratory and field tests and the numerous proposed models for shear strength, no substantial progress has been made to describe accurately the shear behaviour of this single element of a rock mass, taking into account the actual physics governing the shearing of rock discontinuities. The difficulty arises from the presence of asperities, which greatly affect the mechanical behaviour of rock discontinuities during shearing by inducing dilatancy. Many attempts have been made to investigate the effect of asperities on the peak shear resistance, and various

PAGE(S) MISSING IN ORIGINAL

Table 1.1: 10x10 matrix of interactions between various parameters affecting the mechanical behaviour of rock discontinuities

Rock material Type, strength, friction angle etc. **1,1**	strong granites produce very rough surfaces 1,2	hard rocks require high stresses to cause plastic deformation of contacts 1,3	highly permeable rocks may increase overall permeability 1,4	discontinuities in soluble calcitic rocks may produce large quantities of infill 1,5	strength of jointed hard rocks is more dependent on scale than soft rocks 1,6	ductile rocks like halite are more susceptible to creep 1,7	discontinuities in hard silicate rocks are stiffer than in soft argillaceous rocks 1,8	granites near the surface may be decomposed completely 1,9	low-friction rock wall material determines the reinforcement 1,10
rougher joints result in deeper deformed zones at rock contacts 2,1	**Roughness** **2,2**	high stresses are developed at the contacts of rough discontinuities 2,3	dilation of rough discontinuities increases permeability 2,4	strength of filled joints is higher when rock walls are rough 2,5	strength of rough joints is strongly scale-dependent 2,6	rough joints require larger number of loading cycles to reach stability 2,7	degradation of rough rock discontinuities reduces rock mass stiffness 2,8	surface peaks of rough joints may disintegrate more easily 2,9	high degree of interlocking of rough joints reduces support requirements 2,10
concentration of in-situ stress can break intact rock material 3,1	shearing under high stresses reduces roughness 3,2	**In-situ stress** **3,3**	high in-situ stress reduces permeability 3,4	high in-situ stress reduces permeability 3,5	no clear scale effects observed in stress measurements 3,6	weak clayey shales creep at low stress 3,7	high stress increases stiffness 3,8	high stress closes joints and slows down weathering process 3,9	high in-situ stress affects excavation method 3,10
water may reduce friction angle of rock wall material 4,1	water reduces roughness by weathering 4,2	stress is reduced by water pressure 4,3	**Water** water pressure, permeability, **4,4**	high in-situ stress reduces thickness of infill 4,5	hydraulic conductivity reduces with scale 4,6	absorption of water causes swelling 4,7	flow through discontinuities may reduce overall stiffness 4,8	ground water causes weathering of rock walls 4,9	permeability of reservoir slopes affects drainage method 4,10
infill reduces friction angle by masking the rock surface 5,1	thick infills make roughness inactive 5,2	clay-filled joints change stress distribution under a concrete dam 5,3	High water pressure may result due to low-permeability clay infills 5,4	**Infill** type, thickness etc. **5,5**	thick infills reduce scale effect in joint shear strength 5,6	thick clayey infills may swell 5,7	joints with thick infills may considerably reduce rock mass stiffness 5,8	highly permeable infills favour weathering 5,9	discontinuities with thick infills may require drainage 5,10
behaviour of closely jointed rock masses is similar to that of granular soils 6,1	large blocks mobilise roughness of large base-length 6,2	closely fractured rock results in more uniform stress field 6,3	closely fractured rock results in multi-path water flow 6,4	grain size distribution of coarse infills may change due to crushing 6,5	**Scale** rock block size, infill grain size etc. **6,6**	large blocks will swell more than small blocks 6,7	large blocks increase rock mass stiffness 6,8	rock masses consisting of small blocks expose large total surface to weathering 6,9	large blocks are more difficult to remove 6,10
foundation rock may be deformed permanently by fluctuations in reservoir level 7,1	cycling loading reduces roughness by asperity degradation 7,2	stress redistribution following creep may cause successive drop of blocks in a cavern 7,3	the number of normal loading cycles reduce hydraulic conductivity of a discontinuity 7,4	fast strain rate may result in lower strength for clay filled discontinuities 7,5	cycling loading reduces infill mean diameter due to degradation 7,6	**Time** creep, relaxation, swelling, fatigue etc. **7,7**	relaxation reduces stiffness 7,8	cyclic loading accelerates weathering 7,9	swelling foundation requires bolting 7,10
stiff rock mass imposes shearing through intact rock material 8,1	low stiffness allows mobilisation of roughness 8,2	stiff rocks may contain higher stresses 8,3	low stiffness rock mass has higher permeability 8,4	stiff rock masses do not allow clayey infills to swell 8,5	stiff rock masses usually consist of larger blocks than loose rock masses 8,6	stiff rock masses do not allow swelling of clay bearing joints 8,7	**Stiffness** **8,8**	low stiffness rock mass allows water flow which causes weathering 8,9	stiff rocks are difficult to excavate 8,10
soluble rocks are disintegrated by weathering 9,1	discontinuities in weathered rocks are usually not as rough as in fresh rocks 9,2	in-situ stress may be reduced as a result of weathering 9,3	weathering may close water paths and increase water pressure 9,4	thickness of infill increases due to weathering 9,5	strength of weathered joints are less affected by size due to reduced roughness 9,6	weathered joints may reach their fatigue limit after a low number of cycles 9,7	weathering causes loosening of rock mass 9,8	**Weathering** **9,9**	thick infills produced by weathering may require replacement by concrete 9,10
blasting affects rock material intensity 10,1	blasting destroys existing joint roughness 10,2	load of a bridge pier increases in-situ stress 10,3	grout curtains control permeability under a dam 10,4	high foundation loads may reduce infill thickness 10,5	direction of tunnel changes the size of maximum key blocks 10,6	A deep excavation may cause swelling 10,7	excavations may reduce rock mass stiffness 10,8	sprayed concrete protects slope face from weathering 10,9	**Engineering** water pumping, construction method, reservoir filling etc. **10,10**

models both empirical and theoretical have been proposed. The theoretical criteria areoften complicated and difficult to use, so preference is given to empirical. However, they do not consider the physical process involved and their applicability may be limited, so that various modifications may be needed to suit a particular case. Therefore, the use of powerful numerical models developed to describe rock mass behaviour is not beneficial if the input parameters determined from such empirical criteria are not reliable.

It is customary to consider that the peak shear resistance of a rock discontinuity is made up of two components: a) a basic friction component due to frictional resistance of a flat rock surface and b) a roughness component which consists of dilational component and an asperity failure component. The change of shear strength with shear displacement is considered by introducing a ploughing or wear component. While the separation of the shearing resistance into the above components is convenient in qualitative terms, their exact quantitative contribution to the shear strength is extremely difficult to determine, since most of them occur at the same time. The situation becomes more difficult when considering their variation with normal stress and sample size. Understandably, this difficulty made several investigators turn to empirical relationships. It is an objective of this study to investigate separately the role of the frictional and the roughness component on the peak shear strength and attempt to describe the shear behaviour in a rational quantitative way.

Soil-rock interfaces form weak elements between two geomaterials of different class. Interfaces like soil-structures, soil - rock, filled joints etc. are very often the subject of geotechnical engineering problems. Their shear behaviour has been studied by some researchers who investigated mainly the shear characteristics of interfaces between construction materials and soil. In this study some aspects of the behaviour of rock-soil interfaces in shear are investigated, with emphasis in the deformation mechanisms involved. The results are applicable to interfaces at both geological and engineering structures scale.

1.4 Objectives

The main objective of this study is to contribute to a better understanding of the mechanisms involved when a rock-rock or a soil-rock interface is subjected to shearing. To achieve this objective, an experimental programme was set up, based on laboratory direct shear tests on various rock-rock and soil-rock interfaces. A synthetic rock was developed especially for this study and used to represent rock; various granular natural and artificial materials were used as soils.

The main objectives of the first part of the study, which is about the behaviour of rock-rock interfaces, are: (a) to investigate the origin, the magnitude and the relative contribution to shear resistance of the various shear strength components over a wide range of normal stress. (b) to study the effect of scale on peak shear strength and (c) to attempt an incorporation of the results of this study into a rational comprehensive peak shear strength criterion.

The aims of the second part, which concerns the soil-rock interfaces are: a) to investigate the effect of roughness of the rock surface and the grain shape and size of the soil on the shear strength characteristics of the interface. b) to identify deformation mechanisms involved during shearing and c) to attempt to clarify some aspects of the double soil-rock interfaces.

1.5 Method

A systematic laboratory based experimental programme has been the method for this study. Physical modelling of rock joints is commonly used, but various problems in shear behaviour may not be properly accounted for. For example some low strength materials may be unsuitable, in so far as they may produce considerable surface debris or thin smooth surface layers, the effect of which may be inadequately quantified. There is a considerable amount of experimental data on shear strength of rock-rock interfaces and many more are probably not needed. Consequently, the main effort of this study was directed towards the interpretation of high accuracy data produced by the experimental programme, by examining separately the effect of each   strength component on the magnitude of peak shear strength. To achieve this a basic straight-forward, simple and most relevant approach was used: a series of direct shear tests on sets of identical joint samples at various constant normal stresses. A synthetic rock was developed as a rock substitute and used in the experimental programme. Various types of natural rock surfaces were reproduced by casting in a number of identical copies which were then tested at the appropriate normal stress. All samples were tested in the same relative shearing direction, under constant normal stress which varied from very low values up to a sufficiently high to suppress dilation.

A special programme comprising direct shear tests on joints of different sizes and strength of rock was used to examine the effect of scale and rock strength on peak shear strength of rock discontinuities.

The investigation of the shear behaviour of soil-rock interfaces was carried out by means of direct shear tests, using the newly developed synthetic rock to form surfaces with various   roughness, from very smooth to very rough planar and saw-toothed.

OBJECTIVES

Contribution to a better understanding
of the mechanisms involved when a
rock-rock or rock-soil interface is
subjected to shearing

ROCK-ROCK
INTERFACES

SOIL-ROCK
INTERFACES

LITERATURE
REVIEW
(Chapter 3)

DEVELOPMENT OF
A SYNTHETIC ROCK
(Chapter 2)

PHYSICAL
MODELLING

PHYSICAL
MODELLING
(Chapter 4)

SINGLE SOIL-ROCK
INTERFACES
(Chapter 7)

Parameters
examined

Roughness
Normal stress
Rock strength
Sample size

Parameters
examined

Rock surface roughness
Soil grain size
Normal stress

DOUBLE SOIL-ROCK
INTERFACES
(Chapter 8)

DEVELOPMENT OF
A NEW PEAK SHEAR
STRENGTH CRITERION
(Chapter 5)

Published material:
Parameters examined

Rock surface roughness
Soil type
Soil layer thickness
Normal stress

APPLICATION OF THE
NEW CRITERION ON
PUBLISHED RESULTS
(Chapter 6)

Development
of empirical shear
strength criterion

CONCLUSIONS and
RECOMMENDATIONS
regarding
Mechanisms involved and
quantification of shear strength of
rock-rock and soil-rock interfaces
in the laboratory and in-situ

Experimental study of
deformation mechanisms

Improvement
of strength criterion

Figure 1.3: Flow-chart showing components of thesis and their contribution to the research
thrust and conclusions

Granular natural and artificial materials with spherical, round and subround particles of various sizes were used to investigate the effect of grain size as compared to the surface roughness.

1.6 Thesis layout

The thesis is divided in four parts. The development and properties of artificial rock is discussed in part I (Chapter 2). Comparison with natural rocks is made, and critical evaluation of its capabilities and limitations is given.

Part II is about the shear behaviour of rock discontinuities. It consists of Chapters 3, 4, 5 and 6. In Chapter 3 a literature review is attempted, including aspects of the shear behaviour of intact rock and rock discontinuities. Critical review of various peak shear strength models is made. The experimental results from physical modelling and discussion are presented in Chapter 4, whereas the basic characteristics of a new peak shear strength criterion are described in Chapter 5. Well-documented theoretical principles are used to achieve a simple formulation where physically meaningful and easy to determine parameters are used. The theory behind the criterion explains the origin and magnitude of the peak shear strength components. In Chapter 6, the capabilities of the new criterion are tested against a few sets of well-established experimental results, published by various authors.

Part III consists of Chapters 7 and 8. The experimental results and analyses from the experimental programme on single soil-rock interfaces are given in Chapter 7. In Chapter 8 some experimental results and discussion about some aspects of double soil-rock interfaces are presented.

The conclusions of the work and recommendations for engineering practice and further research are given in Part IV, Chapter 9.

The various components of thesis and their contribution to the research thrust and conclusions are given in the form of a flow-chart in Figure 1.3.

CHAPTER 2
DEVELOPMENT OF A SYNTHETIC ROCK

2.1 Introduction

Several model materials have been extensively used in rock mechanics problems. The use of model materials offers the advantage of ease of preparation of identical samples with the same morphological and mechanical characteristics chosen according to the requirements of each particular modelled situation. Stimpson (1970) lists 24 different materials which can provide friction angles from as low as 7° up to 46°. A limitation of this approach exists when modelling at much reducing geometric scales, when, for similitude, the model material is required to be very weak. In this case, a major problem arises from the non-consistent behaviour in shear (e.g. Hencher *et al*, 1993). A more fundamental problem, especially with the rock joints, is the lack of true similitude (Stimpson, 1979). Rock joints are usually rough, and during shearing they produce dilation which must be adequately scaled. The roughness should be modelled directly to the geometric scale. When a modelled surface is produced by direct cast on a natural discontinuity, the corresponding prototype amplitudes may be so high that they become unrealistic. This is a particularly severe problem, where the geometric scale factor is high. It is almost impossible to find a synthetic material whose properties can all be satisfactorily scaled; hence a selection of properties which are most important for the problem concerned must be made. To eliminate some of the aforementioned problems associated with scaling, it was decided to carry out this study by using a relatively strong synthetic cast rock material as a substitute for a natural rock , i.e. by using a scaling factor equal to 1.

2.2 Specification for the synthetic rock properties

In nature, rock-rock interfaces occur in any rock type, from the weakest to the strongest, whereas soil-rock interfaces are formed between soils and relatively weak rocks. Typical natural soil-rock interface are formed by alternate beds of soils with sedimentary rocks such as limestones, sandstones, siltstones, mudstones, shales etc. Therefore, the main requirement for the synthetic rock was to be moderately strong, so that it could be used in a testing program both for rock joints and soil-rock interfaces. The properties set for the synthetic rock, as being representative for such types of rocks are shown in Table 2.1. Another important consideration was that the new material should be stable in water so that it could be used in saturated conditions.

2.3 Selection of constituents
2.3.1 Cementing material

The main model materials most commonly used in rock mechanics problems have a granular "aggregate" and a cementing material such as plaster, cement, resin, oil or

Table 2.1: Specifications of properties of the synthetic rock

No	Property	Units	Value
1	Uniaxial compressive strength	(MPa)	40-80
2	Ratio UCS/UTS	-	10-15
3	Ratio Young's Modulus/UCS	-	100-300
4	Friction angle of planar saw-cut surfaces	(degrees)	30-35
5	Strain at failure	(%)	<0.6
6	Porosity	(%)	<20
7	Density	(Mg/m^3)	2.2-2.7
8	Maximum grain size	(mm)	1

wax (Stimpson, 1970). Recently pure, strong, plaster based materials such as *Hydrostone* (e.g. Kutter & Otto 1990, Huang *et al.* 1993) and *DieKeen* (Handanyan *et al.*, 1990) have been used as rock substitutes in studies of behaviour of rock and rock joints. Johnston & Choi (1986) used a synthetic weak rock substitute by pressing a mix of a natural mudstone powder with different water contents. In the present study an effort was made to develop a cement based material, suitable for substitution of low to medium strength sedimentary rocks commonly encountered in rock - soil interfaces. Unlike plaster, cement is stable in water and can therefore be used in tests with water saturated conditions. Another advantage is the lack of any need for oven curing. However, the time required to gain its full strength, together with low brittleness, make the Ordinary Portland cement unsuitable. A special cement with improved properties, which was adopted for this study is a calcium aluminate cement (CAC) -commonly called High Alumina Cement (HAC)- manufactured in U.K. by Lafarge Special Cements and used mainly in the refractory industry under the trade name *ciment fondu*. The main advantage of calcium aluminate cement over ordinary Portland cement are the higher strength, the faster rate of gain in strength and the lower porosity. It is a rapid hardening cement, but unlike plaster it is not quick setting; its setting time is comparable with that of ordinary Portland cement. However, after CAC has set, it gains strength so rapidly that within 24 hours the compressive strength of the concrete made with it can be as high as 90 per cent of the ultimate strength (Neville, 1975), as shown in Fig. 2.1.

Calcium aluminate cement is a dark grey powder with a bulk density of 1150 kg/m^3 , specific gravity 3.25, an average specific surface area according to BS 915 (1972) 3000 cm^2/g and a residue on 90 micron sieve <8% (Ciment Fondu Lafarge, 1990a, 1990b). The main constituents of CAC are CaO, Al_2O_3, SiO_2, Fe_2O_3 and FeO. Some minor constituents also exist (Table I.1, Appendix I).

The principal mineralogical phase is monocalcium aluminate ($CaO.Al_2O_3$) whereas the secondary phases are:

> $2CaO.SiO_2$ (C_2S)- β calcium silicate
>
> $4CaO.Al_2O_3.Fe_2O_3$ (C_4AF) - calcium ferrites and
>
> $12CaO.7Al_2O_3$ ($C_{12}A_7$)
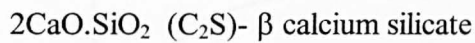
In the abbreviations given in parentheses C stands for CaO, A for Al_2O_3 and F for Fe_2O_3.

The initial setting time for mortar measured on the VICAT needle according to BS 4550:1978 at 20° C is 2 hr 10 mins to 2 hr 30 mins and the final setting 2hr 30 mins to 3 hr 10 mins. For neat cement paste according to BS915:Part 2:1972 the initial set is between 2 and 6hrs and the final set not more than 2 hours after the initial set.

Although the calcium aluminate cement is a rapid hardening cement its setting time is sufficient for controlled casting, cleaning of tools etc.

The total heat of hydration of CAC is in the range 110-120 cal/g which is virtually equivalent to that of Portland cements. However, this heat is liberated within 1 day, compared to 25-50% in the latter case.

The nature of hydrates formed depends on temperature. For hydration below 25°C the following two metastable hexagonal aluminates are formed:

> $CaO.Al_2O_3$ $10H_2O$ (CAH_{10})
>
> $2CaO.Al_2O3$ $8H_2O$ (C_2AH_8)
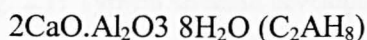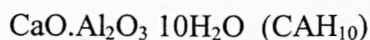
These hydrates change with time to a cubic stable form, following the reactions:

> $3CAH_{10} \rightarrow C_3AH_6 + 2AH_3 + 18H_2O$
>
> $3C_2AH_8 \rightarrow 2C_3AH_6 + AH_3 + 9H_2O$
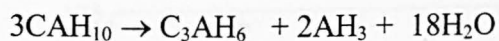
This change - known as "conversion"- takes several years at a temperature of 20°C, but happens much more rapidly as the temperature increases and is accompanied by an increase in the porosity of the cement paste which leads to lower strengths. In a laboratory environment conversion has no any adverse effect on strength if the product (mortar or concrete) is used in less than a year. According to the manufacturer, the shrinkage characteristics of CAC are as follows:

Time	6 hrs	1 day	3 days	7 days	14 days	28 days
Shrinkage (μm/m)	0	200	500	600	680	700

On a standard mortar 1:2.7 (cement : aggregate ratio) with a water/cement ratio = 0.4, the following mechanical properties are obtained:

Age	6hrs	24 hrs	7 days	28 days
Flexural strength (MPa)	4.5-6.5	6.5-8.5	7.5-9	8-12
Compressive strength (MPa)	35-45	60-70	75-85	80-95
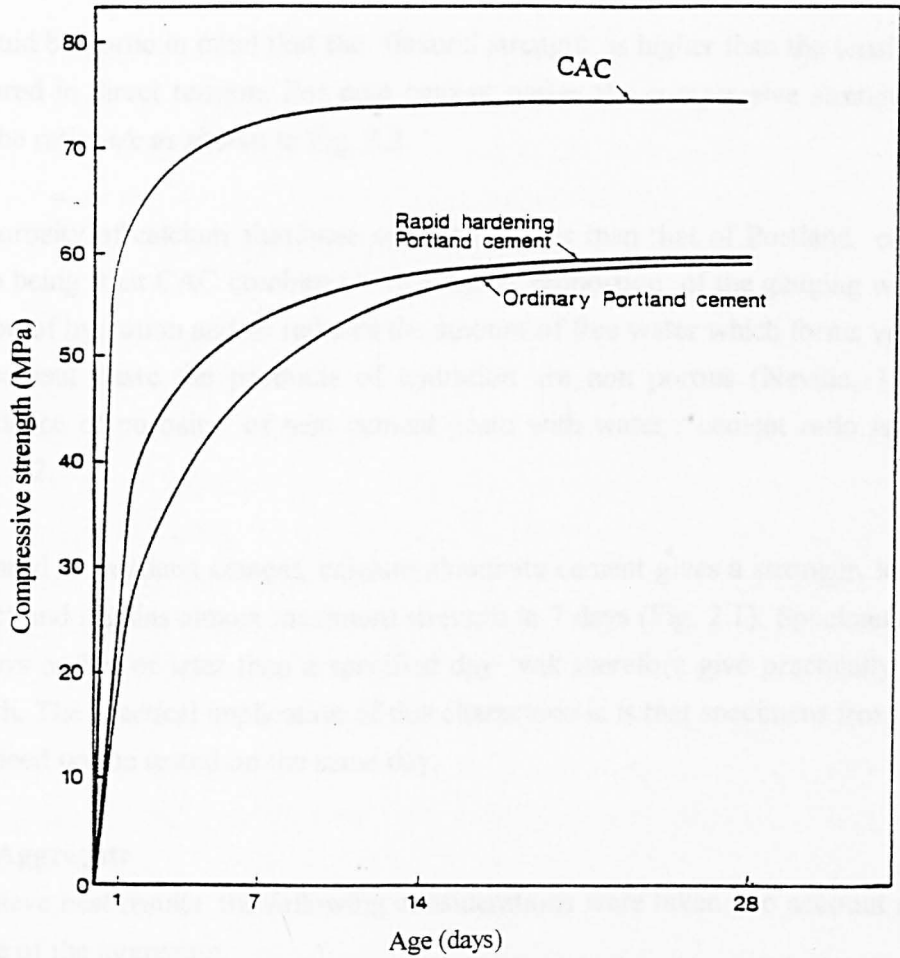
Fig. 2.1: Typical strength development of CAC and Portland cement concrete made with a water/cement ratio of 0.4 (after Neville, 1975)
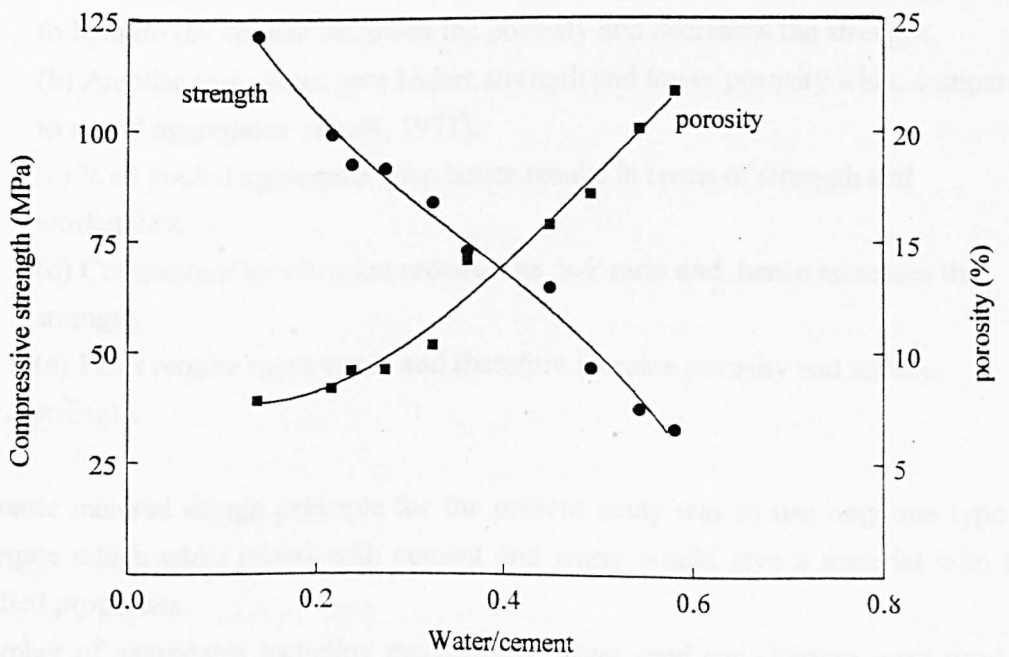
Fig. 2.2: Porosity and compressive strength of neat calcium aluminate cement pastes as a function of water:cement ratio (data from Cottin & Reif, 1980)

It should be borne in mind that the flexural strength is higher than the tensile strength measured in direct tension. For neat cement pastes the compressive strength changes with the ratio *w/c* as shown in Fig. 2.2.

The porosity of calcium aluminate cement is lower than that of Portland cement, the reason being that CAC combines with a higher proportion of the gauging water in the reaction of hydration and so reduces the amount of free water which forms voids. For a neat cement paste the products of hydration are non porous (Neville, 1975). The dependence of porosity of neat cement paste with water / cement ratio is shown in Figure 2.2

Compared to Portland cement, calcium aluminate cement gives a stronger, less porous product and it gains almost maximum strength in 7 days (Fig. 2.1). Specimens tested a few days earlier or later than a specified day will therefore give practically the same strength. The practical implication of this characteristic is that specimens from the same batch need not be tested on the same day.

2.3.2. Aggregate

To achieve best results the following considerations were taken into account regarding the role of the aggregate:

(a) The size of the aggregate should be less than 1 mm for a rock-like material having similar texture to a natural sedimentary rock. The finer the aggregate size the higher water/cement (*w/c*) ratio; the extra water above that required to hydrate the cement increases the porosity and decreases the strength.

(b) Angular aggregates give higher strength and lower porosity when compared to round aggregates (Kraft, 1971).

(c) Well graded aggregates give better results in terms of strength and workability.

(d) Compaction by vibration reduces the *w/c* ratio and hence increases the strength.

(e) Fines require more water and therefore increase porosity and reduce strength.

The basic material design principle for the present study was to use only one type of aggregate which when mixed with cement and water would give a material with the specified properties.

A number of aggregates including marble dust, silver sand and barytes were used as preliminary mixes:

Marble dust consisting of angular particles <1mm, resulted in mixes with higher values for compressive strength, modulus of elasticity and friction angle.

Uniform silver sand with round particles (D<600 μm) gave mixes with lower strength, higher porosity and 8% lower density than the marble dust. Barytes (D_{max} = 300 μm) resulted in product with higher density and similar strength to marble dust.

The results from all these mixes were quite similar with relatively low tensile strength and high strain at failure i.e. reduced brittleness (approaching 1.0%). For each mix the actual values were a function of the cement/aggregate and the water/cement ratios. While these mixes resulted in an acceptable unconfined compressive strength, the tensile strength was relatively low and the axial strain at failure was high. Fortunately, two alternative aggregates which are being used with calcium aluminate cements in the refractory industry, namely andalusite and sillimanite, were employed and gave improved properties. These two minerals have a similar composition and behaviour, and when mixed with CAC and water they gave a material with higher tensile strength, Young's modulus and density and lower strain at failure. As more readily available, andalusite was finally selected, which was mixed only with cement and water to form the synthetic rock.

Andalusite (Al_2SiO_5) appears with the form of coarse prismatic crystals with a nearly square cross section, the prism angle being 89°12' (Mason & Berry, 1968). Some crystals have carbonaceous inclusions arranged so that in cross - section they form a dark cross. This variety is called *chiastolite* (Hamilton *et al.*, 1987*).* Its hardness is 7.5, density 3.15 g/cc and it appears with different colours, the most common being white, grey, pink and brown. It has a vitreous lustre, often dull. Andalusite occurs mainly in contact metamorphosed shales (petites) and occasionally in regionally metamorphosed rocks. It has been recorded from pegmatites and is used in the refractory industry. The andalusite used in the present study had a grey colour and was provided by Sheffield Refractories. The results of a chemical analysis are given in Table I.2 (Appendix I). A microphotograph of the raw andalusite used in the preparation of the synthetic rock, where the shape of the grains can be clearly seen, is shown in Plate 2.1. The grain size was chosen so that 100% passed the 1 mm sieve and 50% was finer than 300 μm. The grain size distribution is given in Fig. I.1 (Appendix I)

2.4 Proportions of constituents

The properties of the synthetic rock vary with the cement:andalusite (*c/a*) ratio and the water cement ratio (*w/c*). A range of *c/a* ratio was used, the main target being to achieve a strong, workable mix, able to copy accurately rough rock surfaces. The main conclusions from these preliminary mixes are as follows:

The compressive strength increases with increasing *c/a* ratio up to a maximum at about 1:1.5, after which it decreases. Young's modulus remains unchanged with *c/a* ratio within the range used. Strain at failure increases with compressive strength. Density decreases with increased *c/a* ratio. Depending on the particular problem to be scaled the appropriate *c/a* ratio can be chosen.

Vibration reduces the amount of mixing water, hence increases strength. The effect is more pronounced for thicker specimens. However, compaction for longer than 1 min may result in segregation. For the present study the main criterion was a high compressive strength material and the final proportions which were selected were:

> Cement   : 1 part by weight
>
> Andalusite   : 1.5 parts by weight
>
> Water/ cement : 0.43

Two slightly different methods were followed for the preparation of the samples: in the first method the mix was poured into steel moulds and placed on an ENDECOTT test sieve shaker and vibrated for 1 minute. In the second method the wet mix was poured into aluminium frames and vibrated by a small hand vibrator for approximately two minutes. The first method was used for the experimental programme on the soil-rock interfaces and the second one on the programme on rock discontinuities. The small vibrator was used because the aluminium frame used for casting the joint replicas was not stiff enough to bear the vibration action and was proved very efficient in removing the air bubbles from the mix; special care was taken to ensure that the size of the pores on the surface of the discontinuity was so small that they were almost invisible.

The strength increases with age as shown in Fig. 2.3. It can be seen that after less than one week the increase in strength is very small and consequently it was decided to test the cast specimens after one week. The proportions finally used resulted in a mix with a good workability. Like all cast materials, some air bubbles remain within the mass of the material even after compaction. However, this has no significant consequence, providing that in the produced rock surface these bubbles are kept to a minimum. The new synthetic rock tends to dry at the free surface and a thin layer becomes dusty. This can be avoided if after setting an anti-drying agent is applied to the free surface.

2.5 Properties of the synthetic rock

2.5.1 Physical Properties

The total porosity was determined with a Micrometrics mercury porosimeter, type AutoPore II 9220. Each of the five samples used was oven dried and evacuated, immersed in mercury, and the mercury pressure on the sample was isostatically
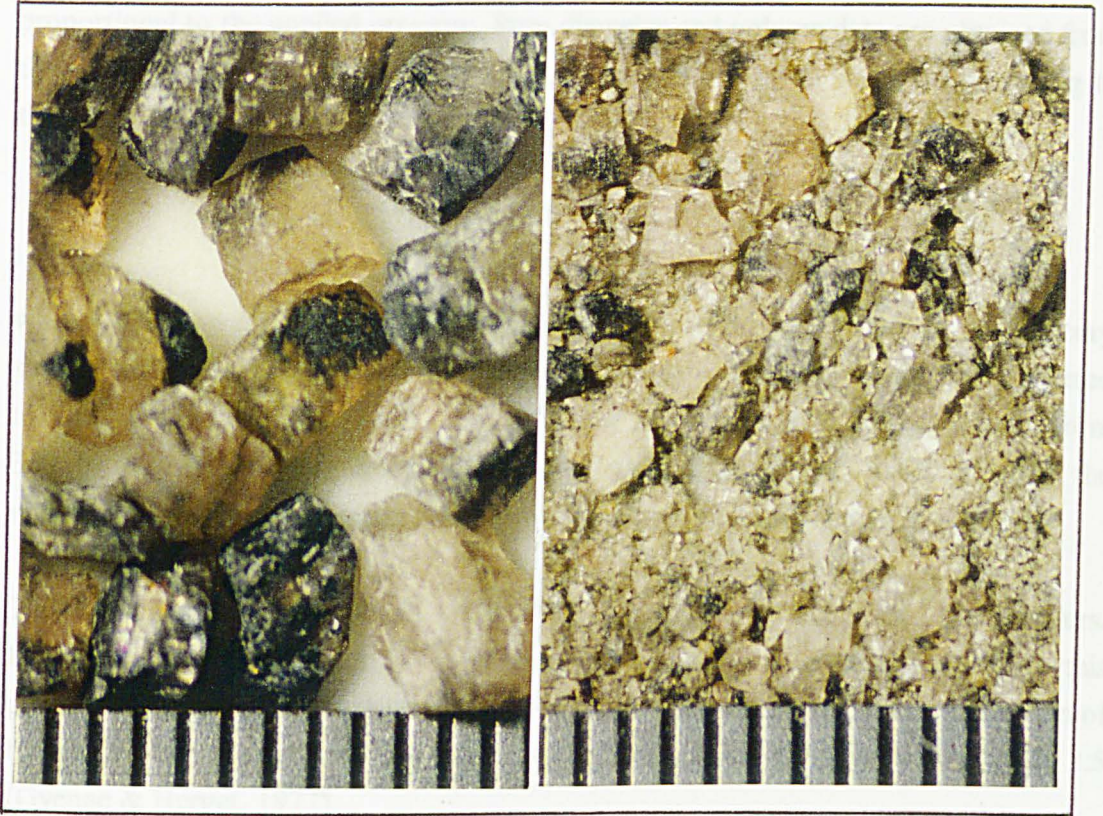
Plate 2.1: Microphotographs of andalusite showing selectected coarse grains (a) and as used (b).
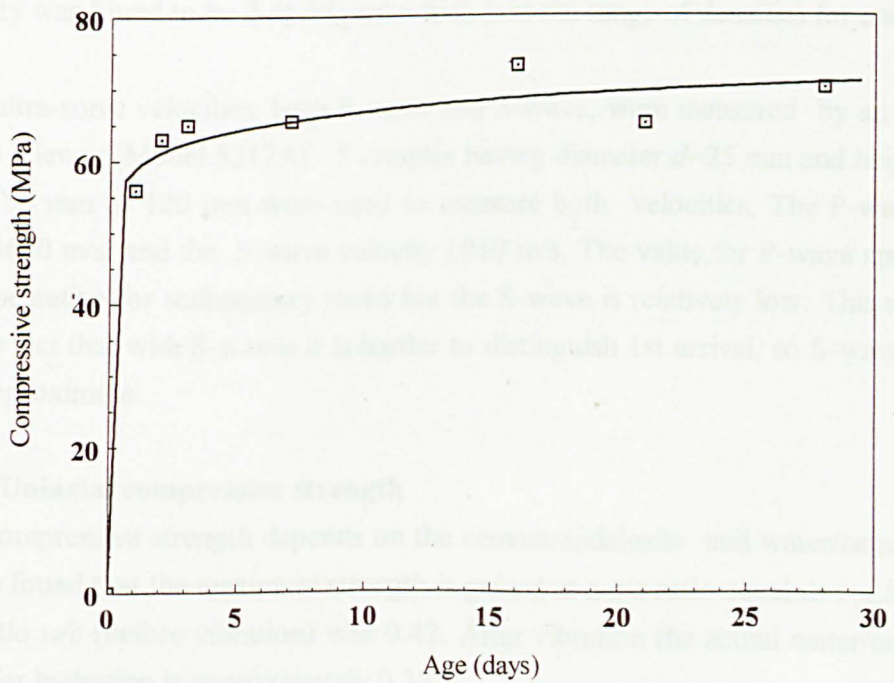
Fig. 2.3: Development of strength with age of the synthetic rock.

increased causing mercury to intrude into the pores. The pore size intruded is inversely proportional to the applied pressure. Pore diameter and volume data are obtained from the equilibrated pressures where mercury intrudes into a given size pore according to the so-called Wasburn equation:

$$D = \frac{-4\gamma \cos\theta}{p} \qquad\qquad (2.1)$$

where D is pore diameter when p is the applied pressure, $\gamma=485$ dyn/cm the mercury surface tension and $\theta=130°$ the interfacial contact angle. The samples are first subjected to low pressure (up to 207 kPa), which allows measurement of pore diameters from 360 to 6 μm and then to high pressure (up to 414 MPa), which extends the measurement of pore diameters from 6 to 0.003μm. Results are shown in Fig. 2.4.

The average porosity was found to be 19%, with specimens oven-dried for 24 hours. During this process the CAC is converted and the porosity is increased. When this porosity is normalised to account for conversion it comes down to 13%. Comparison of the density and porosity of the synthetic with some natural rocks, is shown in Fig. 2.5 (Gyenge & Herget, 1977).

From the same tests the dry density was found equal to 2.27 Mg/m³ whereas the skeletal density was 2.80 Mg/m³. The density of the material "as used", was determined by dividing the mass of a sample by its volume. All the samples tested in compression, tension and triaxial compression (more than 50 samples), were used and the average density was found to be 2.45 Mg/m³ which is in the range of densities for many rocks.

The ultra-sonic velocities, both P-wave and S-wave, were measured by an OYO New Sonic Viewer (Model 5217A). 5 samples having diameter $d=25$ mm and height ranging from 50 mm to 120 mm were used to measure both velocities. The P-wave velocity was 4640 m/s and the S-wave velocity 1910 m/s. The value for P-wave appears to be representative for sedimentary rocks but the S-wave is relatively low. This may be due to the fact that with S-waves it is harder to distinguish 1st arrival, so S-wave velocities are approximate.

2.5.2 Uniaxial compressive strength

The compressive strength depends on the cement/andalusite and water/cement ratios . It was found that the maximum strength is gained at a *c/a* ratio equal to 1:1.5 for which the ratio *w/c* (before vibration) was 0.42. After vibration the actual water/cement ratio used for hydration is approximately 0.38.
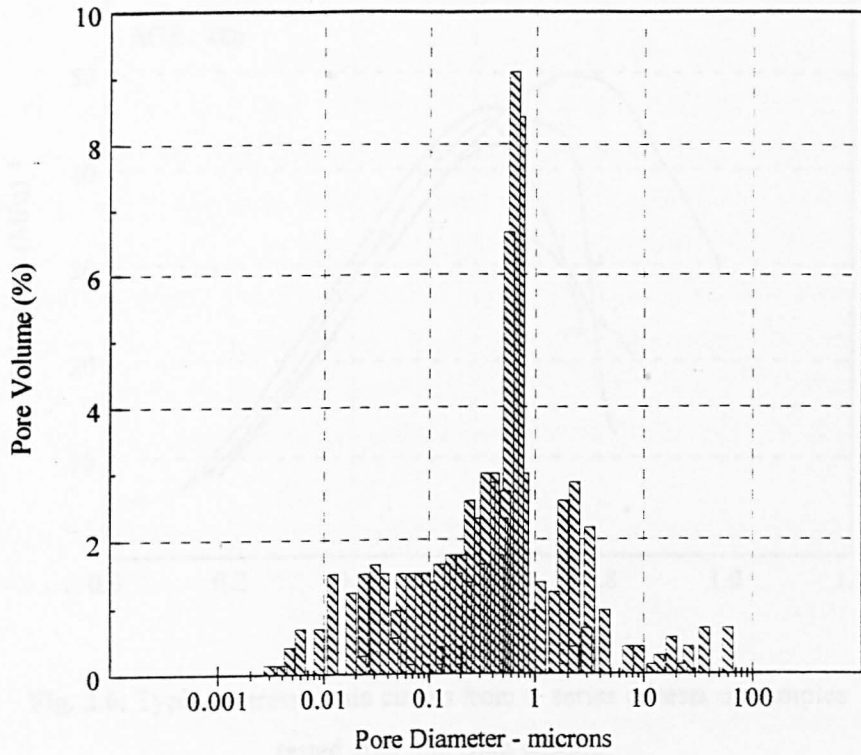
Fig. 2.4: Distribution of pores in the synthetic rock
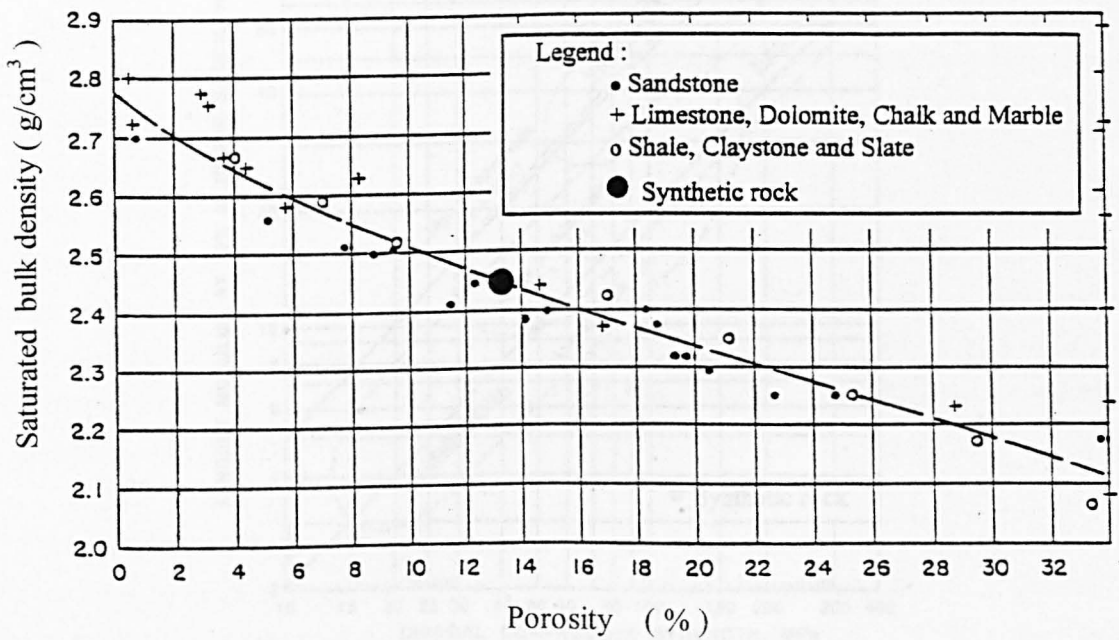
Fig. 2.5: Relationship between porosity and bulk saturated density for various sedimentary rocks (after Gyenge & Herget, 1977)
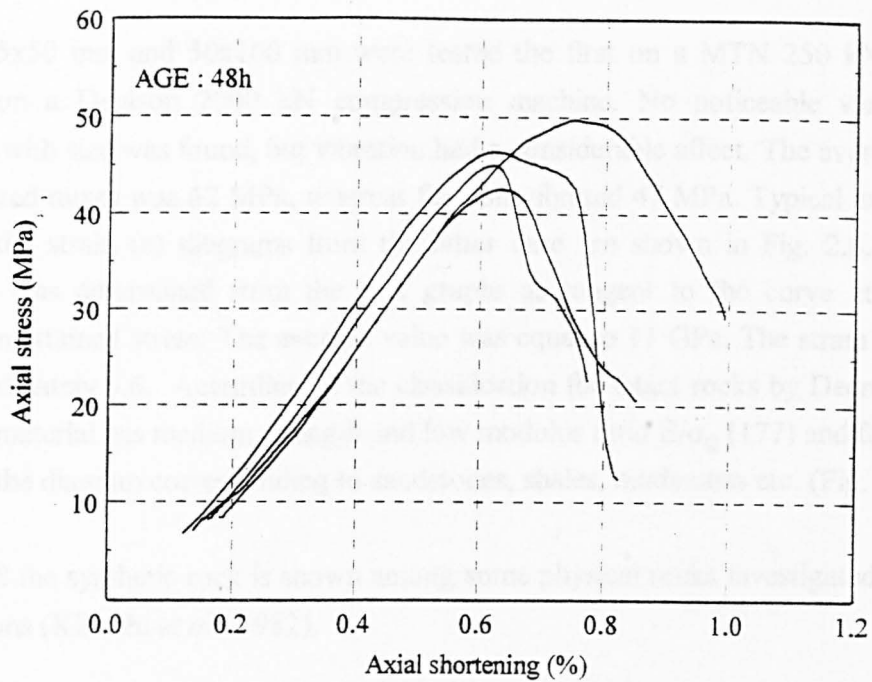
Fig. 2.6: Typical stress-strain curves from a series of tests on samples tested after 48h from casting
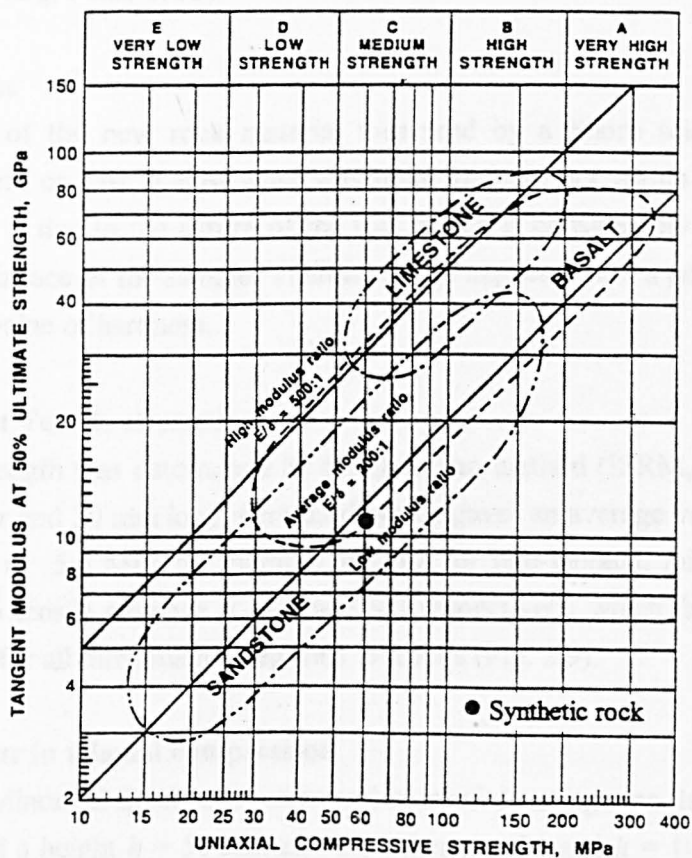
Fig. 2.7. Engineering classification of intact rock based on uniaxial compressive strength and modulus ratio (after Deere & Miller, 1966).

Cores 25x50 mm and 50x100 mm were tested the first on a MTN 250 kN and the second on a Denison 2000 kN compression machine. No noticeable variation of strength with size was found, but vibration had a considerable affect. The average value for vibrated mixes was 62 MPa, whereas for non-vibrated 47 MPa. Typical axial stress (σ) – axial strain (ε) diagrams from the latter case are shown in Fig. 2.6. Young's modulus was determined from the σ–ε graphs as tangent to the curve at 50% of maximum attained stress. The average value was equal to 11 GPa. The strain at failure is approximately 0.6. According to the classification for intact rocks by Deere (1968), the new material has medium strength and low modulus ratio E/σ_c (177) and falls in the areas of the diagram corresponding to sandstones, shales, mudstones etc. (Fig. 2.7).

In Fig 2.8 the synthetic rock is shown among some physical rocks investigated for dam foundations (Kikuchi *et al.*, 1982).

From S- wave velocity and the calculated Young's modulus, Poisson's ratio was found equal to 0.33 (average of 5 specimens), which falls in the range of Poisson's ratio values for limestones (e.g. Pells, 1993).

2.5.3 Hardness
The hardness of the new rock material measured by a Shore scleroscope, on flat surfaces saw-cut or cast against glass was quite variable but within the range 15-25. The variability is due to the nature of the test, which is considerably affected by small pores on the surface of the sample. Therefore, it is expected that a porous material has no consistent value of hardness.

2.5.4 Indirect Tensile strength
The tensile strength was determined by the Brazilian method (ISRM, 1981). Cores 50 mm in diameter and 30 mm long were used which gave an average value of the tensile strength equal to 5.5 MPa for vibrated and 4.8 for non-vibrated mixes. The ratio of compressive to tensile strength is 11.3 and 9.8 respectively, which falls almost on the best-fit curves for all three main categories of rocks (Fig. 2.9).

2.5.5 Behaviour in triaxial compression
Two sizes of cylindrical specimens were used in triaxial testing: one having a diameter $d = 25$ mm and a height $h = 50$ mm and the other $d = 54$ and $h = 100$ mm. The axial stresses are plotted against the confining pressures in Fig. 2.10. The shape of the envelope is concave downwards, but if a Mohr-Coulomb envelope is fitted a cohesion of 16.5 MPa and a friction angle of 30.5° is obtained. As can be concluded from Fig. 2.10, the difference between vibrated and non-vibrated mixes disappears at small
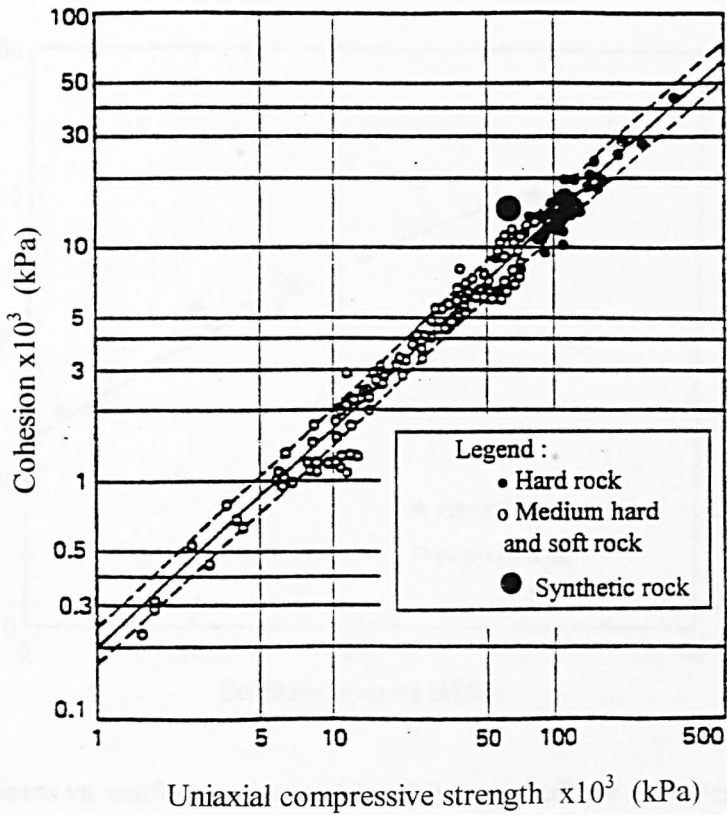
Fig. 2.8: Cohesion value of various rock grades as a function of the uniaxial compressive strength (after Kikuchi *et al.*, 1982)
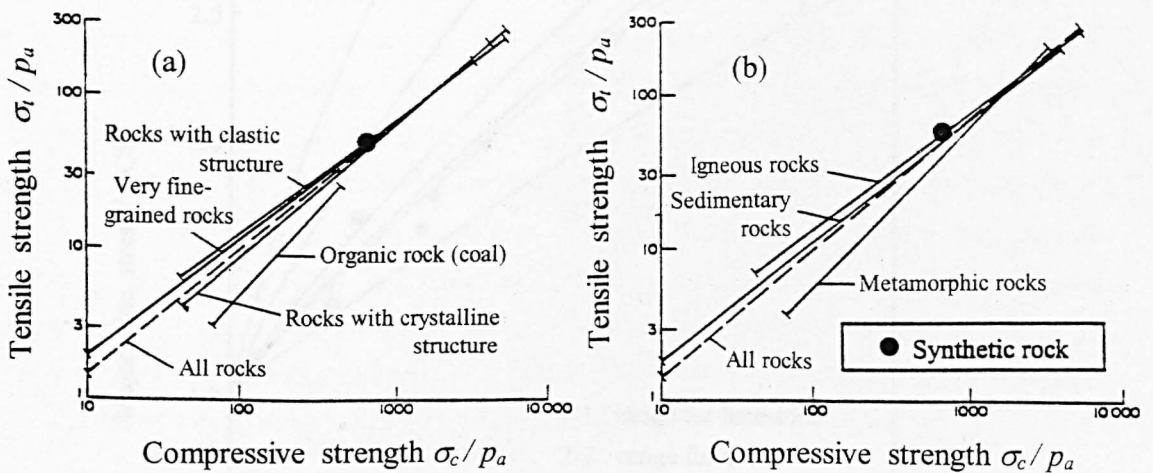
Fig. 2.9: Comparison of best fit relations between uniaxial tensile strengths and uniaxial compressive strengths according to classification based on (a) engineering behaviour and (b) geological origin (after Lade, 1993)
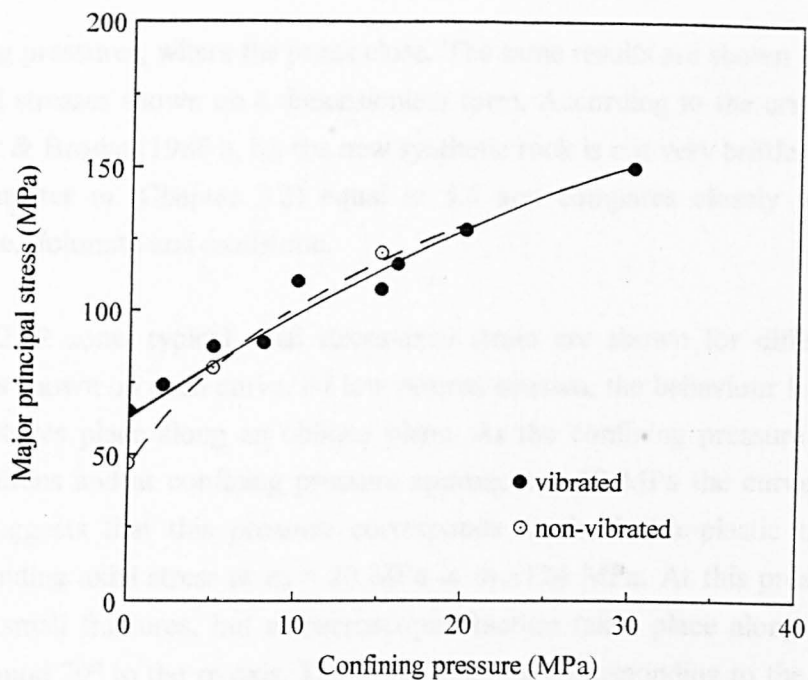
Fig. 2.10: Axial stress vs. confining pressure. Closed symbols indicate results from vibrated mixes, and open symbols from non-vibrated mixes.

1-1 : range for limestone
2-2 : range for dolomite
3-3 : range for sandstone
● synthetic rock
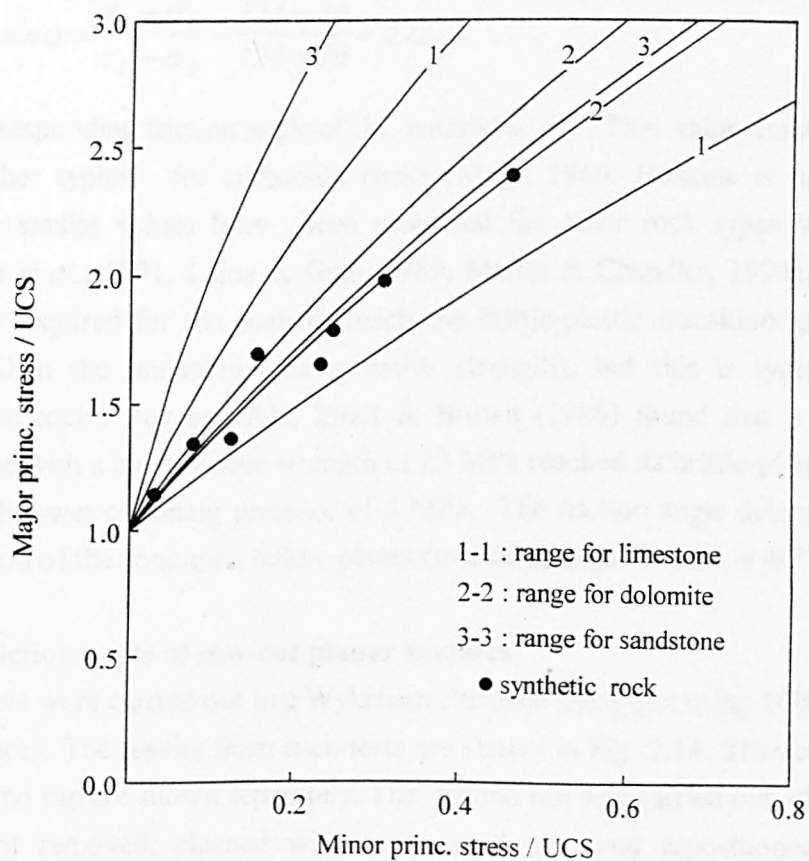
Fig. 2.11: Triaxial behaviour of the synthetic rock

confining pressures, where the pores close. The same results are shown in Fig 2.11 with principal stresses shown on a dimensionless form. According to the criterion proposed by Hoek & Brown (1980 a, b), the new synthetic rock is not very brittle, has a value for the parameter m (Chapter 3.2) equal to 5.9 and compares closely with rocks like limestone, dolomite and mudstone.

In Fig. 2.12 some typical axial stress-axial strain are shown for different confining pressures shown on each curve. At low normal stresses, the behaviour is brittle and the fracture takes place along an oblique plane. As the confining pressure increases, the curve flattens and at confining pressure approaching 20 MPa the curve is horizontal, which suggests that this pressure corresponds to the brittle-plastic transition. The corresponding axial stress at $\sigma_3 = 20$ MPa is $\sigma_1 = 124$ MPa. At this pressure there are multiple small fractures, but a macroscopic fracture takes place along a plane at an angle around 30° to the σ_1 axis. The Mohr diagram corresponding to the state of stress in the brittle-plastic transition is shown in Figure 2.13. The friction angle can be calculated from the tangent to the Mohr circle passing through the origin (Orowan, 1960), which has a slope to the σ axis given by

$$sin\,\phi = \frac{\sigma_1 - \sigma_3}{\sigma_1 - \sigma_3} = \frac{124 - 20}{124 + 20} = 0.72 \qquad (2.2)$$

The corresponding friction angle of the material is 46°. This value may seem high, but it is rather typical for carbonate rocks (Mogi, 1966, Hoskins et al., 1968, etc.), whereas similar values have been measured for other rock types such as granite (Gyenge et al., 1991, Lajtai & Gadi, 1989, Martin & Chandler, 1994). The confining pressure required for the rock to reach the brittle-plastic transition is relatively low (lower than the unconfined compressive strength), but this is typical for porous carbonate rocks. For example, Elliot & Brown (1986) found that a porous oolitic limestone with a compressive strength of 23 MPa reached its brittle-plastic transition at the much lower confining pressure of 5 MPa. The friction angle determined from the orientation of the conjugate failure planes (measured angle $\theta = 63°$) is 46°.

2.5.6 Friction angle of saw-cut planar surfaces

Shear tests were carried out in a Wykeham Farrance shear box using 100x100 mm saw-cut surfaces. The results from such tests are shown in Fig. 2.14. The results from first and second run are shown separately. The second run was carried out after the samples were first removed, cleaned with compressed air and repositioned. Most tests, especially those at the higher normal stresses, exhibited stick-slip behaviour; the magnitude of stick-slip increased with increasing normal stress.
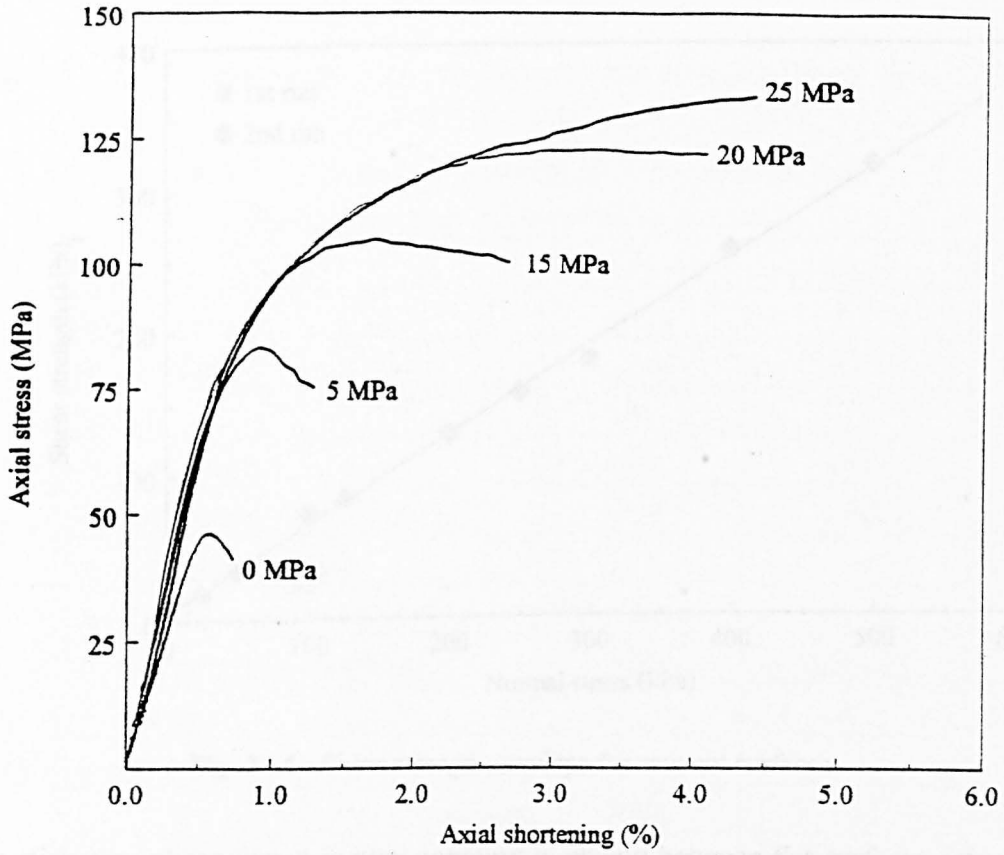
Fig. 2.12. Typical axial stress- axial strain diagrams for different confining pressures shown on each curve
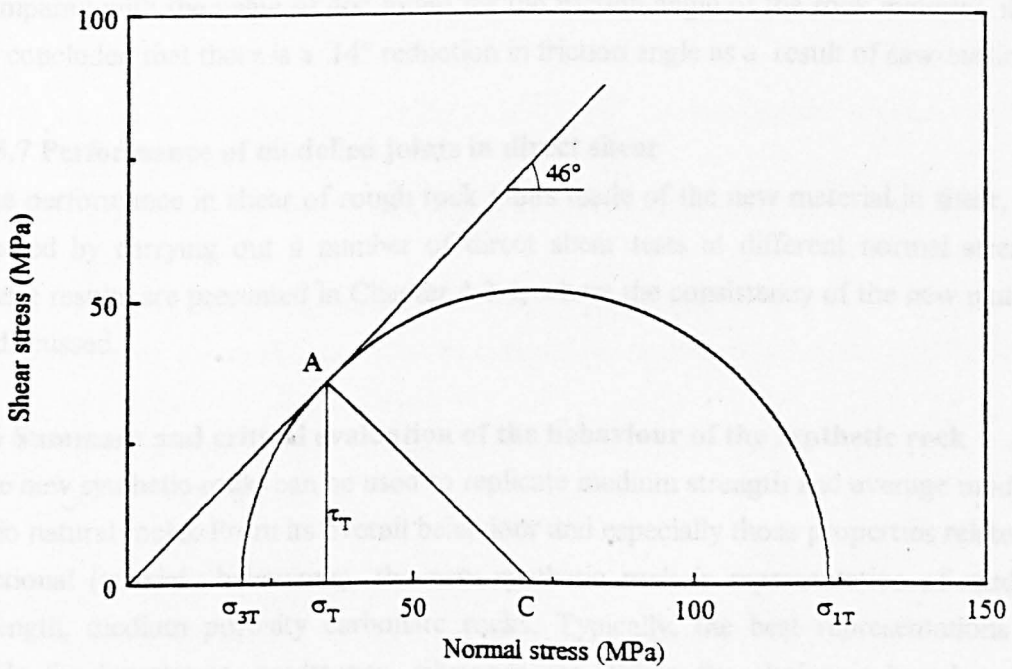
Fig. 2.13. Mohr circle at the brittle-plastic transition
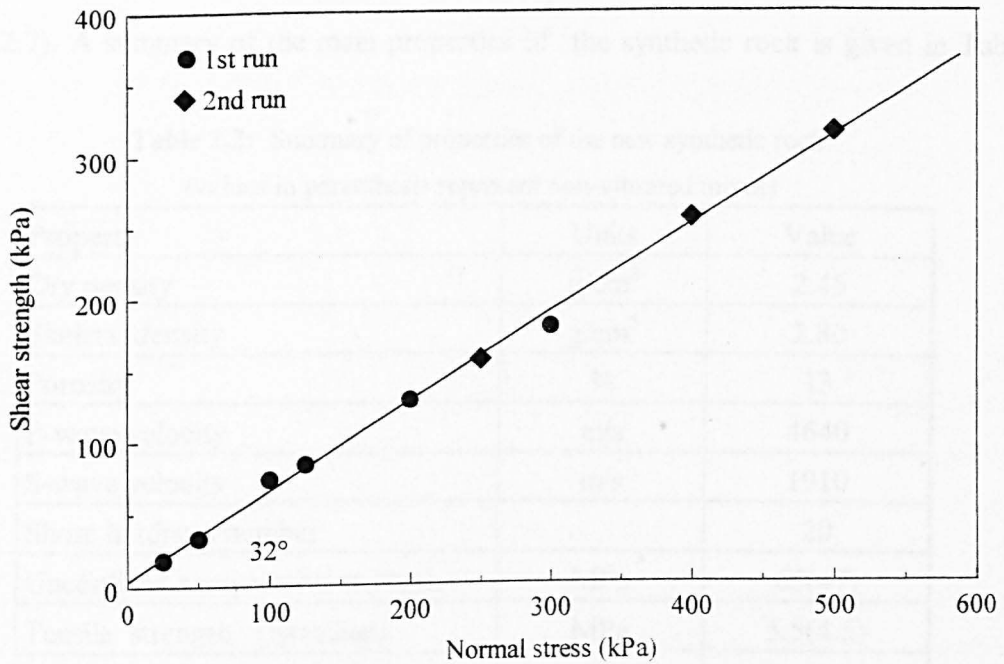
Fig. 2.14 : Shear strength envelope for saw-cut surfaces

The stick-slip phenomenon is very common in sliding between flat surfaces especially at high normal stresses (Lajtai & Gadi 1989). From the plot shown in Fig. 2.14 an average friction angle $\phi=32°$ is derived. Tests on a tilt table on large number (>50) of different saw-cut surfaces gave a similar sliding angle of $32.4°\pm2.3°$. When this value is compared with the value of $46°$ found for the friction angle of the rock material, it can be concluded that there is a $14°$ reduction in friction angle as a result of saw-cutting.

2.5.7 Performance of modelled joints in direct shear

The performance in shear of rough rock joints made of the new material in shear, was studied by carrying out a number of direct shear tests at different normal stresses. These results are presented in Chapter 4.2.4, where the consistency of the new material is discussed.

2.6 Summary and critical evaluation of the behaviour of the synthetic rock

The new synthetic rock can be used to replicate medium strength and average modulus ratio natural rocks. From its overall behaviour and especially those properties related to frictional (triaxial behaviour), the new synthetic rock is representative of medium strength, medium porosity carbonate rocks. Typically, the best representations are made for limestones, mudstones, siltstones etc. When the choice is based on the unconfined compressive strength/Young's modulus ratio, this material can be considered as suitable to represent a wide range of materials such as sandstones, limestones, schists, diabases, basalts etc. and all rock types lying on the same E/σ_c line

(Fig. 2.7). A summary of the main properties of the synthetic rock is given in Table 2.2.

Table 2.2: Summary of properties of the new synthetic rock

(values in parenthesis represent non-vibrated mixes)

Property	Units	Value
Dry density	g/cm^3	2.45
Skeletal density	g/cm^3	2.80
Porosity	%	13
P-wave velocity	m/s	4640
S-wave velocity	m/s	1910
Shore hardness number		20
Unconfined compressive strength	MPa	65(47)
Tensile strength (Brazilian)	MPa	5.5(4.5)
Friction angle	degrees	46
Mohr-Coulomb parameters		
Cohesion	MPa	16.5
Friction angle	degrees	30.5
Friction angle of saw-cut surface	degrees	33

The main advantages of the material include:

(a) It is a simple two component cast material with no special requirements for treatment.

(b) Early development of high strength which practically remains unchanged after the first seven days.

(c) Selection of the desired compressive strength or frictional resistance by adjusting the c/a ratio.

(d) low porosity relatively to other similar materials.

(e) It can be used both as model material at small scaling factors (e.g.<5) and as rock substitute (scaling factor = 1)

(f) Good reproduction of rough joint surfaces, which may be secured by the use of a small vibrator.

On the other hand, the main disadvantages are :

(a) Requirement for curing at temperatures exceeding 25° C, because of the risk of "conversion" . This is not in real problem when the material is being used in the laboratory, where temperature is expected to be lower than 25° C.

(b) Drying of the free surface, necessitating the use of an anti-drying agent if the free surface has to remain unaltered.

CHAPTER 3
SHEAR STRENGTH OF ROCK DISCONTINUITIES

3.1 Introduction

The shear behaviour of rock discontinuities has attracted a great number of investigators over the past three decades. An impressive number of studies have been devoted to all aspects of shearing along joints. Numerous models have been proposed to describe characteristic shear strength parameters, such as peak shear strength, or complete shear and normal behaviour or coupled hydromechanical response. Although, the basic mechanism of shearing along a rock joint is widely accepted and despite the large amount of existing data, the most widely used shear strength criteria remain empirical in nature. Incorporation of these empirical criteria into numerical models of rock mass behaviour make their predictive capabilities, at best, as good as the accuracy of the performance of these empirical models which are based mainly on purely empirical input parameters.

It is customary to consider that the shearing resistance of a rock discontinuity is made up of the following components:
a) a component due to frictional resistance of flat surfaces
b) a dilational component
c) an asperity failure component and
d) a plough component

Most models for predicting shear strength use the first two or three components whereas some recent ones have introduced the plough component to account for changes of shear stress with shear displacement.

While the separation of the shearing resistance into the above components is convenient in qualitative terms, their exact quantitative contribution to the shear strength is extremely difficult, since they all occur at the same time. The situation becomes more difficult when considering their variation with normal stress and scale. Understandably, this difficulty made several investigators turn to empirical relations.

3.2 Shear strength of intact rock
3.2.1 Introduction

The shear characteristics of a rock discontinuity are partly determined by the characteristics of the intact rock material which forms the walls. It is therefore necessary to describe the basic characteristics of the shear behaviour of intact rock. The shear strength of intact rock is best studied by the triaxial compression test where $\sigma_1 > \sigma_2 = \sigma_3$. The complete axial stress (σ_1) - axial strain (ε_1) curves in triaxial

compression at different confining pressures are similar to those obtained by Wawersik & Fairhurst (1970) for Tennessee Marble at different confining pressures (Fig. 3.1). As the confining pressure increases

(a) the peak strength increases;

(b) the type of behaviour changes from typically brittle to fully plastic;

(c) there is a flattening and widening of the region incorporating the peak of the (σ_1)-(ε_1) curve;

(d) the post-peak drop in the stress to the residual strength reduces and disappears at high values of σ_3.

The change in behaviour from brittle to fully ductile (corresponding to $\sigma_3 = 48.3$ MPa in Figure 3.1) is known as the *brittle-ductile transition* or more accurately *brittle - plastic transition* (Rutter, 1986) and varies with the rock type. Generally, the dependence on confining pressure of the maximum differential stress $(\sigma_1-\sigma_3)$ preceding failure is non-linear (Fig. 3.2)

3.2.2 Fracture criteria for isotropic rock

All the fracture criteria used in practice have the following form:

$$\sigma_1 = f(\sigma_3) \tag{3.1}$$

The simplest and most important of the phenomenological criteria is the Coulomb's shear strength criterion, stating that shear failure takes place in that plane for which

$$\tau = c + \sigma_n \tan\phi \tag{3.2}$$

where

c is the "*cohesion*" and ϕ the "*angle of internal friction*" and

τ is the shear strength on the plane.

In terms of principal stresses the criterion is expressed by a linear relation (at least over a moderate range of confining pressure) between σ_1 and σ_3, namely

$$\sigma_1 = \sigma_0 + q\sigma_3 \tag{3.3}$$

where σ_0 is a constant, equal to the unconfined compressive strength C_0, if the relation is obeyed down to zero confining pressure and q a constant with a value usually between 2 and 11 (Paterson, 1978). The parameters in the two expressions of the criterion are related to the following expressions

$$\sin\phi = \frac{q-1}{q+1} \quad \text{(a)} \qquad\qquad c = \frac{C_0}{2\sqrt{q}} \quad \text{(b)} \tag{3.4}$$
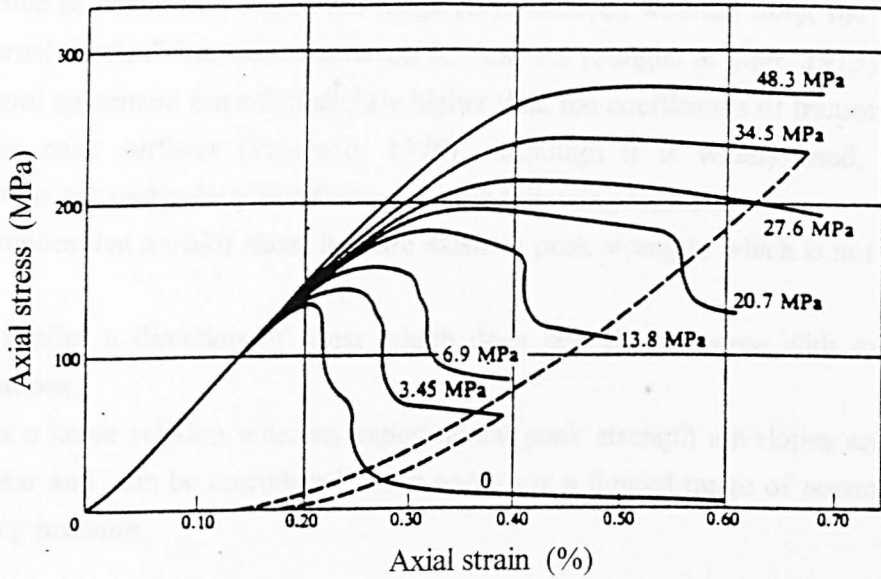
Figure 3.1: Axial stress-axial strain curves of Tennessee Marble at the confining pressures indicated by the numbers on each curve (after Wawersik & Fairhurst, 1970).
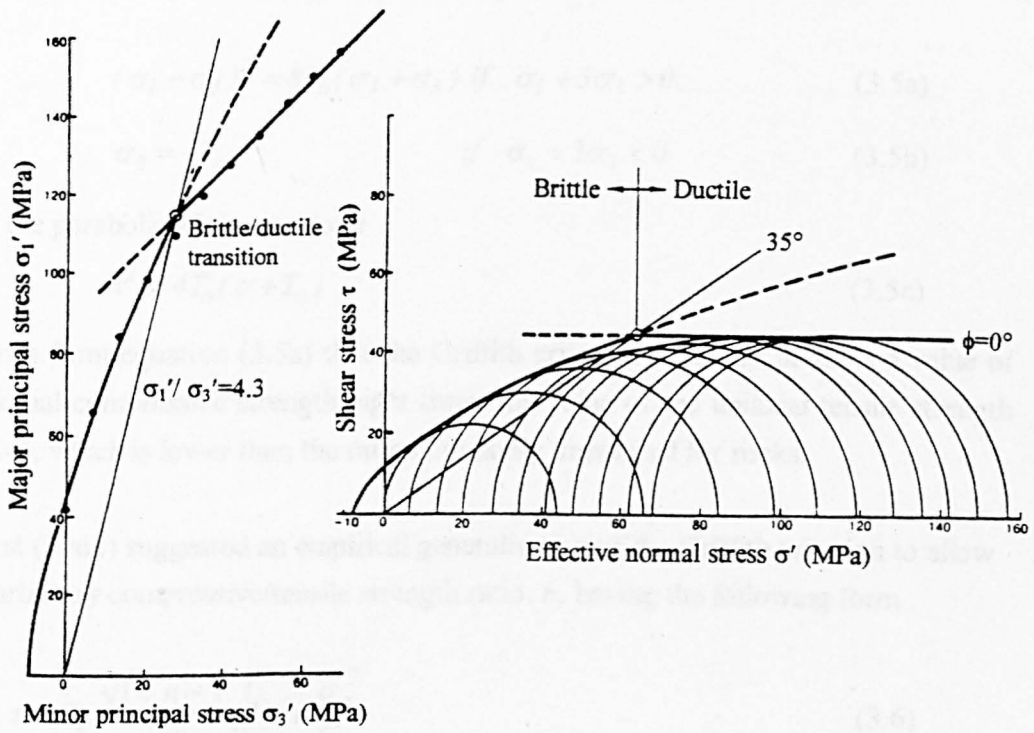
Figure 3.2 Dependence of differential stress at failure in compression on confining pressure for Indiana Limestone illustrating brittle-plastic transition
(Data from Schwartz, 1964, after Hoek , 1983)

The value of cohesion c lies in the range $(0.15\text{-}0.35)C_o$ whereas $tan\phi$, the "coefficient of internal friction" has values between 0.5 and 1.5 (Sangha & Dhir, 1975), which are in general agreement but often slightly higher than the coefficients of friction for sliding between rock surfaces (Paterson, 1978). Although it is widely used, Coulomb's criterion is not particularly satisfactory for the following reasons:

(a) It implies that a major shear fracture exists at peak strength, which is not always the case.

(b) It implies a direction of shear which does not always agree with experimental observations.

(c) It is a linear relation whereas experimental peak strength envelopes are generally non-linear and can be considered linear only over a limited range of normal stress or confining pressure.

Griffith (1921) postulated that fracture of brittle materials is initiated at tensile stress concentrations at the tips of hypothetical minute elliptical cracks (Griffith cracks) in the material. He developed a criterion described by

$$(\sigma_1 - \sigma_3)^2 = 8T_o(\sigma_1 + \sigma_3) \quad if \quad \sigma_1 + 3\sigma_3 > 0 \qquad (3.5a)$$

$$\sigma_3 = -T_o \qquad\qquad if \quad \sigma_1 + 3\sigma_3 < 0 \qquad (3.5b)$$

and to the parabolic Mohr envelope

$$\tau^2 = 4T_o(\sigma + T_o) \qquad (3.5c)$$

It follows from equation (3.5a) that the Griffith criterion of failure predicts a value of the uniaxial compressive strength eight times the value of the uniaxial tensile strength (Fig. 3.4), which is lower than the ratio commonly measured for rocks.

Fairhurst (1964) suggested an empirical generalisation of the Griffith criterion to allow for an arbitrary compressive/tensile strength ratio n, having the following form

$$\tau = C_o \frac{\sqrt{1+n}-1}{n} \sqrt{1 + n\frac{\sigma_n}{C_o}} \qquad (3.6)$$

where

τ is the shear strength

σ_n the normal stress and

C_o the unconfined compressive strength

McLintock & Walsh (1962) modified the Griffith criterion in order to take into account friction forces between the surfaces of closed cracks, since the original criterion was
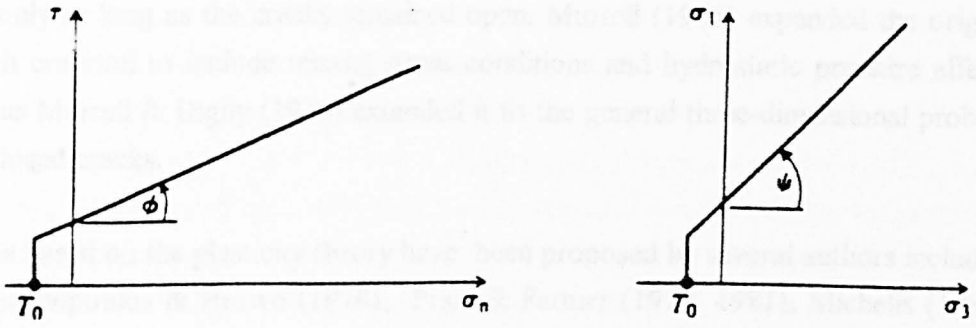
Fig. 3.3: Mohr-Coulomb envelopes with a tensile cut-off

$$(\sigma_1 - \sigma_2)^2 = 8T_0(\sigma_1 + \sigma_2)$$

$$\tau^2 = 4T_0(\sigma_n + T_0)$$
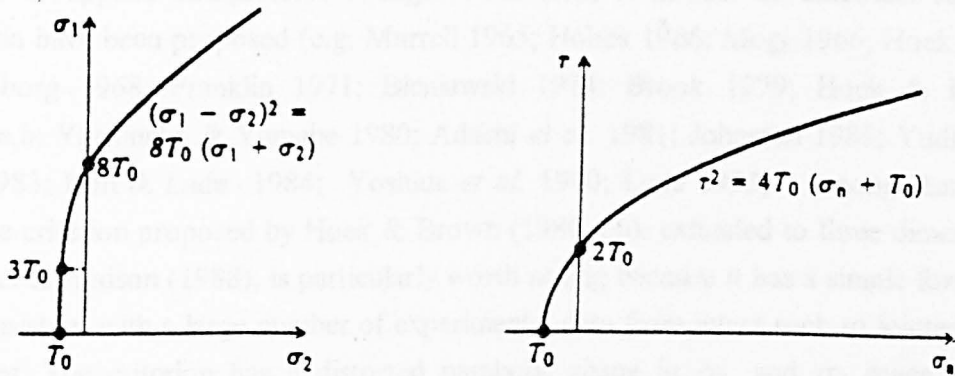
Fig. 3.4: Griffith envelopes

$m = 14.3$
$r^2 = 0.87$
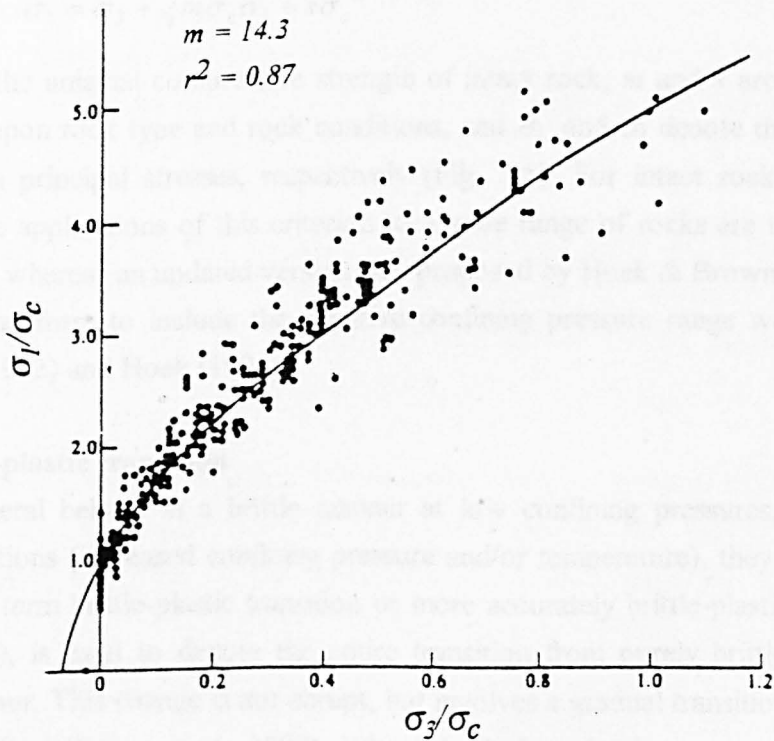
Fig 3.5: Normalised peak strength envelope for sandstones (after Hoek & Brown, 1980 a,b)

valid only as long as the cracks remained open. Murrell (1965) expanded the original Griffith criterion to include triaxial stress conditions and hydrostatic pressure effects, whereas Murrell & Digby (1970) extended it to the general three-dimensional problem with closed cracks.

Criteria based on the plasticity theory have been proposed by several authors including Gerogiannopoulos & Brown (1978), Price & Farmer (1979, 1981), Michelis (1985), and Elliot & Brown (1986).

However, because all these criteria have been found not to apply to rock over a wide range of applied compressive strength conditions, a number of empirical strength criteria have been proposed (e.g. Murrell 1965; Hobbs 1966; Mogi 1966; Hoek 1968; Lundborg 1968; Franklin 1971; Bieniawski 1974; Brook 1979; Hoek & Brown 1980a,b; Yoshinaka & Yamabe 1980; Adachi et al. 1981; Johnston 1985; Yudhbir et al. 1983; Kim & Lade 1984; Yoshida et al. 1990; Lade 1993). Among them, the failure criterion proposed by Hoek & Brown (1980 a,b), extended to three dimensions by Pan & Hudson (1988), is particularly worth noting because it has a simple form and is consistent with a large number of experimental data from intact rock to jointed rock masses. The criterion has a distorted parabolic shape in σ_1 and σ_3 space and is expressed as

$$\sigma_1 = \sigma_3 + \sqrt{m\sigma_c\sigma_3 + s\sigma_c^2} \qquad (3.7)$$

where σ_c is the uniaxial compressive strength of intact rock, m and s are parameters that depend upon rock type and rock conditions, and σ_1 and σ_3 denote the maximum and minimum principal stresses, respectively (Fig. 3.5). For intact rock s is unity. Results of the applications of this criterion to a wide range of rocks are tabulated by Hoek (1983), whereas an updated version was proposed by Hoek & Brown (1988) and a more general form to include the negative confining pressure range was given by Hoek et al. (1992) and Hoek (1994).

3.2.3 Brittle-plastic transition

Rocks in general behave in a brittle manner at low confining pressures, but under suitable conditions (increased confining pressure and/or temperature), they can exhibit ductility. The term brittle-plastic transition or more accurately brittle-plastic transition (Rutter, 1986), is used to denote the entire transition from purely brittle to purely plastic behaviour. This change is not abrupt, but involves a gradual transition through a "semi-brittle" field (Evans et al., 1990). When physical mechanisms are considered, a variety of potential deformation mechanisms in the ductile field and correspondingly a variety in the character of brittle-plastic transition may occur as shown in Table 3.1.

Thus no single view of the brittle-plastic transition can be valid under all conditions (Paterson, 1978). However, there are two simplified views of how a brittle-plastic transition can happen with increasing confining pressure. These cases have been characterised by Mogi (1972, 1974) as A-type and B-type transitions and represent extremes in the range of behaviour that can be expected at relatively low temperatures: A-Type corresponds to rocks which deform in the ductile field entirely by *crystal plasticity* whereas B-type occurs entirely by *cataclastic flow.*

a) A-type rocks (Simple crystal plasticity case, Fig. 3.6a). Crystal plasticity is a term used to describe the permanent deformation of crystalline material by slip and twinning within grains. Both processes are basically simple shearing processes. In this case faulting occurs after some permanent deformation, which increases with increasing pressure. The large permanent strain in the post-yield region before fracture occurs by homogeneous plastic deformation. The brittle-plastic transition may occur when the fracture strength is equal to the yield strength.

b) B-type rocks (simple cataclastic flow case, Fig. 3.6.b). Cataclastic flow is a term describing the permanent straining achieved by the combination of the disturbed fracturing whereas the material is broken into fragments, and the relative movement of fragments. This mechanism is similar to the flow of a granular material (Paterson, 1978). In this case the stress drop occurs just after the yield point and the permanent deformation in the post-yield region occurs by cataclastic flow or frictional sliding. According to Orowan (1960) the brittle-plastic transition pressure is the pressure at which the strength of rock at faulting is equal to the strength due to frictional resistance after faulting.

Some carbonate rocks are A-type, whereas many silicate rocks are B-type but most rocks seem to be intermediate between these two types and near the transition pressure probably both fracturing and plastic deformation contribute to the inelastic deformation just before and after yielding (Mogi, 1974).

For both cases the ductility, which is defined as the ability to undergo large permanent deformation without fracture (Handin, 1966) increases as the confining pressure increases, whereas the stress drop decreases. Orowan (1960) suggested that the stress drop characteristic of fracture does not occur at high pressure because frictional resistance on the fault surface becomes higher than the shearing strength of rock. This idea has been used as a possible explanation of the brittle-plastic transition by Maurer (1965), Mogi (1966) and Byerlee (1968). Mogi (1966) found that the brittle-plastic

Table 3.1: Schematic diagram illustrating the phenomenology of the brittle-plastic transition (after Evans *et al.* 1990)

Failure Mode	< ―――― Brittle ――――― > < ――――――――――――――Ductile―――――――― >
	< ― Semibrittle――― >
Attributes	< ――――――――――― Cataclasis―――――――――――― > < ―――― Plastic ―――― >

	Brittle	Semibrittle / Ductile	Plastic
Permanent Strain before Failure	< ―――― <3% ―――― >	< ―――― >3%―――― >	< ―――― >5% ―――― >
Work Softening	< ―――――――――― >		
Possible Stress Drop	< ―――――― >		
Loss in Cohesion	< ―――――― >		
Microcracking	< ――――――――――――――――――――――――― >		
Dilatancy	< ――――――――――――――――――――――――― >		
Acoustic Emission	< ――――――――――――――――――――――――― >		
Pressure Dependence of Strength	< ――――――――――――――――――――― >		
Temperature Dependence of Strength	< ――――――――――― low ――――――――――― > < ―――― high――― >		
Deformation Mechanisms	Distributed and Localized Microcracking	Distributed Microcracking, Local Plasticity	Fully Plastic
Macroscopic Appearance			
Typical Axial Stress-Strain Curves			
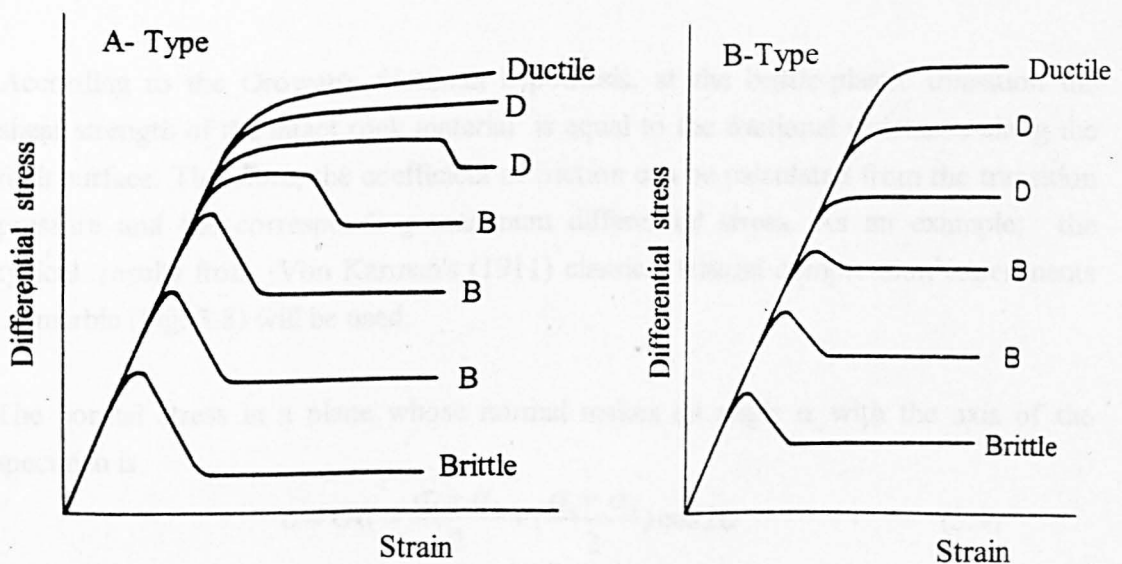
Figure 3.6: Types of transitions : (a) A-type, simple crystal plasticity. (b) B-type, simple cataclastic flow (after Mogi, 1974)

transition boundary in the differential stress vs. confining pressure graph is expressed by the linear curve (Figure 3.7a)

$$\sigma_1 - \sigma_3 \approx 3.4\sigma_3 \qquad (3.8)$$

for various silicate rocks, whereas the transition boundary in carbonate rocks is somewhat different (Figure 3.7b).

Mogi (1972) suggested that the frictional hypothesis can explain the brittle-plastic transition for B-type rocks which deform in the post-yield region by cataclastic flow or frictional sliding, but it may not be applicable to A-type rocks, in which large permanent strain before fracture takes place by homogeneous plastic deformation.

Byerlee (1968) argued that the brittle-plastic transition boundary is independent of rock type, and that Orowan's frictional hypothesis is valid for both silicate and carbonate rocks. The difference in the interpretation of the brittle-plastic behaviour in the two rock types may be due to some confusion about the definition of the brittle or plastic state. Heard (1960) defined brittle or plastic behaviour by using the ductility. The rock specimen is considered brittle if the maximum strain was less than 3%, transitional between 3% and 5%, and plastic above 5%. Using this definition, the frictional hypothesis can explain the B-type behaviour but it may be not applicable to A-type. On the other hand, Byerlee (1968) defined the brittle or plastic state by whether or not stress drop occurs after faulting. In this case, the brittle-plastic transition can be explained by the frictional hypothesis for both A- and B-types, as pointed out by Mogi (1974).

According to the Orowan's frictional hypothesis, at the brittle-plastic transition the shear strength of the intact rock material is equal to the frictional resistance along the fault surface. Therefore, the coefficient of friction can be calculated from the transition pressure and the corresponding maximum differential stress. As an example, the typical results from Von Karman's (1911) classical triaxial compression experiments on marble (Fig. 3.8) will be used.

The normal stress in a plane whose normal makes an angle α with the axis of the specimen is

$$\sigma = OC = \frac{\sigma_1 + \sigma_3}{2} + (\frac{\sigma_1 - \sigma_3}{2})\cos2\alpha \qquad (3.9)$$

and the shear stress is

SILICATE ROCKS

Differential stress (MPa)

$\sigma_1 \approx 4.4\ \sigma_3$

Brittle

Ductile

(a)

Confining pressure (MPa)

CARBONATE ROCKS

Differentia stress (MPa)

Brittle

Ductile

(b)

Confining pressure (MPa)

39
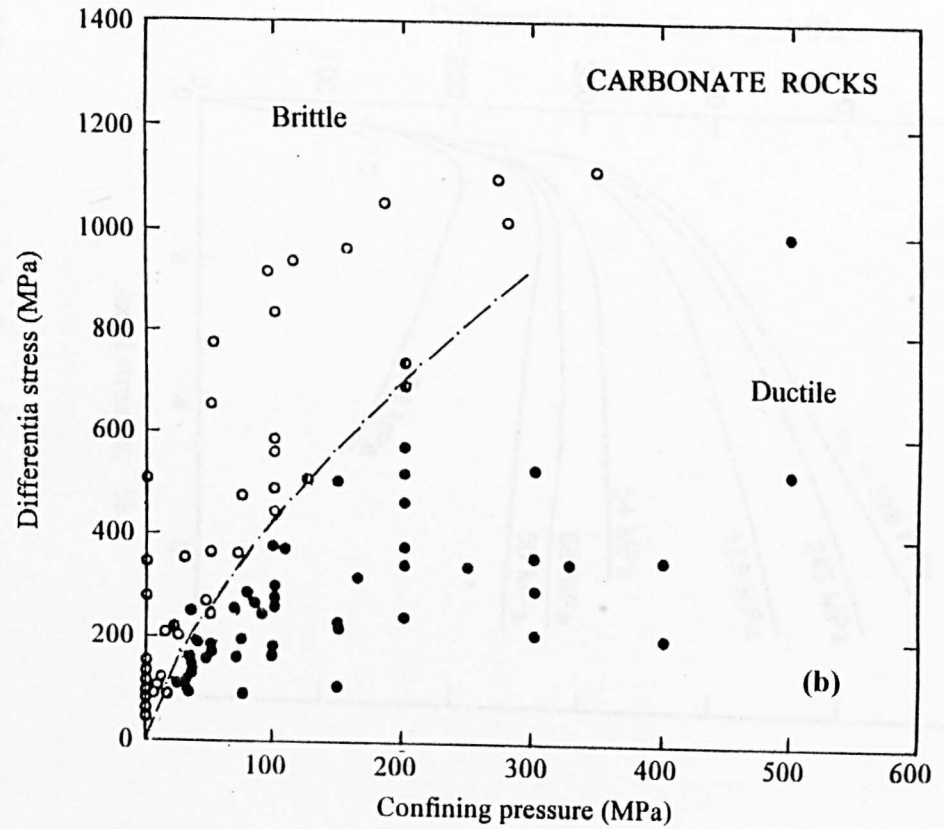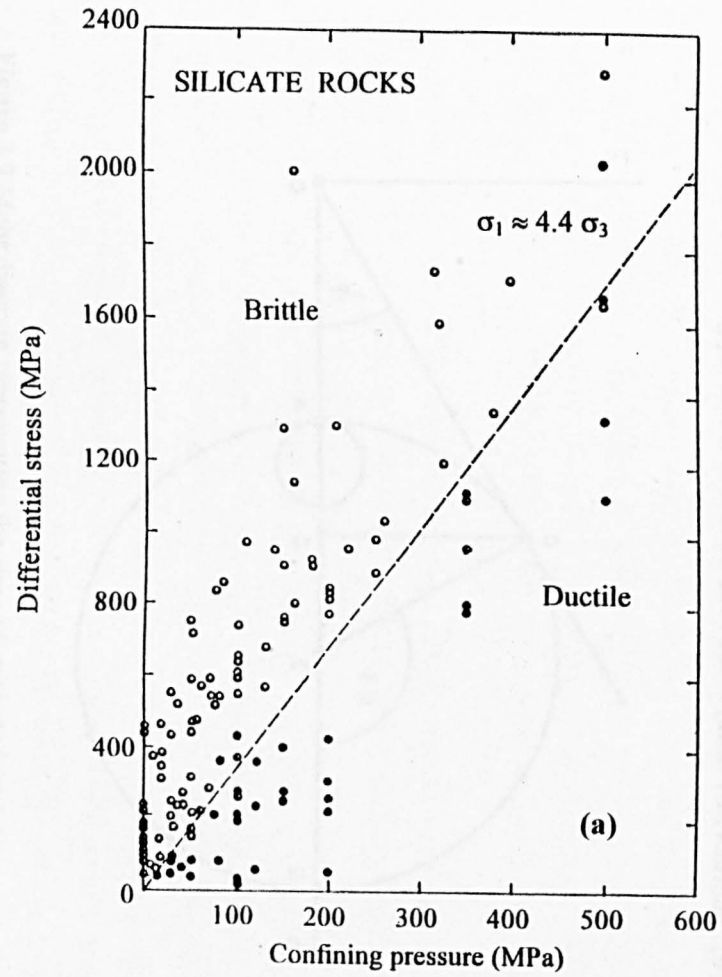
Figure 3.7: Brittle-plastic transition boundary for silicate (a) and carbonate (b) rocks (after Mogi, 1966)
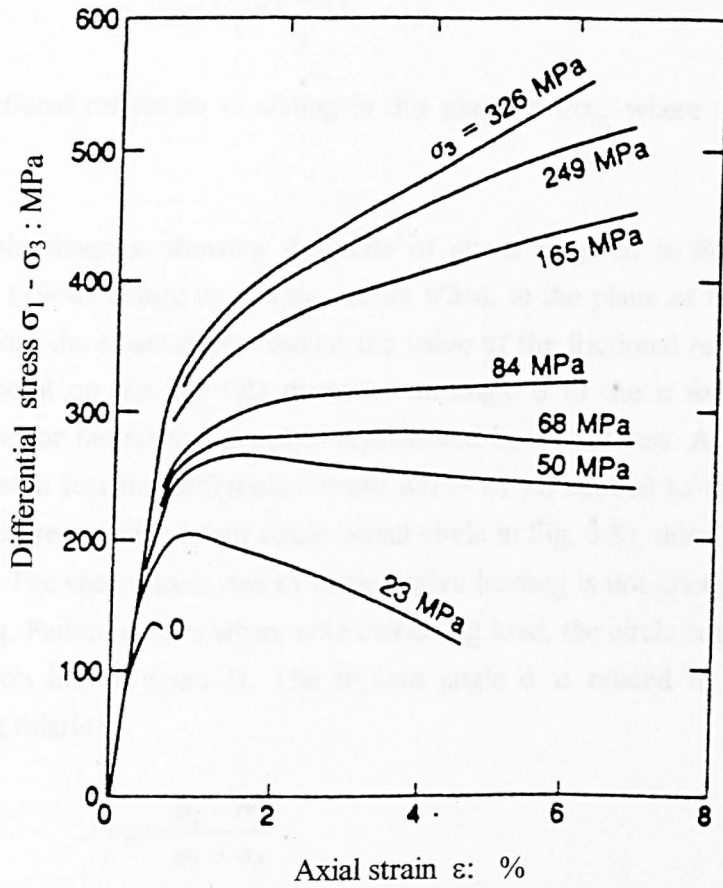
Figure 3.8 Stress-strain curves for Carrara Marble deformed in triaxial compression at different confining pressures shown on each curve (after von Karman, 1911).
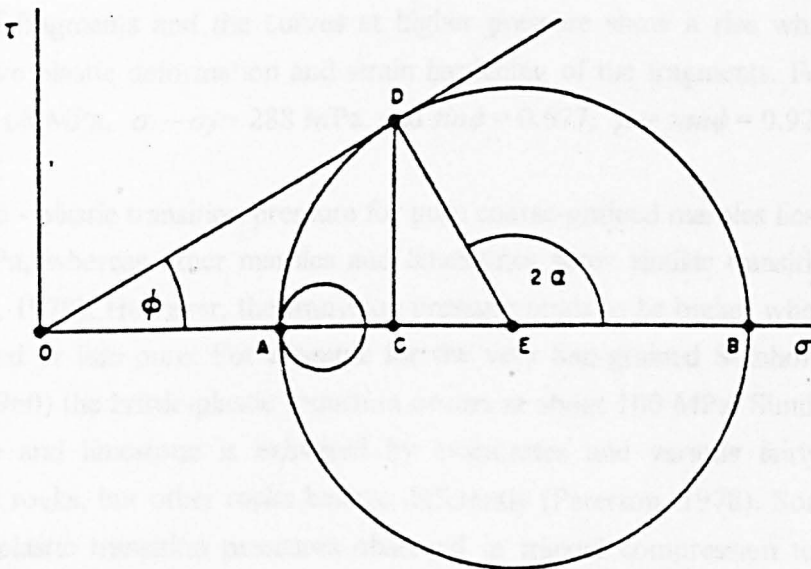
Figure 3.9 Mohr diagram representing the state of stress in triaxial compression tests

$$\tau_a = CD = (\frac{\sigma_1 - \sigma_3}{2}) \sin 2\alpha \qquad (3.10)$$

The frictional resistance to sliding in this plane is $\mu\sigma_\alpha$, where μ is the coefficient of friction.

The Mohr diagram showing the state of stress is given in Fig. 3.9. According to Orowan (1960) failure by sliding occurs when, in the plane of the most unfavourable orientation, the shear stress reaches the value of the frictional resistance. The ordinate of any point on the line OD drawn at an angle ϕ to the σ axis gives the frictional resistance for the normal pressure represented by its abscissa. At the beginning of the compression test the differential stress AB = $\sigma_1 - \sigma_3$ applied to the specimen is small, and the corresponding Mohr circle (small circle in Fig. 3.8) does not reach the friction line OD. The shear stress due to compressive loading is not enough to produce failure by sliding. Failure occurs when, with increasing load, the circle comes into contact with the friction line at point D. The friction angle ϕ is related to σ_1 and σ_3 with the following relation

$$\sin\phi = \frac{\sigma_1 - \sigma_3}{\sigma_1 + \sigma_3} \qquad (3.11)$$

from which the coefficient of friction is obtained.

Of the curves in Figure 3.8, the most appropriate for calculating the coefficient of friction is that at $\sigma_3 = 68$ MPa. The curves at lower pressure show a stress drop which means that the resistance to crushing is still higher than the frictional resistance to sliding of fragments and the curves at higher pressure show a rise which is due to progressive plastic deformation and strain hardening of the fragments. For the curve with $\sigma_3 = 68$ MPa, $\sigma_1 - \sigma_3 = 288$ MPa, and $\sin\phi = 0.677$, $\mu = \tan\phi = 0.92$ ($\phi = 42.6°$).

The brittle - plastic transition pressure for pure coarse-grained marbles lies in the range 20-30 MPa, whereas other marbles and limestones show similar transition pressures (Paterson, 1978). However, the transition pressure tends to be higher when the rock is fine-grained or less pure. For example for the very fine-grained Solnhofen limestone (Heard, 1960) the brittle-plastic transition occurs at about 100 MPa. Similar behaviour to marble and limestone is exhibited by evaporates and various fairly porous or weathered rocks, but other rocks behave differently (Paterson, 1978). Some examples of brittle-plastic transition pressures observed in triaxial compression tests at room temperature are shown in Table 3.2, compiled by Paterson (1978). A more detailed compilation of data on brittle-plastic transition pressures and the resulting friction angles is presented in Chapter 5.

Table 3.2: Examples of typical brittle-plastic transition pressures
(after Paterson, 1978)

Rock	Approximate transition pressures (MPa)
Limestones and marbles	30-100
Dolomite	100-200 or higher
Gypsum	40
Anhydrite	100
Rocksalt	<20
Talc	400
Serpentinite	300-500
Chloritite	300
Argillaceous sandstone (~10% porosity)	200-300
Siltstones and shales of medium to high porosity	<100
Porous lavas	30-100

The more siliceous igneous and metamorphic silicate rocks, such as granite and quartzite, remain brittle at confining pressures in excess of 1000 MPa (Byerlee 1968, Bergues *et al.* 1974). Shimada *et al.*(1983) found that non-porous granite, gabbro, dunite and eclogite remained in the brittle field when tested at room temperature and confining pressures up to 3 GPa.

Transition pressure decreases with porosity. Correlations between transition pressure and porosity of some sandstones are given by Scott & Nielsen (1991), Logan (1987) and Wong (1990).

3.3 Shear strength of rock discontinuities

3.3.1 Introduction

The resistance to sliding between contacting solids has been extensively studied and many attempts have been made to derive a complete theory to account for the phenomenon.

There are two basic laws of frictional behaviour:

    a) The shear resistance between two bodies is independent of the size of the surfaces in contact.

    b) The shear resistance between two bodies is proportional to the normal load between the bodies.

These laws were first stated by Leonardo da Vinci in the late 1400s, largely forgotten, and then rediscovered by the French engineer Amontos in 1699. They are often called *Amontons' laws*.

It is generally accepted that the adhesion theory described below provides the most likely explanation of friction.

3.3.2 The adhesion theory of friction

Terzaghi (1925), and Bowden and Tabor (1950) proposed that friction is due to adhesive forces acting at the points of contact between the opposing surfaces. This theory became known as the *adhesion theory of friction*.

Terzaghi (1925) argued that even smooth surfaces are rough on a molecular scale, and that the actual area of contact is only a small part of the total area of the surface. He suggested that the frictional resistance is caused by physical-chemical interaction between the contacting surfaces, forming firm or semi-firm bridges and concluded that for chemically pure surfaces the bridges are formed by molecular attraction at the points of contact. Thus the frictional resistance is the shear strength of that bridge. This hypothesis of Terzaghi was overlooked for many years, and was independently stated and shown to describe the frictional behaviour of a wide range of materials by Bowden, Tabor and their colleagues starting in the late 1930s. Based on a series of experiments on the friction between surfaces of metallic solids, Bowden and Tabor (1950), suggested that when solid surfaces are brought together they make contact only at a few points (Fig. 3.10). The sum of all these contact areas A_r is much smaller than the apparent area A of the contacting surfaces. It is only A_r, not A, that is responsible for friction. Accordingly, the normal stress acting at these areas is very high, and results in adhesion, welding the surfaces together at "junctions". Bowden and Tabor (op. cit.) have shown how at the contacting regions the deformation will first be elastic, but with materials capable of undergoing plastic flow the smallest loads will produce stresses exceeding the elastic limit and plastic deformation will occur. If the

load is increased the asperities are plastically crushed until they are large enough to support the load by elastic strains in the underlying material. Under these conditions the true area A_r of contact is small and independent of the apparent area of contact A. Bowden & Tabor assumed that the true area of contact, A_r, arose from plastic deformation and that the major force of friction arose from shearing the junctions thus formed.

asperities

(a)

(b)
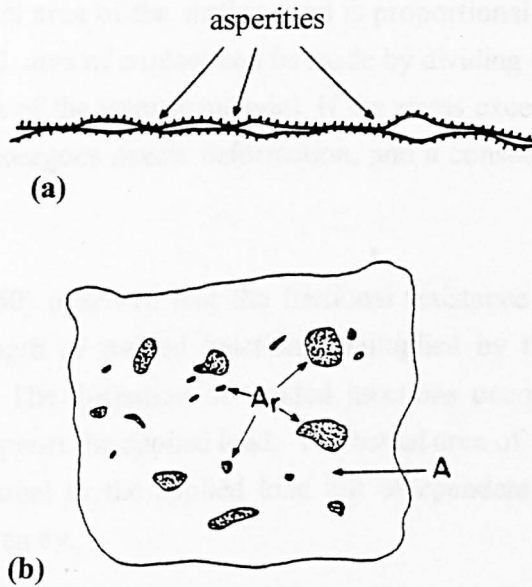
Fig. 3.10. Contact between two rough surfaces

3.3.3 The area of contact between contacting surfaces

Terzaghi (1925), suggested that the frictional resistance of a surface, S, is equal to:

$$S = \mu N \qquad (3.12)$$

where

N is the total load, and

μ is the coefficient of friction.

He observed that sliding could commence only after the shear strength of the weaker material s had been exceeded over the total net area of contact A_r. Thus the frictional resistance of the surface, S, was equal to:

$$S = A_r s \qquad (3.13)$$

or

$$A_r s = \mu N \qquad (3.14)$$

Both the coefficient of friction and the shear strength of the weaker material are constant, thus the frictional resistance of the surface is proportional to both the normal load and the actual area of contact between the surfaces.

Terzaghi reasoned that the stress acting at the points of contact is of the order of the compressive strength of the weaker material and that the actual area of contact is small in comparison to the total area of the surface, and is proportional to the applied load. An estimate of the actual area of contact can be made by dividing the applied stress by the compressive strength of the weaker material. If the stress exceeds the compressive strength, the material undergoes plastic deformation, and a consequent increase in the area of contact.

Bowden and Tabor (1950) observed that the frictional resistance of solid surfaces is equal to the shear strength of welded junctions, multiplied by the area of contact, equation (3.12) above. The formation of welded junctions occurs until the area of contact is sufficient to support the applied load. The actual area of contact between the surfaces, A_r, is proportional to the applied load but independent of the area of the sliding surface, and is given by:

$$A_r = \frac{N}{p}$$
(3.15)

where
A_r is the real area of contact
N is the load acting across the surfaces and
p is the yield strength of the material.

Thus both Terzaghi (1925) and Bowden & Tabor (op. cit.) have shown that the frictional resistance of *plastic surfaces* is a function of the actual contact area, and that the actual contact area is independent of the area of the sliding surface, but proportional to the applied load.

For surfaces which behave elastically, the relationship between the actual area of contact and the normal load is more complex. Archard (1957) found that for a Hertzian contact between a hemispherical asperity and a planar surface, the area of contact A_r and the normal load N are connected with the relation

$$A_r \propto N^{\frac{2}{3}}$$
(3.16)

This relation contradicts Amonton's second law and suggests that, either elastic surfaces do not behave in a Hertzian manner, or some other mechanism of asperity deformation occurs.

In the case of surfaces composed of numerous elastic asperities, Archard (op. cit.) suggested two possible modes of deformation upon the application of a normal load:
a) the number of asperity contacts remains constant with each asperity deforming due to the applied load. In this case the increase in contact area is proportional to two-thirds the applied load (relation 3.16 above).
b) the number of asperities increases with normal load, but the deformation of each asperity remains constant. In this case the area of contact increases proportionally with the normal load.
In a real situation both modes of deformation occur simultaneously as a result of an increase in normal load. Hyett & Hudson (1990) observed that upon the application of a normal load on both rough and smooth joint surfaces consisting of epoxy resin, there was an increase in both the deformation of existing contacts and the creation of new points of contact. Archard (1957 and 1974) showed that for a surface composed of hemispherical asperities the area of contact is given by:

$$A_r \propto N^n \tag{3.17}$$

where $2/3 < n < 1$

For a surface composed of a single scale of asperity, n equals 2/3. For surfaces composed of asperities of numerous scales the value of n increases. When the variation in scale of the asperities displays a gaussian distribution, n is equal to 44/45. Thus the proportionality between load and contact area holds in case of complex elastic surfaces.

Therefore, when any plastic or complex elastic surfaces come into contact, the actual contact area approaches direct proportionality to the normal load and Amonton's laws are obeyed.

3.3.4 The origin of the adhesive forces between solid surfaces
Several investigators other than Bowden and Tabor (1950) and Terzaghi (1925) tried to explain the origin of the adhesive forces between solid surfaces. Hardy and Hardy (1919) and Hencher (1977) attributed adhesion to molecular attraction between surfaces at the points of contact, whereas Allen (1963) and Bailey (1965) to chemical bonding, i.e. metallic, ionic and co-valent bonds forming between molecules in opposing surfaces, and other surface forces, i.e. Van der Waals forces. Tabor and

Winterton (1969) observed that Van der Waals forces acting on mica surfaces contribute significant attractive forces at distances up to 30 nm.

Johnson *et al.* (1971) observed that a force perpendicular to the surfaces is required to separate them, and concluded that the force is equal to the adhesion acting at the points of contact. They observed that adhesion decreases as the surface roughness increases, reasoning that the decrease is due to the roughness preventing intimate contact between the surfaces. Fuller and Tabor (1975) observed that a force acting normally to the surfaces of contacting elastic solids is required to cause their separation and attributed this to adhesion. They noted that adhesion diminishes with increasing roughness.

The occurrence of adhesive forces at the points of contact between mineral surfaces have been recognised by several authors. Horn and Deere (1962) attributed the frictional resistance of minerals to molecular cohesion between the surfaces and observed that the frictional resistance is variable. They reasoned that this is due to the adsorption of contaminants onto the mineral surfaces which reduces the adhesion. Bromwell (1966) suggested that friction is due to adhesive forces and demonstrated that the adhesive forces are diminished by the absorption of gases onto the mineral surface when it is exposed to air. He found that frictional resistance is increased by careful cleaning.

3.3.5 The Greenwood & Williamson model

Greenwood and Williamson (1966) developed a realistic analytical model for contact of a rough surface with a flat surface, where the rough surface was described with a random distribution of asperity heights.

The basic assumptions of this model are:

a) The asperities, at least at their summits, are spherical.

b) All asperity summits have the same radius β

c) The summits are sufficiently apart to deform independently

Based on the Hertzian contact theory between individual asperities (Timoshenko & Goodier, 1951) they showed that for a peak height distribution $\phi(z)$, when the reference planes of the two surfaces are separated by a distance d (Fig. 3.11b), the number of contact spots n, the real area of contact A_r and the total normal load N are given from the following equations respectively

$$n = \eta A \int_d^\infty \phi(z)dz \qquad\qquad (3.18)$$

$$A_t = \pi \eta A \beta \int_d^{\infty} (z - d_o + \delta) \phi(z) dz \tag{3.19}$$

$$N = \frac{4}{3} \eta \ AE'\beta^{\frac{1}{2}} \int_d^{\infty} (z - d_o + \delta)^{\frac{3}{2}} \phi(z) dz \tag{3.20}$$

where

η is he number of asperities per unit area

A is the macroscopic (gross) area of contact

β the radius of the asperity summits

z applies to the rough surface and is the distance from a peak to its reference plane

$\delta = d_o - d$ with d_o the distance between the reference plane and the smooth surface without any stress.

$\int_d^{\infty} \phi(z) dz$ is the probability of an asperity peak having a height greater than d and E' is

a composite modulus of elasticity, given by

$$\frac{1}{E'} = \frac{1 - v_1^2}{E_1} + \frac{1 - v_2^2}{E_2} \tag{3.21}$$

where E_1, v_1 and E_2, v_2 are the modulus of elasticity and the Poisson's ratio for the material of surfaces 1 and 2 respectively.

If the two contacting surfaces are of the same material $E_1 = E_2 = E$, $v_1 = v_2 = v$ and

$$E' = \frac{E}{2(1 - v^2)} \tag{3.22}$$

In the case of an exponential distribution, $\phi(z) = -e^{\frac{s}{s}}$, equations (3.20), (3.21) and (3.22) yield:

$$n = \eta \ Ae^{-h} \tag{3.23}$$

$$A_t = \pi \ (\eta \beta s) Ae^{-h} \tag{3.24}$$

$$\sigma_n = \pi^{\frac{1}{2}} (\eta \beta s) E'(\frac{s}{\beta})^{\frac{1}{2}} e^{-h} \tag{3.25}$$

where

σ_n the apparent normal stress and

s the standard deviation,

$h = (do-\delta)/s$ the standardised separation

Equation (3.27) then yields

$$\delta = A + B \ln \sigma_n \tag{3.26}$$

(a) No stress

Flat surface and reference plane
Reference plane in rough surface

Rough profile

Reference plane below rough surface

(b) Stress σ_n

σ_n
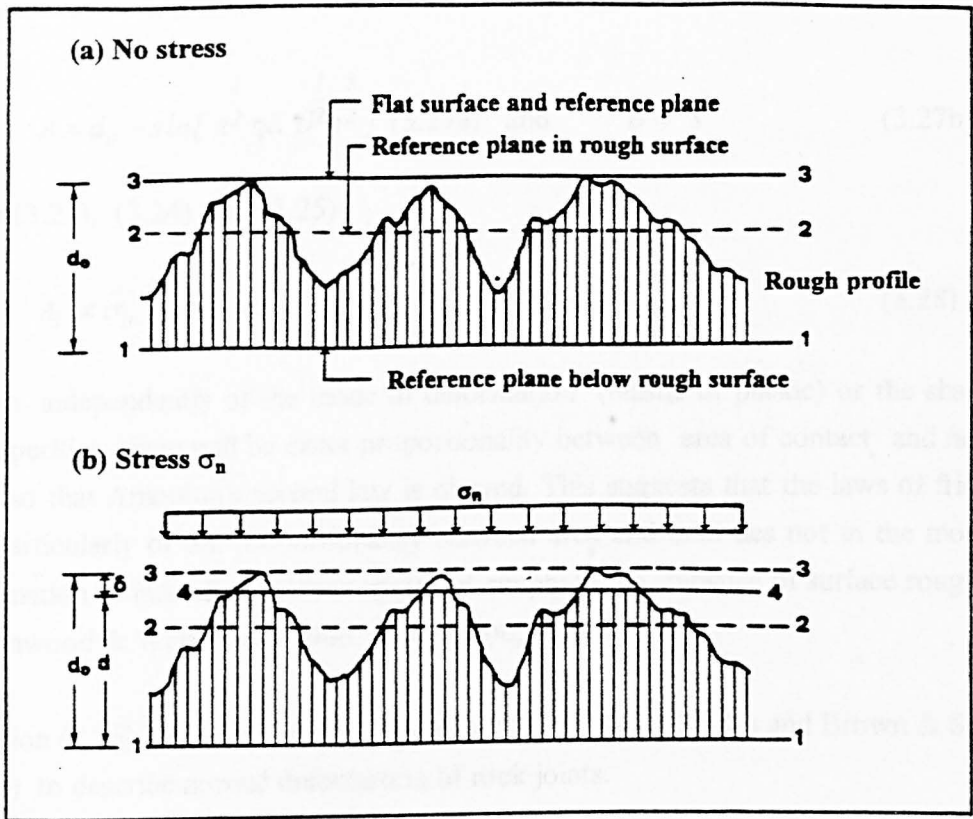
Fig. 3.11. Contact between a rough and a flat surface
(a). No normal stress. (b) Under normal stress σ_n

Reference plane 1

Z_1

d

Z_2

(a)

Reference plane 2

d

$Z=Z_1+Z_2$

(b)
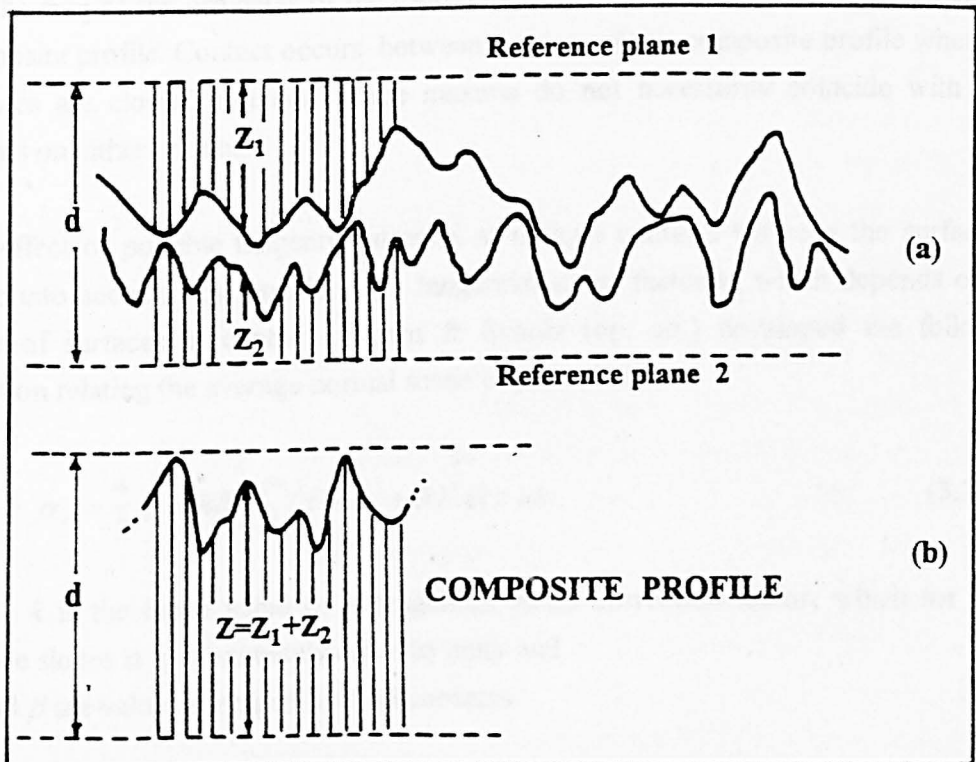
COMPOSITE PROFILE

Fig. 3.12: (a) Sketch of the profiles of two rough surfaces. (b) Sketch of a composite profile, the sum of the ordinates of the two profiles in (a) (after Brown & Scholz, 1985).

where

$$A = d_o - s\ln[\,\pi^{\frac{1}{2}}\,\eta E\,'\beta^{\frac{1}{2}}s^{\frac{3}{2}}\,]\quad (3.27a) \quad \text{and} \qquad B = s \qquad (3.27b)$$

From (3.23), (3.24) and (3.25)

$$A_t \propto \sigma_n \quad ; \quad n \propto \sigma_n \qquad (3.28)$$

and so, independently of the mode of deformation (elastic or plastic) or the shape of the asperities, there will be exact proportionality between area of contact and normal load, so that Amonton's second law is obeyed. This suggests that the laws of friction, and particularly of the proportionality between area and load lies not in the mode of deformation of individual contact spots but simply in the statistics of surface roughness (Greenwood & Williamson, 1966, Greenwood, 1967).

Equation (3.26) has been used by Goodman (1976), Swan (1983) and Brown & Scholz (1986) to describe normal deformation of rock joints.

Brown & Scholz (1985) generalised the theory of Greenwood & Williamson to cover the case of contact between two rough surfaces mated or unmated (Fig. 3.12). They use the sum of the ordinates of the topographic profiles for each surface to generate a composite profile. Contact occurs between maxima of this composite profile where the surfaces are closest together. These maxima do not necessarily coincide with peak heights on either surface.

The effect of possible tangential stresses at oblique contacts between the surfaces is taken into account, by introducing a tangential stress factor k, which depends on the slope of surfaces in contact. Brown & Scholz (op. cit.) developed the following equation relating the average normal stress to joint closure

$$\sigma_n = \frac{4}{3}\eta\ E'k\beta^{\frac{1}{2}}\int_d^\infty (z - d_o + \delta)^{\frac{3}{2}}\phi(z)dz \qquad (3.29)$$

where k is the mean value of a tangential stress correction factor, which for small surface slopes is approximately equal to unity and
E' and β are values averaged over all contacts.

For an exponential probability function $\phi(z)$, equation (3.29) yields again equation (3.26). In this case, the constants A and B are given by

$$A = d_o - s \, ln[\, \pi^{\frac{1}{2}} \eta k E' \beta^{\frac{1}{2}} s^{\frac{3}{2}} \,] \quad (3.30a) \quad \text{and} \quad B = s \quad (3.30b)$$

The peaks in most rough surfaces are essentially of Gaussian distribution rather than exponential. Swan (1983) made careful measurements with a profilometer of the topography of 10 different surfaces of Offerdale slate and showed that the peak heights of asperities fitted a Gausssian distribution. However, an exponential distribution is a fair approximation to the upper quartile of a Gaussian distribution of heights of asperities as suggested by Greenwood & Williamson (1966), who observed in practice (for metal surfaces) the ideal behaviour predicted for an exponential distribution. This quartile is more relevant to the frictional behaviour (Halling, 1978) and an exponential distribution of heights can offer a reasonable approximation for rock joint contacts at low to medium normal stresses (Swan, 1983, Sun et al., 1985).

Greenwood & Williamson (1966) found that plastic flow is expected at high normal loads. Thus under sufficiently high loads, asperities of small curvature may flow plastically even for normally brittle materials, although brittle fracture of the asperities often may intercede (Scholz, 1990).

3.3.6. Plastic deformation of rocks and rock joints

It may be argued that the application to rock surfaces of adhesion theory, which is based upon plastic deformation of the points of contact, to rock surfaces may be problematic, since rocks are normally brittle materials and the asperities may fail by brittle fracture, rather than plastic yielding. However, this brittle behaviour changes to plastic when the applied stress is sufficiently high, as suggested by Bridgman's experiments (Bridgman, 1952). Bowden and Tabor (1964) observed that when NaCl was subjected to high confining pressures, brittle fracturing was prevented, and the NaCl deformed by plastic flow, thus allowing cold welding of the contacts. The same authors have shown experimentally that the deformation of rock salt in the region of sliding is dominated by plastic and not by brittle processes. Brace (1962) observed that quartz crystals subjected to indentation hardness tests displayed apparent plastic deformation in the region of the indentation and concluded that brittle fracturing is restricted by high confining pressures. Based on the results of penetration tests, Scholz and Engelder (1976) proposed that the creep observed was due to plastic flow. According to Gerk & Tabor (1978) under conditions of hardness indentation, brittle materials around the indenter become sufficiently ductile to sustain plastic flow. It appears that this behaviour is independent of the hardness of the material, as suggested by direct observations on the transition of diamond by Vereshhchagen et al. (1974). These observations suggest that if the confining pressure is sufficiently high, the plastic

deformation of the surface required to cause cold welding at the points of contact does occur.

Brown and Scholz (1986) observed that, at low normal stresses, contacting rock surfaces undergo elastic deformation. As the contact stresses increase, the elastic yield strength of the asperities is exceeded and the asperities deform plastically. They noted that macroscopic plasticity when viewed microscopically may involve both brittle fracturing and plastic flow. This is typical of the behaviour in the brittle-ductile transition, as suggested by Evans *et al.* (1990) and shown in Table 3.1 The plastic deformation first occurs when the maximum contact stress exceeds the indentation hardness of the material, and that significant plastic deformation occurs when the mean contact stress exceeds the indentation hardness of the material. The onset of plastic deformation is also dependent upon the shape of the asperities. Asperities with low apex angles deform plastically at lower stresses than those with high apex angles.

From routine shear strength testing there is also enough experimental evidence, that the frictional force of natural rock-rock interfaces arises from shearing of rock under high normal stresses at localised areas of contact. For example Jaeger (1971) estimated that the actual area of contact A_a for a rough joint is of the order of 1% of the apparent area of contact A. Based on laboratory measurements Barton (1971a) estimated that at any stage of sliding the ratio A_a/A is relatively small, whereas Barton & Choubey (1977) pointed out that real normal and shear stress at a conventional rock mechanics problem may be as high as one thousand times as those calculated from the gross area of contact. For example at nominal stresses of 1 MPa, the corresponding real stresses may be as high as 1000 MPa. They found that, over a wide range of rock joints the ratio A_a/A is approximately equal to the normal stress/joint wall compressive strength ratio, in agreement with Terzaghi (1925). Results by Iwai (1976, quoted in Barton *et al.*, 1985) from normal closure tests on granite, indicated ratios of A_a/A of less than 0.1% when effective normal stress as low as 0.26 MPa was applied. At higher normal stress (20 MPa) the ratio of A_a/A was in the range 10-20%. Similar observations were made by McMahon (1985), Yoshinaka *et al.* (1993) and others.

Brown & Scholz (1986) calculated the real area of contact as less than 1% of the nominal surface area of the sample at normal loads exceeding 50 MPa. Logan & Teufel (1986) measured the real area of contact during sliding for three different cases: sandstone sliding on sandstone; limestone on limestone and sandstone sliding on limestone. Their results, shown in Fig. 3.13, indicate that the real area of contact. increases linearly with normal stress in all cases. The approximate values of the real normal stress were from 200 to 2,200 MPa. The fractional area of contact A_a/A at an
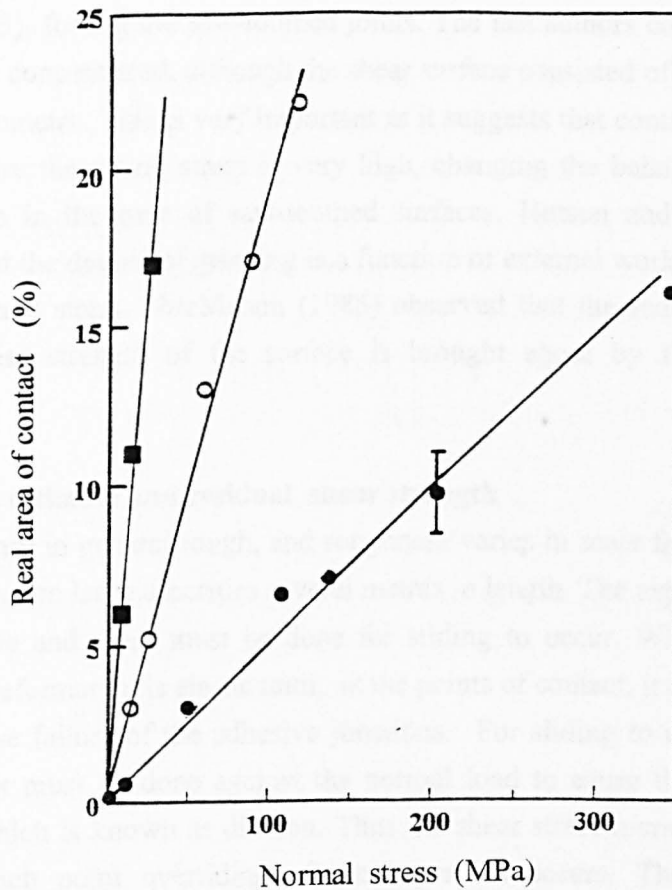
Fig. 3.13: Variation of contact area with normal stress (after Logan & Teufel, 1986)

apparent normal stress of 10 MPa was of the order of 1-7%, and lower at lower normal stresses. The asperities deform by a combination of brittle fracturing, crystal twinning and bending of existing twins.

Stesky and Hannan (1987, 1989) also conducted normal closure tests on joints in marble, alabaster and quartzite, at normal stresses up to half the uniaxial compressive strength of the rock. They found that the relative contact area increased with reaching about 15% at 19 MPa for marble, 30% at a normal stress of 12 MPa for alabaster but quartzite had a permanent relative contact area of less than 1% at 49 MPa, indicating that most of the deformation was elastic. These authors commented that the initial contact stress may be close to the differential stress needed for deformation of this marble rock under sufficient confinement for bulk cataclastic flow to occur, i.e. close to the brittle-ductile transition stress.

McMahon (1985) examined the nature of asperity failure during shear of natural joints and observed that the asperities fail by grinding rather than by shearing through. Similar observations were made by Hutson & Dowding (1990) and Perreira & de

Freitas (1993) for regular saw-toothed joints. The last authors concluded that stresses were locally concentrated, although the shear surface consisted of a number of teeth of the same geometry. This is very important as it suggests that contact points are limited and therefore the acting stress is very high, changing the behaviour from brittle to plastic, even in the case of saw-toothed surfaces. Hutson and Dowding (op. cit.) observed that the degree of grinding is a function of external work, the joint roughness and the normal stress. McMahon (1985) observed that the reduction from peak to ultimate shear strength of the surface is brought about by this grinding of the asperities.

3.3.7 Peak, ultimate and residual shear strength

Rock joints are in general rough, and roughness varies in scale from that of the grain size of the rock to large asperities several metres in length. The asperities interlock to a certain degree and work must be done for sliding to occur. When a shear force is applied the deformation is elastic until, at the points of contact, it becomes sufficiently high to cause failure of the adhesive junctions. For sliding to occur at low normal stresses work must be done against the normal load to cause the overriding of the asperities, which is known as dilation. Thus the shear stress increases to a peak (Fig. 3.14) at which point overriding of the asperities occurs. The shear stress will subsequently reduce; however, further interlocking may produce successive peaks. As the normal stress increases less work is required to cause asperity failure than asperity overriding. Consequently, the dilation is reduced and peak shear stress is mainly due
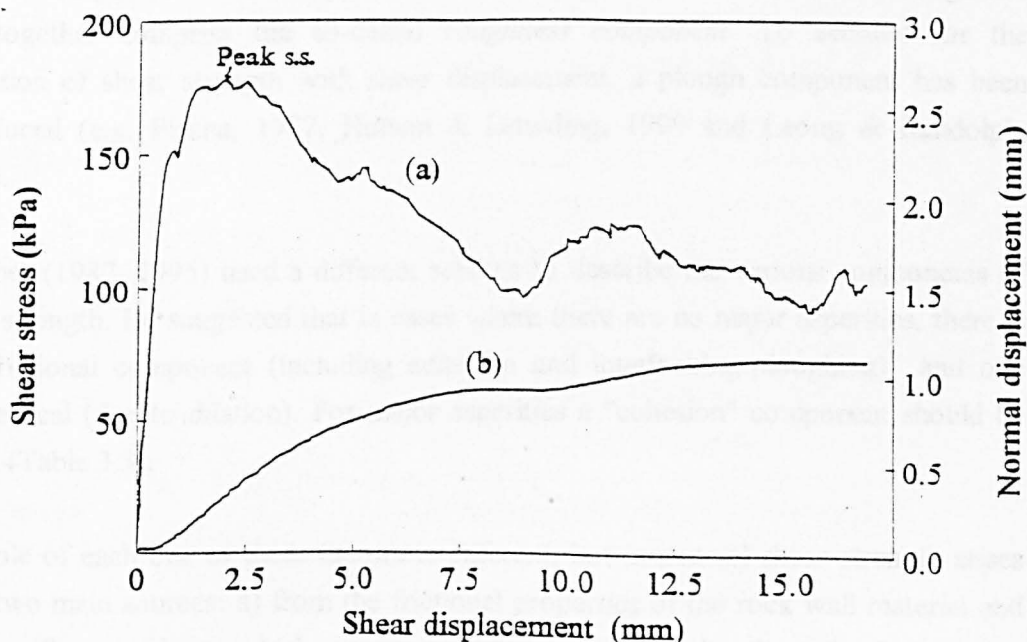
Fig. 3.14: Typical behaviour of a rough rock joint.

(a) shear stress -shear displacement diagram

(b) normal displacement - shear displacement diagram

to the shear strength of the asperities. If the normal stress is sufficiently high, dilation is fully suppressed and the shear strength is solely due to shearing through the asperities. After failure of the asperities has occurred the shear stress reduces to a level at which further sliding will occur with no further increase in shear stress. This is commonly termed the residual shear strength. Krahn and Morgenstern (1979) observed that the residual shear strength of the surface depends upon the original roughness. Hassani and Scoble (1985) observed a similar relationship for shear tests on artificially roughened siltstone discontinuities. Krahn and Morgenstern (op. cit.) recommend that the term ultimate shear strength be used for the post peak shear strength of rock discontinuities.

Barton (1973) proposed that the residual shear strength can be indirectly obtained by direct shear tests of saw cut surfaces. However, saw cutting alters the affects of surface texture and consequently the affects of surface damage and the accumulation of sliding debris during shearing. It is therefore questionable whether a saw-cut surface will give the true residual strength of a rough joint.

3.3.8   The origin of shear strength of rock joints

Ladanyi & Archambault (1970) and Barton (1971a, b) separated the peak shear strength of a rough joint into three components, following a similar for soils (Rowe, 1962): a) one due to sliding resistance between flat surfaces (base friction component) b) one due to dilation (dilation component) and c) one due to shearing through of asperities (asperity failure component). The last two components are due to roughness and together comprise the so-called *roughness component*. To account for the reduction of shear strength with shear displacement, a plough component has been introduced (e.g. Plesha, 1987, Hutson & Dowding, 1990 and Leong & Randolph, 1992).
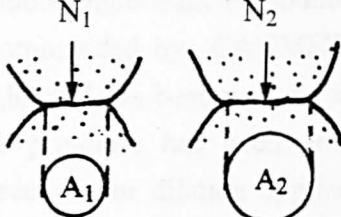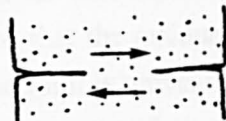
Hencher (1987, 1995) used a different scheme to describe the various components of shear strength. He suggested that in cases where there are no major asperities, there is one frictional component (including adhesion and interlocking-ploughing) and one geometrical (due to dilation). For major asperities a "cohesion" component should be added (Table 3.3).

The role of each one of these factors is different, but in general shear strength arises from two main sources: a) from the frictional properties of the rock wall material and b) the surface roughness which causes overriding and/or shearing through of asperities.

3.3.8.1 The frictional component

The "base" friction angle is used in rock mechanics in a similar way to the mineral friction angle for soils (Rowe, 1962). That is, a block is cut into two and is subjected to shearing. The corresponding friction angle is termed *the basic fiction angle* (Barton 1973), and depends on the surface preparation (degree of grinding and polishing), as has been demonstrated by Ripley & Lee (1962), Coulson (1970), Krahn & Morgenstren (1979) and others. In the case of unweathered joints, this friction angle is taken as being equal to the residual friction angle for unweathered joints (Barton &

Table 3.3: Factors contributing to the shear strength of rock joints (after Hencher, 1995)

1. Adhesion (lower bound friction) increasing normal load→ N_1 N_2 	*- Bonding over true area of contact (A_1, A_2)* • proportional to normal load • does not cause dilation • no reduction with displacement • same for different textural surfaces and roughness
2. Interlocking and ploughing **(additional friction)** increasing normal load→ N_1 N_2 	*- Surface textural component* • proportional to normal load • does not cause dilation • generally decreases with displacement due to damage and the production of debris • increases with rougher surface texture
3. Overriding 	*- Work done due to dilation or compression* • uphill sliding leads to an increase in measured strength and vice versa • purely geometrical effect • decreases with normal load and decreasing wall rock strength reduction with displacement • same for different textural surfaces and roughness
4. Cohesion 	*- Shearing of rock bridges and locked asperities* • not proportional to normal load • independent of dilation • lost after peak strength

Choubey, 1977). The base friction angle is not a fundamental physical property of the material and for a diamond sawcut surface may be a reproducible index for a particular rock type and particular saw blade. In some cases sand-blasted surfaces have been used, for example by Ripley & Lee (1962), Coulson (1972) and others. Hencher *et al.* (1993) reported that the sliding angle of a flat sandstone surface can be reduced from 35° to 12° by repetitive sliding. For weak materials this may not be possible, as the variation in base friction angle may be higher. Toy (1993) demonstrated that the base friction angle of weak plaster-based model materials may vary considerably n the range 9-35° and concluded that this friction angle is variable. Swan & Zongqi (1985) and Reeves (1985) argued that the base friction angle is scale dependent.

Ripley & Lee (1962) used the term *true friction angle* to describe that part of peak friction angle which remains after correction for dilation. The same procedure is recommended by CANMET (Gyenge and Herget, 1977) to define a *basic* friction angle, and has been used by several authors including Ross-Brown & Walton (1975). The principle has been employed by Hencher & Richards (1982, 1989), with correction for dilation applied in an incremental fashion for volumetric work done throughout the test. These authors used the term "basic" friction angle not for sawcut surfaces, but for *naturally textured, non-dilational surfaces*. This angle was found to be about 40° for a number of shear tests on sheeting joints in granite, a value clearly higher than the friction angle of saw-cut surfaces. The method of separation of shear strength into two components is very clear, but Barton (1990) argued that the *textural* strength of Hencher & Richards is scale dependent. However, Papaliangas *et al.* (1994) demonstrated that this strength is independent of scale. This subject is a matter of some debate and it would be true to say that an objective of the present work was to attempt to resolve this problem.

A wide range of values for typical base friction angles is reported in the literature. These values are based on sliding tests on sawcut surfaces, which may have been subjected to lapping or sandblasting, or on residual shear strength. The value of residual shear strength - and consequently the basic friction angle- may be dependent upon the original roughness (Krahn & Morgenstern, 1979, Hassani & Scoble, 1985). Barton (1973) argued that the residual shear strength may not be achieved during a direct shear test due to insufficient shear displacement. Barton & Choubey (1977) proposed that the residual friction angle is equal to the friction angle of sawn surfaces when the joint is unweathered but in the case of weathered joints it can be obtained by direct shear tests of saw cut surfaces and from the Schmidt rebound numbers for the unweathered and weathered surface. Ultimate friction angles measured on different types of joints in the same hard, relatively pure, unaltered limestone ranged from 14°

to 32° (Cruden, 1983). Some basic friction angle ranges for typical rocks are given in Table 3.4. These values may vary considerably with site conditions.

3.3.8.2 The roughness component

Roughness has a dominant effect on the frictional properties of rock joints. It has been argued by Greenwood & Williamson (1965) and Greenwood (1967) that the laws of friction have their origin not in the mode of deformation (brittle fracture or plastic flow) but in the statistics of surface roughness (see Chapter 3.3.5). The random geometry of joint surfaces has been statistically treated by a number of researchers. Several attempts have been made to correlate roughness directly to shear strength, for example Reeves (1985), Swan(1981, 1983), Swan & Zongqi (1985), Dight & Chiu (1981), Chiu & Dight (1983) among them. The effects of roughness on shear strength can be considered on different scales, but they are usually considered on two scales, that of the contacting asperities (microscopic scale) and that scale of the sliding surface (macroscopic scale).

Table 3.4: Typical basic friction angles (after Wyllie, 1990)

Rock type	Typical examples	Basic friction angle
Low-friction rocks	schists (high mica content), shale, marl	20°- 27°
Medium-friction rocks	sandstone, siltstone, chalk, gneiss, slate	27°- 34°
High-friction rocks	basalt, granite, limestone, conglomerate	34°- 40°

On the microscopic scale all surfaces, even the smoothest ones, are rough and the frictional resistance of two contacting surfaces is due to adhesion at the points of contact. On this scale the effect of surface roughness is to reduce the adhesive component of friction. This has been demonstrated by Hardy and Hardy (1919) who observed that the frictional resistance of rough glass surfaces was lower than that of smooth glass. Similar observations were made by Fuller and Tabor (1975), Johnson *et al.* (1971), and Briggs & Briscoe (1976) who attributed this reduction to the higher asperities causing the smaller asperities to separate. This reduces the actual area of contact between the surfaces, and consequently reduces the adhesion. However, when the two surfaces are of different hardness, the shear resistance increases with increasing roughness, as shown by Byerlee (1967a). Due to this difference there is a significant amount of asperity indentation, similar to that described by Scholz and Engelder (1976), which increases the coefficient of friction between the two surfaces.

The macroscopic scale roughness has no effect upon the friction due to adhesion at the points of contact, but work must be done to overcome interlocking of large scale

asperities in order to enable shear displacement to occur. Consequently the effect of large scale roughness is to increase the shear strength of the surfaces. To overcome this interlocking the asperities must either be overridden or sheared through.

Roughness can be characterised by a number of parameters. Many researchers, among them Wu & Ali (1978), Tse & Cruden (1979), Krahn & Morgenstern (1979), Maerz *et al.* (1990) and others have tried statistical parameters such as centre line average value, mean square value, root mean square (RMS) value, mean square of the first derivative, (Z_2) RMS of the first derivative, RMS of the second derivative, probability density function, auto-correlation function, spectral density function, structure function (*SF*), roughness profile index (R_p) and micro-average *i* angle (A_i) to quantify roughness. Ladanyi & Archambault (1970), Reeves (1985), Swan (1981, 1983), Swan & Zongqi (1985), Dight & Chiu (1981), Chiu & Dight (1983) amongst others have used the average asperity slope, which appears to be most relevant to the dilational behaviour of rough surfaces. This parameter can be defined in different ways, but the most common form in use is the root mean square slope gradient (Z_2) defined by:

$$Z_2 = \frac{1}{L} \int_{x=0}^{x-L} \left(\frac{dy}{dx}\right)^2 \qquad (3.31)$$

where

y is the amplitude at a particular point on the roughness profile about the centreline,

x is the tangential distance along the profile and

L is the total length of the profile. The centreline divides the profile such that the sums of areas to either side of it are equal.

Kulatilake *et al.* (1994) feel that Z_2 is a good parameter to quantify small scale roughness, and an additional statistical parameter is needed to quantify large-scale roughness.

The use of the fractal dimension D (Mandelbrot, 1983, 1985, Feder, 1988) to provide a measure of roughness for rock joints has been tried by some researchers including Brown & Scholz (1985), Andrle & Abrahams (1989), Chesters *et al.* (1989), Miller *et al.* (1990), Power & Tullis (1991), Huang *et al.* (1992), Odling (1994), Hsiung *et al.*(1995) and others.

Barton & Choubey (1977) defined a "Joint Roughness Coefficient" (*JRC*) which takes values from 0 for the smoothest to 20 for the roughest surface. They have suggested two methods to choose an appropriate value for *JRC*: the first by visual comparison with a set of 10 typical roughness profiles published by these authors. This visual comparison has been found subjective and unreliable by some workers including Maerz

et al. (1990) and Miller *et al.* (1990). The second method, tilt or pull tests, are carried out on natural joints and an estimate of JRC is made by back analysis of the test results using the empirical criterion suggested by Barton & Choubey (1977), along with the estimations for joint wall compressive strength and basic friction angle on the joint plane. Although purely empirical and strongly scale dependent (Bandis *et al*, 1981), *JRC* has experienced wide application and several attempts have been made to correlate it with other roughness parameters, mainly the average asperity angle (or slope) and the fractal dimension.

Tse & Cruden (1979) found the following relation between JRC and the Root Mean Square (*RMS*) gradient (Z_2) when an asperity base length of 0.5% of the sample length was used:

$$JRC = 32.2 + 32.47 \log(Z_2) \tag{3.32}$$

Various investigators including Turk *et al.* (1987), Carr & Warriner (1989), Lee *et al.* (1990), Wakabayashi & Fukushige (1992), Xie & Pariseau (1992) and Odling (1994) tried to establish correlations between JRC and fractal dimension, in order to develop a quantitative method of specifying surface roughness. A fractal approach would be very useful, as it would enable scale effects on joint roughness to be considered. However, these correlations are not capable of providing a reasonable estimate of JRC value, to be used for the estimation of peak shear strength of rock joints (Hsiung *et al.* , 1993). Furthermore, it must not be forgotten that the nature of *JRC* is purely empirical. Any correlations must be considered as a connection between fractal dimension and a roughness parameter, rather than JRC itself. Hobbs (1993) states the limitations existing when correlating the fractal dimension of a surface with JRC, concluding that as yet there is no case of correlation between *JRC* and the fractal dimension, whereas Miller (1990) emphasises the difficulties in obtaining meaningful measures of fractal dimension. Tanimoto & Kishida (1994) feel that the fractal dimension range corresponding to JRC values (from 0 to 20) is too narrow to distinguish JRC rating, i.e. its resolution is too low to represent the roughness of a joint surface. They suggested an alternative parameter called "power spectrum moment" to describe roughness. Seidel & Haberfield (1995) tried a more meaningful correlation between two physical parameters, namely the fractal dimension and the mean asperity angle and height of rough surfaces. It must be said that the fractal dimension is of little use to the practising engineer, dealing with description and quantification of roughness of rock joints. This is the reason why several such correlations have been suggested between D and JRC or other common roughness parameters.

For a complete description of roughness one single parameter is not adequate. Koura & Omar (1981) found that both the asperity height and the wave length should be considered simultaneously to describe surface roughness adequately. Brown (1987) has pointed out that the fractal dimension D should be considered together with the amplitude of the surface at a particular wave length, in order to specify the roughness of the profile, and similar suggestions were made by Hsiung et al. (1995). However, for design purposes, it would be very convenient to represent the profile of a joint by a single parameter. It appears that, among other single parameters, the average slope of the asperities correlates best with the coefficient of friction (Koura & Omar, 1981, Myers, 1962, Tabor, 1975). In the field of rock engineering, the importance of the average slope angle i of the asperities on shear strength of rock joints is reflected by the great number of studies devoted to it (e.g. Reeves, 1985).

In conclusion, it appears that despite the work devoted to attempt to correlate several surfaces parameters to JRC, which is a purely empirical parameter, the results may be inadequate to describe roughness. It would probably have been more useful if the research had been directed towards the establishment of an alternative to JRC, rather than trying to correlate JRC with various other parameters.

To measure roughness at different scales from laboratory size samples to large exposed surfaces, various techniques have been proposed by several researchers, including Fecker & Rengers (1971), Ross-Brown & Walton (1975), Weisbach (1978), Stimpson (1982), Miller et al (1989) and Maerz et al (1990). The most commonly used methods for in-situ measurement of roughness are:

(a) A compass clinometer with variable-size base plate (Fecker & Rengers, 1971, Richards & Cowland, 1982).

(b) A profilometer clamped to the rock surface (Fecker & Rengers 1971). A stylus or wheel traverses the surface along a line and the roughness is recorded on paper or magnetic medium, by means of a transducer system.

(c) Shadow profilometry (Franklin et al., 1988 and Maerz et al., 1990). A shadow is cast on a rough rock joint facet by a straight edge held against the surface in bright light. Using photoanalysis, the edge of the shadow can be digitised and any required roughness parameter calculated.

(d) Terrestrial photogrammetry, used when the surfaces to be recorded are large (Ross-Brown et al., 1973).

Rock surface roughness comprises a whole spectrum of varying wavelengths and amplitudes. It appears that small samples are influenced mainly by small scale
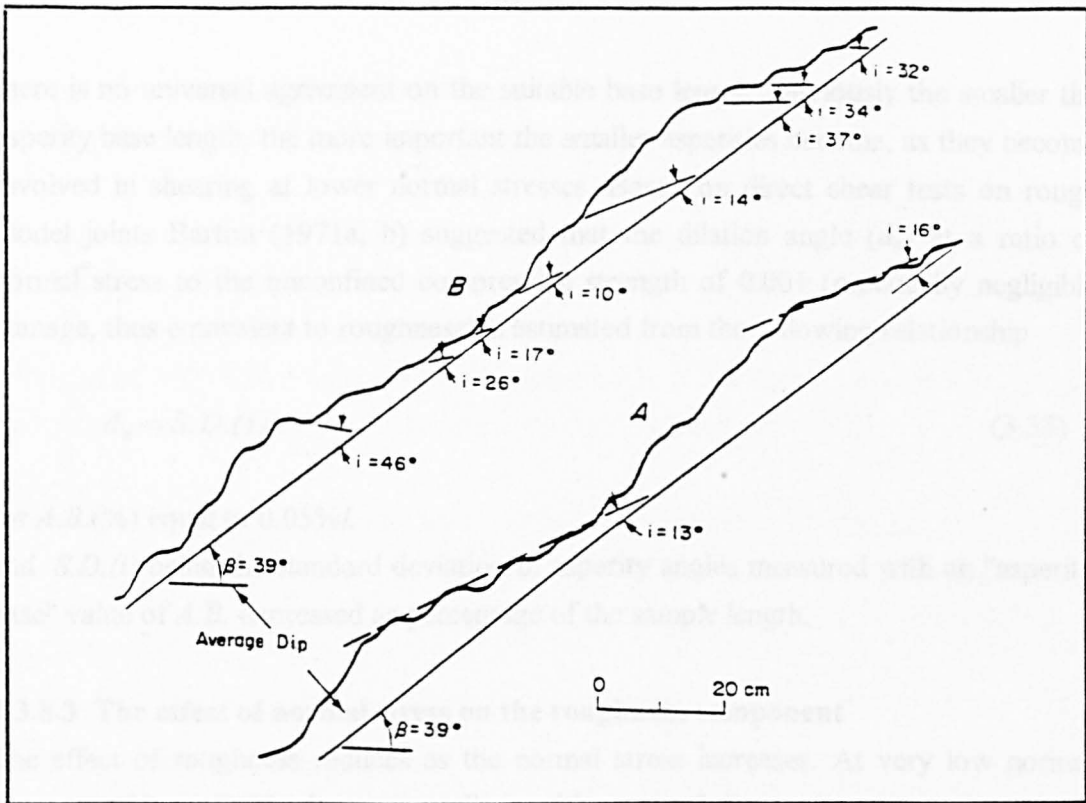
Fig. 3.15: First (A) and second (B) order asperities of a rock joint surface. β = average slope angle, i = angle between surface feature and average dip of discontinuity

(after Patton, 1966a)

roughness and larger samples by large scale asperities. The slope angle of asperities (or the equivalent exhibited dilation angle) is dependent upon the asperity base length over which this angle is determined, as demonstrated by Fecker & Rengers (1971), Barton (1971a), Goodman *et al.* (1972), Richards & Cowland (1982) and others. Patton (1966a) categorised field scale roughness into first-order and second order with wave lengths 1-2% and 0.1-0.3% respectively of the lengths of the failed surfaces he studied. A typical illustration where first order roughness gives an angle of 13° and second order between 10 and 46° is shown in Fig. 3.15. Generally, large asperities have roughness angles which are relatively low (< 20°), and second-order asperities have roughness angles which may be as high as 60°, but more commonly fall in the range 40° - 50° (Selby, 1987). The significance of each of these components of roughness depends upon the strength of asperities and the magnitude of the normal and shear stress. At very low normal stress, the asperities remain intact, but as the normal stress increases in magnitude the second order, and then the first order, become increasingly more important.

Tse & Cruden (1979) in their correlation between *JRC* and the mean asperity gradient Z_2 , used base length equal to 0.5% of the sample length *L*, whereas Sarra Pistone (1990) for an analogous correlation suggested a base length of 2% *L*. It appears that

there is no universal agreement on the suitable base length. Obviously the smaller the asperity base length, the more important the smaller asperities become, as they become involved in shearing at lower normal stresses. Based on direct shear tests on rough model joints Barton (1971a, b) suggested that the dilation angle (d_n) at a ratio of normal stress to the unconfined compressive strength of 0.001 (practically negligible damage, thus equivalent to roughness) is estimated from the following relationship

$$d_n = S.D.(i) \qquad\qquad (3.33)$$

for $A.B.(\%)$ equal to $0.05\%L$
and $S.D.(i)$ being the standard deviation of asperity angles measured with an "asperity base" value of $A.B.$ expressed as percentage of the sample length.

3.3.8.3 The effect of normal stress on the roughness component

The effect of roughness reduces as the normal stress increases. At very low normal stresses, with negligible damage, small asperities control shear strength. As the normal stress increases, larger and larger asperities dominate shear behaviour, and the role of roughness reduces. At a sufficiently high normal stress, all dilation is suppressed, and roughness no longer has an affect on shear strength, and the individuality of joint morphology is lost. Ladanyi & Archambault (1970) suggested that this normal stress is a fraction of the brittle - ductile transition stress, depending on the degree of interlocking. Barton et al. (1985) suggested that at high normal stress dilation is equal to $0.5JRClog_{10} (JCS/\sigma_n)$, which implies that dilation becomes zero when normal stress approaches the compressive strength of the rock wall material. However, there is no experimental evidence for this. On the contrary, several experimental data sets suggest that the normal stress at which dilation becomes zero is much lower. For example, Denby & Scoble (1984) reported that all dilation is suppressed at a normal stress in the range 2.0-3.5 MPa for a large number of joints in Coal Measures with unconfined compressive strengths in the range 40-160 MPa (Hassani & Scoble, 1981). Kutter & Otto (1990), found that dilation in gneiss joints with an unconfined compressive strength of 180 MPa, formed by separation along its schistocity plane tended to zero when the normal stress approached 7.5 MPa. Krsmanovic (1967) presented data from shear tests on rough joints in limestone, which show linearity between shear strength and normal stress for normal stress above 5 MPa. Martin & Millar (1974) found that for joints in weathered greywacke dilation becomes zero at normal stress 3.0 MPa. Gaziev (1976) suggested a formula for the variation of dilation angle with normal stress, which predicts zero dilation when the normal stress is equal to 30-40% of the unconfined compressive strength, and data from Gaziev & Lapin (1986) indicate that dilation becomes zero at about $0.25\sigma_c$. Goodman & Dubois (1972) found that for

sandstones, granites and other rock types dilation is completely prevented at a normal stress far below the brittle-ductile transition stress.

Model joints also show zero dilation at normal stresses lower than the unconfined compressive strength. For example the experimental results published by Bandis *et al.* (1981) based on direct shear tests on model joints with unconfined compressive strength of 2000 kPa, suggest a zero dilation angle in the range 100-250 kPa. Similar conclusions are drawn from the results published by Schneider (1976).

Numerous models have been developed to take account of the variation of the roughness component with normal stress. Some of these models consider separately a component due to dilation and a component due to asperity failure, whereas others do not.

3.3.9 Peak shear strength criteria

Attempts to explain the shear strength of rough rock joints was based on the work of Newland & Allely (1957) who studied the dilatant behaviour of sand and proposed the following linear strength criterion

$$\tau = \sigma_n \, tan(\phi_\mu + i) \tag{3.33}$$

where τ is the peak shear strength

σ_n the normal stress

ϕ_μ the angle of frictional sliding resistance between sand grains

i the average angle of deviation of particle displacements from the direction of the applied shear stress.

Using plaster models with saw-toothed shape, Patton (1966a, b) and Goldstein *et al.* (1966) showed that the peak shear strength envelope at very low normal stresses is linear, and can be represented by:

$$\tau = \sigma_n \, tan(\phi_r + i) \tag{3.34}$$

where

ϕ_r is the angle of frictional sliding resistance along a plane surface or the residual friction angle and

i the asperity inclination angle.

At high normal loads Patton suggested that peak shear stress is given by:

$$\tau = c + \sigma_n \tan \phi_r \tag{3.35}$$

where

   c is the apparent cohesion.

The apparent cohesion is equivalent to the shear strength of the asperities. This component of strength is lost once the asperities have been sheared. Combination of equations (3.34) and (3.35) produces a bi-linear failure envelope for rough rock discontinuities, (Patton 1966, and Rengers 1970).

However, some years before Patton had proposed his bi-linear model, Ripley & Lee (1962) recognised that the effect of roughness was to increase the friction angle by an angle i equal to the angle of inclination of asperities. They tested rough natural joints in sandstone, siltstone and shale and concluded that, when determined from the true normal and tangential forces to the inclined plane of motion, the coefficient of friction does not vary, but when horizontal and vertical stresses are considered the result is an apparent friction coefficient higher than the basic value of the material. They found that what they called the *true coefficient of friction* could be determined by

$$\tan \phi_{true} = \frac{\tan \phi_p - \tan i}{1 + \tan \phi_p \tan i} \tag{3.36}$$

which is equivalent to (3.33) and where

   ϕ_{true} is the *true friction angle*

   ϕ_p is the measured peak friction angle and

   i is the instantaneous dilation angle.

In contrast to the results of Patton, Ripley and Lee found that this equation holds throughout the normal stress range used (up to 1.4 MPa), and Nieble *et al.* (1974) found similar results for large blocks (0.7m x 0.7m and 1.0m x 1.0m) of joints in basaltic rock tested under normal stresses up to 2.5 MPa. The true friction angle is higher than that of artificially prepared (ground and sandblasted) surfaces, as shown in Table 3.5.

The bi-linear failure envelope proposed by Patton (1966 a, b) implies a sharp change from overriding to shearing of the asperities. This is not the case as there is a progressive change from overriding to shearing. Consequently many authors including Jaeger (1971), recommended the use of a curved failure envelope for joints at low stresses.

Table 3.5: Friction angles obtained from flat and rough surfaces
(after Ripley & Lee, 1961)

Rock type	Flat surfaces		Rough natural surfaces	
	Ground smooth	Sand-blasted	Peak non-dilational	Peak Measured
Sandstone	25°	29°	36°	54°
Siltstone	25°	31°	31°-34°	45°-47°
Shale	26°	27°	24°	34°
Shale	26°	27°	35°-39°	35°-39°

Based on multi-stage tests on sheeting joints in Hong Kong granite (Figure 3.16), Hencher & Richards (1982, 1989), suggested that peak shear strength is made up of two components, one frictional and one geometrical. Like Ripley & Lee (1961), they calculated the normal and shear stress along the inclined plane to define the frictional component.

Ladanyi & Archambault (1970) derived a curvilinear, semiempirical shear strength criterion as a function of the strength of intact rock, the degree of interlocking, dilation and the residual friction angle. Following Rowe (1962), they assumed that shear strength is derived from three sources: resistance to sliding along the contacting surfaces of asperities, resistance to shearing of asperities, and work performed by the normal load during dilation or contraction.

$$\tau_p = \frac{\sigma_n(1-a_s)(\dot{v}+\mu)+a_s\eta\tau_r}{1-(1-a_s)\dot{v}} \tag{3.39}$$

where τ_p = peak shear strength

σ_n = normal stress

$\dot{v} = \dfrac{dy}{dx}$ = dilation rate due to shear

μ = average coefficient of friction for the joint wall surfaces

a_s = ratio of area of asperities sheared off to total area.

η = degree of interlocking.

τ_r = the shear strength of the irregularities in the joint wall, given by Fairhurst's parabolic relationship (see chap. 3.2)

$$\tau_r = C_o[\sqrt{1+n}-1)/n]\sqrt{(1+n\sigma_n/C_o)} \tag{3.40}$$

where
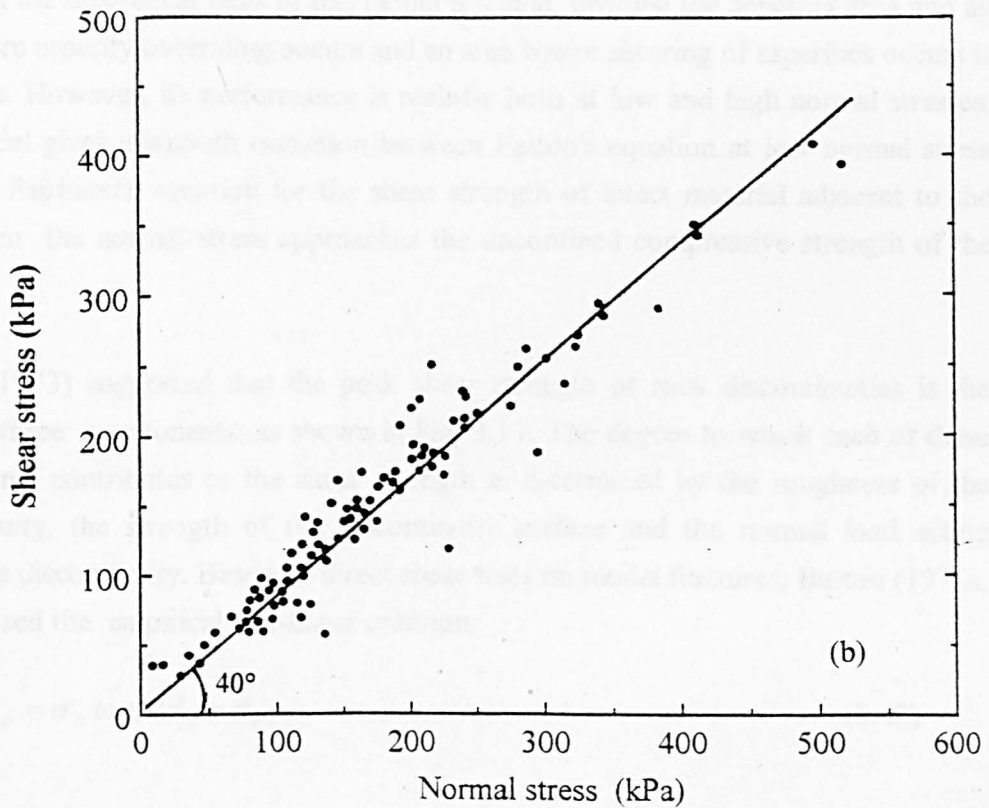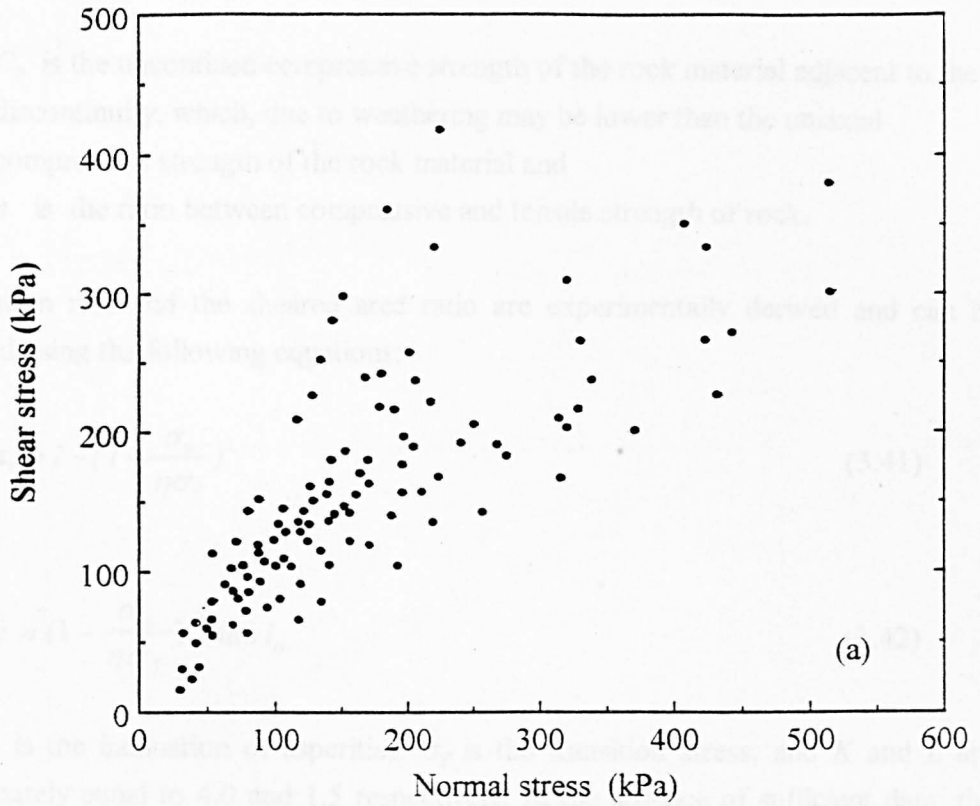
Fig. 3.16: Peak shear strengths from multistage tests on rough joints through granite: (a) measured; (b) dilation-corrected (after Hencher & Richards, 1989).

C_o is the unconfined compressive strength of the rock material adjacent to the discontinuity, which, due to weathering may be lower than the uniaxial compressive strength of the rock material and

n is the ratio between compressive and tensile strength of rock.

The dilation rate and the sheared area ratio are experimentally derived and can be estimated using the following equations:

$$a_s \approx 1-(1-\frac{\sigma_n}{\eta\sigma_T})^L \qquad (3.41)$$

and

$$\dot{v} \approx (1-\frac{\sigma_n}{\eta\sigma_T})^K \tan i_o \qquad (3.42)$$

where i_o is the inclination of asperities, σ_T is the transition stress, and K and L are approximately equal to 4.0 and 1.5 respectively. In the absence of sufficient data, the transition stress can be approximated by the uniaxial compressive strength of the rock. Although the theoretical basis of this model is sound, dividing the apparent area into an area where asperity overriding occurs and an area where shearing of asperities occurs is simplistic. However, its performance is realistic both at low and high normal stresses. This model gives a smooth transition between Patton's equation at low normal stress levels to Fairhurst's equation for the shear strength of intact material adjacent to the joint when the normal stress approaches the unconfined compressive strength of the rock.

Barton (1973) suggested that the peak shear strength of rock discontinuities is the result of three components, as shown in Fig. 3.17. The degree to which each of these components contributes to the shear strength is determined by the roughness of the discontinuity, the strength of the discontinuity surface and the normal load acting across the discontinuity. Based on direct shear tests on model fractures, Barton (1971a, b) proposed the empirical non-linear criterion,

$$\tau_p = \sigma_n \tan(2d_n + \phi_b) \qquad (3.43)$$

where

ϕ_b the *basic* friction angle and

d_n the peak dilation angle

69
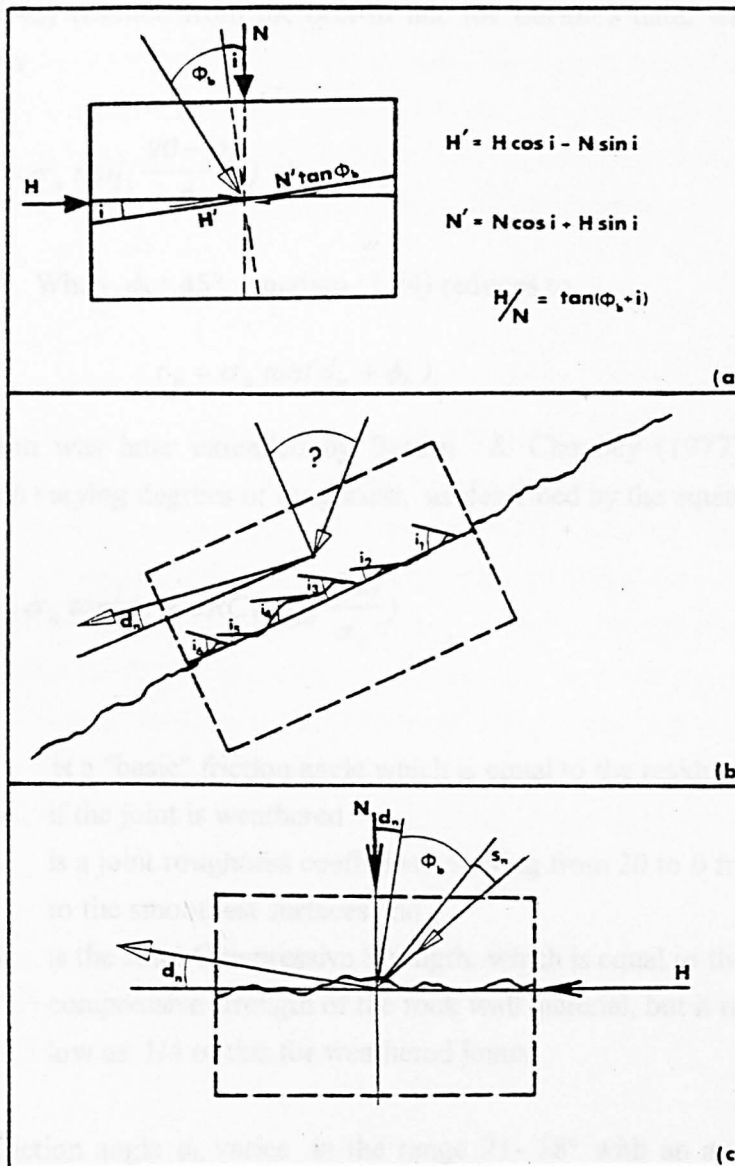
Fig. 3.17: Angular components of rock joint shear strength (after Barton, 1971 a, b)

Relation (3.43) resulted from the best-fit line for Barton's data, which had the more general form

$$\tau_p = \sigma_n \ tan[(\frac{90 - \phi_b}{\phi_b}) \ d_n + \phi_b]$$ (3.44)

for ϕ_b =30°. When ϕ_b= 45° equation (3.44) reduces to

$$\tau_p = \sigma_n \ tan(d_n + \phi_b)$$

This criterion was later extended by Barton & Choubey (1977) to include joint surfaces with varying degrees of roughness, as described by the equation:

$$\tau_p = \sigma_n \ tan(\phi_b + JRC \ log_{10} \frac{JCS}{\sigma_n})$$ (3.45)

where

ϕ_b is a "basic" friction angle which is equal to the residual friction angle ϕ_r if the joint is weathered

JRC is a joint roughness coefficient varying from 20 to 0 from the roughest to the smoothest surfaces and

JCS is the Joint Compressive Strength, which is equal to the unconfined compressive strength of the rock wall material, but it may be as low as 1/4 of this for weathered joints.

The basic friction angle ϕ_b varies in the range 21- 38° with an average of 30°. For unweathered joints, it can be obtained by carrying out residual shear tests on flat sawcut surfaces, whereas for weathered joints, it is replaced by the residual friction angle which can be estimated using the following equation:

$$\phi_r = 10 + \frac{r}{R}(\phi_b - 10)$$ (3.46)

where R and r are the Schmidt rebound values on the unweathered and weathered rock surfaces respectively.

Barton & Choubey suggested that at low normal stresses with little asperity damage, the roughness component $JRC \ log_{10}(JCS/\sigma_n)$ is equal to the peak dilation angle, whereas at higher normal stress the dilation angle decreases and the asperity damage becomes larger.

Barton's criterion fails to predict peak shear strength both at very low and very high normal stresses. At very low normal stresses, the logarithmic term in equation 3.45 tends to infinity and the equation ceases to be valid. Barton suggests that the maximum value of the term in the brackets should be 70°. At normal stresses approaching *JCS* the logarithmic term becomes zero and equation (3.45) predicts

$$\tau_p = \sigma_n \, tan \, \phi_r \qquad (3.47)$$

which is lower than the observed values (Barton, 1973, 1990). Theoretically, this is a serious disadvantage, as it may indicate an underlying fundamental deficiency in the basis of Barton's relation. To overcome this, Barton (1976) suggested that the confined strength (σ_1-σ_3) should be used instead of *JCS*, because of the "more effective confinement" of asperities. Despite its purely empirical nature (see criticism by Reeves, 1985), Barton's criterion gives accurate predictions, when the parameters *JRC* and *JCS*, which according to Bandis *et al.*(1981), are strongly scale dependent, are adjusted to field scale. However, Hencher *et al.* (1993) and Papaliangas *et al.* (1994) have shown that the asperity failure component of the peak shear strength (i.e. *JCS*) is not scale-dependent and this is a matter which will be considered and discussed in detail in this study.

While the vast majority of the proposed models are based on Patton's "$\phi+i$" principle, there are some empirical models of the power law form, for example Nilsen (1985), Lilly (1981), Denby & Scoble (1985)

$$\tau_p = a \, \sigma_n^{\,b} \qquad (3.47)$$

where a and b are constants. These models may fit experimental data quite well but lack any theoretical basis.

Micromechanical models have been proposed which involve an intrinsic frictional strength of the contacts, adhesion, geometrical interlock, asperity failure, and ploughing. As typical examples the models proposed by Yamada *et al.* (1978), Sun *et al.* (1985), Swan & Zongqi (1985), and Boitnott *et al.* (1992) are mentioned. Although these models propose meaningful mechanisms of friction, their application to rock engineering problems seems quite remote.

Many other studies have been devoted to different aspects of shear behaviour of rock joints. They may be summarised :
(a) empirical, in which correlations between variables affecting shear behaviour are derived from existing experimental data, for example Goodman (1974), Schneider

(1976) Barton & Choubey (1977), Barton *et al.* (1985), Leichnitz (1985), Papaliangas *et al.* (1993).

(b) theoretical, where known theories are used to describe the observed behaviour. This approach has been adopted by Roberds & Einstein (1978), Hsu-Sun (1979), Swan (1981), Desai & Fishman (1987), Kane & Drumm (1987), Plesha (1987), Qiu *et al.* (1993) and others. Combination of the two approaches or analytical methods have also been used for example by Pande (1985), Heuze (1979) and others. Basic parameters need to be experimentally or empirically determined, which reduces the confidence on these models.

Strength criteria are required to allow prediction and extrapolation from a few laboratory tests to any combination of stresses found in a rock mass. In the lack of criteria with theoretical basis which match the experimental results satisfactorily and give accurate predictions, the empirical criteria, obtained by curve fitting and for which a large effort is made to rationalise (Kulatilake *et al.* , 1994), are used.

The relation between dilation angles (or roughness angle) and normal stress for some common models is given in Table 3.6, from which it becomes evident that all of them are empirical in nature and require a number of empirical constants to be determined experimentally. In conclusion, the basic criteria for peak shear strength of rock joints remain mostly empirical although a great number of studies have been devoted to it and huge amount of experimental data from both laboratory and in-situ tests are available.

3.4 Summary

The real contact area between two rock rough surfaces is very small and the real normal stress very high. When any plastic or complex elastic surfaces come into contact the actual area of contact is proportional to normal load. Rock joint surfaces have a random geometry, therefore, when in contact, they follow this proportionality law.

The exponential distribution of heights of a surface offers the important advantage that, independent of the mode of deformation and the shape of asperities, they obey Amonton's friction laws. A rock joint surface can be considered as having an exponential distribution, especially at low to intermediate normal stresses.

Enough experimental evidence suggests that shear strength of rock discontinuities arises from shearing of rock wall material under the acting high normal stresses.

Table 3.6 : Proposed relations between dilation and normal stress

Model	Relation	Remarks
1. Ladanyi & Archambault (1970)	$tan\ i\ =\ tan\ i_o(1-\dfrac{\sigma_n}{n\sigma_T})^{k_2}$	$\sigma_T=C_o,\ k=4,$ n = empirical constant
2. Tsytovich $et\ al.$ (1970)	$i\ =\ i_o - a\ln\sigma_n$	a = empirical constant
3. Goodman & Dubois (1972)	$i\ =\ i_o\ (1-\dfrac{\sigma_n}{\sigma_T})^k$	$\sigma_T=C_o,$ k = empirical constant
4. Schneider (1976)	$i\ =\ i_o\ e^{-k\sigma_n}$ $k = a(\sigma_t d)^{-b}$	d = dimensional constant σ_t= tensile strength $a,\ b$ = empirical constants
5. Barton $et\ al.$ (1985)	$i\ =\ 0.5\,JRC\ log\ (\dfrac{JCS}{\sigma_n}\ )$	JRC = Joint Roughness Coefficient JCS = Joint Compressive Strength
6. Leichnitz (1985)	$i\ =\ i_o + c\ln(\dfrac{N}{N_o})$	c = empirical constant $N,\ N_o$= normal forces corresponding to i and i_o
7. Jing $et\ al.$ (1992)	$i\ =\ i_o\ (1-\dfrac{\sigma_n}{C_o})^b$	b = empirical constant
8. Gaziev (1976)	$i\ =\ i_o\ (1-\dfrac{\sigma_n}{\sigma_T})^m$	$m=10\ \ \sigma_T=C_o$
9. Heuze (1979)	$i\ =\ ATAN(A\sigma_n + 2B\sigma_n\ + \\ 3C\sigma_n^2)\ - \phi_r$	$A,\ B,\ C$ = empirical constants
10. Pease & Kulhawy (1984)	$tan\,i\ =\ tan\,i_o\ e^{-\frac{k\sigma_n}{nC_o}}$	$k,\ n$ = empirical constants
11. Reeves (1985)	$i = mz_2(r) = mK(p)(Z_1/xD)$	m = constant, $K(p)=f(p)$ Z_1/xD average asperity gradient
12. Gerrard (1986)	$tan\ i\ =\ tan\ i_o[1-\dfrac{\sigma_n}{\sigma_T}\ ]^n$	$\sigma_T=\sigma_c$ n = empirical constant
13. Leong & Randolph (1992)	$i\ =\ A\ - B\ln\dfrac{\sigma_n}{C_o}$	$A,\ B,$ = empirical constants
14. Kulatilake $et\ al.$(1994)	$i\ =\ A(z_2')^B\,(log\ \dfrac{JCS}{\sigma_n}\ )^C$	$A,\ B,\ C$ = empirical constants

Numerous models exist to describe peak shear strength. Empirical models may not explain the mechanisms involved, whereas theoretical models are complicated and do not accurately fit the experimental data. Due to difficulties in prediction of the effect of roughness on shear strength at any normal stress, there is no simple, accurate model which satisfactorily explains experimental observations in terms of basic theory.

CHAPTER 4
EXPERIMENTAL PROGRAMME

4.1 Introduction

The shear behaviour of rock joints is best studied experimentally by direct shear testing. A great number of studies, devoted to several aspects rock joint behaviour, describe both the method and results of direct shear tests. Notable examples include Patton (1966a), Goodman (1970), Jaeger (1971), Barton (1971a, b) Coulson (1970, 1972), Lama (1978), Krahn and Morgenstern (1979), Bandis et al. (1981), Hassani and Scoble (1985), Hencher and Richards (1989) and Papaliangas et al. (1990, 1993).

The method adopted here is based on direct shear tests on replicas of natural joints. To avoid problems with friability, the synthetic rock described in Chapter 2 was used. Identical samples from several prototype rock surface were prepared and tested in direct shear under different normal stresses. A preliminary testing programme (Papaliangas et al., 1994) and other recent experimental results (Hencher et al., 1993) indicated that previously widely accepted concepts regarding scale dependence of peak shear strength may not be valid, and a special part of the experimental programme was dedicated to this aspect of peak shear strength.

The experimental part of the thesis is a straight-forward testing programme, consisting of three different series of direct shear tests:

a) The first series involves tests on replicas of three natural joints with different roughness, under normal stresses in the range 0-2 MPa.

b) The second series concentrated on the implications of sample size on peak shear strength. A replica of a natural rock joint, 354 mm long and 150 mm wide, was divided into 4 and 12 pieces and all sizes (full, 1/4th and 1/12th) were tested under two different normal stresses, namely 25 kPa and 125 kPa. Three additional normal stress levels, namely 250 kPa, 1.0 MPa and 2.0 MPa were used for the smallest size samples.

c) The third series of tests examines the affect of both the strength of the material and the sample size on peak shear strength. In order to carry out this programme it was necessary to use a weaker model material. Samples from the same joint were prepared in the same way as in b) and the results were compared. An additional small size (1/24th) was used at a normal stress of 125 kPa. The material used was the same as that used by Bandis (1980) and Toy (1993), so that a direct comparison with their results could be made.

4.2 Testing details

4.2.1 Preparation of model joints

A hot rubber melt moulding compound (Vinamold 9525, "Hard" variety) was used to obtain mating negative impressions of natural rock surfaces. From these Vinamold moulds, several identical positive casts was made of the model rock material. Details of the procedure followed to obtain the final pair of copies for each sample can be found elsewhere (Bandis, 1980 and Papaliangas, 1986). The natural rock surface from which impressions were made was a fine micaceous sandstone. For the first two series of tests the new synthetic rock was used. To prepare each one of the two halves of the samples, andalusite was first mixed dry with cement in a 5 litre HOMBART model A210 mixer for 5 minutes. The water was poured slowly and the whole mix continued for another 5 minutes. The mix was then poured into a steel frame surrounding the Vinamold impressions and vibrated with a 16 mm steel bar, attached to a small pneumatic vibrating plate. The time of vibration was ranged between 0.5 and 2.0 minutes, depending on the size of the sample. With vibration, air bubbles were removed and the joint surface was freed of large pores, a problem which is inevitable with casting of materials. Although some water was concentrated on the free surface during compaction, segregation was not noticed. All the joint surfaces used were rough, and this was reproduced in the replicas. However, when seen on a microscopic scale their surfaces were smooth due to the nature of the rubber compound used to reproduce them. With this smooth texture the reproduced samples did not eventually represent the original sandstone surface, but another rock type with similar smooth surface texture and granular underlying material. This is not a problem since the original sandstone surface was used not for studying its shear behaviour but for producing a surface with a realistic natural roughness.

The degree of fit between the two halves of the replicas depends on the accuracy of reproduction of the two halves of the corresponding Vinamold impressions, which were subsequently used for preparation of the replicas. Obviously, a perfect fit between the two halves is impossible, and the larger the sample the worse the joint mating. An acceptable degree of macroscopic fitting was achieved, but occasionally the two halves were rocked slightly. This may be more serious for samples of large size.

4.2.2 Testing equipment

In order to test both large size samples over a wide range of normal stresses, two different direct shear apparatuses were employed in this study.

In the first series of tests where normal stresses up to 2.0 MPa were used, a Golder Associates Direct Shear Box, as described by Hencher and Richards (1989), was

employed (Fig. 4.1). Shearing is caused by pulling the lower surface from beneath a restrained upper surface. A constant normal load is applied by means of dead weights on a hanger at the end of a lever arm with a theoretical mechanical advantage of 11. A yoke driven by a hydraulic ram which enables the tests to be conducted at an approximately constant rate of shear displacement is used to apply the shear force. The maximum normal stress which could be applied for this size of sample was 2.0 MPa. The joints were sheared for up to 15 mm horizontal displacement, at constant normal load, following the recommended ISRM method (ISRM, 1981). The shear force is measured directly from a load cell mounted on the loading yoke and the horizontal and vertical displacements are measured using displacement transducers. The measurements are recorded on a computer via an analogue/digital interface, and are analysed to determine shear stress, dilation angle and other parameters throughout the test. From these results the peak and residual shear strengths, and the peak dilation angle for the discontinuity are determined. The shear rate was maintained at approximately 1 mm per minute, which was found not to have any effect on shear strength if small fluctuations in the shear rate occur (Hencher & Richards, 1989).

In the second and third series of tests, where larger samples were used, the large purpose-built shear box in the Department of Earth Sciences (Bandis, 1980) was used. The loading arrangement of this shear box is given in Fig. 4.2. Shear rate was 0.4 mm/min. The shear load was measured by means of a 5 kN proving ring, on which an LVDT was mounted. Normal load remained constant throughout the tests. Shear displacement was measured by a horizontal LVDT, whereas, for the normal displacement, three LVDTs were employed at three different points on the upper half of the sample. All measurements were recorded on a computer via analogue/digital interface. The shear tests on small samples at 1.0 MPa and 2.0 MPa were carried out on the Golder Associates shear box described above.

4.2.3 Non-dilational shear strength

The values of normal and shear stress acting on the sample are calculated by dividing the normal and shear loads by the apparent area of contact. Due to shear displacement, the apparent area of contact and therefore the normal stress changes continuously throughout the test, even if shearing takes place at constant normal load. This variation of normal stress with shear displacement was taken into account, when stresses were calculated. The calculated stresses differ significantly from the actual stresses acting at the points of contact as the actual area of contact is only a very small proportion of the apparent area of contact. The calculated stresses thus determined were subsequently separated into a dilational and a non-dilational component. The method of separation into these two components has been used by Ripley & Lee (1962), Hencher &
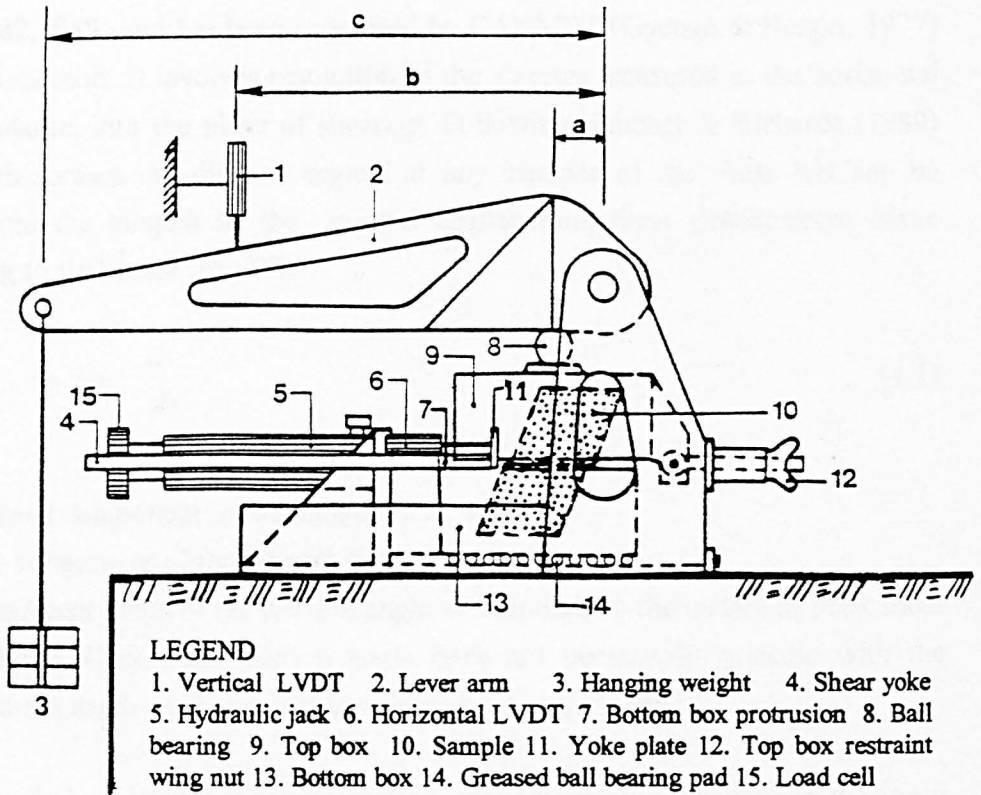
Fig. 4.1: The Golder Associates direct shear box. Theoretical mechanical advantage of lever arm: c/a; amplification of vertical LVDT reading: b/a

LEGEND
1. Vertical LVDT 2. Lever arm 3. Hanging weight 4. Shear yoke
5. Hydraulic jack 6. Horizontal LVDT 7. Bottom box protrusion 8. Ball bearing 9. Top box 10. Sample 11. Yoke plate 12. Top box restraint wing nut 13. Bottom box 14. Greased ball bearing pad 15. Load cell
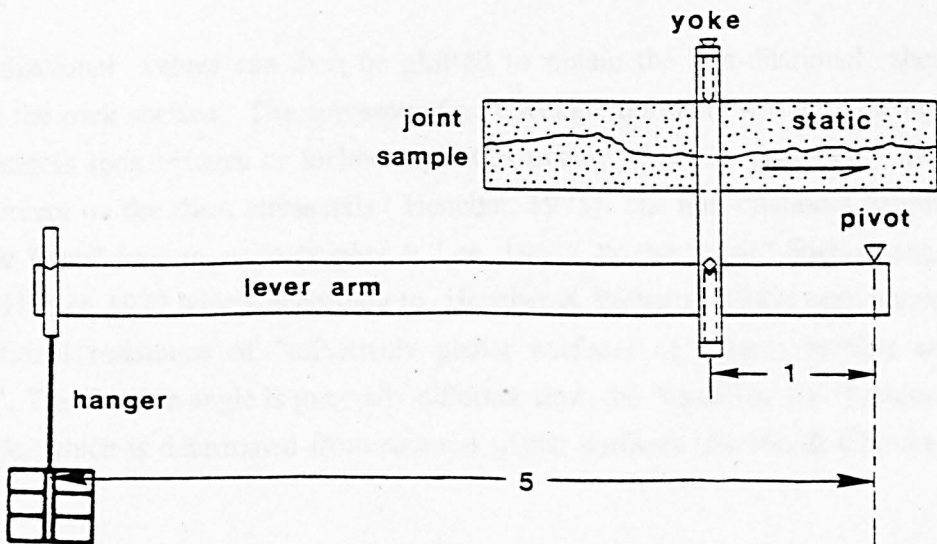
Fig. 4.2: Loading 5x lever arm set-up for the large shear box.

Richards (1982,1989) and has been suggested by CANMET (Gyenge & Herget, 1977) as a standard method. It involves resolution of the stresses measured in the horizontal and vertical planes, into the plane of shearing. Following Hencher & Richards (1989) for any rough surface the dilation angle i at any instance of the shear test can be calculated from the tangent to the normal displacement-shear displacement curve corresponding to that point (Fig 4.3):

$$i = tan^{-1} \frac{dv}{dh} \qquad (4.1)$$

where

dv is the normal component of the tangent line and

dh the shear component of the tangent line.

The more significant value of the dilation angle corresponds to the instant of peak shear strength (Figure 4.3a). This dilation angle does not necessarily coincide with the maximum dilation angle exhibited during a shear test (Arnold, 1992).

The normal and shear stresses acting on the shearing plane at an angle i to the mean joint plane are given by the following equations:

$$\tau_i = (\tau \cos i - \sigma \sin i) \cos i \qquad (4.2a)$$
$$\sigma_i = (\sigma \cos i + \tau \sin i) \cos i \qquad (4.2b)$$

where

τ_i is the shear stress in the plane of shearing and

σ_i the normal stress in the plane of shearing

These non-dilational values can then be plotted to obtain the non-dilational shear strength for the rock surface. The corresponding envelope normally will pass through the origin, unless rock bridges or locked asperities occur, when the envelope has a positive intercept on the shear stress axis (Hencher, 1995). The non-dilational stresses will give the "true" friction angle (Ripley & Lee, 1962), or the "basic" friction angle (Gyenge & Herget, 1977 which, according to Hencher & Richards (1989) corresponds to the frictional resistance of "effectively planar surfaces of natural texture and mineralogy". This friction angle is generally different from the "basic" or the "residual" friction angle, which is determined from saw-cut planar surfaces (Barton & Choubey, 1977).

4.2.4 Shear strength characteristics of rough model joints

The suitability of the model material to replicate the behaviour of rock joints was checked by using four casts of the joint C, which were subjected to direct shear under

Peak

shear stress

200

150

100

50

Shear stress (kPa)

3.0

2.5

2.0

1.5

1.0

0.5

0.0

Normal displacement (mm)

i

normal displacement

(a)

0   5.0   10.0   15.0

Shear displacement (mm)

σ

τ

dv

dh

i

τ

(b)

τ_i

i

τ

σ

σ_i

i

(c)
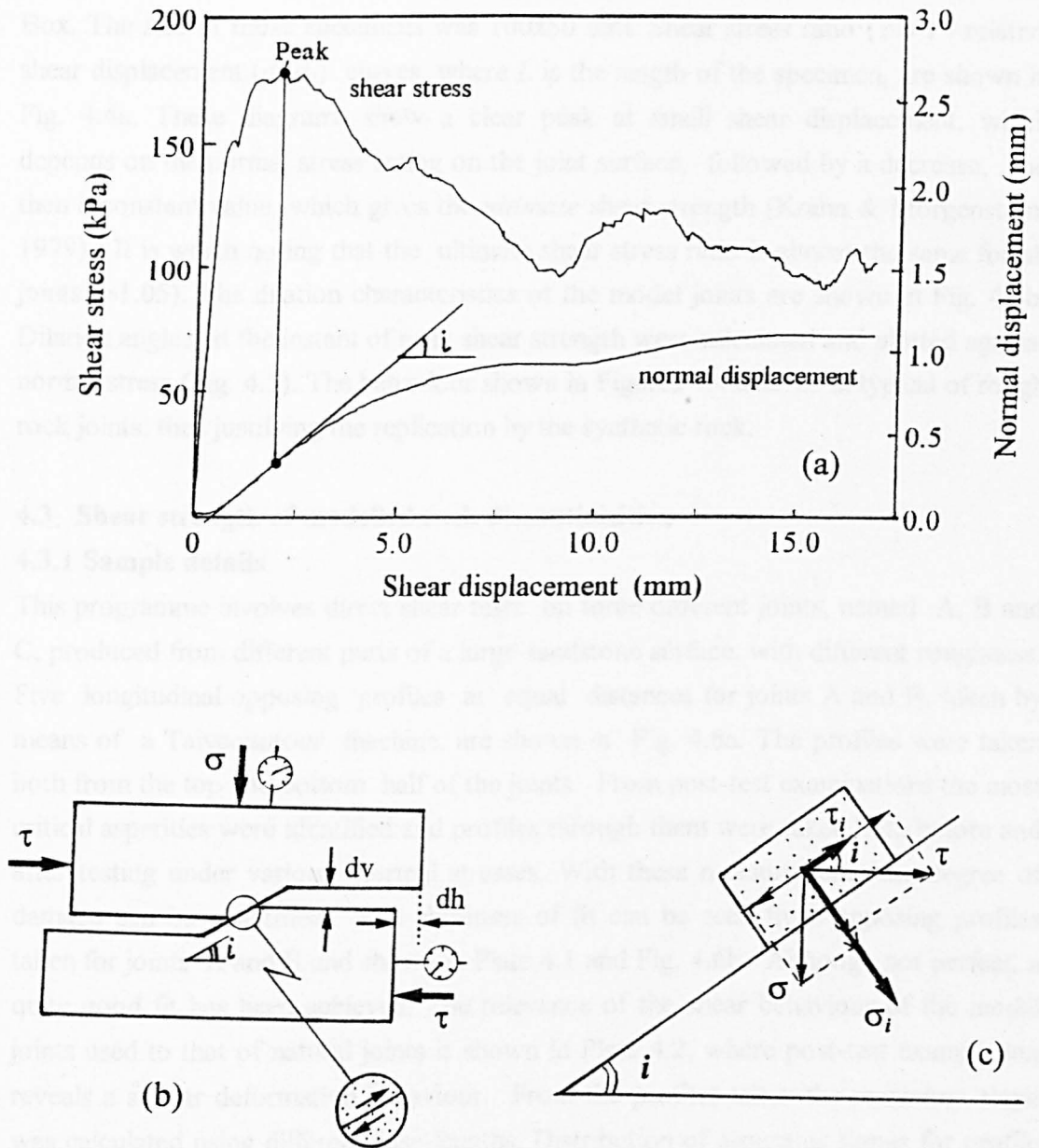
INSTANTANEOUS DILATION ANGLE : $i = tan^{-1}(dv/dh)$

Fig. 4.3 Calculation of the non-dilational shear stress.
(a) Shear stress-shear displacement and normal displacement-shear displacement diagrams.
(b) simplified representation of dilating sample. (c) analysis of forces in the plane of shearing

different normal stresses in the range 0-2.0 MPa, in a Golder Associates Direct Shear Box. The size of those specimens was 100x50 mm. Shear stress ratio (τ/σ) - relative shear displacement (*dh/L*) curves, where *L* is the length of the specimen, are shown in Fig. 4.4a. These diagrams show a clear peak at small shear displacement, which depends on the normal stress acting on the joint surface, followed by a decrease, and then a constant value, which gives the *ultimate* shear strength (Krahn & Morgenstern, 1979). It is worth noting that the ultimate shear stress ratio is almost the same for all joints ($\approx$1.05). The dilation characteristics of the model joints are shown in Fig. 4.4b. Dilation angles at the instant of peak shear strength were calculated and plotted against normal stress (Fig. 4.5). The behaviour shown in Figures 4.4 and 4.5 is typical of rough rock joints, thus justifying the replication by the synthetic rock.

4.3 Shear strength of modelled rock discontinuities

4.3.1 Sample details

This programme involves direct shear tests on three different joints, named A, B and C, produced from different parts of a large sandstone surface, with different roughness. Five longitudinal opposing profiles at equal distances for joints A and B, taken by means of a Talycountour machine, are shown in Fig. 4.6a. The profiles were taken both from the top and bottom half of the joints. From post-test examinations the most critical asperities were identified and profiles through them were taken both before and after testing under various normal stresses. With these measurements the degree of damage can be quantified. The closeness of fit can be seen from opposing profiles taken for joints A and B and shown in Plate 4.1 and Fig. 4.6b. Although not perfect, a quite good fit has been achieved. The relevance of the shear behaviour of the model joints used to that of natural joints is shown in Plate 4.2, where post-test examination reveals a similar deformation behaviour. From the profiles taken the maximum slope was calculated using different base-lengths. Distribution of asperities slopes for profile No 2 of joint A and No 1 of joint B calculated over a base-length equal to 0.2% of the sample length is shown in Figure 4.7.

4.3.2 Peak shear strength

The main testing programme was based on direct shear tests on replicas of joints A, B and C. Pairs of profiles from both top and bottom half are shown in Fig. 4.6. Although not perfect, the fit is quite good. Each test was carried out under constant normal stress and only one test under constant normal stress was carried out on each sample. From each test a number of parameters were determined. Summarised data are given in Tables 4.1a and b, where

σ_n is the normal stress,

τ_p the peak shear strength

σ_i and τ_i the normal stress and shear stress corresponding to non-dilatant behaviour
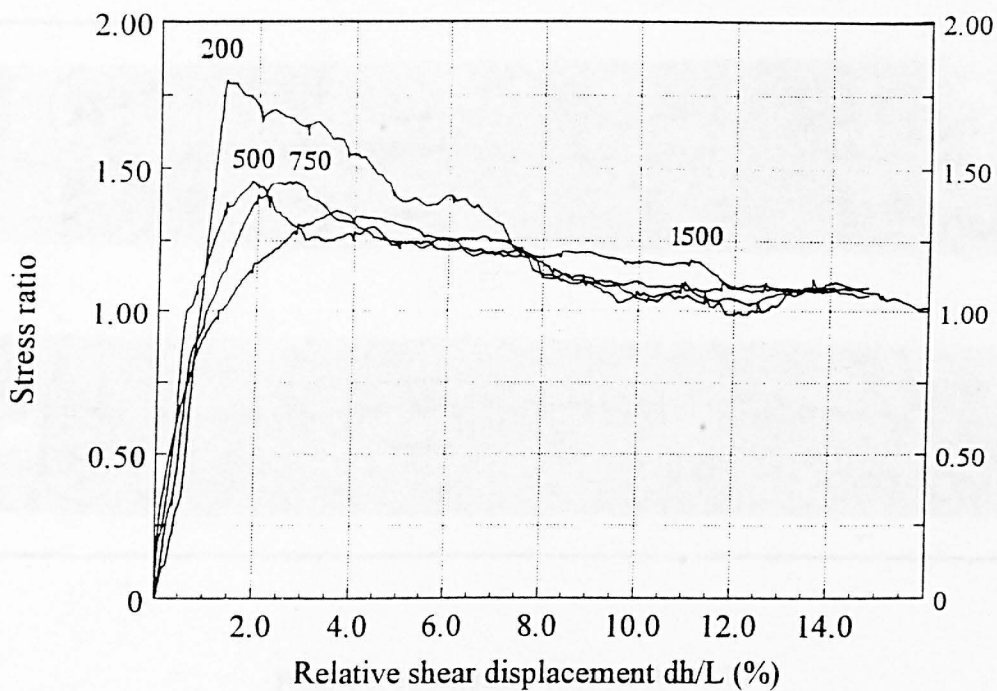
(a)
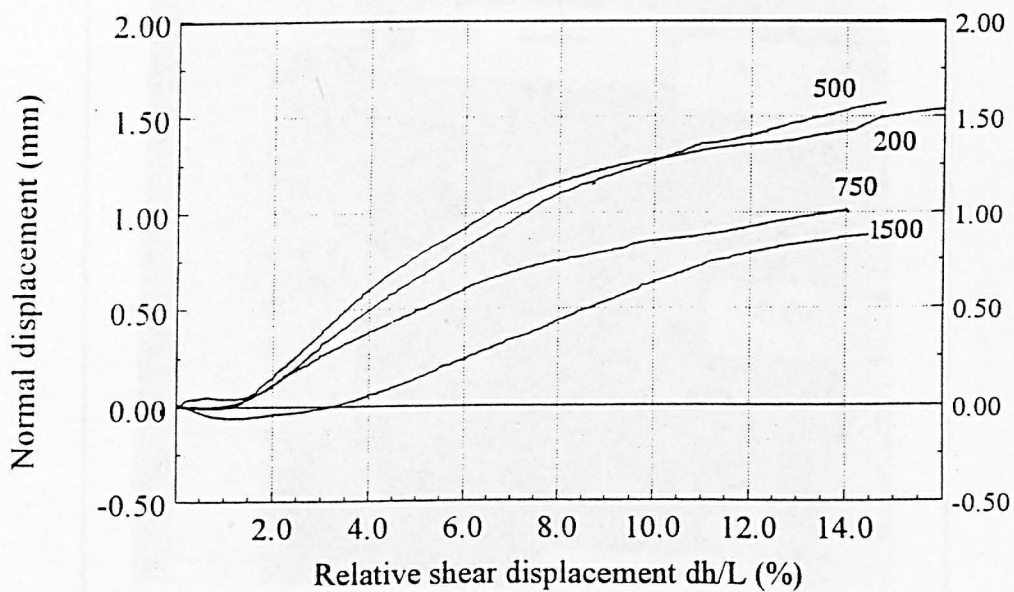
(b)

Fig. 4.4 : shear behaviour of modelled joints.

(a) Shear stress - shear displacement diagrams of model joints

(b): Normal displacement- shear displacement diagrams of model joints
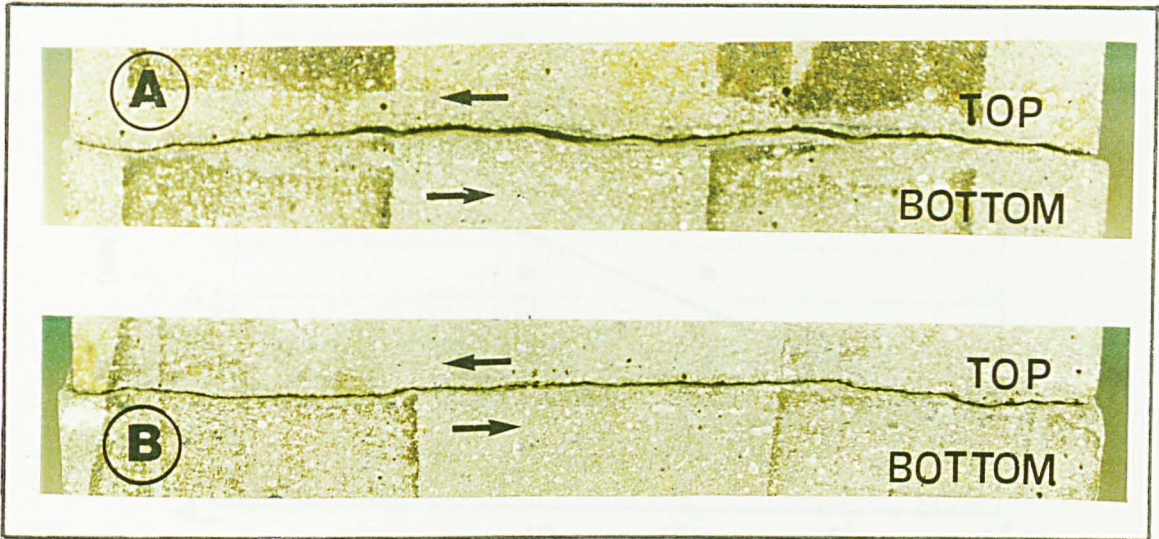
Plate 4.1: Photographs of joints A and B.
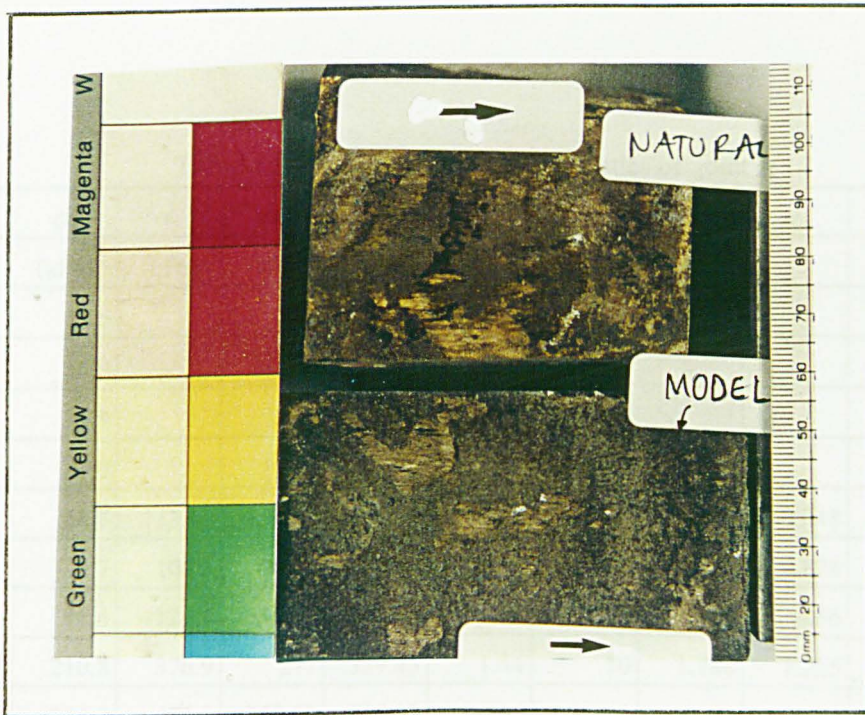
Plate 4.2: Comparison of surface damage caused by direct shear testing of a model and a natural rock joint
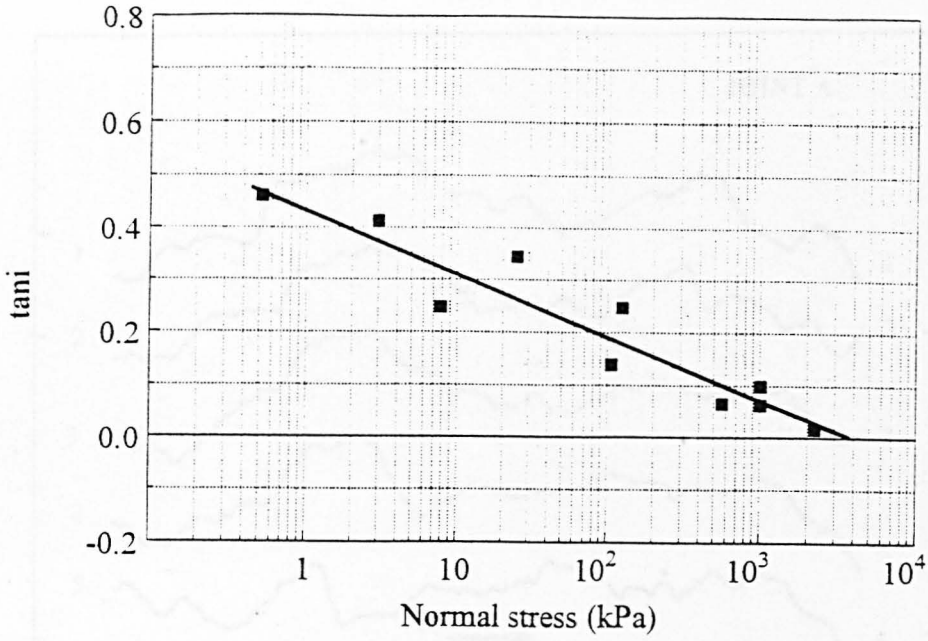
Fig. 4.5: Variation of peak dilation rate with normal stress

Table 4.1a: Shear strength characteristics of joint A

Test	σ_n	τ_p	σ_l	τ_l	dh_p	ψ	μ_p	μ_m	ψ_{max}	$dh_{\psi max}$
	(kPa)	(kPa)	(kPa)	(kPa)	(mm)	(°)			(°)	(mm)
A_00	0.6					35.6			35.6	
A_01	6.9					36.8			36.8	0.9
A_02	6.9					21.9			21.9	0.45
A_03	6.9					34.1			34.1	1.15
A_04	68.7	113.02	94.82	89.9	1.15	14.3	1.646	0.948	19	1.067
A_05	69.7	104.3	96.03	79.49	1.48	16.9	1.511	0.828	19.3	1.39
A_06	91.4	123.6	118.51	101.98	1.99	12.8	1.353	0.86	13.2	1.63
A_07	210.8	376.9	277	339.45	1.44	10	1.788	1.225	14.2	3.01
A_08	264.3	473.3	359.99	396.12	0.66	13.1	1.791	1.1	14.5	0.93
A_09	492.9	717.3	619.2	644.32	1.88	9.4	1.455	1.041	10.5	2.17
A_10	760.3	1105	1013.3	942.1	2.64	12.6	1.453	0.93	12.99	2.71
A_11	1001	1200	1176	1158	2.83	4.6	1.198	0.985	7.3	3.05
A_12	1456.4	1771.5	1907	1875	4.71	6.1	1.216	0.983	7.66	6.54
A_13	1500	2033	1757	2076	3.6	3.8	1.355	1.182	7.2	4.46
A_14	2070	2378	2155	2298	3.8	2.1	1.154	1.073	2.63	3.79
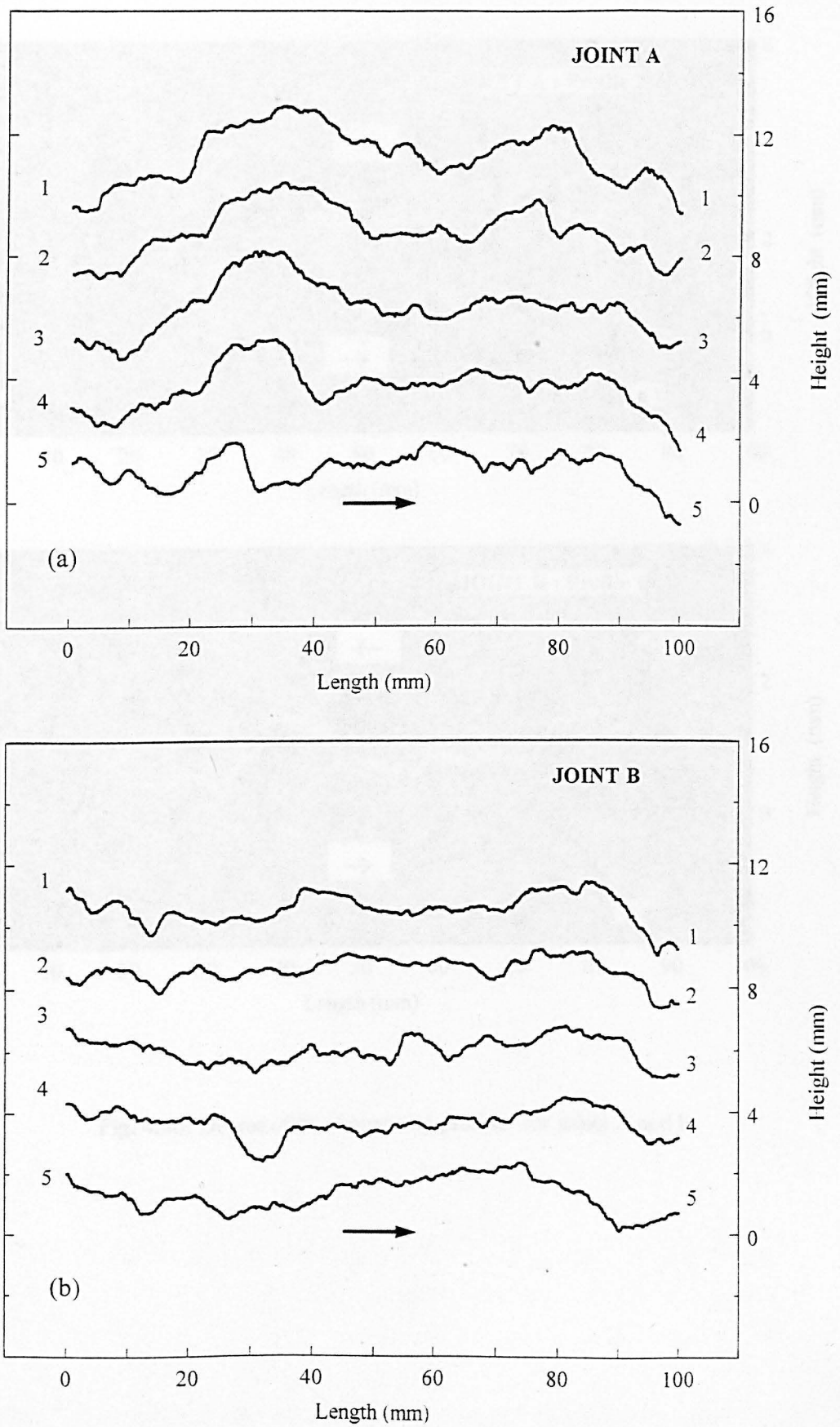
Fig 4.6a: Profiles of bottom halves at equal distances of the rock joints used (arrows show the direction of shearing): (a) Joint A. (b) Joint B.
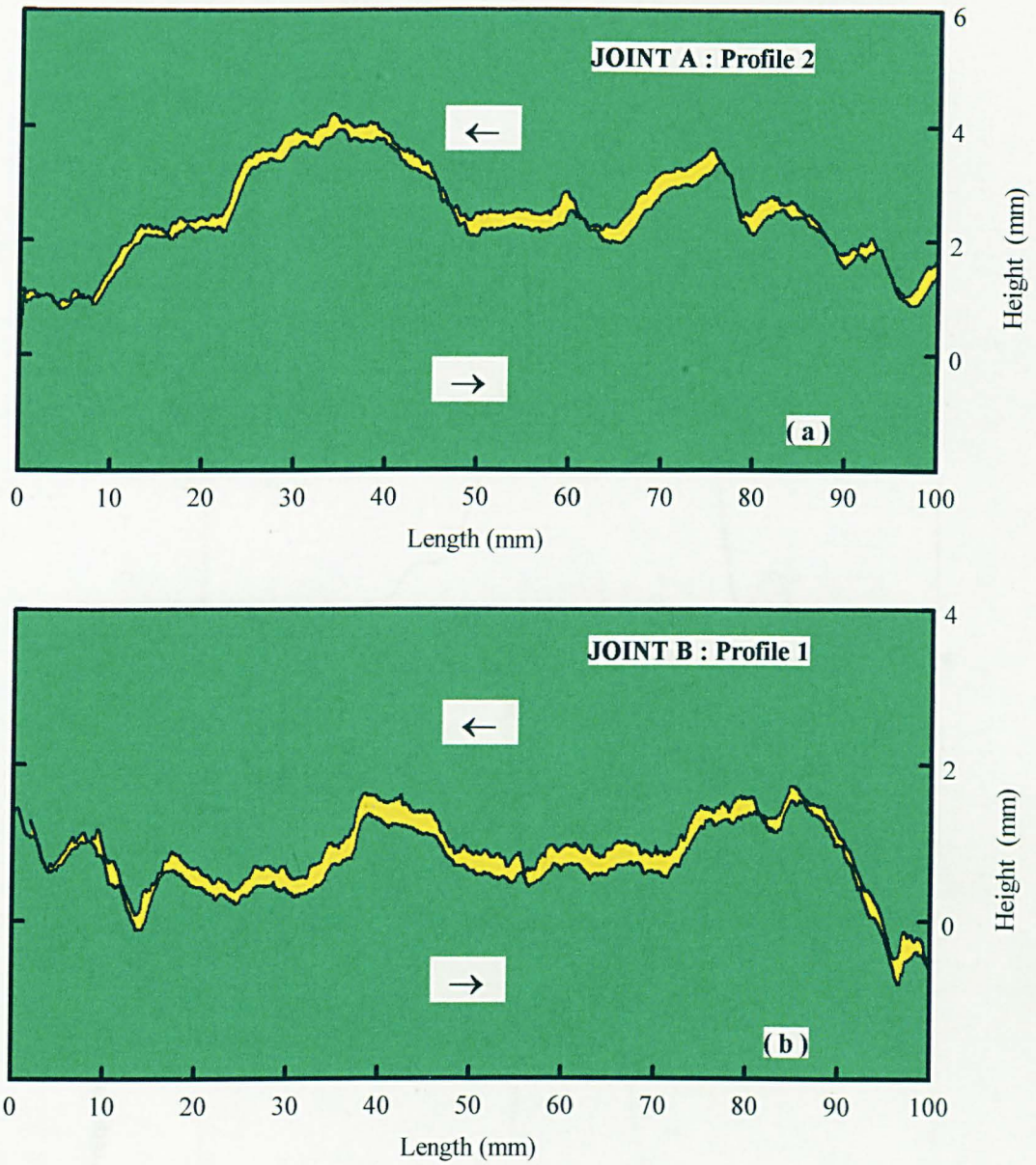
Fig. 4.6b: Degree of fit of opposing profiles for joints A and B.

dh_u the peak shear displacement

a_p the measured peak ratio ratio (h_p/h_0)

ρ_p the non-dilational stress ratio

ψ the dilation angle at peak shear stress

ψ_{max} the maximum dilation angle

dh_{max} the shear displacement corresponding to ψ_{max}
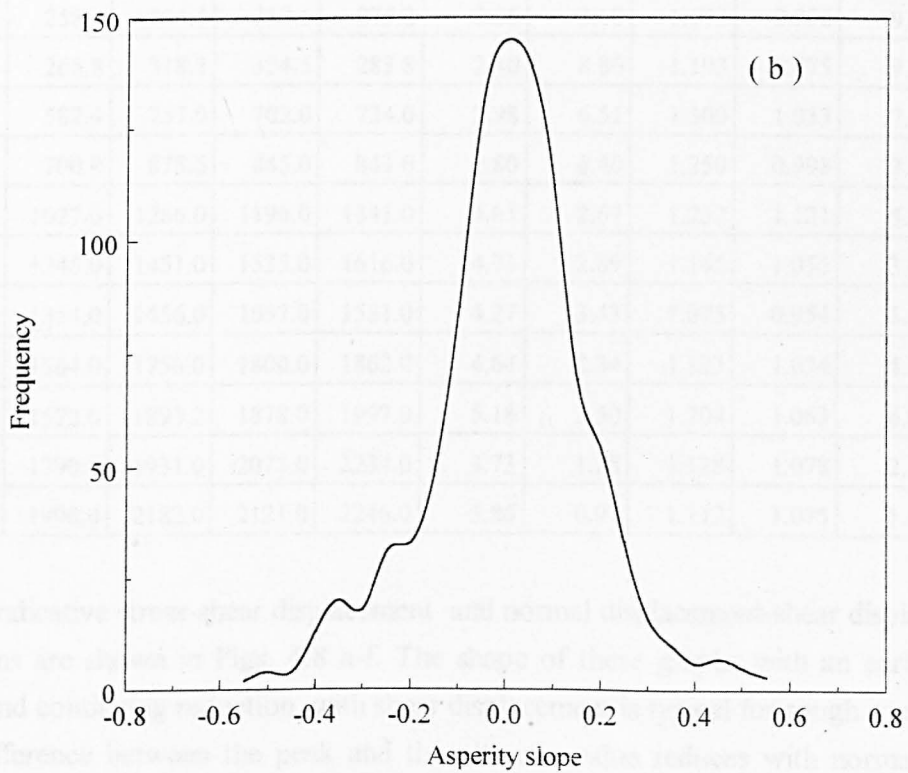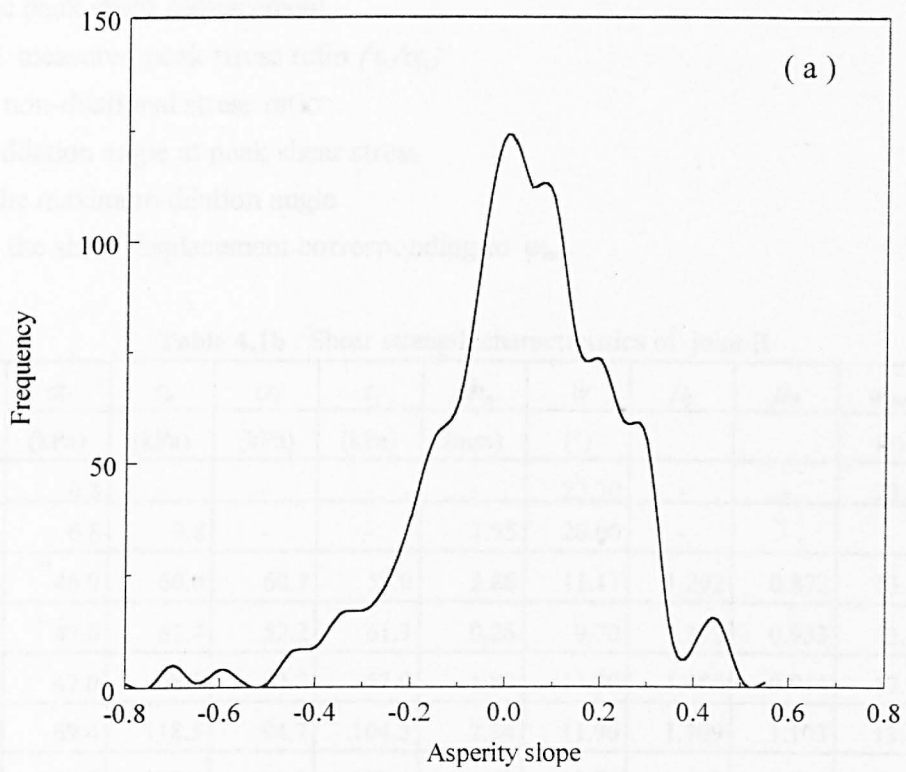
Fig 4.7: Distribution of asperity slopes for a base-length of 0.2% of the sample length.
(a) Joint A. (b) Joint B.

dh_p the peak shear displacement

μ_p the measured peak stress ratio (τ_p/σ_n)

μ_m the non-dilational stress ratio

ψ the dilation angle at peak shear stress

ψ_{max} the maximum dilation angle

$dh_{\psi max}$ the shear displacement corresponding to ψ_{max}

Table 4.1b : Shear strength characteristics of joint B

Test	σ_n	τ_p	σ_l	τ_l	dh_p	ψ	μ_p	μ_m	ψ_{max}	$dh_{\psi max}$
	(kPa)	(kPa)	(kPa)	(kPa)	(mm)	(°)			(°)	(mm)
B_00	0.8	-	-	-	-	23.30	-	-	23.30	-
B_01	6.8	9.8	-	-	1.95	20.00	-	-	-	-
B_02	46.9	60.6	60.7	53.0	2.86	11.17	1.292	0.872	13.27	3.46
B_03	47.0	61.7	52.2	61.7	0.26	9.70	1.312	0.933	13.10	0.43
B_04	47.0	68.8	62.2	57.0	1.89	13.20	1.463	0.916	17.10	1.64
B_05	69.4	118.5	94.7	104.5	2.34	11.90	1.709	1.103	13.60	1.80
B_06	93.0	132.2	120.9	109.4	1.59	12.70	1.422	0.905	16.70	1.70
B_07	258.4	304.6	310.6	275.2	2.36	8.10	1.179	0.896	9.89	2.65
B_08	266.8	318.3	324.5	283.8	2.40	8.86	1.193	0.875	9.89	2.22
B_09	582.4	757.0	702.0	724.0	2.98	6.51	1.300	1.033	7.35	3.32
B_10	700.0	875.6	845.0	843.0	2.80	6.40	1.250	0.998	7.85	3.11
B_11	1027.0	1266.0	1196.0	1341.0	4.65	2.67	1.232	1.121	5.55	5.24
B_12	1245.0	1451.0	1535.0	1616.0	4.71	2.89	1.165	1.053	3.36	5.27
B_13	1354.0	1456.0	1657.0	1581.0	4.27	3.43	1.075	0.954	5.41	8.31
B_14	1564.0	1756.0	1800.0	1862.0	4.64	2.34	1.123	1.034	4.38	3.90
B_15	1572.0	1893.2	1878.0	1997.0	5.18	3.50	1.204	1.063	6.00	5.68
B_16	1790.0	1931.0	2071.0	2234.0	3.73	1.28	1.128	1.078	2.39	5.98
B_17	1990.0	2182.0	2121.0	2246.0	5.86	0.97	1.112	1.075	1.88	4.88

Some indicative stress-shear displacement and normal displacement-shear displacement diagrams are shown in Figs. 4.8 a-f. The shape of these graphs with an early peak value and continuing reduction with shear displacement is typical for rough rock joints. The difference between the peak and the ultimate value reduces with normal stress, corresponding to values of the ratio peak/ultimate stress from as high as 2.0 at low normal stresses to about 1.0 at higher normal stresses. The non-dilational shear stress is more or less constant for the whole range of shear displacement with the exception of the initial pre-peak region, where generally an increased value is obtained. The resolution of the non-dilational shear stress versus horizontal displacement graph depends on the step-size used to calculate the dilation angle. This step-size must be
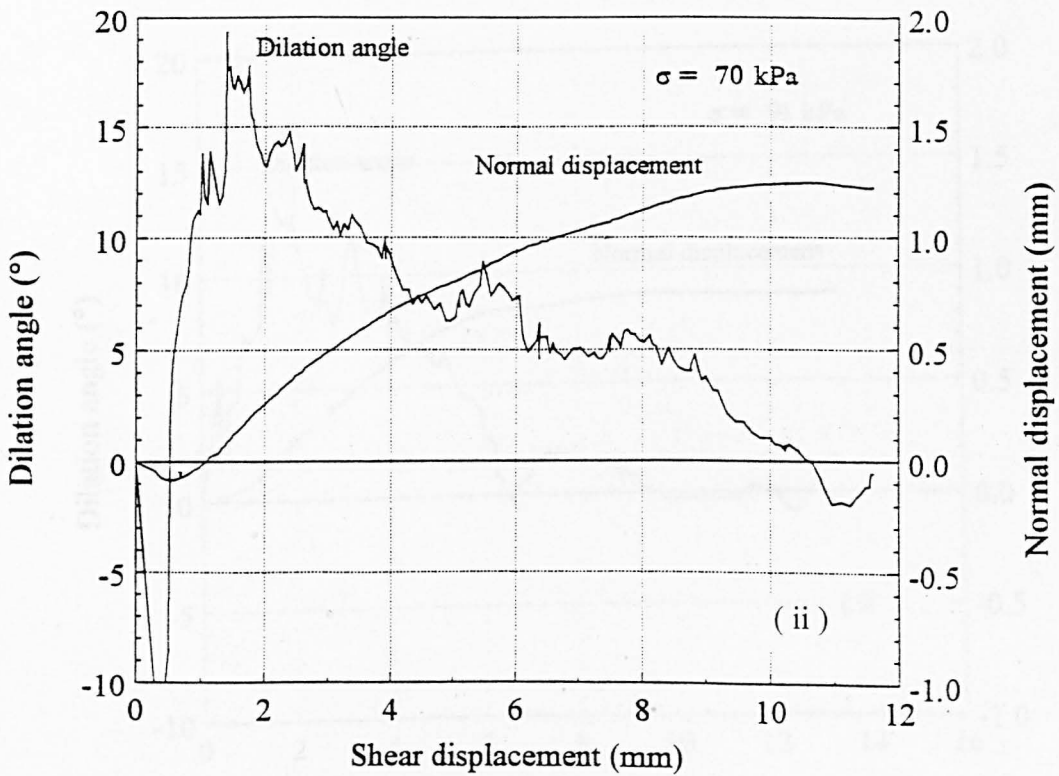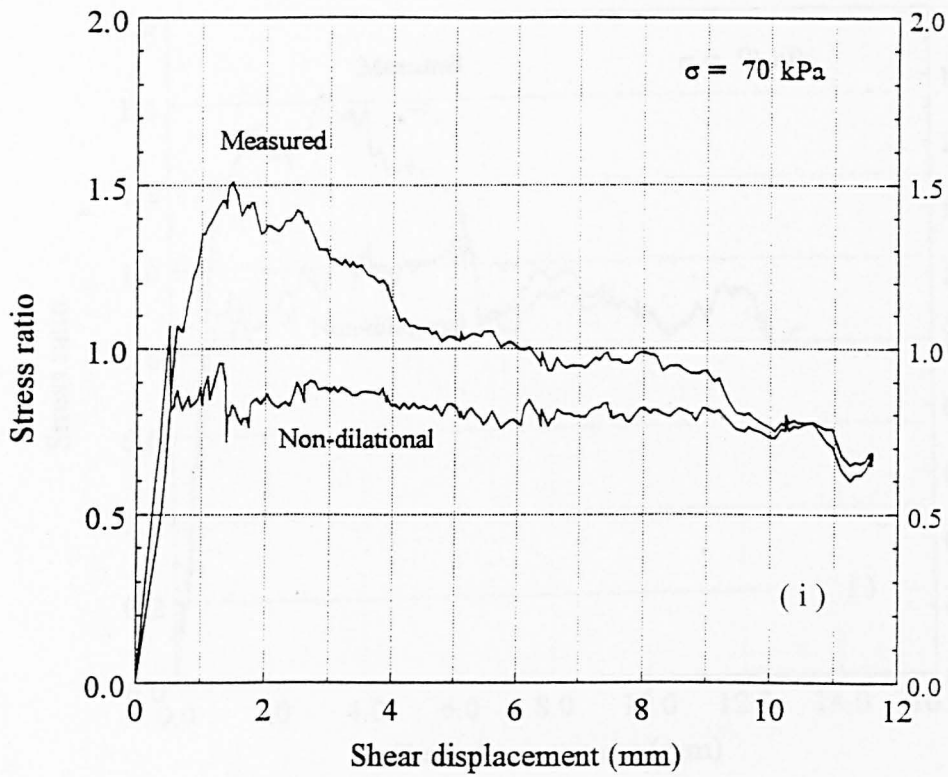
Fig. 4. 8a: Shear characteristics of joint A ($\sigma_n = 70$ kPa)

(i). Stress ratio (τ/σ_n)- shear displacement diagram

(ii). Normal displacement-shear displacement diagram
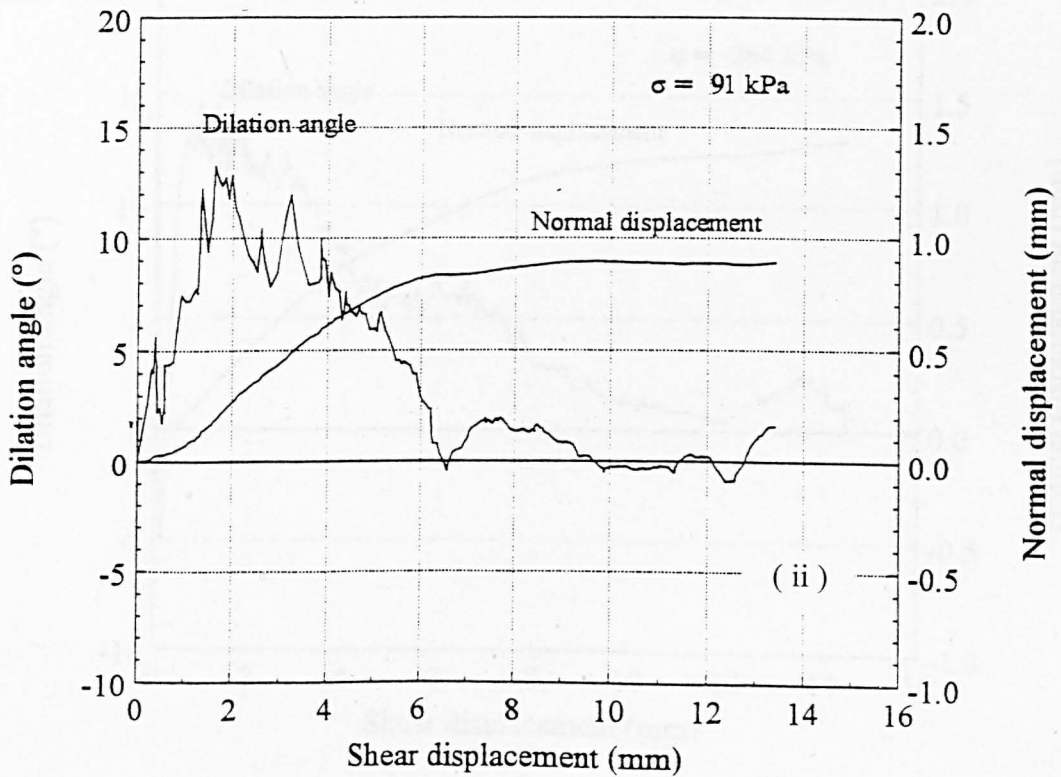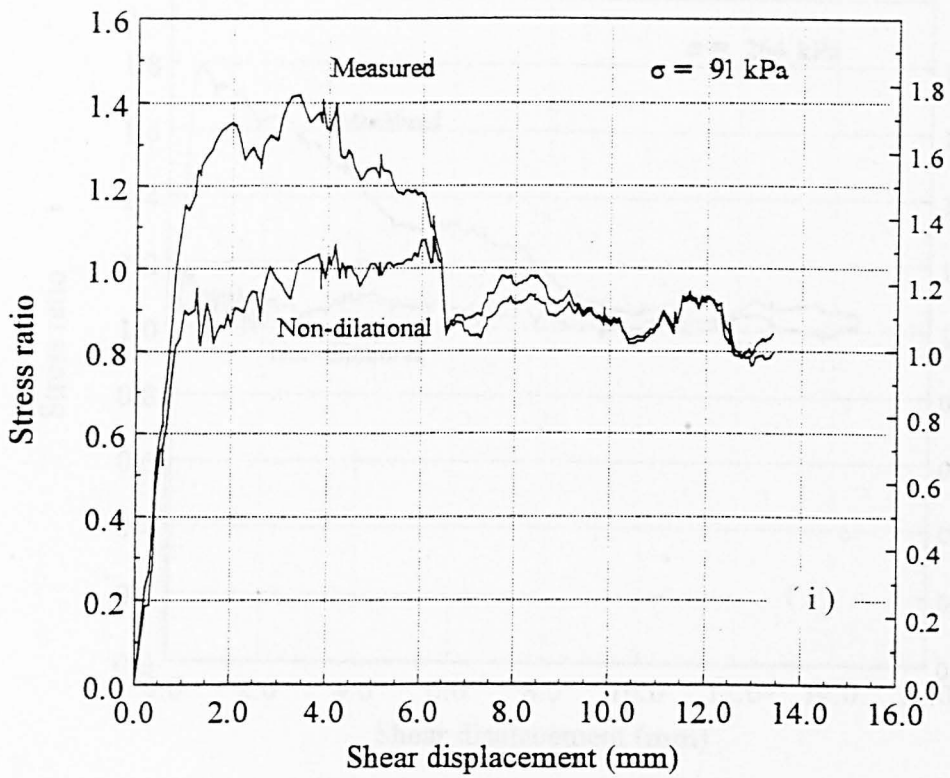
Fig. 4. 8b: Shear characteristics of joint A ($\sigma_n = 91$ kPa)

(i). Stress ratio (τ/σ_n)- shear displacement diagram

(ii). Normal displacement-shear displacement diagram
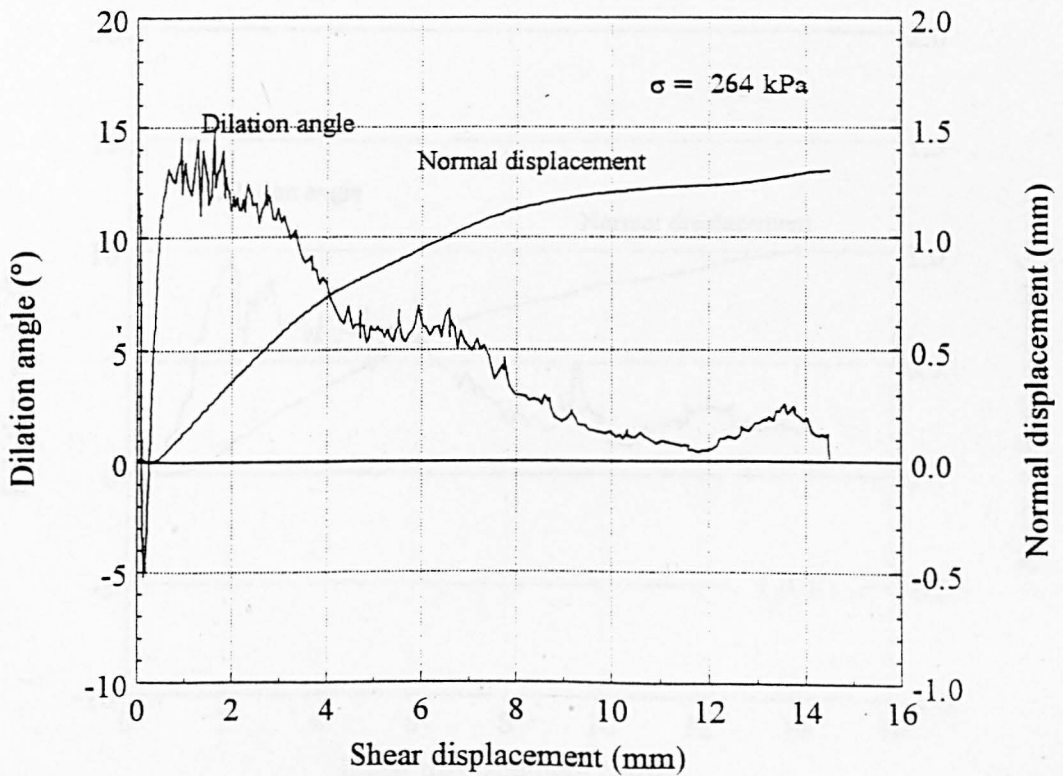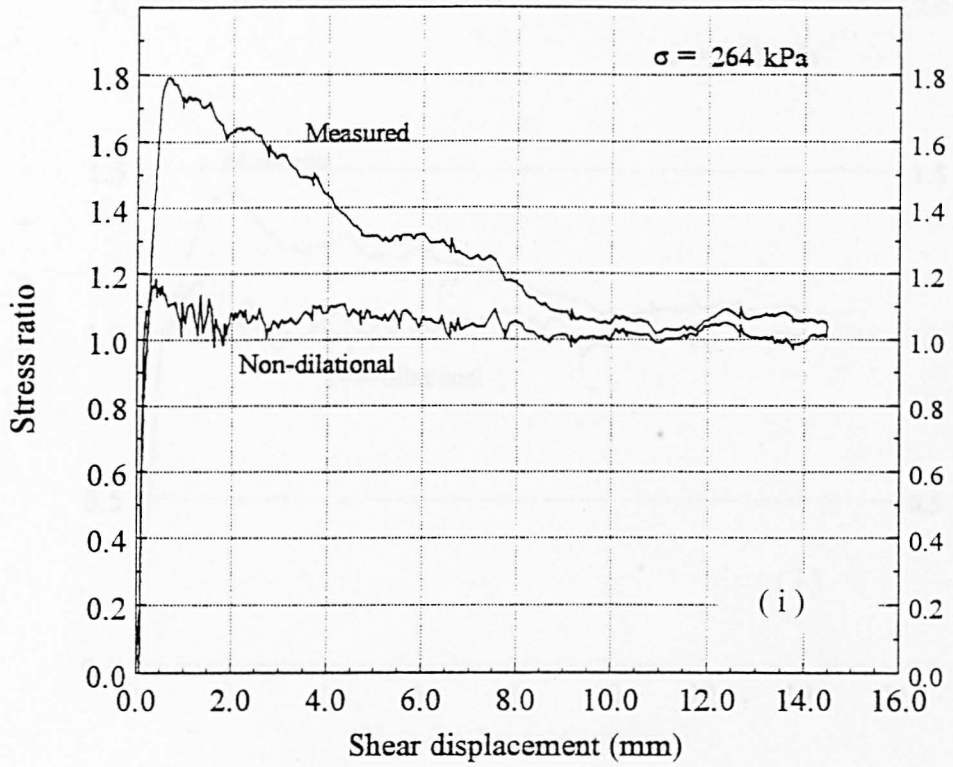
Fig. 4. 8c: Shear characteristics of joint A ($\sigma_n = 264$ kPa)

(i). Stress ratio (τ/σ_n)- shear displacement diagram

(ii). Normal displacement-shear displacement diagram
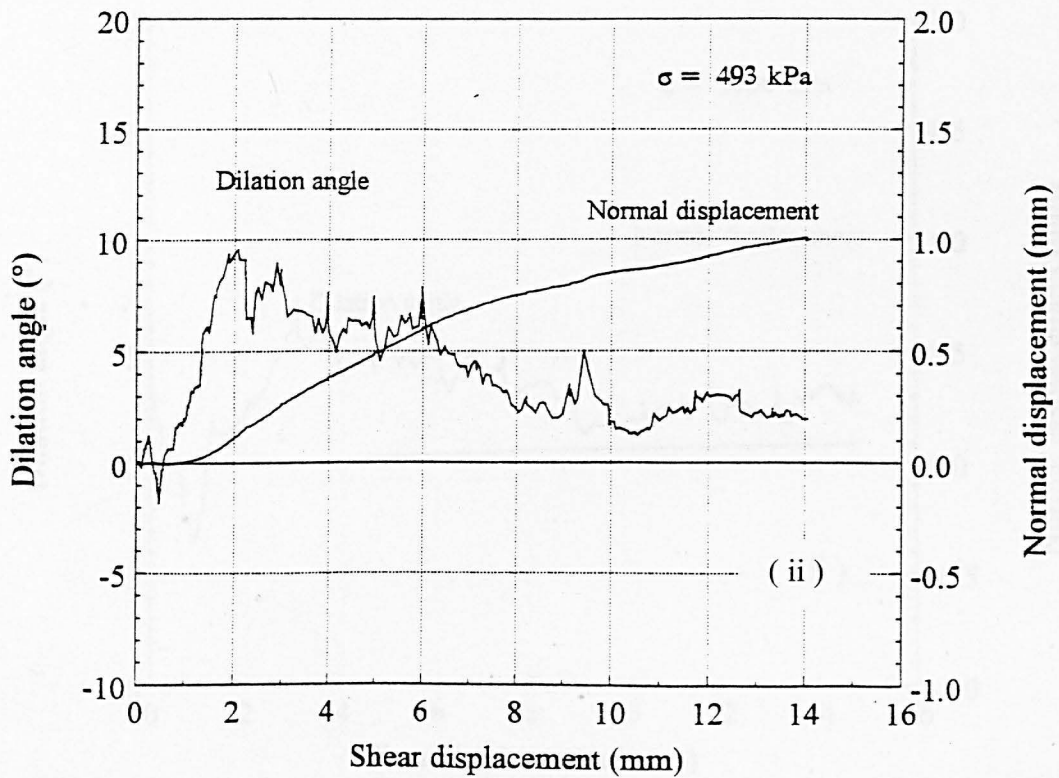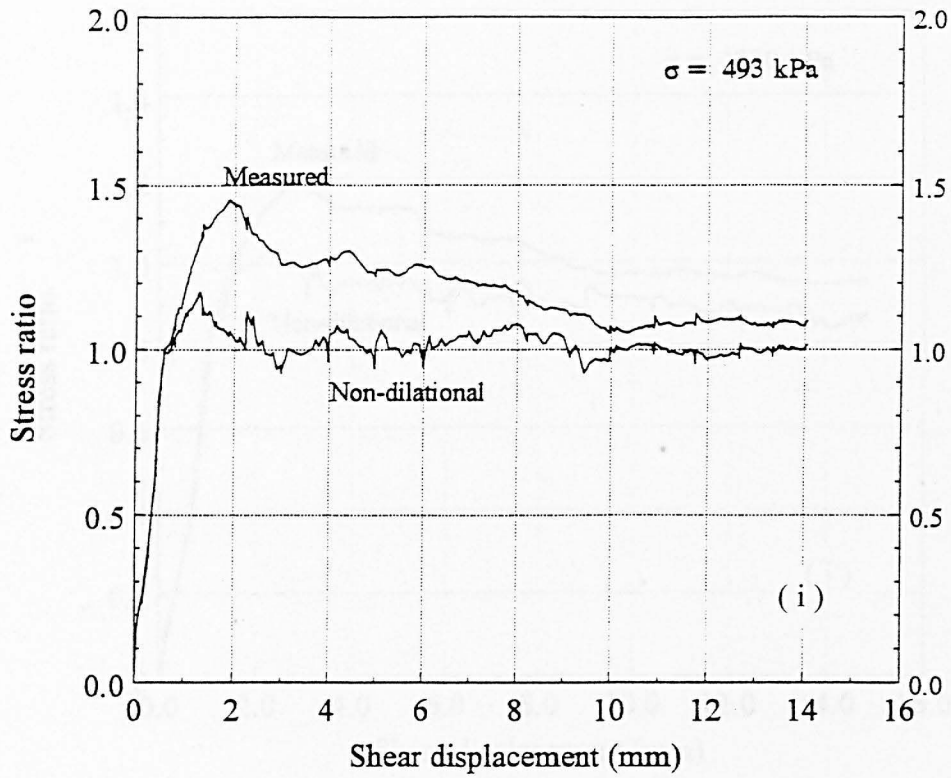
Fig. 4. 8d: Shear characteristics of joint A (σ_n = 493 kPa)

(i). Stress ratio (τ/σ_n)- shear displacement diagram

(ii). Normal displacement-shear displacement diagram
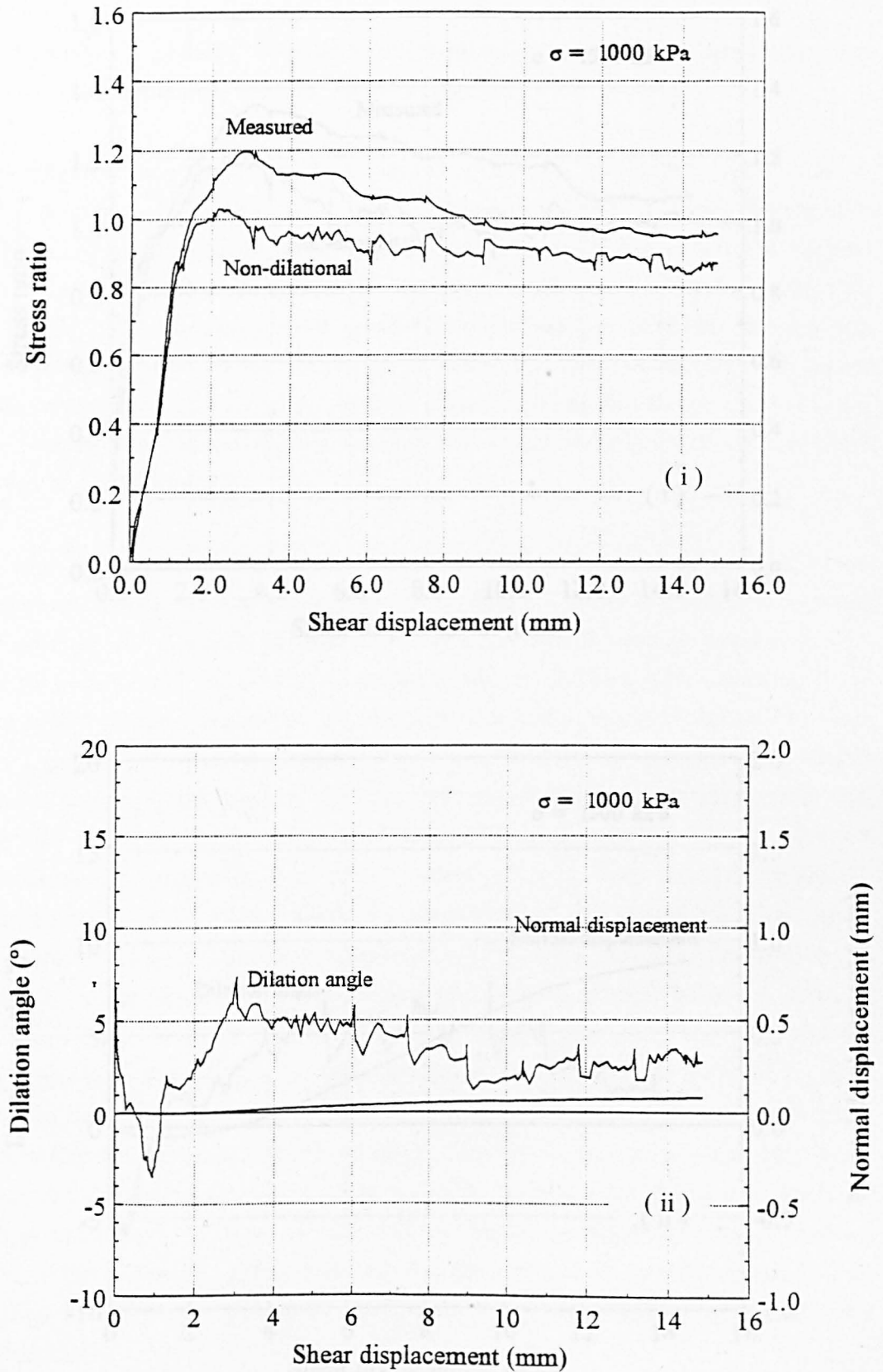
Fig. 4. 8e: Shear behaviour of modelled rock joints

(i). Shear stress-shear displacement diagrams

(ii). Normal displacement-shear displacement diagrams
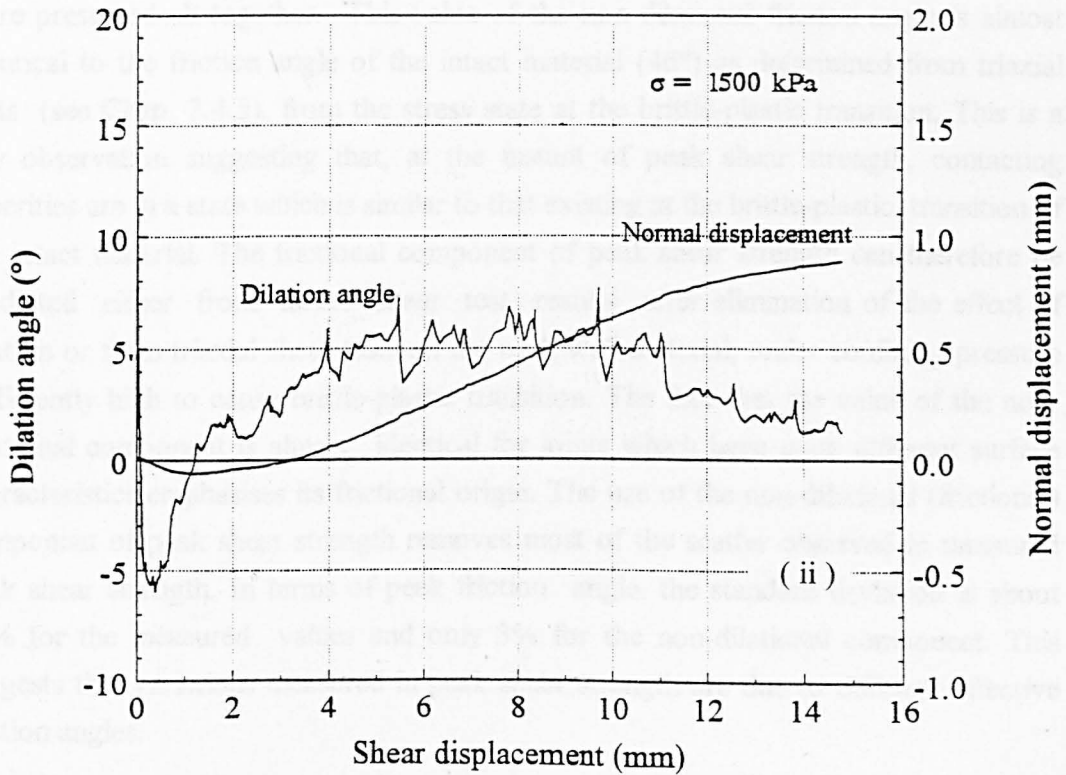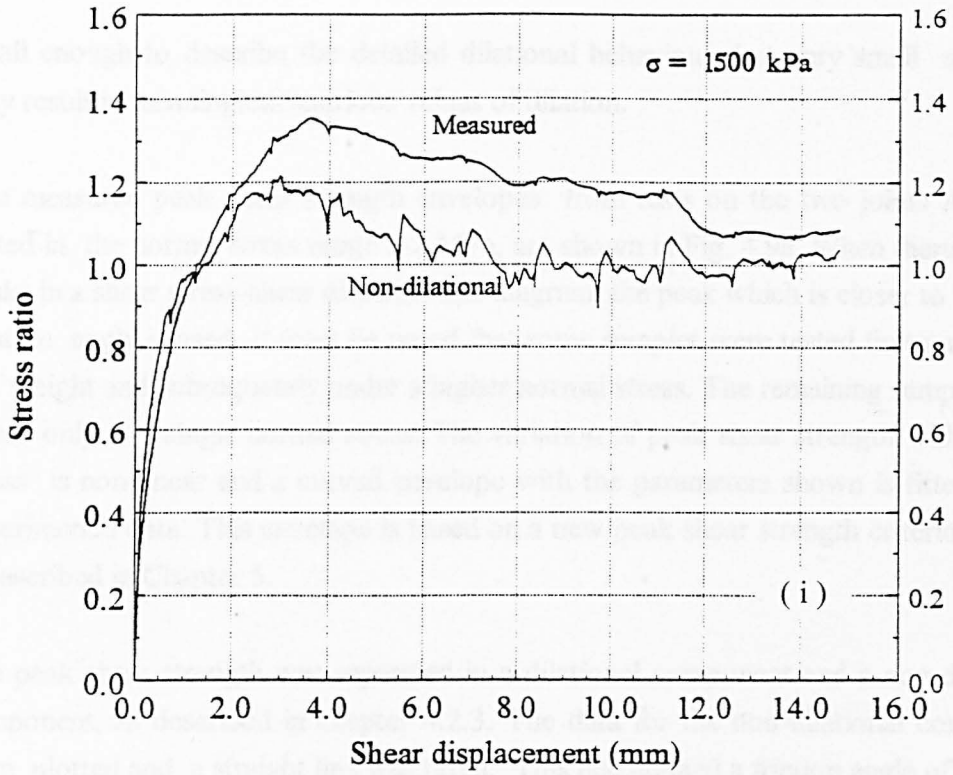
Fig. 4. 8f: Shear behaviour of modelled rock joints

(i). Shear stress-shear displacement diagrams

(ii). Normal displacement-shear displacement diagrams

small enough to describe the detailed dilational behaviour, but very small step-sizes may result in meaningless spurious values of dilation.

The measured peak shear strength envelopes from tests on the two joints A and B, tested in the normal stress range 0-2 MPa, are shown in Fig. 4.9a. When there are two peaks in a shear stress-shear displacement diagram, the peak which is closer to the peak dilation angle is used. It must be noted that some samples were tested first under their self weight and subsequently under a higher normal stress. The remaining samples were tested only at a single normal stress. The variation of peak shear strength with normal stress is non-linear and a curved envelope with the parameters shown is fitted to the experimental data. This envelope is based on a new peak shear strength criterion which is described in Chapter 5.

The peak shear strength was separated in a dilational component and a non-dilational component, as described in chapter 4.2.3. The data for the non-dilational component were plotted and a straight line was fitted. This line defined a friction angle of 46.6° for joint A and 46.2° for joint B, as shown in Fig. 4.10. The results from joint C are quite similar to those of joint B, and this suggested that it would be better if the data were presented all together. This value of the non-dilational friction angle is almost identical to the friction angle of the intact material (46°) as determined from triaxial tests (see Chap. 2.4.5), from the stress state at the brittle-plastic transition. This is a key observation suggesting that, at the instant of peak shear strength, contacting asperities are in a state which is similar to that existing at the brittle-plastic transition of the intact material. The frictional component of peak shear strength can therefore be predicted either from direct shear test results after elimination of the effect of dilation or from triaxial shear tests on the rock wall material, under confining pressure sufficiently high to cause brittle-plastic transition. The fact that the value of the non-dilational component is almost identical for joints which have quite different surface characteristics emphasises its frictional origin. The use of the non-dilational (frictional) component of peak shear strength removes most of the scatter observed in measured peak shear strength. In terms of peak friction angle, the standard deviation is about 10% for the measured values and only 3% for the non-dilational component. This suggests that variations measured in peak shear strength are due to different effective dilation angles.

4.3.3 Deformation of modelled rock discontinuities
4.3.3.1 Peak rate of dilation
For each test the rate of dilation was calculated at every point from the normal displacement- shear displacement diagram. The dilation angle is a function of the shear

Joint A
Joint B
Joint C and other

peak shear strength (MPa)

Normal stress (MPa)

$\phi_m = 46.1°$

$\sigma_{nT} = 3.8$ MPa

46.1°

Joint A
Joint B
Joint C and other

Non-dilational peak shear strength (MPa)

Normal stress (MPa)

$\tau = 1.04\,\sigma$

$(r^2 = 0.991)$

46.1°
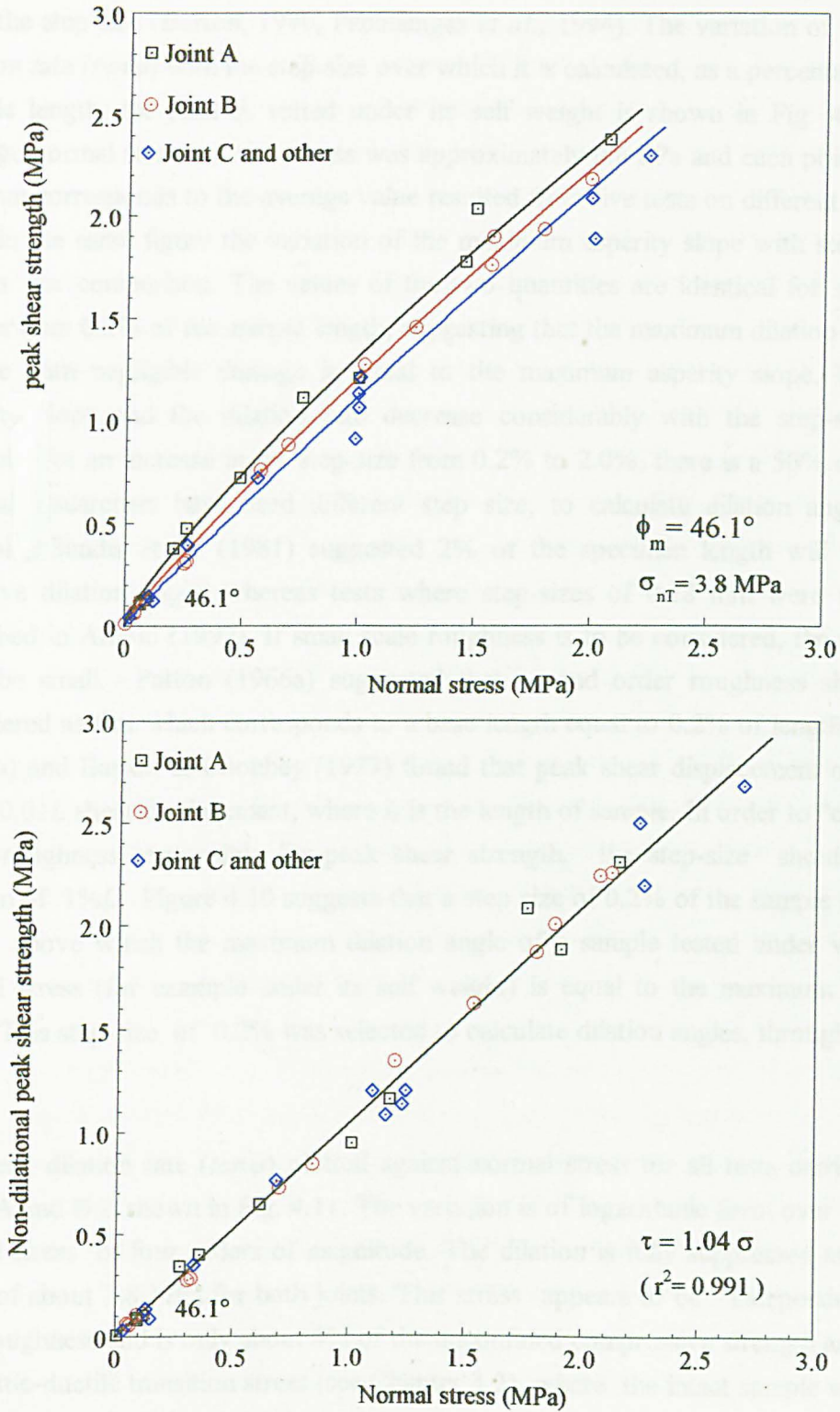
Fig. 4.9: Peak shear strength envelopes for modelled rock joints

(a) Measured peak shear strength.   (b) Non-dilational peak shear strength

distance - step size over which is calculated and is known to decrease logarithmically with the step size (Barton, 1990, Papaliangas *et al.*, 1994). The variation of the peak dilation rate (*tan ψ*) with the step-size over which it is calculated, as a percentage of the sample length, for joint A tested under its self weight is shown in Fig. 4.10. The average normal stress on these tests was approximately 0.6 kPa and each point on the diagram corresponds to the average value resulted from five tests on different samples. Also in the same figure the variation of the maximum asperity slope with step-size is shown for comparison. The values of the two quantities are identical for step-sizes greater than 0.2% of the sample length, suggesting that the maximum dilation rate of a sample with negligible damage is equal to the maximum asperity slope. Both the asperity slope and the dilation rate decrease considerably with the step-size. For example, for an increase in the step-size from 0.2% to 2.0%, there is a 50% decrease. Several researchers have used different step size, to calculate dilation angles. For example, Bandis *et al.* (1981) suggested 2% of the specimen length will give the effective dilation angle, whereas tests where step-sizes of 0.18 mm were used are described in Arnold (1992). If small scale roughness is to be considered, the step size must be small. Patton (1966a) suggested that second order roughness should be considered as that which corresponds to a base length equal to 0.2% of length. Barton (1971a) and Barton & Choubey (1977) found that peak shear displacement occurs at about $0.01L$ shear displacement, where L is the length of sample. In order to "catch" all micro-roughness responsible for peak shear strength, the step-size should be a fraction of $1\%L$; Figure 4.10 suggests that a step size of 0.2% of the sample length is a limit above which the maximum dilation angle of a sample tested under very low normal stress (for example under its self weight) is equal to the maximum asperity slope. This step-size of 0.2% was selected to calculate dilation angles, throughout this study.

The peak dilation rate (*tan ψ*) plotted against normal stress for all tests carried out on joints A and B is shown in Fig. 4.11. The variation is of logarithmic form over a range of normal stress of four orders of magnitude. The dilation is fully suppressed at a normal stress of about 3.8 MPa for both joints. This stress appears to be independent of the joint roughness and is only about 8% of the unconfined compressive strength and 11% of the brittle-ductile transition stress (see Chapter 3.2), where the intact sample will behave in a purely frictional manner. Assuming that at the brittle-ductile stress there is 100% contact between the two surfaces, and proportionality between area and load exists, as it occurs when an exponential distribution of asperity heights is assumed (Greenwood & Williamson, 1966), these data indicate that dilation is fully suppressed when the area of contact is approximately 11% of the gross area of the sample. The highest dilation rates were obtained from tests at "no load" conditions, i.e. where only the self weight of the

sample was acting. This was equivalent to 0.6 kPa for joint A and 0.8 kPa for joint B (average of 5-8 tests). There is a wide scatter at low normal stresses as the two samples have different roughness and exhibit different dilation angles, but as the normal stress increases, this scatter reduces considerably. This occurs in natural joints as well, as shown very clearly in Fig. 4.12, for the experimental data sets published by three different authors, shown on the figure. In this figure data from various sources on natural joints and artificially produced tensile fractures in natural rocks are included, which indicate that dilation is fully suppressed at a normal stress of about 10 MPa, which is about one order of magnitude lower than the unconfined compressive strength, assumed to be 100 MPa. These results are in agreement with the results shown in Fig. 4.11 for the artificial joints produced by the synthetic rock. Data published by other workers such as Goodman & Dubois (1972), Martin & Millar (1974), Schneider (1976), Bandis *et al.* (1981), Denby & Scoble (1984) and Hassani & Scoble (1985) are in line with these findings. Kutter & Otto (1990) suggested that the stress able to suppress all dilation is equal to the tensile strength of the rock material. This seems to be realistic as tensile strength is approximately one order of magnitude lower than the compressive strength, and for the synthetic material used (tensile strength 4.5 MPa and normal stress corresponding to zero dilation 3.8 MPa) this suggestion may lead to a reasonable approximation. However, in the authors opinion, this is a matter of actual area of contact and brittle-plastic transition stress, rather than tensile strength and compressive strength. In contrast, the assumption that dilation is fully suppressed only when the averaged normal stress is equal to the unconfined compressive strength, as assumed in some models, for example the JRC-JCS model (Barton & Bandis, 1990), is not confirmed and may be unrealistic for most natural joints.

A better correlation between dilation rate and normal stress is obtained if a graph of the normalised dilation rate $tan\psi/tan\psi_o$ and $log\sigma_n$ is plotted. In this way individuality of joints at low normal stress is lost and the critical normal stress σ_{nT} can be estimated more confidently, as shown in Figure 4.13 in which the data plotted in Figure 4.11 have been used. This logarithmic relation holds over four orders of magnitude of normal stress. A value of ψ_o for each individual sample can be obtained by self-weight tests prior to main testing at the appropriate normal stress. From the data presented, it is evident that the affect of roughness diminishes at normal stresses higher than σ_{nT}. The value of σ_{nT} is dependent upon the normal stress required to cause plastic deformation over the area around the tips of the most critical (contacting) asperities. The results shown in Figure 4.8 suggest that σ_{nT} is independent of roughness; similar results were obtained by Kutter & Otto (1990).
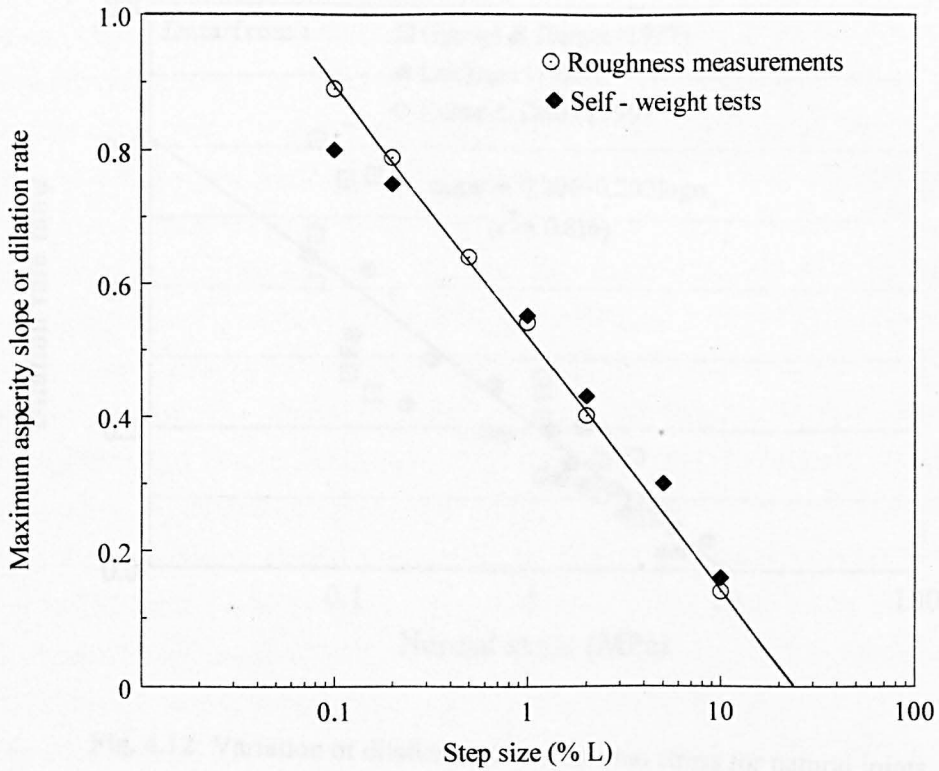
Fig. 4.10: Comparison between the maximum dilation angle calculated from self weight tests and the maximum asperity slope calculated from roughness measurements. The step -sizes are given as percentages of the sample length.
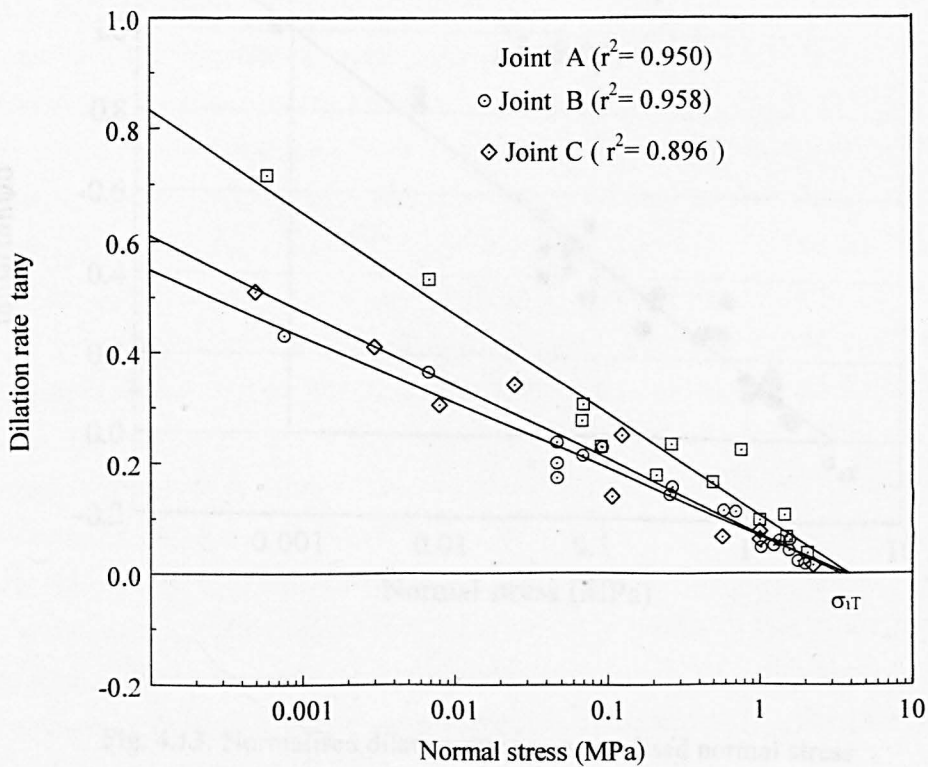
Fig. 4.11: Variation of peak dilation rate with normal stress for modelled joints
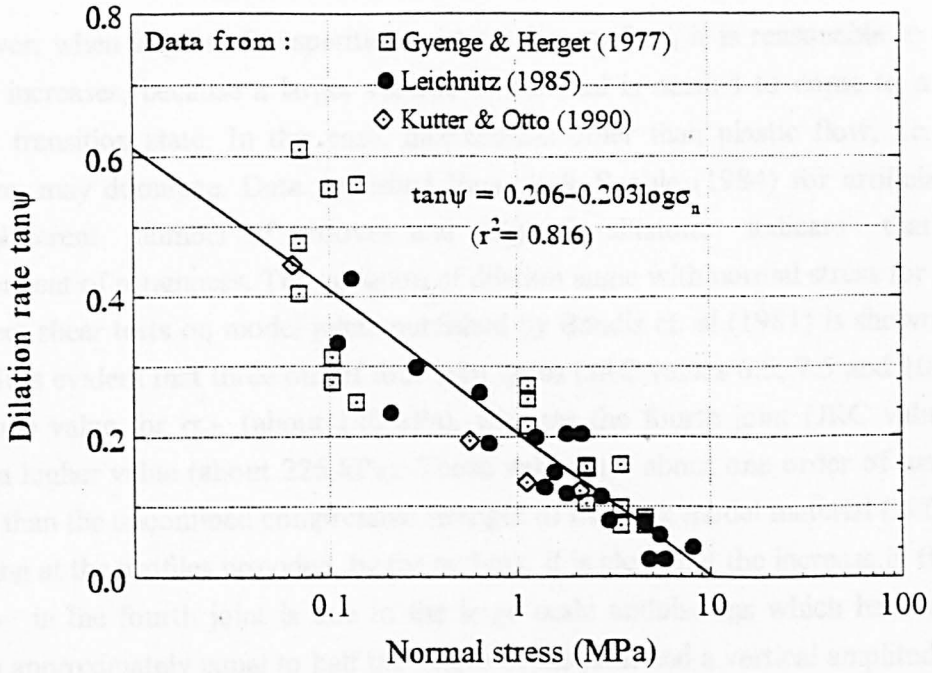
Fig. 4.12: Variation of dilation rate with normal stress for natural joints
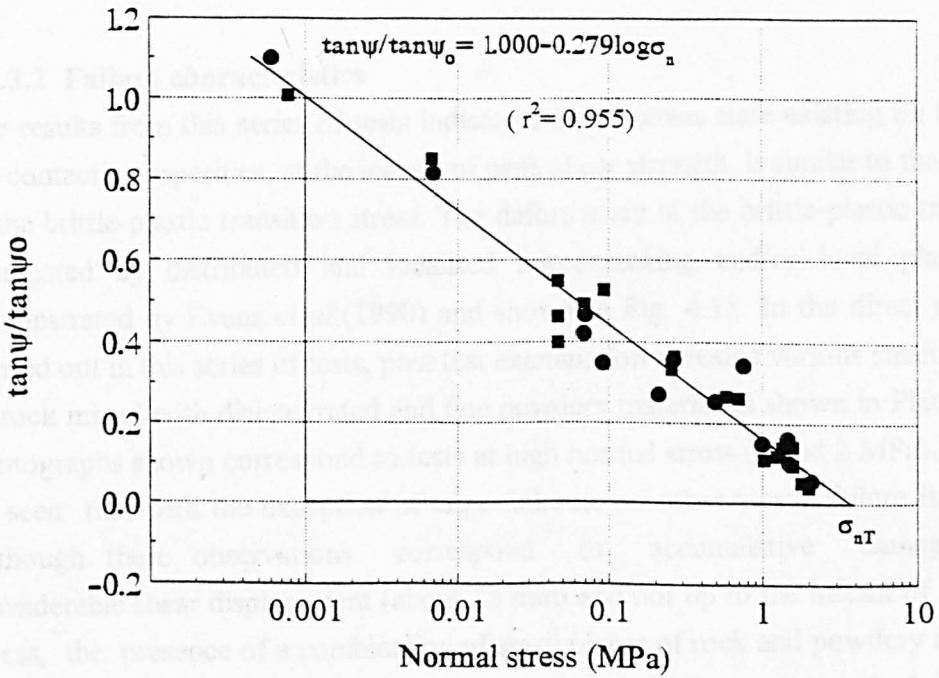
Fig. 4.13: Normalised dilation rate vs. normalised normal stress

However, when large scale asperities exist on the surface, it is reasonable to assume that it increases, because a larger volume of material is needed to come to a brittle-plastic transition state. In this case, mechanisms other than plastic flow, i.e. tensile fracture, may dominate. Data published Hassani & Scoble (1984) for artificial joints with different number of grooves and ridges in siltstone indicate that σ_{nT} is independent of roughness. The variation of dilation angle with normal stress for a series of direct shear tests on model joints published by Bandis et. al (1981) is shown in Fig. 4.14. It is evident that three out of four joint types (JRC values 6.5, 7.5 and 10.6) give the same value for σ_{nT} (about 140 kPa), whereas the fourth joint (JRC value 16.6) gives a higher value (about 225 kPa). Those values are about one order of magnitude lower than the unconfined compressive strength of the rock model material (2000 kPa). Looking at the profiles provided by the authors, it is clear that the increase in the value of σ_{nT} in the fourth joint is due to the large scale undulations which have a wave length approximately equal to half the length of the joint and a vertical amplitude larger than 1/20th of that. At prototype scale these parameters represent a joint with a wavelength of about 1.35 m and a vertical amplitude of about 0.15 m, which are quite uncommon. Consequently, it can be assumed that, in general, the value of σ_{nT} is independent of the joint roughness, unless large scale steep asperities exist on the surface, when this value will be higher.

4.3.3.2 Failure characteristics

The results from this series of tests indicate that the stress state existing on the tips of the contacting asperities, at the instant of peak shear strength, is similar to that occuring at the brittle-plastic transition stress. The deformation at the brittle-plastic transition is dominated by distributed and localised microcracking and/or local plasticity, as demonstrated by Evans et al.(1990) and shown in Fig. 4.15. In the direct shear tests carried out in this series of tests, post test examination revealed various small fragments of rock mixed with disintegrated and fine powdery material as shown in Plate 4.3. The photographs shown correspond to tests at high normal stress (1 and 2 MPa), and it can be seen that with the exception of edge failures, no other tensile failure is observed. Although these observations correspond to accumulative damage after a considerable shear displacement (about 15 mm) and not up to the instant of peak shear stress, the presence of a combination of small pieces of rock and powdery material on the sheared joint surface is indicative of a stress state similar to that at the brittle-plastic state where distributed and localised microcracking occur simultaneously. Similar observations have been made on many occasions in natural rock joints (see for example Plate 4.2 and Chapter 3.3).
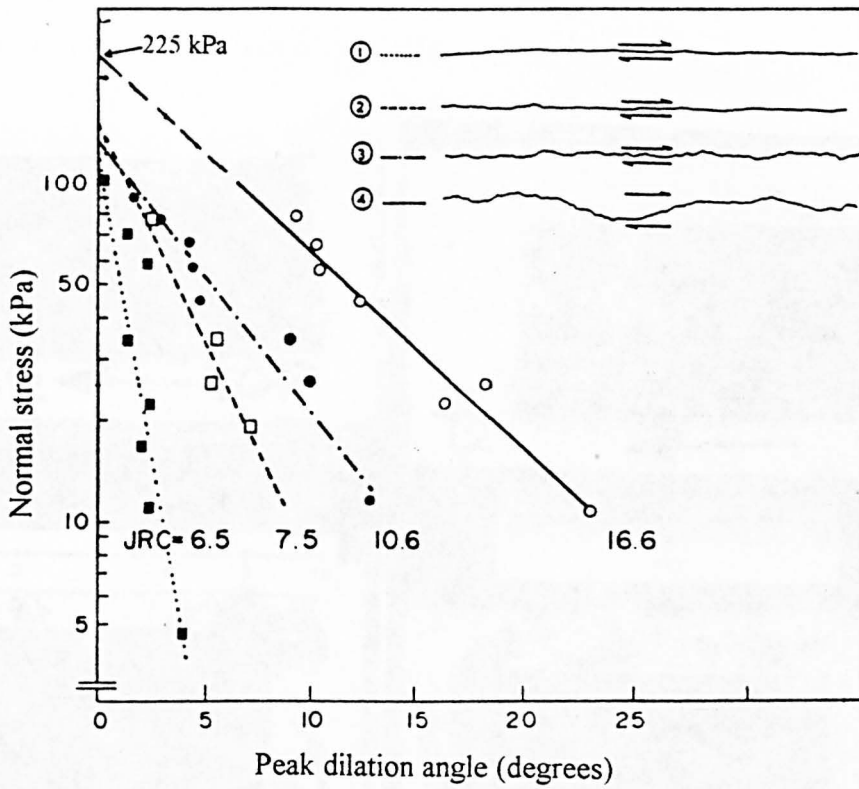
Fig. 4.14: Variation of peak dilation angle with normal stress (after Bandis *et al.*, 1981)

(a)   (b)
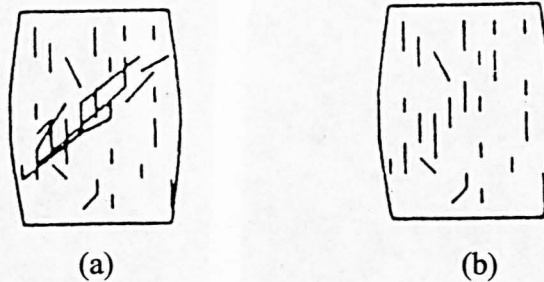
Fig 4.15: Deformation of intact rock samples at the brittle-plastic transition.

(a) distributed and localised microcracking. (b) distributed microcracking, local plasticity.

(a) $\sigma = 1$ MPa

(b) $\sigma = 2$ MPa

(c) $\sigma = 2$ MPa

(d) $\sigma = 2$ MPa
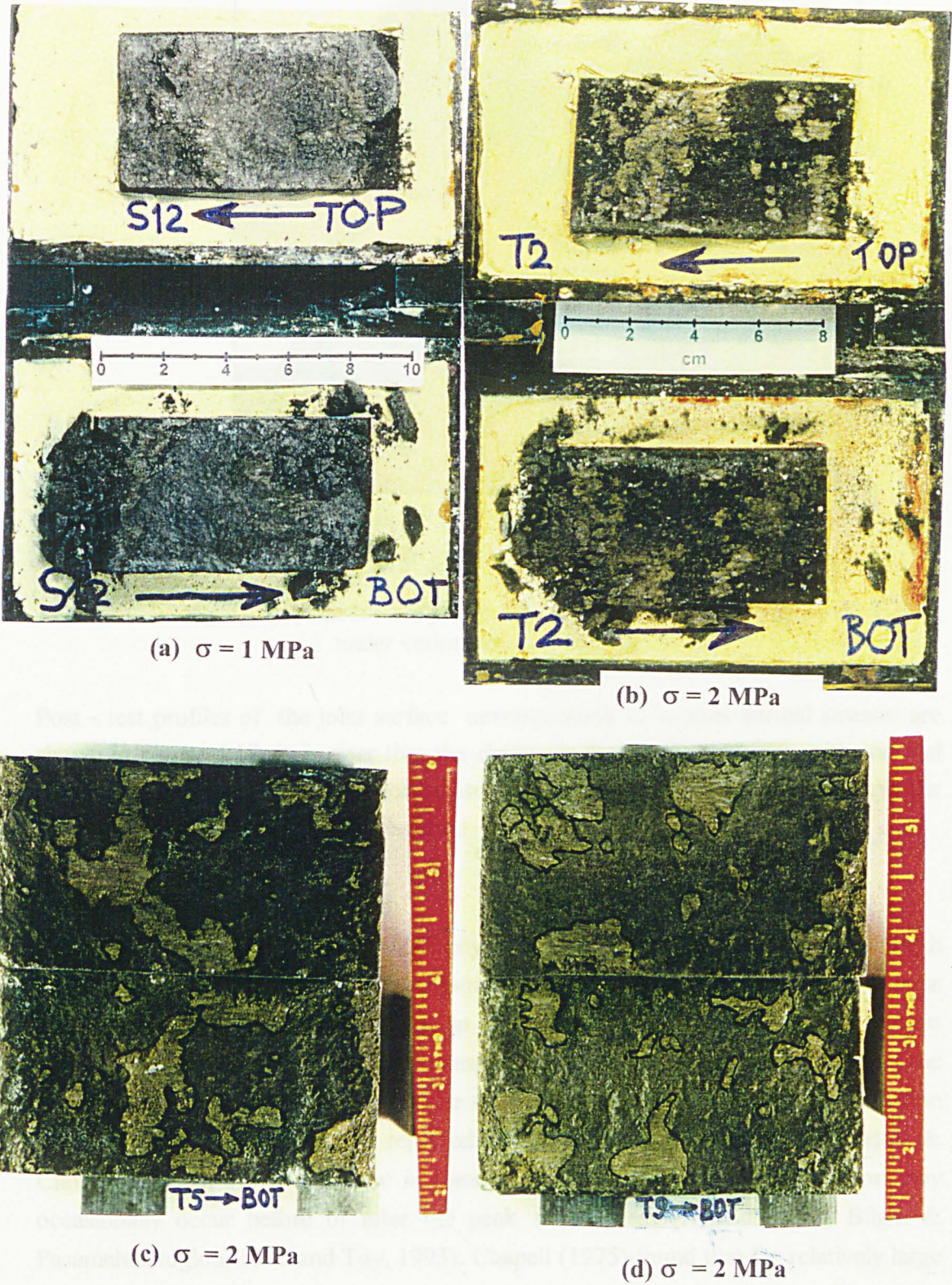
Fig. 4.16: Post-test photographs of joints sheared under various normal stresses
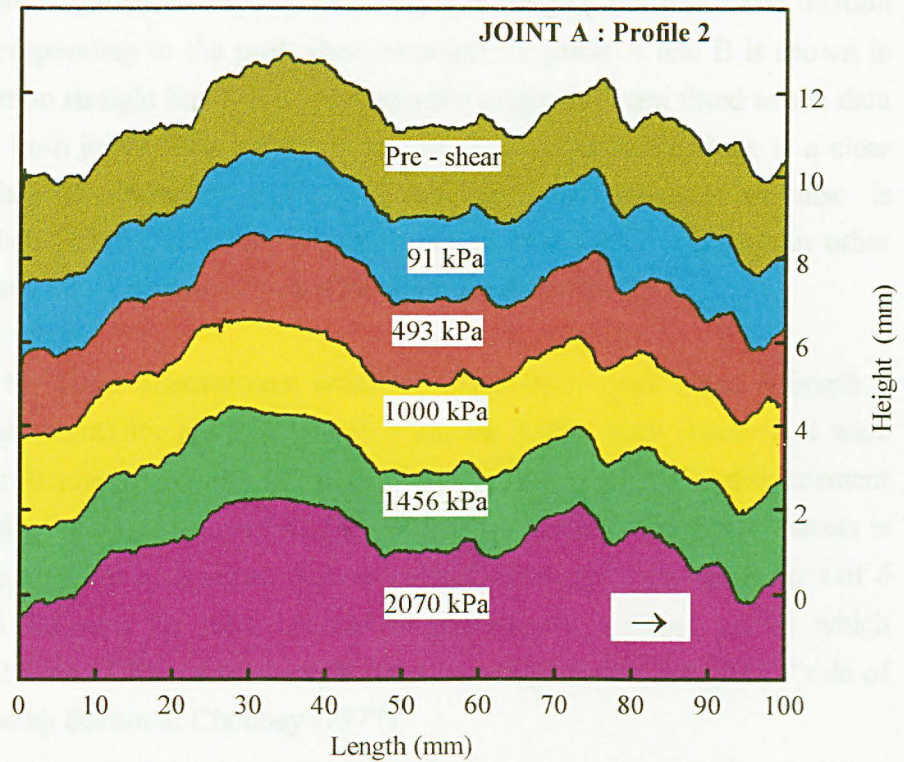
Fig. 4.17: Profile No 2 of joint A before testing and after testing under various normal stresses

Post - test profiles of the joint surface corresponding to various normal stresses are shown in Figure 4.17. It is clear that the change in the profile increases with normal stress and at even at the highest normal stress where dilation approaches zero, only the highest part of the asperities are flattened.

4.3.3.3 Peak shear displacement

From the experimental results of this study, it has been shown that peak shear strength can be considered as a two component parameter over the whole range of normal stress where joint behaviour is dilational (i.e. up to 3.8 MPa). Since the frictional component is proportional to normal load, peak shear strength should occur at the instant of the full mobilisation of roughness, i.e. at the same shear displacement as the peak dilation angle. This is most commonly reported in the literature (for example, Barton & Choubey, 1977). However, there is some evidence that the maximum dilation may occasionally occur before or after the peak shear stress (Arnold, 1992, Bilgin & Pasamehmetoglou, 1990 and Toy, 1993). Chapell (1975) found that for relatively large joints, peak shear strength does not coincide with maximum dilation. The phase difference in the two quantities is probably due to the degree of interlocking at the commencement of sliding. A tightly interlocked joint will cause an initial suppression of dilation, and peak shear strength will be reached well before the maximum dilation angle.

The relation between the shear displacement corresponding to the maximum dilation rate and that corresponding to the peak shear strength for joints A and B is shown in Fig. 4.18. A common straight line passing through the origin has been fitted to the data corresponding to both joints. There is some scatter in the results, but there is a clear trend that the shear displacement required for the maximum dilation to mobilise is slightly larger (about 15%) than that corresponding to peak shear strength. In other words the maximum dilation angle occurs after the peak shear strength.

The variation of the shear displacement which corresponds to peak shear strength δ (peak shear displacement) for joints A and B is shown in Fig. 4.19. There is a wide scatter but a clear increase with normal stress of the δ exists. Peak shear displacement values are lower for the rougher joint (A), but the rate of increase with normal stress is approximately the same for both joints. At zero normal stress the projected values of δ are 1.2 mm and 1.8 mm for joints A and B respectively. These values which correspond to 1.2% and 1.8% of the sample length are higher than the 1% L "rule of thumb" suggested by Barton & Choubey (1977).

4.3.4 Concluding remarks
The peak shear strength of rock joints can be considered as comprising two components, one frictional and one dilational, over the whole range of normal stress where dilation occurs. Therefore the " $\phi+i$ " principle is applicable over the whole range of dilatant shearing, with ϕ representing the friction angle of the rock wall material and i the dilation angle (geometrical component) at peak shear strength. Consequently, at least for rock joints similar to those used in this study, the "asperity failure component " can not be separated from the "basic friction component".

The non-dilational component of peak friction angle is equal to the friction angle of the rock wall material, determined from the stress state at the brittle-plastic transition. This suggests that brittle-plastic transition state occurs at the tips of the contacting asperities and therefore, the frictional component of peak shear strength can be determined either from triaxial tests under sufficiently high confining pressure to produce a brittle-plastic transition stress or from direct shear tests after elimination of the effect of dilation.

The friction angle of the synthetic rock used in this study is found from triaxial tests or direct shear tests after the effect of dilation is removed. The value of friction angle thus determined (46°) is 14° degrees higher than that of saw-cut surfaces and can be considered as representative of relatively soft artificial rock materials. Also it compares well with friction angle values corresponding to relatively soft natural rocks such as limestones, dolomites, marbles etc. Therefore, if the findings of this work are generally
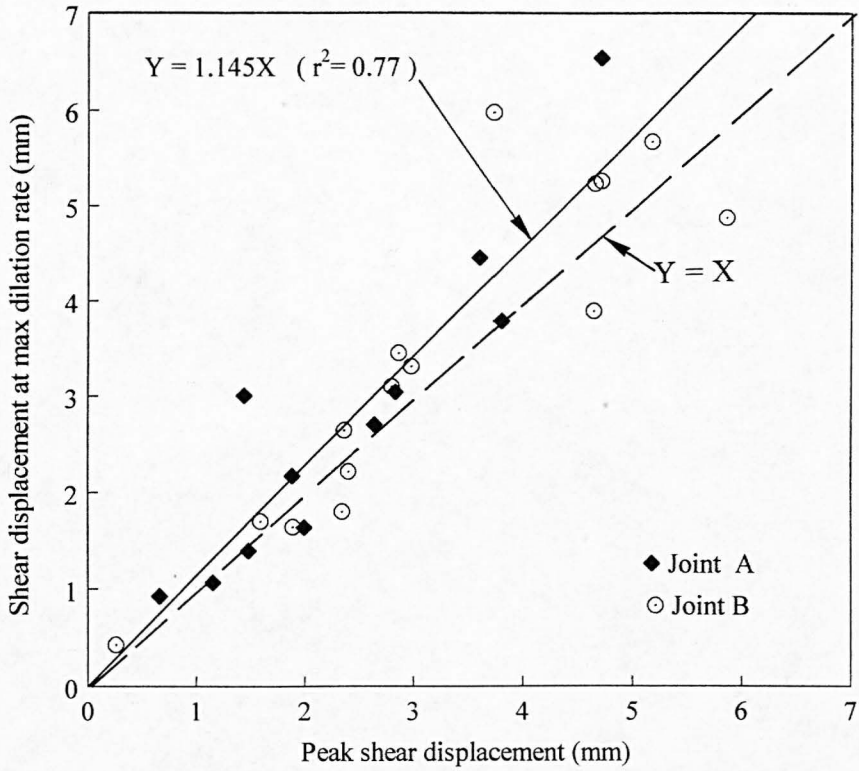
Fig. 4.18: Shear displacement at maximum dilation rate vs. shear displacement
at peak shear strength
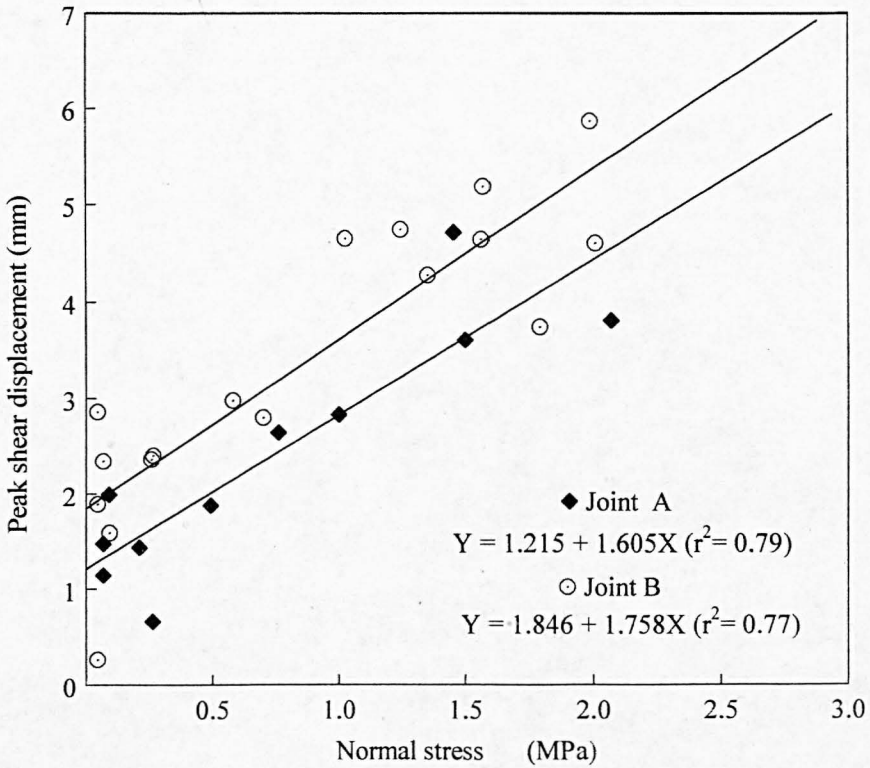
Fig. 4.19: Variation of peak shear displacement with normal stress

applicable, the use of the friction angle of a saw-cut surface in rock joint shear behaviour may be inappropriate.

The dilation at peak shear strength reduces logarithmically with normal stress, over four orders of magnitude. The normal stress at which the specimen ceases to dilate is much lower than the unconfined compressive strength, and about one order of magnitude lower than the brittle-plastic transition stress. It appears to be independent of roughness and can be experimentally derived from a series of direct shear tests.

For the joints tested the peak shear strength occured slightly earlier than the peak dilation rate.

The peak shear displacement increases with normal stress. For the synthetic rock used, at low normal stress it is about 1-2% of the sample length and becomes about 4-5% of the sample length at a normal stress of 2.0 MPa.

4. 4. The effect of sample size on peak shear strength: discontinuities modelled by the strong synthetic rock

4.4.1 Introduction

The strength values obtained from testing of rock samples of different volume are known to reduce with the sample size used. This is usually termed "scale effect" on rock strength, and is due to the nature of rock materials. Rocks are composed of crystals and grains in a fabric including cracks and fissures. Therefore, rather large samples are required to obtain statistically complete collections of all the components that influence strength. Unconfined compression tests carried out in the field by Bieniawski (1968) and Pratt et al. (1972) have shown that a reduction in strength of up to one order of magnitude may result from samples of different size.

Experimental work by several investigators including Pratt *et al.*(1974), Leichnitz & Natau (1979), Bandis (1980), Bandis *et al.*(1981), Muralha & Cunha (1990), Maerz & Franklin (1990) and Yoshinaka *et al.*(1993), have shown that there is also an apparent reduction in peak shear strength of model and natural rock discontinuities with increasing sample size. Positive scale effects (increasing strength with increasing size) or no scale effect have also been reported, for example by Locher & Rieder (1970), Kutter & Otto (1990), Gianni *et al.*(1992) and Ohnishi *et al.* (1993). The studies of Swan (1983, 1985) and Swan & Zongqi (1985) indicate that scale has negligible influence on predicted joint behaviour for surfaces of engineering interest. The fundamental mechanisms involved in the shearing of rock joints at different normal stresses have not yet been resolved; scale effect is a subject which remains controversial.

It is widely accepted that the scale effect in peak shear strength is most marked for rough joints, and disappears for planar, smooth, residual surfaces, as does dilation. The results presented in Chapter 4.3 illustrate that dilation is the only cause for variations in peak shear strength. If this is true, then scale effect will be a result of different dilation mobilised by joints of different size. Joints in the same rock exhibiting the same peak dilation angle will have the same peak shear strength. If for some reason samples of different lengths, from the same rock surface, exhibit the same peak dilation angle, then they will have the same peak shear strength, as occurs in the case of saw-toothed joints (Ohnishi *et al.*, 1993).

Based on the reduction in unconfined compressive strength with scale reported by Pratt *et al.*(1972), Barton & Choubey (1977) interpreted experimental results on scale effects in peak shear strength of rock joints, published by Pratt *et al.* (1974), on the basis of a scale dependence of both peak dilation angle d_n and asperity failure component. A

reduction of 60-75% in peak shear strength with scale was attributed to the reduction in the asperity failure component and the remaining 40-25% to the dilation angle. Direct shear tests on plaster modelled rock joints, carried out by Bandis (1980), and interpreted in the same way, confirmed the above findings of Barton (Fig. 4.20). Assuming that the value of ϕ_b is constant, the asperity failure component was calculated in angular form, from the formula

$$s_n = \phi_p - \phi_b - d_n \qquad (4.1)$$

where

ϕ_p is the measured peak friction angle

ϕ_b the "basic" friction angle and

d_n the peak dilation angle.

The reduction in the dilation angle and the asperity failure component was quantified by Barton & Bandis (1982), by using the following empirical relationships

$$JRC_n \approx JRC_o \left(\frac{L_n}{L_o}\right)^{-0.02 JRC_o} \qquad (4.2)$$

$$JCS_n \approx JCS_o \left(\frac{L_n}{L_o}\right)^{-0.03 JRC_o} \qquad (4.3)$$

where JRC_o and JCS_o correspond to laboratory scale sample and JRC_n and JCS_n to field scale. The graphical form of equations (4.2) and (4.3) is shown in Figure 4.21.

Hencher *et al.* (1993) discussed tests carried out by Toy (1993) to investigate the mechanisms contributing to changes in strength with size of sample. The tests were carried out on replicas of a natural limestone joint made with the same model material, in the same shear box and under the same conditions as used by Bandis (1980), i.e. the same normal stress (24.2 kPa) and at a shear rate of 0.4 mm/min. Tests were conducted on full size (354 mm x 150 mm), quarter size (4 blocks 177 mm x 75 mm each) and 1/12th size (12 blocks 88.5 mm x 50 mm each). Profiles of the joint surface and positions of numbered samples at the different scales are given in Fig. 4.22. Within the limitations of the data, Hencher *et al.* (op. cit.) confirmed the broad negative scale dependence of measured strength data reported by Bandis. However, following detailed analysis, they found no evidence of a scale-dependent asperity failure component as postulated by Bandis *et al.*(1981). Furthermore, they found that there was a wide scatter in measured friction values, which for sanded flat surfaces was in the range 9°-34° (Fig 4.23). They concluded that this model material had severe limitations for accurately and consistently simulating shear behaviour of most rocks. For the same
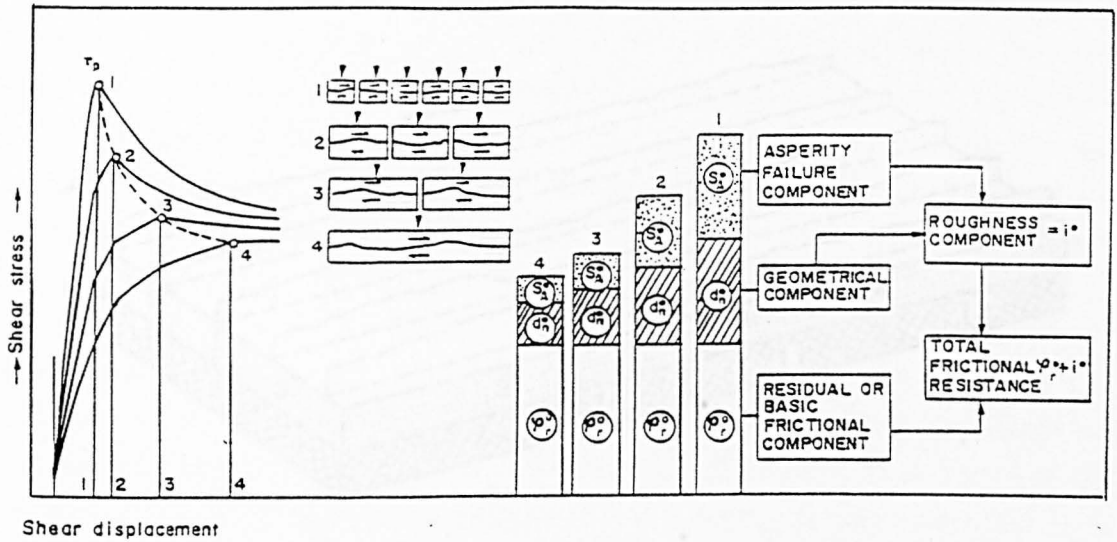
Fig. 4.21: Scale effect on peak shear strength of model joints (after Bandis *et al.*, 1981)
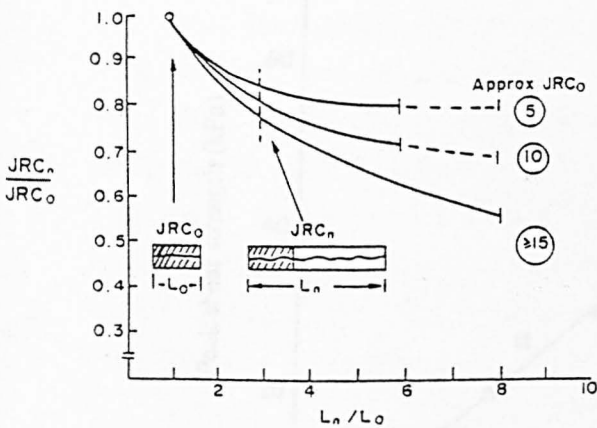
Fig. 4.21 Estimation of JRC_n value for larger sizes of rock joint, based on laboratory-size values (JRC_o) after Bandis *et al* (1981).
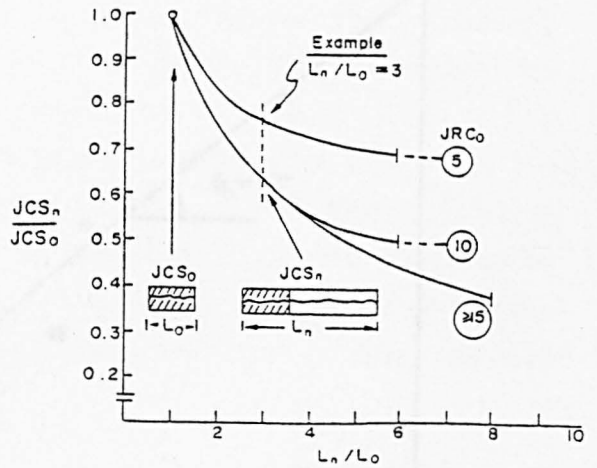
Fig. 4.22 Estimation of JCS_n value for larger sizes of rock joint, based on laboratory-size values (JCS_o) after Bandis *et al* (1981).
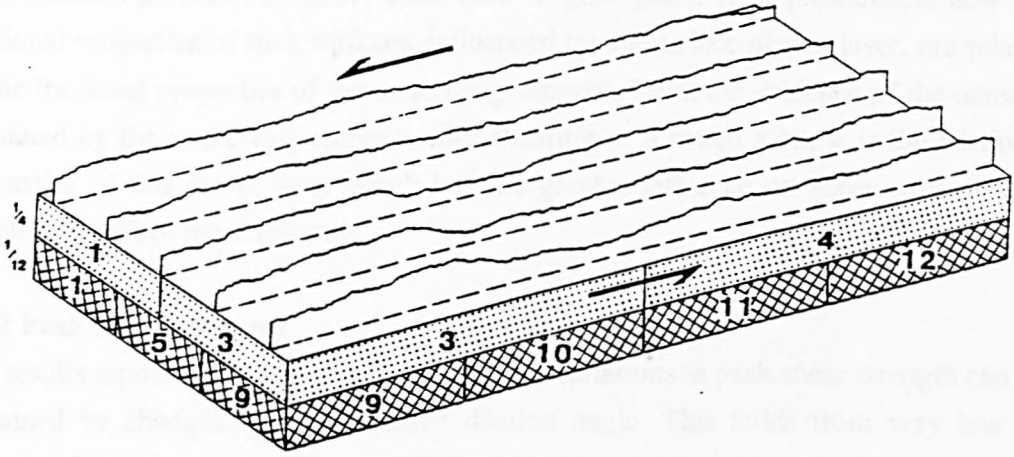
Fig. 4.23: Joint profiles indicating sub-samples positions and sizes (after Toy, 1993)
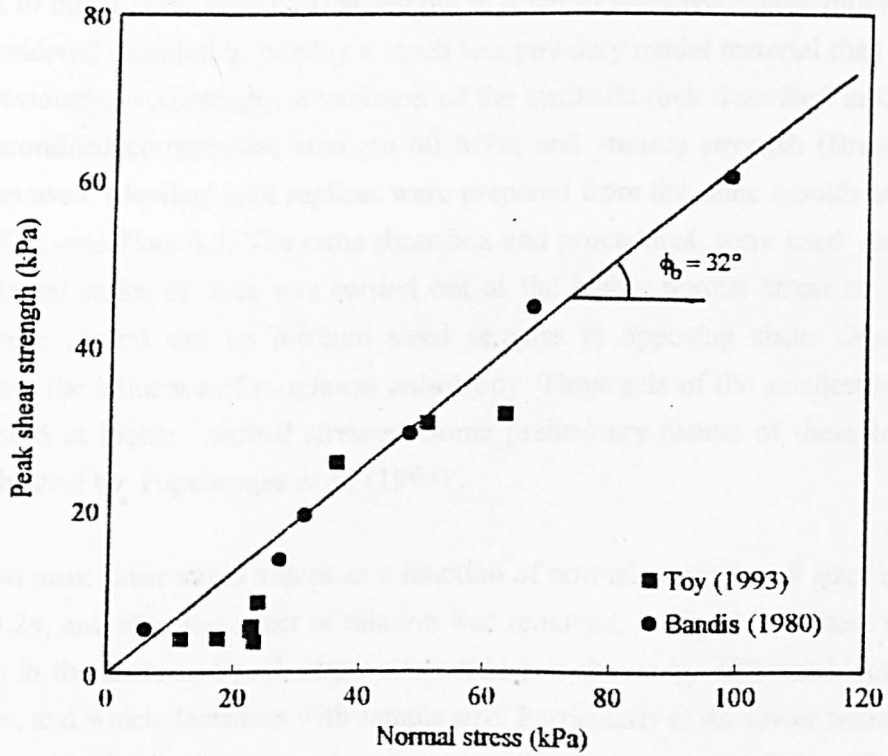
Fig. 4.24: Variation in shear strength of sanded flat surfaces with normal stress
(after Toy, 1993)

model material, Bandis (1980) used a basic friction angle of 32°, which was determined from surfaces prepared by direct casts onto a glass plate. It is questionable how the frictional properties of such surfaces, influenced by the surface plaster layer, are related to the frictional properties of the underlying material. From the evidence of the damage sustained by the underlying material after shearing of a rough joint, it is the frictional properties of this lower layer which has the greater influence on shear strength and which is therefore more relevant.

4.4.2 Peak shear strength

The results reported in Chapter 4.3 suggest that variations in peak shear strength can be explained by changes in the mobilised dilation angle. This holds from very low to stresses high enough to eliminate dilation. If this argument is true, then there is a contradiction with the scale effect on the asperity failure component found by Bandis (op. cit.) and the basic assumption of the JRC-JCS model (Barton & Bandis, 1990) where not only the dilation component (expressed by JRC) but also the asperity failure component (as expressed by JCS) is stated to be scale dependent (equations 4.2 and 4.3 and Figures 4.20, 4.21).

A series of direct shear tests was carried out in order to investigate these differences. It was considered essential to employ a much less powdery model material than had been used previously. Accordingly, a variation of the synthetic rock described in Chapter 2 with unconfined compressive strength 60 MPa, and tensile strength (Brazilian) 5.5 MPa was used. Identical joint replicas were prepared from the same moulds as used by Toy (1993) -see Plate 4.2. The same shear box and procedures were used except that an additional series of tests was carried out at the higher normal stress of 125 kPa. Tests were carried out on medium sized samples in opposing shear directions to investigate the influence of roughness anisotropy. Three sets of the smallest block size were tested at higher normal stresses. Some preliminary results of these tests have been published by Papaliangas et al. (1994) .

Measured peak shear stress values as a function of normal stress for all sizes are given in Fig. 4.24, and after the effect of dilation was removed, in Fig. 4.25. There is a wide variation in the measured peak shear stress which is shown by different blocks of the same size, and which decreases with sample size. Particularly at the lower normal stress level, the peak shear stress ratio shows a generally negative scale effect, although the medium size blocks gave the highest average value (Table 4.2). Non-dilational data at all scales gave consistent average friction angles to within ±0.5°. The difference in the average value of friction angle at 24.5 kPa and 125 kPa is attributed to the variations in surface finish produced by different mixtures. It is worth noting that samples with quite
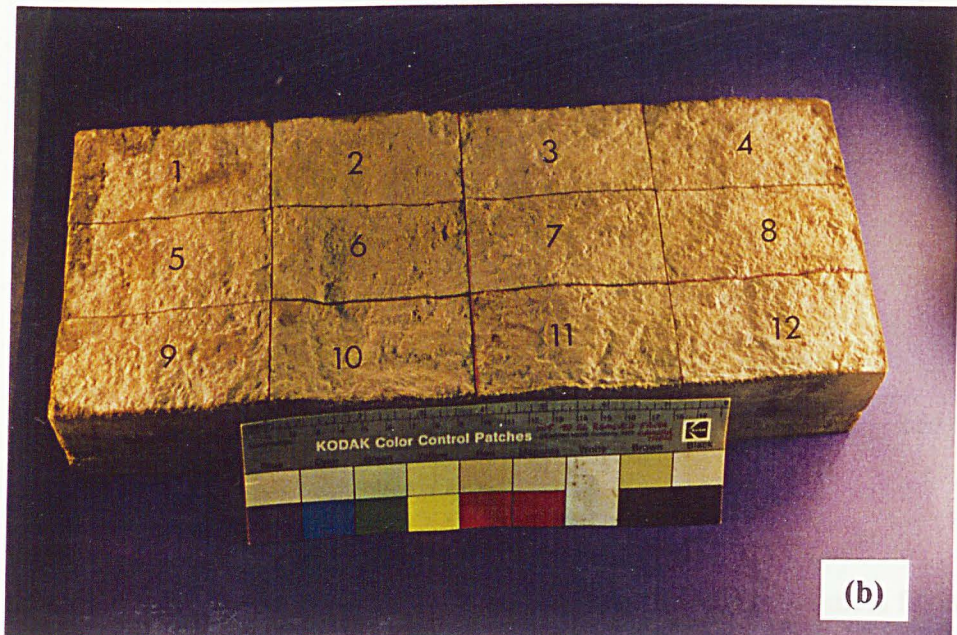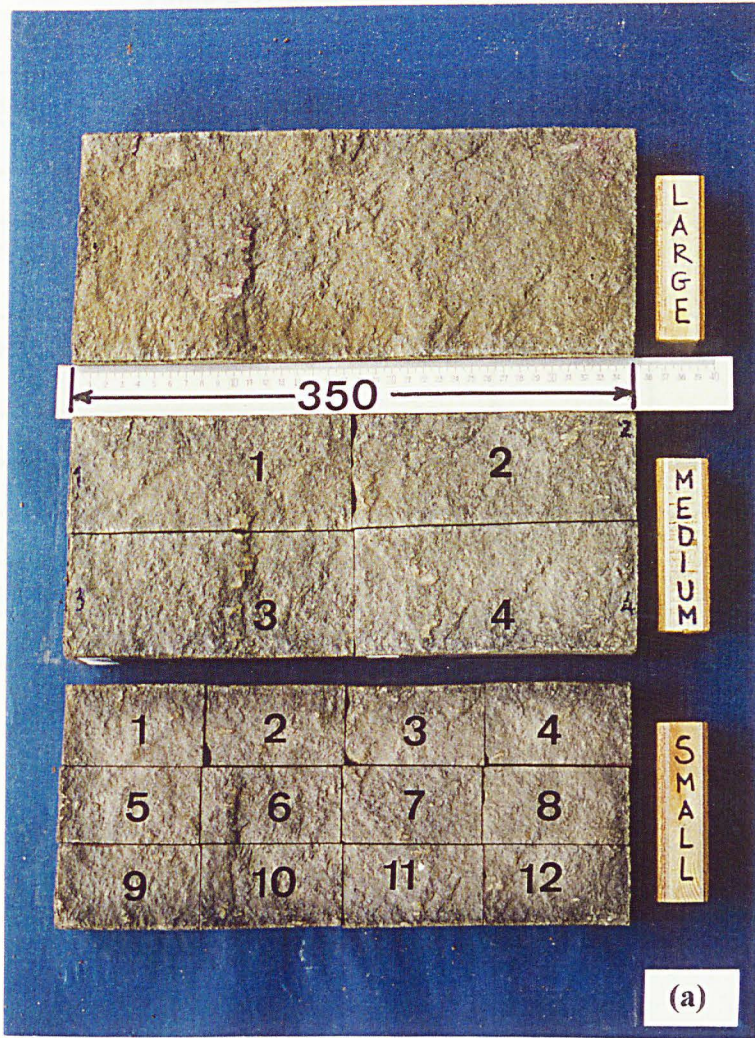
Plate 4.3 : (a) Sample sizes and positions of individual blocks.

(b) texture of model joint surface.

Table 4.2: Summary of peak shear stress ratios

Block size	Peak measured			Non- dilational		
	Range	Mean	St.dev.	Range	Mean	St.dev.
			σ = 24.2 kPa			
Small	1.38-3.32	1.81	0.54	0.50-1.03	0.83	0.16
Medium-forward	1.08-2.79	1.87	0.76	0.72-1.02	0.83	0.14
Medium-reverse	1.17-1.61	1.42	0.22	0.71-1.00	0.84	0.09
Large	1.45-1.62	1.53	0.08	0.77-0.94	0.84	0.09
			σ = 125 kPa			
Small	1.00-2.78	1.42	0.51	0.53-1.14	0.78	0.19
Medium	1.04-2.03	1.42	0.47	0.77-0.82	0.80	0.02
Large	1.46	1.46	-	0.77	0.77	-
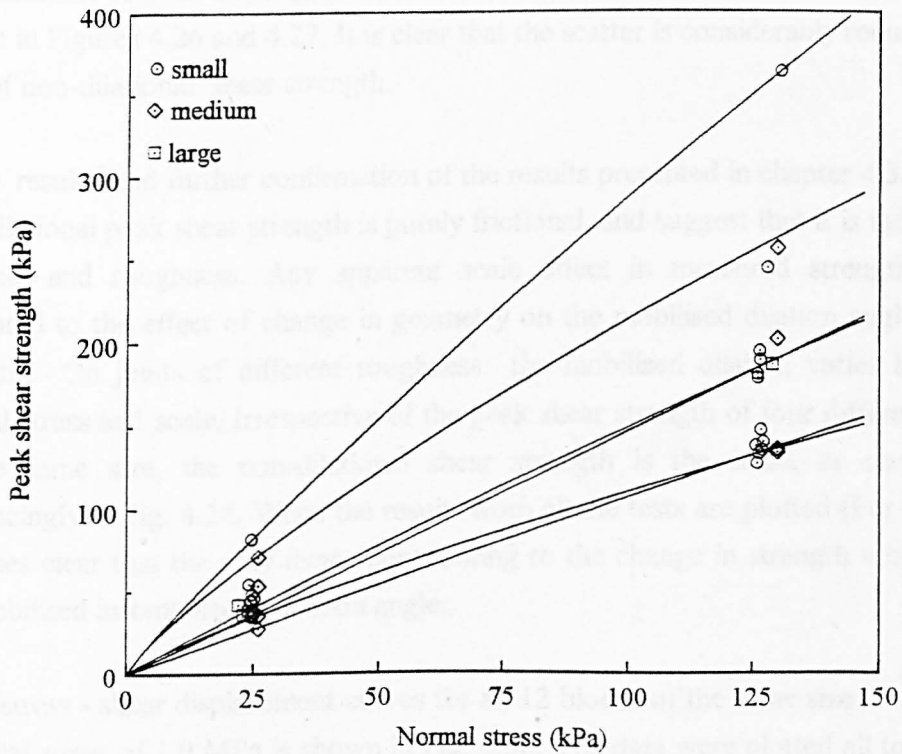
Figure 4.25: Variation of measured peak shear strength with normal stress for all sizes

different peak shear strength give almost the same non-dilational friction angle. For example, the small block with the highest peak friction angle (with a peak friction angle of 73° at normal stress 25 kPa and 70° at 125 kPa), has a non-dilational friction angle of 38.7° and 39.8° respectively. The relatively high value of mean peak measured stress ratio and standard deviation, shown by the medium size blocks, is due to a dominant asperity on the joint surface (see Fig. 4.22 and Plate 4.4). When the same blocks were sheared in the reverse direction, where this asperity has no effect, the mean and the standard deviation of peak shear strength was considerably reduced.

The non-dilational peak shear strength data for the two normal stress levels and all scales are all very close and define a friction line of 38.7° with a correlation coefficient of 0.906 (Fig. 4.25a). For reasons of clarity, the data have been redrawn in Figures 4.25b (small samples) and 4.25c (medium and large samples). The data for the small samples show some scatter, especially at normal stress 125 kPa, but large and medium (forward and reverse direction) size blocks show a remarkable correlation with a coefficient of friction equal to 0.80 (friction angle approximately 39°).

The variation of peak shear stress ratio with scale for the two normal stress levels is shown in Figures 4.26 and 4.27. It is clear that the scatter is considerably reduced in the case of non-dilational shear strength.

These results lend further confirmation of the results presented in chapter 4.3, that the non-dilational peak shear strength is purely frictional, and suggest that it is independent of scale and roughness. Any apparent scale effect in measured strength can be attributed to the effect of change in geometry on the mobilised dilation angle at peak strength. On joints of different roughness the mobilised dilation varies both with normal stress and scale. Irrespective of the peak shear strength of four different blocks of the same size, the non-dilational shear strength is the same, as shown very convincingly in Fig. 4.28. When the results from all the tests are plotted (Fig. 4.29), it becomes clear that the only factor contributing to the change in strength with scale is the mobilised instantaneous dilation angle.

Shear stress - shear displacement curves for all 12 blocks of the same size tested under a normal stress of 1.0 MPa is shown in Fig. 4.30. The data were plotted all together in order to obtain the general trend of the relation between peak shear stress and shear displacement. Two clear trends can be seen: a) the peak shear displacement depends on the roughness of the sample. As the roughness (and the peak shear strength) decreases, the peak shear displacement increases (Fig. 4.30 a). From a comparison between Figures 4.30a and 4.21 it becomes evident that the effects on peak shear
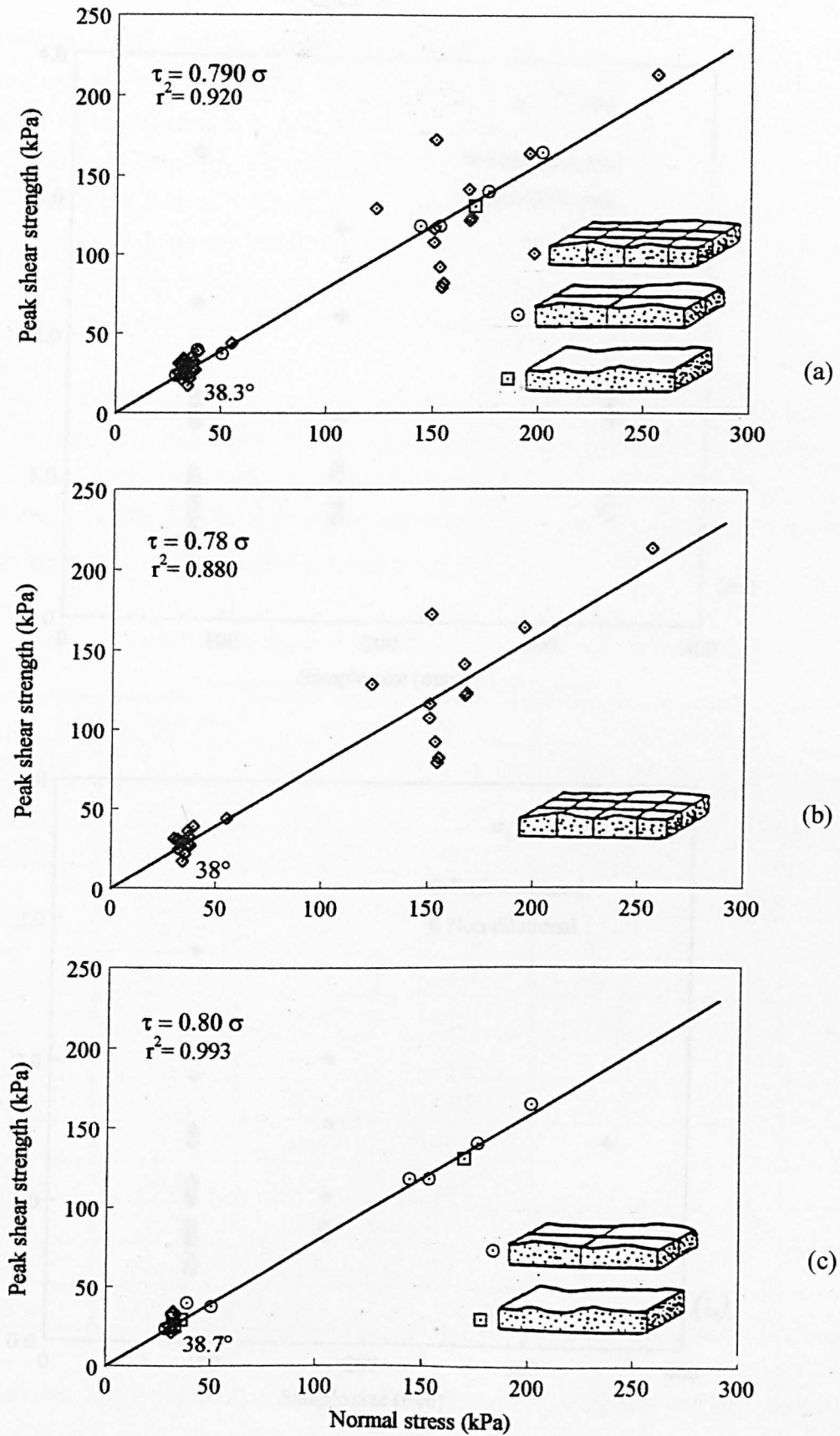
Figure 4.26: Variation of non-dilational peak friction angle with normal stress for all sizes (a). All sizes (40 samples). (b) Small size only (24 samples). (c) Medium and large samples (14 samples).

displacement of the sample and that the shape of dilation are scale specific. This implies that a possible explanation of the equivalent roughness is that the intrinsic roughness is reached at different scales. The values of shear stress displacement in these 12 blocks are between 2.0 mm to 4.0 mm, after which the shear stress drops after a small after-peak fall to a constant value for the remaining shear displacement. This constant value is generally reached before the measured peak shear strength, and irrespective of the sample roughness, it falls within a narrow band corresponding to an average value of shear stress / normal stress ratio of about 1.0.

Peak friction angles for measured and non-dilational (friction) at normal stress 1.0 MPa, 2.0 MPa and minimum dilation angles under self-weight stress (0.9 kPa) are shown in Table 4.3. The average non-dilational peak friction angle values for the two normal stresses differ only by 0.1°, and by less than 1° from the value obtained from the main testing programme presented in Chapter 4.3 (46.1°).

Figure 4.27. Variation of peak shear stress ratio with sample size.
(a) σ=24.5 kPa. (b) σ=125 kPa.

displacement of the sample size and the sample roughness are quite similar. This implies that a possible explanation of the scale effect seen in Fig. 4.21 is the different roughness mobilised at different scales. The values of peak shear displacement for these 12 blocks are between 2.0 mm an 4.0 mm. b) the non-dilational shear stress after a small initial peak falls to a constant value for the remaining shear displacement. This constant value is generally reached before the measured peak shear strength, and irrespective of the sample roughness, it falls within a narrow band corresponding to an average value of shear stress / normal stress ratio of about 1.0.

Peak friction angles both measured and non-dilational (frictional) at normal stress 1.0 MPa, 2.0 MPa and maximum dilation angles under self-weight tests (0.9 kPa) are shown in Table 4.3. The average non-dilational peak friction angle values for the two normal stresses differ only by 0.1° and by less than 1° from the value obtained from the main testing programme presented in Chapter 4.3 (46.1°).

Table 4.3: Peak friction angles of individual small sub-samples (85 mm long) at normal stress 1.0 and 2.0 MPa (degrees)

σ	σ_n=0.9 kPa	σ_n = 1.0 MPa		σ_n = 2.0 MPa	
Block No	a°	measured	non-dilational	measured	non-dilational
1	41.9	51.1	47.2	44.2	45.9
2	29.5	44.2	44.8	47.5	45.6
3	32.9	51.8	42.4	45.6	43.3
4	37.5	54.8	44.20	46.2	43.3
5	45.6	53.0	44.3	52.1	42.1
6	51.0	56.5	43.0	53.8	47.2
7	29.5	55.5	44.2	42.1	42.7
8	33.4	46.5	43.0	46.5	45.3
9	27.6	54.6	44.2	50.0	49.9
10	40.9	59.6	46.0	52.3	43.3
11	34.2	50.6	47.1	50.2	46.4
12	41.0	53.6	44.4	44.9	46.4
Mean	37.1±6.9	52.7±4.1	44.6±1.5	48.0±3.5	45.1±2.2

The difference in the value of the non-dilational friction angle at low and high normal stress is attributed to the thin cement layer existing on the surface, whose properties are different than those of the underlying material. The smooth layer was formed as a result of casting (the aggregate grains are covered by cement and are not exposed to the free surface) and the smooth texture of the Vinamold impressions produce samples which
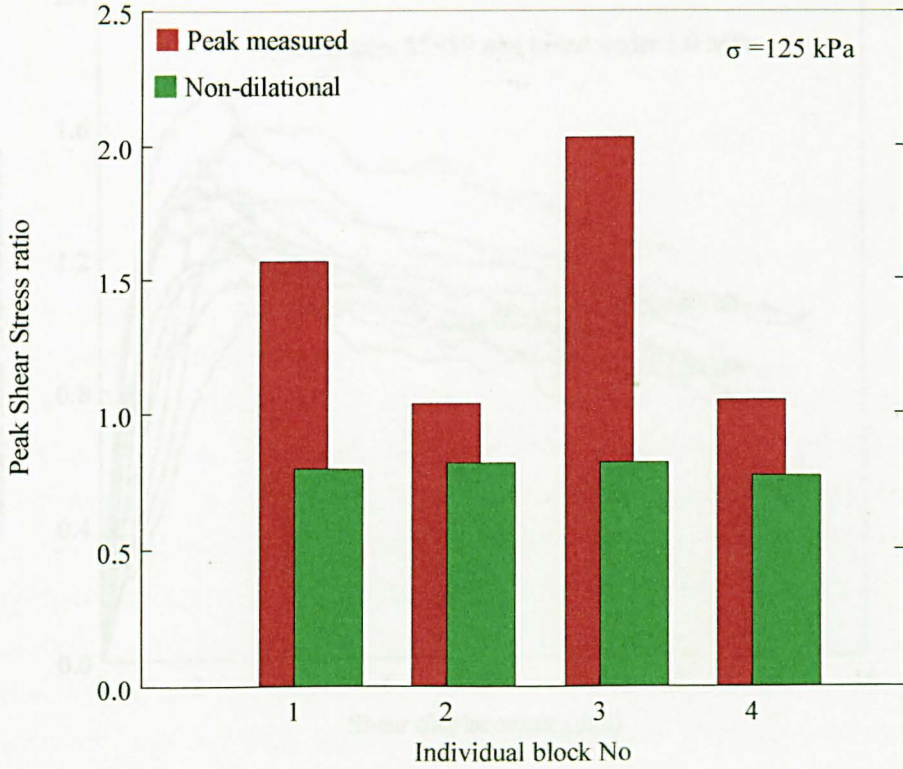
Figure 4.28. Peak shear stress ratios of individual medium sized blocks at normal stress 125 kPa
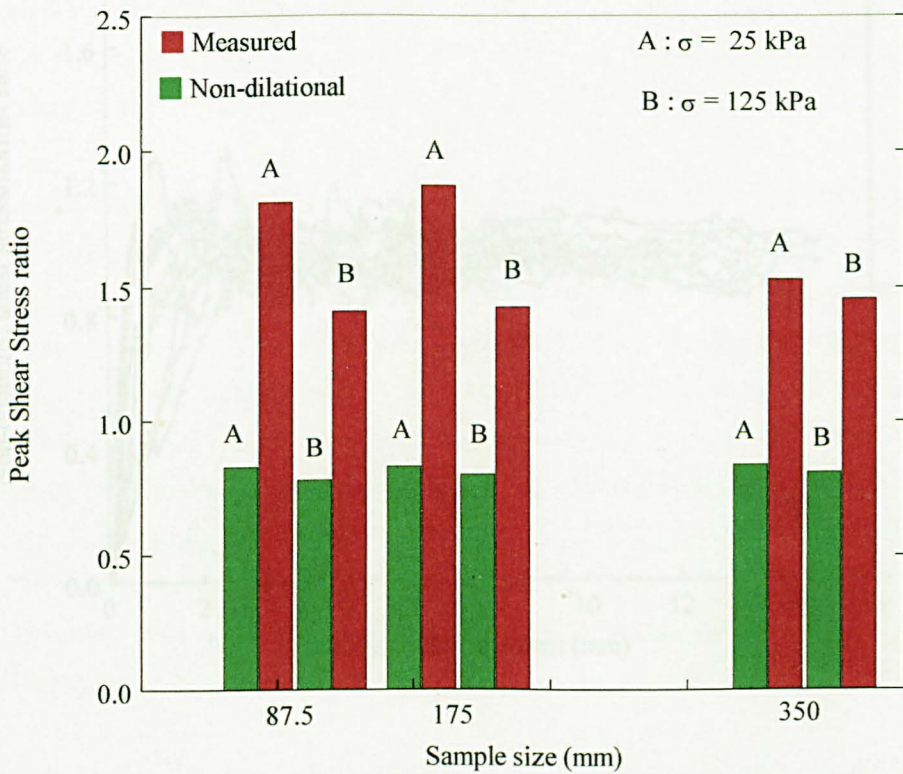
Figure 4.29. Average peak shear stress ratios of all block sizes at normal stresses 24.5 kPa and 125 kPa.

12 samples 85x50 mm tested under 1.0 MPa

Measured shear stress/normal stess

Shear displacement (mm)

(a)

12 samples 85x50 mm tested under 1.0 MPa

Non-dilational shear stress/normal stess

Shear displacement (mm)

(b)
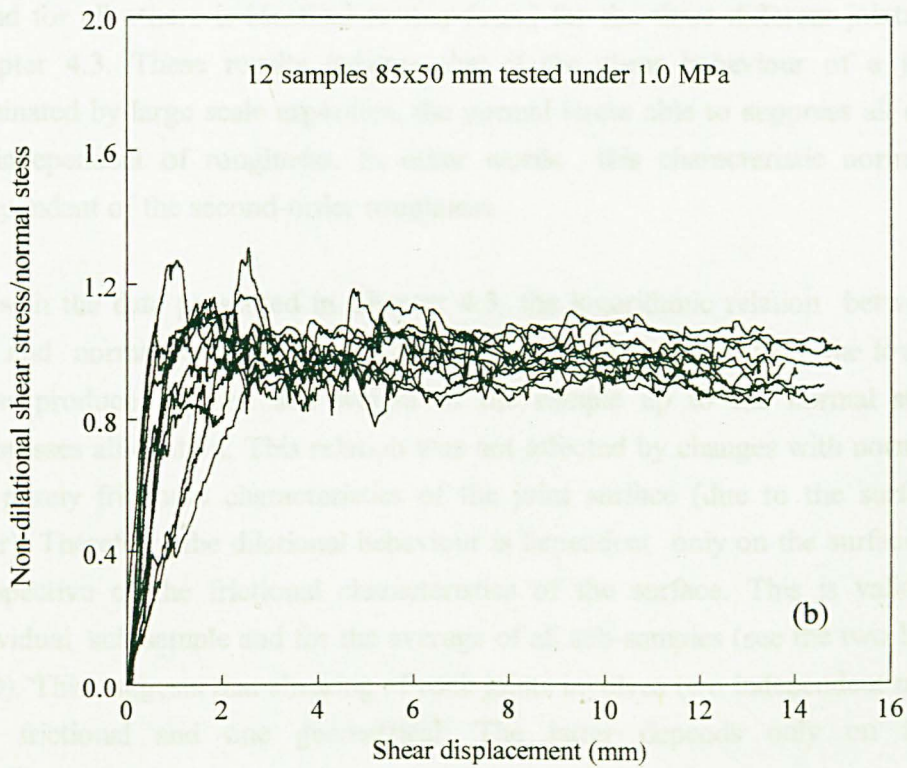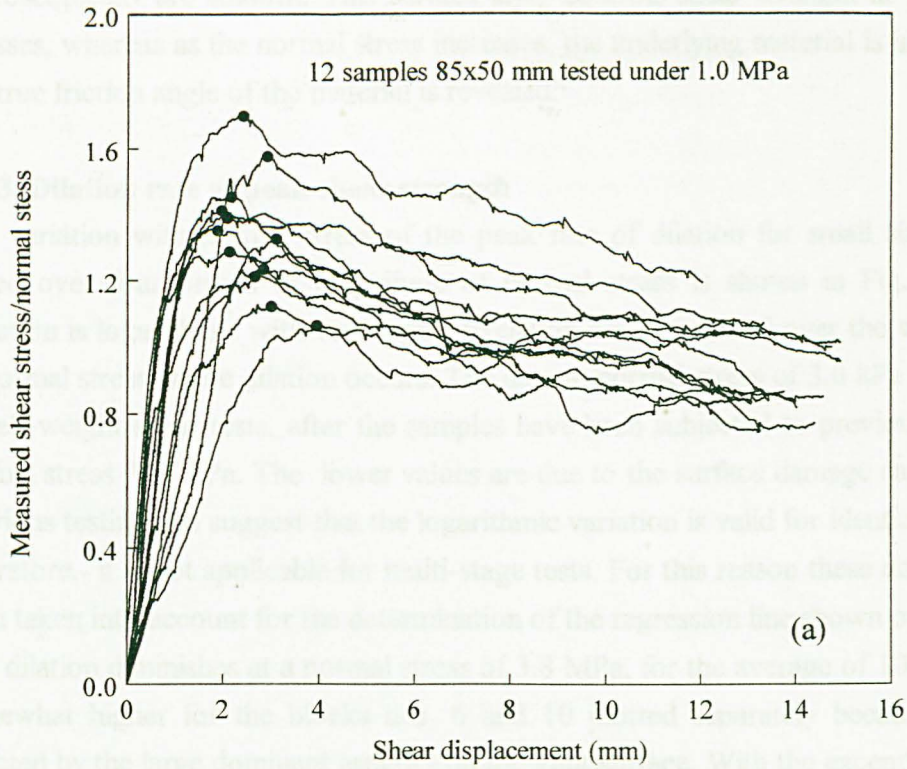
Fig. 4.30: Shear stress / normal stress ratio vs. shear displacement for 12 blocks 85x50 mm
tested under a normal stress of 1.0 MPa: (a) Measured. (b) Non-dilational

microscopically are smooth. This surface layer controls shear strength at low normal stresses, whereas as the normal stress increases, the underlying material is involved and the true friction angle of the material is revealed.

4.4.3. Dilation rate at peak shear strength

The variation with normal stress of the peak rate of dilation for small size samples, tested over four orders of magnitude of normal stress is shown in Fig. 4.30. The variation is logarithmic with very high correlation coefficient and over the whole range of normal stress where dilation occurs. The data at normal stress of 3.0 kPa correspond to self-weight shear tests, after the samples have been subjected to previous tests at a normal stress 24.5 kPa. The lower values are due to the surface damage caused by the previous testing and suggest that the logarithmic variation is valid for identical surfaces. Therefore, it is not applicable for multi-stage tests. For this reason these data have not been taken into account for the determination of the regression line shown on Fig. 4.30. The dilation diminishes at a normal stress of 3.8 MPa, for the average of 10 blocks and somewhat higher for the blocks nos. 6 and 10 plotted separately because they are affected by the large dominant asperity on the joint surface. With the exception of these two blocks, the average value of normal stress where dilation becomes zero (3.8 MPa), found for all others is identical to that found for the three different joints studied in Chapter 4.3. These results indicate that if the shear behaviour of a joint is not dominated by large scale asperities, the normal stress able to suppress all dilation will be independent of roughness. In other words this characteristic normal stress is independent of the second-order roughness.

As with the data presented in Chapter 4.3, the logarithmic relation between dilation rate and normal stress holds over four orders of magnitude, from the lowest normal stress produced by the self weight of the sample up to the normal stress which suppresses all dilation. This relation was not affected by changes with normal stress in the purely frictional characteristics of the joint surface (due to the surface cement layer). Therefore, the dilational behaviour is dependent only on the surface geometry, irrespective of the frictional characteristics of the surface. This is valid for every individual sub-sample and for the average of all sub-samples (see the two lines on Fig. 4.30). This suggests that shearing of rock joints involves two independent mechanisms: one frictional and one geometrical. The latter depends only on the surface characteristics and the normal stress.

Shear tests under the self-weight of the samples, were carried out for all the samples prior to main testing, and the maximum dilation angle was calculated. This angle can be used as a reference value for the peak dilation angles measured at higher normal

stresses. The average normal stress at these data points were 8.8 kPa for the small size samples, 1.6 kPa for the medium-size and 1.0 kPa for the full-size sample. The peak-dilation angle for these samples, extracted from shear tests was found to decrease logarithmically with the sample size (filled data symbols). This data were all normalised at 8.8 kPa normal stress, exhibiting logarithmic decrease with normal stress and a value of zero-dilation normal stress of 3.8 MPa. The data points shown in Figure 4.31 are too few to define a reliable relation which correlates the peak dilation rate with the sample length. However, if we assume that the relation shown in Figure 4.31 holds at larger scales, then extrapolation of this relation results in a scale-free block length of about 3.9 m. This value of scale-free block length is believed to be affected by the large dominant asperity on the surface, so this may be atypical for more regular natural joints. A crude estimation of scale effect can be made if the blocks affected by the large asperity are considered. For the small samples, 2 of 12 blocks (17%) are affected, 1 out of 4 (25%) for the medium size samples, and the whole (100%) for the largest sample extrapolation. The scale-free block length typical of more typical roughness may be obtained if these blocks are not taken into account. In this case the resulted scale-free block length is approximately 2.4 m (open symbols in Figure

Fig. 4.31a: Variation of dilation rate tanψ with normal stress for small size samples
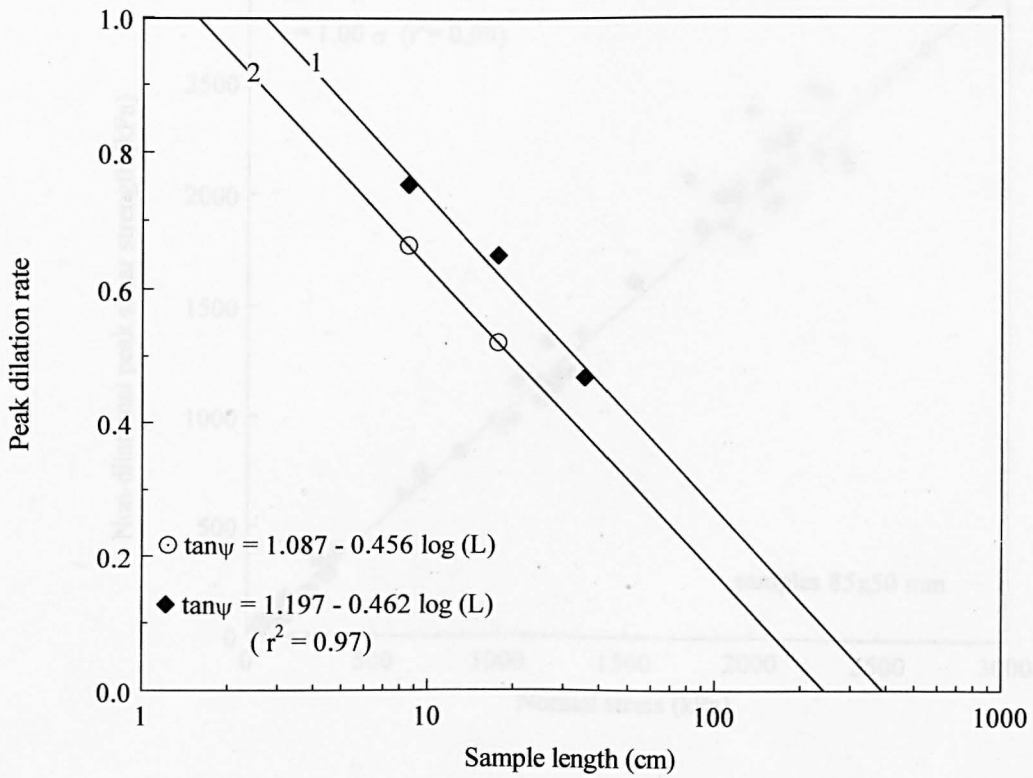
Fig. 4.31b: Variation of dilation angle at "no normal load" condition with sample size.

stresses. The average normal stress at these self-weight tests were 0.9 kPa for the small size samples, 1.6 kPa for the medium-size samples and 2.9 kPa for the full-size sample. The maximum dilation angle for these eventually damage-free shear tests was found to decrease logarithmically with the sample length (Fig. 4. 31, closed symbols). The data were all normalised at 0.9 kPa normal stress, assuming logarithmic decrease with normal stress and a value of zero-dilation normal stress of 3.8 MPa. The data points shown in Figure 4.31 are too few to define a reliable relation which correlates the peak dilation rate with the sample length. However, if we assume that the relation shown in Figure 4.31 holds at larger scales, then extrapolation at zero dilation results in a scale-free block length of about 3.9 m. This value of scale-free block length is believed to be affected by the large dominant asperity on the surface and thus may be atypical for more regular natural joints. A crude estimation of this effect can be made if the blocks affected by the large asperity are considered. For the small sub-samples 2 of 12 blocks (17%) are affected, 1 out of 4 (25%) for the medium size sub-samples and the whole (100%) full-size sample. An estimation of the scale-free block length for joints of more typical roughness may be obtained if these blocks are not taken into account. In this case the resulted scale-free block length is approximately 2.4 m (open symbols in Figure. 4.31).
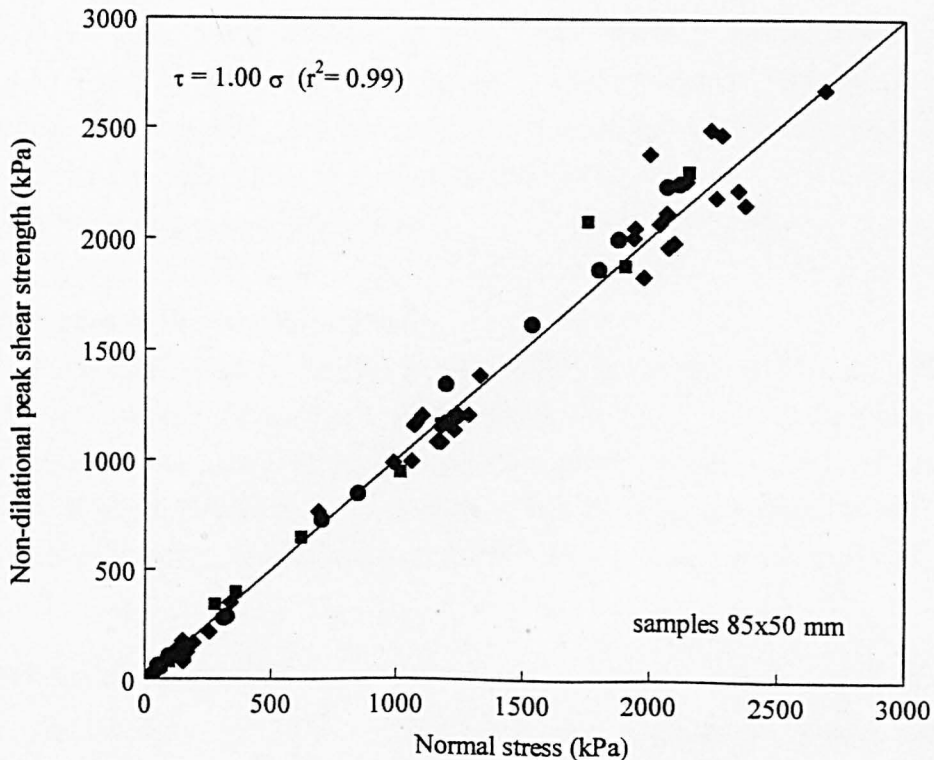
Fig. 4.32: Non-dilational peak shear strength for samples of different roughness and size tested under various normal stresses

The non-dilational peak shear strength for all samples of this series is shown in Figure 4.32. The data represent samples of various roughness and lengths from 85 mm to 354 mm, tested under various normal stresses in the range 0-2.0 MPa. Also the results described in section 4.3 are included. These data indicate clearly that the non-dilational shear strength is independent of roughness, normal stress and scale.

4. 5. The effect of sample size on peak shear strength: discontinuities modelled by a weak artificial model material

4.5.1 Introduction

The results reported in Chapters 4.3 and 4.4 have shown that the "asperity failure" component of peak shear strength can not be separated from the "basic friction" component; together they are independent of normal stress, scale, and roughness. This contradicts the basic assumption of the JRC-JCS model that asperity failure component is scale dependent. The normal stresses used in the previous investigation were 24.5 kPa and 125 kPa, corresponding to a ratio of compressive strength to normal stress equal to 1918 and 376 respectively. Although these ratios are relatively low, visual post-test examinations revealed surface damage which was larger at the higher normal stress. Dilation was fully suppressed at a normal stress of about 3.8 MPa and this value was only 30 times higher than the highest normal stress used. Therefore, asperity damage took place.

In order to confirm previous findings at higher normal stress: compressive strength ratios, a new series of direct shear tests was undertaken. Given the sample dimensions chosen and the capacity of the available direct shear test equipment, this could only be achieved if a weaker artificial material was used. The model material used in the Department of Earth Sciences of The University of Leeds for an investigation of the scale effect on peak shear strength of rock joints (Bandis, 1980), was recently employed by Toy (1993) and was readily available. Thus it was very convenient to use this material, which would give the additional advantage of comparison of the experimental results with those obtained by Bandis (1980) and Toy (1993), and extend them over a wider range of normal stress.

4.5.2. Properties of the model material

The model material consisted of: silver sand 1000 gr., barytes 375 gr., calcined alumina 125 gr., plaster of Paris 157.5 gr. and water 375 cm³. The following properties were measured by Bandis (1980): density 1.85 g/cm³, porosity 36%, unconfined compressive strength 2.0 MPa, strain at failure: 0.36%, Young's modulus 867 MPa, modulus ratio $E/\sigma_c \approx 421$, tensile strength 0.288 MPa and basic friction angle 32°.

4.5.2.1 Frictional properties

According to Bandis *et al.* (1981), the basic friction angle of the model material, determined from direct shear tests on surfaces produced by direct casting of the wet mix against a glass plate, was 32° (Figure 4.33a). However, Toy (1993) found the basic frictional behaviour of the same material quite unreliable, with friction angles varying from 9° to 35° (Fig. 4.33b). He used both sanded surfaces and casts against glass and
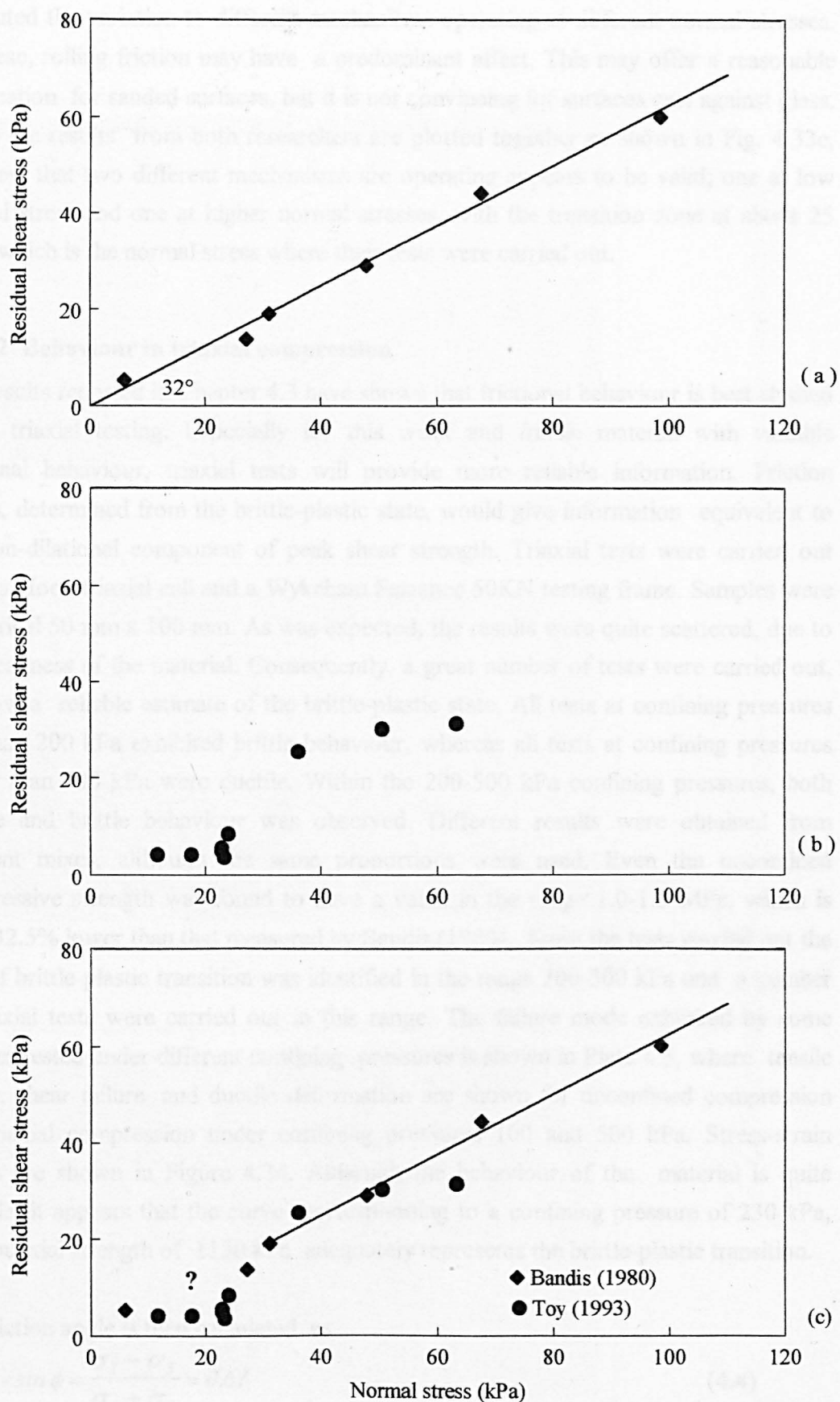
Figure 4.33: Friction angle of flat surfaces of the model material (a) Based on casts against glass (after Bandis, 1980). (b) Based mainly on sanded surfaces (after Toy, 1993).

(c) Combined data.

attributed the variation to different mechanisms operating at different normal stresses. Of these, rolling friction may have a predominant affect. This may offer a reasonable explanation for sanded surfaces, but it is not convincing for surfaces cast against glass. When the results from both researchers are plotted together as shown in Fig. 4.33c, the view that two different mechanisms are operating appears to be valid; one at low normal stress and one at higher normal stresses, with the transition zone at about 25 kPa, which is the normal stress where their tests were carried out.

4.5.2.2 Behaviour in triaxial compression

The results reported in Chapter 4.3 have shown that frictional behaviour is best studied under triaxial testing. Especially for this weak and friable material with variable frictional behaviour, triaxial tests will provide more reliable information. Friction angles, determined from the brittle-plastic state, would give information equivalent to the non-dilational component of peak shear strength. Triaxial tests were carried out using a Hoek triaxial cell and a Wykeham Farrance 50KN testing frame. Samples were cylindrical 50 mm x 100 mm. As was expected, the results were quite scattered, due to the weakness of the material. Consequently, a great number of tests were carried out, to allow a reliable estimate of the brittle-plastic state. All tests at confining pressures less than 200 kPa exhibited brittle behaviour, whereas all tests at confining pressures higher than 500 kPa were ductile. Within the 200-500 kPa confining pressures, both ductile and brittle behaviour was observed. Different results were obtained from different mixes, although the same proportions were used. Even the unconfined compressive strength was found to have a value in the range 1.0-1.3 MPa, which is 50%-32.5% lower than that measured by Bandis (1980). From the tests carried out the area of brittle-plastic transition was identified in the range 200-300 kPa and a number of triaxial tests were carried out in this range. The failure mode exhibited by some samples tested under different confining pressures is shown in Plate 4.5, where tensile failure, shear failure, and ductile deformation are shown for unconfined compression and triaxial compression under confining pressures 100 and 500 kPa. Stress-strain curves are shown in Figure 4.34. Although the behaviour of the material is quite variable, it appears that the curve corresponding to a confining pressure of 230 kPa, with an axial strength of 1150 kPa adequately represents the brittle-plastic transition.

The friction angle is then calculated as

$$sin\,\phi = \frac{\sigma_1 - \sigma_3}{\sigma_1 + \sigma_3} = 0.67 \tag{4.4}$$

and $\phi \approx 42°$. This value is 10° higher than that corresponding to the smooth surface produced by direct casting against glass (Fig. 4.33).
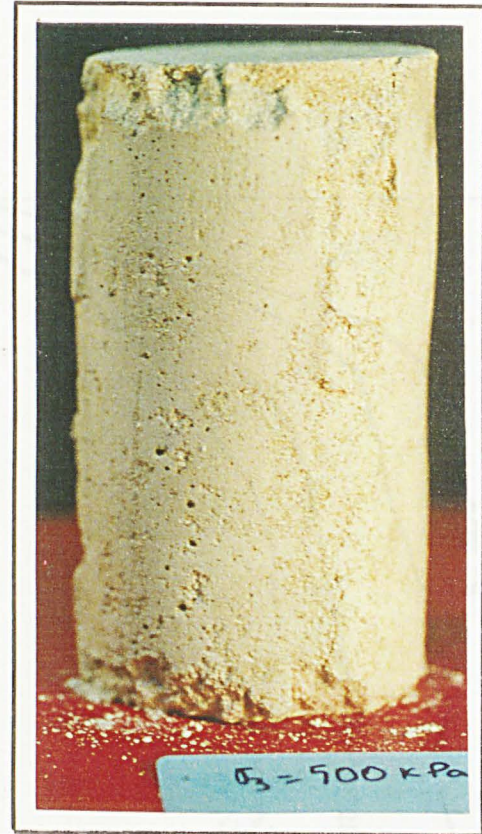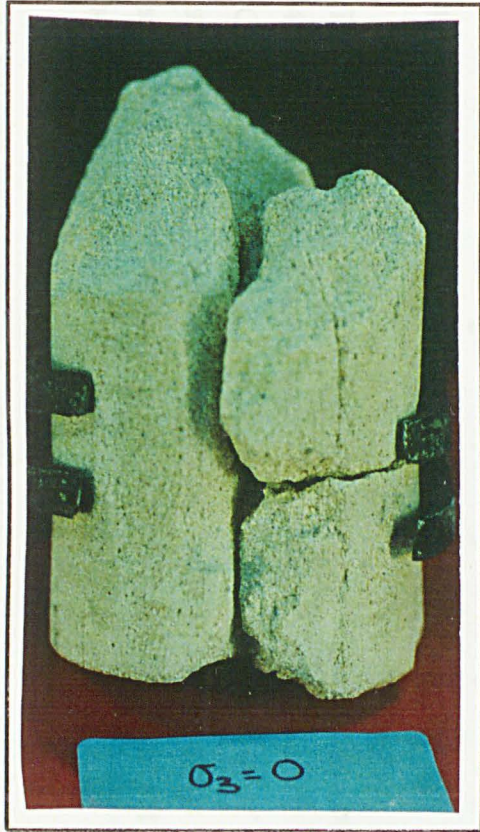
Plate 4.4: Failure of 50x100 mm cylindrical samples in triaxial compression under different confining pressures
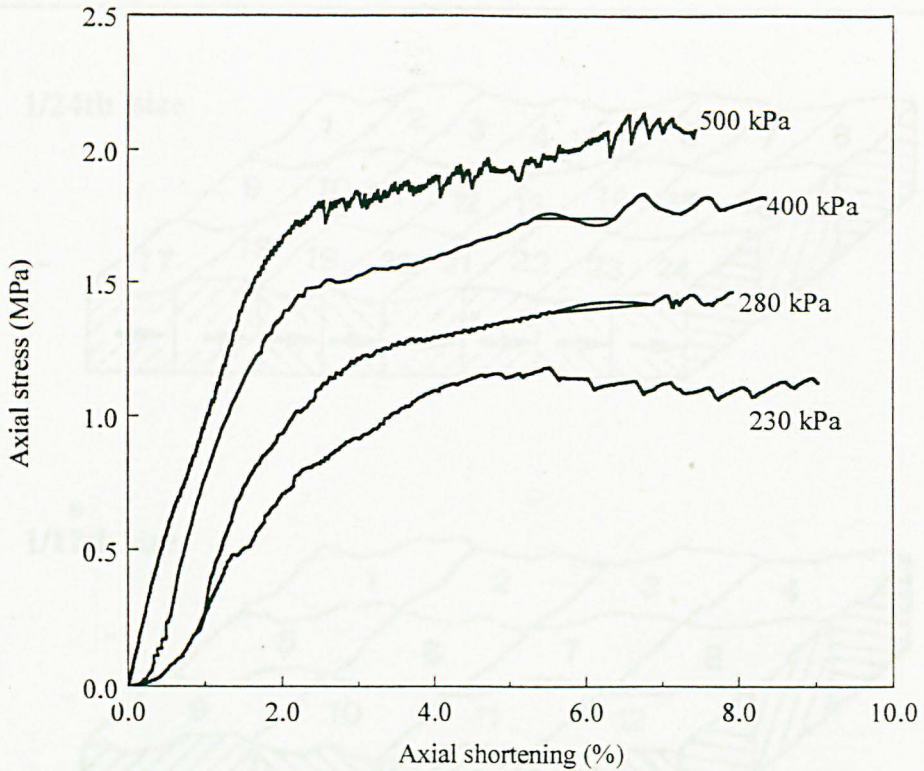
Figure 4.34: Axial stress - axial strain curves of the model material at the confining pressures indicated on each curve

4.5.3. Testing details

This series of tests was a duplicate of those described in Chapter 4.4, with the exception of the model material used. The same prototype large joint surface was used, of approximate dimensions 354x150mm, which was divided into 4 and 12 pieces (Fig. 4.22). Each joint block was tested in direct shear at a shearing rate of 0.40 mm/min under constant normal stress conditions. An additional size was added to the testing programme, by cutting the blocks of 1/12th size into two, thus four different sizes were available as shown in Figure 4.35, namely full size (354x150), quarter size (177x75), 1/12th size (88.5x50) and 1/24th size (44x50).

The surface texture produced by the Vinamold negative impressions was smooth (Plate 4.6). The degree of smoothness varied depending upon the number surface pores Careful preparation and compaction resulted in reduction of pores existing on the surface and consequently in a smoother texture. The fit of the two sample halves was satisfactory, but occasionally some pairs rocked slightly. Misfit increased with sample size, and may become a serious problem at larger sizes.

All samples were tested at a normal stress of 125 kPa, which corresponds to a ratio of compressive strength to normal stress equal to 16, if a value of 2.0 MPa is assumed for the compressive strength. But since the unconfined compressive strength found here
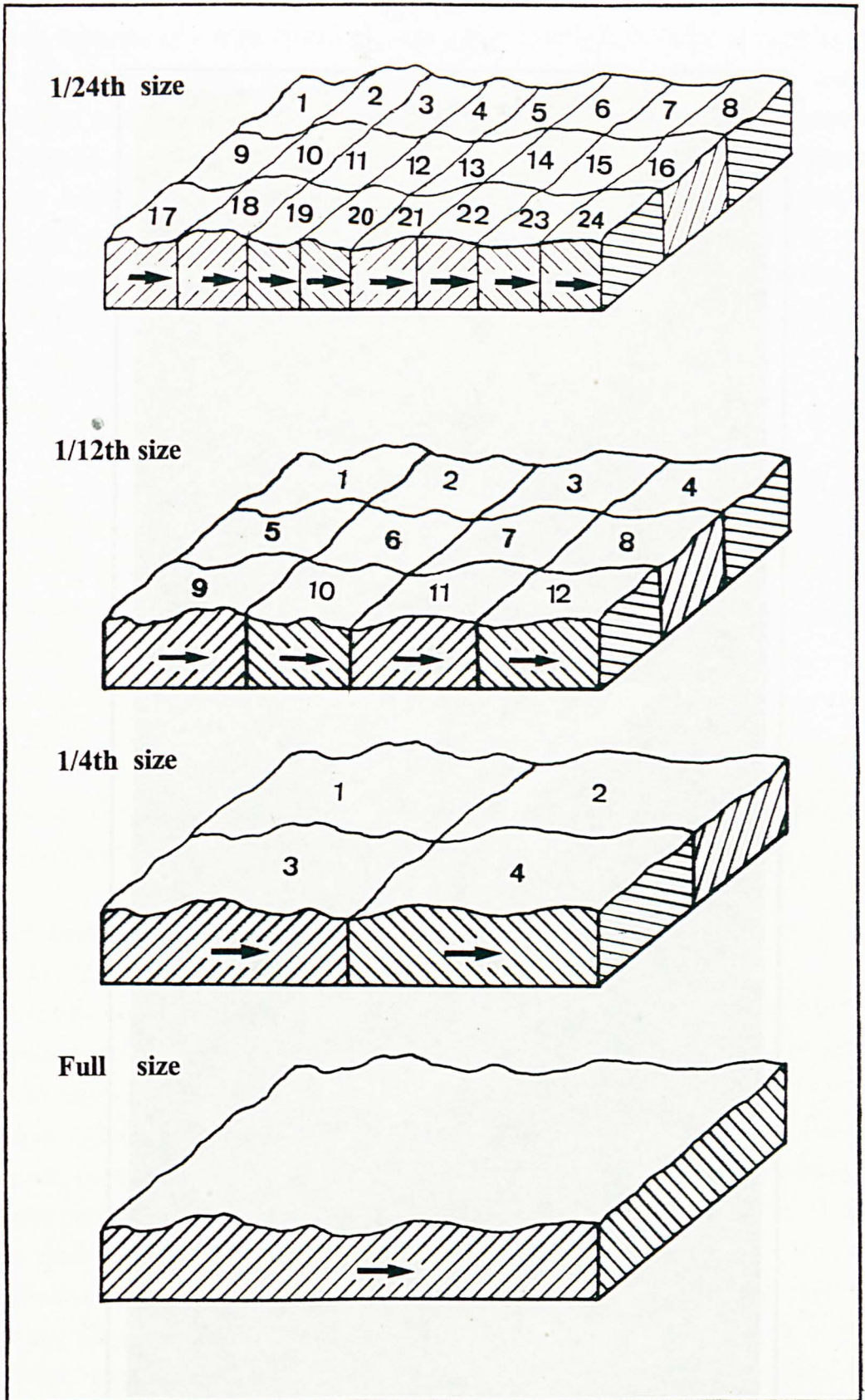
Fig. 4.35: Full size, 1/4th, 1/12th and 1/24th sub-samples used
with the weak modelling material

Plate 4.5: Photograph indicating different textures of the surface layer
and the underlying material

was of the order of 1 MPa these ratio was approximately 8. A series of samples from the three larger sample sizes was subjected to self-weight direct shear tests to determine their maximum dilation angle. The ratio of lengths between the largest and the smallest sample was 8. All four sizes were tested under 125 kPa and under self-weight conditions and when combined with tests carried out by Toy (1993) on the same joint and using the same material, adequate data was available for analysis. The whole range of tests carried out is shown in Table 4.4, where the actual average dimensions of each size are shown. These dimensions were generaly smaller than the nominal ones for all sub-samples, due to loss of material during cutting.

Table 4.4: Tests carried out on all sizes of sub-samples produced
from the same original full-size sample

Sample size	Full	Quarter	1/12th	1/24th
Actual average Dimensions (mm)	354x150	177x75	85x50	42.5x50
0.5 kPa (self weight)	√	√	√	
24.5 kPa (Toy, 1993)	√	√	√	
125 kPa	√	√	√	√

Some quarter size sub-samples were tested independently under additional normal stress, in order to define a more complete shear strength envelope.

4.5.4. Peak shear strength
4.5.4.1. Tests on 42.5 mm blocks

These blocks were produced by splitting small blocks 85x50 mm which had been previously sheared under 24.5 kPa. Sub-samples A_1 and B_1 were produced by splitting the 85 mm sub-sample no 1, A_2 and B_2 were produced by splitting the 85 mm sub-sample no 2 and so on. They are the only samples which had been previously sheared at a lower normal stress. Thus they had suffered some previous surface damage, and results on dilation angles are not directly comparable with unused samples. Provision was made to ensure that all samples were sheared with their mean plane either horizontal or at a positive angle (uphill sliding) to the mean shearing plane. This ensured some minimum surface damage during shearing and elimination of of any possible "surface effects" due to the superficial plated layer formed on the sample surface due to casting. A total of 24 blocks were tested. The results of measured peak friction angle and non-dilational friction angle are given in Table 4.5 and Fig. 4.36. The average value of measured peak friction angle is $\phi_p = 46.4° \pm 5.1°$ whereas the average non-dilational friction angle $\phi_m = 42.6° \pm 1.4°$. The difference in the average values of measured and non-dilational peak friction angle is only 3.8°, which is due to previous testing at 24.5 kPa. However, the standard deviation from 5.1° (11.0 %) in the first

Fig. 4.36: Measured (a) and non-dilational (b) peak friction angle
for the 42.5x50 mm sub-samples tested at normal stress σ_n=125 kPa

case reduces to only 1.4° (3.3 %) in the case of the non-dilational friction angle. This is a direct indication that variation in peak shear strength is due to dilation. The value of 42.6° found for the non-dilational friction angle is very close to the value of friction angle of the material determined from triaxial tests (42°).

Table 4. 5: Measured and non-dilational peak friction angles of
24 blocks 42.5 mm long tested at 125 kPa (in degrees, standard deviation in parenthesis)

Block	measured	non-dilational	Block	measured	non-dilational
A1	48.2	43.6	B1	51.1	44.3
A2	38.7	42.1	B2	43.9	39.6
A3	43.3	43.3	B3	49.0	44.2
A4	39.4	43.0	B4	50.4	41.6
A5	42.0	41.3	B5	43.1	42.4
A6	52.8	42.7	B6	52.8	43.7
A7	46.2	43.2	B7	44.5	43.0
A8	43.4	42.7	B8	46.1	42.1
A9	39.8	40.7	B9	47.1	43.0
A10	57.1	40.4	B10	49.1	42.4
A11	46.6	44.5	B11	37.5	40.9
A12	46.5	44.9	B12	54.5	43.4
Mean of 24 blocks				46.4(5.1)	42.6(1.4)

4.5.3.2. Tests on 85 mm long sub-samples

The results from two series of tests carried out at 125 kPa normal stress are shown in Table 4.6 and Fig. 4.37 plotted all-together, for peak friction angles both as measured and non-dilational. The average value for the measured peak friction angle is 46.3°. The values for the non-dilational friction angle for the two different mixtures are 40.7° and 42.9° with an average of 41.8°, very close to the predicted from triaxial testing value of 42°. It can be seen that a whole 2.8° difference in the frictional properties is due to the variability of the material. There are two exceptions: two blocks (no 6 and 10) which contained the large steep asperity gave considerably higher non-dilational friction angles (average 50.9°), which suggests that a different mechanism operates in this case. The same applies for 3 blocks (B3, B7 and B9), all from the same original parent sample, which gave a lower average value for the non-dilational friction angle of 35.7°. These latter samples were actually sheared downslope, and this resulted in less surface damage, so that the smooth surface plaster layer reduced the overall peak friction angle (both measured and non-dilational). In contrast, when blocks are sheared upslope, the material underneath the surface layer is involved in shearing; thus the true

Fig. 4.37: Measured (a) and non-dilational (b) peak friction angle
for the 85x50 mm sub-samples tested at normal stress σ_n=125 kPa

Table 4.6: Measured and non-dilational peak friction angles
of 2 sets of 12 blocks 85 mm long tested at 125 kPa (in degrees)

Block	measured	non-dilational	Block	measured	non-dilational
A1	43.3	40.0	B1	43.0	39.7
A2	43.0	42.2	B2	48.1	42.7
A3	47.2	43.1	B3	40.8	34.8
A4	46.3	40.9	B4	45.9	43.3
A5	51.3	39.0	B5	40.2	40.2
A6	58.0	45.3	B6	55.3	50.5
A7	42.4	44.2	B7	40.4	36.9
A8	48.8	44.6	B8	45.4	43.0
A9	45.7	43.7	B9	38.5	35.5
A10	55.5	51.3	B10	47.7	40.1
A11	53.0	40.3	B11	42.6	39.4
A12	45.1	40.3	B12	43.4	41.8
12 blocks	48.3(4.9)	42.9(3.2)	12 blocks	44.3(4.4)	40.7(4.0)
10 blocks	47.6(4.6)	41.8(1.9)	10 blocks	42.8(2.8)	39.7(2.9)

friction angle controls the shear behaviour. To check the validity of this argument, in the second series of tests (series B), provision was made for these three blocks to have their mean plane horizontal. The results obtained were then in line with that of the remaining sub-samples. The results for series B shown in Table 4.9 are more consistent, and more representative of the true friction angle of the material. The average non-dilational friction angle is 42.9°, reducing to 42.1°, if the highest value of 51.3° corresponding to block no 10 (affected by the large asperity) is excluded from the sample population. This value is almost identical with the friction angle of the model material, determined from triaxial tests, and to that found for the 42.5 mm long sub-samples.

With regard to the behaviour of the sub-samples containing the large asperity, no explanation could be offered. The shear stress-shear displacement and normal displacement - shear displacement diagrams for the block A6 (Table 4.6), which gave a non-dilational friction angle are shown in Fig. 4.38a, together with calculated dilation angles and non-dilational shear stress. For a more detailed observation, the portions of the same diagrams corresponding to the instant of peak shear strength are shown in Fig. 4.38b. It can be seen that peak shear strength occurs at a shear displacement of 2.8 mm, whereas the maximum dilation angle (approximately 16°) occurs at about 2.4 mm. As the peak shear strength is approached, the dilation angle drops and the sample is not
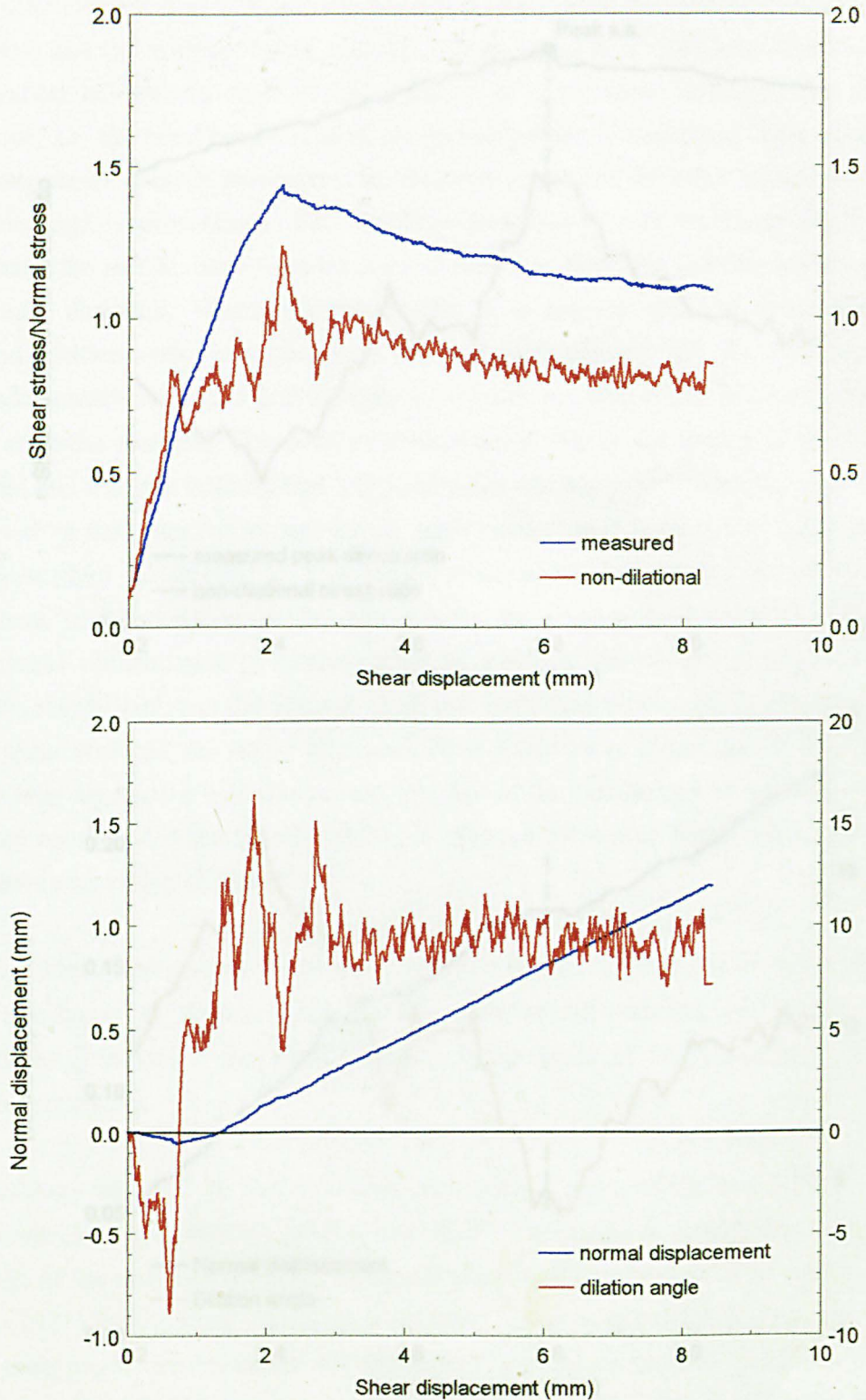
Fig. 4.38a: Shear behaviour of block No 6 containing an unusually high asperity

(a) Shear stress ratio - shear displacement

(b) Normal displacement - shear displacement
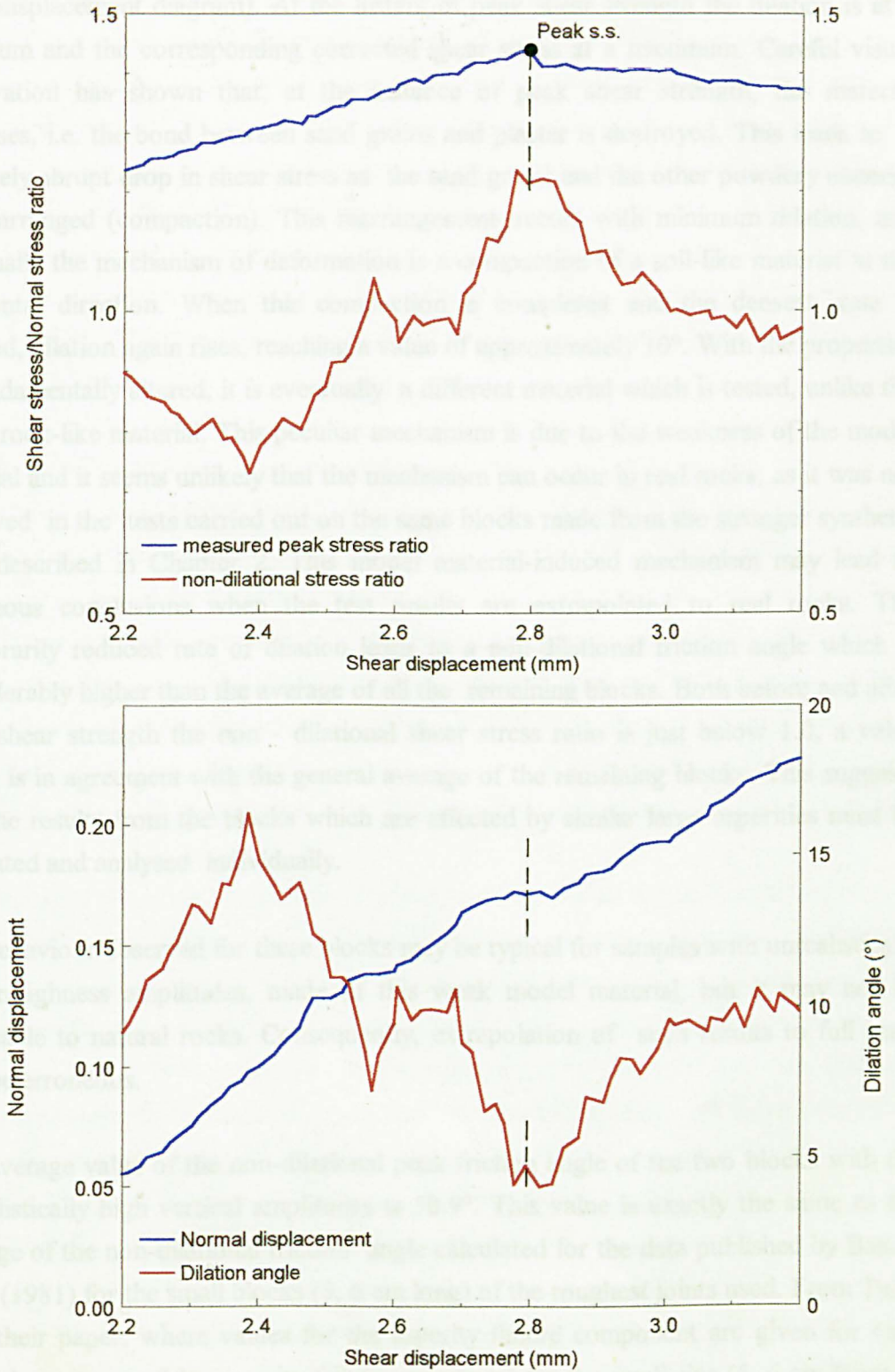
Fig. 4.38: Shear behaviour near the peak shear strength

of block no 6 containing an unusually high asperity

(a). Shear stress ratio - shear displacement

(b). Normal displacement - shear displacement

moving in the normal direction (see the small plateau on the normal displacement - shear displacement diagram). At the instant of peak shear strength the dilation is at a minimum and the corresponding corrected shear stress at a maximum. Careful visual observation has shown that, at the instance of peak shear strength, the material collapses, i.e. the bond between sand grains and plaster is destroyed. This leads to a relatively abrupt drop in shear stress as the sand grains and the other powdery material are rearranged (compaction). This rearrangement occurs with minimum dilation, and eventually the mechanism of deformation is a compaction of a soil-like material in the horizontal direction. When this compaction is completed and the densest state is reached, dilation again rises, reaching a value of approximately 10°. With the properties so fundamentally altered, it is eventually a different material which is tested, unlike the initial rock-like material. This peculiar mechanism is due to the weakness of the model material and it seems unlikely that the mechanism can occur in real rocks, as it was not observed in the tests carried out on the same blocks made from the stronger synthetic rock described in Chapter 2. This model material-induced mechanism may lead to erroneous conclusions when the test results are extrapolated to real rocks. The temporarily reduced rate of dilation leads to a non-dilational friction angle which is considerably higher than the average of all the remaining blocks. Both before and after peak shear strength the non - dilational shear stress ratio is just below 1.0, a value which is in agreement with the general average of the remaining blocks. This suggests that the results from the blocks which are affected by similar large asperities must be separated and analysed individually.

The behaviour observed for these blocks may be typical for samples with unrealistically high roughness amplitudes, made of this weak model material, but it may not be applicable to natural rocks. Consequently, extrapolation of such results to full scale may be erroneous.

The average value of the non-dilational peak friction angle of the two blocks with the unrealistically high vertical amplitudes is 50.9°. This value is exactly the same as the average of the non-dilational friction angle calculated for the data published by Bandis *et al.* (1981) for the small blocks (5, 6 cm long) of the roughest joints used. From Table 2 of their paper, where values for the asperity failure component are given for each joint, the average of the asperity failure component for the small size (5, 6 cm long) of the roughest 8 joints (nos. 1-8), described as strongly or moderately undulating, very rough to moderately rough, is 18.9°±1.3°, which if added to the assumed basic friction angle of 32° gives 50.9°. Of the remaining three joints, no 9 had a similar magnitude of asperity failure component (16.3°), no 10 had 13.1° resulting in a non-dilational friction angle of 45.1°, and no 11 had 7.5° which gives a non-dilational peak friction angle of 39.5°. This remarkable agreement may suggest that the values of non-dilational

friction angle obtained by the authors may be due to the peculiar deformation mechanism described earlier, which is indicative of samples with unusually high asperities in a weak model material. Indeed, some of the full-size model joints used were unrealistically rough when considered at full scale. Obviously, the problem becomes much more serious when the full size joints are cut into 6 or 8 to produce the smallest sub-samples. For example model no 1 at full scale had a wave length of 3.5 m and a vertical amplitude 25 cm. When the full size length was reduced to 1/6th, the length obtained was 58 cm, but the vertical amplitude remained 25 cm. Such a joint is very unlikely to occur in nature, and the simulation may fail adequately to describe real joint behaviour. This emphasises the difficulties and the care which must be taken when roughness is to be scaled.

4.5.3.3. Tests on 175 mm long sub-samples

These blocks were tested under self-weight, 48 kPa and 125 kPa, which when combined with the results from tests at 24.5 kPa carried out by Toy (1993), they can define a complete shear strength envelope. The results are shown in Table 4.7 and Fig. 4.39. There is a wide scatter for the measured peak friction angle from 39° to 65°. It appears that the measured peak friction angle changes with each mix, as shown by the two data sets at 125 kPa, where a difference of 2.9° is observed, which diminishes when the non-dilational friction angle is considered. Nominally identical samples may differ in the non-dilational friction angle by 5° (compare sub-samples MB3 and MG3).

Differences of the same magnitude (3°) may be observed in the non-dilational friction angle at different normal stresses. These differences are attributed to the variability in the strength of the material and the degree of surface smoothness achieved. The latter depends on the number of pores, and the degree of damage suffered on removal of the Vinamold. Toy (1993) attributed similar differences in measured and non-dilational peak shear strength for nominally identical samples to the model material properties, the quality of the cast and the degree of mating fit. The average non-dilational friction angle for all the samples under the normal stresses used is 41.8° (41.7° if block no 3 is not included).

Some blocks were separately tested under higher normal stresses (200-400 kPa), are shown in the left bottom of Table 4.7. At this high normal stress the resistance to sliding is higher than that required for the material to disorder and deform in compression, as shown in Plate 4. 5 where the total shear displacement was equal to the shortening of the top-half. In these tests the joint is not the weakest element and thus the results can not be used for direct comparison with the rest shown on the same Table. Actually this behaviour is also seen in some tests at $\sigma = 125$ kPa, where fracture of the top half in many fragments takes place in addition to sliding along the
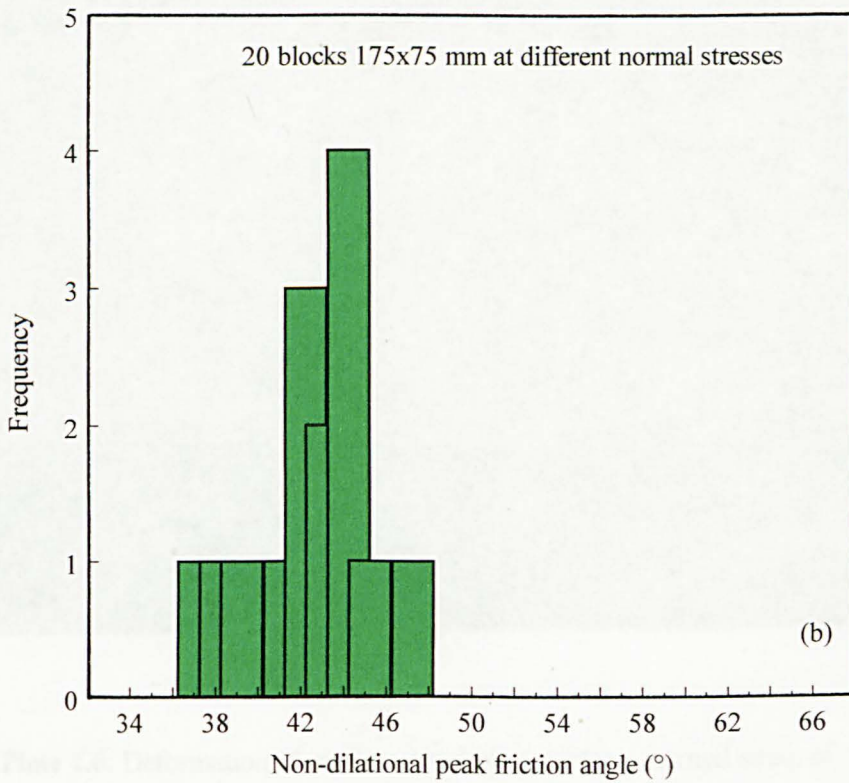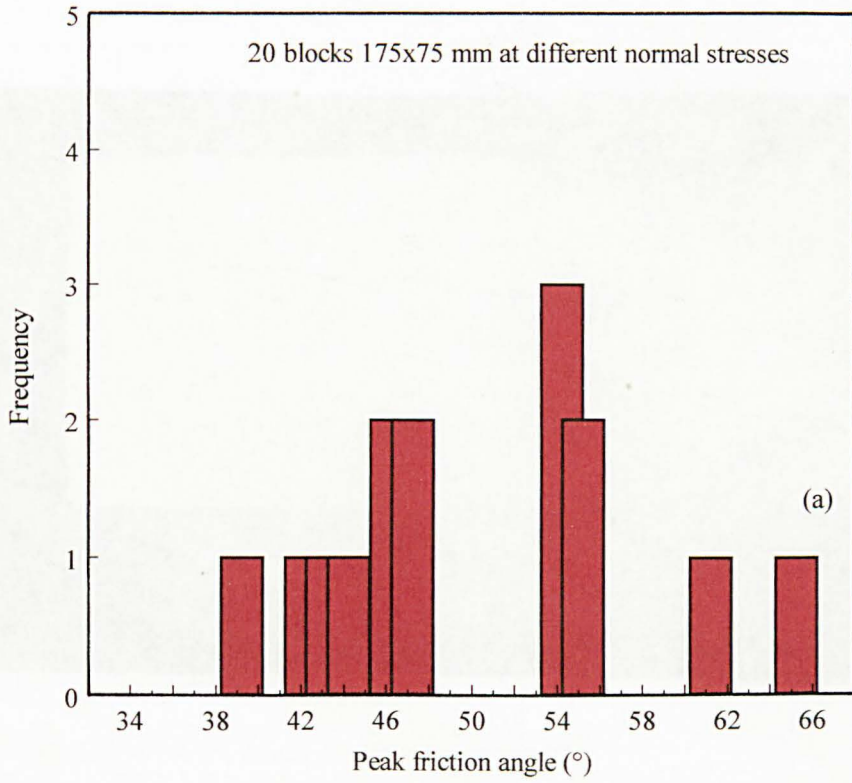
Fig. 4.39: Measured and non-dilational peak friction angle for the 175x75 mm sub-samples tested under various normal stresses

Table 4.7: Measured and non-dilational peak friction angles of 4 sets of 4-blocks 175 mm long tested at different normal stresses 125 kPa (in degrees)

Block No	measured	non-dilational	Block No	measured	non-dilational

Δl

| | | | | | |
| Mean | 42.6 (41.2) | 40.5 (39.3) | Mean | | |

$\sigma_n = 200\text{-}400\ kPa$

MH125.02
BOTTOM
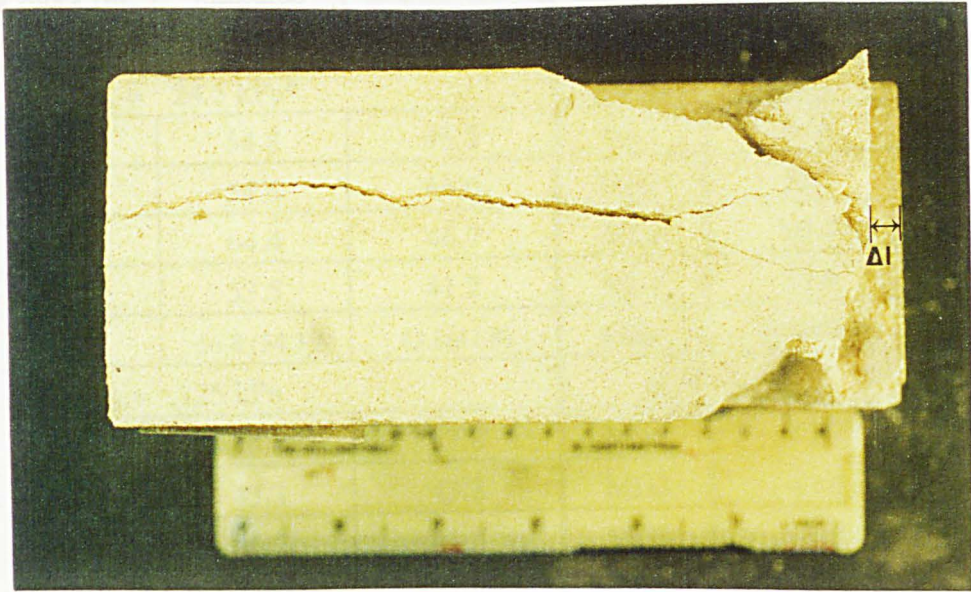
Plate 4.6: Deformation of medium-sized block under a normal stress of 125 kPa

4.5.3.5 Comparison of results

The values of the non-dilational peak shear strength obtained from tests on samples are very close. The non-dilational peak friction angles at this stress level give a consistent average value of 40-41° which is identical to the friction angle of the intact material obtained from triaxial tests at the homogeneous condition. These results further confirm that the effect of scale on peak shear strength is the result of different dilation angles mobilised at different scales.

Table 4.7: Measured and non-dilational peak friction angles of 4 sets of 4 blocks 175 mm long tested at different normal stresses 125 kPa (in degrees)

Block No	measured	non-dilational	Block No	measured	non-dilational
$\sigma_n =$ 24.5 kPa*			$\sigma_n =$ 48 kPa		
MA1	54.8	43.2	ME1	N/A	N/A
MA2	54.6	44.0	ME2	52.2	43.1
MA3	64.4	46.7	ME3	60.4	44.7
MA4	53.5	41.2	ME4	53.6	42.4
Mean	56.8 (54.3)	43.8(42.8)	Mean	55.4(52.9)	43.4(42.8)
$\sigma_n =$ 125 kPa			$\sigma_n =$ 125 kPa		
MB1	38.8	37.8	MG1	45.9	40.2
MB2	43.3	43.3	MG2	42.6	42.0
MB3	46.2	41.5	MG3	46.9	36.5
MB4	41.9	38.7	MG4	46.0	42.1
Mean	42.6 (41.3)	40.3(39.9)	Mean	45.5(45.0)	40.2(41.4)
$\sigma_n =$ 200-400 kPa					
A4/200	53.5	44.1	A3/300	45.4	43.2
A4/400	46.0	40.8	B4/300	50.5	43.8
Mean	48.9	43.0	*After Toy (1993)		

* Results after Toy (1993) - In brackets mean values without block no 3

joint surface (Plate 4.7). This situation is equivalent to the state at the brittle-plastic transition stress.

4.5.3.4 Tests on full-size samples (L=354 mm)

Two full-size samples were tested at 125 kPa, which gave values for the non-dilational friction 43.5° and 40.0° correspondingly, with an average of 41.8°, which is in agreement with other sizes.

4.5.3.5 Comparison of results

The values of the non-dilational peak shear strength obtained from tests on samples having a length varying from 42.5 mm to 354 mm (i.e. over one order of magnitude) are very close. The non-dilational peak friction angles at four different sizes give a consistent average value of 42°±0.5° which is identical to the friction angle of the intact material obtained from triaxial tests at the brittle-plastic transition. These results further confirm that the effect of scale on peak shear strength is the result of different dilation angles mobilised at different scales.

A plot of peak stress ratio (τ_p/σ) both measured and non-dilational for all the data of this series is shown in Fig. 4.40, from which the following conclusions can be drawn:
a) A wide scatter of the experimental results exists at all scales, but it reduces with scale. The consistency of the data for the smallest scale is due to the more uniform surface finish, resulted from previous shearing of these samples, so the true friction angle of the underlying material is involved. The same reason explains the slightly above average mean value of this group.

The average non-dilational friction angle is shown to be independent of scale.

Due small variations in the preparation procedure, the model material used could not give identical surface finish properties, resulting in samples with different degree of surface smoothness and number of pores.

4.5.4. Peak shear strength envelopes

Peak shear strength envelopes from all tests in this series are shown in Fig. 4.41 both for the measured and the non-dilational peak shear strength. The best fit straight line for the non-dilational data falls very close to the friction line corresponding to 42°.
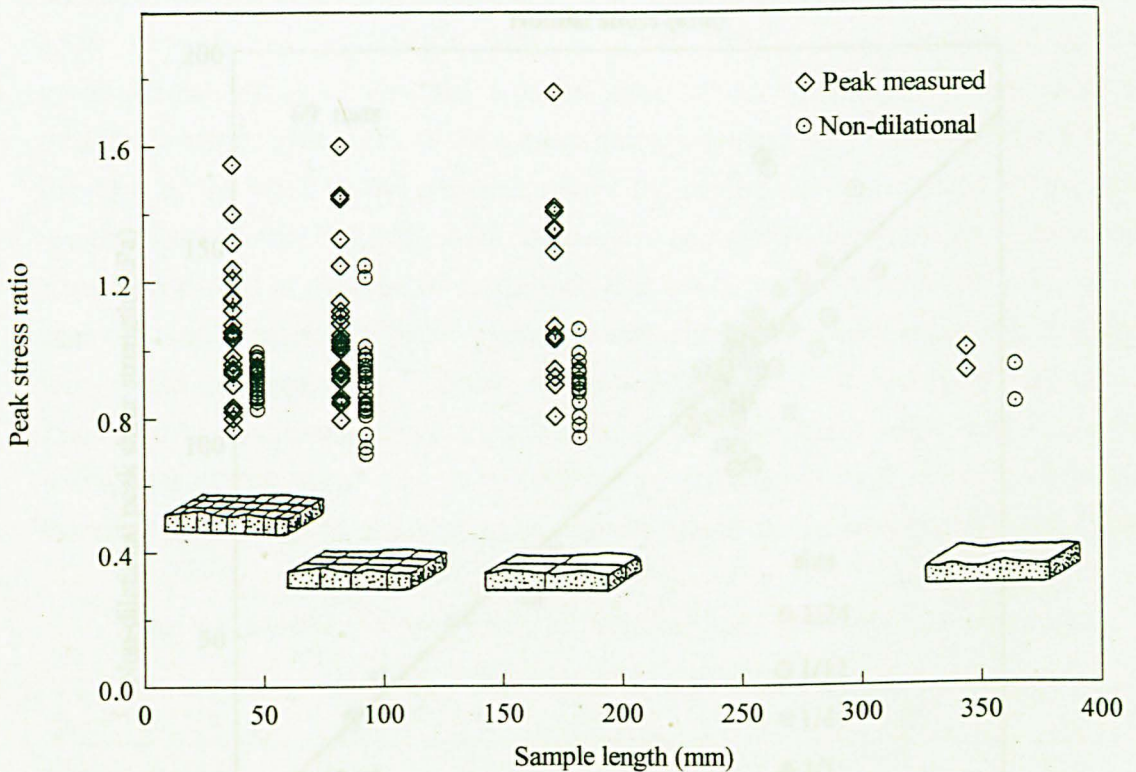
Fig. 4.40 : Measured and non-dilational peak stress ratio (τ_p/σ) versus sample size

145
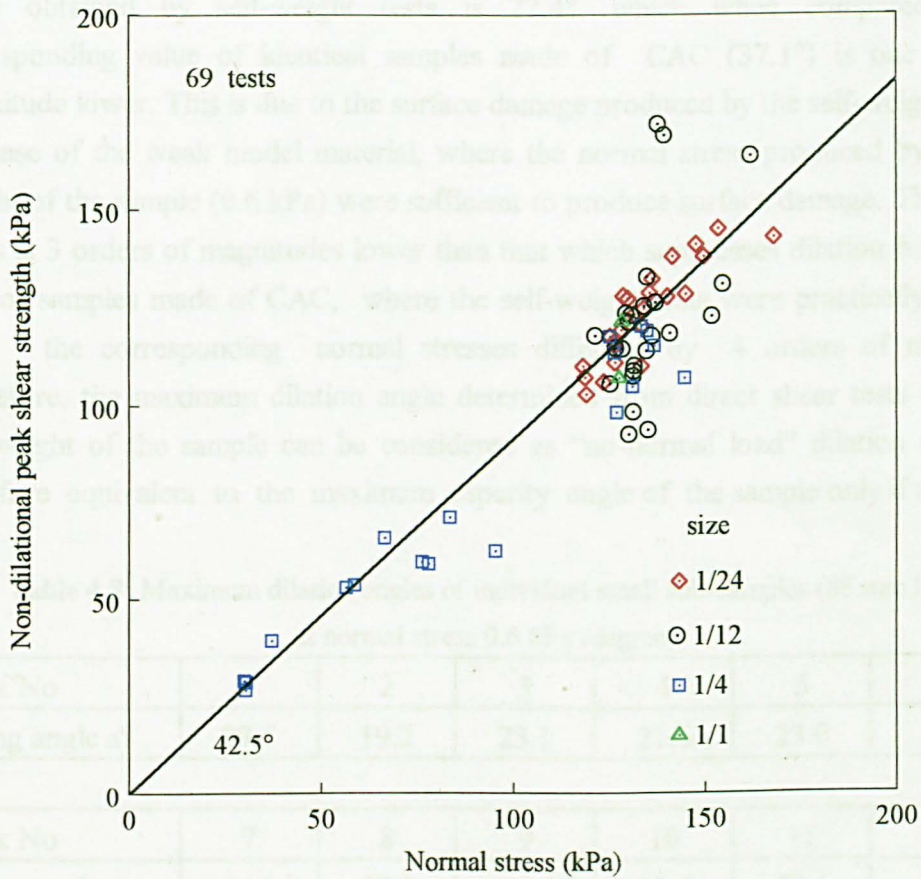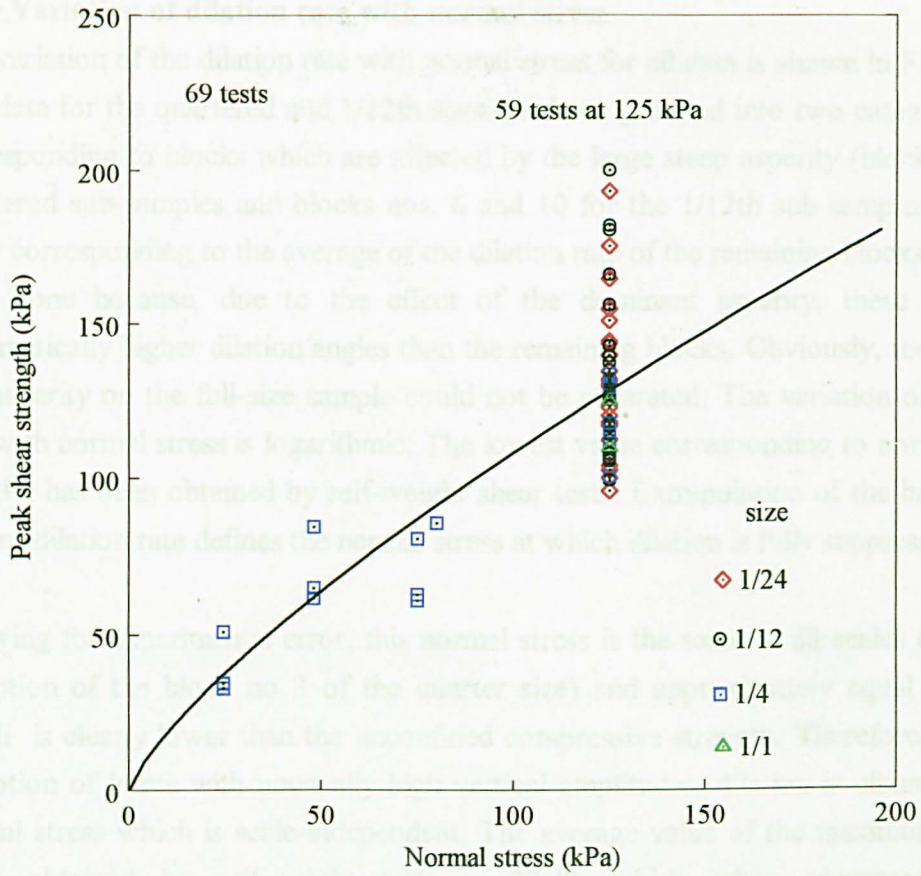
Fig. 4.41: Peak shear strength envelopes (a) Measured   (b) Non-dilational

4.5.5 Variation of dilation rate with normal stress

The variation of the dilation rate with normal stress for all data is shown in Figure 4.43 The data for the quartered and 1/12th sizes has been grouped into two categories: one corresponding to blocks which are affected by the large steep asperity (block no 3 for quartered sub-samples and blocks nos. 6 and 10 for the 1/12th sub-samples) and the other corresponding to the average of the dilation rate of the remaining blocks. This has been done because, due to the effect of the dominant asperity, these produced systematically higher dilation angles than the remaining blocks. Obviously, the affect of this asperity on the full-size sample could not be separated. The variation of dilation rate with normal stress is logarithmic. The lowest value corresponding to normal stress 0.6 kPa has been obtained by self-weight shear tests. Extrapolation of the best-fit line to zero dilation rate defines the normal stress at which dilation is fully suppressed.

Allowing for experimental error, this normal stress is the same at all scales (with the exception of the block no 3 of the quarter size) and approximately equal 400 kPa, which is clearly lower than the unconfined compressive strength. Therefore, with the exception of joints with unusually high vertical amplitudes, dilation is eliminated at a normal stress which is scale-independent. The average value of the maximum dilation angle obtained by self-weight tests is 27.4°, which when compared to the corresponding value of identical samples made of CAC (37.1°) is one order of magnitude lower. This is due to the surface damage produced by the self-weight tests in the case of the weak model material, where the normal stress produced by the self-weight of the sample (0.6 kPa) were sufficient to produce surface damage. This normal stress is 3 orders of magnitudes lower than that which suppresses dilation fully. In the case of samples made of CAC, where the self-weight tests were practically damage-free, the corresponding normal stresses differed by 4 orders of magnitude. Therefore, the maximum dilation angle determined from direct shear tests under the self-weight of the sample can be considered as "no-normal load" dilation angle and therefore equivalent to the maximum asperity angle of the sample only if the acting

Table 4.8: Maximum dilation angles of individual small sub-samples (85 mm long) at normal stress 0.6 kPa (degrees)

Block No	1	2	3	4	5	6
Sliding angle a°	29.5	19.2	23.1	21.6	23.0	52.4

Block No	7	8	9	10	11	12
Sliding angle a°	24.9	27.8	20.7	39.5	23.6	23.9

Average of 12 blocks: 27.4°±9.9°	Average of 10 blocks: 23.7°±3.1°
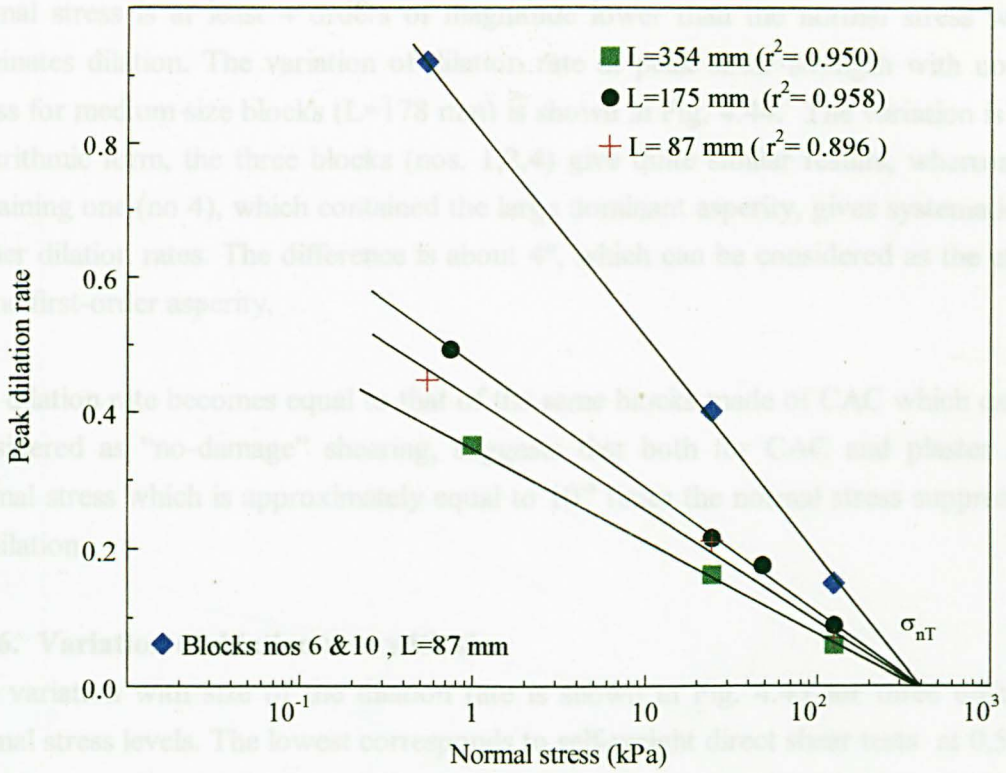
Fig. 4.43. Variation of dilation rate *tanψ* with normal stress
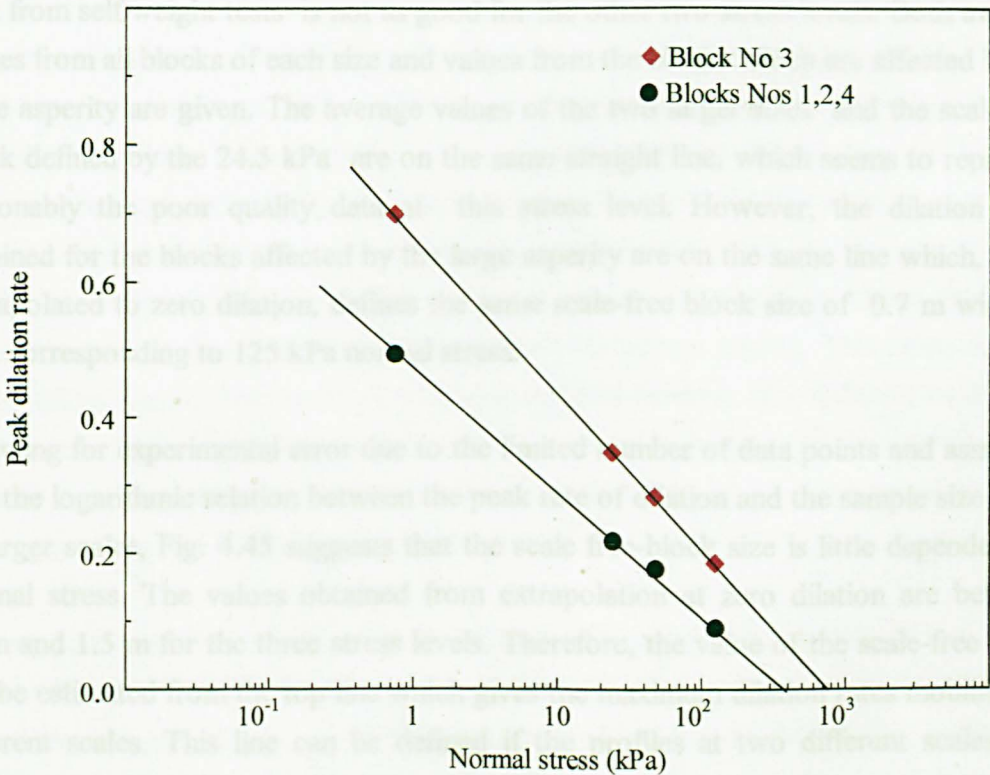
Fig. 4.44. Variation of dilation rate *tanψ* with normal stress, for different blocks of medium size sub-samples (L=178mm)

normal stress is at least 4 orders of magnitude lower than the normal stress which eliminates dilation. The variation of dilation rate at peak shear strength with normal stress for medium size blocks (L=178 mm) is shown in Fig. 4.44. The variation is of a logarithmic form, the three blocks (nos. 1,2,4) give quite similar results, whereas the remaining one (no 4), which contained the large dominant asperity, gives systematically higher dilation rates. The difference is about 4°, which can be considered as the effect of the first-order asperity.

The dilation rate becomes equal to that of the same blocks made of CAC which can be considered as "no-damage" shearing, suggests that both for CAC and plaster at a normal stress which is approximately equal to 10^{-4} times the normal stress suppressing all dilation.

4.5.6. Variation of dilation rate with size

The variation with size of the dilation rate is shown in Fig. 4.45 for three different normal stress levels. The lowest corresponds to self-weight direct shear tests at 0.5-1.0 kPa, the second at 24.5 kPa and the third at 125 kPa. A good logarithmic correlation exists for the data at 24.5 kPa and 125 kPa. The best-fit lines define a zero dilation sample length of 0.7 m and 1.5 m respectively, which give the scale-free length L_{cr}, if the assumption that these relations hold at larger sizes is made. The correlation for the data from self weight tests is not as good for the other two stress levels. Both average values from all blocks of each size and values from the blocks which are affected by the large asperity are given. The average values of the two larger sizes and the scale-free block defined by the 24.5 kPa are on the same straight line, which seems to represent reasonably the poor quality data at this stress level. However, the dilation rates obtained for the blocks affected by the large asperity are on the same line which, when extrapolated to zero dilation, defines the same scale-free block size of 0.7 m with the data corresponding to 125 kPa normal stress.

Allowing for experimental error due to the limited number of data points and assuming that the logarithmic relation between the peak rate of dilation and the sample size holds at larger scales, Fig. 4.45 suggests that the scale free-block size is little dependent on normal stress. The values obtained from extrapolation at zero dilation are between 0.7m and 1.5 m for the three stress levels. Therefore, the value of the scale-free block can be estimated from the top line which gives the maximum dilation rates mobilised at different scales. This line can be defined if the profiles at two different scales (for example at laboratory and field sise) are available.

Blocks with length greater than that, will exhibit a purely frictional shear behaviour, as described in Chapter 5.
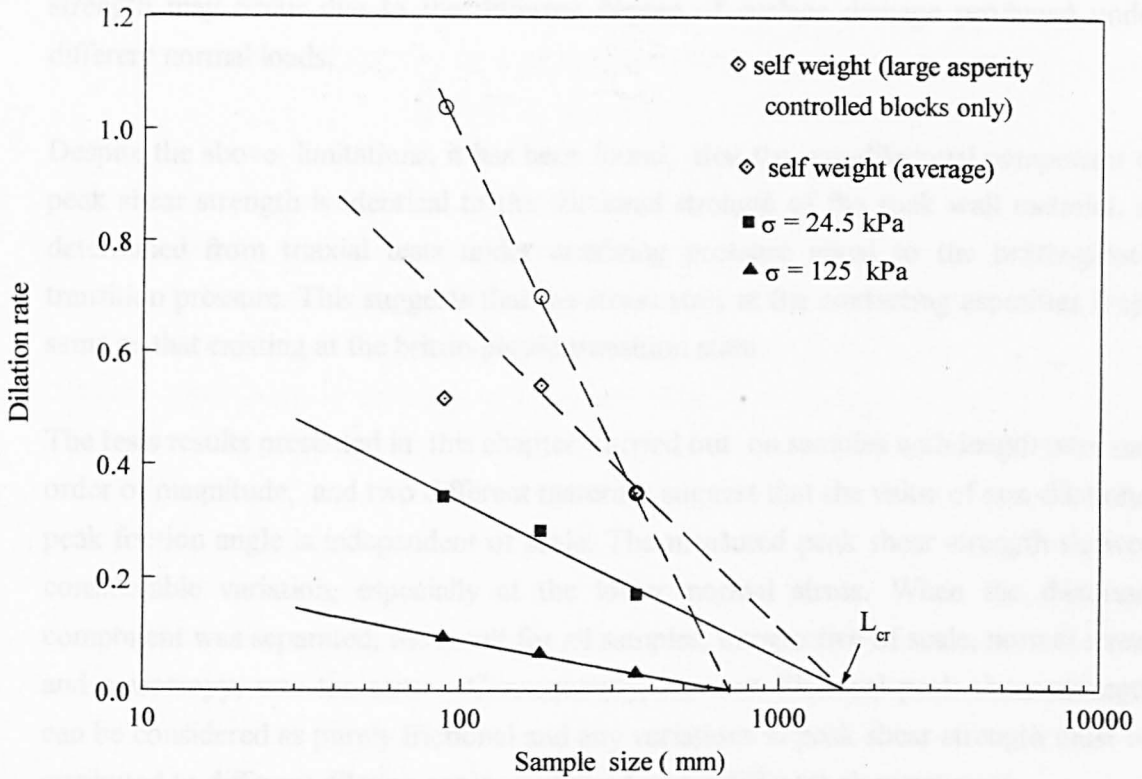
Fig. 4.45. Variation of dilation rate $\tan\psi$ with size, at different normal stress levels

4.6 Concluding remarks

The model material used for this part of the research was proved to be inadequate to represent the frictional behaviour of rock joints with sufficient accuracy. Its friction angle was not consistent, and mechanisms such as reduction of friction angle due the smooth plaster layer formed on the surface or rolling friction due to the weak bonding between the sand particles and the plaster may cause problems in the interpretation of the measured shearing resistance, especially at low normal stresses. The procedure of producing artificial joints by casting against a rubber compound produces smoothly-textured surfaces, due to a surface layer formed by the wet plaster. This exists only up to a shallow depth, whereas the underlying material behaves in a different manner. A difference in friction angle of the order of $10°$ appears to be possible due to this effect. Therefore such surfaces as well as similar surfaces produced by casting against glass, can not give the real friction angle of the material.

The properties of the material are quite variable differing even from one mix to another. Eventually they can not be accurately reproduced. Nominally identical samples may give different peak friction angles both as measured and non-dilational. The reasons for these variations are the strength of the material, the surface smoothness which depends on the number of pores (a result of the degree of compaction) and the surface damage produced on removal of the rubber mould. Variations with normal stress in peak shear

strength may occur due to the different degree of surface damage produced under different normal loads.

Despite the above limitations, it has been found, that the non-dilational component of peak shear strength is identical to the frictional strength of the rock wall material, as determined from triaxial tests under confining pressure equal to the brittle-plastic transition pressure. This suggests that the stress state at the contacting asperities is the same as that existing at the brittle-plastic transition state.

The tests results presented in this chapter, carried out on samples with length over one order of magnitude, and two different materials suggest that the value of non-dilational peak friction angle is independent of scale. The measured peak shear strength showed considerable variation, especially at the lower normal stress. When the dilational component was separated, the result for all samples, irrespective of scale, normal stress and anisotropy, was the same. Consequently, the non-dilational peak shear strength can be considered as purely frictional and any variations in peak shear strength must be attributed to different dilation angles mobilised under different circumstances.

The limited number of data points is not enough to establish an accurate relation between the peak rate of dilation and normal stress, however the results indicate that a logarithmic relation exists and the peak dilation rate tends to zero at a critical normal stress which with the exception of joints with asperities of large scale waviness, is independent of scale.

The experimental results suggest that the scale-free block length obtained from extrapolation of dilation-sample size data is relatively small (for the joint tested less than 2-3 m) and appears to be independent of normal stress. Therefore, it can be estimated from self weight tests or from profiles of samples of different size. This suggestion is based on the results of one single joint surface; other surfaces may exhibit different behaviour, If the conclusion that the effect of scale dies out at small block lengths is generally valid, then natural blocks exceeding this critical length, will exhibit purely frictional behaviour and therefore, the field shear strength can be estimated from the frictional component only, i.e. by ignoring the effect of dilation. However, if large scale undulations exist on the joint surface, then the roughness is expected influence the shear resistance of larger blocks.

CHAPTER 5
A NEW COMPREHENSIVE CRITERION FOR PEAK SHEAR STRENGTH
OF ROCK DISCONTINUITIES

5.1 Introduction

A new, simple, comprehensive peak shear strength criterion for rock joints is proposed. The criterion is derived from experimental results produced in by this study and accurately fits published shear strength data on natural rock joints. It is based on a realistic mechanism of shearing, which is that peak shear strength at any normal stress is the result of two components, one purely frictional, and one dilational. The origin and magnitude of the frictional component are explained by the adhesion theory, whereas the dilational component may be predicted from consideration of surface morphology and normal contact theory. The maximum asperity slope, which is easily determined from surface measurements, is used as the sole parameter to describe roughness. The criterion is developed without reference to empirical parameters but all parameters used are physically meaningful.

5.2. Mechanism of shearing of rough rock discontinuities

In the following analysis only rough fresh, unweathered, uncoated and unfilled joints with unrestricted dilation are considered.

When two rock surfaces are brought together surface roughness causes contact to occur at discrete contact spots. The true contact area is the aggregate of the individual contact spot areas. Deformation occurs in the region of contact spots, establishing stresses which oppose the applied load. The mode of deformation may be either elastic, plastic or mixed elastic-plastic and depends on normal load, surface roughness and material constants (Young's modulus, Poisson's ratio and the hardness). At low normal loads the deformation is elastic, but beyond a certain load plastic flow starts within an asperity, and as the load is increased the zone of plastic flow increases until eventually the entire asperity deforms plastically. Since surface roughness is a random process there will inevitably be some high, sharp asperities which deform plastically even at the lightest loads. Therefore, rough rock surfaces will have some plastically deformed asperities at any normal load. The magnitude of normal load required to cause plastic flow of the rock substance is that which corresponds to brittle-plastic transition. The deformation at this state may be macroscopically plastic, but microscopically brittle fracture occurs as well. Under these circumstances, the adhesion theory originally proposed for metals (Bowden & Tabor, 1950), can be used for friction of rock surfaces.
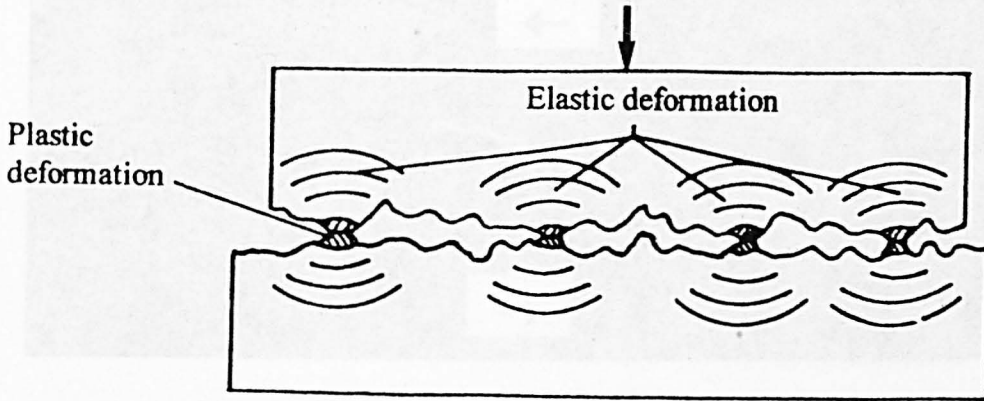
Fig. 5.1: Formation of friction junctions at the regions of real contact
(after Bowden & Tabor, 1973)

In the case of macroscopically flat joints, the regions of contact are under high normal stress and adhered to form "junctions", as shown in Fig. 5.1. The shearing resistance S, will then be

$$S = A_r s \qquad (5.1)$$

where A_r is the area of contact and s the shear strength of junctions.

In the case of macroscopically rough rock joints, upon the application of a normal load, the asperities of opposing rock walls deform, resulting in an area of contact, the magnitude of which depends on the normal stress and the roughness.

As shearing begins, the joint dilates, the contact area decreases and the normal stress increases accordingly until, at the instant of peak shear strength, the regions of real contact reach their brittle-plastic transition stress (Chap. 3.2.3). At this state, the joint ceases to be the weak element and the contacting asperities are adhered together to form junctions. These junctions are now formed on the sides of the asperities. The average slope of these inclined areas, define the mean angle of sliding relative to the shearing direction, i.e. the dilation angle. The plastically deformed areas extend only to a certain depth which depends on the normal stress, whereas the surrounding regions are deformed elastically (Fig. 5.2). At low normal stresses, this depth is small and the inclination of the mean plane of sliding is large, close to the maximum inclination of asperities without any deformation. At high normal stress, where the asperities deform heavily, the inclination will be small. In any case it can be determined from shear and normal displacement measurements. As shearing proceeds, different contact regions are deformed at a different rate, i.e. smaller asperities will deform faster than larger ones, therefore the average sliding angle will continuously change and therefore it must be

(a)

DETAIL A

Brittle-plastic transition state

Elastic deformation

(b)

(c)
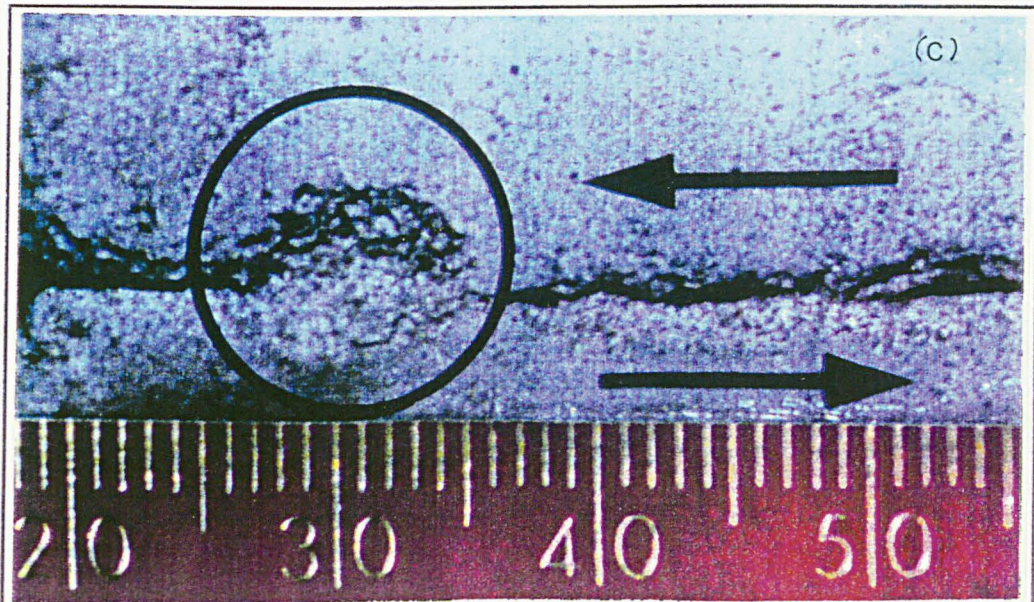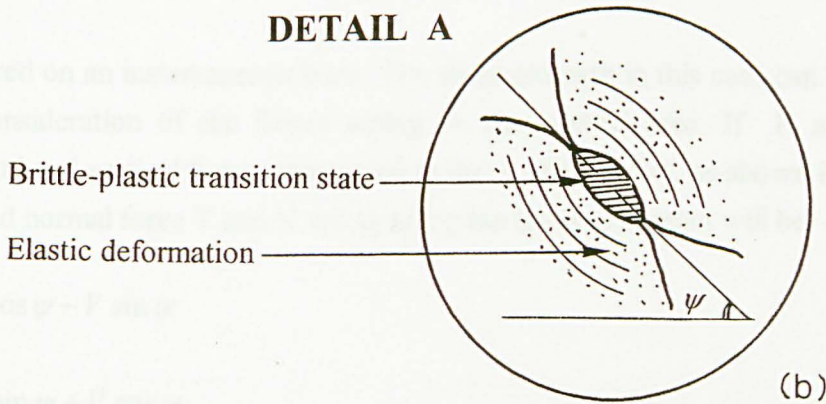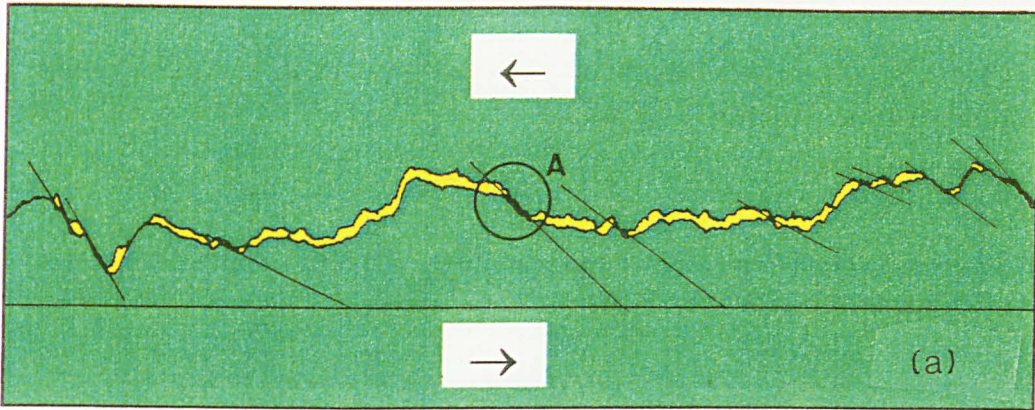
Fig. 5.2 : Deformation of asperities during shearing

(a) contacts with different inclination. (b) detail of an individual contact with assumed brittle-plastic transition state. (c) deformation of a model joint tested under a normal stress of 125 kPa.
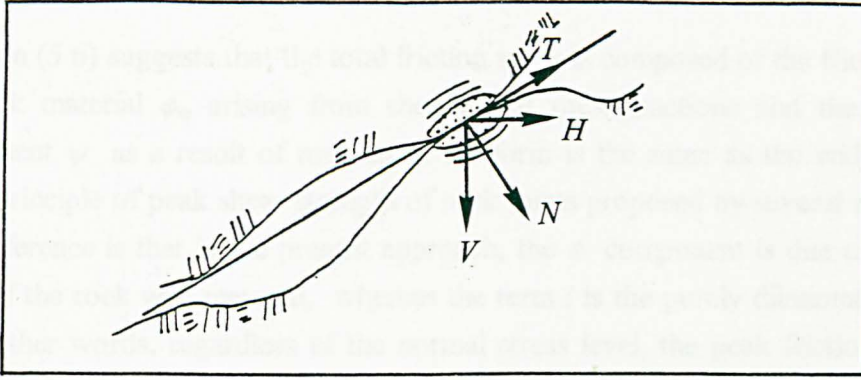
Fig. 5.3: Analysis of forces on an inclined plane

considered on an instantaneous basis. The shear strength in this case can be determined from consideration of the forces acting on the contact area. If H and V are the horizontal and vertical forces (measured in direct shear tests), as shown in Fig. 5.3, the shear and normal force T and N acting along the inclined contact will be:

$$T = H \cos \psi - V \sin \psi$$

$$(5.2)$$

$$N = H \sin \psi + V \cos \psi$$

$$\frac{T}{N} = \frac{H \cos \psi - V \sin \psi}{H \sin \psi + V \cos \psi} \quad (5.3)$$

$$\frac{T}{N} = \frac{\dfrac{H}{V} - \tan \psi}{\dfrac{H}{V} \tan \psi + 1} \quad (5.4)$$

Due to the existing stress state existing on the contacts (brittle-plastic transition stress) the shear strength of the rock material is equal to the frictional strength, thus

$$\frac{T}{N} = \tan \phi_m$$

whereas

$$\frac{H}{V} = \tan \phi_p$$

where $tan\phi_p$ is the measured peak coefficient of friction. Therefore, equation (5.4) gives

$$\tan \phi_p = \frac{\tan \phi_m + \tan \psi}{1 - \tan \phi_m \tan \psi} = \tan(\phi_m + \psi) \quad (5.5)$$

or

$$\phi_p = \phi_m + \psi \qquad\qquad (5.6)$$

Equation (5.6) suggests that the total friction angle is composed of the friction angle of the rock material ϕ_m arising from shearing of rock junctions and the geometrical component ψ as a result of roughness. Its form is the same as the widely accepted "$\phi+i$" principle of peak shear strength of rock joints proposed by several investigators. The difference is that in the present approach, the ϕ component is due to the friction angle of the rock wall material, whereas the term i is the purely dilational component ψ. In other words, regardless of the normal stress level, the peak friction angle of a rock joint is the sum of the friction angle of the rock wall material, plus the dilation angle. The friction angle ϕ_m is higher than that of a saw-cut. The peak shear strength will be given by the formula

$$\tau_p = \sigma_n \ tan(\phi_m + \psi) \qquad\qquad (5.7)$$

where

τ_p is the peak shear strength

σ_n the effective normal stress

ϕ_m the friction angle of the rock wall material and

ψ the dilation angle at the instant of peak shear strength

It is emphasised that this relation is valid over the whole range of normal stress. At low normal stress, the dilation angle will be high and the area and the number of contacts small. As apparent normal stress increases, so the area and the number of contact increases, and a larger total area reaches the brittle-plastic state.

5.3 The frictional component of peak shear strength

The *brittle-plastic transition pressure* is the confining pressure at which friction along the sliding surface is equal to the shear strength of intact rock (Orowan 1960, Byerlee 1967). Accordingly, the fracture envelope of the rock material and the envelope of frictional strength are intersected at the normal stress σ_T which corresponds to the brittle ductile transition state. Since at this high normal stress joints are not the weak elements, their shear strength envelope will pass through the same point. Above this stress, dilation is zero and the shear strength of the joint coincides with that of the intact material. If this transition stress is known, the friction angle of the joint can be found from the shear strength envelope of the intact rock (Fig. 5.4).

The shear strength of the rock material can be determined by any of the existing criteria, some of which have been described in Chapter 3.2. If, for simplicity, the parabolic criterion described in Chap. 3.2 (Fairhurst, 1964) is used
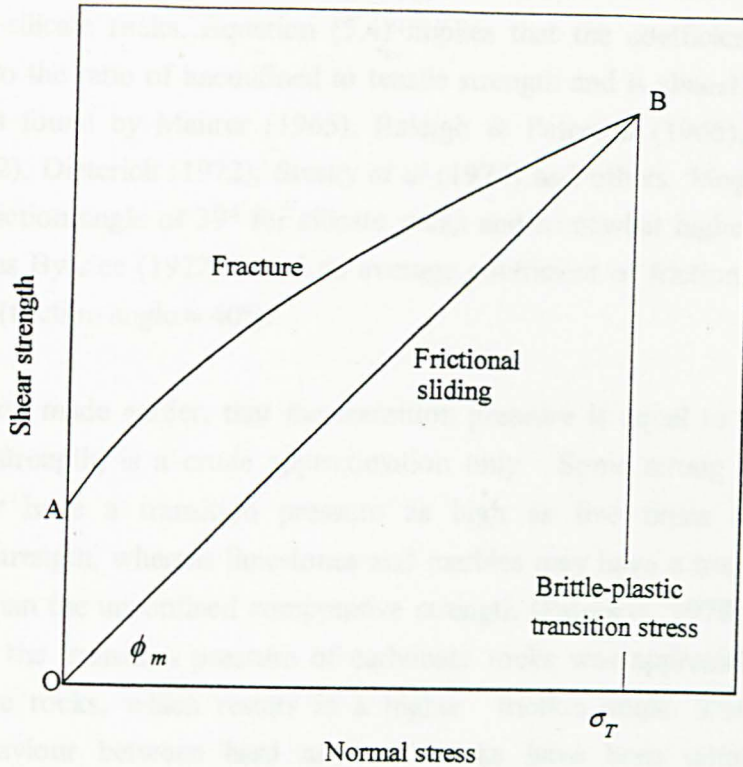
Fig. 5.4: Shear strength and frictional strength of intact rock

$$\tau_r = C_o \frac{(\sqrt{1+n}-1)}{n}\sqrt{(1+n\frac{\sigma_n}{C_o})} \tag{5.8}$$

and, at first approximation, the transition pressure is considered to be equal to the unconfined compressive strength, as proposed by Ladanyi & Archambault (1970), Goodman (1976), Franklin & Dusseault (1989) and others, equation (5.3)

$$\mu_m = \frac{\sqrt{1+n}-1}{n}\sqrt{1+n} \tag{5.9}$$

where μ_m is the coefficient of friction of the rock material.

The friction coefficient μ_m ranges from 0.71 ($\phi_m = 35.4°$) when $n = 5$, to 0.91 ($\phi_m = 42.3°$) for $n = 100$. For an average ratio of compressive to tensile strength $n = 15$, the coefficient of friction is $\mu_m = 0.8$ ($\phi_m = 38.7°$). Using the summarised data given by Kulhawy (1976) for several rock types, equation (5.9) produces the results shown in Table 5.1. An average material friction angle for all rock types is equal to $\phi_m = 39.2°$. This value is in a remarkable agreement with a friction angle 39° at the brittle-plastic transition found by Mogi (1966) for a number of silicate rock types. Therefore

Fairhurst's criterion appears to give a good prediction of the friction angle of the material, for silicate rocks. Equation (5.4) implies that the coefficient of friction is related only to the ratio of unconfined to tensile strength and is almost independent of rock type, as found by Maurer (1965), Raleigh & Paterson (1965), Mogi (1966), Byerlee (1972), Dieterich (1972), Stesky et al.(1974) and others. Mogi (1966) found an average friction angle of 39° for silicate rocks and somewhat higher for carbonate rocks, whereas Byerlee (1972) found an average coefficient of friction for many rock types of 0.85 (friction angle ≈ 40°).

The assumption made earlier, that the transition pressure is equal to the unconfined compressive strength, is a crude approximation only. Some strong rocks, such as granites, may have a transition pressure as high as five times the unconfined compressive strength, whereas limestones and marbles may have a transition pressure much lower than the unconfined compressive strength (Paterson, 1978). Mogi (1966) observed that the transition pressure of carbonate rocks was appreciably lower than that of silicate rocks, which results in a higher friction angle. The difference in frictional behaviour between hard and soft rocks have been noticed in sliding experiments by many investigators, including Patton (1966a), Hoskins et al. (1968), Coulson (1970), Ohnaka (1975) and Scholz & Endelger (1976).

Table 5.1: Average friction angles for different rock types determined by equation (5.9)

ROCK TYPE	Compres. strength (MPa)	Tensile strength (MPa)	Compressive/ tensile strength	μ_m	φ_m (°)	Average φ_m (°)
1.Igneous						
Plutonic	145.4	9.1	15.09	0.81	38.8	
Volcanic	123.9	9.0	13.77	0.79	38.4	38.6
2.Metamorhic						
Non-foliated	150.0	5.6	25.79	0.84	40.0	
Foliated	79.6	7.5	10.61	0.77	37.7	38.9
3.Sedimentary						
Clastic	95.3	3.0	32.10	0.85	40.4	
Chemical	88.1	3.9	22.59	0.83	39.7	40.0
Average	114.1	5.4	20.32	0.81	39.2	39.2
St. Deviation	30.37	2.60	8.26	0.03	1.04	0.75

The actual transition pressure can be determined experimentally from triaxial tests under different confining pressures. The pressure at which the frictional strength becomes equal to the shear strength corresponds to the brittle-plastic state. However, the shear strength of some rocks such as granite and quartzite is so high that often exceeds the friction at the maximum confining pressure that can be applied in most laboratories and the transition from brittle to plastic failure can not be produced.

A compilation of published data on brittle-plastic transition for a number of rock types is given in Table 5.2. Friction angles and transition stresses have been determined from more than 110 data sets from triaxial tests on 26 different rock types where the confining pressure was sufficiently high to produce a brittle-plastic state. The friction angles range from 14° to 55°, depending on the rock type. Lack of sufficient number of tests from each set does not allow an accurate determination of the transitional state, so the values shown must be used as approximate. Increased reliability is obtained where a larger number of data of the same lithological type exists. The values given in Table 5.2.b were produced on this basis and correspond to rock types with 5 or more data sets, excluding shale, because of its unusual behaviour (Maurer, 1965, Mogi, 1966). It becomes evident that for carbonate rocks (dolomite, limestone and marble) the friction angle is well within 41.5° and 43° with an average value of 42°. On the other hand the average values obtained for silicate rocks (sandstones and granites) are in the range 32°-34°. The average value for the seven rock types shown in Table 5.2b is 39°. This value is in good agreement with that of 40° found for a number of different rock types by Byelee (1978), who concluded that friction angle has little or no dependence on rock type. The results shown in Table 5.2 suggest that friction angles depend on rock type and clearly that carbonate rocks have higher friction angles than silicate. However, with the exception of some low friction rocks such as chlorite, graphite and talc which may have friction angles lower than 20° and rock salt for which a very high value (55°) was obtained, friction angles are in the range 30° - 43°. The transition stress is between $0.80C_o$-$1.4C_o$ for carbonate rocks and $3.1C_o$-$5.2C_o$ for silicates, where C_o is the unconfined compressive strength. Therefore the assumption made often that the transition stress is approximately equal to the unconfined compressive strength of the rock (Ladanyi & Archambault, 1970, Goodman, 1976 etc.) is reasonable for carbonates but not for silicates.

It must be born in mind that these values have been derived from triaxial tests on fresh rocks, thus they may not be valid for weathered rocks, which are expected to have lower values.

Table 5.2: Approximate transition stress and friction angle for various rock types

No	Rock type	No of values	Mean σ_T (MPa)	Estimated Friction angle (°) range	Estimated Friction angle (°) mean	Ratio σ_T/C_o range	Ratio σ_T/C_o mean	References
1	Andesite	1	165	-	43.2	-	1.5	1
2	Anhydrite	3	185	33.9-41.8	38.6	2.1-2.4	2.2	2,3,4
3	Basalt	1	420	-	37.6	-	2.3	5
4	Chalk	4	9.5	37.9-39.5	36.7	0.9-2.4	1.5	6,7
5	Chlorite	2	375	16.9-20.9	18.9	5.9	5.9	8,9
6	Claystone	4	84	32.0-37.2	34.1	1.3-2.2	1.8	10
7	Dolomite	5	234	39.7-44.9	41.5	0.3-2.0	1.3	4,11
8	Dunite	2	940	37.9-40.3	39.1	3.1-8.5	5.6	12,13
9	Eclogite	1	3020	-	31.2	-	15.1	12
10	Gabbro	2	821	29.2-33.4	31.3	1.9-5.4	3.6	12,13
11	Granite	5	1243	27.7-37.3	32.0	3.3-6.8	5.2	13,14,15,16,17
12	Graphite	1	135	-	22.0	-	-	18
13	Gypsum	1	53	-	30.2	-	1.1	9
14	Limestone	17	138	34.6-48.6	41.6	0.4-4.0	1.4	3,4,13,18,19,20,21, 22,23,24,25,26
15	Liparite	2	160	38.4-40.5	39.4	1.3-2.1	1.7	10
16	Marble	11	64	39.9-45.7	42.9	0.5-1.1	0.8	1,11,18,24,27,28,29
17	Marl	1	22	-	34.6	-	2.2	22
18	Quartzite	1	952	-	35.9	-	2.8	30
19	Rock salt	2	55	48.8-61.2	55.0	0.3-0.8	0.6	31,32
20	Sandstone	20	186	26.2-41.6	34.2	1.8-4.1	3.1	4,10,18,19,27,33, 34,35,36,37
21	Serpentinite	5	441	33.1-45.6	37.7	1.3-4.3	2.5	9,38,39
22	Shale	11	200	25.2-38.4	32.1	1.2-7.6	2.9	3,4,10
23	Siltstone	2	214	22.5-36.6	29.5	1.7-2.1	1.9	4,10
24	Talc	1	240	-	14.0	-	-	18
25	Trachyte	1	59	-	40.5	-	-	1
26	Tuff	8	53	38.3-52.5	43.2	0.8-1.9	1.2	1,10

σ_T is the brittle-plastic transition stress determined from the principal stresses σ_1 and σ_3 as shown in Figure 2.13 (page 27)

C_o is the unconfined compressive strength

Table 5.2a.: Sources of data in Table 5.2

1	Mogi (1965)	2	Muller & Siemes (1974)	3	Bredthauer (1957)
4	Handin & Hager (1957)	5	Shimada (1986)	6	Siwak et al.(1993)
7	Loe et al. (1992)	8	Murphy (1971)	9	Murrell & Ismail (1976)
10	Hoshino et al. (1972)	11	Mogi (1971)	12	Shimada et al. (1983)
13	Byerlee (1968)	14	Bergues et al. (1974)	15	Ryabinin et al.(1971)
16	Shimada (1981)	17	Tullis & Yud (1977)	18	Edmond & Paterson(1972)
19	Blanton (1981)	20	Bernaix (1967)	21	Elliot (1982)
22	Price (1979)	23	Chitty & Blouin (1992)	24	Friedrich et al. (1990)
25	Mogi (1972)	26	Robertson (1955)	27	von Karman (1911)
28	Mogi (1964)	29	Paterson (1958)	30	Hadizabeh et al. (1983)
31	Handin (1953)	32	Campos de Orellana(1996)	33	Friedman & Logan (1973)
34	Murell (1965)	35	Stavropoulou (1988)	36	Shock et al. (1973)
37	Gowd & Rummel(1980)	38	Raleigh & Paterson (1965)	39	Rummell et al (1978)

Table 5.2b. Friction angle and transition stress for rock types of Table 5.2
with more than 5 data sets

No	Rock type	No of values	Estimated friction angle (°)		Transition stress σ_T (MPa)		Ratio σ_T/C_o	
			mean	st. dev.	mean	st. dev.	mean	st. dev.
1	Dolomite	5	41.5	2.1	234	109	1.3	0.7
2	Limestone	17	41.6	4.0	138	77.3	1.4	1.1
3	Marble	11	42.9	2.1	64	20.5	0.8	0.2
4	Granite	5	32.0	3.4	1243	492	5.2	1.9
5	Sandstone	20	34.2	3.3	186	110	3.1	0.6
6	Serpentinite	5	37.7	4.8	441	163	2.5	1.3
7	Tuff	8	43.2	4.3	89.3	52.3	1.2	0.4
	AVERAGE		39.0	4.5				

Transition pressure decreases with porosity. Correlations between transition pressure and porosity of some sandstones are given by Scott & Nielsen (1991), Logan(1987) and Wong (1990).

The use of Fairhurst's equation for an estimate of friction angle is satisfactory for many rock types, when the transition stress is taken equal to the unconfined compressive strength. However, when the transition pressure is appreciably higher or lower than the unconfined compressive strength, this equation fails to make accurate predictions. For example, for the synthetic rock used in this study, which had a ratio of unconfined compressive to tensile strength equal to 11, Fairhurst's equation predicts $\mu_m = 0.78$ ($\phi_m = 38°$), which is much below the measured value (46°). However, if the same equation is used not with the unconfined compressive strength but with the actual transition stress, it predicts a value of 43° approximately, for the friction angle of the rock material which is closer to the measured value of 46°. When the transition stress is much higher than the unconfined compressive strength, the predictions are unrealistically low.

The empirical criterion proposed by Hoek & Brown (1980), may provide a little better estimate of the friction angle. The criterion is expressed as

$$\sigma_1 = \sigma_3 + \sqrt{m\sigma_c\sigma_3 + s\sigma_c^2} \tag{5.10}$$

where σ_c is the uniaxial compressive strength of intact rock, m is an empirical constant that depends upon rock type and rock conditions, and σ_1 and σ_3 denote the maximum and minimum principal stresses. The parameter m is a measure of the inclination of the $\sigma_1 - \sigma_3$ envelope near the σ_1 axis and values for a number of rock types have been published by Hoek et al. (1992) and Hoek (1994b). A correlation between the friction angle ϕ_m given in Table 5.2 and the parameter m is given in Fig. 5.5. It can be seen that, with the exception of claystone and siltstone, all other rock types fall within a narrow band. A curved line has been fitted to the data, which is described by the equation

$$\phi_m = 69.2m^{-0.225} \tag{5.11}$$

The adhesion theory provides an explanation of the fact that friction coefficient is quite similar for a wide range of different rock types. The friction coefficient is given by equation (3.13)

$$\mu = s / p$$
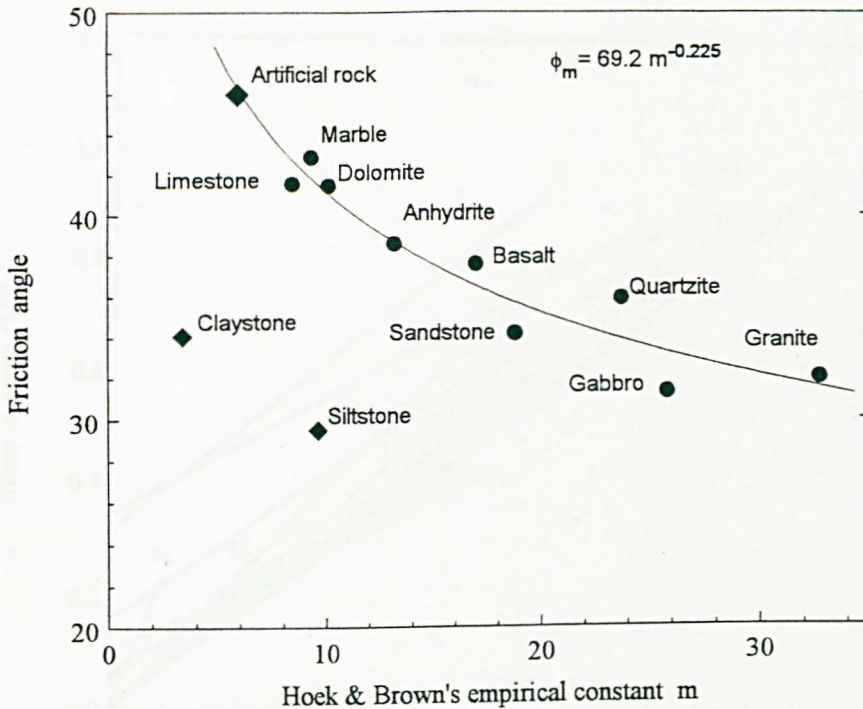
Fig. 5. 5: Relation between estimated friction angle and Hoek & Brown's parameter m

Both s (shear strength) and p (penetration hardness) are very similar quantities depending in almost the same way on such properties of the materials as bond strength, nature of dislocations etc. (Rabinowicz, 1995). Thus, materials with quite different values of s and p have nearly the same ratio of these quantities. Rabinowicz (op. cit.) mentioned the case of two metals (lead and low carbon steel) which vary by nearly a factor of 100 in shear strength and penetration hardness, but the coefficient of friction, representing the ratio of these two quantities, is nearly the same for steel (1.0) as is for lead (1.2). This may offer the explanation for observing quite similar friction coefficients for most rocks. The average value of 0.80 which is supposed to be a mean representative value for rocks, is also typical for contacts between identical unlubricated metal surfaces (Rabinowicz, 1995).

From the above analysis and the values given in Table 5.2b, it is clear that an average friction angle for some common rock types is 39°. This means that joints in fresh rock, if they do not exhibit any dilation will have an average friction angle of this magnitude and a shear strength envelope described by the 39° friction angle will be a typical lower bound for shear strength of unwethered rock joints. Baldovin (1970) carried out direct shear tests on joints from 20 different, mainly weak rocks, under normal stresses in the range 0-1 MPa. When contacts having the same rock type in both sides are considered, all the contacts define a lower bound of 39°. Similarly, Gianni (1992) presented data from several rock types, including some weak ones (Fig. 5.6).
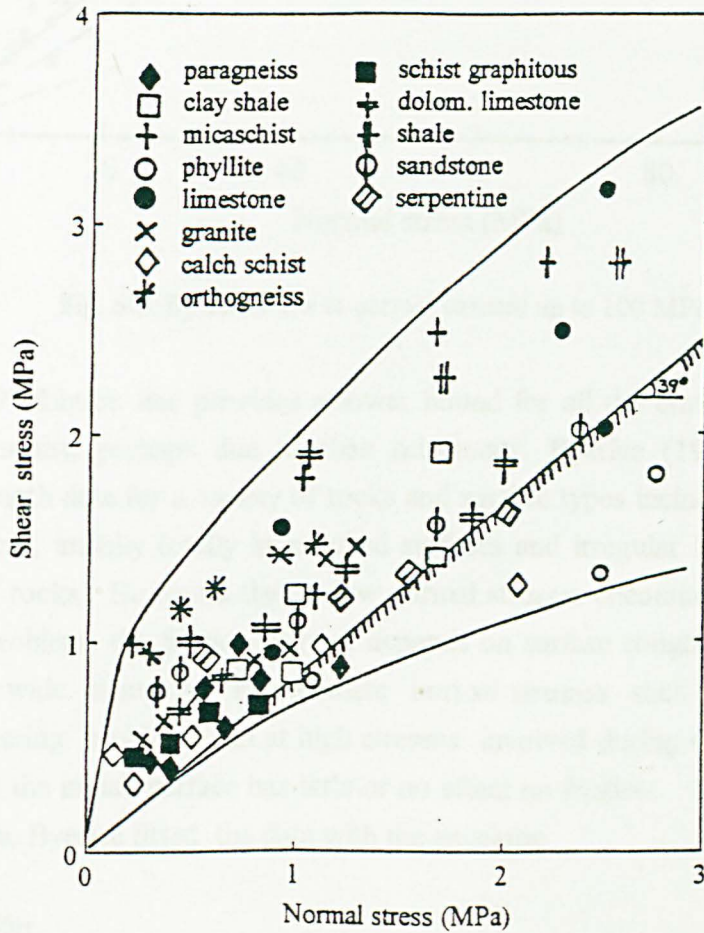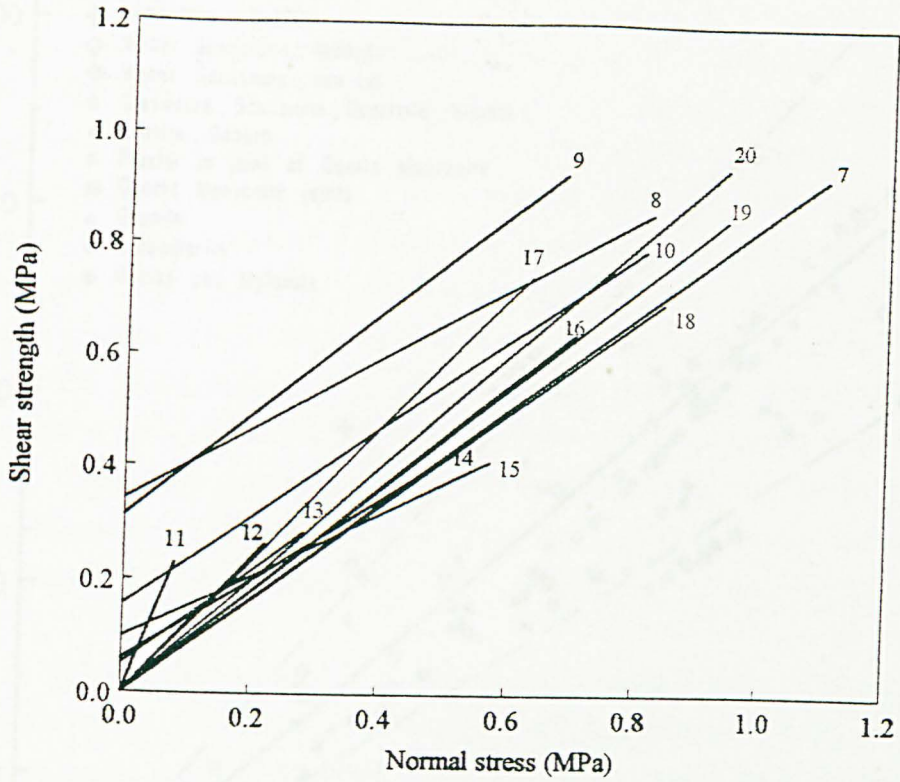
Fig. 5.6: Peak shear strength envelopes for a number of different rock contacts

(a) after Baldovin (1970)   (b) after Giani (1992)
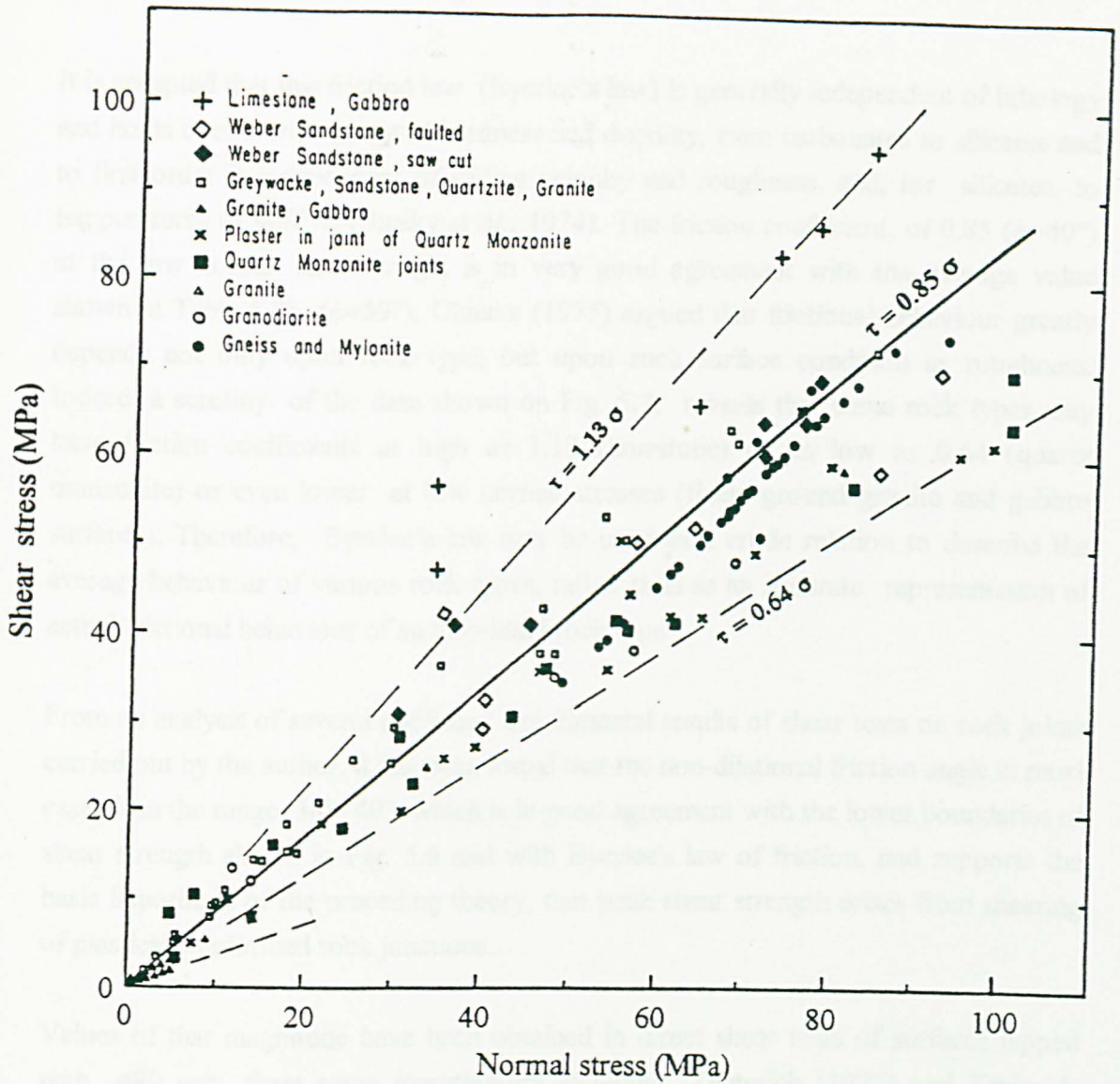
Fig. 5.7: Byerlee's law at normal stresses up to 100 MPa

Again, the 39° friction line provides a lower bound for all the envelopes, except for phyllite and schist, perhaps due to their schistosity. Byerlee (1978) summarised frictional strength data for a variety of rocks and surface types including initially finely ground surfaces, initially totally interlocked surfaces and irregular faults produced in initially intact rocks. He found that at low normal stresses encountered in most civil engineering problems the friction of rock depends on surface roughness and can vary between very wide limits. At intermediate normal stresses such as encountered in mining engineering problems and at high stresses involved during sliding on faults in the deep crust the initial surface has little or no effect on friction. At normal stresses up to 200 MPa, Byerlee fitted the data with the envelope

$$\tau = 0.85\sigma \tag{5.11}$$

It is accepted that this friction law (Byerlee's law) is generally independent of lithology and holds over a wide range of hardness and ductility, from carbonates to silicates and to first order is independent of sliding velocity and roughness, and, for silicates, to temperatures of 400° C (Stesky *et al.*, 1974). The friction coefficient, of 0.85 ($\phi=40°$) at the low normal stress range, is in very good agreement with the average value shown in Table 5.2b. ($\phi\approx39°$). Ohnaka (1975) argued that frictional behaviour greatly depends not only upon rock type, but upon such surface condition as roughness. Indeed, a scrutiny of the data shown on Fig. 5.7, reveals that some rock types may have friction coefficients as high as 1.13 (limestone) or as low as 0.64 (quartz monzonite) or even lower at low normal stresses (finely ground granite and gabbro surfaces). Therefore, Byerlee's law may be used as a crude relation to describe the average behaviour of various rock types, rather than as an accurate representation of actual frictional behaviour of an individual rock type.

From an analysis of several published experimental results of shear tests on rock joints carried out by the author, it has been found that the non-dilational friction angle in most cases is in the range 38°- 40°, which is in good agreement with the lower boundaries of shear strength shown in Fig. 5.6 and with Byerlee's law of friction, and supports the basic hypothesis of the preceding theory, that peak shear strength arises from shearing of plastically deformed rock junctions.

Values of that magnitude have been obtained in direct shear tests of surfaces lapped with #80 grit from some investigators including Dieterich (1972) and Krahn & Morgenstern (1976), but Ripley & Lee (1962) demonstrated that the non-dilational friction angle is higher than that obtained from sand-blasted surfaces (see Table 3.5) .

5.5 The dilational component of shear strength

The frictional term in equation 5.7 has been defined and its origin explained. It now remains to determine and explain the dilational term ψ, at any normal stress level, so that a full criterion for peak shear strength can be developed.

Consider an individual asperity with a base-length equal to $2L$ (Fig. 5.8a). Under a certain normal stress σ_n, the asperity will deform and a total normal deformation (closure) equal to d will take place. Assuming that the highest point B will be normally displaced by δ (Fig. 5.8b) whereas the lowest point will remain in place, sliding will then occur along the plane AB', inclined at an angle ψ to the horizontal, which will be equal to the instantaneous measured dilation angle.

From the simplified geometry of deformation shown in Fig 5.8b, the closure δ can be expressed as

$$\delta = L(\tan \psi_o - \tan \psi) \tag{5.12}$$

It is assumed that the distribution of peaks of the rock surface is of exponential form, and according to the model proposed by Greenwood & Williamson (1966) - see Chap. 3.3.5-

$$\delta = A + B \ln \sigma$$

or

$$L(\tan \psi_o - \tan \psi) = A + B \ln \sigma \tag{5.13}$$

and

$$\tan \psi = \tan \psi_o - C - D \ln \sigma_n \tag{5.14}$$

where

$C=A/L$,

$D=B/L$ and

$2L$ the base length of the asperity.

When the normal stress is small enough to guarantee that deformation of asperities will be negligible,

$\sigma_n = \sigma_{no} \rightarrow 0$,

$\tan \psi \approx \tan \psi_o$

where ψ_o is the maximum asperity angle before any deformation of the initial surface and equation (5.14) becomes:
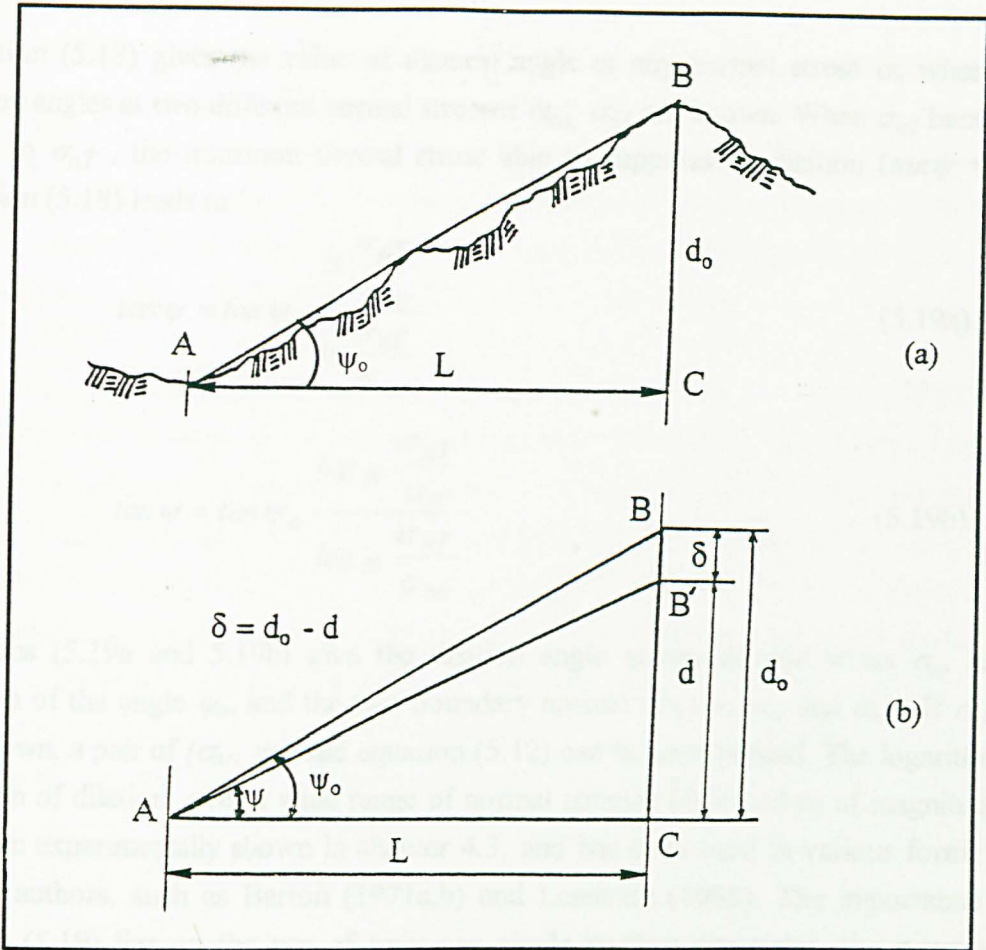
Fig. 5.8 Simplified geometry of asperity deformation

$$C = -D \ln \sigma_{no} \tag{5.15}$$

The value of σ_{no} can not be equal to zero but to a minimum "seating pressure" (Goodman, 1976), for example 1 kPa. The constant D can be obtained if the dilation angle $\psi = \psi_1$ at a normal stress σ_{n1} is known. In this case the relations (5.14) and (5.15) give

$$\tan \psi_1 = \tan \psi_o + D(\ln \sigma_{no} - \ln \sigma_{n1}) \tag{5.16}$$

or

$$D = \frac{\tan \psi_o - \tan \psi_1}{\ln \dfrac{\sigma_{n1}}{\sigma_{no}}} \tag{5.17}$$

Equation (5.14) then becomes

$$\tan \psi = \tan \psi_o + (\tan \psi_1 - \tan \psi_o) \frac{\ln \dfrac{\sigma_{n1}}{\sigma_n}}{\ln \dfrac{\sigma_{n1}}{\sigma_{no}}} \tag{5.18}$$

Equation (5.18) gives the value of dilation angle at any normal stress σ_n when the dilation angles at two different normal stresses σ_{no}, σ_{n1} are known. When σ_{n1} becomes equal to σ_{nT}, the transition normal stress able to suppress all dilation ($tan\psi = 0$), equation (5.18) leads to

$$tan\,\psi = tan\,\psi_o \frac{\ln \dfrac{\sigma_{nT}}{\sigma_n}}{\ln \dfrac{\sigma_{nT}}{\sigma_{no}}} \qquad (5.19a)$$

or

$$tan\,\psi = tan\,\psi_o \frac{\log_{10} \dfrac{\sigma_{nT}}{\sigma_n}}{\log_{10} \dfrac{\sigma_{nT}}{\sigma_{no}}} \qquad (5.19b)$$

Relations (5.19a and 5.19b) give the dilation angle at any normal stress σ_n, as a function of the angle ψ_o, and the two boundary normal stresses σ_{no} and σ_{nT}. If σ_{nT} is not known, a pair of (σ_{n1}, ψ_1) and equation (5.12) can be used instead. The logarithmic variation of dilation over a wide range of normal stresses (four orders of magnitude), has been experimentally shown in chapter 4.3, and has been used in various forms by several authors, such as Barton (1971a,b) and Leichnitz (1985). The importance of relation (5.19) lies on the use of only one single surface parameter, the maximum asperity slope, which can be directly measured for any surface, to determine dilation angle at any given normal stress. The strong correlation of the asperity angle with shear strength has been stressed by several authors including Myers (1962), Tabor (1975) and Koura & Omar (1981).

The angle ψ_o is the dilation angle of a rock joint when all the roughness is mobilised (negligible surface damage), and can be obtained from a shear test under nominally zero normal loading conditions. It is a physical parameter used in constitutive laws of shearing of rock joints (Plesha, 1987, Qiu et al., 1993) and can be most satisfactorily determined by surface measurements on the actual joint samples. Methods employing photogrammetric techniques (Ross-Brown et al., 1973, Patton, 1966a), profilometer (Fecker, 1970, Rengers, 1970) can be used to provide an appropriate value of ψ_o. The value of this angle depends on the base-length over which is calculated and a problem arising from this is the magnitude of the base length to be used for the determination of the angle ψ_o. Measurements on second order (base length 0.2%L) joint asperities made by Patton (1966a) indicated a typical range of values between 10° and 46°, although values up to 60° might be expected, especially for tensile fractures (Barton, 1973, Barton & Choubey, 1977, Selby 1987, Aydan & Kawamoto, 1990 etc.), at laboratory scale. It appears that this base length is appropriate, for small scale roughness and has been used throughout in this study. Rengers' (1970) method for calculating the slope

angle envelopes provides information, which is approximately equivalent to that obtained by performing a shear test under a very low normal stress which causes no asperity damage (Swan & Zongqi, 1985). This method has been used by Schneider (1976) and adopted for the experimental programme conducted in this study. The value of $tan\psi_o$ was obtained from the normal displacement-shear displacement diagram for a shear displacement step-size equal to 0.2% of the sample length.

Several authors including Ladanyi & Archambault (1970) and Barton (1971a,b) suggested that the normal stress able to suppress all dilation, σ_{nT}, is equal to the unconfined compressive strength of the rock wall, and this has been incorporated in their models. Goodman (1974) stated that this stress is of the order of the unconfined compressive strength of the rock wall material. The experimental data of the present study indicate that the dilation is fully suppressed at a much lower normal stress, i.e. when the normal stress is approximately 3.8 MPa which is less than 10% of the unconfined compressive strength. It is believed that this normal stress is related to the real area of contact and to the plastic deformation of asperities and it is inappropriate to equate or even correlate with the compressive strength. Rather it should be related to the brittle-plastic transition stress.

Assuming that the logarithmic variation of $tan\psi$ with normal stress over four orders of magnitude, found for the experimental data of this study is general, i.e. $\sigma_{no} = 10^{-4}\sigma_{nT}$ equations (5. 19a, b) then become

$$tan\psi \approx \frac{tan\psi_o}{9.21}ln\frac{\sigma_{nT}}{\sigma_n}$$
(5.20a)

or

$$tan\psi = \frac{tan\psi_o}{4}log_{10}\frac{\sigma_{nT}}{\sigma_n}$$
(5.20b)

For normal stress above σ_{nT}, the peak shear stress is proportional to normal stress until the brittle-plastic transition stress, , i.e.

$$\tau = \sigma_n\, tan\,\phi_m$$
(5.21)

Beyond the brittle-plastic transition stress, the shear strength of the joint is equal to that of the intact rock material.

At very low normal stresses and high values of ψ_o equations 5.19a and 5.19b tend to infinity. For practical purposes the suggestion of Barton (1973) to use a total peak

friction angle of 70° can be adopted. Typical families of curves for different parameters of the new criterion is shown in Fig. 5.9.

The data shown in Chapter 4.5.6 suggested that the geometrical component of shear strength diminishes when the size of the sample approaches a critical value of a few meters. If this is generally true, then the field shear strength of rock blocks larger than this critical value can be considered as frictional only and predicted by equation (5.21). This conclusion is supported by the results of back-analyses of failed slopes published by several authors including Krahn & Morgenstern (1976) and McMahon (1985).

5.6 Transition from dilational to pure frictional sliding

The experimental data of this work show that dilation becomes zero when the apparent normal stress is about 3.8 MPa, i.e. at normal stresses in excess of 3.8 MPa roughness has no effect on shear strength. Zero dilation implies that all critical asperities have reached their transitional state. This value of σ_{nT} may be representative for some soft and weak rocks, with a behaviour similar to that of the artificial rock used in this study, but for harder rocks is expected to be higher.

Proportionality between normal stress and real area of contact gives

$$\frac{A_r}{A} = \frac{\sigma_{nT}}{\sigma_T} = \frac{3.8}{34} \approx 0.10$$

The joints tested here had a maximum roughness angle in the range of 20°- 40°, and the value of σ_{nT} appeared to be independent of roughness. Most natural joints are of similar roughness and if this 10% "rule of thumb" holds, then some strong rocks, such as granite, with a transition pressure of the order of 1000 MPa or higher, will be expected to have σ_{nT} values of the order of 100 MPa, whereas most rocks, with a transition stress in the range 100-200 MPa, will be expected to have a zero-dilation normal stress σ_{nT} between 10 and 20 MPa.

Analyses of experimental results of natural joints are in agreement with this argument. It has been shown in Chapter 4 that σ_{nT} is independent of scale. However, in cases where large scale asperities dominate the behaviour of the joint, higher stress is required to bring it to a plastic state, and as a result of this, the values of σ_{nT} will be higher.

In cases where the joint is mated and asperities are locked, dilation is prevented partly or fully, the contact area is large and the formation of plastic junctions is not possible.
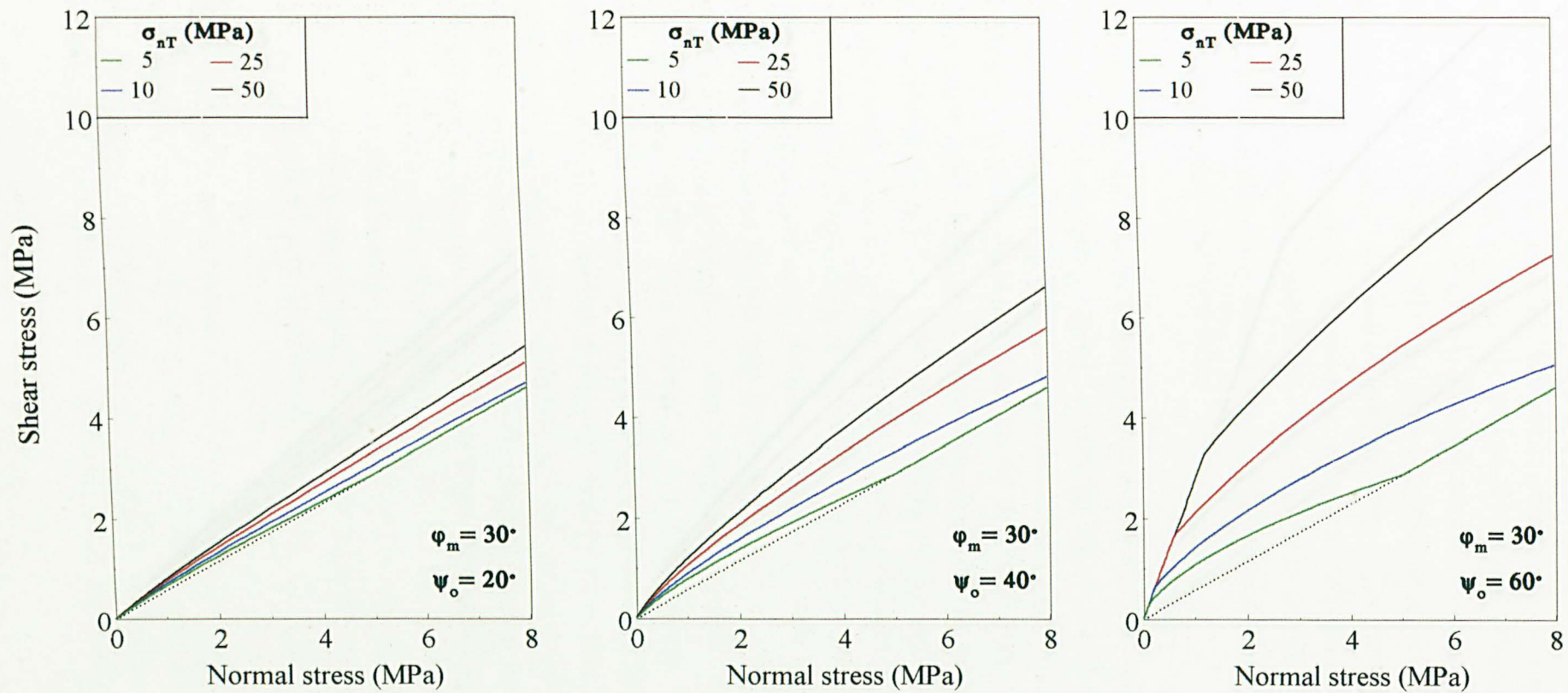
Fig. 5.9a : Typical families of curves for different parameters of the new criterion ($\phi_m = 30°$)
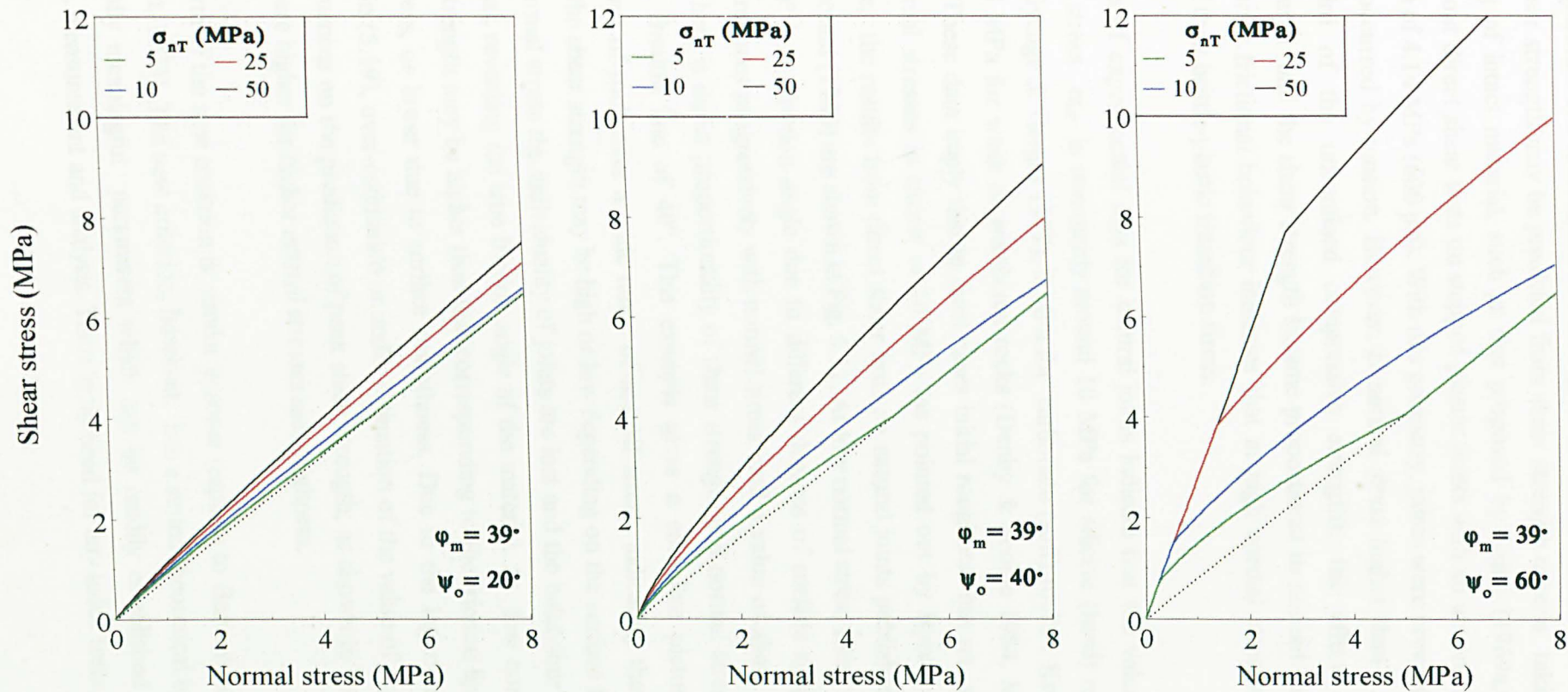
Fig. 5.9b : Typical families of curves for different parameters of the new criterion ($\phi_m = 39°$)

In this case the peak shear strength will be due to deformation or shearing through of large asperities. The mechanism of shearing described in Chapter 5.2 does not operate, and shear strength may be predicted from shear strength criteria taking into account shearing of intact material, such as that proposed by Lajtai (1969a,b). This author carried out direct shear tests on stepped plaster joints with an unconfined compressive strength of 4.14 MPa (600 psi). With this geometry, joints were prevented to dilate and failure occurred by tension. However, at normal stress higher than 1.4 MPa (about one third of the unconfined compressive strength), the effect of interlocking disappeared and the shear strength became proportional to normal stress (Fig. 5.10). This purely frictional behaviour indicates that at high normal stresses, the asperities reached their brittle-plastic transition stress.

Analysis of experimental data for natural joints indicate that the value of the critical normal stress σ_{nT} is commonly around 10 MPa for silicate (hard) rocks (Leichnitz, 1985, Gyenge & Herget 1977), 5 MPa for carbonate (soft) rocks (Krsmanovic 1967) and 2-3 MPa for weak or weathered rocks (Denby & Scoble 1984, Martin & Millar, 1974). These data imply that in most cases initial roughness has no significant affect for normal stresses in excess of 10 MPa (as pointed out by Byerlee 1978). As an example, the results from direct shear tests on natural joints published by Yamaguchi & Shimotani (1986) are shown in Fig. 5.11. At low normal stress there is a wide scatter (20°-60°) in friction angle due to different degrees of surface roughness, but this scatter reduces progressively with normal stress until a value of about 8 MPa, beyond which there is direct proportionality of shear strength and normal stress, and uniquely defined friction line of 40°. This example gives a complete picture of the shear behaviour of rock over a wide range of normal stress, indicating that at low normal stress the shear strength may be high or low depending on the surface finish whereas at high normal stress the individuality of joints are lost and the behaviour becomes purely frictional, revealing the true friction angle of the material. At low normal stresses the shear strength may be higher than that corresponding to the friction line due to surface roughness, or lower due to surface smoothness. Due to the logarithmic form of the equation (5.19), over-estimation or under-estimation of the value of σ_{nT} has no serious consequences on the prediction of peak shear strength, as shown in Tables 5.3a and b. Errors are higher for higher normal stresses and roughness.

The form of the new criterion is similar in some respects to Barton's empirical formula (Barton, 1973). The new criterion, however, has a sound theoretical base and employs physically meaningful parameters which can be readily established through careful testing, measurement and analysis. There is no need for any index tests or preparation
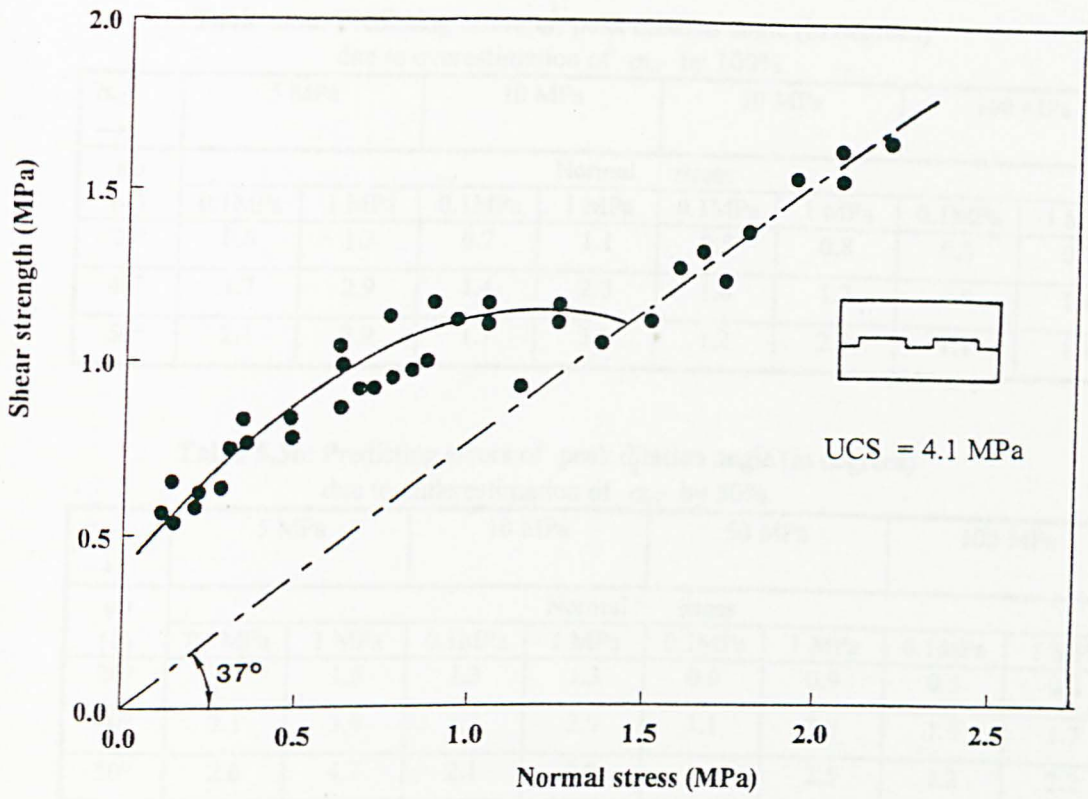
Fig. 5.10: Shear strength envelopes for stepped joint in plaster (after Lajtai, 1969a)
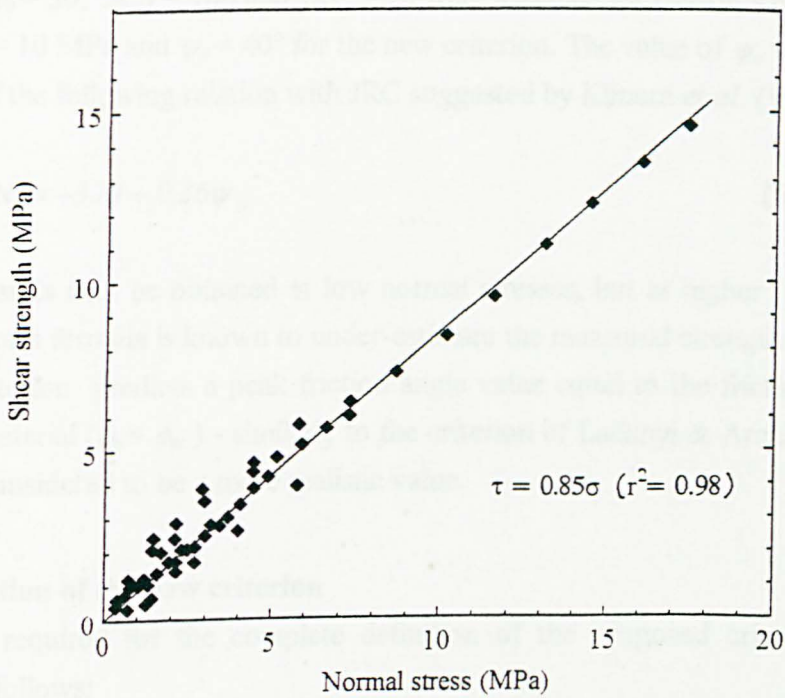
Fig. 5.11: Shear strength envelopes for natural joints

(after Yamaguchi & Shimotani, 1986)

Table 5.3a: Predicting errors of peak dilation angle (in degrees)
due to overestimation of σ_{nT} by 100%

σ_{nT} $\rightarrow$	5 MPa		10 MPa		50 MPa		100 MPa	
ψ_0 ($\downarrow$)	Normal	stress						
	0.1MPa	1 MPa	0.1MPa	1 MPa	0.1MPa	1 MPa	0.1MPa	1 MPa
20°	0.8	1.3	0.7	1.1	0.5	0.8	0.5	0.7
40°	1.7	2.9	1.4	2.3	1.0	1.7	0.9	1.4
50°	2.1	3.9	1.7	3.2	1.2	2.2	1.1	1.9

Table 5.3b: Predicting errors of peak dilation angle (in degrees)
due to underestimation of σ_{nT} by 50%

σ_{nT} $\rightarrow$	5 MPa		10 MPa		50 MPa		100 MPa	
ψ_0 ($\downarrow$)	Normal	stress						
	0.1MPa	1 MPa	0.1MPa	1 MPa	0.1MPa	1 MPa	0.1MPa	1 MPa
20°	1.0	1.5	1.3	1.3	0.6	0.9	0.5	0.8
40°	2.1	3.4	1.7	2.9	1.1	2.0	1.0	1.7
50°	2.6	4.7	2.1	3.9	1.4	2.5	1.2	2.2

of surfaces. A comparison between the two criteria is shown in Figure 5.10.

Values of $\phi_b = 30$, $JCS = 100$ and $JRC = 10$ were assumed for Barton's criterion, and ϕ_m = 39°, $\sigma_{nT} = 10$ MPa and $\psi_0 = 40°$ for the new criterion. The value of ψ_0 was selected on the basis of the following relation with JRC suggested by Kimura *et al.* (1993):

$$JRC = -3.74 + 0.36\psi_0 \tag{5.22}$$

Identical results may be obtained at low normal stresses, but at higher normal stresses where Barton's formula is known to under-estimate the measured strength (Barton, 1976) the new criterion predicts a peak friction angle value equal to the friction angle of the rock wall material ($\phi_p = \phi_m$) - similarly to the criterion of Ladanyi & Archambault (1970) - which is considered to be a more realistic value.

5.7 Application of the new criterion

The values required for the complete definition of the proposed criterion may be obtained as follows:

The angle ϕ_m from triaxial tests at confining pressures sufficiently high for the rock to reach its brittle-plastic transition state. The values given in Table 5.2 can be used as guide. This Table will be expanded later to include more data, as such data become available. Alternatively, ϕ_m can be deduced from careful direct shear testing after correction for dilation of the measured peak shear strength . This correction reveals the

1- New criterion

$\varphi_m = 39°$

$\psi_o = 40°$

$\sigma_{nT} = 10$ MPa

2 - Barton's equation

$\varphi_r = 30°$

JRC = 10

JCS = 100 MPa

(a)

φ_m

1- New criterion

$\varphi_m = 39°$

$\psi_o = 40°$

$\sigma_{nT} = 10$ MPa

2 - Barton's equation

$\varphi_r = 30°$

JRC = 10

JCS = 100 MPa

(b)

σ_{nT}
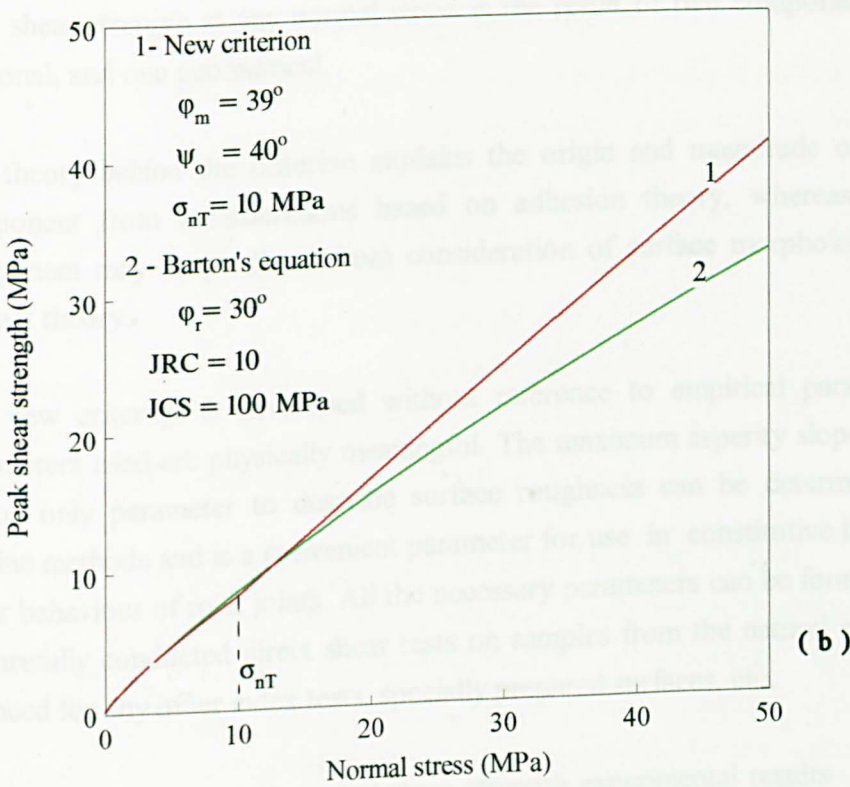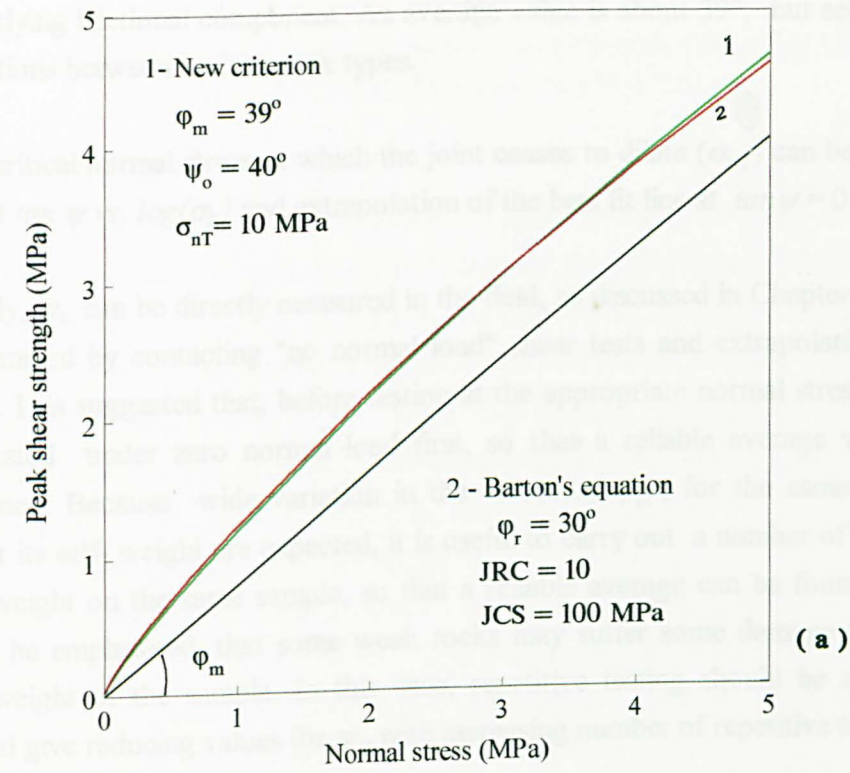
Figure 5.12. Comparison of proposed criterion with Barton's model

(a) Low normal stress   (b) High normal stress

underlying frictional component. An average value is about 39°, but see Table 5.2 for variations between various rock types.

The critical normal stress at which the joint ceases to dilate (σ_{nT}) can be deduced from a plot $tan\ \psi$ vs. $log(\sigma_n)$ and extrapolation of the best fit line at $tan\psi = 0$ (Fig. 4.11).

Finally, ψ_o can be directly measured in the field, as discussed in Chapter 3, or it can be determined by contacting "no normal load" shear tests and extrapolation to the field scale. It is suggested that, before testing at the appropriate normal stress, each sample be tested under zero normal load first, so that a reliable average value of ψ_O is obtained. Because wide variation in the values of ψ_O, for the same sample tested under its self- weight are expected, it is useful to carry out a number of tests under the self-weight on the same sample, so that a reliable average can be found. However, it must be emphasised, that some weak rocks may suffer some damage even under the self-weight of the sample. In this case, repetitive testing should be avoided (which would give reducing values for ψ_O with increasing number of repetitive tests).

5.8 Concluding remarks

A new, simple, theoretical, comprehensive peak shear strength criterion for rock joints has been proposed. It is based on a realistic mechanism of shearing, which suggests that peak shear strength at any normal stress is the result of two components, one purely frictional, and one geometrical.

The theory behind the criterion explains the origin and magnitude of the frictional component from considerations based on adhesion theory, whereas the dilational component may be predicted from consideration of surface morphology and normal contact theory.

The new criterion is developed without reference to empirical parameters but all parameters used are physically meaningful. The maximum asperity slope which is used as the only parameter to describe surface roughness can be determined in-situ by routine methods and is a convenient parameter for use in constitutive laws concerning shear behaviour of rock joints. All the necessary parameters can be found from a series of carefully conducted direct shear tests on samples from the natural surface, without the need for any other index tests, specially prepared surfaces, etc.

The good agreement with typical shear strength experimental results implies that the proposed theory contains the essential physics of the rock joint shearing.

CHAPTER 6
APPLICATION OF THE NEW CRITERION ON PUBLISHED EXPERIMENTAL RESULTS

6.1 Introduction

The basic principle of the new criterion is that variations in peak shear strength of rock joints are due to dilation only, and what remains after that is purely frictional, i.e. proportional to normal load. In order to test the validity of this principle and the ability of the new criterion to describe adequately the peak shear strength in joints other than those used in the present study, the author carried out analyses of a number of published experimental data sets both from natural and artificial joints. Five examples based on well-known experimental data, are presented below:

a) Artificial tensile fractures in sandstone (Kutter, 1974)

b) Artificial tensile fractures in a weak model material (Barton, 1971)

c) Natural joints through weathered granite (Barton & Choubey, 1977)

Two data sets are examined with regard to the effect of scale on peak shear strength.

d) Natural joints in quartz diorite (Pratt et al., 1974)

e) Artificial joints in a weak cast material (Bandis et al., 1981)

Finally, results from tightly interlocked joints through quartz syenite (Arnold, 1992) are analysed and the behaviour of coated joints is discussed.

6.2 Tensile fractures on sandstone (Kutter, 1974)

Kutter (1974) carried out direct shear tests on artificial tensile fractures on Darley Dale sandstone, on a specially designed 100 ton capacity shear box at Imperial College. These test results superficially appear strange, as they show a concave upwards peak shear strength envelope. When the non-dilational peak shear strength was considered, a straight line of 36.5° was obtained (Fig. 6.1). Ripley & Lee (1962) found a non-dilational friction angle of 36° for sandstone and Ross-Brown & Walton (1975) a friction angle of 33° for saw-cut and sandblasted surfaces of Darley Dale sandstone. These three values are in good agreement and compare quite well with the average predicted value for sandstone given in Table 5.2 (34.1°).

6.3 Tensile fractures on a weak model material (Barton, 1971a)

Barton (1971a) carried out direct shear tests on tension fractures generated in different strengths of a weak, brittle model material. Peak dilation angles and peak friction angles were calculated for eight different joint types of the model material, shown in Table 6.1 in descending order of roughness. The distribution of data for peak $arctan(\tau/\sigma_n)$ versus peak dilation angle (d_n) is shown in Fig. 6.1 and the variation of peak dilation angle with the ratio normal stress/compressive strength in Fig. 6.2.
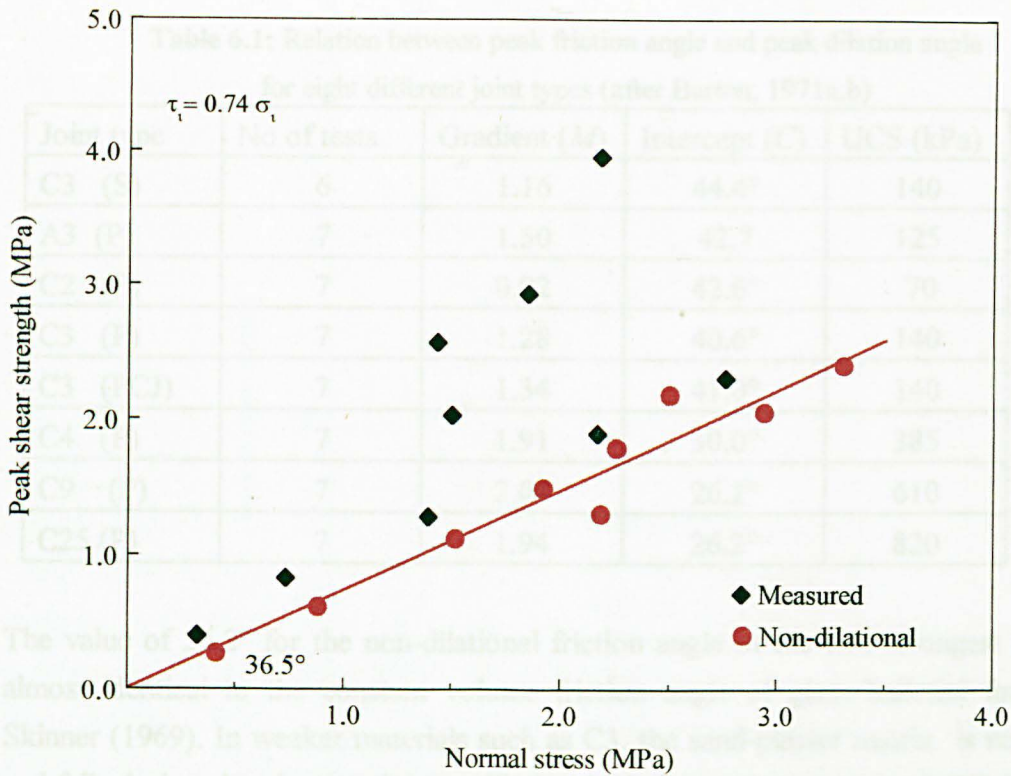
Fig. 6.1 Measured and non-dilational peak shear strength for tensile fractures in Darley Dale sandstone (data from Kutter, 1974)

The best-fit straight lines of the form

$$arctan(\frac{\tau}{\sigma_n}) = C + Md_n \qquad (6.1)$$

for each joint type were fitted and the gradients M and the intercepts C are shown in Table 6.1. The values of these parameters suggest that the frictional behaviour of the eight joint types can be classified into two groups: the first group consists of the first five joint types which have unconfined compressive strength 70-140 kPa and give a consistent value of intercept C between 40.6° and 44.4°. The second group consists of the remaining three joint types which have a compressive strength between 385 and 820 kPa (average 594 kPa) and values for the intercept 26.2°-30.0°. The difference in the values of intercept C, which gives the non-dilational friction angle of each model type, indicates that two shear mechanisms operate. It is believed that these mechanisms are related to the role of the glass ballotini filler, which was used for the preparation of the samples C. Although more regular, the stronger model joints (C4, C9 and C25) exhibit higher peak dilation angle than that of the weaker ones at the same normal stress/compressive strength ratio, whereas their peak friction angle is lower, as shown in Fig. 6.2a and b. This can be explained by an increased affect of the glass ballotini, which was used for the preparation of these models. In stronger mixes, the plaster matrix is strong and shearing takes place mainly along glass-glass contacts.

Table 6.1: Relation between peak friction angle and peak dilation angle
for eight different joint types (after Barton, 1971a,b)

Joint type	No of tests	Gradient (M)	Intercept (C)	UCS (kPa)
C3 (S)	6	1.16	44.4°	140
A3 (P)	7	1.50	42.7	125
C2 (P)	7	0.92	42.6°	70
C3 (P)	7	1.28	40.6°	140
C3 (PCJ)	7	1.34	41.0°	140
C4 (P)	7	1.91	30.0°	385
C9 (P)	7	2.04	26.2°	610
C25 (P)	7	1.94	26.2°	820

The value of 26.2° for the non-dilational friction angle of the two strongest mixes is almost identical to the constant volume friction angle of glass ballotini found by Skinner (1969). In weaker materials such as C3, the sand-plaster matrix is not strong and fails during shearing, so the non-dilational friction angle (average of 42°) is related to the friction angle of sand-plaster mixes (see Chapter 4.5). This value is in very good agreement with that of the similar model material described in chapter 4.5 and with that of limestone (Table 5.2) which the material C3 resembles (Barton, 1970). Therefore, in the case of this particular model material, stronger types (group II) when compared to weaker ones (group I), show lower peak friction angle and higher peak dilation angle, and as a result the gradient M in equation 6.1 is higher whereas the intercept is lower. Accordingly, the data shown in Figures 6.2a and b were analysed as two independent groups and the following best-fit straight lines were obtained (the data were obtained from the graphs provided by Barton, thus they may carry a small approximation). The results for the first group which comprises the majority of the whole sample population, are in line with the results presented in Chapter 4, conforming to the general relationship

$$\phi_p = \phi_m + \psi \tag{6.2}$$

Table 6.2: Relation between peak friction angle and peak dilation angle
for two groups of joint types

Group	No of points	Gradient (M)	Intercept (C)	UCS (kPa)
I	34	1.06	44.7°	123
II	21	1.74	31.5°	605

For the second group, the deviation from this relation is attributed to the special role of the glass ballotini, which is not expected to occur in most natural rock joints. Barton
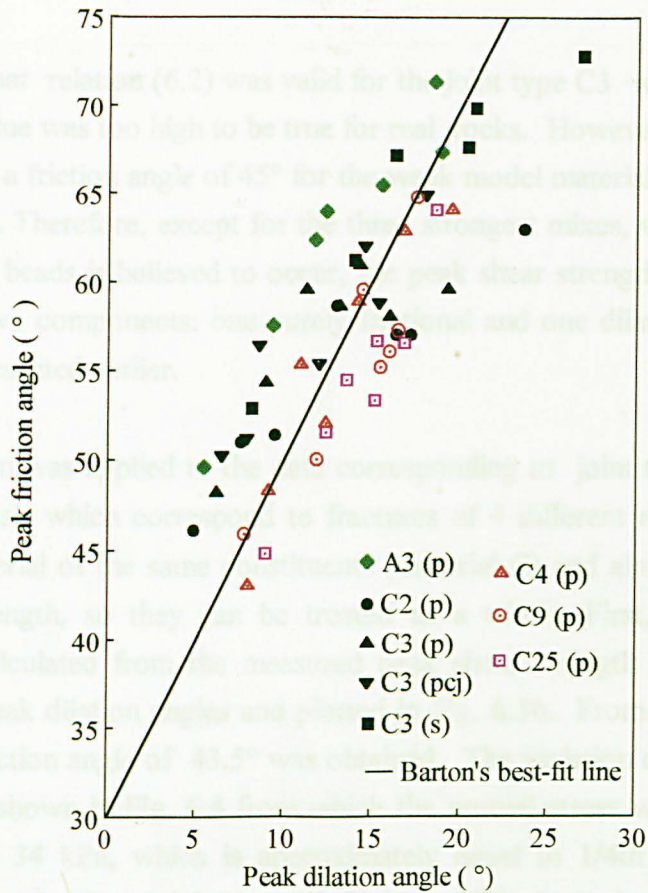
Fig. 6.2a: The relation between peak friction angle and peak dilation angle for eight different types of model joints (after Barton, 1971a,b)
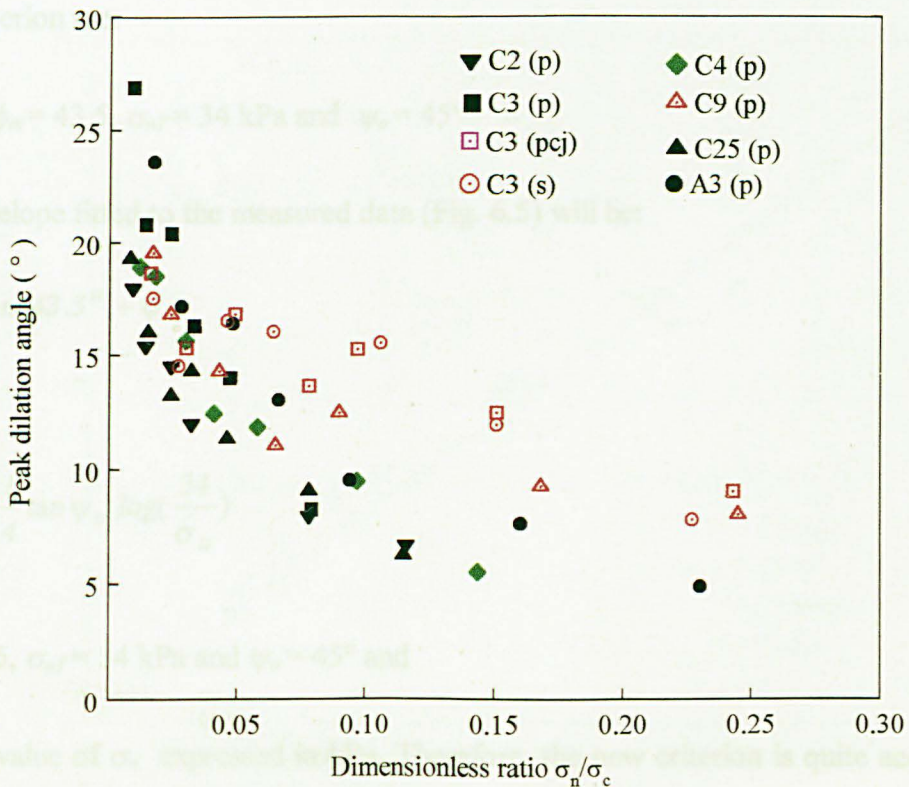
Fig. 6.2b: Variation of peak dilation angle with ratio of normal stress to compressive strength (after Barton, 1971a,b)

(1971a) found that relation (6.2) was valid for the joint type C3 with $\phi_m = 45°$ but he felt that this value was too high to be true for real rocks. However, as the results of this study show, a friction angle of 45° for the weak model material found by Barton is quite reasonable. Therefore, except for the three strongest mixes, where a very special role of the glass beads is believed to occur, the peak shear strength can be considered as comprising two components: one purely frictional and one dilational, as suggested by the theory presented earlier.

The new criterion was applied to the data corresponding to joint types C2(p), C3(p), C3(pcj) and C3(s), which correspond to fractures of 4 different roughness produced from model material of the same constituents (material C) and almost with the same compressive strength, so they can be treated as a whole. First, the non-dilational stresses were calculated from the measured peak shear strength (fig. 6.3a) and the corresponding peak dilation angles and plotted in Fig. 6.3b. From the best - fit line a non-dilational friction angle of 43.5° was obtained. The variation of dilation rate with normal stress is shown in Fig. 6.4 from which the normal stress which suppresses all dilation is about 34 kPa, which is approximately equal to 1/4th of the unconfined compressive strength of material C3 and half that of C2. Assuming that zero surface deformation occurs at a normal stress $\sigma_{no} = 10^{-4} \sigma_{nT}$, the corresponding value for the maximum asperity slope $tan\psi_o$ is equal to 1.00 ($\psi_o = 45°$), which seems quite reasonable for these rough tensile fractures. Therefore the parameters necessary for the new criterion are:

$$\phi_m = 43.5, \ \sigma_{nT} = 34 \text{ kPa and } \psi_o = 45°$$

The envelope fitted to the measured data (Fig. 6.5) will be:

$$\tau = \sigma \ tan(43.5° + \psi)$$

where

$$tan \ \psi = \frac{1}{4} tan \ \psi_o \ log(\frac{34}{\sigma_n})$$

with

$\phi_m = 43.5, \ \sigma_{nT} = 34$ kPa and $\psi_o = 45°$ and

and the value of σ_n expressed in kPa. Therefore, the new criterion is quite accurately applicable to this set of experimental data.
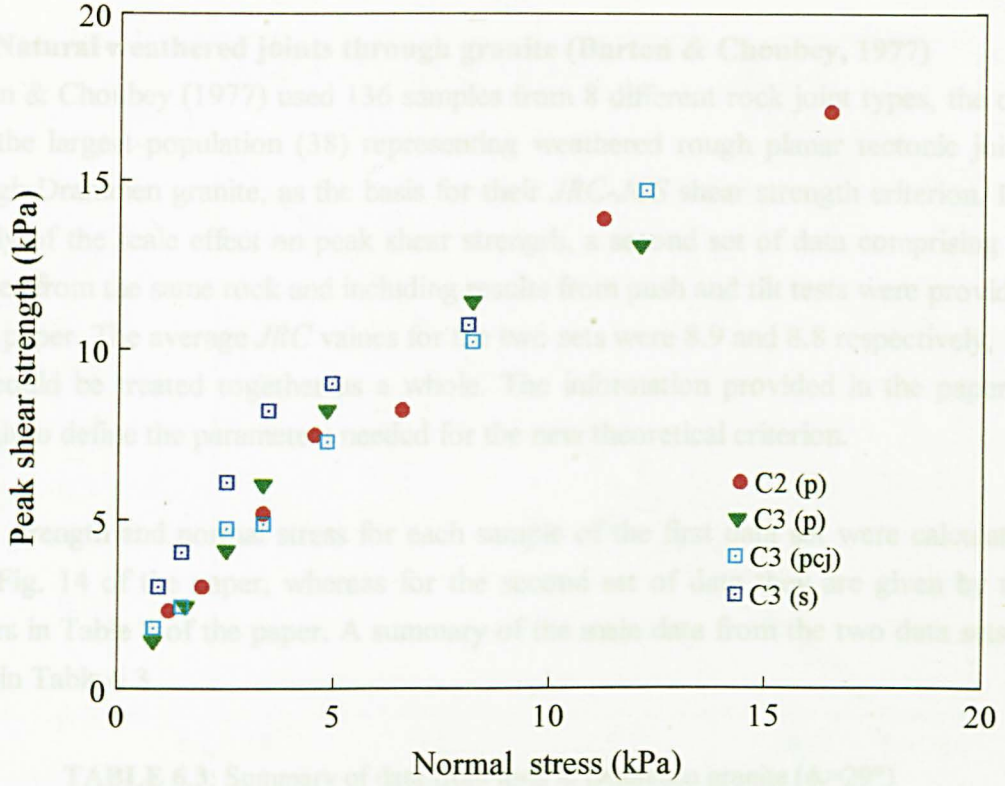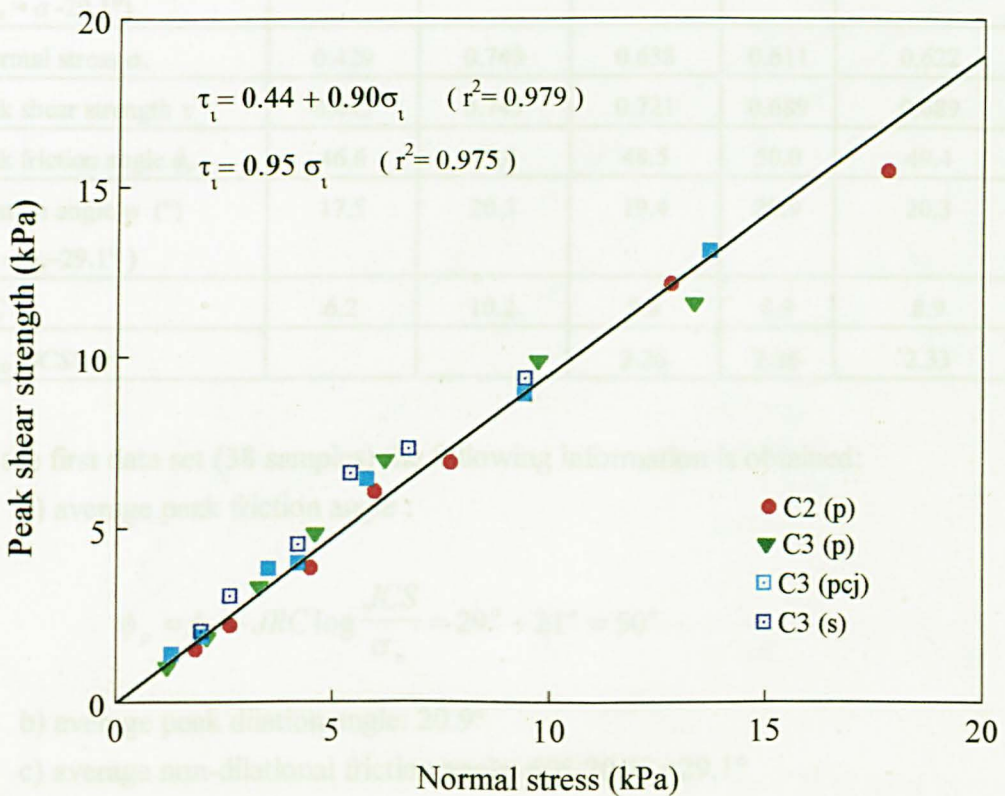
6. 4 Natural weathered joints through granite (Barton & Choubey, 1977)

Barton & Choubey (1977) used 136 samples from 8 different rock joint types, the one with the largest population (38) representing weathered rough planar tectonic joints through Drammen granite, as the basis for their *JRC-JCS* shear strength criterion. For a study of the scale effect on peak shear strength, a second set of data comprising 18 samples from the same rock and including results from push and tilt tests were provided in the paper. The average *JRC* values for the two sets were 8.9 and 8.8 respectively, so they could be treated together as a whole. The information provided in the paper is enough to define the parameters needed for the new theoretical criterion.

Shear strength and normal stress for each sample of the first data set were calculated from Fig. 14 of the paper, whereas for the second set of data they are given by the authors in Table 8 of the paper. A summary of the main data from the two data sets is given in Table 6.3.

TABLE 6.3: Summary of data from tests in Drammen granite (ϕ_r=29°)

DATA SET	SET 1			SET 2	COMBINED
Type of test	Tilt/shear	Push/shear	Combined	shear	shear
No of tests	6	12	18	38	56
Sliding angle α (°)	67.2	70.5	69.4		
Max asperity angle ψ_o (°) ($\psi_o = a$ -29.1°)	38.1	41.4	40.3		
Normal stress σ_n	0.429	0.743	0.638	0.611	0.622
Peak shear strength τ	0.445	0.743	0.721	0.689	0.689
Peak friction angle ϕ_p	46.6	49.4	48.5	50.0	49.4
Dilation angle ψ (°) ($\psi = \phi_p$–29.1°)	17.5	20.3	19.4	20.9	20.3
JRC	6.2	10.2	8.8	8.9	8.9
$\log_{10}$ (JCS/σ_n)			2.26	2.36	2.33

From the first data set (38 samples) the following information is obtained:

    a) average peak friction angle :

$$\phi_p = \phi_r + JRC \log \frac{JCS}{\sigma_n} = 29° + 21° = 50°$$

    b) average peak dilation angle: 20.9°

    c) average non-dilational friction angle: 50°-20.9° =29.1°

Fig. 6.4 Variation of dilation rate with normal stress

Figure axes — Peak dilation rate (0.0, 0.2, 0.4, 0.6, 0.8, 1.0, 1.2) versus Normal stress (kPa) (σ_{no}, 10^{-2}, 10^{-1}, 1.0, 10.0, σ_{nT}, 10^{2}).

$$y = 0.385 - 0.251\log x \quad (r^2 = 0.802)$$

$\tan \psi_o$

Legend: C2 (p), C3 (p), C3 (pcj), C3 (s)

Figure axes — Peak shear strength (kPa) (0, 5, 10, 15, 20) versus Normal stress (kPa) (0, 5, 10, 15, 20).
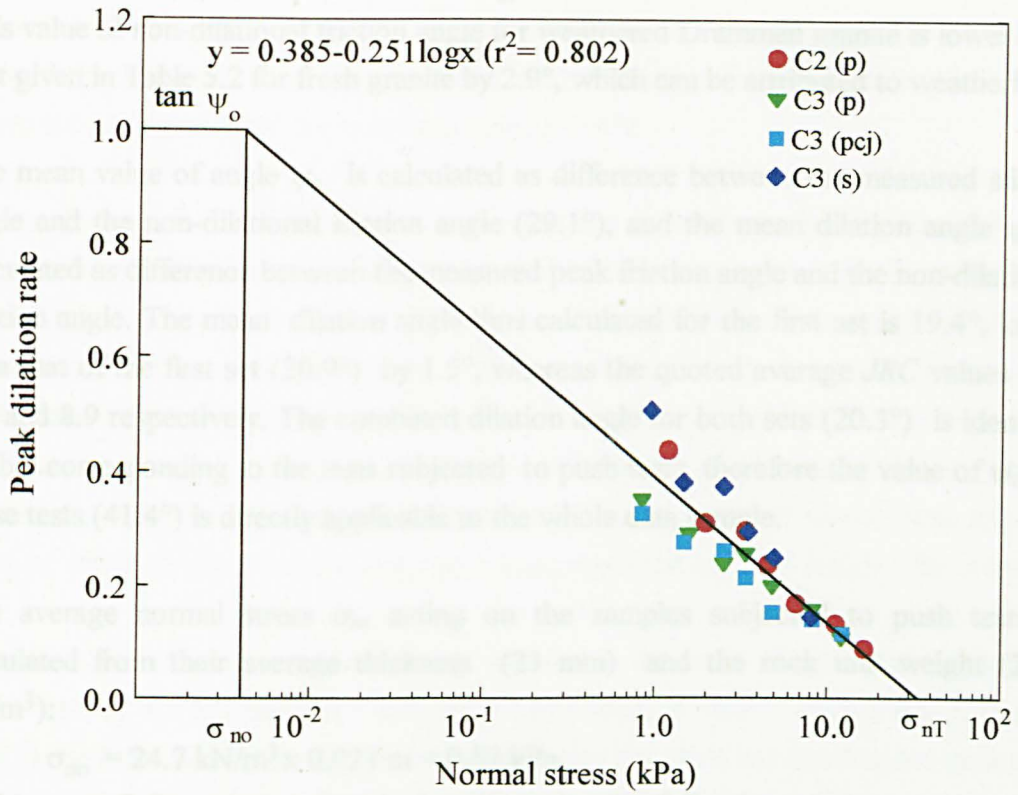
Legend: C2 (p), C3 (p), C3 (pcj), C3 (s)
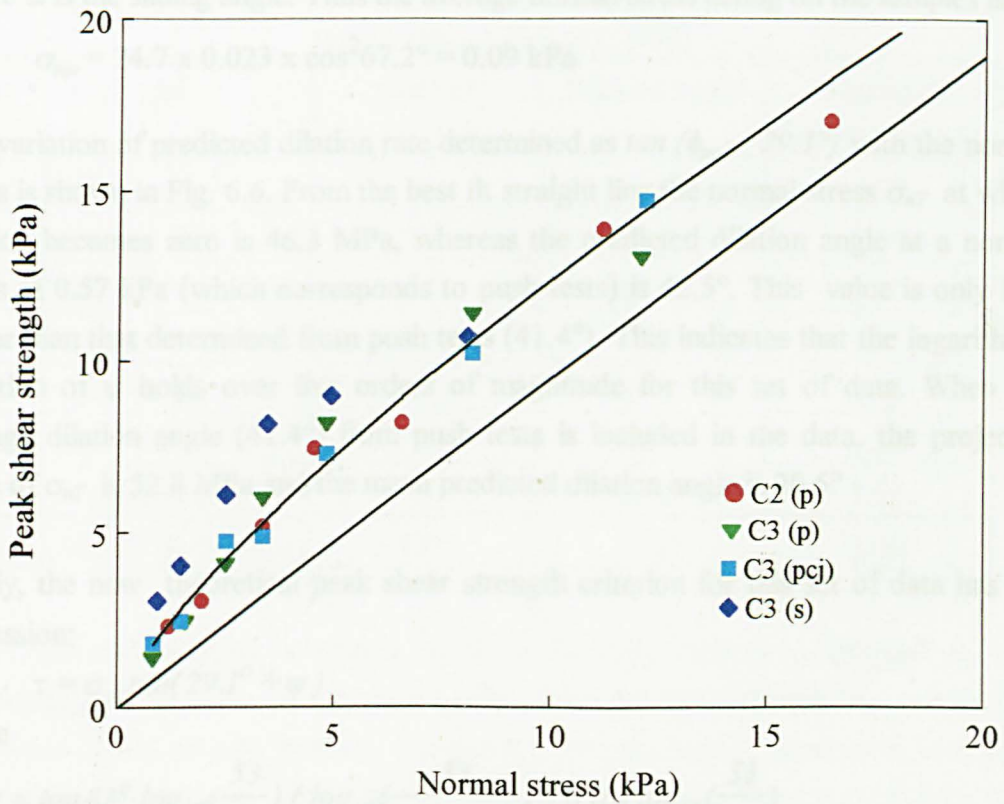
Fig. 6.5: Fitted envelope to data shown on Fig. 6.3a with $\phi_m = 43.5°$, $\sigma_{nT} = 34$ kPa and $\psi_o = 45°$

This value of non-dilational friction angle for weathered Drammen granite is lower than that given in Table 5.2 for fresh granite by 2.9°, which can be attributed to weathering.

The mean value of angle ψ_o is calculated as difference between the measured sliding angle and the non-dilational friction angle (29.1°), and the mean dilation angle ψ is calculated as difference between the measured peak friction angle and the non-dilational friction angle. The mean dilation angle thus calculated for the first set is 19.4°, lower than that of the first set (20.9°) by 1.5°, whereas the quoted average *JRC* values are 8.8 and 8.9 respectively. The combined dilation angle for both sets (20.3°) is identical to that corresponding to the tests subjected to push tests, therefore the value of ψ_o for these tests (41.4°) is directly applicable to the whole data sample.

The average normal stress σ_{no} acting on the samples subjected to push tests is calculated from their average thickness (23 mm) and the rock unit weight (24.7 kN/m³):

$$\sigma_{no} = 24.7 \text{ kN/m}^3 \times 0.023 \text{ m} = 0.57 \text{ kPa}$$

In the case of tilt tests σ_{no} is calculated by using the following relation suggested by Barton & Choubey (1977) :

$$\sigma_{no} = \gamma\, h\, cos^2\alpha \qquad\qquad (6.3)$$

where α is the sliding angle. Thus the average normal stress acting on the samples is

$$\sigma_{no} = 24.7 \times 0.023 \times cos^2 67.2° = 0.09 \text{ kPa}$$

The variation of predicted dilation rate determined as *tan* (ϕ_{peak} - 29.1°) with the normal stress is shown in Fig. 6.6. From the best fit straight line the normal stress σ_{nT} at which dilation becomes zero is 46.3 MPa, whereas the predicted dilation angle at a normal stress of 0.57 kPa (which corresponds to push tests) is 42.5°. This value is only 1.1° higher than that determined from push tests (41.4°). This indicates that the logarithmic variation of ψ holds over five orders of magnitude for this set of data. When the average dilation angle (41.4°) from push tests is included in the data, the projected value of σ_{nT} is 52.8 MPa and the mean predicted dilation angle is 20.5°

Finally, the new theoretical peak shear strength criterion for this set of data has the expression:

$$\tau = \sigma_n\, tan(29.1° + \psi)$$

where

$$tan\,\psi = tan\,42° \, log_{10}(\frac{53}{\sigma_n}) \, / \, log_{10}(\frac{53}{5.7 \times 10^{-4}}) = 0.181\, log_{10}(\frac{53}{\sigma_n})$$

and σ_n is the normal stress in MPa. Using this equation for the prediction of peak shear strength for each individual shear test, the resulted average peak friction angle is 49.6° which is 0.2° higher than the measured value (49.4°).

The quality of the fit is shown in Fig. 6.7 where the data from both sets (56 tests) have been included. The example illustrates the ability of the new criterion to predict accurately shear strength from only a series of direct shear tests on samples from natural joints. Barton and Choubey (1977), used additional shear tests on saw-cut surfaces and Schmidt hammer tests to estimate the basic or residual friction angle and the joint compressive strength (*JCS*) used in their model. As shown, all the parameters needed for the new criterion can be obtained from a series of direct shear tests on samples which, prior to main testing, have been subjected to "self-weight" shear tests.

It has also shown that the basic principle adopted in this study that peak shear strength is the sum of a frictional and a dilational component is valid. Barton and Choubey (1977) used the *damage coefficient M* to describe the observed relation between peak friction angle (ϕ_p) and peak dilation angle (ψ) for the seven joint types used.

$$\phi_p = \phi_r + M\psi$$

Table 6.4: Mean dilation angle and damage coefficient for different rock types
(after Barton & Choubey, 1977)

No	Rock type	Number of samples	Dilation angle d_n	Damage coefficient M
1	Aplite	36	25.5°	0.92
2	Granite	38	20.9°	1.00
3	Hornfels	17	26.5°	0.99
4	Gneiss	17	17.3°	1.01
5	Calc. Shale	11	14.8°	1.39
6	Slate	7	6.8°	0.78
7	Soapstone	5	16.2°	1.53
8	Model fractures	130	13.2°	2.00

They found that M varies between 1 and 2, as shown in Table 6.4. Although ϕ_m is in general different than ϕ_r it is apparent from Table 6.4 that the first four natural rock joint types (aplite, granite, hornfels and gneiss), with the largest population, have an M value which is exactly or very close to unity. The remaining three natural joint types (calcareous shale, slate and soapstone) have M values higher or lower than 1.0 but the number of samples is considerably lower, so the reliability is lower. It may not be coincidental that the largest deviation from 1.0 (1.53) corresponds to the rock type
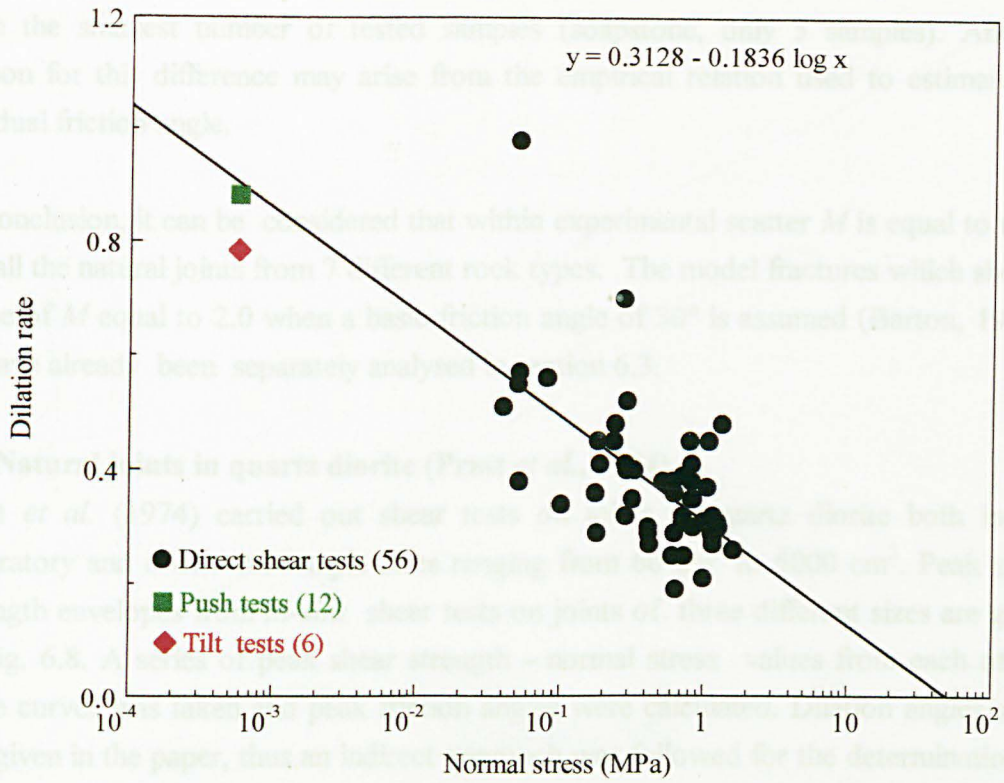
Fig. 6.6: Variation of assumed dilation rate with normal stress for shear tests in Drammen granite
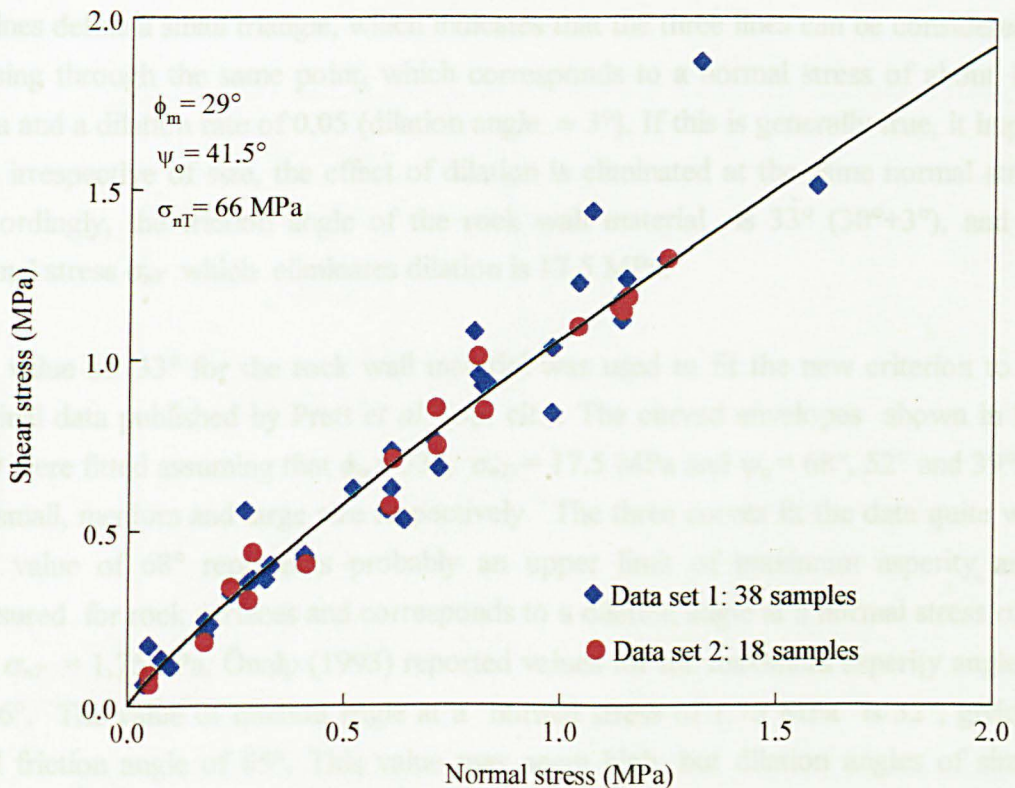
Fig. 6.7: Shear strength data and fitted envelope for natural joints in Drammen granite

with the smallest number of tested samples (soapstone, only 5 samples). Another reason for this difference may arise from the empirical relation used to estimate the residual friction angle.

In conclusion, it can be considered that within experimental scatter M is equal to unity for all the natural joints from 7 different rock types. The model fractures which show a value of M equal to 2.0 when a basic friction angle of 30° is assumed (Barton, 1971a, b) have already been separately analysed in section 6.3.

6.5 Natural joints in quartz diorite (Pratt *et al.*, 1974)

Pratt *et al.* (1974) carried out shear tests on joints in quartz diorite both in the laboratory and *in-situ* on sample sizes ranging from 60 cm^2 to 5000 cm^2. Peak shear strength envelopes from *in-situ* shear tests on joints of three different sizes are given in Fig. 6.8. A series of peak shear strength - normal stress values from each of the three curves was taken and peak friction angles were calculated. Dilation angles were not given in the paper, thus an indirect approach was followed for the determination of ϕ_m and σ_{nT}. Assuming an arbitrary friction angle of 30° for the rock wall material, a graph of the corresponding dilation rate, calculated as $tan (\phi_{peak}-30°)$, versus normal stress was plotted (Fig. 6.9). The calculated dilation rates reduced logarithmically with normal stress for the three different sizes. The points of intersection of the three best-fit lines define a small triangle, which indicates that the three lines can be considered as passing through the same point, which corresponds to a normal stress of about 17.5 MPa and a dilation rate of 0.05 (dilation angle $\approx 3°$). If this is generally true, it implies that irrespective of size, the effect of dilation is eliminated at the same normal stress. Accordingly, the friction angle of the rock wall material is 33° (30°+3°), and the normal stress σ_{nT} which eliminates dilation is 17.5 MPa.

The value of 33° for the rock wall material was used to fit the new criterion to the original data published by Pratt *et al.* (op. cit.). The curved envelopes shown in Fig. 6.10 were fitted assuming that $\phi_m= 33°$, $\sigma_{nT} = 17.5$ MPa and $\psi_o= 68°$, 52° and 39° for the small, medium and large size respectively. The three curves fit the data quite well. The value of 68° represents probably an upper limit of maximum asperity angle measured for rock surfaces and corresponds to a dilation angle at a normal stress $\sigma_{no} = 10^{-4} \sigma_{nT} = 1.75$ kPa. Önalp (1993) reported values for the maximum asperity angle up to 76°. The value of dilation angle at a normal stress of 1.75 MPa is 32°, giving a total friction angle of 65°. This value may seem high, but dilation angles of similar magnitudes have been reported in the literature for tensile fractures. For example, the value of dilation angle corresponding to the normal stress of 1.4 MPa for the tensile fractures in sandstone shown in Fig. 6.1 is 30° and to normal stress of 2.2 MPa is 25°.
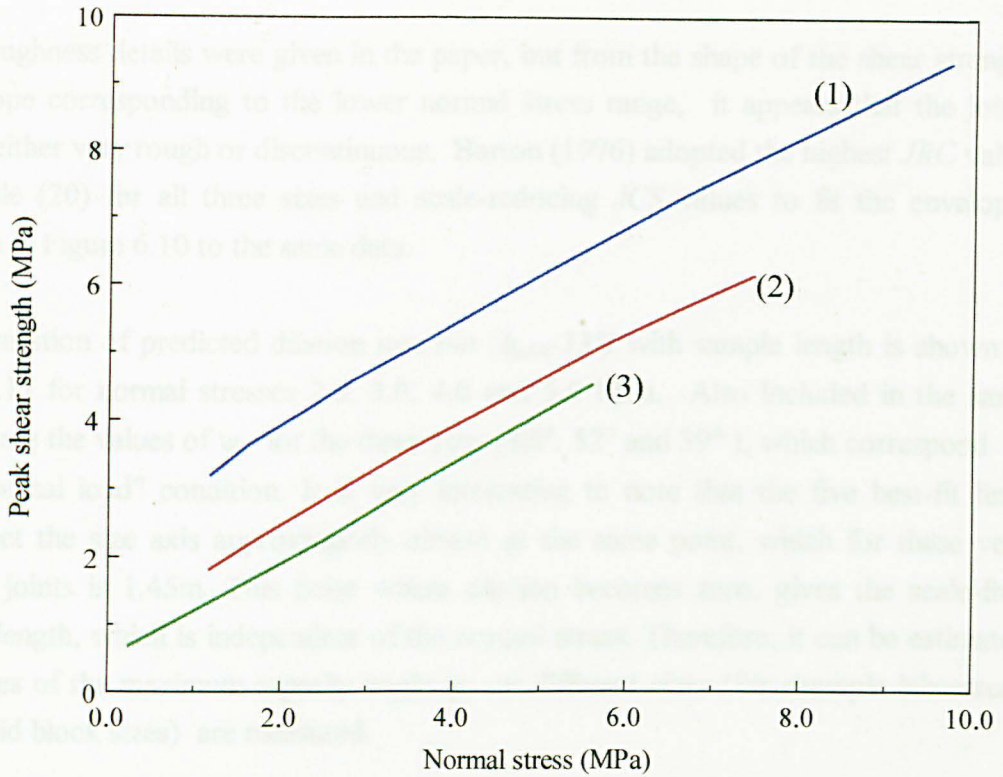
Fig. 6.8: Friction envelopes developed from *in-situ* shear tests on joints in quartz diorite.
(1) average area 200 cm^2. (2) average area 1500 cm^2. (3) average area 5000 cm^2
(after Pratt *et al.*, 1974)
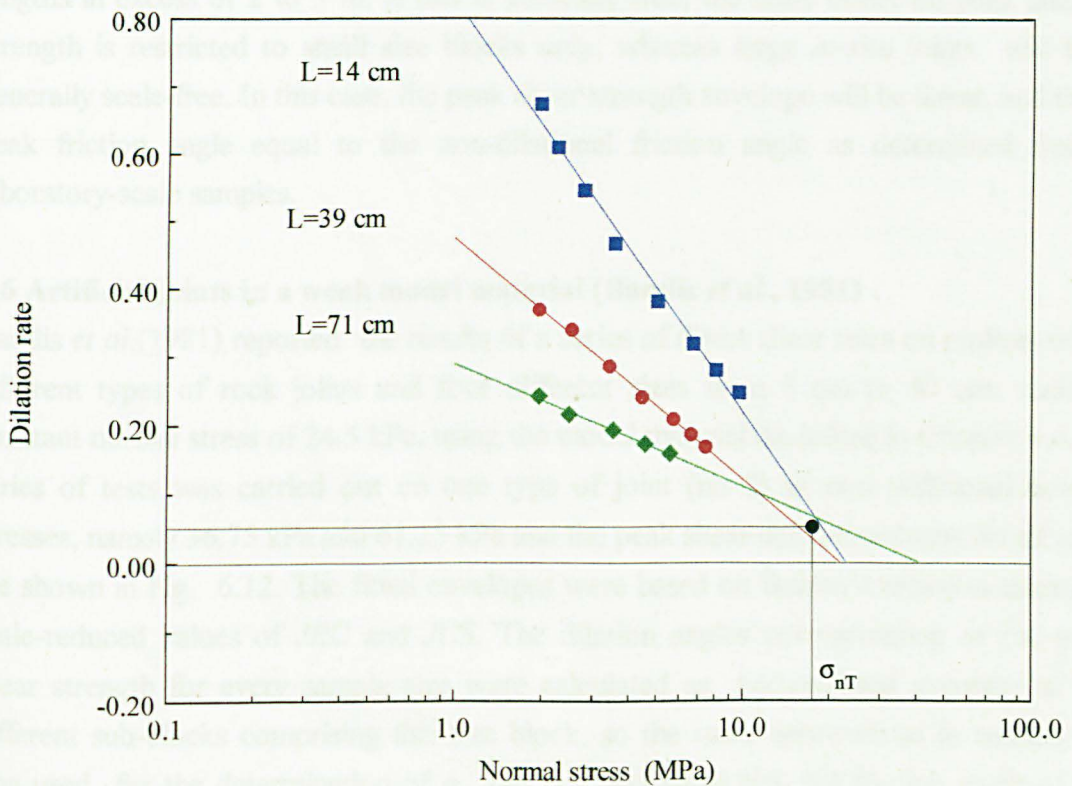
Fig. 6.9: Variation of back-calculated dilation rate with normal stress

No roughness details were given in the paper, but from the shape of the shear strength envelope corresponding to the lower normal stress range, it appears that the joints were either very rough or discontinuous. Barton (1976) adopted the highest *JRC* value possible (20) for all three sizes and scale-reducing *JCS* values to fit the envelopes shown in Figure 6.10 to the same data.

The variation of predicted dilation rate *tan (ϕ_{peak}-33°)* with sample length is shown in Fig. 6.11 for normal stresses 2.0, 3.0, 4.0 and 5.0 MPa. Also included in the same figure are the values of ψ_o for the three sizes (68°, 52° and 39°), which correspond to "no normal load" condition. It is very interesting to note that the five best-fit lines intersect the size axis approximately almost at the same point, which for these very rough joints is 1.45m. This point where dilation becomes zero, gives the scale-free block length, which is independent of the normal stress. Therefore, it can be estimated if values of the maximum asperity angle ψ_o at different sizes (for example laboratory and field block sizes) are measured.

The value of 1.45 m for the scale-free block found for the data of Pratt *et al.* (1974) is in agreement with that found for the model joints used in this study (see Figures 4.31b, 4.45) and according to the proposed theory suggests that the effect of scale disappears for relatively small block lengths. Following a different approach, Barton (1976) suggested that for the same experimental data, scale effect might die out for joint lengths in excess of 2 to 3 m. If this is generally true, the scale effect on peak shear strength is restricted to small size blocks only, whereas large *in-situ* joints will be generally scale-free. In this case, the peak shear strength envelope will be linear, and the peak friction angle equal to the non-dilational friction angle as determined from laboratory-scale samples.

6.6 Artificial joints in a weak model material (Bandis *et al.*, 1981)

Bandis *et al.*(1981) reported the results of a series of direct shear tests on replicas of 11 different types of rock joints and four different sizes from 5 cm to 40 cm, under a constant normal stress of 24.5 kPa, using the model material described in Chapter 4.4. A series of tests was carried out on one type of joint (no 2) at two additional normal stresses, namely 36.75 kPa and 61.25 kPa and the peak shear stress envelopes for all sizes are shown in Fig. 6.12. The fitted envelopes were based on Barton's criterion assuming scale-reduced values of *JRC* and *JCS*. The dilation angles corresponding to the peak shear strength for every sample size were calculated as accumulated averages of the different sub-blocks comprising this size block, so the same approach as in section 6.5 was used for the determination of ϕ_m and σ_{nT}. Assuming that the friction angle of the rock wall material was 32°, as suggested by the authors, a graph of the corresponding
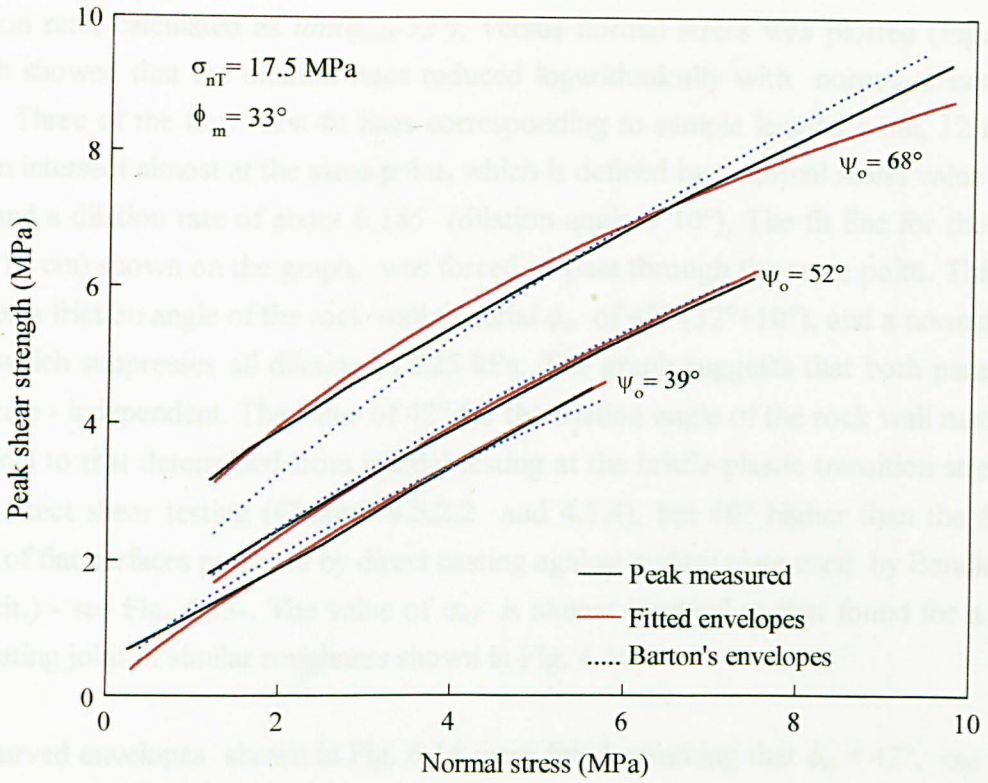
Fig. 6.10: Peak shear strength envelopes obtained from the new criterion, with values of ψ_o as shown and values of $\phi_m=33°$ and $\sigma_{nT}=17.5$ MPa
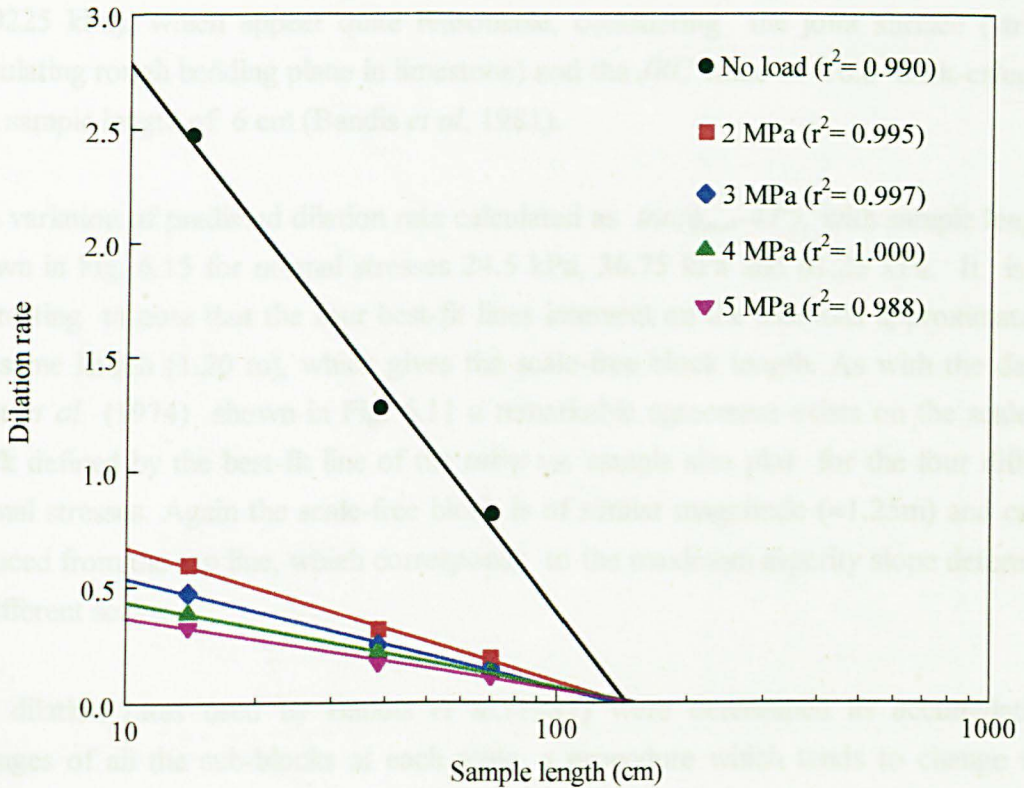
Fig. 6.11: Variation of dilation rate with sample length

dilation rate, calculated as $tan(\phi_{peak}-32°)$, versus normal stress was plotted (Fig. 6.13), which showed that the dilation rates reduced logarithmically with normal stress for all sizes. Three of the four best-fit lines corresponding to sample lengths 6 cm, 12 cm and 36 cm intersect almost at the same point, which is defined by a normal stress value of 225 kPa and a dilation rate of about 0.185 (dilation angle ≈ 10°). The fit line for the fourth size (18 cm) shown on the graph, was forced to pass through the same point. This point defines a friction angle of the rock wall material ϕ_m of 42° (32°+10°), and a normal stress σ_{nT} which suppresses all dilation of 225 kPa. The graph suggests that both parameters are scale - independent. The value of 42° for the friction angle of the rock wall material is identical to that determined from triaxial testing at the brittle-plastic transition stress and from direct shear testing (Chapter 4.5.2.2 and 4.5.4), but 10° higher than the friction angle of flat surfaces prepared by direct casting against a glass plate used by Bandis *et al*. (op. cit.) - see Fig. 4.33-. The value of σ_{nT} is almost identical to that found for a rough undulating joint of similar roughness shown in Fig. 4.16.

The curved envelopes shown in Fig. 6.14 were fitted assuming that ϕ_m = 42°, σ_{nT} = 225 kPa for all sizes and ψ_o = 60°, 51°, 46° and 36° for the 6 cm, 12 cm, 18 cm and 36 cm long samples respectively. The curve fitting is at least as good as that shown in Fig. 6.12, which was based on variable *JCS* values (compare the envelopes corresponding to the smallest sample size). The values of ψ_o correspond to a normal stress $\sigma_{no}=10^{-4}\sigma_{nT}$ (0.0225 kPa), which appear quite reasonable, considering the joint surface (strongly undulating rough bedding plane in limestone) and the *JRC* value of 16.8 back-calculated at a sample length of 6 cm (Bandis *et al*, 1981).

The variation of predicted dilation rate calculated as $tan(\phi_{peak}-42°)$, with sample length is shown in Fig. 6.15 for normal stresses 24.5 kPa, 36.75 kPa and 61.25 kPa. It is very interesting to note that the four best-fit lines intersect on the size axis approximately at the same length (1.20 m), which gives the scale-free block length. As with the data of Pratt *et al* (1974) shown in Fig. 6.11 a remarkable agreement exists on the scale-free block defined by the best-fit line of the *tanψ* vs. sample size plot for the four different normal stresses. Again the scale-free block is of similar magnitude (≈1.25m) and can be deduced from the top line, which corresponds to the maximum asperity slope determined at different scales.

The dilation rates used by Bandis *et al*.(1981) were determined as accumulative averages of all the sub-blocks at each scale, a procedure which tends to change the typical S-shaped normal displacement-shear displacement curve in a more linear form, so giving systematically lower values than the maximum dilation angle corresponding to the individual samples. A direct comparison between the predictions made with the

Curve No	L (cm)	JRC	JCS (kPa)
1	6	16.8	2000
2	12	14.4	1550
3	18	13	1330
4	36	12	1120
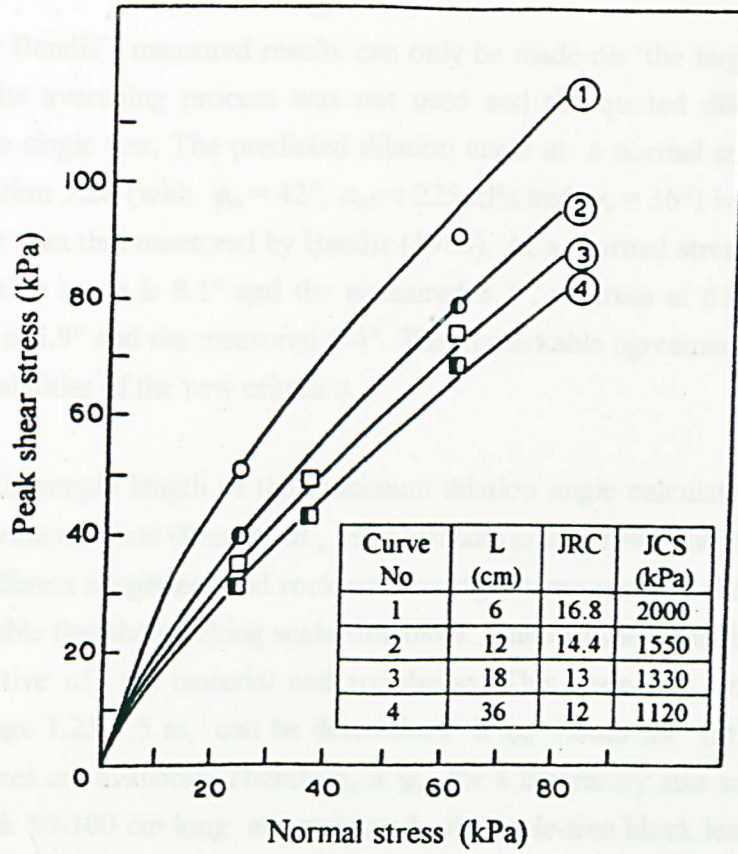
Fig. 6.12: Theoretical envelopes fitted to experimental data using scale-reduced values of *JRC* and *JCS* (after Bandis *et al.*, 1981)
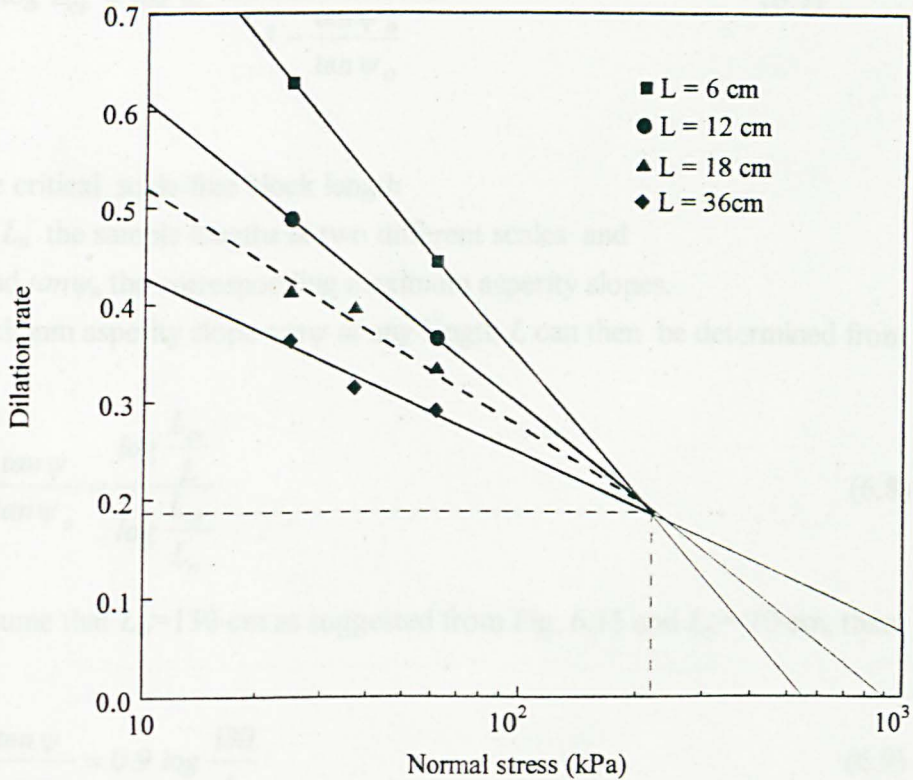
Fig. 6.13: Variation of assumed dilation rate with normal stress

new criterion and Bandis's measured results can only be made on the largest size (36 cm), for which the averaging process was not used and the quoted dilation angles correspond to one single test. The predicted dilation angle at a normal stress of 24.5 kPa using the relation 5.20 (with $\phi_m = 42°$, $\sigma_{nT} = 225$ kPa and $\psi_o = 36°$) is 9.9°, which is only 0.1° higher than that measured by Bandis (1980). At a normal stress 36.75 kPa the predicted dilation angle is 8.1° and the measured 8.2°, whereas at 61.25 kPa the predicted dilation is 5.9° and the measured 6.4°. This remarkable agreement underlines the predicting capabilities of the new criterion.

The variation with sample length of the maximum dilation angle calculated for three independent experimental sets (Pratt *et al.*, 1974, Bandis *et al.*, 1981 and this study), where joints of different roughness and rock wall strength were used, is shown in Fig. 6.16. It is remarkable that the resulting scale-free block is almost the same for the three data sets, irrespective of the material and roughness. This scale-free block length, which is in the range 1.25-1.5 m, can be determined if ψ_o values for (at least two) different sample sizes are available. Therefore, if ψ_o for a laboratory size sample (e.g. 10 cm) and a block 50-100 cm long are measured, the scale-free block length can be deduced from a graph like that shown in Fig. 6.15 or by the equivalent formula:

$$\log L_{cr} = \log L_o \frac{\dfrac{\log L_n}{\log Lo} - \dfrac{\tan \psi_n}{\tan \psi_o}}{1 - \dfrac{\tan \psi_n}{\tan \psi_o}}$$ (6.7)

where
L_{cr} is the critical scale-free block length
L_o and L_n the sample lengths at two different scales and
$tan\psi_o$ and $tan\psi_n$ the corresponding maximum asperity slopes.
The maximum asperity slope $tan\psi$ at any length L can then be determined from

$$\frac{tan\psi}{tan\psi_o} = \frac{\log \dfrac{L_{cr}}{L}}{\log \dfrac{L_{cr}}{L_o}}$$ (6.8)

If we assume that $L_{cr}=130$ cm as suggested from Fig. 6.15 and $L_o = 10$ cm, then

$$\frac{\tan \psi}{\tan \psi_o} = 0.9 \log \frac{130}{L}$$ (6.9)

where L is the sample length in cm.

196
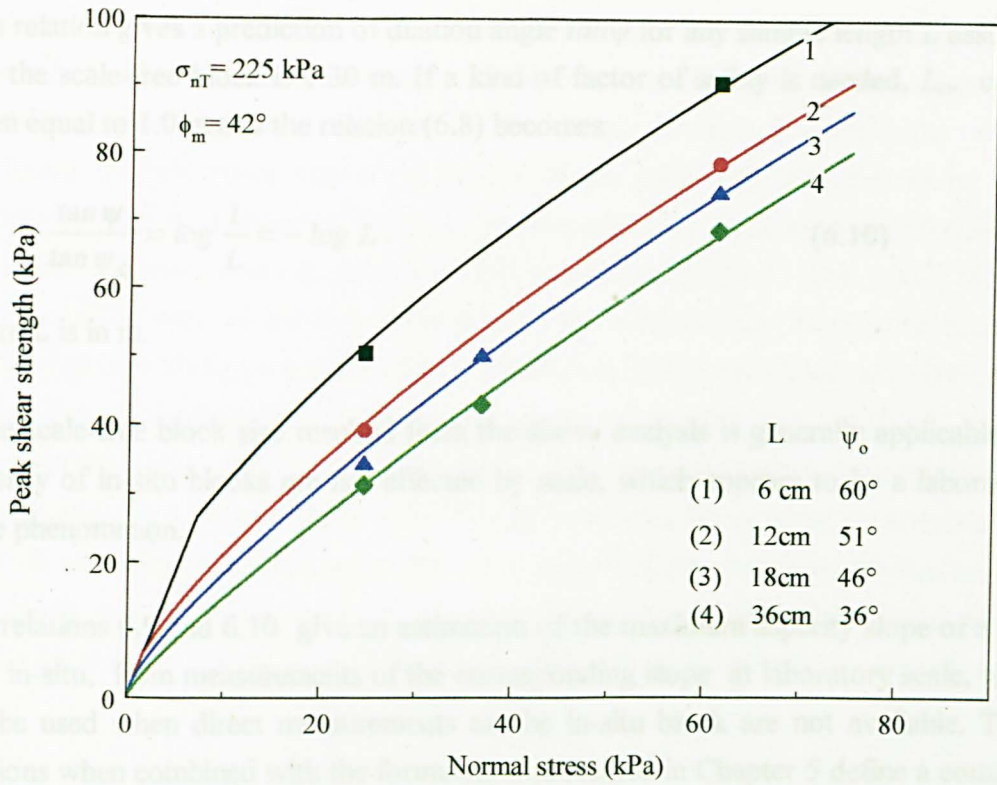
Fig. 6.14: Peak shear strength envelopes obtained from the new criterion, with values of ψ_o as shown and values of $\phi_m=42°$ and $\sigma_{nT}=225$ kPa
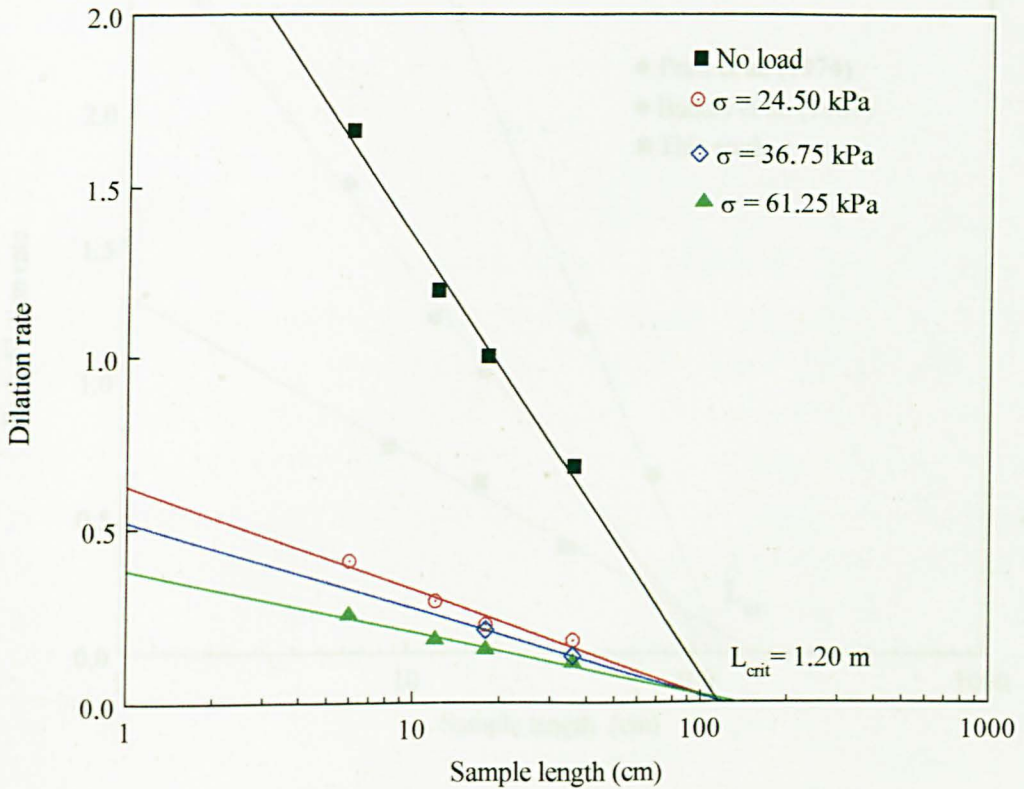
Fig. 6.15: Variation of dilation rate with sample length

This relation gives a prediction of dilation angle *tanψ* for any sample length L assuming that the scale-free block is 1.30 m. If a kind of factor of safety is needed, L_{cr} can be taken equal to 1.0 m and the relation (6.8) becomes

$$\frac{\tan \psi}{\tan \psi_o} = \log \frac{1}{L} = - \log L \qquad (6.10)$$

where L is in m.

If the scale-free block size resulted from the above analysis is generally applicable, the majority of in-situ blocks are not affected by scale, which appears to be a laboratory-scale phenomenon.

The relations 6.9 and 6.10 give an estimation of the maximum asperity slope of a rock joint in-situ, from measurements of the corresponding slope at laboratory scale, which can be used when direct measurements on the in-situ block are not available. These relations when combined with the formulation presented in Chapter 5 define a complete peak shear strength criterion, which takes into account the effect of scale.
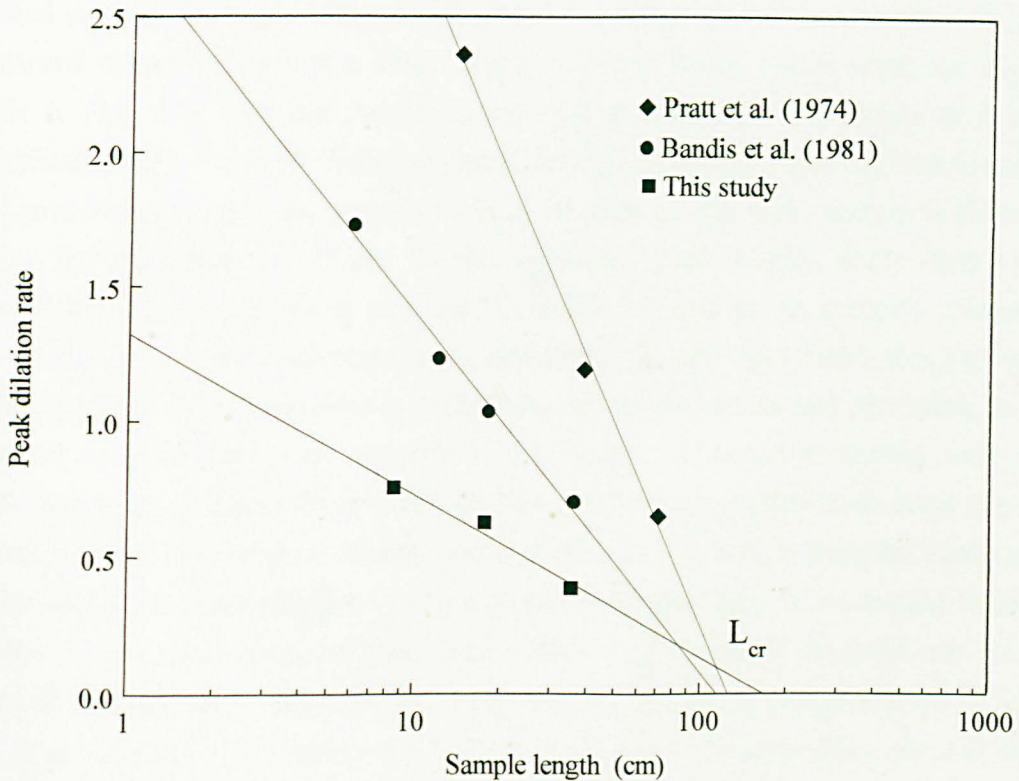
Fig. 6.16: Scale-free block size determined from three different experimental data sets.

The data shown here suggest that the geometrical component of shear strength diminishes when the size of the sample approaches a critical value of a few meters (say less than 3.0 m), i.e. the scale effect on peak shear strength is a parameter which is irrelevant to field scale, where the length of the joints are expected to be larger. Therefore, the field shear strength can be determined by measuring the friction angle ϕ_m in the laboratory and ignoring the field roughness. This will give a safe value for design. In the case of joints with large-scale undulations, the large scale roughness angle must be added to the value of ϕ_m. McMahon (1985) back-analysed natural failed slopes and concluded that only large-scale roughness (with a base length of 2% of the length of the sliding block) contributes to the field shear strength. More specifically the friction angle of a natural slope with 1° large scale roughness which occurred along a joint in quartzite was found to be 36°. Therefore, the non-dilational friction angle for this block was 35°. This value is in very good agreement with the friction angle of quartzite given in Table 5.2 (35.9°), although the latter is based only in one data set.

6.7 Tightly interlocked joints

When the maximum asperity angle ψ_o of a rock surface is so high that the total friction angle $(\phi_m + \psi_o)$ approaches 90°, it is impossible for the dilation to mobilise fully. The asperities are forced to shear through, even at extremely low normal stresses, and a cohesion component is introduced. This is the case with some tensile fractures, where asperities are "locked" and prevent free dilation at the initial stage of the shearing process. After some shear displacement when enough asperity deformation has taken place, free dilation may occur. The result is that the maximum dilation appears with a hysteresis relative to peak shear strength. Joints of this type i.e. tight, unweathered hard-surfaced joints, are found in nature, for example in jaspers, cherty limestones, and granitic rock masses (Obert et al., 1976). In this case, besides the frictional and the dilational component, the peak measured strength will include an extra component due to cohesion of locked asperities (Hencher, 1995). This extra component substitutes a part of the potential -but suppressed- dilational component.

A typical example of this category of joints is shown in Fig. 6.17, where a single direct shear test is presented from a series of tests on an artificial tensile fracture through very strong quartz syenite carried out by Hencher and reported by Arnold (1992). Dilation angles calculated over horizontal displacements of 0.18 mm and ratios of shear to normal stresses (measured and non-dilational) are shown. It can be seen that the peak measured strength occurs at a shear displacement of about 1 mm when the dilation angle is only 13°, whereas the maximum dilation angle of 30° occurs at a shear displacement of 1.5 mm when the measured strength is already reducing. The measured and non-dilational peak shear strength from 15 runs on the same sample is shown in Fig. 6.18. The value of 55° for the non-dilational peak friction angle (line 1) is considerably higher than those predicted in Table 5.2, and in the author's opinion, is due to the extra cohesional component introduced by the tight interlocking of small scale asperities. This component is independent of normal stress and therefore, in this case the non-dilational shear strength is not purely frictional in nature, even if it appears to be proportional to normal load over the limited normal stress range used, as shown in Fig. 6.18. The more realistic value of 39° (line 2) for the frictional component is obtained if the shear strength due to maximum dilation angle is subtracted from the measured peak shear strength. This value which would result if the joint was free to dilate, is in agreement with the predicted values for many rock types given in Table 5.2. The variation of the maximum dilation rate and that corresponding to peak shear strength with normal stress is shown in Fig. 6.19. Since the data correspond to one single sample which was repeatedly tested under different normal stresses, the reliability of the "peak strength" results is not the same for all tests. The first test carried out at a normal stress equal to 60 kPa corresponds to the initial surface; the remainder

corresponds...
shearing. So,... and maximum dilation angles are lower
than those corresponding to the initial undamaged surface. This is clear that the two
tests at the lowest normal stress shown in Figure 6.1... maximum dilation
rate from 0.8 ($\psi = 41°$) at the first run carried out... stress $\sigma_n = 60$ kPa,
reduces to 0.6 ($\psi = 31°$) at the second run ($\sigma_n = 160$ kPa), and 0.11 ($\psi = ...$) at the
third run $\sigma_n = 60$ kPa. So a decrease of 12° has taken place between two runs (run 2
and 3) at the same normal stress (60 kPa), after a previous normal stress of 160 kPa has
taken place between the run. This is in agreement with what is... corresponding to
the first set of experiments... shown in Figure 6.19. On the other hand, the
data for the dilation angles corresponding to peak shear strength are relatively low
for this type of test (extension fracture) and are not seen to be affected by previous
shearing, as illustrated by the data points corresponding to the two runs carried out
under 60 kPa normal stress. The maximum dilation rate tends to zero at a normal stress
σ_n of about... a maximum dilation rate corresponding to the peak shear strength
at a normal stress which is one order of... The corresponding projected
values at a normal stress $\sigma_n = 10$ kPa are about 1.5 (56°) and 0.95 (43.5°).

Fig. 6.17: Single test of repeated, multistage shear test on induced fracture in quartz syenite
(after Arnold, 1992)

(1) $y = 1.46x$ ($r^2 = 0.98$)
(2) $y = 0.81x$ ($r^2 = 0.98$)
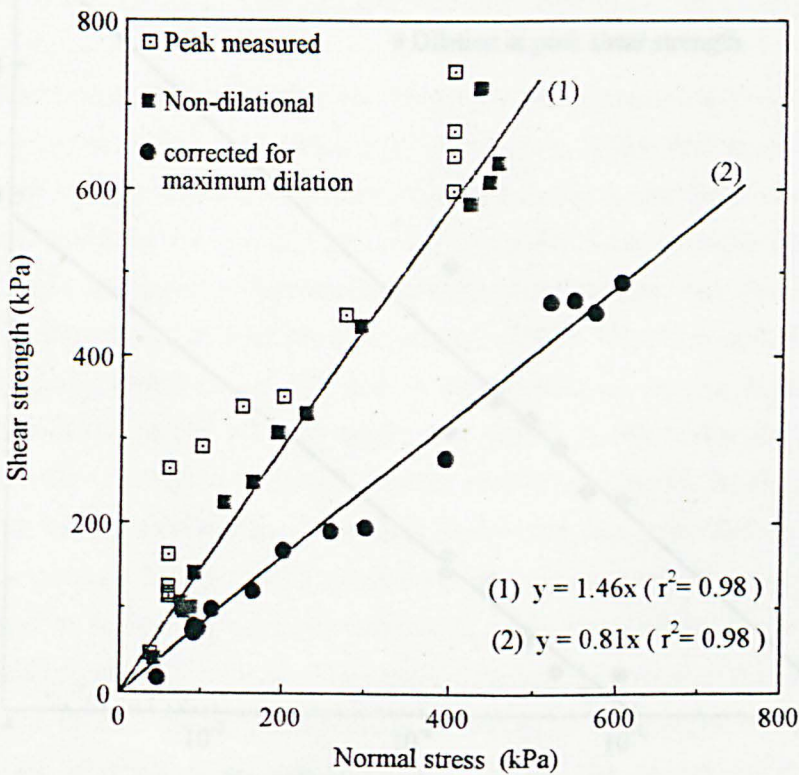
Fig. 6.18: Measured and non-dilational peak friction angle for tensile fractures
in quartz syenite (data from Arnold, 1992).

corresponds to joints which have been smoothened to some degree by the previous shearing. So, except for the first run, the measured maximum dilation angles are lower than those corresponding to the initial undamaged surface. This is clear from the two tests at the lowest normal stress shown in Figure 6.19, where the maximum dilation rate from 0.87 ($\psi = 41°$) at the first run carried out at a normal stress $\sigma_n = 60$ kPa, reduces to 0.60 ($\psi = 31°$) at the second run ($\sigma_n = 100$ kPa) and 0.55 ($\psi = 29°$) at the third run ($\sigma_n = 60$ kPa). So a decrease of 12° has taken place between two runs (nos. 1 and 3) at the same normal stress (60 kPa), after a run at normal stress of 100 kPa has taken place between them (run no 2). For this reason, only the data corresponding to the first test at each normal stress are included in Figure 6.19. On the other hand, the data for the dilation angles corresponding to the peak shear strength are relatively low for this type of joints (extension fractures) and are not seen to be affected by previous shearing, as suggested by the data points corresponding to the two runs carried out under 60 kPa normal stress. The maximum dilation rate tends to zero at a normal stress σ_{nT} of about 5MPa whereas the dilation rate corresponding to the peak shear strength at a normal stress which is one order of magnitude lower. The corresponding projected values at a normal stress $\sigma_{no}=10^{-4}\sigma_{nT}$ are about 1.5 (56°) and 0.95 (43.5°).
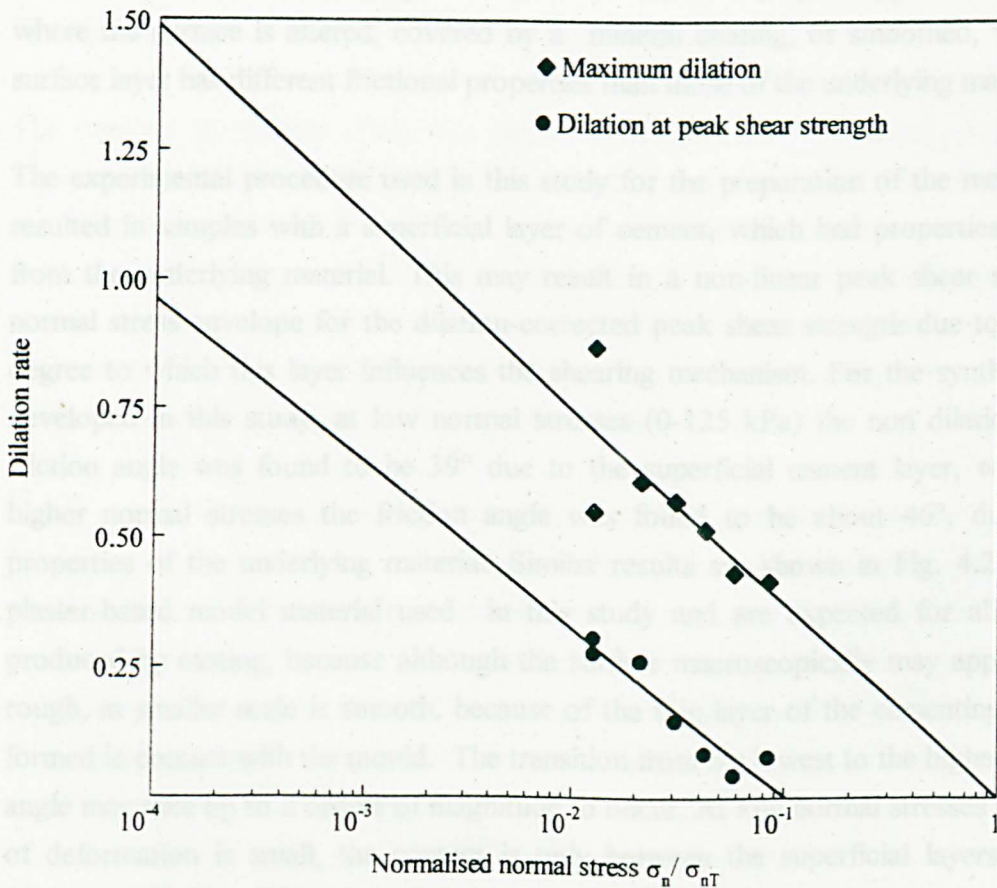
Fig. 6.19: Variation of dilation rate with normal stress for tensile fractures in quartz syenite (data from Arnold, 1992)

The value of 43.5° combined with a friction angle of 40° gives a value of 83.5° for the total friction angle, which can be considered as a practically maximum value (the theoretical maximum value being 90°). The two best fit lines are almost parallel, their difference in the $tan\psi$ axis giving the suppressed amount of dilation or the equivalent cohesional component (independent of normal stress). This suggests that the cohesional component can be estimated as a difference between the maximum asperity angle ψ_o and the maximum permitted dilation angle (maximum $90-\phi_m$).

A similar behaviour is observed in rock/concrete contacts (see for example Krsmanovic & Popovic, 1966, Ruiz *et al.* 1968 and Tsytovic *et al.*, 1970), where true cohesion is provided by the adhesion between rock and concrete. This adhesion is important at low normal stresses but has no significant effect at higher normal stresses (Krsmanovic & Popovic, 1966).

6.8 Joints with coated surfaces

The values for the friction angle of the rock wall material determined from triaxial tests and the non-dilational component of the peak friction angle determined from direct shear tests coincide if the frictional properties of the superficial layer in contact are the same as those of the underlying material. However, there are joint types, such as those where the surface is altered, covered by a mineral coating, or smoothed, where the surface layer has different frictional properties than those of the underlying material.

The experimental procedure used in this study for the preparation of the model joints resulted in samples with a superficial layer of cement, which had properties different from the underlying material. This may result in a non-linear peak shear strength - normal stress envelope for the dilation-corrected peak shear strength due to different degree to which this layer influences the shearing mechanism. For the synthetic rock developed in this study, at low normal stresses (0-125 kPa) the non dilational peak friction angle was found to be 39° due to the superficial cement layer, whereas at higher normal stresses the friction angle was found to be about 46°, due to the properties of the underlying material. Similar results are shown in Fig. 4.21 for the plaster-based model material used in this study and are expected for all surfaces produced by casting, because although the surface macroscopically may appear to be rough, at smaller scale is smooth, because of the thin layer of the cementing material formed in contact with the mould. The transition from the lowest to the highest friction angle may take up to 2 orders of magnitude to occur. At low normal stresses the depth of deformation is small, the contact is only between the superficial layers and the friction coefficient will be that of the layer. As the normal stress increases the thin layer breaks down, the deformation extends to the underlying material, and the frictional

resistance will be somewhere between that of thin layer and that of the underlying material. The relative contribution of each one of these coefficients will depend on the value of normal stress. The friction coefficient will increase with normal stress, and at some normal stress level will become equal to that of the underlying material.

Natural joints covered by mineral coatings behave in a similar manner. Such coatings consist of a continuous layer of minerals which form an entirely new surface of small thickness whose frictional properties may be quite different from those of the underlying material. In most cases the friction coefficient of a coating is lower than that of the rock itself, but the reverse may occur especially in iron stained rock surfaces (Brown et al., 1977). According to Welsh (1994), if the surface is coated with massive minerals, i.e. quartz, feldspar, calcite etc. the friction coefficient of the coating does not differ from that of natural rock surfaces, but if it is coated with platy minerals, i.e. mica, chlorite etc., the coefficient of friction of the surface will be much less than that for the massive minerals. In such cases, the value of friction angle determined from triaxial tests on intact samples does not reflect the frictional properties of the surface coating and therefore is not as reliable as that determined from direct shear tests. The difference is more pronounced at lower normal stresses where the surface material is more relevant to the shearing process and may be diminished at higher normal stresses where the adjacent wall material plays an increasingly important role.

The analogy in metallic friction is the case of an oxide film covering a surface. According to Bowden & Tabor (1964) the overriding factor which determines whether a coating will support a given load depends on the hardness of the coating relative to that of the underlying material. In the case of a soft and plastic coating covering the surface of a harder rock material, the coating will fracture progressively with normal load and the friction coefficient will be low at low normal stresses, but as the normal stress increases, the friction coefficient will increase.

In this case the peak shear strength envelope is curved upwards, which shows that with increasing normal stress the underlying material has a greater influence. Such curved envelopes have been observed in data reported by a number of different authors, such as Manolopoulou (1994) for kaolin coated model rock joints, Hencher & Richards (1989) for bitumen/calcite coated joints in dolomite and Arnold (1992) for iron-coated joints in quartz syenite. The results shown in Figure 4.33 may be interpreted on the same basis.
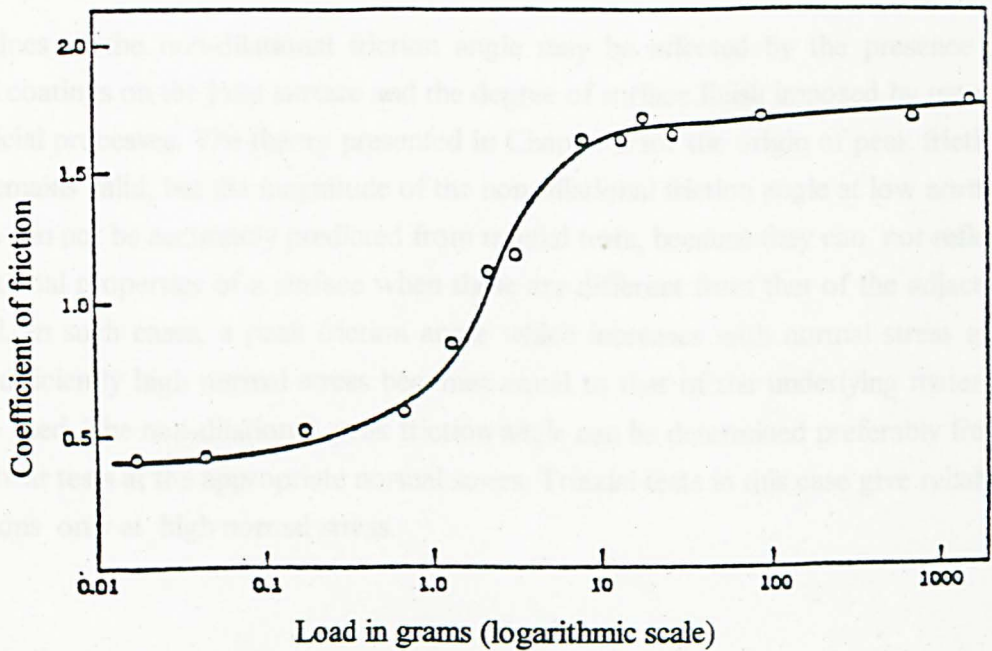
Fig. 6.20 :Variation of friction coefficient with normal load for copper covered with oxide film
(after Bowden & Tabor, 1964)

6.9. Concluding remarks

The new peak shear strength criterion has been successfully applied to a number of published experimental data. The basic principle that peak friction angle is a two-component parameter proved valid throughout. Variations in peak shear strength can therefore be attributed to changes in the dilation, whereas the frictional component remains constant.

The experimental results used as the basis for the *JRC-JCS* model, where both dilation angle and joint wall compressive strength are considered to be scale-dependent, have been used to show that the effect of sample size on peak shear strength is due to different dilation mobilised at different scales, and therefore *JCS* is scale-independent.

The scale-free block length can be determined from measurements of the maximum asperity slope on samples at different scales. Quite good agreement between different data sets on the magnitude of the scale-free block length (in the range 1.0-1.5 m) has been found.

A simple relation is proposed to estimate the maximum asperity slope at any scale from the maximum asperity slope of a laboratory-size sample. The experimental results indicate that in-situ shear strength of joints is dilation-free and therefore in-situ shear strength can be predicted from the frictional component only.

The values of the non-dilational friction angle may be affected by the presence of mineral coatings on the joint surface and the degree of surface finish imposed by natural or artificial processes. The theory presented in Chapter 5 for the origin of peak friction angle remains valid, but the magnitude of the non-dilational friction angle at low normal stresses can not be accurately predicted from triaxial tests, because they can not reflect the frictional properties of a surface when these are different from that of the adjacent material. In such cases, a peak friction angle which increases with normal stress and under sufficiently high normal stress becomes equal to that of the underlying material must be used. The non-dilational peak friction angle can be determined preferably from direct shear tests at the appropriate normal stress. Triaxial tests in this case give reliable predictions only at high normal stress.

CHAPTER 7
SINGLE SOIL-ROCK INTERFACES

7.1 Introduction

Interfacial problems are encountered in many geotechnical projects at different scales. Soil-rock interfaces involve contacts between two different lithological units one of which is classified as soil and the other one as rock. The distinction between soil and rock is not clear as the boundary between a weak rock and a hard soil is not defined. Interfaces usually have lower strength than the parts they separate and provide the weakest stress path in various circumstances. Some examples of such interfaces involve natural boundaries between rock and soil layers, transition zones in weathering profiles between soil-like and adjacent rock-like zone, boundaries between infill and rock wall in filled joints, etc. Such interfaces are commonly responsible for large scale landslides. Another type of interface which is of primary importance in civil engineering is that between soil and structures such as embankments, dams, retaining structures, foundations, grouting, bored piles etc. Usually, it forms a weak element in the transmission of forces from the structure to the ground. The extensive use of geosynthetics in recent years gave rise to interfacial problems between the geosynthetic liner and the soil. Some typical examples of interfaces between soils and rocks or construction materials are given in Figure 1.1. Contacts between natural rock and concrete structures such as pier sockets, tunnel linings, grouting etc. form an artificial discontinuity between two rock-like materials. The behaviour of these contacts is similar to that of natural rock discontinuities (Johnston Lam, 1989a and b) which has been discussed in Part I. The case of interfaces between two different soils is not considered here.

A number of investigators including Potyondy (1961), Brumund & Leonards (1973), Kulhawy & Peterson (1979), Desai (1981), Acar et al. (1982), Kishida & Uesugi (1987) and Al-Douri & Poulos (1991) have studied the shear behaviour of soil-structure interfaces, mainly aiming to resolve problems related to the shearing resistance between soil (particularly sand) and various construction materials (steel, wood, concrete, mortar etc.) as applied to foundation engineering. Kanji (1970 and 1974) and Bosscher & Ortiz (1987) used geological materials (granite, limestone, sandstone) and sand and kaolinite as soils. A number of numerical models have been proposed to describe characteristic shear behaviour of interfaces (e.g. Desai, 1987, Aydan et al., 1990). The relation between the shear strength of infill-rock wall interfaces and the shear strength of an infilled joint has been discussed by Kutter & Rautenberg (1979) and Papaliangas et al. (1990 and 1993).

7.2 Parameters affecting the shear behaviour of interfaces

As a boundary between different materials, a rock-soil interface is affected by both the properties of the rock and the soil. As far as the rock is concerned, the surface roughness is of primary importance (as discussed in Part I). Generally, a smooth interface has lower friction angle than a rough interface. Sowers & Sowers (1970) suggested that for a "smooth" concrete-sand interface the friction angle δ can be taken as equal to $(1/2-2/3)\phi$, where ϕ is the friction angle of the sand, whereas in the case of a "rough" interface δ can be taken as equal to ϕ. Brumund & Leonards (1973) compared the surface roughness to the grain size and concluded that when the rock surface is rough in comparison to the grain size of the sand, the interface friction angle exceeds the friction angle of the sand and the failure surface will be within the sand. In the case of interfaces between geotextiles and soils the shear strength of the interface is in the range $0.60 tan\phi \leq tan\delta \leq tan\phi$, where ϕ is the friction angle of the soil (Jewell, 1996), whereas the minimum direct sliding resistance is obtained for soils siding on a smooth metal surface and is of the order of $tan\delta \approx 0.4 tan\phi$ (Potyondi, 1961; Kishida & Uesugi, 1987).

The quantification of an interface roughness imposes some difficulties, as both the roughness of the rock surface and the grain size, shape and texture of the soil must be considered. Kulhawy & Peterson (1979) defined a relative roughness of the interface as follows

$$R_R = R_{structure}/R_{soil} \tag{7.1}$$

where

$R_{structure}$ is the roughness of the structural face and

R_{soil} the roughness of the soil described as

$$R = D_{60}D_{10}/D_{50}$$

where R is the roughness and D_{60}, D_{10} and D_{50} the 60%, 10% and 50% finer particle sizes. A soil-soil interface gives $R_R=1$ and is the boundary between smooth ($R_R<1$) and rough ($R_R>1$) interfaces . They found that in general for a smooth interface ($R_R<1$) δ/ϕ <1 and for a rough interface ($R_R>1$) $\delta/\phi \geq 1$.

Kishida & Uesugi (1987) used a normalised roughness R_n, to describe the behaviour of sand-steel interfaces. This is defined as

$$R_n = R_{max(L=D)}/D_{50} \tag{7.2}$$

where $R_{max(L=D)}$ is the R_{max} value of steel surface with gauge length $L=D_{50}$. A high correlation between R_n and the coefficient of interface friction over a wide range of sand diameter ($D_{50} = 0.16$-1.82 mm) was found. When $R_{max(L=0.2mm)}$ is larger than 100-150 times shear failure occurs in the sand, which is the weakest element.

The parameters which affect the shear strength of a soil such as voids ratio, grain size, angularity and surface texture of soil particles, grain-size distribution and normal stress also influence the shear behaviour of a soil-rock interface as found by several researchers, including Brumund & Leonards (1973), Kulhawy & Peterson (1979), Acar *et al.* (1982) and Al-Douri & Poulos (1991). For the same density, the interface friction angle is affected by the mineralogy of both the rock and the soil. For example Al-Douri & Poulos (1991) found that for the same density the interface friction angle for calcareous sand is greater than that for silica sand. This is in agreement with the results obtained by Koerner (1970) for quartz and calcite sands in triaxial tests and also with the results presented in Chapter 5, where silicate rocks were found to have lower friction angles than carbonates. Some rock surfaces covered with low friction minerals such as talc, chlorite etc. may experience much lower friction angle than most other rocks with clean surfaces.

Most studies related to the soil-rock interfaces are oriented to the determination of friction properties of construction materials faces (mainly steel and concrete) against sand. The purpose of the present series of tests is to examine the effect on the shear strength and deformation of roughness at larger scale, applicable to interfaces between various rocks and soils such as those between a rockfill dam and its foundation rock.

7.3 Experimental procedure

7.3.1 Materials tested

The experimental programme of this series of tests involves direct shear tests of soils of different size on rock surfaces with different roughness, including smooth planar, saw-toothed, and rough planar. Two different materials were used as soils, namely Leighton Buzzard standard sand and glass ballotini.

7.3.1.1 Soil Characteristics

Leighton Buzzard sand is a pure siliceous material with almost spherical particles, specific gravity 2.65 and bulk density 1.40 g/cm^3. The following standard grades, used for testing cement according to BS 4550:Part 5, were employed:

a) fine sand (S1) : 150/90μm, Fraction E, having a mean particle diameter of 115μm, and a uniformity coefficient of 1.4

b) medium/coarse sand (S2) : 1.18mm/600μm, Fraction B having a mean particle diameter of 850 μm and a uniformity coefficient of 1.5 and

c) coarse sand (S3) : 2.36/1.18 mm, Fraction A, which had a mean particle diameter of 1.70 mm and a uniformity coefficient of 1.5.

The range of grain size distribution for the three sands is shown in Figure 7.1.
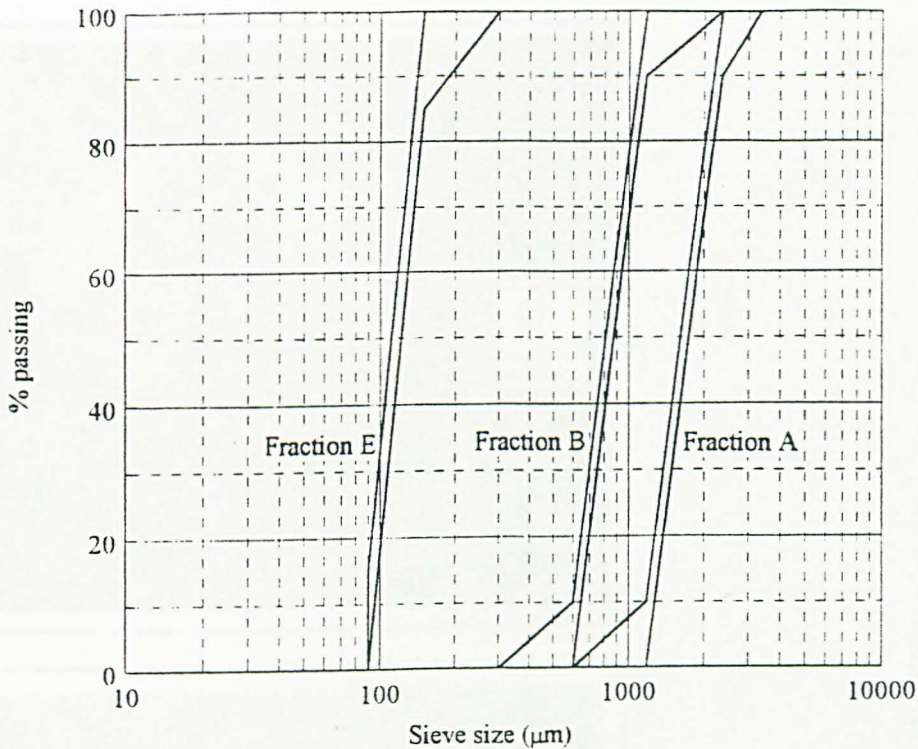
Figure 7.1: Grain size distribution of sands

Soda-lime glass ballotini with almost spherical particles (less than 3% max by number angular particles), was used in 2 different sizes with D = 1mm and D=3 mm which according to the manufacturer has a specific gravity 2.45-2.55 g/cm^3, bulk density 1.5 g/cc approx. and hardness Mohs 6, Rockwell 47 HRC or Knoop 518 kg/mm^2. The static and dynamic coefficient of friction is 0.9-1.0 and 0.7-0.8 respectively. Young's modulus (tensile) is $6.89x10^4$ N/mm^2, the rigidity modulus (flexural) $2.96x10^4$ N/mm^2 and Poisson's ratio is 0.21. A typical analysis gives the following composition: SiO_2 72.5%, NaO 13.7%, CaO 9.8%, MgO 3.3%, Al_2O_3 0.4%, $FeO;Fe_2O_3$ 0.2%, K_2O 0.1%.

The two soil materials were chosen for the following reasons:

1) Their behaviour (ballotini and uniform sands) is easier to understand than non-uniformly graded soils because the different shapes and particle sizes bring more complicated interparticle mechanisms.

2) They have been used as standard materials in research. As a consequence their behaviour is very well documented by high quality experimental data reported in the literature e.g. Skinner (1969), Stroud (1971), Jewell (1980), Palmeira (1987) and others. On the contrary, the idealised shape of the soil particles make the use of the results in a real situation questionable. However, the main aim of this study is to examine the mechanisms involved when a soil is sheared against a rock surface and in this context the selection is appropriate. Microphotographs of the three sands and the two glass ballotini grades used are shown in Plates 7.1 and 7.2.
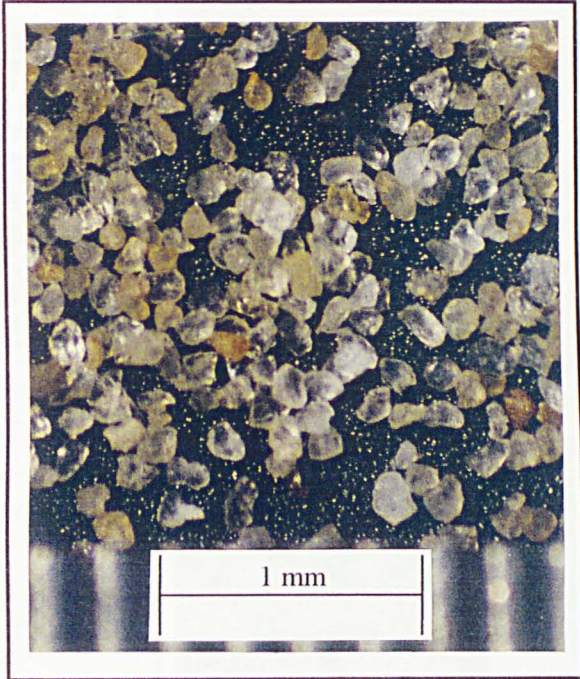
Sand 1

Sand 2

Sand 3

Plate 7.1: Microphotographs of the sands tested
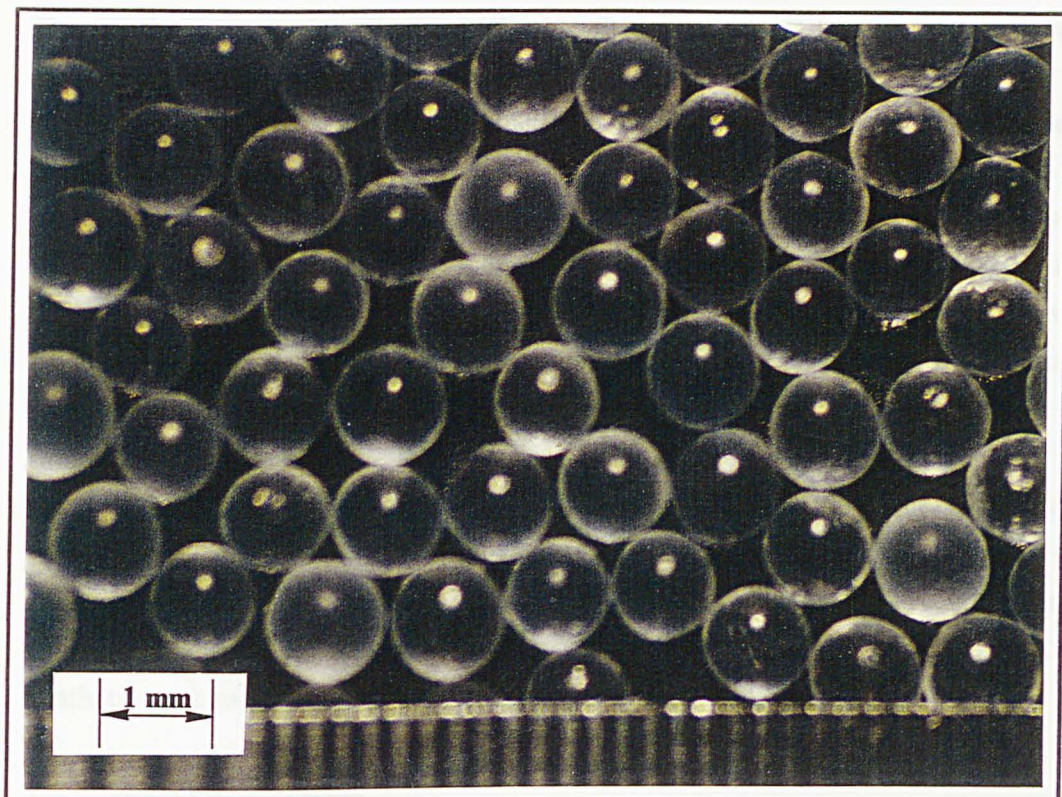
(a)
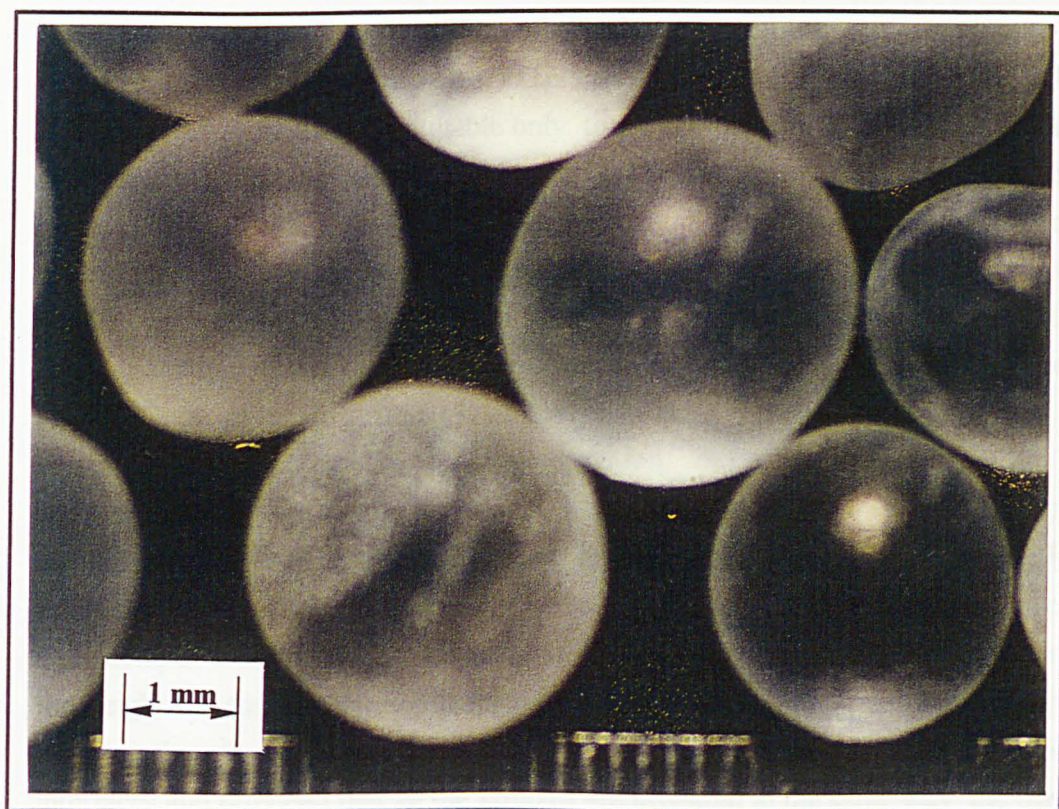
(b)

Plate 7.2: Microphotographs of glass ballotini: (a) D = 1 mm. (b) D = 3 mm.

7.3.1.2 Rock Characteristics

The synthetic rock described in Chapter 2 was used to produce several surface roughness configurations, saw-toothed and random. It was easy to use and could produce samples with repeatable geometrical and mechanical properties. The following different types of surfaces were used:

(a) Planar (P1): smooth planar surfaces produced by direct casting against a glass plate

(b) Indented (I): Three surfaces of saw-teeth shape were used having inclinations 10°, 20° and 30° (and occasionally 5°), as shown in Figure 7.2. The surfaces were first produced in an aluminium block by machining, from which an impression was made by using VINAMOLD. This impression was then used as mould to produce as many samples as required. The procedure is described in detail in Section 4.2.1.

(c) Rough (R): These surfaces were produced by brushing the free surface of the sample from the synthetic rock after setting and hardening, so that the aggregate grains were exposed at the surface. By changing the size of the aggregate, surfaces with different roughness could be produced. Brushing the surface of sample was easy as the synthetic rock tends to dry on the free surface if it is left to dry in the free air.

7.3.2 Sample preparation

A standard Wykeham Farrance shear box was used for all tests of this series. The sample size was 100x100mm and the shear load was applied by pulling of the lower half. This mode was found to be more reliable than the pushing mode (West, 1992). Automatic recording system with LVDT's was used. According to Kishida & Uesugi (1987), direct shear tests are suitable only to obtain the peak friction angle and not for modelling the full behaviour of the interface, since the measured shear displacement includes the deformation of the soil within the frame as well as the sliding displacement of the interface. The height of the soil mass would influence this value. However, the results compare well with those obtained from simple shear tests. Peak shear strength and frequently residual shear strength occurred at relatively small shear displacements (<5% of the shear box length) and well within the range of movements which corresponds to an acceptable level of deformation, with respect to the boundary effect. Serious reliability problems may occur when the grain size of the soil is large. The coarser material used in this study is the 3 mm glass ballotini. According to Roscoe (1970) the shear band thickness is approximately 10 times the diameter of the soil. For a diameter $D = 3$ mm, the estimated band thickness is about 30 mm, which is less than the height of the sample (about 40 mm). since the main purpose of this study is to examine the effect of roughness and soil size on the shear behaviour of soil-rock interfaces and provided that all the samples are prepared in the same way, the use of the direct shear apparatus is very advantageous. In addition, there are several published direct shear tests results for comparison. All tests of this series were performed by the author at normal stresses in the range 0-400 kPa and shearing rate 0.36 mm/min.

I1

10°

I2

20°

I3

30°

← 25 mm → | ← 25 mm → | ← 25 mm → | ← 25 mm →

← 100 mm →
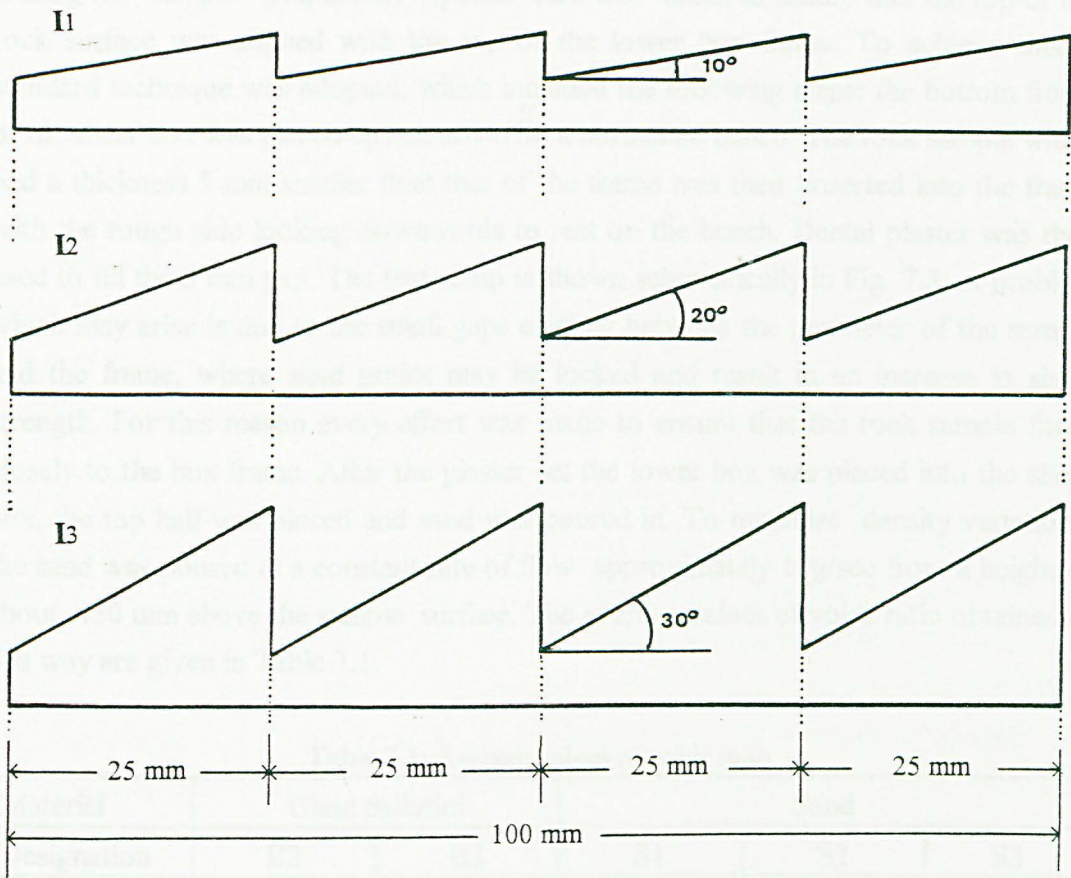
Figure 7.2: Shapes of saw-toothed modelled rock surfaces

Soil

Rock

Plaster
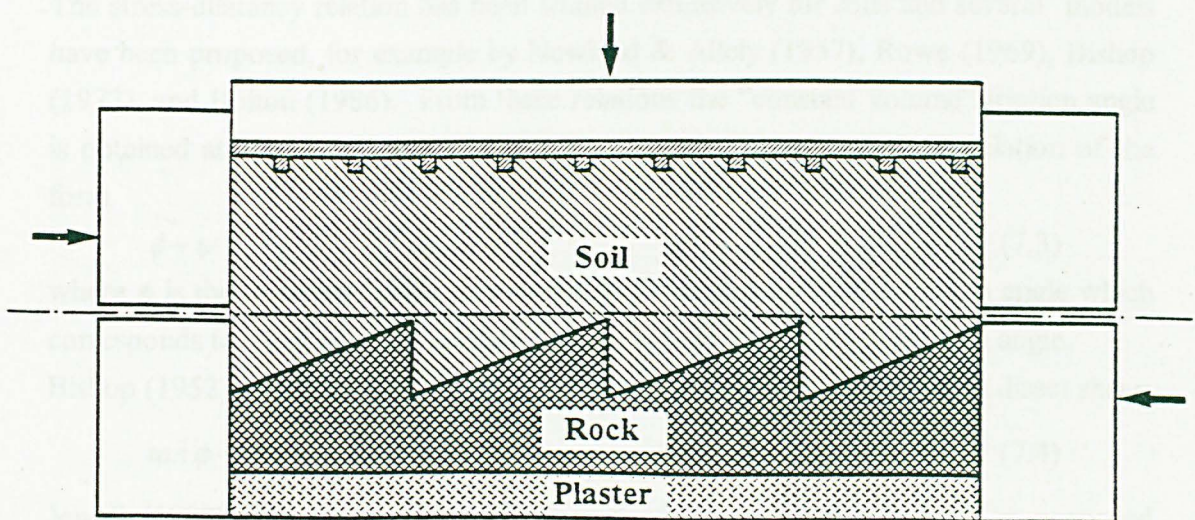
Figure 7.3: Direct shear test set-up

During the sample preparation special care was taken to ensure that the top of the rock surface was aligned with the top of the lower box frame. To achieve this, a standard technique was adopted, which included the following steps: the bottom frame of the shear box was placed upside down on a horizontal bench. The rock sample which had a thickness 5 mm smaller than that of the frame was then inserted into the frame with the rough side looking downwards to rest on the bench. Dental plaster was then used to fill the 5 mm gap. The test setup is shown schematically in Fig. 7.3. A problem which may arise is due to the small gaps existing between the perimeter of the sample and the frame, where sand grains may be locked and result in an increase in shear strength. For this reason every effort was made to ensure that the rock sample fitted closely to the box frame. After the plaster set the lower box was placed into the shear box, the top half was placed and sand was poured in. To minimise density variations, the sand was poured at a constant rate of flow approximately 10g/sec from a height of about 450 mm above the sample surface. The average values of voids ratio obtained in this way are given in Table 7.1.

Table 7.1: Average values of voids ratio

Material	Glass ballotini		Sand		
Designation	B2	B3	S1	S2	S3
Initial	0.46±0.02	0.45±0.00	0.86±0.05	0.73±0.03	0.64±0.02
After consolidation	0.45±0.02	0.44±0.00	0.82±0.05	0.71±0.03	0.62±0.02

7.3.3 Methods of analyses

The stress-dilatancy relation has been studied extensively for soils and several models have been proposed, for example by Newland & Allely (1957), Rowe (1969), Bishop (1972), and Bolton (1986). From these relations the "constant volume" friction angle is obtained at zero dilatancy. Newland & Allely (1957), proposed a relation of the form

$$\phi - \psi = \phi_{cv} \qquad (7.3)$$

where ϕ is the observed angle of shearing in direct shear, ϕ_{cv} the friction angle which corresponds to shearing with constant volume and ψ the observed dilation angle.

Bishop (1952) proposed the following relation to describe the behaviour in direct shear:

$$tan\,\phi - tan\,\psi = tan\,\phi_{cv} \qquad (7.4)$$

Jewell (1989) derived the following formula from the energy correction proposed originally by Taylor (1948):

$$tan\,\phi - tan\,\psi = sin\,\phi_{cv} \qquad (7.5)$$

Finally Bolton (1986) suggested the following empirical formula

$$tan\phi = tan\ (\phi_{cv} + 0.8\,\psi)\ cos\phi_{cv} \qquad\qquad (7.6)$$

The relations 7.3 to 7.6 can be used to analyse direct shear test results on granular materials. The relation 7.3 proved to describe very accurately the stress-dilatancy relation of rock joints, at any normal stress and independent of the joint roughness and scale (Part I). However, according to Bolton (1986), when applied to granular soils, for a certain constant volume friction angle ϕ_{cv}, it overestimates the observed $\phi - \phi_{cv}$ by about 20%. This happens because the assumption that shearing is equivalent to sliding along an inclined plane is accurate for rock joints but not for soils due to the wide range of inclinations of sliding contacts.

A comparison of the relations 7.3 - 7.6 s shown in Figure 7.4. A constant value of 0.60 is assumed for the shear stress/normal stress ratio at zero dilation for all relations, so that 7.4 and 7.5 become equivalent. According to Jewell (1989) the relation 7.5 is the most convenient to describe the behaviour of Leighton Buzzard sand in direct shear. However, shearing of interfaces may involve sliding of sand along the rock surface, and thus relation 7.3 may give acceptable results. For the purpose of analysis, the instantaneous dilation rate at failure $tan\,\psi$ was calculated as the ratio of the vertical dy to horizontal dx increments. The increment dx used was about 0.20 mm, which gives a quite detailed dilation curve, but smooth enough to be meaningful, as smaller intervals result in spurious values of dilation. The dilation angle at failure ψ_f was calculated as $arctan(dy/dx)$. The direct shear angle of friction ϕ can be determined by using the constant volume angle of friction ϕ_{cv} and the measured dilation angle ψ. Throughout the analysis in this work, the peak friction angle is meant to be the secant value, which results from the ratio of the peak shear stress to the normal stress (τ_p/σ). This must be clarified since the peak friction angle of soils is normal stress dependent (e.g. Lupini *et al.*, 1981 and Bolton, 1986).

7.4. Results and discussion on glass interfaces
7.4.1 Preliminary tests
A set of tests were carried out to determine the basic properties of ballotini. A number 5 mm soap washed glass ballotini were put in a cylindrical aluminium tin 60 mm diameter x 20 mm deep, and oven dried. Immediately after removing from the oven, a glass plate was placed on top and the whole system was turned upside down and placed on the tilt table. The mean value of sliding angle was equal to 10°. No particle rotation during sliding was observed from underneath the transparent tilting table. The same sample cleaned with water and tested in the same way in wet condition resulted in an average value of sliding of 24°. In a third configuration 100 glass spheres (5 mm dia) were fixed on a 10x10mm grid in mortar and subjected to sliding against a glass plate (cleaned with acetone) on the tilt table. The average value of the friction angle

The equations in the figure:

1. $\tan\phi = \sin\phi_{cv} + \tan\psi$

2. $\tan\phi = \tan\phi_{cv} + \tan\psi$

3. $\tan\phi = \tan(\phi_{cv} + 0.8\psi)\cos\phi_{cv}$

4. $\phi = \phi_{cv} + \psi$

Y-axis: shear stress/normal stress

X-axis: Rate of dilation
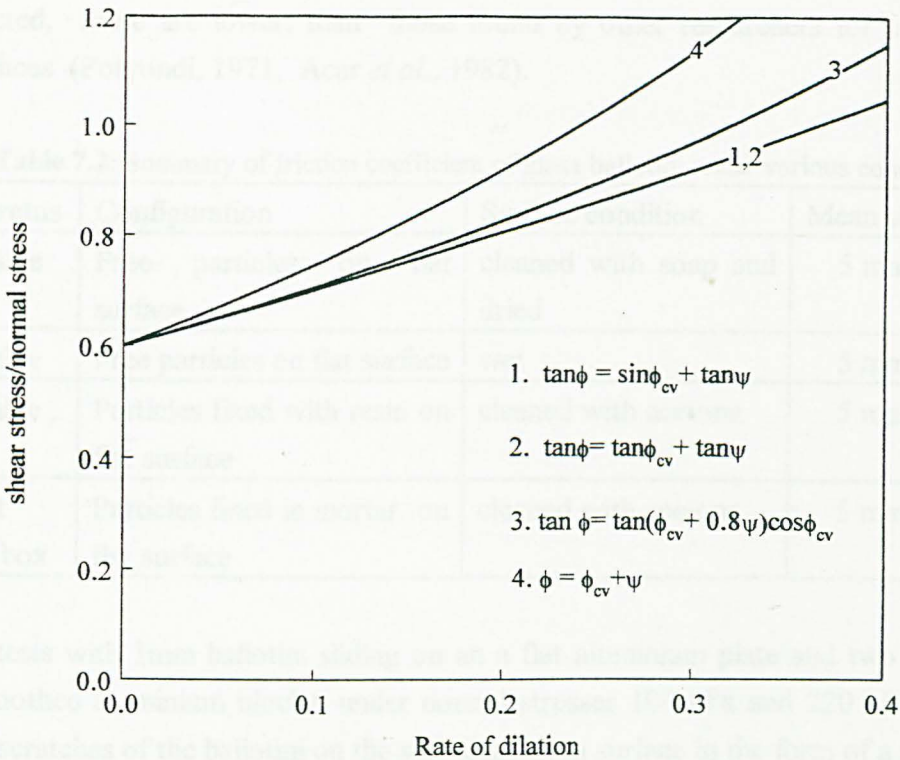
Figure 7.4: Comparison between various stress-dilatancy relations corresponding to a shear stress/ normal stress ratio of 0.6

obtained was $16°\pm2°$. Rolling-free sliding was secured, since the balls were fixed. In another configuration 5 mm glass balls were fixed with resin on a planar mortar block, washed with liquid soap and tested against a cleaned (with acetone) glass plate in the Wykeham Farrance shear box, with a total weight of 2365 g, which corresponds to a normal stress of 2.32 kPa. This resulted in a friction angle of 36°. These values suggest that the surface conditions largely affect the friction coefficient as noticed by many researchers (Skinner, 1969, Procter & Barton, 1974 and others). Clean dry particles have lower values than wet by a factor of 2. One of the disadvantages of the tilt table is that independent of the rate of tilting, small vibrations may occur, but the results obtained here are in very good agreement with published results by Procter & Barton (1974) who found for particle to plane sliding a mean value of friction angle of 15.5° for saturated balls and 5-10° for dry sample and for particle to particle sliding 17.9° (saturated) and 5°-10° (dry). Rowe (1962) reported values of 15° for 5 mm glass ballotini cleaned with soap, water and acetone. This value is higher than that observed in the tilt tests. A summary of results from these preliminary tests is given in Table 7.2.

The results from some direct shear tests on 1mm and 3mm glass balls sliding against a "smooth" steel plate under normal stresses up to 500 kPa are shown in Figure 7.4. The peak friction coefficient is 0.192 ($\phi = 10.9°$) for 1 mm balls and 0.181 ($\phi = 10.3°$) for 3mm. The residual value is somewhat lower: $\mu_r = 0.15$ ($\phi_r = 8.5°$) for both sizes. As

expected, these are lower, than those found by other researchers for steel - sand interfaces (Potyondi, 1971, Acar *et al.*, 1982).

Table 7.2: Summary of friction coefficient of glass ballotini under various conditions

Apparatus	Configuration	Surface condition	Mean size	ϕ_μ
Tilt table	Free particles on flat surface.	cleaned with soap and dried	5 mm	10°
Tilt table	Free particles on flat surface	wet	5 mm	24°
Tilt table	Particles fixed with resin on flat surface	cleaned with acetone	5 mm	16°
Direct shear box	Particles fixed in mortar on flat surface	cleaned with acetone	5 mm	36°

Two tests with 1mm ballotini sliding on an a flat aluminium plate and two others on saw-toothed aluminium blocks, under normal stresses 100 kPa and 220 kPa revealed small scratches of the ballotini on the soft aluminium surface in the form of a number of small lines parallel to the direction of sliding, showing particle parallel movement. The peak shear strength of the saw-toothed interface with 20° inclination was 6.3° higher than that of the flat interface, whereas the residual and non-dilational shear strength were about the same. The residual shear strength is almost identical for both flat (μ_p = 0.39) and saw-toothed interface (μ_p = 0.38) and equal to that of ballotini. Obviously the inclination of the teeth (20°) induces a dilation angle which is much lower (9°).

7.4.2 Direct shear tests on glass ballotini alone

In order to determine the frictional properties of a mass of ballotini particles $D = 1$ mm and $D = 3$mm a series of tests was carried out. A summary of the results are given in Table 7.3. The average voids ratio for these tests was $e_d = 0.46\pm0.02$ and $e_d = 0.45\pm0.01$ respectively. The shear stress - shear displacement and normal displacement - shear displacement diagrams shown in Figures 7.5 and 7.6 are of typical dense granular materials. The tests were run at normal stresses up to 500 kPa. It can be seen that for $D = 3$mm stick-slip occurs, which is characterised by an increasing with normal stress amplitude of oscillations. A similar phenomenon was not be observed for $D = $ 1mm. Stick-slip is a function of natural friction behaviour of a material, in that coefficient of static and kinetic friction differ, allied to the stiffness of the apparatus (Jaeger, 1971), which is the prime cause of the phenomenon (Byerlee, 1970). According to Procter & Barton (1974) it is inherent in all single contact friction tests and particularly so for glass ballotini, perhaps due to rapidly varying surface conditions.

For ballotini with $D = 3$ mm stick-slip behaviour is observed at all normal stresses. Typically, it begins when the shear stress approaches its peak value. The mechanism of
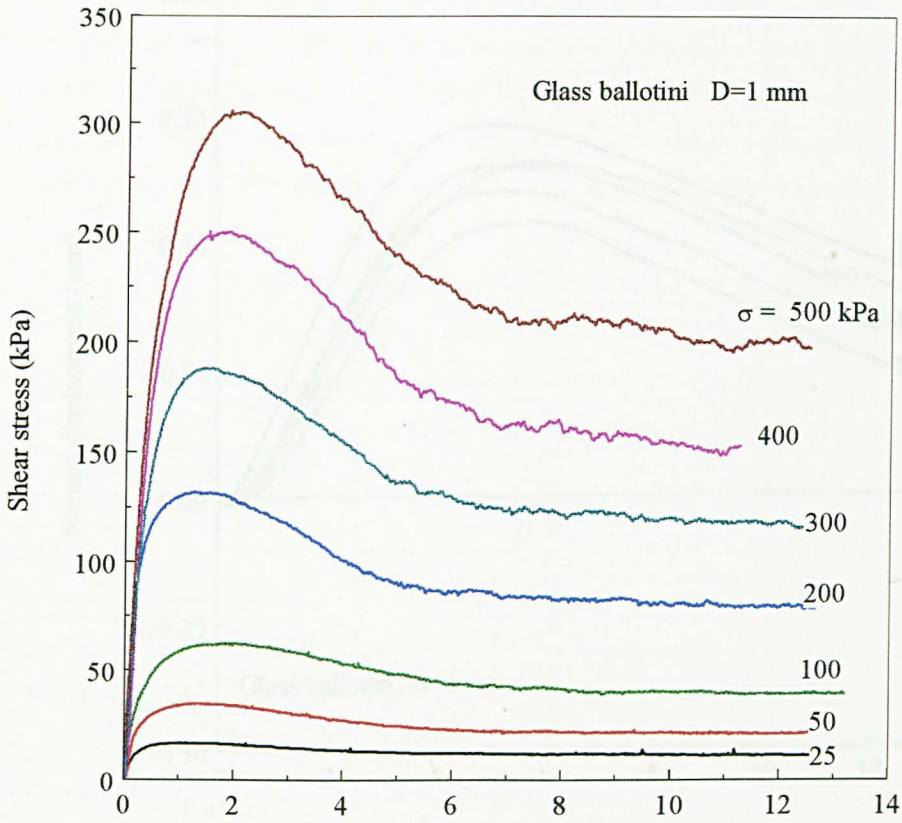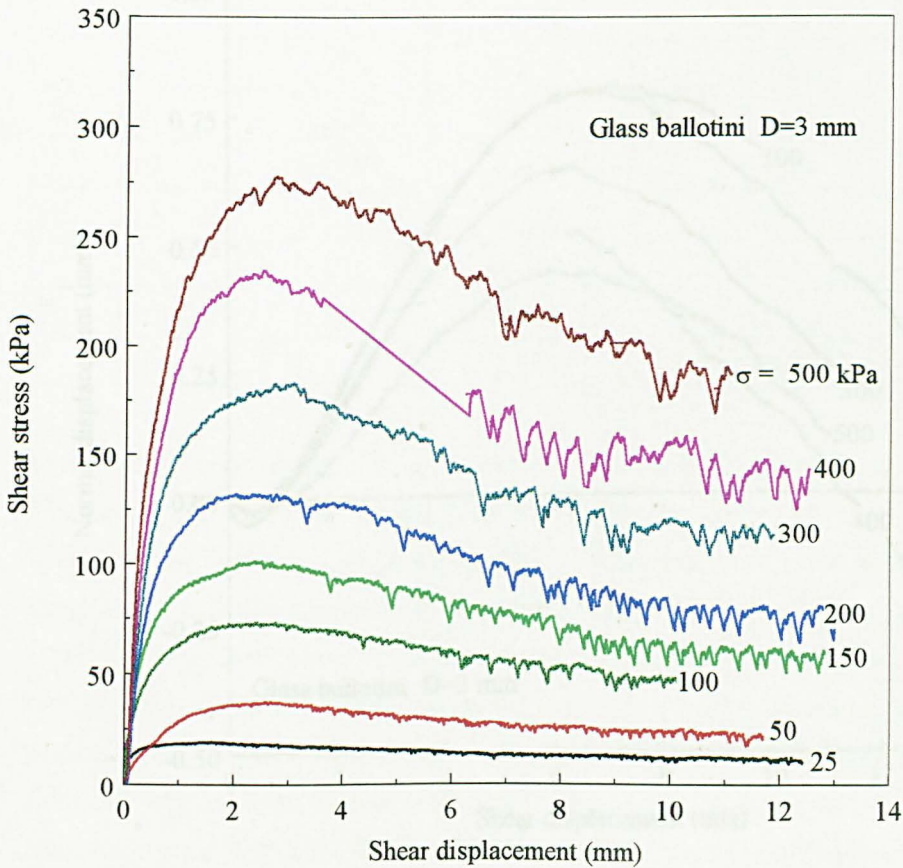
Figure 7.5: Shear stress-shear displacement diagrams for glass ballotini under various normal stresses shown on each curve: a) $D = 1$mm (b) $D = 3$ mm.

Normal displacement (mm)

1.00
0.75
0.50
0.25
0.00
-0.25
-0.50

200
400
100
300
500

(a)

Glass ballotini D=1 mm

0   2   4   6   8   10   12   14

Normal displacement (mm)

1.00
0.75
0.50
0.25
0.00
-0.25
-0.50

100
200
300
500
400

(b)

Glass ballotini D=3 mm

0   2   4   6   8   10   12   14
Shear displacement (mm)
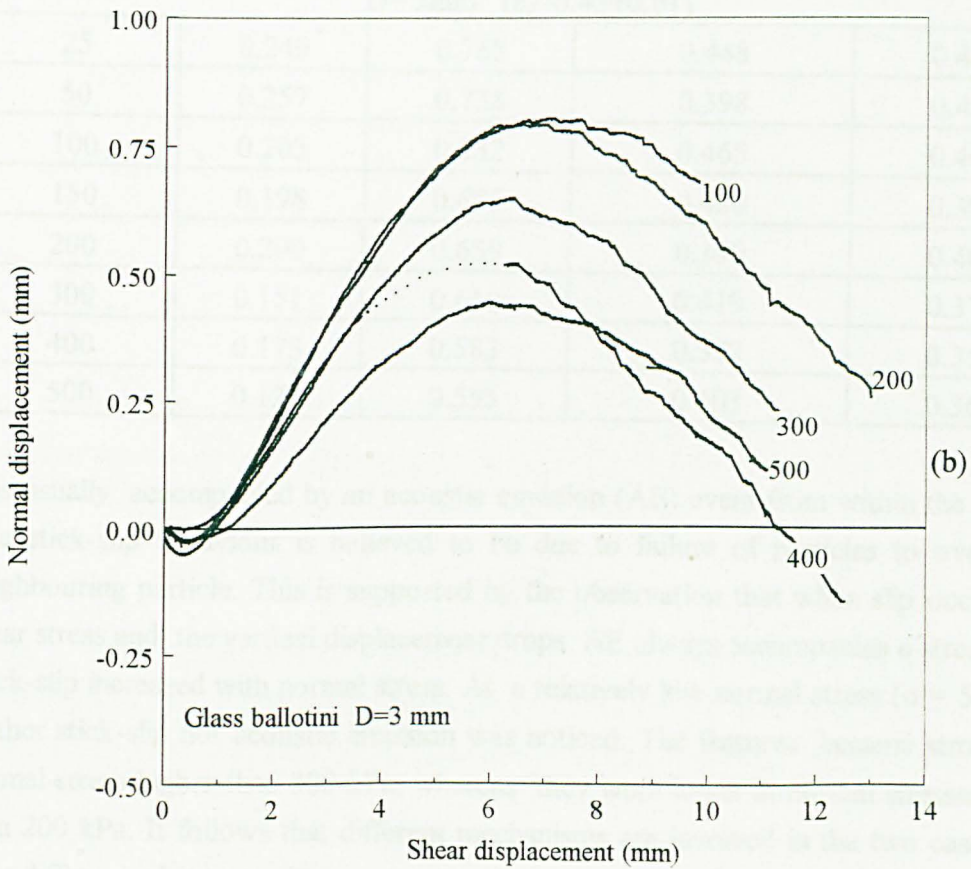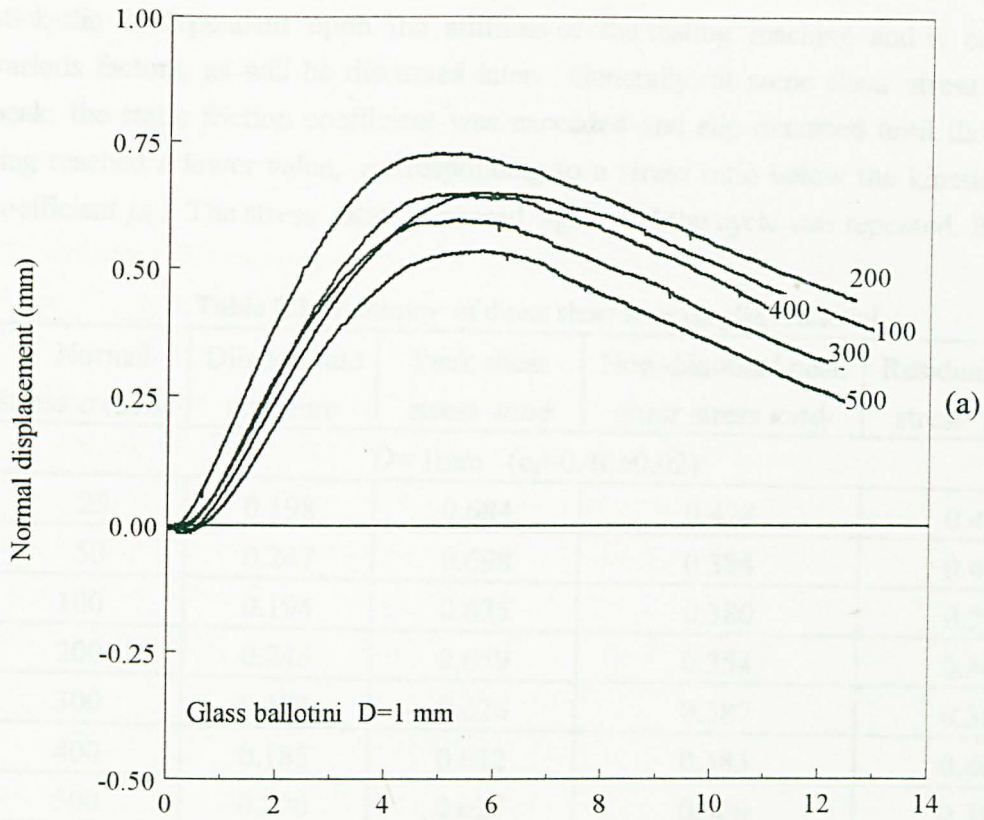
Figure 7. 6: Normal displacement-shear displacement diagrams for glass ballotini under various normal stresses shown on each curve: a) $D = 1$mm (b) $D = 3$ mm.

stick-slip is dependent upon the stiffness of the testing machine and is caused by various factors, as will be discussed later. Generally, at some shear stress near the peak, the static friction coefficient was exceeded and slip occurred until the proving ring reached a lower value, corresponding to a stress ratio below the kinetic friction coefficient μ_k. The stress ratio increased again and the cycle was repeated. Each slip

Table 7.3: Summary of direct shear tests on glass ballotini

Normal stress σ (kPa)	Dilation rate at failure	Peak shear stress $tan\phi$	Non-dilational peak shear stress $tan\phi_f$	Residual shear stress $tan\phi_{ds}$
$D=$ 1mm (e_d=0.46±0.02)				
25	0.198	0.684	0.428	0.46
50	0.247	0.698	0.384	0.42
100	0.194	0.625	0.380	0.39
200	0.246	0.659	0.354	0.40
300	0.193	0.626	0.387	0.38
400	0.185	0.612	0.383	0.40
500	0.200	0.627	0.380	0.39
$D=$ 3mm (e_d=0.45±0.01)				
25	0.240	0.768	0.448	0.440
50	0.257	0.738	0.398	0.420
100	0.203	0.732	0.465	0.460
150	0.198	0.675	0.420	0.393
200	0.200	0.659	0.399	0.400
300	0.151	0.610	0.419	0.373
400	0.173	0.583	0.372	0.350
500	0.125	0.555	0.403	0.360

was usually accompanied by an acoustic emission (AE) event from within the sample. The stick-slip behaviour is believed to be due to failure of particles to override a neighbouring particle. This is supported by the observation that when slip occurs, the shear stress and the vertical displacement drops. AE always accompanies a stress drop. Stick-slip increased with normal stress. At a relatively low normal stress (σ = 50 kPa), neither stick-slip nor acoustic emission was noticed. The features became stronger at normal stress higher than 300 kPa, whereas they were lower at normal stresses lower than 200 kPa. It follows that different mechanisms are involved in the two cases. The only difference between these two cases is the size of the particles and at the same normal stress, the load per particle is higher in the case of the coarser particles. Assuming that there are only two ways in which a particle can move relative to its neighbours, i.e. sliding or rolling, the balance of these two mechanisms differs in the

two cases. At high normal stresses particle crushing occurred which was proved by glass fragments found after the tests. Acoustic emission was generally stronger at peak shear stress. This event can be due either to a sudden movement e.g. particle rolling or failure to override neighbouring particles.

The variation of measured stress ratio at failure τ_p/σ with the dilation rate is given in Figure 7.7, from which the constant volume friction angle of glass ballotini is obtained by extrapolating the best fit line to zero dilation rate. The resulting value of τ/σ is 0.431 which is equivalent to a constant volume friction angle $\phi_{cv} = 25.5°$ if it is calculated as $asin(\tau/\sigma)$ as the relation (7.5) suggests or 23.3° if it is calculated as $atan(\tau/\sigma)$, according to the relation 7.4. When a plot of ϕ versus $tan\psi$ was produced the resulting value for ϕ_{cv} was 24.5°. This may suggest that the true constant volume friction angle is somewhere between the values predicted by the two stress dilatancy relations. The values of constant volume friction angle for glass ballotini obtained here are in agreement with those obtained by other authors. Rowe (1972) mentioned a value of 23° whereas Skinner (1969) found a value of 26°.

Peak shear strength envelopes are given in Figure 7.8. A straight friction line has been fitted for $D=1$ mm, corresponding to a friction angle of 31.8°, whereas for the residual shear strength the best-fit straight line passes through the origin and corresponds to 21°. This linear relation, which passes through the origin, indicates that errors associated with frictional resistance in the equipment are negligible. For glass ballotini $D=3$ mm the peak shear strength envelope decreases with increasing normal stress. No differences in the non-dilational shear strength or residual shear strength envelope for the two sizes of ballotini are observed.

Scott (1963) calculated the apparent coefficient of friction for a hexagonal close-packed array of equal spheres as:

$$\mu_{obs} = \frac{\sqrt{3} + 4\sqrt{2}\mu}{2(\sqrt{6} - \mu)} \tag{7.7}$$

where μ is the coefficient of mineral (particle to particle) friction for the spheres. Assuming that for 1 mm ballotini the mineral coefficient of friction is 0.18 ($\phi_\mu = 10°$), as suggested by Table 7.2, then the resulted coefficient of friction for the pack will be

$$\mu_{obs} = \frac{\sqrt{3} + 4\sqrt{2} \ \ 0.18}{2(\sqrt{6} - 0.18)} = 0.606$$

which corresponds to a friction angle of 31.2°. This is in a very good agreement with value of 31.8° for the peak shear strength which was calculated from the direct shear tests. If this is not a coincidence, then it suggests that theoretical predictions can be

made for the friction angle of a mass of particles when they are considered as spheres. From the direct tests it is seen that although the friction coefficient is often a very sensitive to surface condition, the shear behaviour of a mass of glass ballotini was adequately reproduced. According to Procter & Barton (1974) the dry conventional laboratory tests the dry behaviour of a single sand grain is analogous to the behaviour of a large mass of particles. This conclusion is fully supported by the results of this study. Skinner (1969) showed that a change of friction angle between particle contacts by a factor of at least four does not significantly change the ultimate shear strength of the material. Even then, this testing programme could be carried out without any reservations about special precautions about the surface condition of the glass balls.

7.4.3. Interaction between glass ballotini and flat glass surfaces

A number of tests were carried out on 1 mm glass ballotini sliding on a glass plate. A typical shear stress – shear displacement diagram shows a clear peak followed by a drop to a residual value (Figure 7.9). The values of the friction angle obtained were in the range 10-15°, which is comparable with the results obtained in the tilt table. After the end of the tests, scratches on the surface could be observed by visual examination.

Figure 7.7: Variation of measured peak shear stress ratio with the rate of dilation

In the figure: $(\tau/\sigma) = 0.431 + 1.132\tan\psi$

$\phi_{cv} = 23.3°$

♦ Ballotini D = 1mm
⊙ Ballotini D = 3 mm

Axes: τ/σ (vertical), Peak dilation rate (horizontal)

Ballotini D=1mm
♦ Peak $\tau = 0.621\,\sigma$ ($r^2 = 1.00$)
● Non-dilational $\tau = 0.380\,\sigma$ ($r^2 = 1.00$)
▲ Ballotini 1mm on glass plate
▽ Ballotini 1 mm on steel plate

Labels on envelopes: 31.8°, 21°, 10°

Axes: shear stress (kPa) (vertical), Normal stress (kPa) (horizontal)
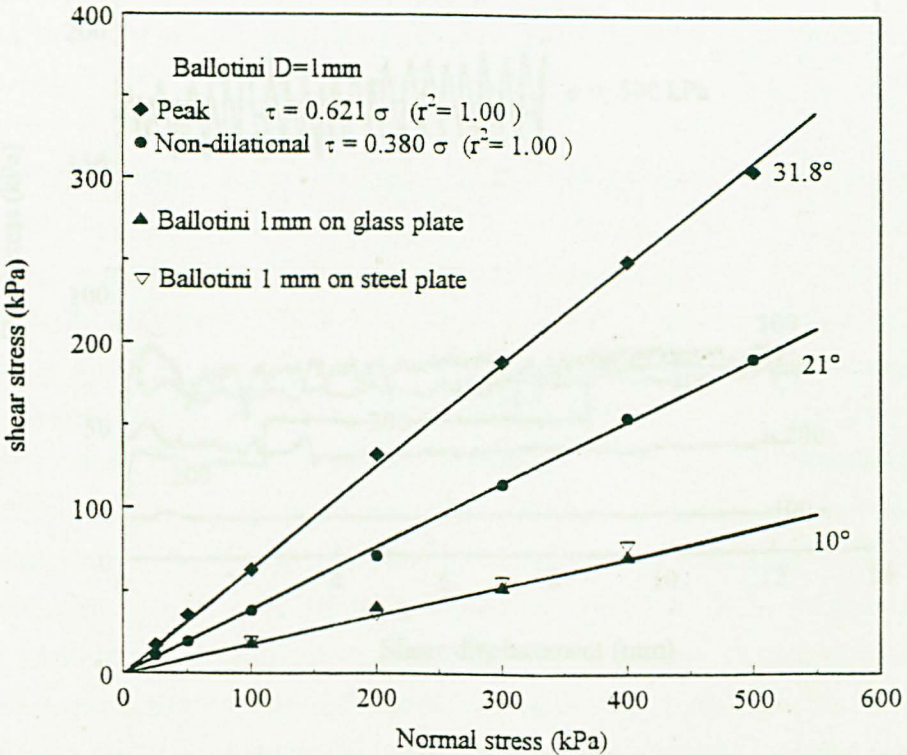
Figure 7.8: Shear strength envelopes for glass ballotini

made for the friction angle of a mass of particles when they are considered as spheres. From the above tests it is seen that although the friction coefficient of glass is very sensitive to surface condition, the shear behaviour of a mass of glass ballotini was adequately reproduced. According to Procter & Barton (1974), in any conventional laboratory test the dry behaviour of a single contact point is irrelevant to the behaviour of a large mass of particles. This conclusion is fully supported by the results of this study. Skinner (1969) showed that a change of friction angle between particle contacts by a factor of at least 5 does not significantly change the effective shear strength of the mass. Given this, this testing programme could be carried out without any reservations regarding special precautions about the surface condition of the glass balls.

7.4.3. Interfaces between glass ballotini and flat glass surfaces

A number of tests were carried out on 1 mm glass ballotini sliding on a glass plate. A typical shear stress - shear displacement diagram shows a clear peak followed by a drop to a residual value (Figure 7.9). The values of the friction angle obtained were in the range 10-15°, which is comparable with those obtained in the tilt table. After the end of the tests, scratches on the surface could be observed by visual examination.
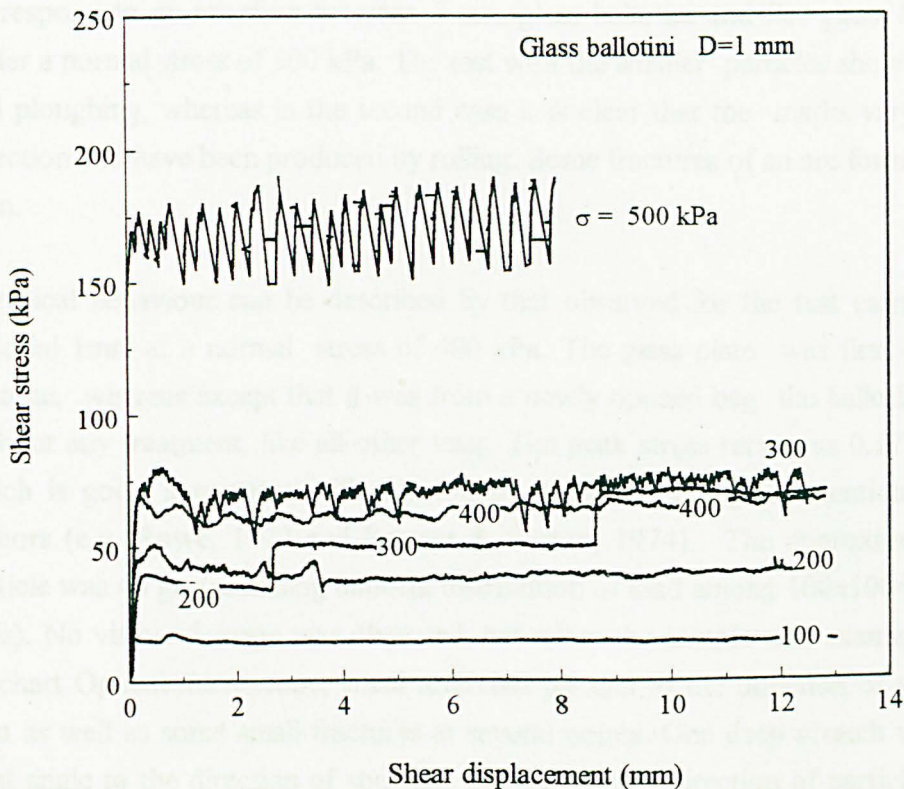
Figure 7.9: Shear stress shear displacement diagrams for glass ballotini 1mm, sliding on flat glass under various normal stresses, shown on each curve.

Their number increased with increasing normal stress. Stick-slip was shown to be favoured by high normal stress and smoothness of the surface and was noticeable for tests at normal stress above 200 kPa. The mechanism of stick-slip of a mass of particles subjected to shearing is irrelevant to that of ballotini sliding on glass plate. In the latter case, it appears that stick-slip correlates with indentation and ploughing. The phenomenon became more intense as the normal stress increased, where indentation and ploughing were considerable. At 500 kPa the stick-slip oscillation is about 5% of the value of peak shear stress. These results are in agreement with those of Engelder (1976) who showed that stick-slip for polished granite and quartzite occurs above a minimum normal load able to cause indentation and ploughing. This normal stress for the present series of tests was about 200 kPa. Microscopic observations suggest that stick-slip is associated with the brittle fracture of the flat glass surface, which according to Engelder & Scholz (1976) occurs in the flat surface regardless of the hardness contrast between the two contacting surfaces. Indentation is possible if the soil particle is small and the normal stress high. For large particles, indentation is not favoured, and sliding resistance becomes very high due to the high normal load applied. The alternative possible mechanism is rolling. An illustration of the different shear mechanisms observed is given in Plate 7.3, in which the top mark (a) corresponds to an interface between 1 mm glass ballotini and flat glass, whereas the other three correspond to an interface between 5 mm glass ballotini and flat glass, both sheared under a normal stress of 500 kPa. The test with the smaller particles shows indentation and ploughing, whereas in the second case it is clear that the marks vary in size and direction and have been produced by rolling. Some fractures of an arc form can also be seen.

A typical behaviour can be described by that observed for the test carried out with ballotini 1mm at a normal stress of 400 kPa. The glass plate was first cleaned with acetone, whereas except that it was from a newly opened bag the ballotini was used without any treatment, like all other tests. The peak stress ratio was 0.177 ($\phi_p = 10°$) which is good agreement with the friction angle for dry glass mentioned by other authors (e.g. Rowe, 1972 and Procter & Barton, 1974). The approximate load per particle was 40 gr. (assuming uniform distribution of load among 100x100=10000 glass balls). No visible damage was observed, but when the sample was examined under a Reichart Optical microscope, small scratches parallel to the direction of shearing was seen as well as some small fractures at several points. One deep scratch was about at right angle to the direction of shearing, showing either direction of particle movement or crack propagation between fractures caused by neighbour particles. The density of small spot fractures was not the same but it was concentrated on one quarter of the sample, showing non-uniform load distribution during shearing, which is one of the

Plate 7.3: Grooves produced on a glass plate by shearing of a mass of glass ballotini under a
normal stress of 500 kPa. (a) Ballotini 1 mm. (b)-(d) Ballotini 5 mm.

Their number increased with increasing normal stress. Stick-slip was shown to be favoured by high normal stress and smoothness of the surface and was noticeable for tests at normal stress above 200 kPa. The mechanism of stick-slip of a mass of particles subjected to shearing is irrelevant to that of ballotini sliding on glass plate. In the latter case, it appears that stick-slip correlates with indentation and ploughing. The phenomenon became more intense as the normal stress increased, where indentation and ploughing were considerable. At 500 kPa the stick-slip oscillation is about 5% of the value of peak shear stress. These results are in agreement with those of Engelder (1976) who showed that stick-slip for polished granite and quartzite occurs above a minimum normal load able to cause indentation and ploughing. This normal stress for the present series of tests was about 200 kPa. Microscopic observations suggest that stick-slip is associated with the brittle fracture of the flat glass surface, which according to Engelder & Scholz (1976) occurs in the flat surface regardless of the hardness contrast between the two contacting surfaces. Indentation is possible if the soil particle is small and the normal stress high. For large particles, indentation is not favoured, and sliding resistance becomes very high due to the high normal load applied. The alternative possible mechanism is rolling. An illustration of the different shear mechanisms observed is given in Plate 7.3, in which the top mark (a) corresponds to an interface between 1 mm glass ballotini and flat glass, whereas the other three correspond to an interface between 5 mm glass ballotini and flat glass, both sheared under a normal stress of 500 kPa. The test with the smaller particles shows indentation and ploughing, whereas in the second case it is clear that the marks vary in size and direction and have been produced by rolling. Some fractures of an arc form can also be seen.

A typical behaviour can be described by that observed for the test carried out with ballotini 1mm at a normal stress of 400 kPa. The glass plate was first cleaned with acetone, whereas except that it was from a newly opened bag the ballotini was used without any treatment, like all other tests. The peak stress ratio was 0.177 ($\phi_p = 10°$) which is good agreement with the friction angle for dry glass mentioned by other authors (e.g. Rowe, 1972 and Procter & Barton, 1974). The approximate load per particle was 40 gr. (assuming uniform distribution of load among 100x100=10000 glass balls). No visible damage was observed, but when the sample was examined under a Reichart Optical microscope, small scratches parallel to the direction of shearing was seen as well as some small fractures at several points. One deep scratch was about at right angle to the direction of shearing, showing either direction of particle movement or crack propagation between fractures caused by neighbour particles. The density of small spot fractures was not the same but it was concentrated on one quarter of the sample, showing non-uniform load distribution during shearing, which is one of the

disadvantages of the direct shear test. Due to this problem, the marks of any shape on the surface are mainly concentrated one half of the surface.

7.4.4. Interfaces between glass ballotini and saw-toothed modelled rock surfaces

Several tests on interfaces between glass ballotini and saw-toothed surfaces were carried out. It must be born in mind, when interpreting these results, that the surfaces of the saw-toothed blocks were smooth, because they were produced originally from a smooth aluminium block from which a VINAMOLD impression was made, which gives always a smooth finish (Chapter 4.2.1).

Values of the secant peak friction angle of the glass ballotini ($tan\phi$), the interface ($tan\delta$) and the ratio $tan\delta/tan\phi$ at different normal stresses are given in Tables 7.5a and 7.5b.

The friction angle of the interface is always lower than that of the glass ballotini, irrespective of normal stress and angle of inclination of the rock surface. The ratio of $tan\delta/tan\phi$ is between 0.757 and 0.923. Higher values correspond to rougher surface and lower normal stress. When the normal stress is high the particles are forced to move along the interface, the failure path thus involves higher proportions along the interface. Peak shear strength envelopes are shown in Figure 7.10.

Only one type of saw-toothed surface with $i=30°$ was used with ballotini $D = 3$ mm. The results are shown in Table 7.5.b, from where it is seen that the shear stress ratio of the interface is about the same with that of the ballotini itself. This is because, the inclined rock surface due its steepness does not offer an easier path, thus failure plane entirely through the sand is established.

Table 7.5a: Peak values of $tan\phi$, $tan\delta$ and ratio $tan\delta/tan\phi$ for rock saw-toothed surfaces with ballotini $D = 1$ mm

Normal stress (kPa)		100	200	300	400
Glass ballotini	$tan\phi$	0.625	0.659	0.626	0.612
Glass ballotini vs.	$tan\delta$	0.540	0.499	0.497	0.488
saw-toothed 10° (I1B2)	$tan\delta/tan\phi$	0.864	0.757	0.794	0.797
Glass ballotini vs.	$tan\delta$	0.540	0.525	0.516	0.495
saw-toothed 20° (I2B2)	$tan\delta/tan\phi$	0.864	0.797	0.824	0.809
Glass ballotini vs.	$tan\delta$	0.577	0.589	0.558	0.538
saw-toothed 30° (I3B2)	$tan\delta/tan\phi$	0.923	0.894	0.891	0.879

Peak shear stress
◇ i = 30°
○ i = 20°
□ i = 10°
· Ballotini 1mm

Shear stress (kPa)

Residual shear stress
◇ i = 30°
○ i = 20°
□ i = 10°
· Ballotini 1mm

Shear stress (kPa)
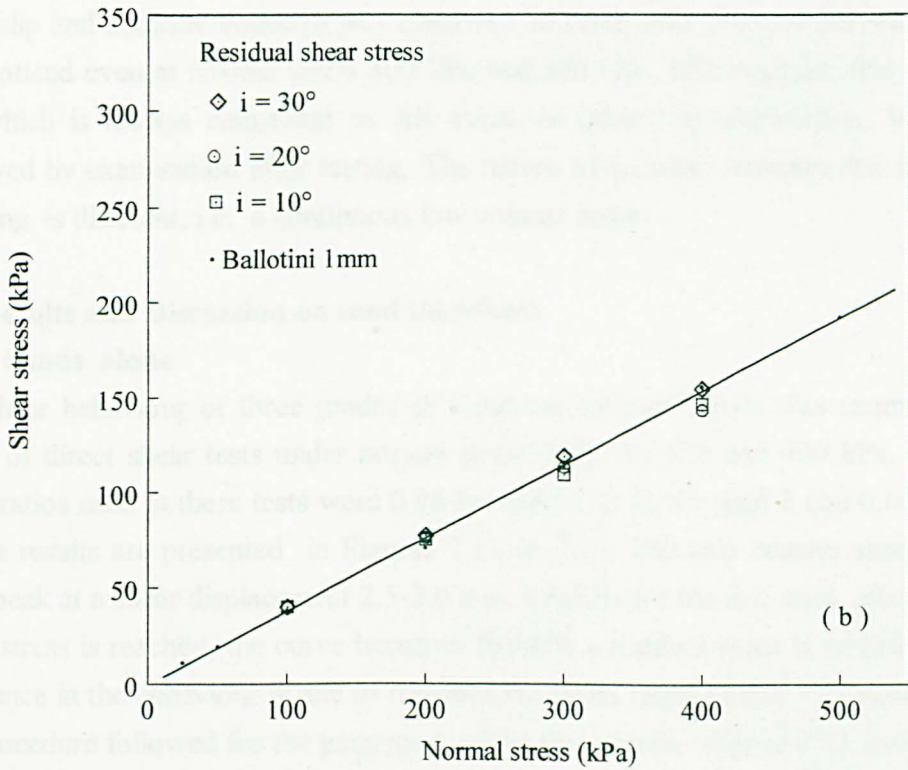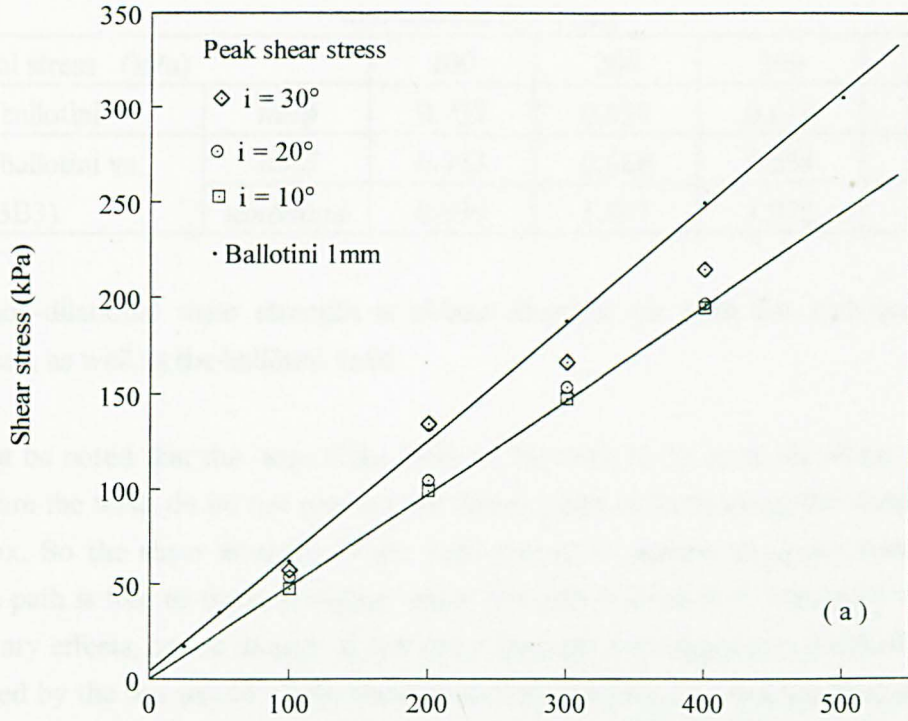
Normal stress (kPa)

Figure 7.10: Shear strength envelopes for glass ballotini/saw-toothed interfaces:
(a) Peak   (b) Residual

Table 7.5b: Peak stress ratio *tanφ*, *tanδ* and ratio *tanδ/tanφ* for rock saw-toothed surfaces
with ballotini *D* = 3 mm

Normal stress (kPa)		100	200	300	400
Glass ballotini	*tanφ*	0.732	0.659	0.610	0.583
Glass ballotini vs.	*tanδ*	0.733	0.668	0.654	0.579
30°(I3B3)	*tanδ/tanφ*	0.999	1.013	1.072	0.993

The non-dilational shear strength is almost identical for both flat and saw-toothed
interface, as well as the ballotini itself.

It must be noted that the top of the teeth of the rock block is on the shear plane and
therefore the teeth do no not prevent the failure plane to form along the shear plane of
the box. So the shear strength of the sand should be always an upper bound, if the
failure path is free to form. If higher shear strength is measured, this must be due to
boundary effects, or the sample is due shear through rock asperities. Boundary effects
imposed by the top platen of the shear box may generate load-bearing bridges formed
by particles. This is of special interest for the case of double soil-rock interfaces.

Stick-slip and acoustic emission was observed in these tests , but no particle crushing
was noticed even at normal stress 400 kPa and 500 kPa. This suggests that the stick-
slip which is always connected to AE event, is caused by indentation, which was
observed by examination after testing. The nature of acoustic emission due to particle
crushing is different, i.e. a continuous low volume noise.

7.5. Results and Discussion on sand interfaces
7.5.1. Sands alone

The shear behaviour of three grades of Leighton Buzzard sands was examined by a
series of direct shear tests under normal stress 100,200, 300 and 400 kPa. the initial
voids ratios used in these tests were 0.86 for sand 1, 0.73 for sand 2 and 0.64 for sand
3. The results are presented in Figures 7.11 to 7.13. The two coarser sands show a
clear peak at a shear displacement 2.5-3.0 mm, whereas for the fine sand, after a certain
shear stress is reached, the curve becomes flat and a residual value is established. The
difference in the behaviour is due to the different voids ratios (Table 7.1) resulted from
the procedure followed for the placement of the three sands. Figure 7.11 indicates that
there is a tendency for stick-slip behaviour as the normal stress and the grain size
increases, similar to that observed for ballotini (see Figure 7.5). The reason for this
stick-slip is attributed to particle breakage, which occur at high normal stresses. This
deformation mechanism is common in structures like tall earth dams which subject the
underlying soils to significant stresses, resulting in significant changes in the grain-
size curve of the original soil (Lade *et al.*, 1996). Uniform sands like those used in this
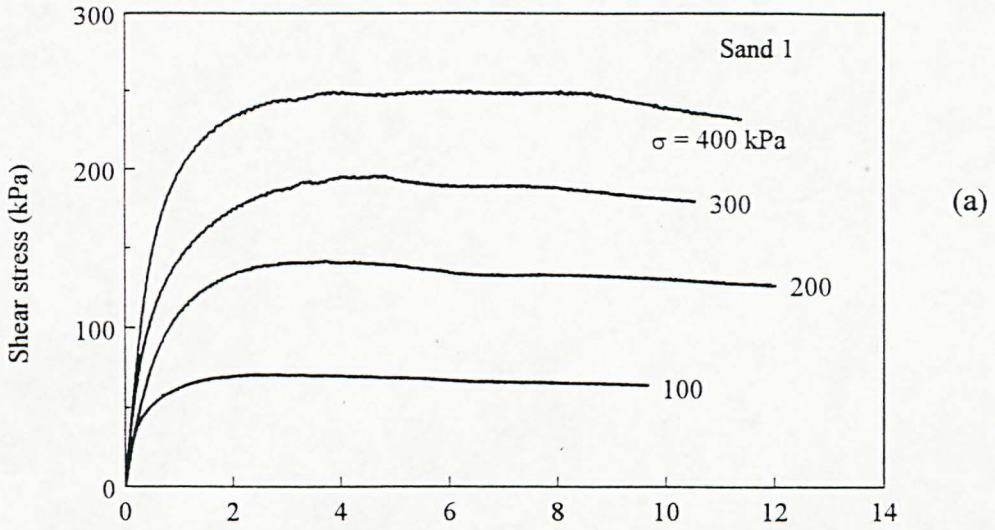
Figure 7.11: Shear stress - shear displacement diagrams for sands

1. $\sigma = 100$ kPa
2. $\sigma = 200$ kPa
3. $\sigma = 300$ kPa
4. $\sigma = 400$ kPa

Sand 1

(a)

1. $\sigma = 100$ kPa
2. $\sigma = 200$ kPa
3. $\sigma = 300$ kPa
4. $\sigma = 400$ kPa

Sand 2

(b)

Normal displacement (mm)

Sand 3

1. $\sigma = 100$ kPa
2. $\sigma = 200$ kPa
3. $\sigma = 300$ kPa
4. $\sigma = 400$ kPa

(c)

Shear displacement (mm)

Figure 7.12: Normal displacement - shear displacement diagrams for sands

study, are more susceptible to particle breakage than uniformly graded ones, because there are lesser interparticle contacts and the load per contact is more than those in a well-graded soil (Lambe & Whitman, 1969). For the same reason coarse particles of sand are more prone to particle crushing than finer particles.

For the coarser sand (S3) the average peak friction angle is 43.5° and the corresponding instantaneous dilation angle 12.4°, occurring at an average shear displacement of 2.8 mm. The range of the peak shear displacement is between 2.5 and 3.1 mm, with the larger values corresponding to higher normal stresses. For sand 2 the average peak friction angle is 37.6° and the average dilation angle 8°. The mean peak shear displacement is somewhat lower than that of the coarser sand (2.5 mm) and again increases with normal stress. Similarly, for sand 1 the average peak friction angle is 33° and the dilation 2.3°. In this case, the average peak shear displacement is 3.9 mm, which is higher than that corresponding to other sizes, due to the flat shape of the shear stress - shear displacement graphs and some uncertainty on the exact position of the peak caused by this. . With the above three sets of ϕ–ψ values, a comparison of the stress-dilatancy relations referred to in Section 7.3.4 is made. From Table 7.6, the results shown in column 3, correspond to the relation 7.4, proposed by Bishop (1972). The value for the constant volume friction angle for the three sand grades vary from 31.3° to 36°, with an average of 33.2°.

The results shown in column 5 correspond to the relation proposed by Bolton (1986), which gives very consistent and realistic results. It must be noted that Bolton (1986) suggests $\phi_{cv} = 33°$ for quartz sand, whereas Jewell (1989) accepts values of ϕ_{cv} between 33° and 35°. The sand 2 specifically is the same with that tested by several researchers at Cambridge (e.g. Stroud, 1971, Jewell, 1980, Palmeira, 1987 etc.) and the accepted value of constant volume friction angle is 35°, which matches very closely the value resulted from these tests by using Bolton's relationship. According to Jewell (1989), differences up to 1.5° in the value of the constant volume friction angle of Leighton Buzzard sand can occur even between different batches of the same sand. The relation 7.5 gives unacceptably high values (column 4), whereas it is worth to note the consistent values for the three sands obtained by using the relation 7.3 (column 2), which however, are about 20% lower than that obtained by Bolton's relation.

The peak shear strength and residual shear strength envelopes are shown in Figure 7.13. The residual values are taken from the last portion of the shear stress - shear displacement diagram. Generally, the results from direct shear tests become increasingly inaccurate with shear displacement due to rotation of the upper box, material lose etc. Therefore, values of shear stress obtained at large shear displacement are unreliable but they can be used for comparison with values of the same or other materials
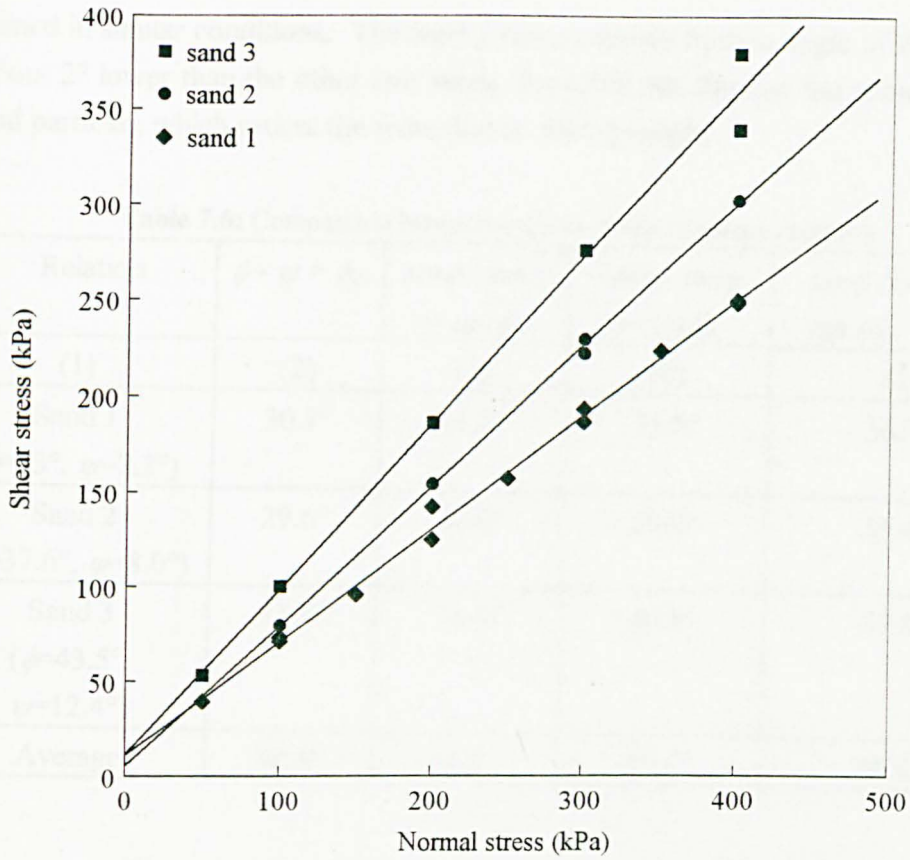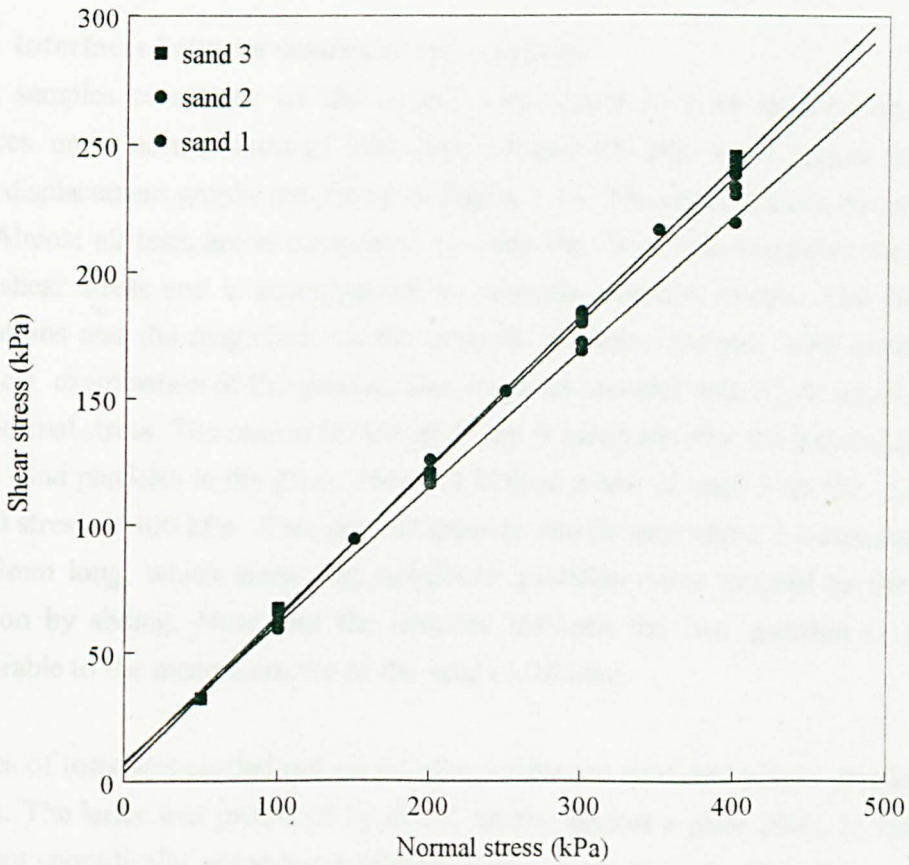
Figure 7.13: Shear strength envelopes for sands : (a) Peak. (b) Residual

obtained in similar conditions. The sand 2 has a residual friction angle of 28.5°, which is about 2° lower than the other two sands. Probably this fraction has somewhat more round particles, which causes the reduction in friction angle.

Table 7.6: Comparison between various stress-dilatancy relations

Relation	$\phi - \psi = \phi_{cv}$	$\tan\phi - \tan\psi$ $= \tan\phi_{cv}$	$\tan\phi - \tan\psi$ $= \sin\phi_{cv}$	$\tan\phi / \cos\phi_{cv} =$ $\tan(\phi_{cv} + 0.8\psi)$
(1)	(2)	(3)	(4)	(5)
Sand 1 (ϕ=33°, ψ=2.3°)	30.7°	31.3°	37.5°	36.7°
Sand 2 (ϕ=37.6°, ψ=8.0°)	29.6°	32.2°	39.0°	35.4°
Sand 3 (ϕ=43.5°, ψ=12.4°)	31.1°	36.0°	46.8°	37.8°
Average	30.5°	33.2°	41.1°	36.6°

7.5.2 Interfaces between sands and flat surfaces

Eight samples consisted of the coarser sand (sand 3) were sheared on flat glass surfaces under normal stress of 100, 200, 300 and 400 kPa. Some typical shear stress-shear displacement graphs are shown in Figure 7.14. The resulted peak friction angle is 32°. Almost all tests are accompanied by stick-slip. Stick-slip begins in the region of peak shear stress and is accompanied by acoustic emission events. The shear stress oscillations and the magnitude of the acoustic emission increase with normal stress. Post-test examination of the glass surface revealed grooves with depth which increases with normal stress. The reason for the stick-slip is believed to be the indentation caused by the sand particles in the glass. Plate 7.4 is from a test of sand 3 on flat glass under normal stress of 400 kPa. Two parallel grooves can be seen about 1.2 mm apart and at least 3mm long, which show that neighbour particles move parallel to the shearing direction by sliding. Note that the distance between the two grooves (1.2 mm) is comparable to the mean diameter of the sand (1.70 mm).

A series of tests was carried out on interfaces between sand and planar modelled rock surface. The latter was produced by direct casting against a glass plate. It had smooth finish but sporadically some pores of various sizes were present. Only the coarser sand (sand 3) was used in these tests. An interesting feature is that the peak shear strength envelope is curved upwards. This shows an increasing with normal stress involvement of the subsurface material which is caused by indentation. A similar mechanism operates in rock joints with smooth surface and the reason is the same: At low normal
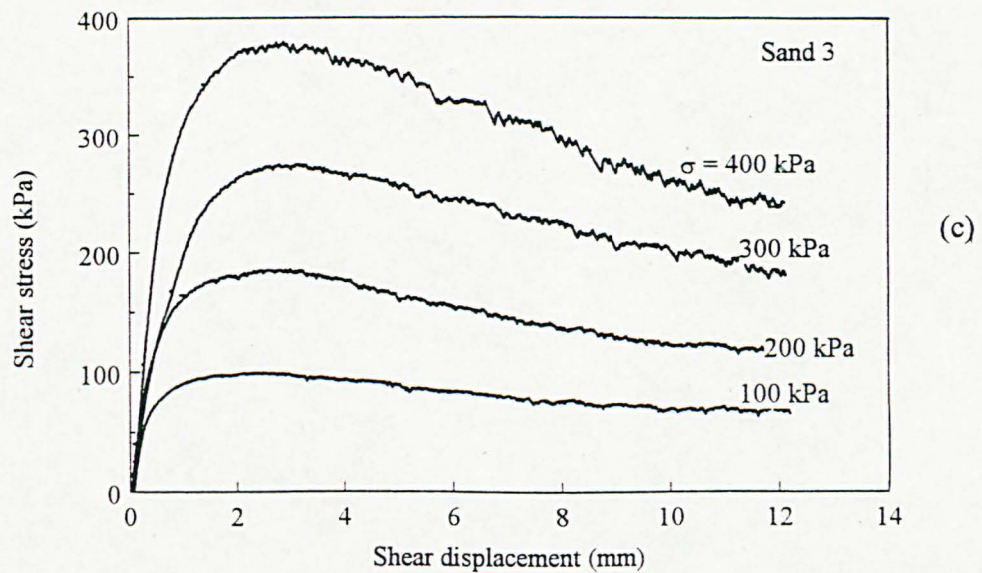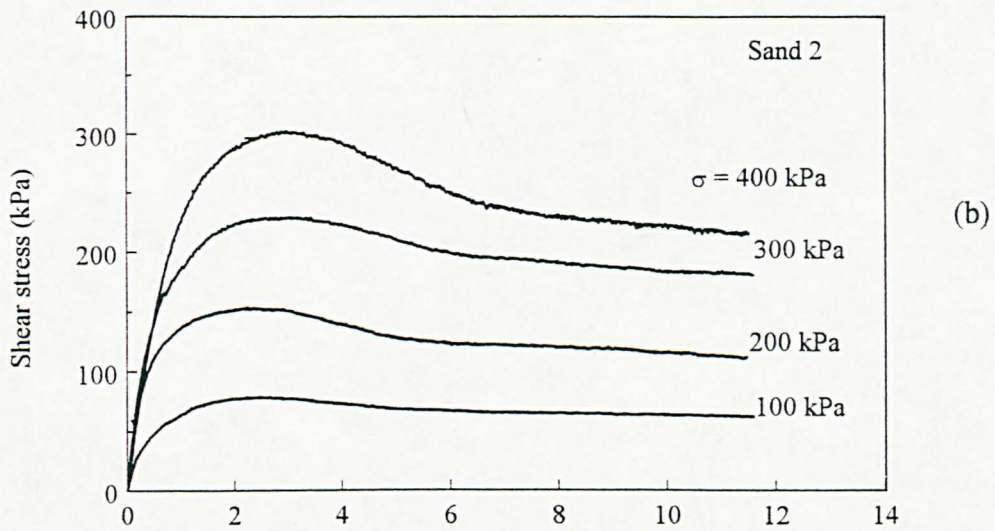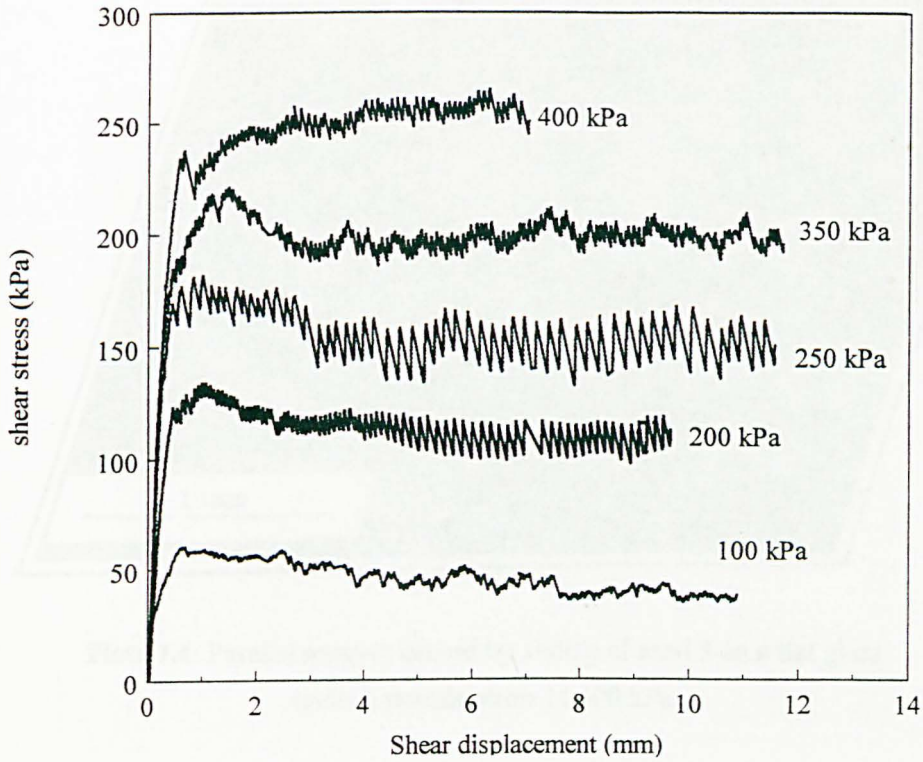
Figure 7.14: Shear stress-shear displacement diagrams for interfaces between sand and flat rock surfaces
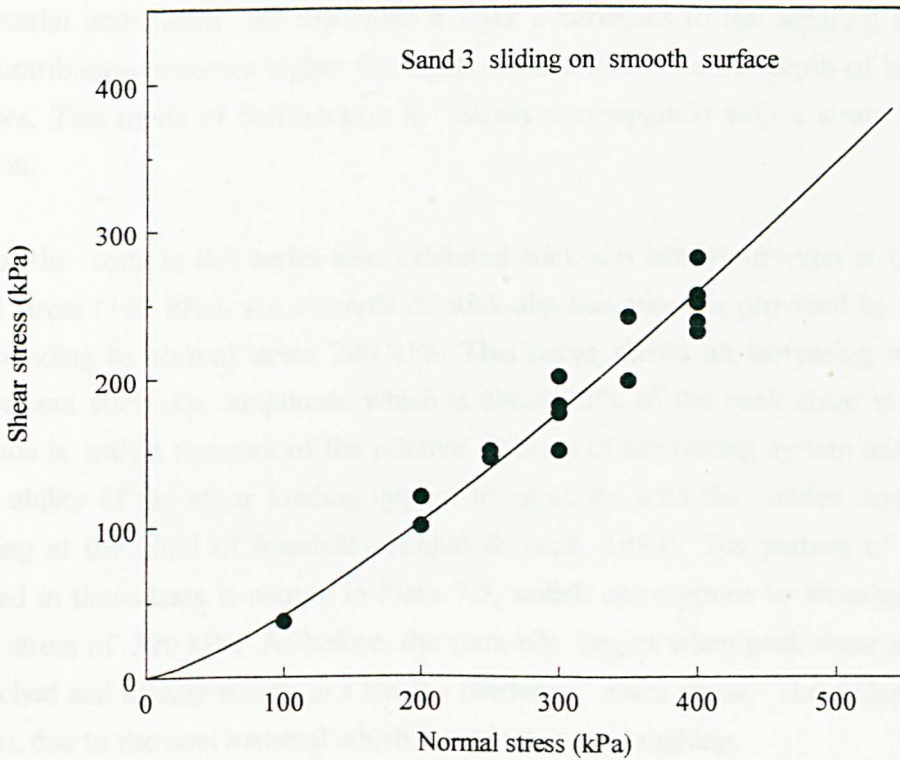
Figure 7.15: Peak shear strength envelopes for interfaces between sand and flat rock surfaces
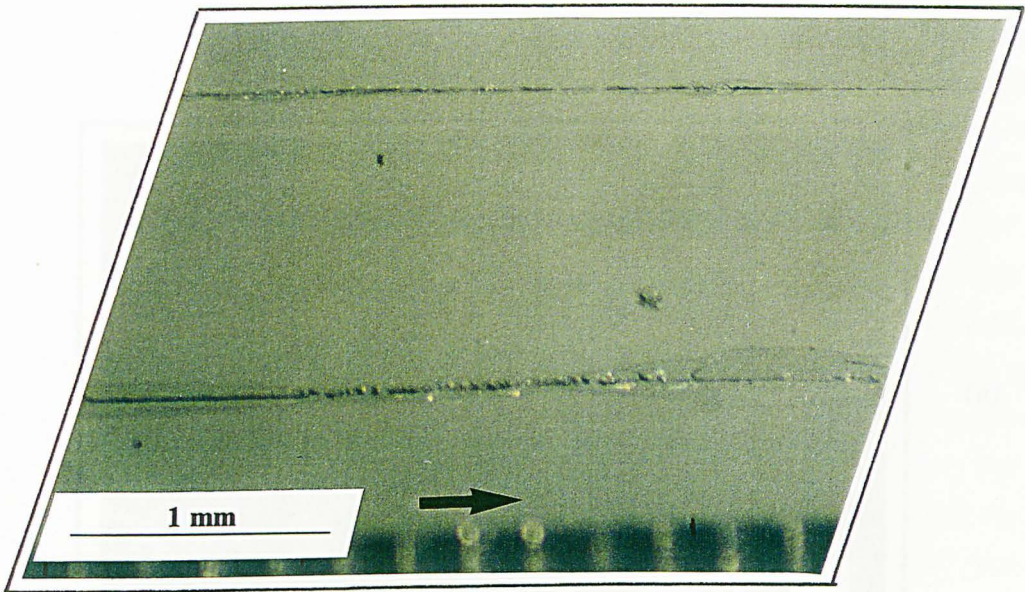
Plate 7.4: Parallel grooves caused by sliding of sand 3 on a flat glass
under a normla stress of 400 kPa

stresses the sand particles slide on the smooth surface and the coefficient of friction is
relatively low. As the normal stress increases, indentation and ploughing occurs, and
the material underneath the top smooth layer contributes to the shearing resistance.
This contribution becomes higher for higher normal stress, as the depth of indentation
increases. This mode of deformation is usually accompanied with a strain hardening
behaviour.

Most of the tests in this series also exhibited stick-slip behaviour even at the lowest
normal stress (100 kPa). An example of stick-slip behaviour is provided by the curve
corresponding to normal stress 200 kPa. This curve shows an increasing with shear
displacement stick-slip amplitude which is about 15% of the peak shear stress. This
amplitude is only a measure of the relative stiffness of the testing system and depends
on the ability of the shear loading system to catch up with the sudden displacement
occurring at the point of instability (Lajtai & Gadi, 1989). The pattern of scratches
observed in these tests is shown in Plate 7.5, which corresponds to shearing under a
normal stress of 300 kPa. As before, the stick-slip begins when peak shear strength is
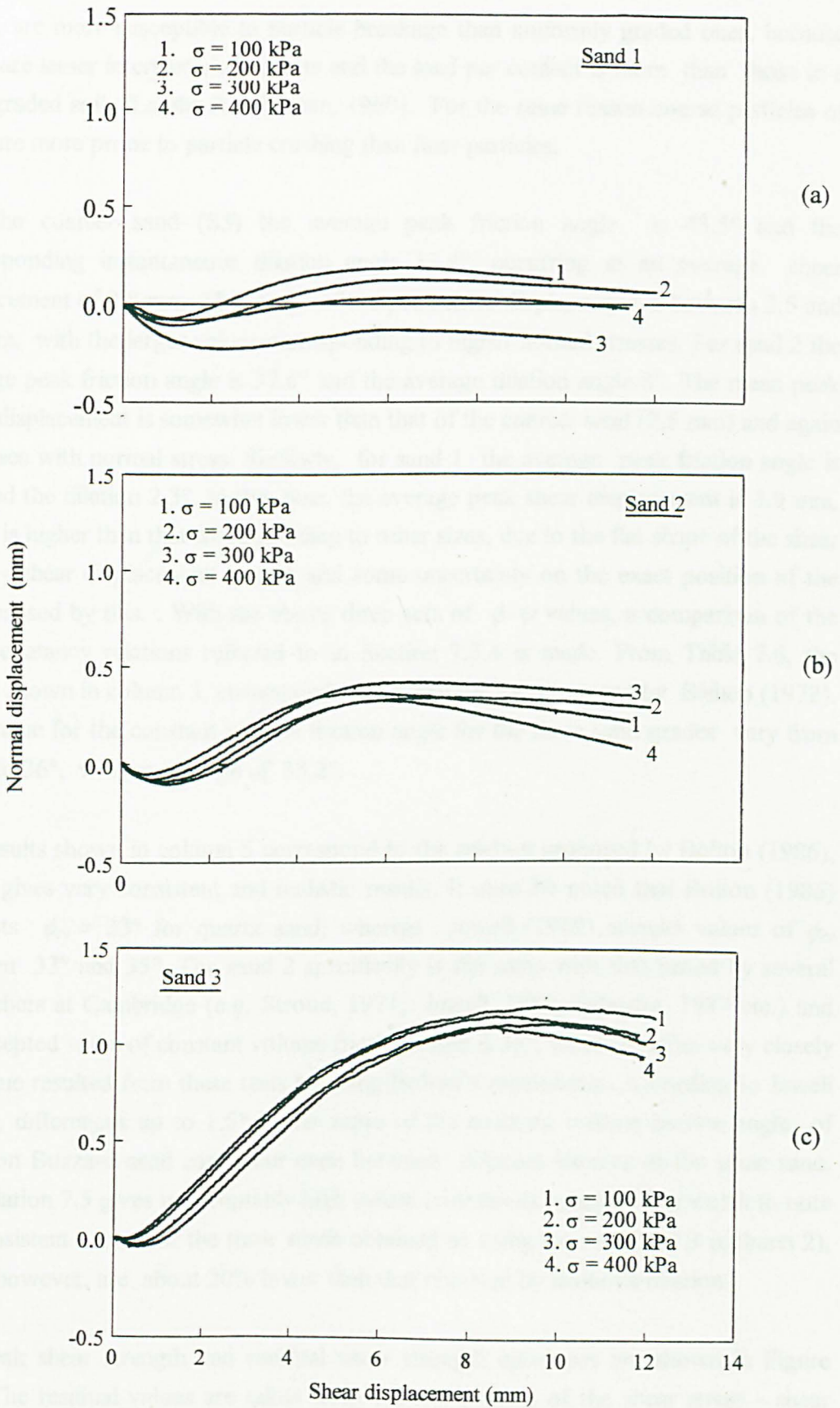approached and usually results in a strain - hardening shear stress - shear displacement
diagram, due to the new material which is subjected to ploughing.

Microscopic post-test examination of the surface revealed some fine grooves parallel
to the sliding direction, with small amount of crushed (or worn) sand on the surface.
At higher normal stresses, much deeper grooves were observed and also cross

(a)

2.5 mm

2.5 mm
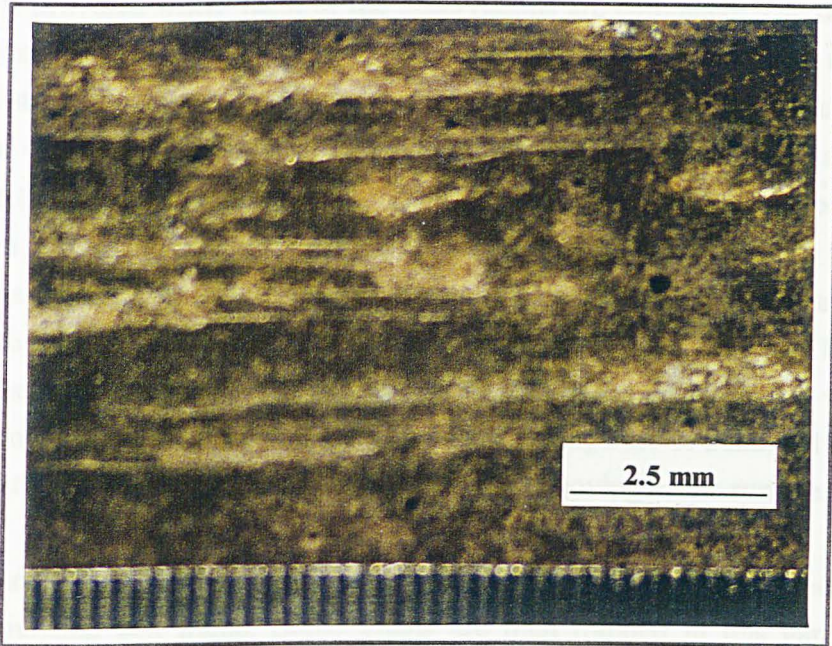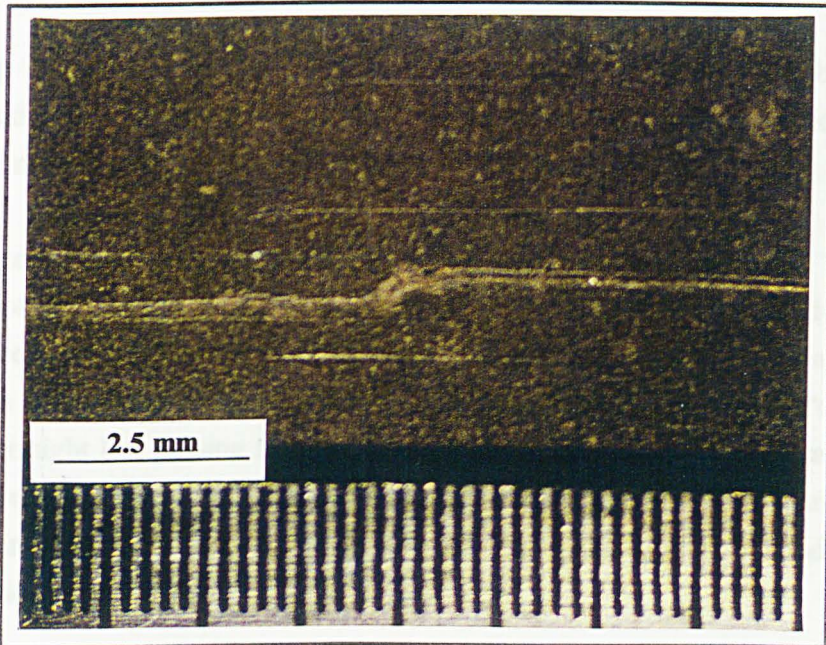
(b)

Plate 7.5: Typical grooves of interfaces between sand and flat rock surface
from two samples (a) and (b) tested under 400 kPa normal stress

fracturing at some points. This could be associated with the stick-slip occurring at the peak shear stress. Acoustic emission events accompany each slip, with loudness proportional to the amplitude of the oscillations. A possible explanation of the observed phenomena is provided when most of the observations are combined. The occurrence of grooves implies that indentation by sand grains has taken place. The increasing with normal stress ploughing brings andalusite grains (hardness 7) from the synthetic rock with the quartz sand grains (hardness 7) and this may cause stick-slip, as contact between quartz surfaces is conductive to stick-slip (Paterson, 1978), maybe because of the sudden brittle failure of small irregularities (Byerlee, 1970). Evidence for this is given by some white marks on the tested rock surface which are due to quartz-quartz contact, in contrast to other brown marks due to sand crushing or wear. From this mechanism the sand particles are worn and new finer particles are produced which are seen in the grooves. Similar observations were made by Engelder & Scholz (1976) who suggested that stick-slip movement is associated with grooving of the surface.

Fracture of sand grains may be caused in case of existing gap between the rock sample and the surrounding box frame. Some grains are then trapped in this gap and are subjected to high stresses which cause fracture. For this reason, the rock has to fit precisely in the shear box frame.

The stick-slip is normal stress dependent. The normal stress where stick-slip begins can not be defined easily. For the finer sand, no such phenomenon was observed, even at the very high normal stress of 500 kPa, which was occasionally used.

7.5.3. Interfaces between sand and saw-toothed modelled rock surfaces

Three types of sand were used for each of the three different saw-toothed surfaces. The results are shown in Figures 7.16-7.17 and Tables 7.8a and 7.8b. The peak friction angle reduces with normal stress for all three sands, resulting in a small "cohesion" intercept. A straight line passing through the origin was fit to the data. For sand 1, the peak shear strength is lower than that of the sand at normal stresses lower than 200 kPa but becomes increasingly higher at normal stresses above 200 kPa. This is independent of the inclination of the surface.

The range of the peak stress ratio $\tau_{peak}/\sigma = tan\delta$ for the interfaces involving the finer grade (sand 1), is between 0.91 and 1.11 of that of the sand alone. The lower values correspond to the lower normal stress (100 kPa) and the highest to the highest normal stress. More specifically, for normal stress 100 kPa $tan\delta$ is lower and for the higher stresses higher than that of the sand alone. From the Table 7.8b , it becomes clear that the same trend exists for the peak rate of dilation, where the range now is much
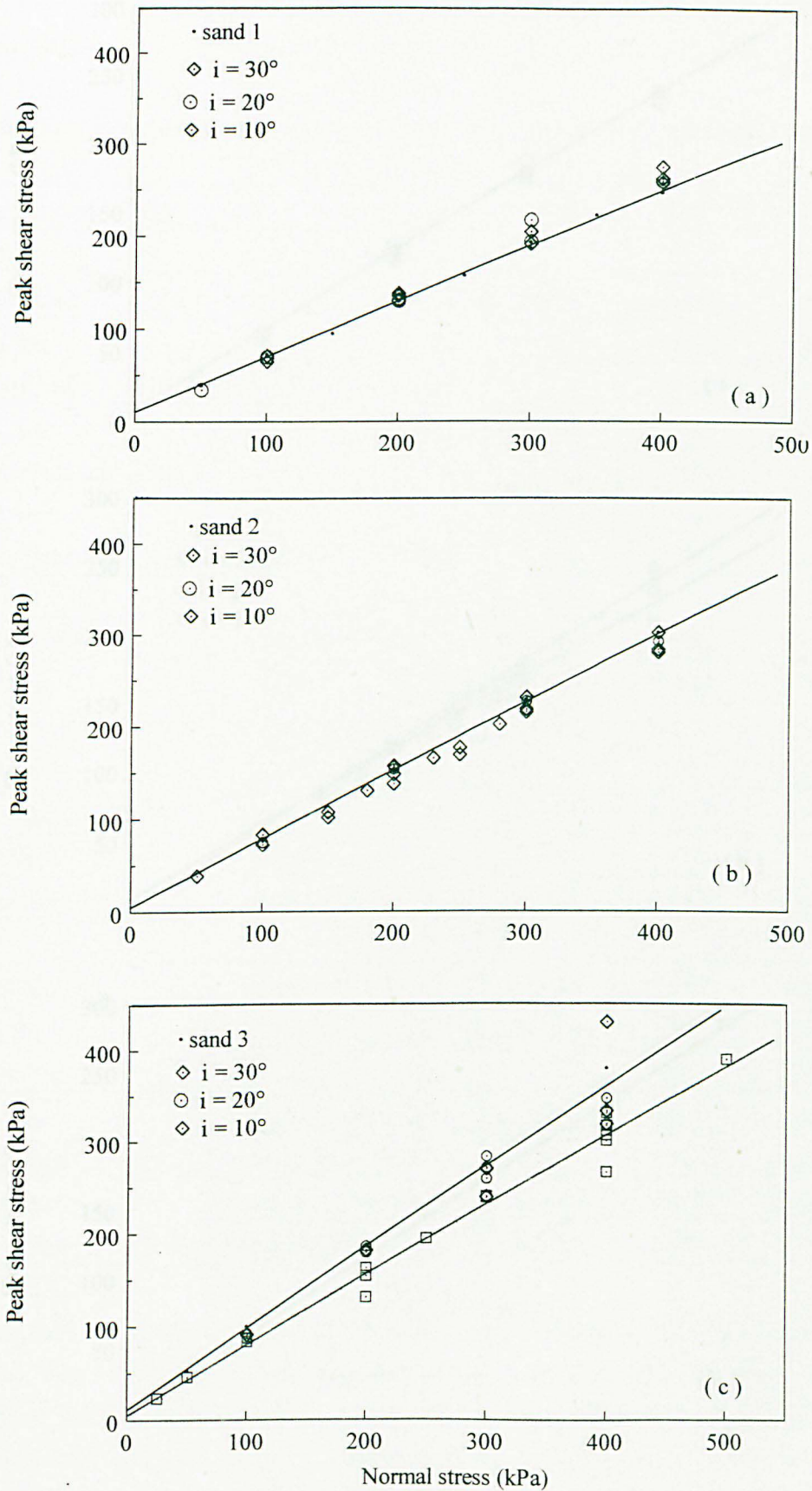
Figure 7.16: Peak shear strength envelopes for interfaces between sands and saw-toothed rock surfaces: (a) sand 1. (b) sand 2. (c) sand 3.
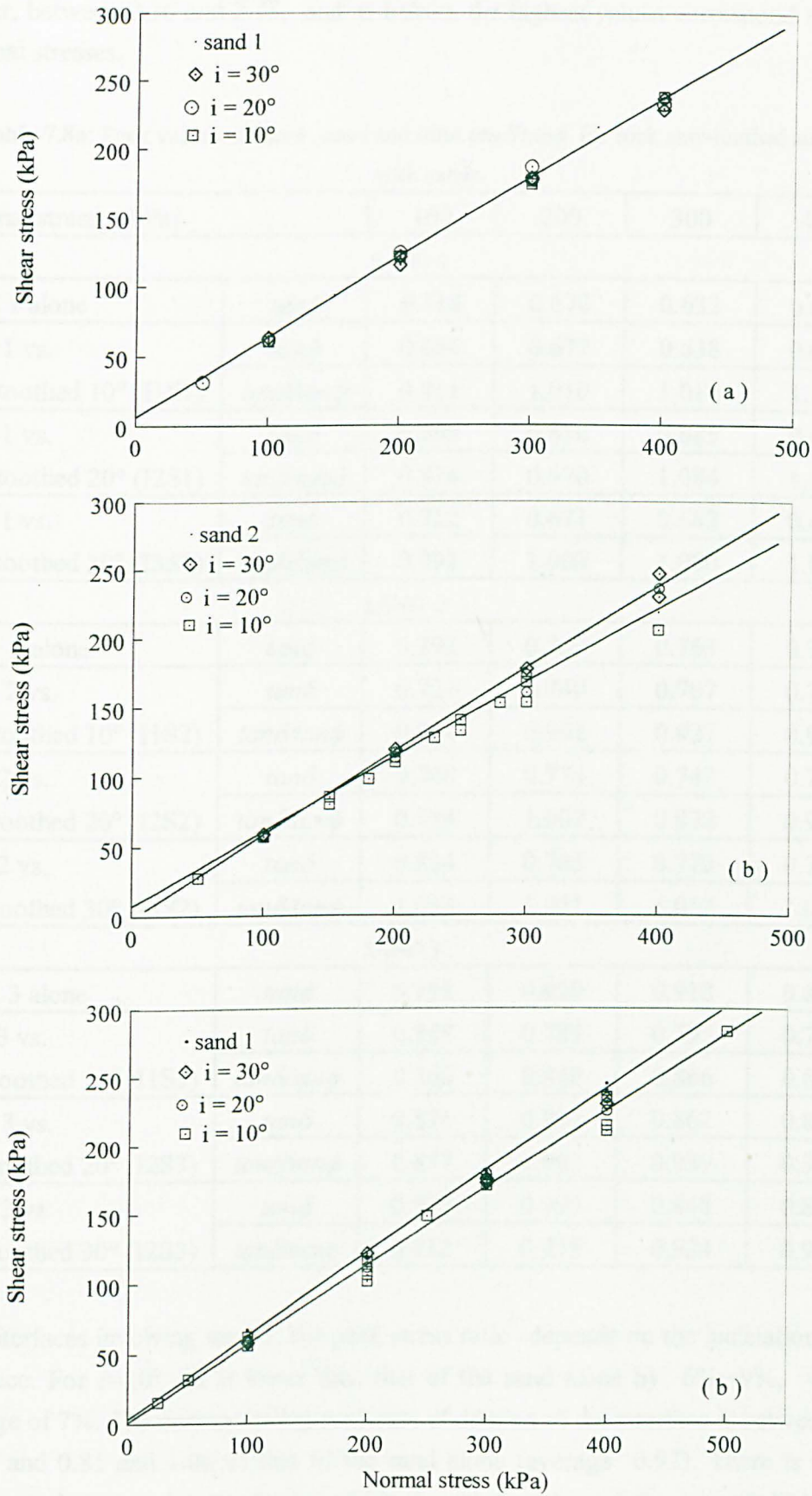
Figure 7.17: Residual shear strength envelopes for interfaces between sands and saw-toothed rock surfaces: (a) sand 1. (b) sand 2. (c) sand 3.

wider, between 0.36 and 2.78, and as before, the highest values correspond to higher normal stresses.

Table 7.8a: Peak values of $tan\phi$, $tan\delta$ and ratio $tan\delta/tan\phi$ for rock saw-toothed surfaces with sands

Normal stress (kPa)		100	200	300	400
SAND 1					
Sand 1 alone	$tan\phi$	0.718	0.670	0.632	0.622
sand 1 vs.	$tan\delta$	0.654	0.677	0.638	0.689
saw-toothed 10° (I1S1)	$tan\delta/tan\phi$	0.911	1.010	1.010	1.108
sand 1 vs.	$tan\delta$	0.699	0.650	0.685	0.651
saw-toothed 20° (I2S1)	$tan\delta/tan\phi$	0.974	0.970	1.084	1.047
sand 1 vs.	$tan\delta$	0.712	0.671	0.682	0.652
saw-toothed 30° (I3S1)	$tan\delta/tan\phi$	0.992	1.000	1.080	1.048
SAND 2					
Sand 2 alone	$tan\phi$	0.792	0.769	0.763	0.755
sand 2 vs.	$tan\delta$	0.724	0.740	0.707	0.708
saw-toothed 10° (I1S2)	$tan\delta/tan\phi$	0.914	0.962	0.927	0.938
sand 2 vs.	$tan\delta$	0.748	0.774	0.742	0.731
saw-toothed 20° (I2S2)	$tan\delta/tan\phi$	0.944	1.007	0.972	0.968
sand 2 vs.	$tan\delta$	0.834	0.785	0.772	0.755
saw-toothed 30° (I3S2)	$tan\delta/tan\phi$	1.053	1.021	1.012	1.000
SAND 3					
Sand 3 alone	$tan\phi$	0.998	0.929	0.918	0.898
sand 3 vs.	$tan\delta$	0.858	0.789	0.795	0.796
saw-toothed 10° (I1S3)	$tan\delta/tan\phi$	0.860	0.849	0.866	0.886
sand 3 vs.	$tan\delta$	0.876	0.893	0.862	0.831
saw-toothed 20° (I2S3)	$tan\delta/tan\phi$	0.877	0.961	0.939	0.925
sand 3 vs.	$tan\delta$	0.910	0.906	0.848	0.814
saw-toothed 30° (I2S3)	$tan\delta/tan\phi$	0.912	0.975	0.924	0.906

For interfaces involving sand 2, the peak stress ratio depends on the inclination of the interface. For $i=10°$, it is lower than that of the sand alone by 6% -9%, with an average of 7%. The corresponding peak rate of dilation of the interface is between 19% lower and 0.81 and 1.06 of that of the sand alone (average 0.92). There is a good agreement between the amount by which the stress ratio and the rate of dilation are reduced (7% and 8% respectively) and this indicates that the difference is mainly due to dilation.

Table 7.8b: Dilation rate at peak shear stress for sands $tan\,\psi_\phi$ and saw-toothed surfaces $tan\,\psi_\delta$

Normal stress (kPa)		100	200	300	400
SAND 1					
Sand 1 alone	$tan\,\psi_\phi$	0.097	0.043	0.025	0.032
sand vs.	$tan\,\psi_\delta$	0	0.056	0.040	0.089
saw-toothed 10° (I1S1)	$tan\,\psi_\delta/tan\,\psi_\phi$	0	1.318	1.600	2.781
sand vs.	$tan\,\psi_\delta$	0.061	0.019	0.046	0.054
saw-toothed 20° (I2S1)	$tan\,\psi_\delta/tan\,\psi_\phi$	0.629	0.442	1.840	1.688
Glass ballotini vs.	$tan\,\psi_\delta$	0.035	0.044	0.038	0.028
saw-toothed 30° (I3S1)	$tan\,\psi_\delta/tan\,\psi_\phi$	0.361	1.023	1.52	0.875
SAND 2					
Sand 2 alone	$tan\,\psi_\phi$	0.139	0.132	0.129	0.148
sand 2 vs.	$tan\,\psi_\delta$	0.112	0.112	0.137	0.142
saw-toothed 10° (I1S2)	$tan\,\psi_\delta/tan\,\psi_\phi$	0.806	0.848	1.062	0.959
sand 2 vs.	$tan\,\psi_\delta$	0.125	0.133	0.137	0.098
saw-toothed 20° (I2S2)	$tan\,\psi_\delta/tan\,\psi_\phi$	0.899	1.008	1.062	0.662
sand 2 vs.	$tan\,\psi_\delta$	0.167	0.130	0.125	0.125
saw-toothed 30° (I3S2)	$tan\,\psi_\delta/tan\,\psi_\phi$	1.201	0.985	0.969	0.845
SAND 3					
Sand 3 alone	$tan\,\psi_\phi$	0.224	0.229	0.211	0.189
sand 3 vs.	$tan\,\psi_\delta$	0.243	0.200	0.212	0.157
saw-toothed 10° (I1S3)	$tan\,\psi_\delta/tan\,\psi_\phi$	1.085	0.873	1.005	0.831
sand 3 vs.	$tan\,\psi_\delta$	0.232	0.235	0.228	0.220
saw-toothed 20° (I2S3)	$tan\,\psi_\delta/tan\,\psi_\phi$	1.036	1.026	1.081	1.164
Sand 3 vs.	$tan\,\psi_\delta$	0.220	0.238	0.225	0.182
saw-toothed 30° (I3S3)	$tan\,\psi_\delta/tan\,\psi_\phi$	0.982	1.039	1.066	0.963

For $i=20°$, the stress ratio of the interface is less than that of the sand by an average of 3%, whereas the peak rate of dilation by about 10%. In the latter case however, the value of the rate of dilation is in disagreement with the general trend, and this may be due to experimental error. It must be noted that most of the values given for each case in Tables 7.8a and b are based in one single test, and may not agree with other values, due to small density variations or other experimental errors. Finally, for $i=30°$ the peak stress ratio of the interface is equal or up to 5% higher than that of the sand (with an average of 2%). The corresponding ratio of dilation rate ranges between 0.85 and 1.20 (average 1.00) of that of the sand. This suggests that the dilational characteristics of the interface and the sand are the same, which means that eventually the failure path must be entirely within the sand. The interface is so steep that eventually is not involved in the shearing process.

For the coarser sand (sand 3) the stress ratio of the interface is in all cases lower than that of the sand, whereas the rate of dilation is about the same. The ratio $tan\delta/tan\phi$ has an average value of 0.86 (ranges between 0.85 and 0.89) for $i = 10°$, 0.93 for $i = 20°$ and $i = 30°$ (ranges 0.88-0.96, and 0.91-0.97 respectively). The ratio of the rate of dilation of the interface to the rate of the dilation of the sand $(tan\psi_\delta/tan\psi_\phi)$ is between 0.83 and 1.06 (with an average of 0.95) for $i=10°$, between 1.03 and 1.16 (average 1.08) for $i=20°$ and between 0.96 and 1.07 (average 1.01) for $i=30°$.

The peak friction angle on the inclined interface is lower than that of the sand alone. Therefore, sand particles tend to move along the interface, so that the failure paths are composite though the sand and along the interface. When the inclination of the interface is low, larger portions of the failure path will be along the interface, whereas for steeper planes, this may occur only near the tips of the interface. The movement along the interface may occur by sliding or rolling. In both cases increased dilation angles will be observed. This is clear for the finest sand, where this mechanism appears to be favoured by increased normal stress, because the strength difference is larger.

On microscopic examination the mechanisms described earlier were also present in this case. For some tests involving the coarser sand fine grooves parallel to the direction of sliding and brown dust was observed on the surface, as a result of sand crushing or wear. Stick-slip and acoustic emission events also accompanied these tests. The latter was small at the beginning of the tests but increased as the sample dilated. As a main cause of dilation is particle rolling, it seems that at higher normal stresses the stick-slip occurred as a result of sand particle rolling on the surface.

It was also observed that when the sand was removed from the rock surface, there was most of the times, a certain amount of sand in the rock valleys which was so highly stressed that on turning the sample upside down, it remained in place (Plate 7.6). It can be assumed that this area is totally excluded from the shearing process and is an indication of the lower boundary of the potential shear zone. Really, from observations on the rock teeth there was no sign of particle movement in this area, whereas several scratches were seen in the top part of the teeth. The shear band was experimentally defined by using ballotini and sand of the same size but of different colour. From examination of the deformed sample after the end of the test, the shear band thickness was measured. The results, shown in Figure 7.19, compare quite well with similar results for sands given by Palmeira & Milligan (1989). Based on this results, possible modes of shear bands are suggested, as shown in Figure 7.20.
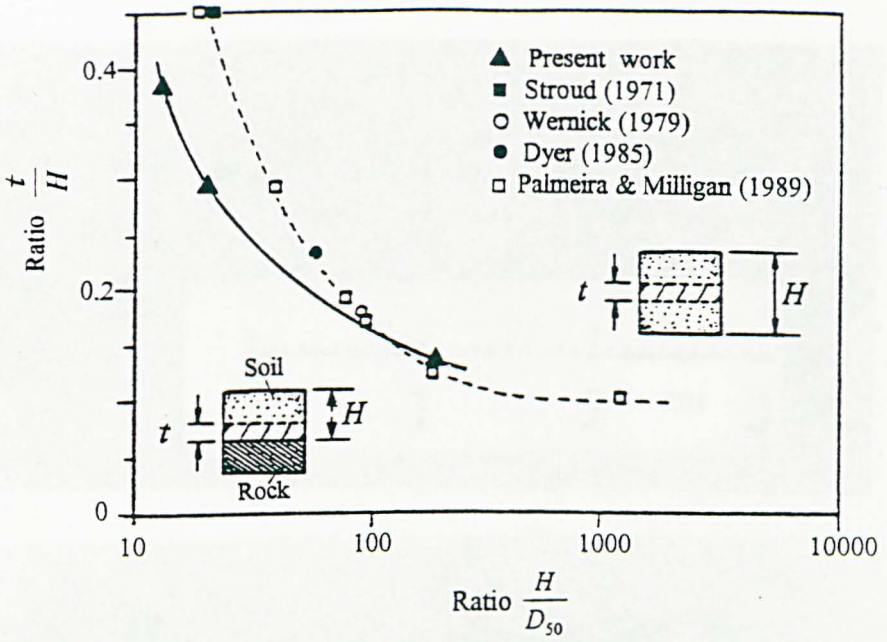
Figure 7.18: Relation between shear band thickness and mean particle diameter.
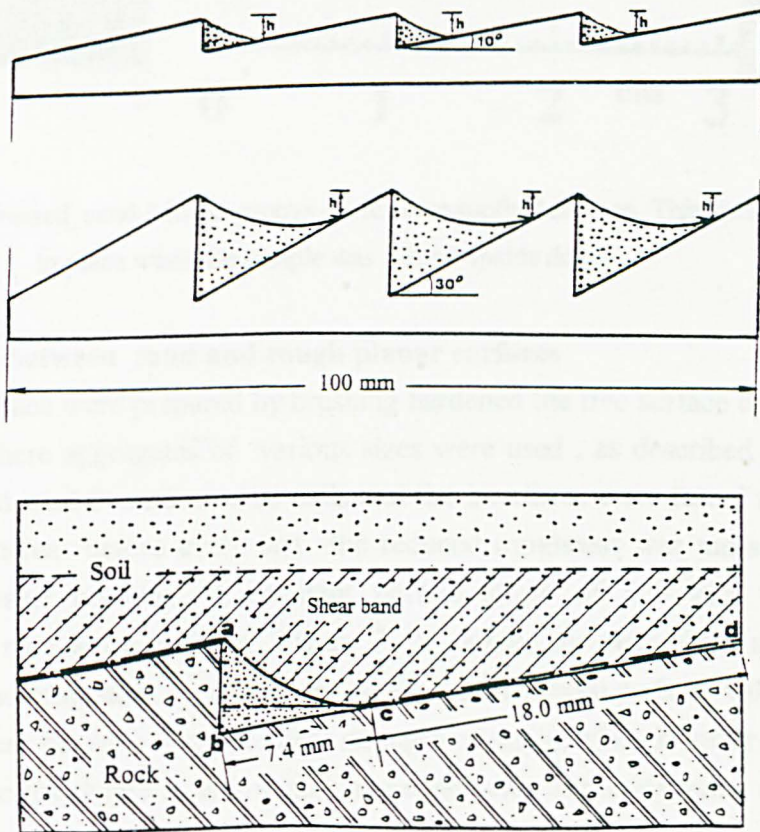
Figure 7.19: Composite failure paths in soil-rock interfaces
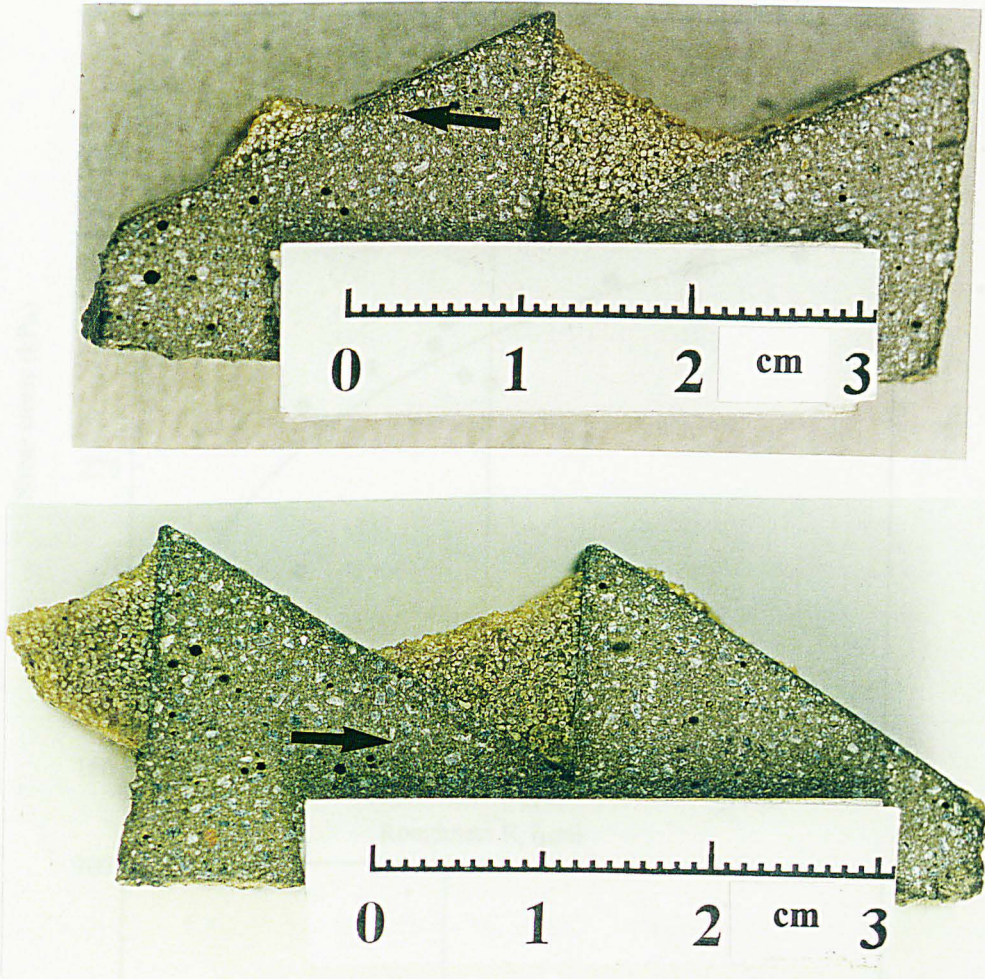
Plate 7.6: Highly stressed sand 1 in the groove of the saw-toothed surface. This sand remained in place when the sample was turned upside down

7.5.4 Interfaces between sand and rough planar surfaces

Rough planar surface were prepared by brushing hardened the free surface of hardened synthetic rock where aggregates of various sizes were used , as described in section 7.3.2. Sand 2 and sand 3 were used as soils and the interfaces were tested repeatedly several times, whereas before every test the reduced roughness was measured by a stylus type Talysurf machine. A constant normal stress of 300 kPa was used throughout. The results are given in Figure 7. 20, where the peak shear strength is plotted against the roughness R_t, which represents the maximum peak to valley height of the profile. It can be seen that the shear strength of the interface is lower of that of the sand when the roughness R_t is low and increases with increasing value of R_t. If a normalised roughness R_n is used defined as

$$R_n = \frac{R_t}{D_{50}}$$

(7.7)
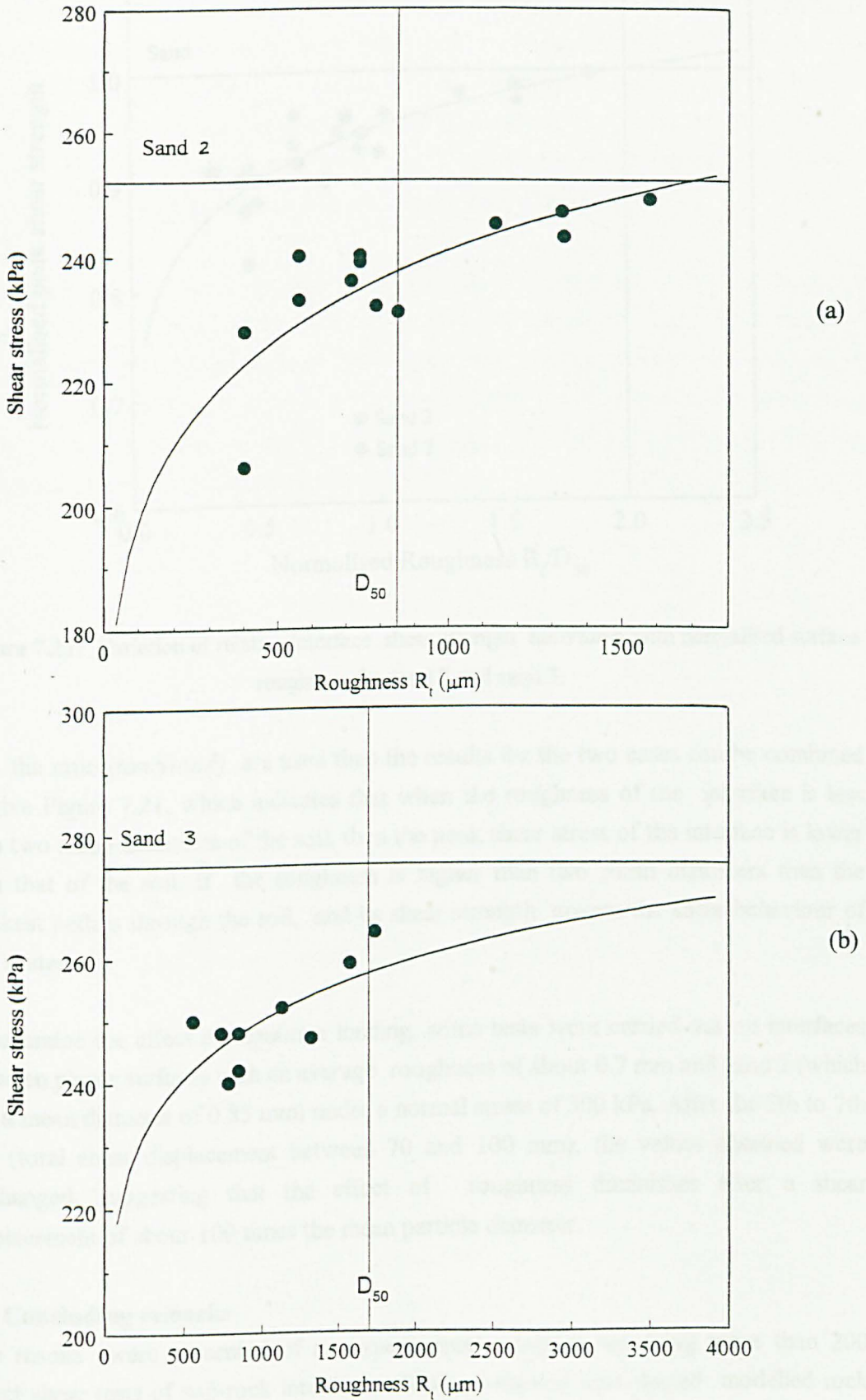
Figure 7.20: Variation of peak shear strength with surface roughness for interfaces involving
(a) sand 2 and (b) and sand 3.
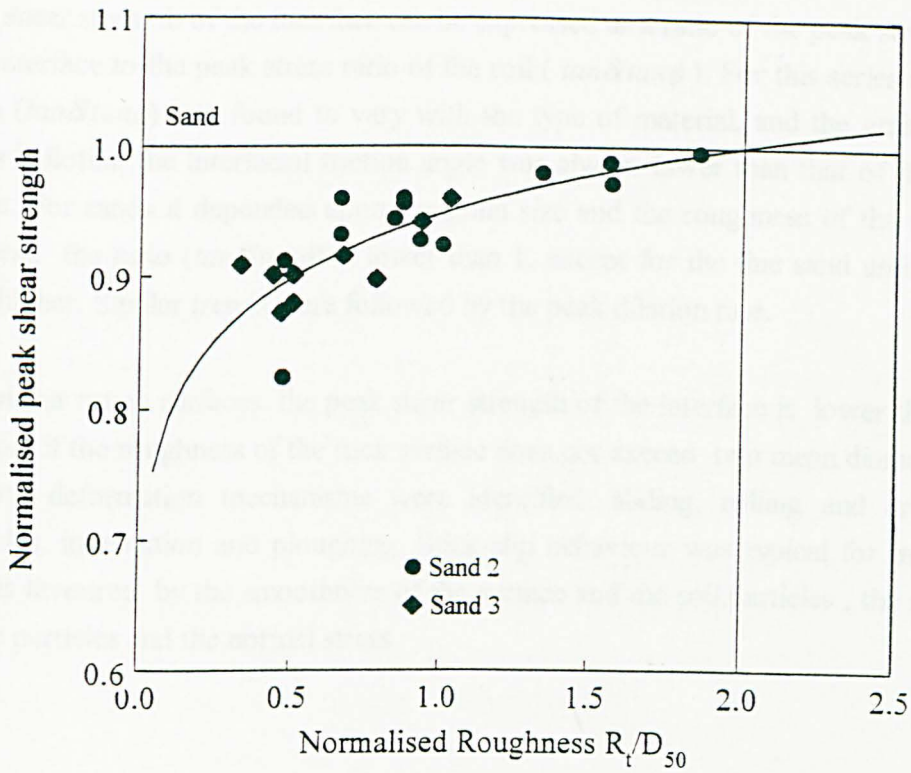
Figure 7.21: Variation of relative interface shear strength *tanδ/tanφ* with normalised surface roughness for sand 2 and sand 3.

and the ratio (*tanδ/tanφ*) are used then the results for the two cases can be combined to give Figure 7.21, which indicates that when the roughness of the interface is less than two mean diameters of the soil, then the peak shear stress of the interface is lower than that of the soil. If the roughness is higher than two mean diameters then the weakest path is through the soil, and its shear strength govern the shear behaviour of the system.

To examine the effect of repetitive loading, some tests were carried out on interfaces between planar surfaces with an average roughness of about 0.7 mm and sand 2 (which has a mean diameter of 0.85 mm) under a normal stress of 300 kPa. After the 5th to 7th run (total shear displacement between 70 and 100 mm), the values obtained were unchanged, suggesting that the effect of roughness diminishes after a shear displacement of about 100 times the mean particle diameter.

7.6 Concluding remarks

The results were presented of an experimental program, involving more than 200 direct shear tests of soil-rock interfaces. Various flat and saw-shaped modelled rock surfaces were used and various sand types and glass ballotini.

The shear strength of the interface can be expressed as a ratio of the peak stress ratio of the interface to the peak stress ratio of the soil ($tan\delta/tan\phi$). For this series of tests the ratio ($tan\delta/tan\phi$) was found to vary with the type of material, and the grain size. For glass ballotini, the interfacial friction angle was always lower than that of the ballotini alone. For sands it depended upon the grain size and the roughness of the surface. In general, the ratio ($tan\delta/tan\phi$) is lower than 1, except for the fine sand used, where it was higher. Similar trends were followed by the peak dilation rate.

For planar rough surfaces the peak shear strength of the interface is lower than that of the soil, if the roughness of the rock surface does not exceed two mean diameters. Several deformation mechanisms were identified: sliding, rolling and crushing of particles, indentation and ploughing. Stick-slip behaviour was typical for many tests. This is favoured by the smoothness of the surface and the soil particles , the roundness of the particles and the normal stress.

CHAPTER 8
DOUBLE SOIL-ROCK INTERFACES

8.1 Introduction

Double soil-rock interfaces in this work are defined occurrences where a soil layer is contained between two rock strata. Soil thickness is relatively small, so that interaction between the two adjacent rock walls is possible. This interaction may make the shear strength of the system different to the shear strength of the soil itself or the single soil-rock interface. Particular examples of such interfaces which are of geotechnical interest are filled rock joints. The author has investigated and published the main findings of this research in a number of papers where relative information can be found. Three of these papers are listed below, and must be considered to be part of the thesis. Reprints are attached at the end of this chapter.

No 1. Papaliangas T., Lumsden A.C., Manolopoulou S. and Hencher S.R. (1990). Shear strength of modelled filled joints. *Rock Joints; Proc. Int. Symp. on Rock Joints*, Loen, Norway (Barton N. & Stephansson O., Eds), pp. 275-282. Balkema, Rotterdam.

No 2. Papaliangas T., Hencher S.R.. & Lumsden A.C. (1995). Laboratory testing and parameters controlling the shear strength of filled rock joints. Discussion. *Géotechnique* 45, No 1, 175-183.

No 3. Papaliangas T., Manolopoulou, S. (1995). Side resistance of bentonite-coated pile-rock interfaces. Proc. 11th ECSMFE, Copenhagen, Vol. 2, Bull. 11, pp. 107-112.

In the following sections an outline of the shear behaviour of filled joints will be given, some recent result will be presented and some aspects of the shear behaviour will be discussed.

8.2. Parameters affecting the shear behaviour of double soil-rock interfaces

As with the single soil-rock interfaces both the properties of the soil layer and the adjacent rock walls affect the shear behaviour of double soil-rock interfaces. An additional effect arises from the geometry of the interface, i.e. the thickness of the soil layer as compared to the rock wall roughness. The effect of these parameters is briefly discussed below.

The obvious effect of a thin soil layer between two rock walls is to keep the two rock surfaces apart. If the soil thickness is smaller than the mean roughness amplitude of the rock walls, then contact between the two rock surfaces is possible after some shear displacement. The introduction of the soil layer between the two rock walls causes a reduction in shear strength in the following ways: a) by change of the frictional properties of the rock surface caused by the different value of particle friction. b) by reducing the micro-roughness, i.e. the effect of surface textural interlocking and c) by reducing the "effective roughness", i.e. caused by a continuous layer between the two rock walls. Consequently a certain amount of shear displacement is required for rock-rock contact to establish.

The following factors were found to affect the shear behaviour of double interfaces.
a) the nature and the shear strength of the soil alone when the thickness of the soil layer is large relative to the roughness of the rock wall and the failure path passes entirely through the soil.
b) the shear strength of the interface when the thickness is large and the failure path passes entirely through the soil-rock interface. As shown in Chapter 7 the shear strength is usually lower than that of the soil alone.
c) both the above, which is most common, when the failure path passes partly along the interface and partly though the infill.
d) the strength and roughness of the rock walls and
e) the thickness of the soil layer as compared to the surface roughness of the wall. Although not a definitive parameter, in filled joint practice the mean roughness amplitude (a) of a rock surface is commonly used to characterise roughness.

An experimental investigation of the above parameters involved direct shear tests on modelled filled joints. These tests have been carried out on a large shear box especially modified to accommodate model filled joints up to 40 mm long (Figure 8.1). Various model joints, infill materials and rock model materials were used. The results from tests on a modelled rock joint with mean roughness amplitude 7 mm and as soil artificial material with round particles, namely pulverised fuel ash, are shown in Figure 8.2. It can be seen that the shear strength of the interface is clearly lower than that of the soil alone. The influence of the roughness of the rock surface is demonstrated by the two shear strength envelopes nos. 5 and 6, of which the first corresponds to saw-cut rock surface/ PFA interface and the second to a smooth surface-PFA interface. The smooth surface was produced by direct casting against glass. The shear strength of the filled joint is always lower than that of the soil alone and higher than that of the interface, as shown in Figure 8.3, and this is so irrespective of the normal stress. similar observations have been made by Kanji (1970 and 1974).
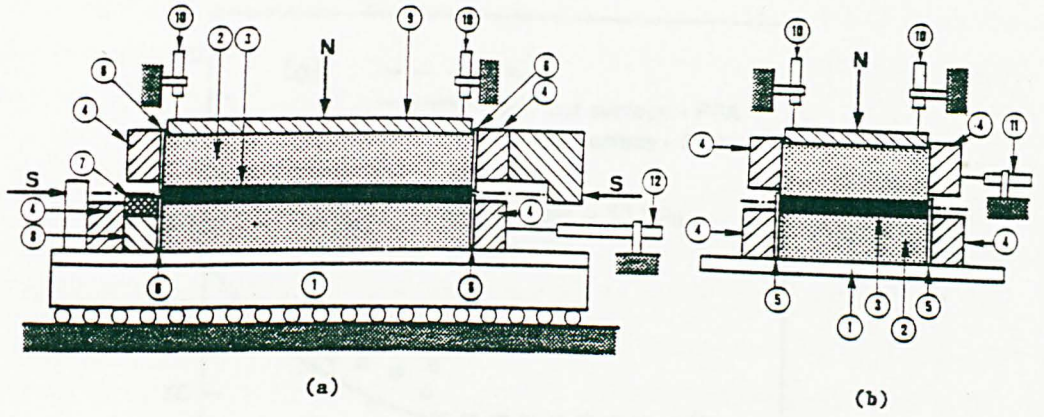
LEGEND:
1)Trolley 2)Rock sample 3) Filling material 4)Sample carriers 5)Longitudinal teflon-coated wooden strips 6)Transverse teflon-coated wooden strips 7)Deformable rubber piece 8)Spacer 9)Steel plate 10) Normal displacement measurements 11)Lateral horizontal displacement measurements and 12)shear displacement measurements.
S=Shear load, N=Normal Load

Figure 8.1: Direct shear box set-up for testing filled joints
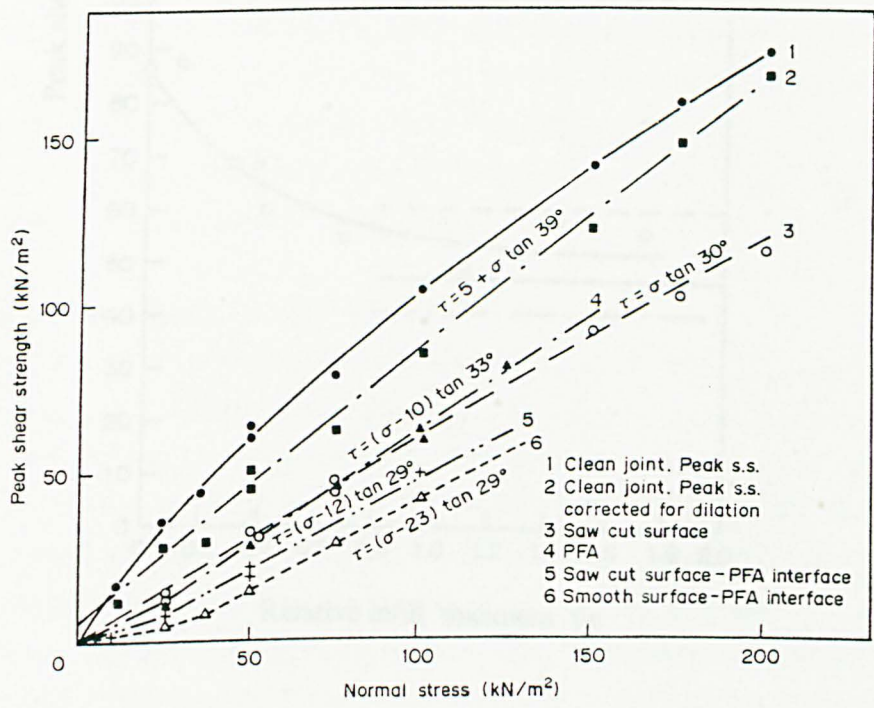
Figure 8.2: Peak shear strength envelopes of rock surfaces, soil, and single soil-rock interfaces
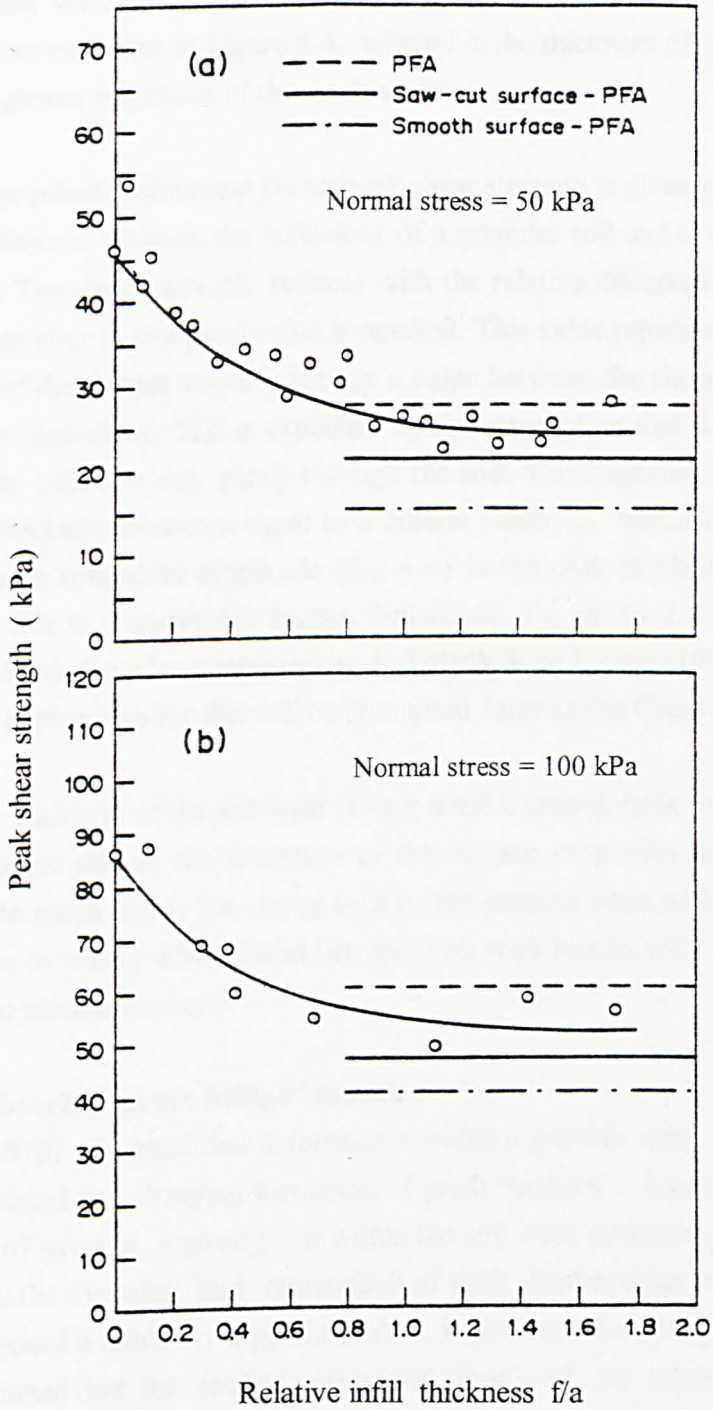
Figure 8.3: Comparison of peak shear strength of system components and peak shear strength of filled joint, with different values of relative thickness f/a.

The general shear behaviour of double interfaces with a granular soil infill is given by the typical *f/a* curves shown in Figure 8.4, where f is the thickness of the soil layer and a the mean roughness amplitude of the rock walls.

The effect of the relative thickness *f/a* on peak shear strength is given in Fig.8.5, where the striking difference between the behaviour of a granular soil and a weak wet clayey soil is obvious. The shear strength reduces with the relative thickness of the soil, and remains constant after a minimum value is reached. This value represents the minimum shear strength of the system which is usually a value between the shear strength of the interface and the soil alone. This is explained by the assumption that the failure path is partly along the interface and partly through the soil. The minimum value is reached when the soil thickness becomes equal to a critical value f_{crit} which is approximately equal to the mean roughness amplitude ($f_{crit} = a$) in the case of clayey soils, but for granular soils, this is considerably higher. Values of f_{crit} up to 2.3 times the mean roughness amplitude have been reported by de Toledo & de Freitas (1995), as shown in Figure 8.6. An explanation for this will be attempted later in this Chapter.

Even when the thickness of the soil layer is very small a considerable reduction in shear strength may occur due to the alteration of the surface properties of the rock. This reduction maybe much higher for clayey soils or for granular soils with round particles which are prone to rolling when placed between two rock blocks with a spacing about the same as the particle diameter.

8.3 The load bearing "grain bridge" model

Mandl *et al.* (1970) observed that deformation within a granular mass in a rotary shear box is by continual and changing formation of grain "bridges". Large fluctuations in the magnitude of stress at a given point within the soil were measured, which may be associated with the formation and destruction of such load-bearing bridges. Biegel *et al.* (1989) proposed a model to explain the shear behaviour of a simulated fault gouge, where it is assumed that the applied normal and shear loads are supported by a finite number of "grain bridges" which span the soil layer and carry the applied load. Rotation of a bridge increases the stress which it supports until it fails and the stress is supported by other newly formed bridges. Such structures have been described by Gallagher *et al.* (1974), Oda & Konishi (1974) and others. According to this model a grain bridge can fail in any of the following modes (Figure 8.8) : a) crushing of particles b) slip between particles c) slip along the interface and d) failure of the surface of rock. The contribution of each one of these four mechanisms to the overall deformation depends on various parameters such as normal stress, particle size distribution, the soil layer thickness, the roughness of the rock surface and the sliding
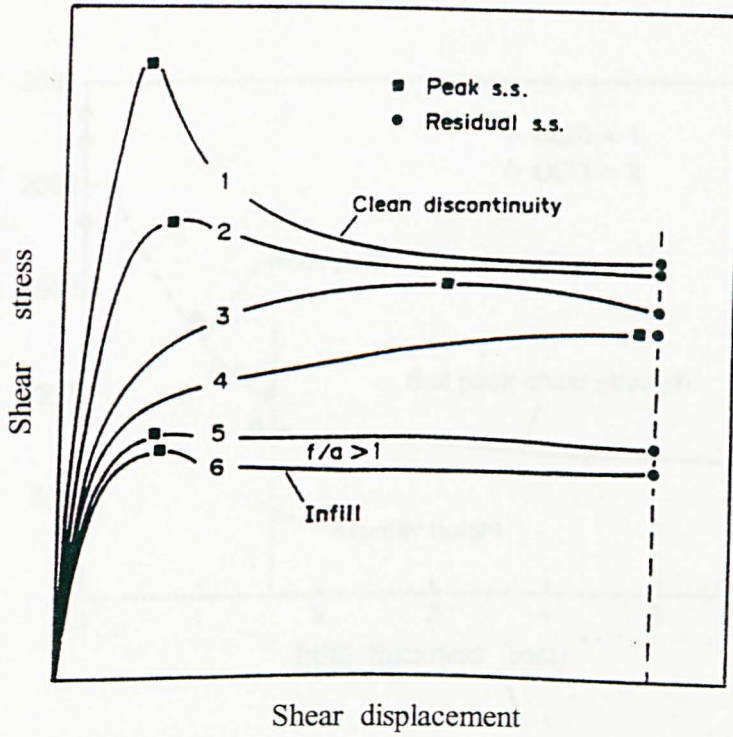
Figure 8.4: Typical shear stress - shear displacement curves for various relative thickness f/a.
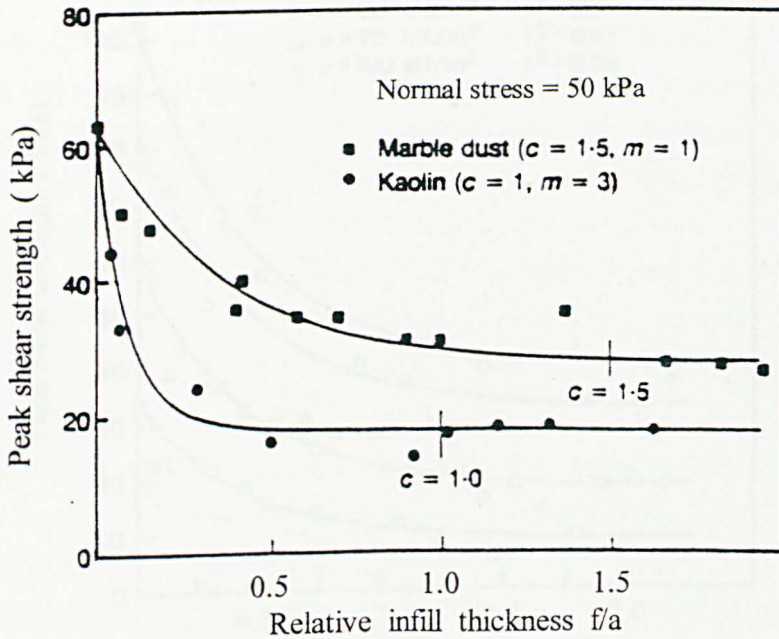
Figure 8.5: Peak shear strength as a function of the relative infill thickness f/a for a granular and a clayey material
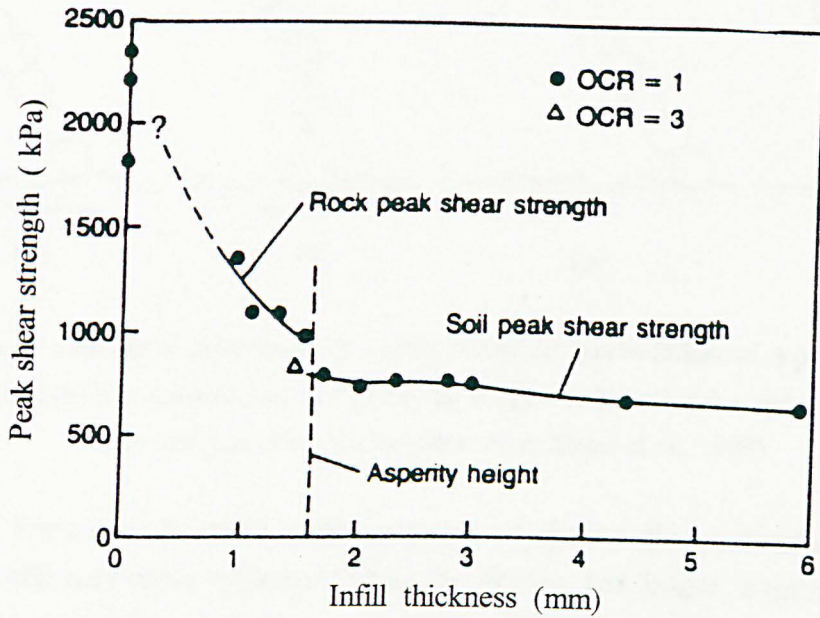
Figure 8.6: Peak shear stress of saw-toothed joint filled with clayey sand plotted against infill thickness for two ovrconsolidated ratios (after de Toledo & de Freitas, 1995)
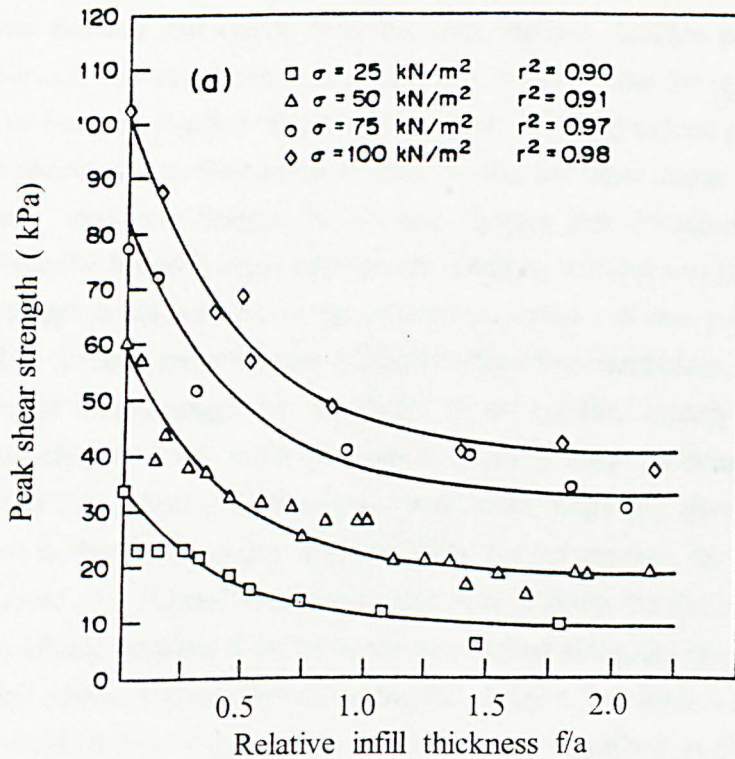
Figure 8.7: Peak shear stress of naturally rough model joint filled with pulverised fuel ash plotted against infill thickness for various normal stresses
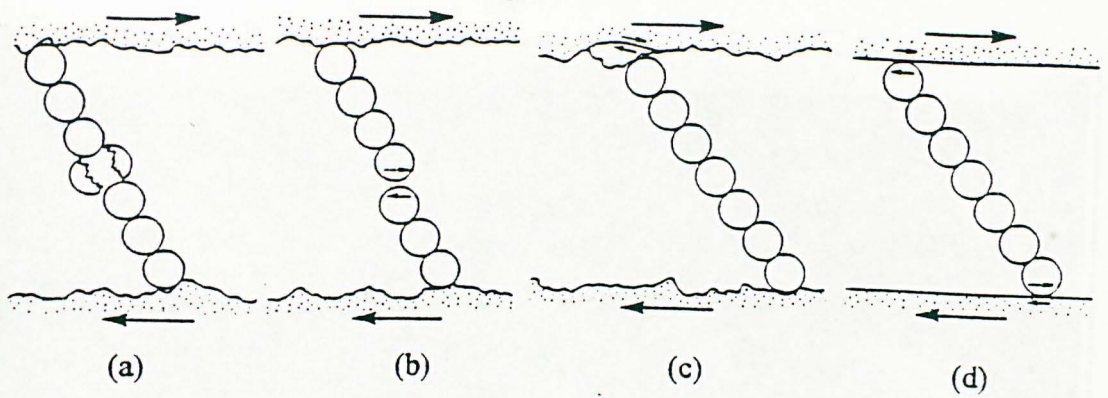
Figure 8. : Modes of deformation of a grain bridge: (a) tensile failure of a particle under compression; (b) slip between particles within the bridge; (c) failure of the rock surface; and (d) slip along the soil-rock interface (after Biegel et al., 1989).

velocity. For a smooth interface, failure occurs along the soil-rock interface. For rough surfaces slip may occur anywhere within the bridge. The longer a grain bridge, the higher the probability of finding a weak link within it, and therefore the lower the observed coefficient of friction.

A few direct shear tests were carried out on interfaces consisting of saw-toothed surfaces and a mass of 3 mm diameter steel rods placed on top. A specially designed transparent shear box 100x100x50 mm, developed by West (1992), was used. Detailed observations showed that during shearing, rods formed bridges between the bottom rock sample and the top platen of the shear box, which forms the upper boundary. The bridges start from the loading edge (right on Plate 8.1) and extend progressively to the rest of the specimen. As they advance, they rotate and after some shear displacement they collapse and new bridges are formed. During this continuous rearrangement, some rods may be found floating between the bridges, without carrying any load. Many of them are kept in place by the bridge action (i.e. contact at two point only) as shown in Figure 8.9. In tests were the saw-toothed surface was aluminium, only two from the four modes of failure suggested by Biegel *et al.* (1989), namely sliding along the interface and between rods, could be possible. Both of these patterns were observed as shown in Plate 8.1, where the deformation at an initial stage and after some 6 mm shear displacement is shown. Note that after the initial rearrangement, the rods tend to form bridges at about 45°. Failure was taking place mainly along the interface by sliding and rolling or by sliding between rods. Note that movement along the interface, begins from the right and advances progressively to the left. Plate 8.2 is from a similar test where the saw-toothed surface was from the synthetic rock described in Chapter 2. In this case tensile fracture of the rock teeth of the type shown in figure 8.6c occurs from right to left. These observations indicate that the stress state in the mass is not homogeneous and progressive failure occurs. Note also that the a number of rods in
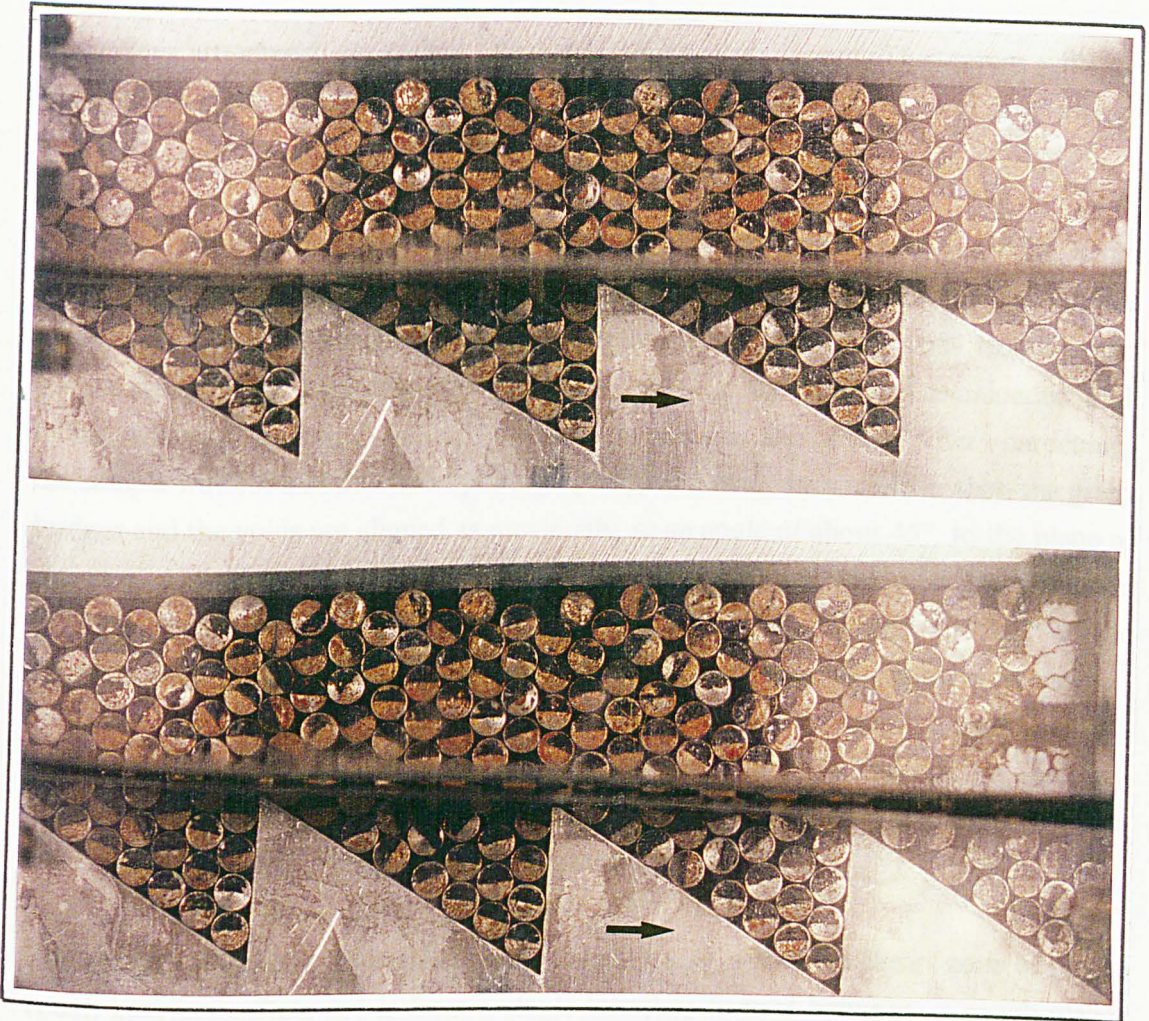
Plate 8.1: Deformation of an assembly of 3 mm steel rods sheared on an aluminium saw-toothed surface under a normal stress of 400 kPa:
(a) after 1 mm shear displacement. (b) after 6 mm shear displacement

Plate 8.2: Tensile failure of teeth of a rock saw-toothed surface sheared with an assembly of 3 mm steel rods under a normal stress of 400 kPa

the valleys are almost untouched after some shear displacement. This agrees with the observation made in tests on sand/saw-toothed rock interfaces, already discussed in Chapter 7.5.4.

A similar deformation pattern is also seen in Plate 8.3, which corresponds to an interface between Leighton Buzzard sand 3 (see Chapter 7) and a saw-toothed surface made from the synthetic rock with inclination 30°. The interface was tested under normal stress of 400 kPa, and after the end of the test, the sample was unloaded and a thin resin was poured to occupy the spaces between the grains. After hardening, the sample was cut and the microphotograph shown was taken. Note that the grain bridges and the voids are aligned as previously, at an angle of about 45° to the plane of shearing. Mandl *et al.* (1977) measured the stress orientation within a granular mass in simple shear and found that the principal stress σ_l was inclined at 45±2° to the interface such that all planes parallel to the boundary are planes of maximum shear. It is believed that joints filled with granular material have shear strength higher than that of the soil alone even if there is no rock-rock contact, due to the mechanism described earlier. As the thickness of the soil increases so the bridge weakens and there is a thickness beyond which there is no any effect of the rock walls.

The bridge pattern of deformation seems to occur also within the shear zone of planar rough interfaces. Plate 8.4 is from a single interface formed between a rough planar surface (Chapter 7.5.4) and sand 3 tested under a normal stress of 400 kPa. The shear zone is seen clearly on the bottom (right) about 4 grains thick above the rock surface (grey coloured). Grain bridges are seen to link the rock surface with the soil mass above the shear zone. It seems that these bridges continue well beyond the shear band boundary. Therefore this mechanism appears to be a typical one at least for the materials tested.

8.4. Critical thickness of soil layer

The question now is what is the magnitude of the soil thickness beyond which the rock walls have no any effect. A simple estimation can be made if we consider the thickness of the shear band which is formed when granular materials are subjected to shearing. Measurements of the shear zone in some tests on single soil-rock interfaces were made and the results are shown in Figure 7.18, together with results from other researchers. The case of double interfaces is not exactly the same as the single rock-soil interface, where the failure plane may be well defined. The state existing in a soil is more appropriate. The effect of the rock walls will diminish when the distance between them is such that the shear zone within the soil does not reach the rock walls (Figure 8.9). According to Roscoe (1970) the thickness of the shear band is about 10 times the mean
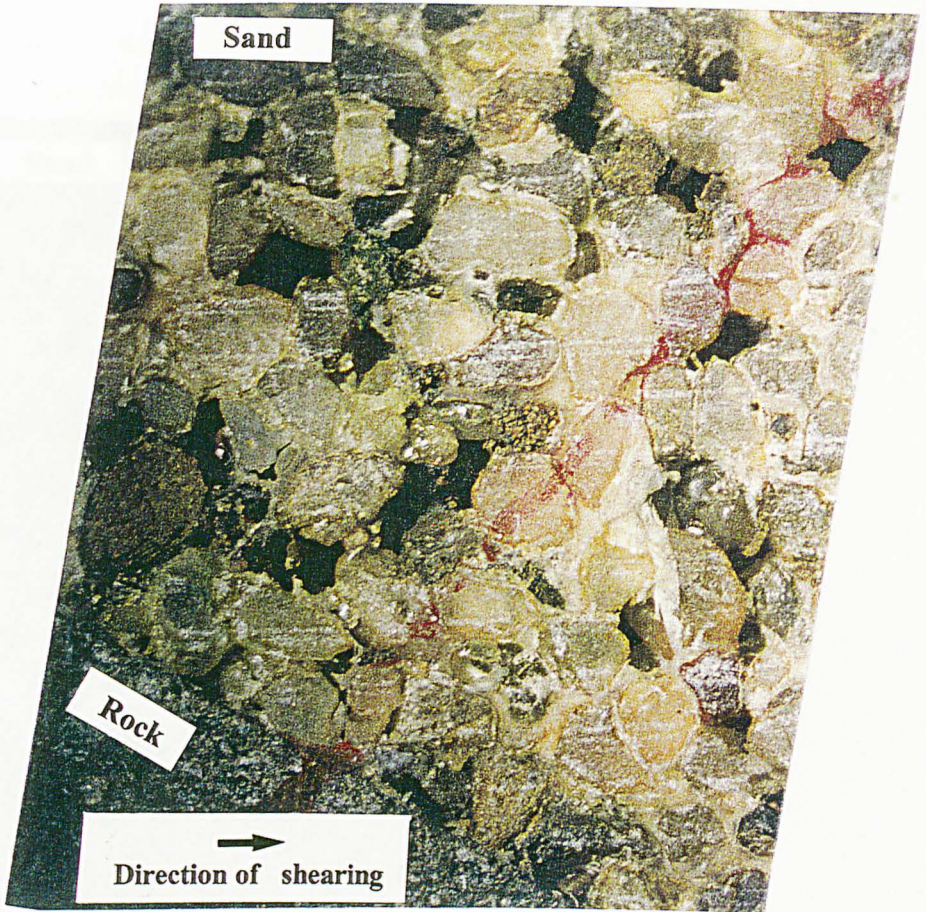
Plate 8.3: Load bearing bridges formed when a sand is sheared on top of a rock saw-toothed surface under a normal stress of 400 kPa

Plate 8.4: Deformation near a single interface between a rough planar rock surface and sand, tested under a normal stress of 400 kPa.

diameter of the soil. Wernick (1979) suggested 14 times the mean diameter, whereas Muhlhaus & Vardulakis (1987) and Bridgwater (1980) predicted similar values. If this value is accepted, then the critical relative thickness will be given by

$$\frac{f_{crit}}{a} = 10\frac{D_{50}}{a} + 1 \tag{8.1}$$

where D50 is the mean diameter of the soil and
a the mean roughness amplitude of the joint.
For cohesive materials

$$\frac{f_{crit}}{a} = 1 \tag{8.2}$$

Where the roughness amplitude is 20 times the mean diameter of the soil, equation (8.1) predicts a value of 1.50 for the critical relative thickness, which is a value quite commonly found in the literature. The results shown in Figure 8.6 , from de Toledo & de Freitas (1995) correspond to tests on saw-toothed surfaces with a mean roughness amplitude $a = 1.6mm$ and infill with a mean diameter of 0.2 mm. From equation 8.1 the value of (f_{crit}/a) is 2.25. The above authors mentioned a value of 2.3. The relation does not take into account the inclination of the asperities, which is at least equally relevant to shearing as is the roughness amplitude. However, given the uncertainties of the problem and the current practice of using only the roughness amplitude to describe roughness, it can be considered as an adequate approximation The very good agreement with the experimental results is an indication that it may be applicable in general, and this may be proved quite useful in predicting the shear strength of infilled joints, by eliminating one unknown in the from the existing empirical criteria.

8.5. Empirical criterion for peak shear strength of filled joints

An empirical criterion was developed which can be applied in the case of double soil-rock interfaces, with the soil layer consisting either granular or clayey material. Detailed description of the criterion is presented in the accompanying papers.

There is a debate on the shape of the shear strength - relative infill thickness envelope The empirical criterion gives an envelope of exponential form concave upwards (Figure 8.10) De Toledo and de Freitas (1993) presented data which show that the opposite may occur and a discussion on this matter is presented in Paper No 3. From Figure 8.7 they used the curve corresponding to a normal stress of 25 kPa to indicate that this is true also for data presented by the author. However, these data correspond to a thin layer of an artificial material (PFA) with spherical particles, which was tested between two rock walls. Obviously, the constant values for the shear strength obtained in the

$$f_{crit} = a + t \approx a + 10D$$
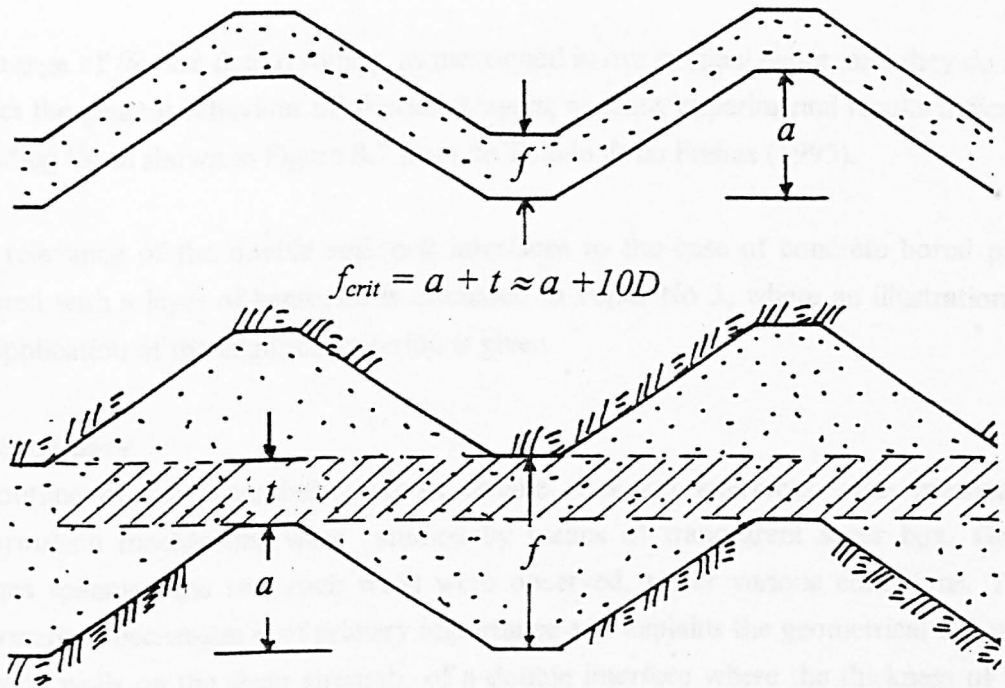
Figure 8.9: A simplified model for the calculation of the critical infill thickness

$$\mu = \mu_{mn} + (\mu_{max} - \mu_{mn})^n$$

$$n = (1 - (fa)/c)^m$$

Typical values
Frictional infills: $c = 1\cdot5$, $m = 1\cdot0-1\cdot5$
Clayey infills: $c = 1\cdot0$, $m = 2\cdot0-4\cdot0$

Stress ratio $\mu = \tau/\sigma$ (%)

Relative infill thickness f/a
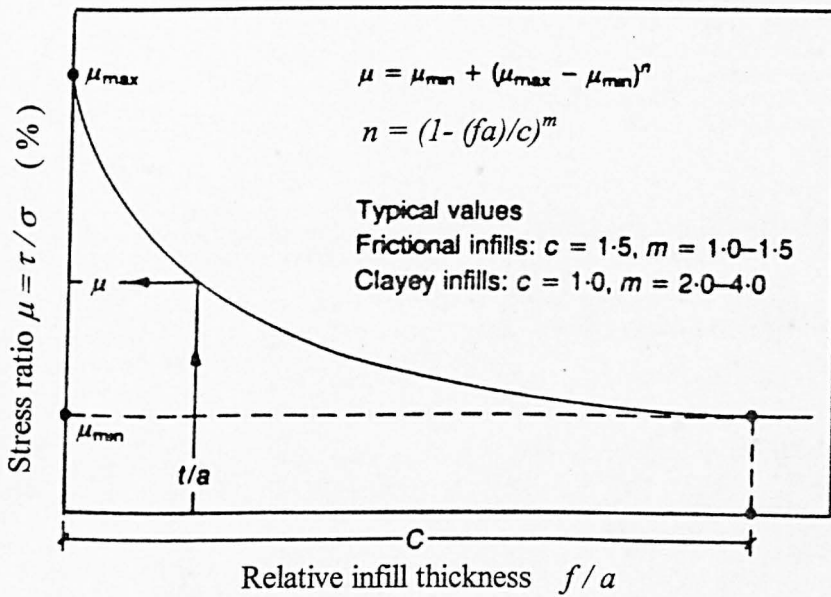
Figure 8.10: Empirical criterion for predicting peak shear strength of filled rock joints

low range of *f/a*, are due to rolling, as mentioned in our original paper, and they do not reflect the general behaviour of frictional layers, as many experimental results indicate, including those shown in Figure 8.7 from de Toledo & de Freitas (1995).

The relevance of the double soil-rock interfaces to the case of concrete bored piles covered with a layer of bentonite is discussed in Paper No 3, where an illustration of the application of the empirical criterion is given .

8.6. Summary

An outline of the shear behaviour of double rock-soil interfaces was presented. Deformation mechanisms were   studied by means of transparent shear box. Grain bridges spanning the two rock walls were observed, under various conditions. This deformation mechanism is of primary importance and explains the geometrical effect of the rock walls on the shear strength of a double interface where the thickness of the soil layer is thick enough not to allow contact between the adjacent rock walls. A simple expression was derived for the estimation of the critical thickness of the soil layer beyond which, the rock walls do not affect the shear strength of the interface.

8.7 Published work on shear behaviour of filled joints

Shear strength of modelled filled rock joints

T.Papaliangas
Department of Earth Sciences, University of Leeds, UK
& Department of Civil Engineering, Technological Education Institute, Thessaloniki, Greece

A.C.Lumsden & S.R.Hencher
Department of Earth Sciences, University of Leeds, UK

S.Manolopoulou
Department of Civil Engineering, Aristotelian University, Thessaloniki, Greece

ABSTRACT: The experimental results of direct shear tests on models of rock joints with two different mean roughness amplitudes (a) and using pulverised fuel ash (PFA), marble dust and kaolin as infill show that the shear strength decreases with increasing infill thickness (f). For kaolin-filled joints, shear strength reduced by 50% from that of the clean joint with f/a as low as 0.1 and continues to decrease slowly with increasing f/a. For frictional infill, decrease in shear strength is much less rapid and overall loss of strength is much smaller. The lowest strength of the infilled joint system lies between the strengths of infill alone and the fill-rock interface. This minimum shear strength is approached when f/a approaches 1.0 for kaolin and 1.5 for marble dust and PFA. A simple empirical relation is derived from the experimental results and is proposed for the prediction of the shear strength of infilled joints.

1 INTRODUCTION

The most obvious effect of a filling material is to separate the discontinuity walls and thereby reduce rock-rock contact, but shear strength will also be influenced by the surface texture, the nature of the filling material itself and the characteristics of the wall-fill interface. Because of the lack of reliable and realistic theoretical or empirical relationships and the difficulties in obtaining and testing representative samples, engineers generally rely on judgement, often taking the shear strength of the infill itself on the assumption that this is a conservative lower bound. The results of a systematic study of the shear behaviour of infilled, rough discontinuity models are reported in this paper. Models were used to ensure uniform geometrical and strength characteristics throughout the test programme. The number of variables was reduced by using a dry cohesionless fill material and shearing the system at 4 different normal stress levels. To provide data for comparison, a second model material with different properties, representing a second rock type, was prepared and sheared with different filling material under one normal stress.

2 EXPERIMENTAL PROCEDURE

Impressions of 2 natural coarse grained sandstone (Millstone Grit) discontinuity surfaces were prepared using VINAMOULD 9525 (hard variety), a rubber hot melt compound, and used to cast joint surface models. The specimens were obtained from Bramhope Quarry, West Yorkshire. Roughness profiles are shown in Figure 1.
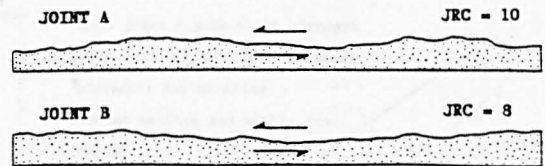
Fig. 1 Profiles of joint surfaces

Joint roughness coefficients are 10 and 8 for joints A and B respectively. The mean roughness amplitudes determined as an average from the profiles according to I.S.R.M. recommendations (1981) were found to be 7.0 mm for joint A and 6.0 mm for joint B. Details of the procedure used to prepare filled model joints are given by Bandis (1980), Bandis et al. (1981) and Papaliangas (1986). Extrusion of fill during shearing occurred only to a very

limited extent and then only when fills were thick and under high normal stress. Ratios of fill thickness (f) to mean roughness amplitude (a) of between 0.05 and 2 were used. The test programme consisted mainly of shearing discontinuities filled to several thicknesses of filling material under a range of normal stresses. For joint A with PFA infill, the normal stresses used were 25, 50, 75 and 100 kN/m^2, and for joint B with marble dust or kaolin, the normal stress was 50 kN/m^2. Preliminary tests were carried out to determine the shear characteristics of the clean discontinuities, saw-cut planar surfaces of the model material, the filling material alone and the interfaces between rock and infill material.

The purpose-built shear box for testing model materials provides shear and normal loads up to 8 kN and accomodates specimens up to 400 mm in length. A maximum stress of about 170 kN/m^2 could be applied to the specimens which were 120 mm wide x 250 mm long. The maximum shear displacement was 36 mm, i.e. 15% of the specimen length. Constant shear rate was 0.4 mm/min. The shear load was measured by means of a 5 kN proving ring, and shear, normal and lateral displacements were recorded throughout the tests.

3 PROPERTIES OF MATERIALS

3.1 Model material

Two different multi-component model materials were used for modelling the discontinuities: A was plaster based and B was cement based. The measured properties for A and B respectively are: density 1.85 and 2.23 Mg/m^3; unconfined compressive strength 3.5 and 6.0 MN/m^2; Young's Modulus 0.6 and 2.0 GN/m^2; friction angle of saw cut, planar surfaces 30.0 and 33.0 degrees.

3.2 Shear strength of model joints

Results of direct shear tests on joints A and B are presented in Figure 2 and Figure 3 respectively.

Peak strength data are presented both uncorrected (as measured) and with stresses corrected for dilation as proposed by Hencher and Richards (1989). The corrected data points describe essentially frictional behaviour, once dilation is accounted for, with a friction angle of 39 degrees (A) and 38 degrees (B).
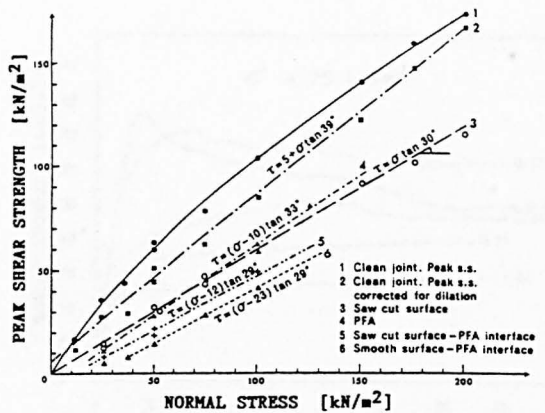
Fig. 2 Shear strength evelopes for joint A and PFA

As discussed by Hencher (1987) and Hencher and Richards (1989), that corrected value will include a component due to surface textural interlocking (non-dilational). Tests on smoother textured saw-cut surfaces define a much lower friction angle of 30 degrees.

3.3 Infill material

Pulverised fuel ash (PFA) from Eggborough Power Station, South Yorkshire, was used as infill material for joint A. PFA is a non-cohesive, fine-grained material with almost spherical particles of glass, specific gravity of 2.39 Mg/m^3 and mean particle diameter 10 micrometres. Marble
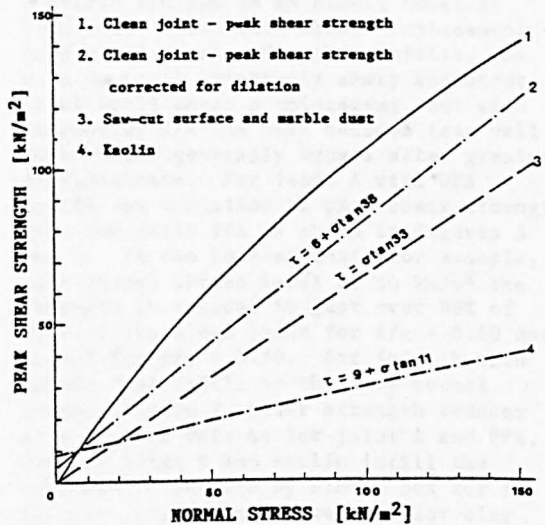
Fig. 3 Shear strength envelopes for joint B, marble dust and kaolin

dust and kaolin were used with joint B. Marble dust was used as a denser frictional material with angular particles and kaolin with a moisture content of 50% was used as weak non-frictional infill. Full details of composition, grain size, etc. of the infill materials can be found in Papaliangas (1986) and Manolopoulou (1990).

The shear strength of the PFA was determined by placing a thick layer (200-400 mm) between flat surfaces of the model material and consolidating under 200 kN/m^2 for one hour before shearing. Results are presented in Figure 2, together with results obtained from shearing model/fill interfaces for two types of joint wall surface, the first using planar saw-cut surfaces, the second using smooth surfaces (formed by pouring the model material against a glass plate). In both cases the interface shear strengths were below that of the PFA itself, which suggests that in infilled joints the weakest part of the system may not always be within the fill material. The tests involving the use of PFA all resulted in linear strength envelopes with apparent negative intercepts (extrapolated) on the shear strength axis. The explanation is probably that used by Hencher (1977) i.e. uplift pressure cause by trapped air.

The shear strengths for marble dust and kaolin are presented in Figure 3.

4 EXPERIMENTAL RESULTS

Normal and shear stresses were calculated from normal and shear loads divided by the gross area of contact adjusted for shear and lateral horizontal displacement. The data were corrected for dilation in the manner described by Hencher and Richards (1989), as mentioned earlier.

Correcting data to remove the effect of dilation, which is a sample variable, allows the fundamental basic shear strength to be measured. Considering the tests reported here, for cohesionless filling materials the values represent the shear strength due to internal friction only, and for a filled joint the shear strength under conditions of constant volume during shearing. Because of the variation in dilation angle, correction of the data produced considerable variation in normal stress values which were normalised and referred to a common nominal normal stress, i.e. the normal stress at the beginning of the test.

Shear stress-horizontal displacement curves for joint A with PFA infill, with normal stress at 75 kN/m^2 and corrected
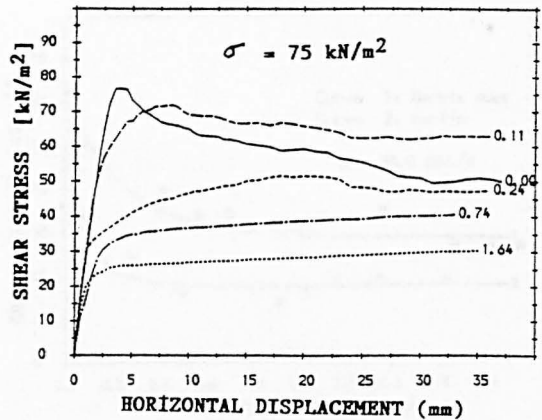
Fig. 4 Shear stress-shear displacement graphs for PFA infilled joint A (corrected for dilation)

for dilation are shown for illustration in Figure 4. These curves show that under shear the infilled joint may behave in various ways, primarily according to the ratio of fill thickness to roughness amplitude. Various aspects of this behaviour are discussed below.

4.1 Shear strength

Peak shear strength is defined as the maximum shear strength at any stage in the test. Peak shear strength is mobilised at different shear displacements, according to f/a ratio. For clean joints shear strength rose to a clear peak followed by a steady decline to an almost constant (residual) value with shear displacement (corrected data). For thin infills, the peak is still relatively sharp and occurs after small shear displacement, but with increasing f/a the peak becomes less well defined and generally occurs after greater displacements. For joint A with PFA infill the variation of peak shear strength with the ratio f/a is shown in Figures 5 and 6. It can be seen that, for example, at a normal stress level of 50 kN/m^2 the strength is reduced to just over 80% of that of the clean joint for f/a = 0.10 and to 45% for f/a = 0.50. For joint B with marble dust infill at the same normal stress, Figure 7, shear strength reduces at a similar rate as for joint A and PFA, but for joint B and kaolin infill the strength is reduced by almost 50% for f/a of only 0.10. Similar results for clay infilled joints have been reported by Lama (1978).
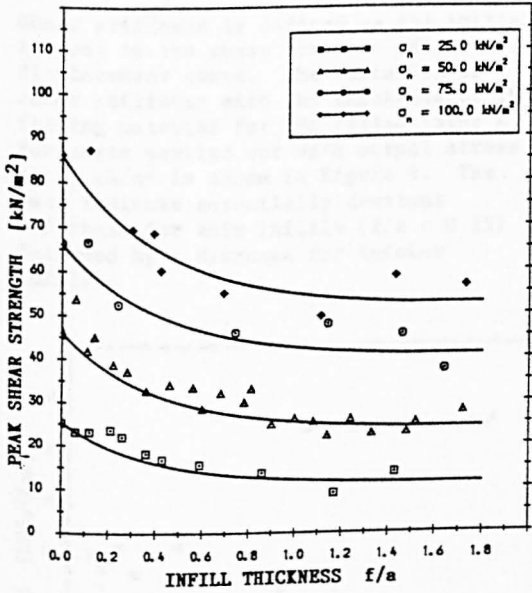
Fig. 5 Effect of infill thickness on peak shear strength. Joint A/PFA (corrected)
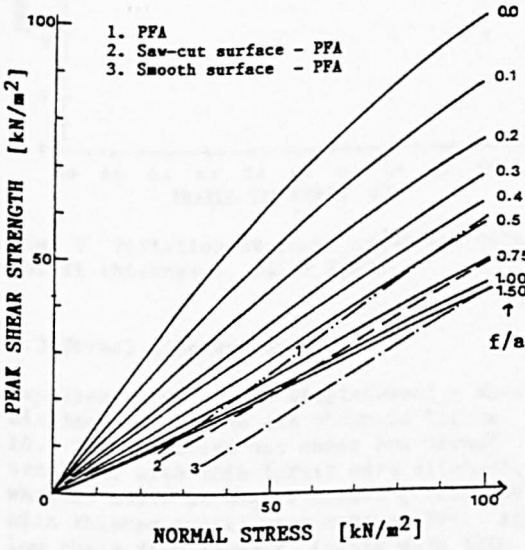
Fig. 6 Shear strength envelopes for various thicknesses of infill

For joint A/PFA and B/marble dust, peak shear strength approaches a constant minimum value for f/a between 1.25 (low normal stress) and 1.50 (higher normal stress). For B/kaolin, peak shear strength approaches a constant minimum when f/a = 0.6.

In the joint A/PFA system, for high f/a ratios and high normal stress levels,
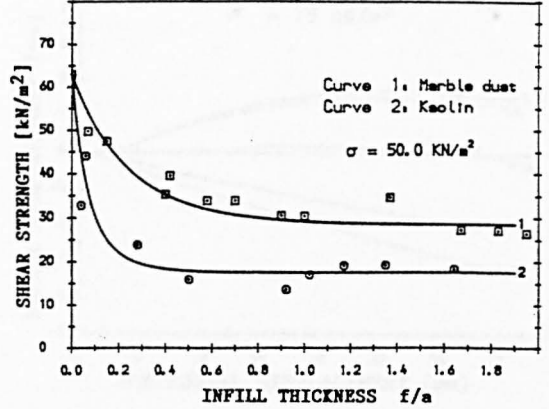
Fig. 7 Effect of infill thickness on the shear strength of joint B.
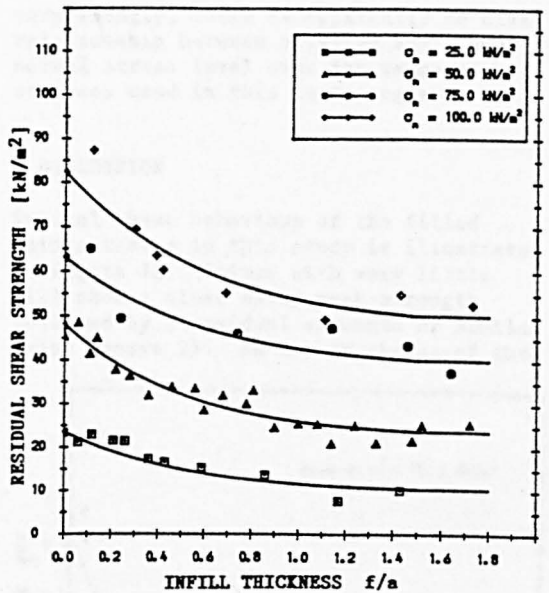
Fig. 8. Effect of infill thickness on the residual shear strength of PFA filled joint A (corrected)

measured shear strengths were lower than that for the PFA alone.

Residual shear strength is taken here as the shear strength at maximum shear displacement, although the term is perhaps misleading because of the strain hardening behaviour observed in many tests. Residual shear strength is plotted against the ratio f/a in Figure 8. For f/a > 1, where the influence of rock walls is unlikely to be significant, residual shear strength is almost constant and would be unlikely to decrease further with continued shearing.

4.2 Shear stiffness

Shear stiffness is defined as tne initial tangent to the shear stress - shear displacement curve. The variation of shear stiffness with the thickness of the filling material for PFA filled joint A for tests carried out with normal stress at 50 kN/m^2 is shown in Figure 9. The data indicate essentially constant stiffness for thin infills (f/a < 0.25) followed by a decrease for thicker infills.
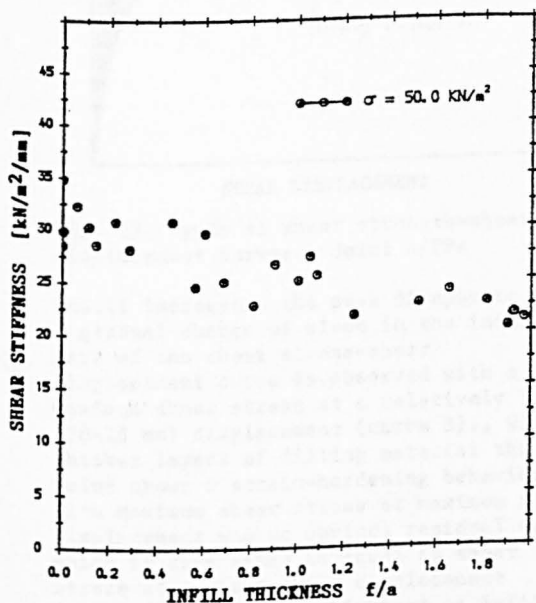
Fig. 9 Variation of shear stiffness with infill thickness. Joint A/PFA

4.3 Normal displacement

Representative normal displacement - shear displacement graphs are shown in Figure 10. Tests carried out under low normal stress or with thin infill were dilatant, whereas tests at higher normal stress and with thicker infill were compressive. At low shear displacement, joints with thin infill showed slightly less compression than the unfilled joints. This is due to the filling material occupying the space between the imperfectly matching joints, limiting the initial closure and is more evident for tests carried out at higher normal stresses. The dilation angle at peak shear strength for different f/a ratios is shown in Figure 11, indicating a change in behaviour from dilatant to compressive for f/a > 0.25. Rather
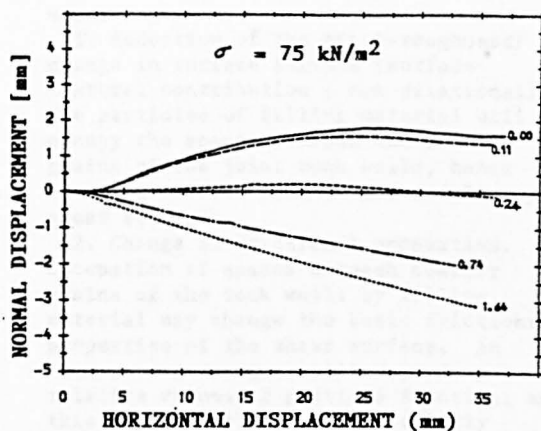
Fig. 10 Normal displacement-shear displacement curves for different f/a ratios. Joint A/PFA

surprisingly, there is apparently no clear relationship between dilation angle and normal stress level over the range of stresses used in this test programme.

5 DISCUSSION

Typical shear behaviour of the filled joints tested in this study is illustrated in Figure 12. Joints with very little fill show a clear early peak strength followed by a residual strength of similar value (curve 2). As the thickness of the
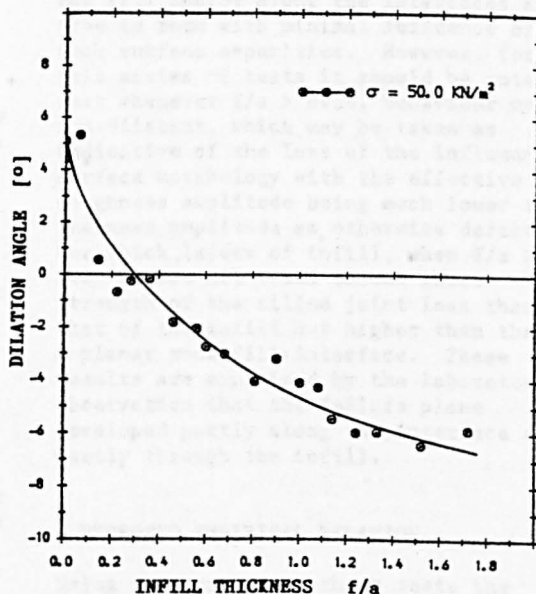
Fig. 11 Effect of infill thickness on dilation angle. Joint A/PFA
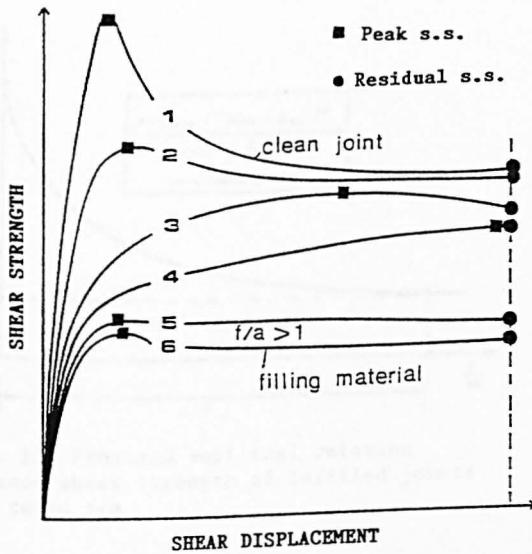
Fig. 12 Types of shear strength-shear
displacement curves. Joint A/PFA

infill increases, the peak disappears and
a gradual change of slope in the initial
part of the shear stress-shear
displacement curve is observed with a
maximum shear stress at a relatively large
(20-25 mm) displacement (curve 3). With
thicker layers of filling material the
joint shows a strain-hardening behaviour
with maximum shear stress at maximum shear
displacement and no obvious residual value
which is then taken as equal to shear
stress at maximum shear displacement
(curve 4). When the thickness of infill
approaches mean asperity amplitude a
residual value is usually reached at
relatively small shear displacements (5 to
10 mm , depending upon the normal stress).
When the infill thickness is greater than
mean asperity amplitude the shear stress-
shear displacement graph shows a small
initial peak followed by a constant
residual value (curve 6). While these
results are considered of general interest
and illustrative of the true behaviour of
naturally infilled joints, the behaviour
might be expected to be affected by the
detailed morphology of the discontinuity
walls and not simply the ratio f/a.

Generally, the shear strength decreases
with increasing fill thickness and lies
between a maximum value, which is the peak
strength of the same unfilled joint, and a
minimum value which is in the strength
range between filling material and the
shear strength of the rock-fill interface.
The filling material may reduce shear
resistance of a joint in the following

ways:
1. Reduction of the micro-roughness/
change in surface texture (surface
textural contribution - non dilational).
The particles of filling material will
occupy the spaces between the coarser
grains of the joint rock walls, hence
altering surface texture and reducing peak
shear strength.
2. Change in frictional properties.
Occupation of spaces between coarser
grains of the rock walls by filling
material may change the basic frictional
properties of the shear surface. An
increase or decrease will depend upon the
relative values of particle friction, and
this may have played a particularly
important role in the very marked decrease
in strength noted for joint B with thin
layers of kaolin infill. The introduction
of a layer of freely mobile particles
may cause a reduction in friction due to
rolling, and this must be a particularly
important consideration for fillings like
PFA which have round particles.
3. Reduction of the "effective
roughness". The presence of fill will
change the geometry of the shear surface,
allowing shear displacement with lower
dilation than for the clean discontinuity.
The effect is greater with increasing f/a.
For idealised discontinuity geometry,
when the thickness of the fill is greater
than the mean roughness amplitude,
rock-rock contact does not normally occur
and the internal failure planes through
the fill and/or along the interfaces are
free to form with minimal influence of the
rock surface asperities. However, for
this series of tests it should be noted
that whenever f/a > 0.28, behaviour was
non-dilatant, which may be taken as
indicative of the loss of the influence of
surface morphology with the effective
roughness amplitude being much lower than
the mean amplitude as otherwise defined.
For thick layers of infill, when f/a >
1.0, almost all tests showed shear
strength of the filled joint less than
that of the infill but higher than that of
a planar rock-fill interface. These
results are explained by the laboratory
observation that the failure plane
developed partly along the interface and
partly through the infill.

6 PROPOSED EMPIRICAL RELATION

Using the results of these tests the
relationship shown in Figure 13, expressed
in terms of percentages of stress ratios,
is proposed for the prediction of the
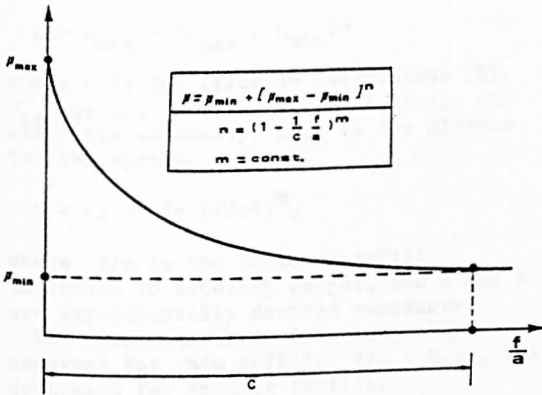
Fig. 13 Proposed empirical relation between shear strength of infilled joints and ratio f/a

Fig. 14 Application of proposed relation on published data (Lama, 1978)

shear strength of filled rock joints.

$$\mu = \mu_{min} + (\mu_{max} - \mu_{min})^n, \qquad (1)$$

where $\mu = (T/\sigma) \times 100$, $\mu_{max} = (T_{max}/\sigma) \times 100$, $\mu_{min} = (T_{min}/\sigma) \times 100$ and n is a function of the filling thickness:

$$n = [1 - 1/c \; (f/a)]^m \qquad (2)$$

for $0 < f/a < c$, where f = thickness of filling material, and a = mean roughness amplitude of the discontinuity.

T_{max} is the maximum shear strength of the system which is the same as the peak shear strength of the same joint unfilled. T_{min} is the potential minimum shear strength of the system for a critical thickness of infill, which varies with the thickness of the rock walls and the normal stress. T_{min} may be the strength of the fill of the shear strength of the rock-fill interface. For rough, undulating joints or strongly stepped discontinuities it is reasonable to assume T_{min} equal to the shear strength of the fill, but for planar or slightly undulating discontinuities T_{min} will be equal to the strength along the interface, which is often lower than the shear strength of the infill.

The constant c, which is the critical ratio f/a for minimum shear strength of the system, Figure 13, depends on the properties of the filling material, the normal stress and the roughness of the joint surface. For the tests reported here the value of c can be taken as 1.5 for PFA and marble dust, and 1.0 for kaolin.

From the curves shown in Figures 5, 7,

and 8 the values of m, which indicates the rate of decrease in shear strength with increasing filling thickness, are 1.0 and 0.75 for peak and residual shear strengths respectively for joint A/PFA and 1.5 and 3 for the peak shear strengths of joint B/marble dust and joint B/kaolin.

The proposed relation can be applied for peak and residual shear strength, using the appropriate values for μ_{max} and μ_{min}. For f/a = 0, $\mu = \mu_{max}$ which gives the peak shear strength of the clean joint. As the ratio f/a increases the curve tends to μ_{min}, where f/a = c. When the above equation is applied with f/a = c, which is the upper limit for f/a, the result is an over-estimation of strength by 1% of μ_{min}. The above relationship provides a good fit to the experimental data on rough, infilled joints presented by Lama (1978), with c = 1 and m = 3, as shown in Figure 14.

7 CONCLUSIONS

The tests reported here were carried out on carefully scaled models and indicate that the shear strength of a joint infilled with frictional material will fall somewhere between the shear strength of the clean joint and the minimum shear strength of the system which is particularly difficult to determine as in some cases shear resistance along the interface between fill and rock wall will be lower than that through the fill material itself.

Friction coefficients (peak and residual) are expressed as percentages and may be predicted by an equation of the form:

$$\mu = \mu_{min} + (\mu_{max} - \mu_{min})^n$$

where μ is the friction coefficient (%), μ_{max} is the friction coefficient for the clean discontinuity, μ_{min} is the minimum for the system, and

$$n = (1 - 1/c \ [f/a])^m,$$

where f/a is the ratio of infill thickness to asperity height, and c and m are experimentally derived constants.

The shear stiffness is essentially constant for thin infills, $f/a < 0.25$, and decreases for thicker infills.

The dilation angle at peak shear strength indicates a change in behaviour from dilatant to compressive for $f/a > 0.25$.

REFERENCES

Bandis, S.C. 1980. Experimental studies of scale effects on the shear strength and deformation of rock joints. Ph.D. Thesis, University of Leeds, Dept. Earth Sciences. Unpublished.

Bandis, S.C., Lumsden, A.C. and Barton, N.R. 1981. Experimental studies of scale effects on the shear behaviour of rock joints. Int. J. Rock Mech. Min. Sci. & Geomech. Abstr. 18, 1-21.

Hencher, S.R. 1977. The effect of vibration on the friction between planar rock surfaces. Ph.D. Thesis, University of London, Imperial College. Unpublished.

Hencher, S.R. and Richards, L.R. 1989. Laboratory direct shear testing of rock discontinuities. Ground Engineering, 22, 2, 24-31

Hencher, S.R. 1987. The implications of joints and structures for slope stability. Chapter 5 in Slope Stability. Editors M.G. Anderson and K.S. Richards. John Wiley and Sons Ltd.

International Society for Rock Mechanics. 1981. Suggested methods for the quantitative description of discontinuities in rock masses. In Rock Characterisation, Testing and Monitoring - ISRM Suggested Methods. E.T. Brown editor. Pergamon, Oxford.

Lama, R.D. 1978. Influence of clay fillings on shear behaviour of joints. Proc. 3rd. Int. Conf. International Association of Engineering Geology, Madrid. Vol.2, Paper II-43, 27-34

Manolopoulou, S.B. 1990. Shear behaviour of filled joints in rock. Ph.D. Thesis, Aristotle University of Thessaloniki, Dept.of Civil Engineering (In preparation).

Papaliangas, T. 1986. The effect of frictional filling materials on shear behaviour of rock discontinuities. M.Sc. Dissertation, University of Leeds, Dept. Earth Sciences. Unpublished.

DISCUSSION

Laboratory testing and parameters controlling the shear strength of filled rock joints

T. Papaliangas, *University of Leeds and Technological Education Institute, Thessaloniki, Greece,* **and S. R. Hencher and A. C. Lumsden,** *University of Leeds*

The Authors provide an account of the parameters affecting the behaviour of infilled rock joints when subjected to shear. Results of rotary shear box tests on an idealized saw-toothed joint infilled with overconsolidated clay show the different influences of the rock walls and the infill material on shear behaviour. On the shear stress-displacement diagram in Fig. 10 two peaks are observed: the first relates to yielding of the infill at an early stage and the second apparently results from contact with the rock walls. We offer some explanation for these results and discuss their relevance to the shear strength of rough, natural infilled joints.

The data in Fig. 21 indicate that the peak shear strength of the unfilled joint is reduced by about 40% by the introduction of only a thin (about 0.13 mm) infill. Similar results, partly reproduced as Fig. 19, were presented by Papaliangas, Lumsden, Hencher & Manolopoulou (1990), who attributed a reduction of almost 50% in strength to a fundamental change in frictional properties of the shear surface by the introduction of kaolin. Such a reduction is not usually seen with granular infills unless the particles are rounded, in which case a considerable decrease in strength may be observed as a result of rolling friction (Papaliangas et al., 1990).

Unfortunately, except for those shown in Fig. 21, the Authors do not provide any new data. Nevertheless, they propose a model (Fig. 22) which, it is suggested, is general and applicable for all types of infill (clayey or granular) and joint (regular saw-toothed or natural rough). There is little discussion of the origin or physical meaning of the various parameters. Furthermore, the proposed general relationship $\tau_2 \rightarrow \phi_{unfilled} + \phi_{soil} - \phi_{basic}$ seems to be of questionable use when several data sets for the shear behaviour of filled joints indicate that $\tau_2 \rightarrow \tau_1$ (Figs 14 and 18–20).

In order to understand any differences between the behaviour of filled natural rough and idealized saw-toothed joints it must first be accepted that the ratio of thickness of infill to mean rough-

ness amplitude t/a is by itself unlikely to account for variations in shear behaviour, just as it is not reasonable to try to predict the behaviour of a rough unfilled joint solely from the mean roughness amplitude a. The frictional behaviour between sliding rough surfaces will be influenced by the number, shape and distribution of the peaks on the surfaces (Halling, 1978). In the case of a regularly saw-toothed joint, the number, shape and distribution of peaks remain unchanged as the infill thickness increases, whereas they change dramatically in the case of rough natural joints for which there is a relatively rapid reduction in effective roughness (the equivalent of bearing areas of Abbot & Firestone, 1933) with increasing infill thickness (Papaliangas et al., 1990), as shown in Fig. 23.

Differences in shear behaviour for regular and irregular joints can be related to the areas of damage to the two rock walls during shearing. To investigate the area of damage for saw-toothed joints, a few direct shear tests were carried out in a Golder Associates shear box (Hencher & Richards, 1989). Before shearing the two sample halves (unfilled) were brought into contact, but with asperity tips and troughs separated by a ver-
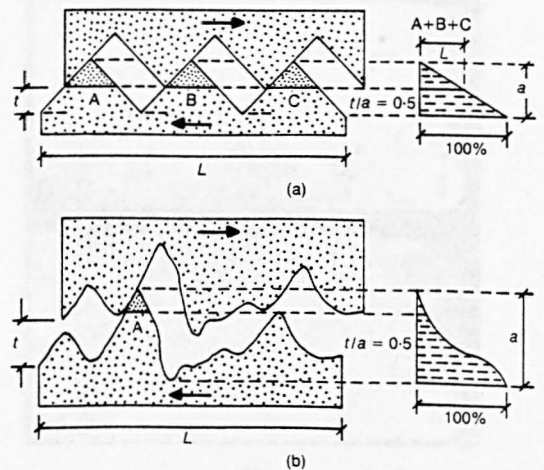
Fig. 23. Bearing area diagrams: (a) saw-toothed surface; (b) irregular rough surface

DISCUSSION

176
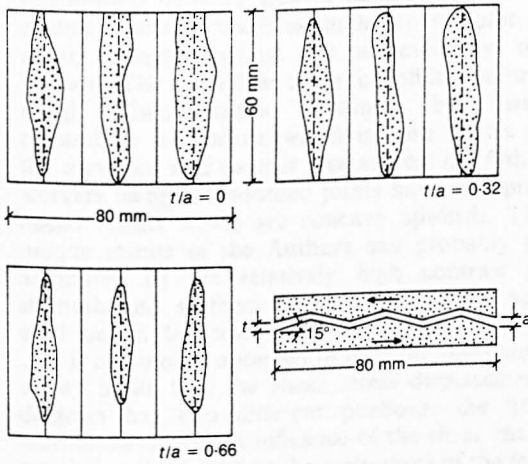
Fig. 24. Damaged areas for different ratios of t/a for a regular saw-toothed joint

tical distance t. With this special test arrangement the pure geometrical effect of the rock wall separation for saw-toothed joints can be seen. After shearing, areas of damage to asperities were measured (Fig. 24). Areas of joint wall damage were also measured for natural rough joints filled with pulverized fuel ash of various thicknesses of infill (Fig. 25); the results are given in Fig. 26 for comparison with those from saw-toothed surfaces. It is clear that, with increasing infill thickness, the reduction in rock wall contact is more rapid for natural rough joints than for saw-toothed joints. Consequently, the critical thickness of infill t_{crit} at which the rock walls cease to affect strength is smaller for natural rough than for saw-toothed surfaces. This also explains why the step in the shear strength envelope at $t = a$ reported in the Paper is not seen in the case of natural rough joints.

(a)

(b)
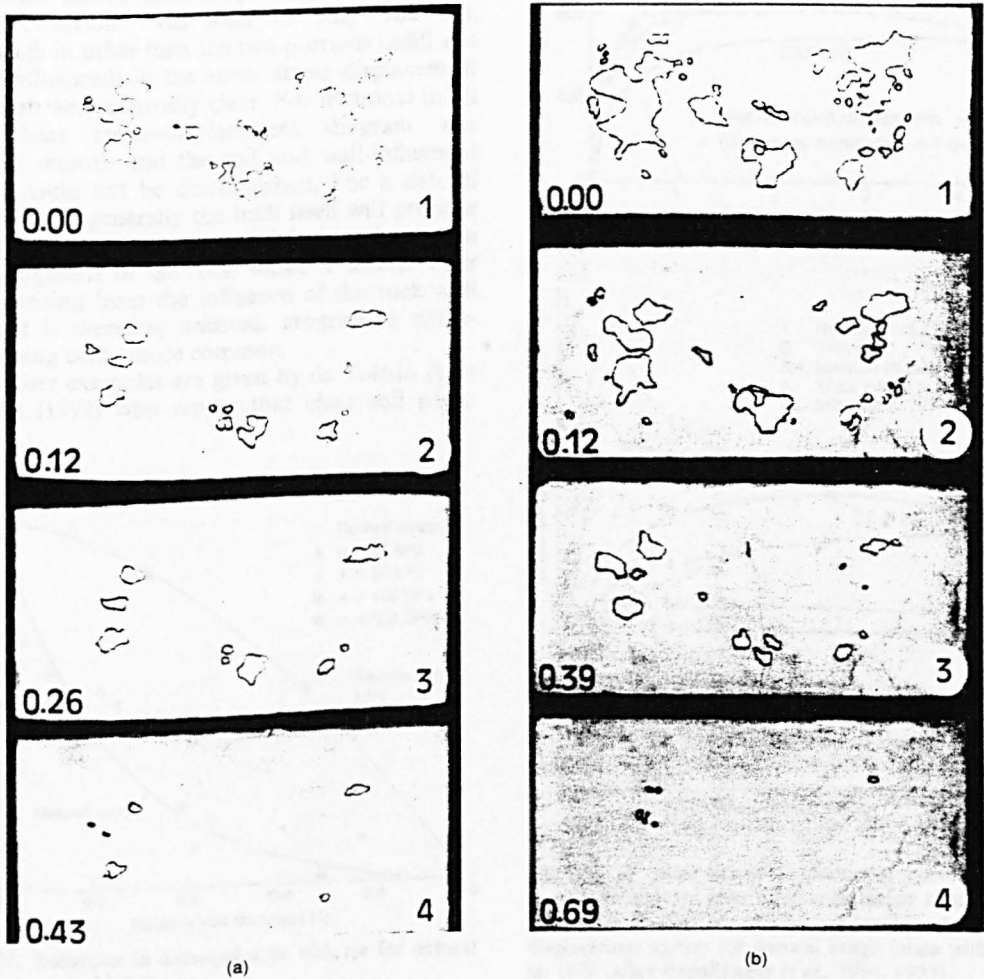
Fig. 25. Reduction in damaged areas for a natural joint filled with pulverized fuel ash (t/a shown in bottom left-hand corner of each specimen): (a) $\sigma = 25$ kPa; (b) $\sigma = 100$ kPa

In the case of the saw-toothed surfaces, the relationship between area of damage and t/a is convex upwards, which is similar to the plot of shear strength against t/a achieved by the Authors. The equivalent curve for infilled, natural rough discontinuities obtained by many researchers is concave, which in turn relates to the curve for wall contact area against t/a. Other workers using saw-toothed joints have also produced results which are concave upwards. The unique results of the Authors can probably be attributed to the relatively high contrast in strength and stiffness between rock walls and infill used in their tests.

It is commonly observed in tests on joints with clayey infills that the shear stress–displacement diagram has two different portions; the first reflects the dominant influence of the shear characteristics of the infill at the early stage of the test and the second shows the increasing influence of the rock walls during later stages. However, two distinct peaks are seldom seen. In the tests carried out with kaolin infill (Papaliangas et al., 1990) such behaviour was seen in only one test, although in other tests the two portions (infill and wall influenced) in the shear stress–displacement diagram were generally clear. For frictional infills the shear stress–displacement diagram was always smooth and the soil and wall-influenced zones could not be distinguished. For a natural rough joint, generally the infill itself will produce a clear peak only when it is thick enough to mask the roughness of the rock walls. A second clear peak arising from the influence of the rock wall contact is therefore unusual, progressive strain-hardening being more common.

Further examples are given by de Toledo & de Freitas (1992) who report that clear soil peaks were not observed in tests on saw-toothed joints infilled with either normally consolidated Gault clay or clayey sand. These results (Fig. 27(a)) are for medium to thick infills and are very similar to the relevant general curves (curves 3–6 in Fig. 27(b)) proposed by Papaliangas et al. (1990) and Papaliangas, Hencher, Lumsden & Manolopoulou (1993) for irregular rough joints with granular infill. The peak shear strength–infill thickness envelope from de Toledo & de Freitas (1992) (Fig. 28) is concave upwards (with $\tau_2 \rightarrow \tau_1$) and not convex (with $\tau_2 \rightarrow \phi_{\text{unfilled}} + \phi_{\text{soil}} - \phi_{\text{basic}}$), as is proposed to be the general case in the Paper. The model in the Paper may perhaps be valid only for the special condition of a saw-toothed joint with

(a)

1. No infill (clean joint)
2. Thin infill
3,4. Medium thickness infill
5. Thick infill ($t > a$)
6. Infill alone

■ Peak shear strength
● Residual shear strength

Shear displacement

(b)
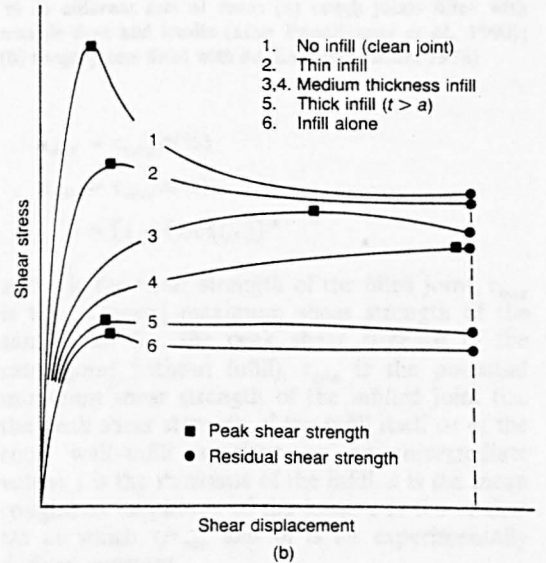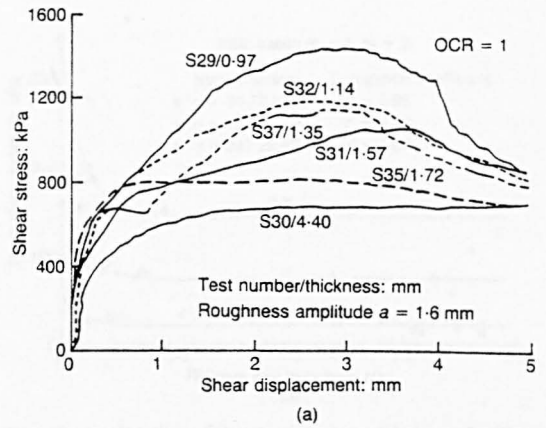
Fig. 27. (a) Shear stress–displacement curves for normally consolidated joint filled with clayey sand (after de Toledo & de Freitas, 1992); (b) typified shear stress–displacement curves for natural rough joints with granular infill (after Papaliangas et al., 1990, 1993)

Fig. 26. Reduction in damaged area with t/a for natural and saw-toothed joints
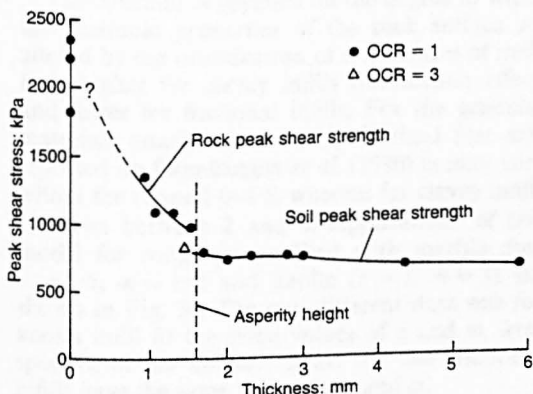
Fig. 28. Peak shear stress of saw-toothed joint filled with clayey sand plotted against infill thickness for two over-consolidation ratios (after de Toledo & de Freitas, 1992)
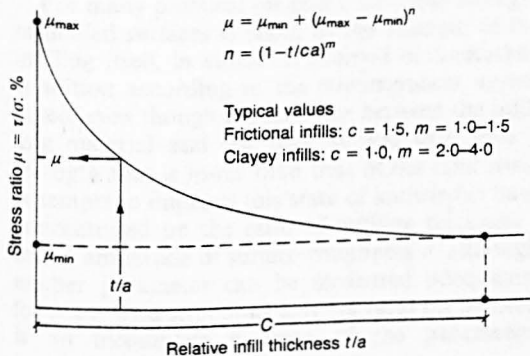
Fig. 29. Empirical model for the prediction of the shear strength of filled joints (after Papaliangas et al., 1990, 1993)

overconsolidated clayey infill tested in the ring shear box.

In summary, various well-documented aspects of shear behaviour of infilled joints, particularly those of natural roughness, do not comply with the model proposed in the Paper based on results from saw-toothed joints infilled with over-consolidated clay.

As suggested by the Authors, the infill–rock wall interface may often represent the weakest part of a filled joint system. In an empirical model proposed by Papaliangas et al. (1990, 1993) for the prediction of the shear strength of a filled rock joint, this aspect was given special consideration. This simple model (Fig. 29) is applicable to all infilled joints regardless of the thickness of infill and not solely to the interfering region as reported by the Authors. The model has the form

$$\mu = \mu_{min} + (\mu_{min} - \mu_{min})^n$$

where

$$\mu = \tau/\sigma(\%)$$
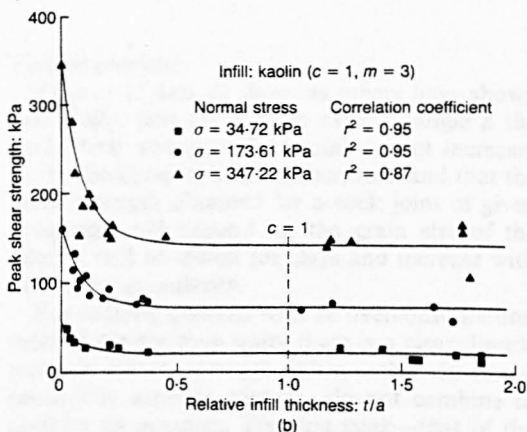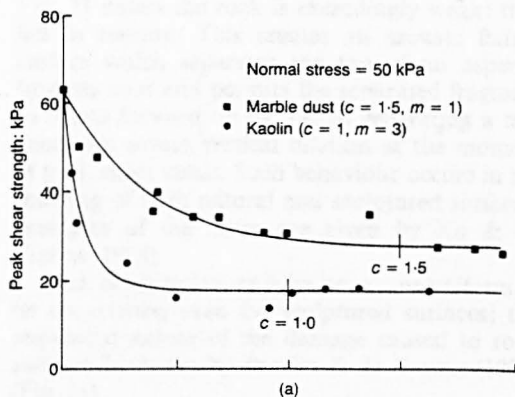
Fig. 30. Application of the empirical model shown in Fig. 29 to different sets of data: (a) rough joints filled with marble dust and kaolin (after Papaliangas et al., 1990); (b) rough joints filled with kaolin (after Lama, 1978)

$$\mu_{max} = \tau_{max}/\sigma(\%)$$

$$\mu_{min} = \tau_{min}/\sigma(\%)$$

$$n = [1 - (1/c)(t/a)]^m$$

and τ is the shear strength of the filled joint, τ_{max} is the potential maximum shear strength of the same joint (i.e. the peak shear strength of the same joint without infill), τ_{min} is the potential minimum shear strength of the infilled joint (i.e. the peak shear strength of the infill itself or of the rock wall–infill interface or an intermediate value), t is the thickness of the infill, a is the mean roughness amplitude of the joint, c is the critical t/a at which τ/τ_{min} and m is an experimentally derived constant.

The critical thickness ratio c varies with the nature of the infill, the roughness of the rock walls and the normal stress. Experimental results indicate that in practice c can be taken as 1·0 for clayey infills and 1·5 (in the range 1·2–2·0) for granular infills.

The constant m depends on the degree to which the frictional properties of the rock surface are altered by the introduction of a thin layer of infill. It is higher for clayey infills (lubrication effect) and lower for frictional infills. For the granular materials (marble dust and pulverized fuel ash) reported by Papaliangas et al. (1990) m may vary within the range 1·0–1·5, whereas for clayey infills m varies between 2 and 4. Applications of this model for rough joints filled with marble dust ($c = 1·5$, $m = 1·0$) and kaolin ($c = 1$, $m = 3$) are shown in Fig. 30. The two different data sets for kaolin infill fit the same values of c and m, irrespective of the normal stress; the two frictional infills have the same values for c and m.

Authors' reply

For many practical purposes the shear strength of infilled surfaces is taken as the strength of the infilling itself, in either its drained or undrained condition according to the circumstances anticipated, even though the interface between the infilling material and the rock surface can have a strength that is lower than that of the infill itself. Attempts to improve this state of knowledge have concentrated on the ratio of infilling thickness t to the amplitude of surface roughness a, although neither parameter can be measured adequately for many field situations and the ratio t/a by itself is an incomplete measure of the parameters involved.

All experimental work has shown the general trend of decreasing shear strength with increasing values of the ratio t/a. Powerful though such empirical approaches are in providing a value of immediate relevance to the problem in hand, they usually prove less useful for revealing the mechanics of the system they quantify and, as stated in the introduction to the Paper, our work, which was based on the performance of 61 tests, was designed to investigate the mechanisms involved in the failure of an infilled joint.

The Paper, which records work done independently from that of Papaliangas et al. (1993), shows significant agreement between the factual results obtained; in many respects the two data sets are complementary.

Rock failure

One of the difficulties with this work is knowing how to separate the relative contributions of soil deformation and asperity interaction from the overall result of shear strength at a given displacement. This cannot be done easily using natural joints and was one reason why we did not use them. Rock asperities rarely fail as shown in Fig. 23 unless the rock is exceedingly weak: they fail in tension. This creates an arcuate failure surface which separates the top of an asperity from its root and permits the separated fragment to rotate forward on its toe, so generating a tendency for severe vertical dilation at the moment of peak shear stress. Such behaviour occurs in the shearing of both natural and sculptured surfaces; examples of the latter are given by Xu & de Freitas (1988).

Rock asperity failure is by no means uniform in its occurrence, even for sculptured surfaces; the sequential nature of the damage caused to rock surfaces is shown by Pereira & de Freitas (1993) (Fig. 31).

Failure envelopes

Figures 21 and 22 show, as others have shown previously, that for a given asperity angle β the peak shear strength of an infilled joint increases as the thickness of infilling decreases, and that the shear strength obtained for a rock joint of given roughness will depend on the grain size of the filler; it will be lowest for clays and increase with increasing granularity.

For infilling material with an overconsolidation ratio of greater than unity there is a clear double peak in shear strength when other factors—principally asperity contact—do not combine to disguise its presence. The first peak—that of the infilling material—increases its contribution to the shear strength at small displacements with decrease in its thickness. However, this contribution cannot continue indefinitely, and for the surfaces we tested its presence becomes indistinguishable from that of the second peak below a relative thickness t/a of about 0·1.

The second peak is controlled by asperity contact. When this occurs the shear strength rapidly increases towards that defined by their failure, shown as the envelope for rock peaks in Fig. 21. A dramatic rise in shear strength occurs as soon as any trace of infilling is removed from the sliding surfaces (see the highest values of shear strength: 2200–2400 kPa).

The validity of such results for natural surfaces has been questioned and Fig. 26 presented as evidence of the difference in behaviour between natural and saw-toothed profiles. Care has to be exercised here for three reasons. First, the results in Fig. 26 were obtained using a range of normal loads under which conditions the surfaces would be expected to behave differently; to draw the conclusions that Messrs Papaliangas, Hencher & Lumsden make, the profiles should have been tested at the same normal loads. Second, as shown in Fig. 31, damage to a rock surface develops sequentially, even on regular surfaces,
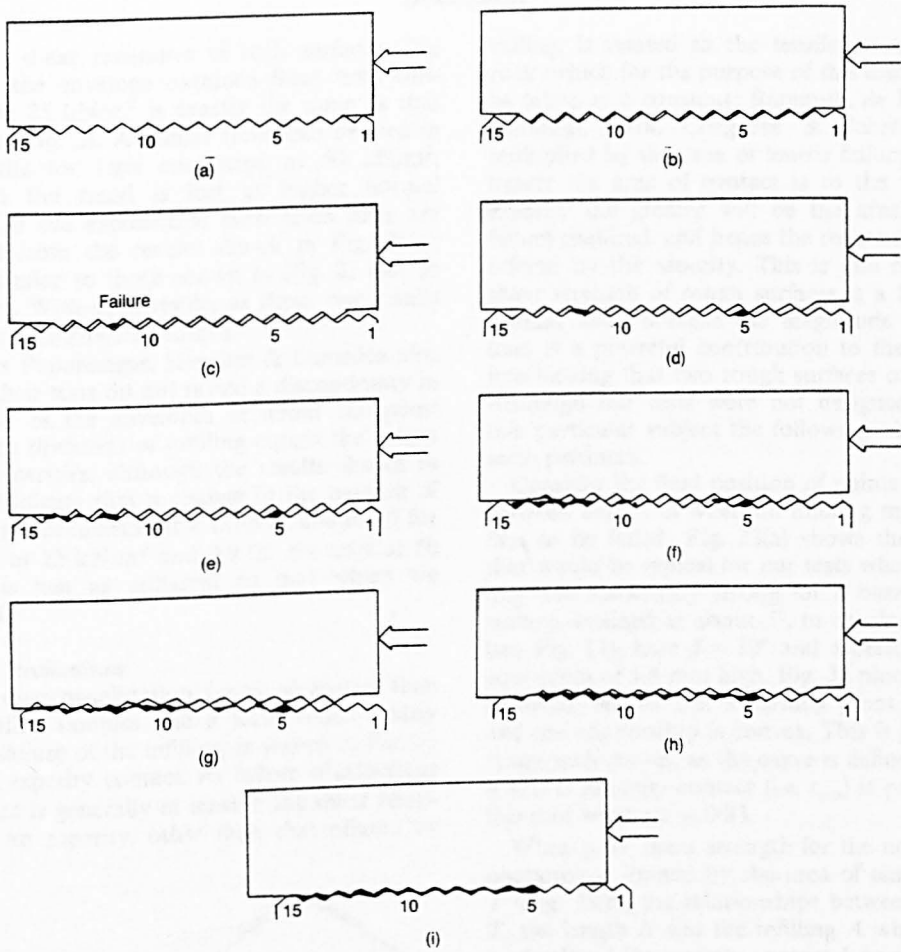
Fig. 31. Progressive destruction of uniform teeth loaded in direct shear: material and teeth dimensions as used in the Paper, normal load 1200 kPa (from Pereira & de Freitas, 1993)
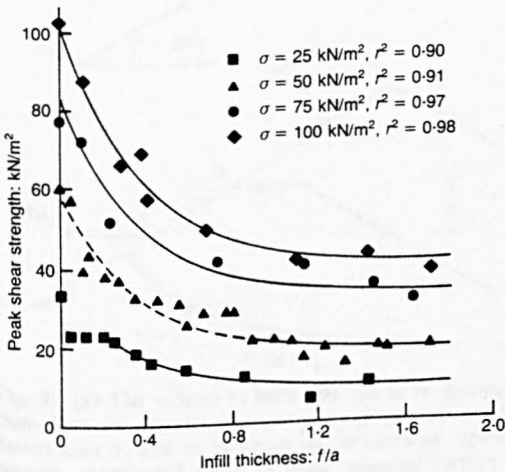
Fig. 32. Effect of infill thickness on peak shear strength (from Papaliangas et al., 1993).

because the magnitude, orientation and distribution of stress close to points of asperity contact constantly change with displacement (Pereira & de Freitas, 1993). Figs 24 and 25 are presented as evidence of the differences between the behaviour of natural and unnatural profiles although they show only the damage accumulated after a given displacement. Conclusions concerning t_{crit} cannot be drawn from such data because it is the total resistance to shear from all the points of contact at the moment of peak failure that defines t_{crit}. Third, Messrs Papaliangas, Hencher & Lumsden present a form of results using moulds of natural surfaces which is similar to the results we obtained using saw-cut profiles. Fig. 32 reproduces data of Papaliangas et al. (1993) before treatment to remove the effects of dilation; in this form it is most comparable with the data in the Paper, which do not have the effects of dilation removed, such effects being work of relevance to

the total shear resistance of such surfaces. The form of the envelope obtained from tests conducted at 25 kN/m^2 is exactly the same as that shown in Fig. 21. A similar trend can be seen in the results for tests conducted at 50 kN/m^2, although the trend is lost at higher normal stresses. If the exponential correlation lines are removed from the results shown in Fig. 30(a), trends similar to those shown in Fig. 21 can be discerned. With such results as these, our results cannot be described as unique.

Messrs Papaliangas, Hencher & Lumsden also believe their tests do not reveal a discontinuity in the trend of the envelopes at about the point where the thickness of infilling equals the height of the asperities, although the results shown in Fig. 32 indicate that a change in the balance of operating mechanisms at a ratio of about 0·5 for the tests at 25 kN/m^2 and 0·9 for the tests at 50 kN/m^2 is just as apparent as that which we recorded.

Possible mechanisms

With overconsolidation ratios of greater than unity, failed samples had a form which clearly implied failure of the infilling as shown in Fig. 33 prior to asperity contact. As failure of asperities in contact is generally in tension the shear resistance of an asperity, other than that offered by

sliding, is related to the tensile strength of the rock (which for the purpose of this discussion can be taken as a constant; Butenuth, de Freitas, Al-Samahiji, Park, Cosgrove & Schetelig, 1993) multiplied by the area of tensile failure. Thus the nearer the area of contact is to the root of an asperity the greater will be the area of tensile failure required, and hence the resistance to shear offered by the asperity. This is one reason why shear strength of rough surfaces is a function of normal load, because the magnitude of normal load is a powerful contribution to the degree of interlocking that two rough surfaces can achieve. Although our tests were not designed to study this particular subject the following observations seem pertinent.

Consider the final position of points of contact between asperities when an infilling material has first to be failed: Fig. 33(a) shows the situation that would be typical for our tests when the infilling was sufficiently strong for a basal shearing surface, inclined at about 5°, to develop within it (see Fig. 11); here $\beta = 30°$ and asperities are the equivalent of 1·6 mm high. Fig. 34 plots the areas involved against t/a; a turning point is present and the relationship is convex. This is just one of many such curves, as the curve is defined by both a and t. Asperity contact (i.e. t_{crit}) is predicted in this case when $t/a = 0·83$.

When peak shear strength for the normal load operating is limited by the area of tensile failure T (Fig. 33(b)) the relationships between the area T, the length L and the infilling A which has to be displaced for asperity contact L to occur, have to be considered. If the area A has a convex relationship with t/a (Fig. 34) shear strength might also be expected to exhibit a convex
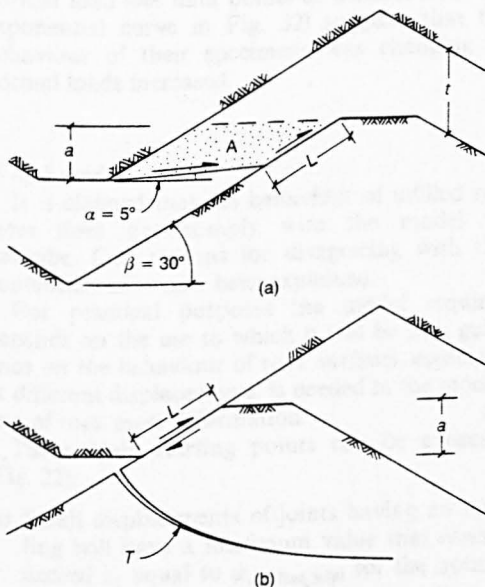
Fig. 33. (a) The volume of infill that has to be squeezed from between advancing asperities, represented by the dotted area A, and its influence on the areas of asperity contact, represented by L (a basal shearing surface α exists, inclined at 5°); (b) the resulting contact (failure then develops either as a sliding interface or as failure in tension T)
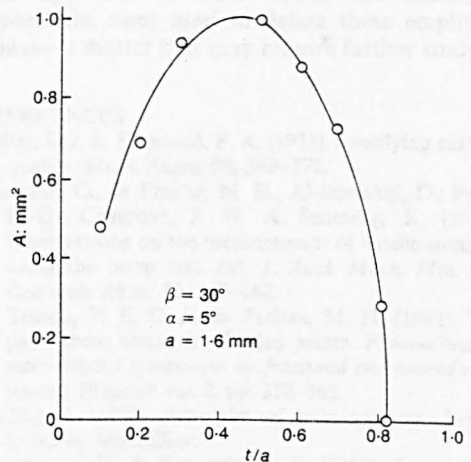
Fig. 34. Area of infill to be removed, as defined in Fig. 33(a), plotted against t/a for $\beta = 30°$ and $\alpha = 5°$

relationship with t/a, and this is evident (Figs 21 and 32) when the overconsolidation ratio is greater than unity.

For normally consolidated infillings the first peak is rarely seen as noted by us previously (de Toledo & de Freitas, 1992) and shown in Fig. 27. Furthermore, the rock peak envelope appears to be concave. We do not know whether these features are linked but suspect that they may be because normally consolidated materials deform differently from overconsolidated materials when they are between rough rock surfaces. Numerical simulations are currently being undertaken to study this aspect (Moosavi, 1992). Messrs Papaliangas, Hencher & Lumsden believe this smooth, concave envelope is the correct response for infilled rough rock surfaces and cite our work (Fig. 28) as further evidence of this, even though data from their tests (Fig. 32) and ours show that this is not so: the smooth concave envelope is just one type of response.

When clayey infilling is either overconsolidated or strengthened by some other means, the envelope is more variable (Figs 21 and 32). When more granular infilling is involved (the results in Fig. 28 were for joints filled with clayey sand) the envelope assumes a smoother concave form, even in overconsolidated conditions. The fact that Papaliangas et al. (1993) record envelopes which become progressively smoother with increasing normal load (see data points as distinct from the exponential curve in Fig. 32) suggests that the behaviour of their specimens was changing as normal loads increased.

Which model?

It is claimed that the behaviour of infilled surfaces does not comply with the model we describe. Our reasons for disagreeing with this contention have now been explained.

For practical purposes the model required depends on the use to which it will be put; guidance on the behaviour of rock surfaces, especially at different displacements, is needed in the modelling of rock mass deformation.

Three basic starting points can be expected (Fig. 22).

(a) Small displacements of joints having no infilling will have a maximum value that cannot exceed τ_1 equal to $\phi_{\text{unfilled joint}}$ for the normal load operating.

(b) When peak shear strength requires shear displacements to squeeze infilling from between the asperities, even if t/a is very small, the shear strength will be unlikely to exceed τ_2, equal to $\phi_{\text{unfilled joint}}$, but one which has been smeared, plus ϕ_{soil} minus ϕ_{basic} for the rock.

(c) When shear displacements are associated with a value of t/a that permits the infilling to generate its own perceptible peak, shear strength is unlikely to exceed τ_3, equal to ϕ_{soil} plus the angle of sliding β.

With increasing values of t/a conditions (b) and (c) will tend to develop as shown in Fig. 22 although, as shown in Figs 33 and 34, the form of the envelopes at small displacements will reflect the inclination and amplitude of roughness operating at the normal loads used. This is evident from the results reported in Fig. 32; as normal stress increases so the form of these envelopes changes to even increasingly smoother concavity. The same trend occurs with increasing granularity of the infill.

Conclusions

Messrs Papaliangas, Hencher & Lumsden draw attention to their approach for providing an overall description of the shear strength of infilled surfaces as a function of infilling thickness and surface roughness, and in so doing question our experimental results. However, beneath their exponential curves many similarities appear to exist between the performance of their tests and our own, which is interesting as their results are for copies of natural surfaces and ours are not. The difference between the work does not appear to lie in the mechanisms operating, so far as they can be discerned, and the data sets obtained, but in the interpretation and use of the data. We related the data to the mechanisms perceived, whereas they have concentrated on defining an overall description for the behaviour of their surfaces. It seems evident that the constants they define with the exponential function incorporate a mixture of mechanisms, making the extension of their approach to other scales and materials beyond the ones used to define these empirical values—a matter that may require further study.

REFERENCES

Abbot, E. J. & Firestone, F. A. (1933). Specifying surface quality. *Mech. Engng* **55**, 569–572.

Butenuth, C., de Freitas, M. H., Al-Samahiji, D., Park, H.-D., Cosgrove, J. W. & Schetelig, K. (1993). Observations on the measurement of tensile strength using the hoop test. *Int. J. Rock Mech. Min. Sci. Geomech. Abstr.* **30**, 157–162.

de Toledo, P. E. C. & de Freitas, M. H. (1992). The peak shear strength of filled joints. *Proceedings of international symposium on fractured and jointed rock masses*, Preprint vol. 2, pp. 358–365.

Halling, J. (1978) *Principles of tribology*, pp. 1–401. London: Macmillan.

Hencher, S. R. & Richards, L. R. (1989). Laboratory direct shear testing of rock discontinuities. *Ground Engng* **22**, 24–31.

Lama, R. D. (1978). Influence of clay fillings in shear behaviour of joints. *Proc. 3rd Int. Conf. Int. Ass. Engng Geol., Madrid* **2**, 27–34.

Moosavi, S. M. (1992). *Numerical modelling of shear behaviour of infilled joints*. Internal report for MPhil–PhD transfer, Imperial College, London.

Papaliangas, T., Lumsden, A. C., Hencher, S. R. & Manolopoulou, S. (1990). Shear strength of modelled filled rock joints. *Rock joints* (eds N. Barton & O. Stephansson), pp. 275–282. Rotterdam, Balkema.

Papaliangas, T., Hencher, S. R., Lumsden, A. C. & Manolopoulou, S. (1993). The effect of frictional fill

thickness on the shear strength of rock discontinuities. *Int. J. Rock Mech. Min. Sci. Geomech. Abstr.* **30**, No. 2, 81–91.

Pereira, J. P. & de Freitas, M. H. (1993). Mechanisms of shear failure in artificial fractures of sandstone and their implication for models of hydromechanical coupling. *Rock Mech. Rock Engng* **26**, 195–214.

Xu, S. & de Freitas, M. H. (1988). Shear strength characteristics of rough joints subjected to large displacements. *Proceedings of conference on applied rock engineering*, pp. 269–282. London: Institute of Mining and Metallurgy.

Side resistance of bentonite-coated pile-rock interfaces

T. Papaliangas
Department of Civil Engineering, Technological Educational Institution of Thessaloniki, Greece

S. Manolopoulou
Department of Civil Engineering, Aristotle University of Thessaloniki, Greece

SYNOPSIS: The behaviour of concrete pile-rock interfaces covered by a layer of bentonite, is simulated by direct shear tests on naturally rough rock joints filled with a soft clayey material. These tests indicate a considerable reduction in shear strength even when the infill is very thin. A comparison is made with results from in-situ tests reported in the literature. A simple empirical model for the prediction of the side resistance of pile-rock interface covered with a layer of bentonite is proposed. This model uses simple and easy to measure parameters, both in the laboratory and the field, such as the shear strength and roughness of the clean interface, and the shear strength and thickness of the bentonite layer.

1. INTRODUCTION

A considerable portion of the applied load on a concrete pile socketed in rock is carried by the side wall resistance of the concrete-rock interface. The excavation of such sockets may require drilling and concreting under bentonite slurry and as a result loose drill cuttings and/or bentonite cakes may be present on the rock wall surface. The various devices developed by contractors for cleaning socket wall are not as effective as desired and drill cuttings may be removed by washing the socket with water jets, but bentonite cakes of various thicknesses often remain on the rock wall. The presence of these bentonite cakes may significantly reduce the side resistance of rock sockets, by preventing the contact between rock and concrete. Thin bentonite cakes act as lubricants and may significantly reduce the friction angle of the rock-concrete contact (Papaliangas et al, 1990). In some cases bentonite cakes may be as thick as 100 mm (Holden, 1981) and may completely prevent the contact between concrete and rock. The

mechanism of side resistance of socketed piles is a special case of the general problem concerning the shear behaviour of rock joints (Johnston & Lam, 1989). Rough rock joints tend to dilate and shear strength at a particular normal stress is the result of a purely frictional (normal stress-independent) and a dilational component which is a function of the surface roughness and the normal stress (Papaliangas et al., 1994a). In a socketed pile, dilation is generated either by the elastic deformation of the pile due to the applied compressive load or by the shear displacement of the pile relative to the rough rock wall. The degree of dilation that occurs depends on the roughness of the walls of the socket and the strength of the rock that forms the asperities.

Because of the state of confinement existing around the pile, dilation causes an increase in normal (radial) stress. Simulations of the behaviour of rock sockets have been carried out in laboratory tests using constant normal stiffness (CNS) direct shear tests (Ooi & Carter, 1987, Lam & Johnston, 1987). Similarly, the behaviour of a pile-rock interface covered with
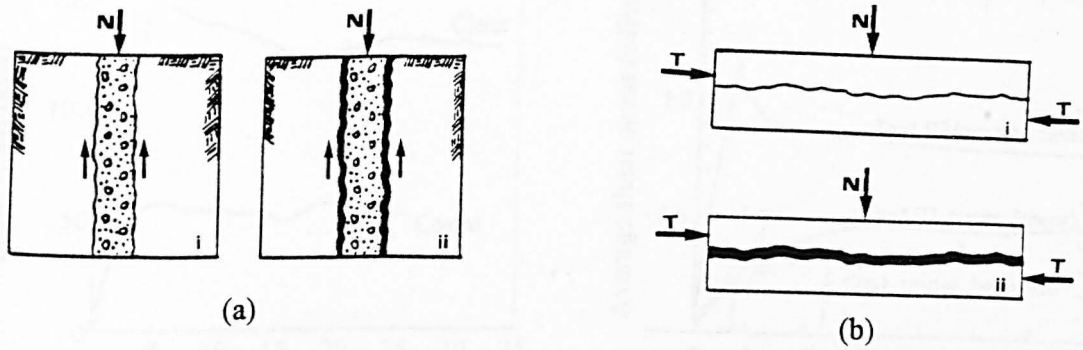
Figure 1. (a) Pile-rock interface: (i) clean (ii) covered with bentonite. (b) Rock joint: (i) clean (ii) filled.

a layer of bentonite may be simulated by the behaviour of a rock joint filled with a soft clayey material. Although the normal load acting on the socket wall is not necessarily constant, a condition of constant normal load (CNL) can be used as a first approximation.

The factors which greatly affect the shear behaviour of filled rock joints are: a) the roughness of the rock wall and b) the nature and thickness infill (Papaliangas et al., 1990, 1994b). The effect of roughness on the side resistance of piles socketed in rock has been illustrated by published laboratory and in-situ test results (Ooi & Carter, 1987, Williams & Pells, 1981).

In practice, an increase in side resistance of smooth sockets may be achieved by grooving, for example 20mm deep helical grooves at 500 pitch. Such grooving may be fairly readily achieved by the action of either a specially fitted oversize drill tooth on the auger, or by utilising a specially fitted hinged reamer type device, usually fitted to the top of a bucket auger (Kingwell & Albrecht, 1989). With grooving, pile-rock contact is established after some shear displacement and there is no significant adverse effect of bentonite on side resistance. However, in sockets drilled by auger, a layer of bentonite on the walls of the socket may cause a reduction in strength as high as 75% (Williams & Pells, 1981).

In the present paper some data are presented on the effect of the thickness of soft coatings on shear resistance of naturally rough joints and an empirical model is proposed to predict the shear resistance from parameters related to the roughness of the socket wall and the characteristics of the coating.

2. EXPERIMENTAL RESULTS

A research programme on naturally rough filled rock joints was carried out, consisted of a series of direct shear tests on modelled rock joints. Replicas of natural joint surfaces were made and a layer of wet kaolin was placed between the rock walls to simulate coatings of various thicknesses. A special cement mortar was used to model walls with: density 2.2 Mg/m³, unconfined compressive strength 6.0 MPa, tensile strength (Brazilian) 0.9 MPa, point load strength 0.9 MPa, porosity 30% and friction angle of flat saw-cut surfaces 33°. The emphasis of the programme was on the effect of the thickness of coating and the roughness of the rock wall on the shear strength under different constant normal stresses. Details of the procedure followed and experimental data for smooth and naturally rough kaolin-coated modelled joints are given elsewhere (Manolopoulou, 1991, 1994).

Figure 2a shows typical shear stress-shear displacement diagrams corresponding to a
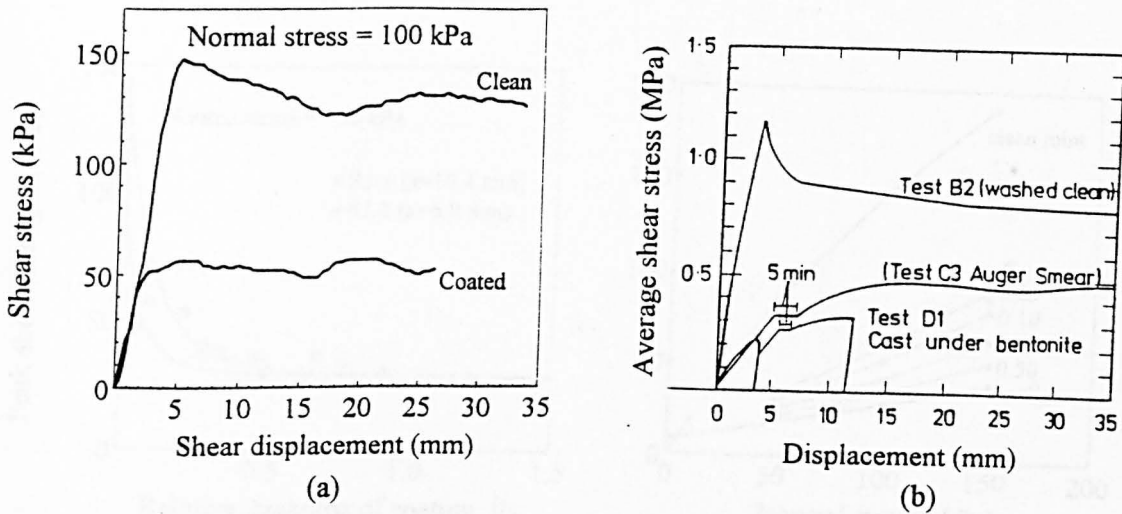
Figure 2. (a) Typical shear stress-shear displacement diagrams for clean and coated joints.
(b) Effect of bentonite on shear resistance of rock sockets (after Williams & Pells, 1981).

rough rock joint (RJ1) having a mean roughness amplitude of 10.4 mm and tested both clean (uncoated) and with a kaolin coating having a thickness of less than 0.5mm, under constant normal stress $\sigma=100$ kPa. The peak shear strength of the coated joint is considerably lower (approximately 35%) than that of the uncoated joint (lubrication effect). For thicker layers of kaolin the shear strength is even lower, approaching a value of the order of only 25% of that of a clean joint.

The shear stress-shear displacement diagram is similar to that given by Williams & Pells (1981) for sockets in sandstone covered with bentonite (Figure 2b). In practice, it is difficult to remove completely bentonite cakes from rock walls, therefore a considerable strength reduction might be expected, even when the bentonite layer is very thin.

The variation of shear strength with the thickness of coating for two surfaces with different roughness (RJ1 and RJ2) is shown in Figure 3a, and peak shear strength envelopes for joint RJ1 filled with kaolin of different thickness express as ratio thickness:mean roughness amplitude is shown in Figure 3b. For thick layers (say greater than 0.5a, where a is the mean roughness amplitude of the surface), the shear strength of the filled joint approachesa a minimum value, equal to the shear strength of

coating (29 kPa), which when compared to the shear strength of the two clean joints (105 and 142 kPa) is only 27.6% and 20.4% (or 24% average). This is in close agreement with the value of 25% suggested byWilliams & Pells (op. cit.) for sockets covered with bentonite or smear layers formed by augering in slightly moist rock.

3. PROPOSED MODEL

The empirical model for the prediction of the side resistance of concrete piles proposed here, is a special case of a general model for filled rock joints (Papaliangas et al., 1993, 1994b). This model has been successfully tested for a number of experimental data sets published by different authors. The model is based on the following principle: the shear resistance of a filled rock joint falls between two limits, τ_{max} , the maximum shear strength of the same joint unfilled (clean) and τ_{min} the potential minimum shear strength of the system, and varies with the thickness and type of the infill, the roughness of the rock walls and the normal stress. The potential minimum shear strength τ_{min} may be the shear strength of the infill, but it may be lower in cases where the shear strength of the rock-infill interface is lower. The shear strength of a rough filled joint
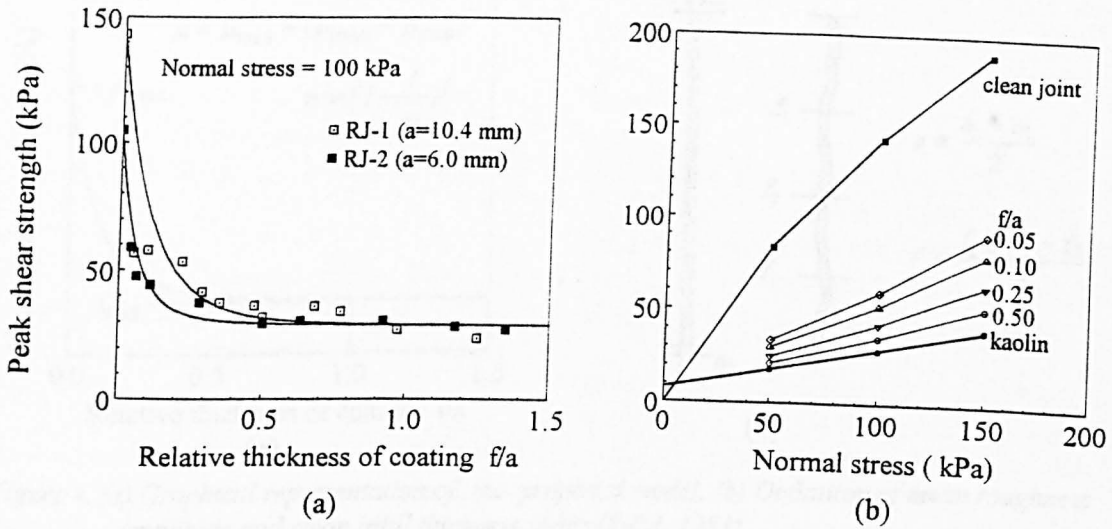
Figure 3. (a) Effect of thickness of coating on shear strength. (b) Peak shear strength envelopes for joints with different f/a ratios shown on each curve.

at a particular normal stress level, is a function of τ_{max} and τ_{min} and the thickness of the infill, and can be expressed as follows:

$$\mu = \mu_{min} + (\mu_{max} - \mu_{min})^n \qquad (1)$$

where μ, μ_{max} and μ_{min} the corresponding stress ratios (τ/σ) expressed as percentages and

$$n = (1 - \frac{1}{c}\frac{f}{a})^m \qquad (2)$$

where f is the mean thickness of infill, and a the mean roughness amplitude of the rock surface.

The constant c depends mainly on the nature of infill and for bentonite it can be taken equal to unity, whereas m gives the rate of decrease in shear strength with the thickness of infill and has a value of about 4 for a very low shear strength material like bentonite.

For f/a=0, $\mu=\mu_{max}$, which gives the shear strength of the joint unfilled.

For f/a>c, μ should be taken equal to μ_{min} which gives the minimum shear strength of the system.

In the case of a pile socketed in rock:
μ is the stress ratio of the coated concrete-

rock interface μ_{min} the stress ratio of the bentonite layer,

μ_{max} the stress ratio of the clean (uncoated) concrete-rock interface,

f the mean thickness of the bentonite layer, and a the mean roughness amplitude of the rock wall.

Equation (2) in this case becomes

$$n = (1 - \frac{f}{a})^4 \qquad (3)$$

The mean roughness amplitude of the rock socket and the average thickness of coating can be measured according to the ISRM recommendations (ISRM, 1981), as shown in Figure 4b.

The shear strength of the clean concrete-socket contact may be estimated by one of the various methods existing for rock joints, for example Barton & Choubey (1977), Hencher & Richards (1989), Johnston & Lam (1989) etc. whereas the shear strength of bentonite may be determined by employing soil mechanics principles and testing methods.

Example

A socket in sandstone having a mean

$$\mu = \mu_{min} + (\mu_{max} - \mu_{min})^n$$

$$n = (1 - \frac{f}{a})^4$$

(a)

$$a = \frac{a_1 + a_2}{2}$$

$$f = \frac{f_1 + f_2 + f_3}{3}$$

(b)
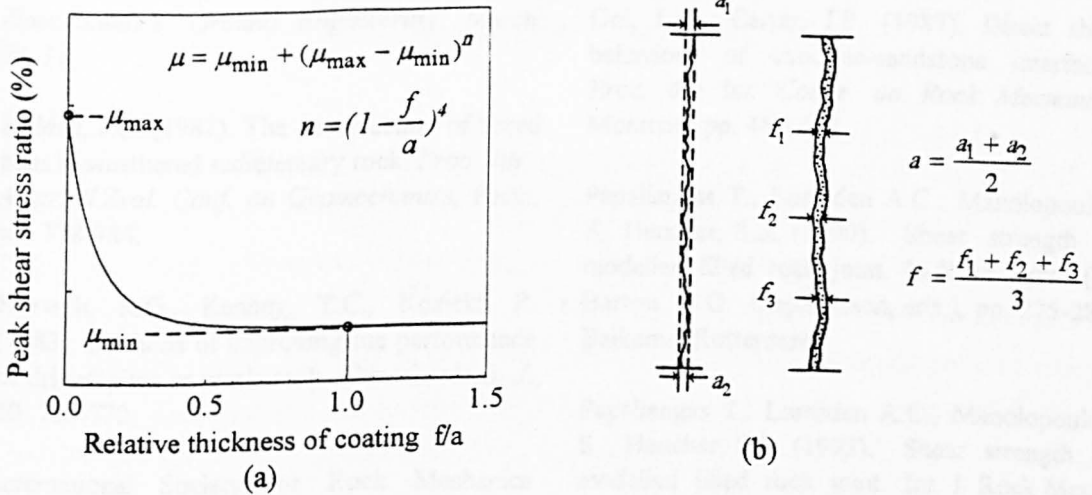
Figure 4. (a) Graphical representation of the proposed model. (b) Definition of mean roughness amplitude and mean infill thickness (after ISRM, 1981).

roughness amplitude of 20mm and a peak friction angle of 45°, is covered with a layer of bentonite 10 mm thick and having a friction angle of 6°.

The maximum stress ratio μ_{max} of the socket is $\mu_{max}= \tan45°\times100=100$ (%)

The minimum stress ratio μ_{min} is

$\mu_{min} = \tan6°\times100 = 10.5$ (%)

n is given by

$$n = (1 - \frac{10}{20})^4 = 0.0625$$

and the stress ratio for the coated socket is

$$\mu = 10.5 + (100 - 10.5)^{0.0625} = 11.32(\%)$$

If a normal stress of 500 kPa is acting around the socket, the side resistance of the coated interface will be
τ=500 x 0.1132= 56.6 kPa

4. CONCLUSIONS

Experimental results from direct shear tests on rough rock joints filled with a soft clayey material were used to simulate the behaviour of pile-socket interfaces with rock walls covered with a layer of bentonite. These tests showed that even a thin coating of a soft material may

cause a considerable reduction in shear strength of the pile-socket interface. For thick layers of coating, where maximum concrete-rock contact is prevented, shear strength decreases with the thickness of coating, up to a minimum value, which is equal to the shear strength of the soft layer. Comparison with results from in-situ tests indicated a similar behaviour of rock-pile interfaces covered with bentonite or smear layers formed by augering in slightly moist rock.. A simple empirical model is proposed for the prediction of the side resistance of pile-socket interface covered with a layer of bentonite. All the parameters used by this model (shear strength and roughness of the clean pile-socket interface, and shear strength and thickness of the bentonite layer), are simple, clearly defined and easy to measure both in the laboratory and the field.

5. REFERENCES

Barton, N., Choubey, V. (1977). The shear strength of rock joints in theory and practice. *Rock Mech.* 10, 1-54.

Hencher, S.R., Richards, L.R. (1989). Laboratory direct shear testing of rock

discontinuities. *Ground Engineering*, March, 24-31.

Holden, J.C. (1983). The construction of bored piles in weathered sedimentary rock. *Proc. 4th Austr.-N.Zeal. Conf. on Geomechanics*, Perth, pp. 378-384.

Horvath, R.G., Kenney, T.C., Kozicki, P. (1983). Methods of improving the performance of drilled piers in weak rock. *Can. Geotech. J.* 20, 758-772.

International Society for Rock Mechanics (1981). Suggested methods for the quantitative description of discontinuities in rock masses. In *Rock Characterisation, Testing and Monitoring - ISRM Suggested Methods* (E.T. Brown, ed.). Pergamon, Oxford.

Johnston, I.W., Lam, T.S.K. (1989). Shear behaviour of regular triangular concrete/rock joints-Analysis. *J.Geotech. Engng*, ASCE 115, No 5, 711-727.

Kingwell, W.J., Albrecht, F.A.A. (1989). Large diameter machine bored piles in Australia. *Proc. Int. Conf. on Piling and Deep Foundations*, London (J.B. Burland & J.M. Mitchell, eds), Vol. 1, pp. 299-307. Balkema, Rotterdam.

Lam, T.S.K., Johnston, I.W. (1989). Shear behaviour of regular triangular concrete/rock joints-Evaluation. *J.Geotech. Engng.*, ASCE 115, No 5, 711-727.

Manolopoulou, S. (1991). *Experimental investigation of shear behaviour of filled rock joints*. Ph. D. thesis, Department of Civil Engineering, Aristotle University of Thessaloniki, Greece (in Greek).

Manolopoulou, S. (1994). The effect of soft coatings on shear strength of rock joints. *Proc. 7th Int. IAEG Congress*, Lisbon, Vol. 2, pp. 913-917. Balkema, Rotterdam.

Ooi, L.H., Carter, J.P. (1987). Direct shear behaviour of concrete-sandstone interfaces. *Proc. 6th Int. Congr. on Rock Mechanics*, Montreal, pp. 467-470.

Papaliangas T., Lumsden A.C., Manolopoulou S., Hencher, S.R. (1990). Shear strength of modelled filled rock joint. In *Rock Joints* (N. Barton & O. Stephansson, eds.), pp. 275-282. Balkema, Rotterdam.

Papaliangas T., Lumsden A.C., Manolopoulou S. , Hencher, S.R. (1993). Shear strength of modelled filled rock joint. Int. J. Rock Mech. Min. Sci. & Geomech. Abstr. 30, No 2, 81-91.

Papaliangas, T., Hencher, S.R., Lumsden, A.C. (1994a). Scale independent shear strength of rock joints. *Proc. Int. Conf. on Integral Approach to Applied Rock Mechanics*. Santiago, Chile, V.1, pp. 123-134.

Papaliangas, T., Hencher, S.R., Lumsden, A.C. (1994b). Laboratory testing and parameters controlling the shear strength of filled rock discontinuities. Discussion. *Géotechnique* (in press).

Williams, A.F., Pells, P.J.N. (1981). Side resistance rock sockets in sandstone, mudstone and shale. *Can. Geotech. J.* 18, 502-513.

CHAPTER 9
SUMMARY AND CONCLUSIONS

9.1 Aim of work

Rock-rock and rock-soil interfaces occur in many geotechnical environments, yet their shear behaviour has not been fully explored and certainly not accurately quantified. The origin and magnitude of the various components of shear strength of rock discontinuities is a matter of dispute. The effect of scale on peak shear strength still remains a controversial subject. The use of empirical relations proved to be inadequate to describe the shear behaviour of rock discontinuities, as they do not consider the physical mechanisms involved. This study has been aimed at

- separately investigating the role of the various strength components by studying the fundamental mechanisms of deformation of rock discontinuities and thus becoming able to explain the effects of various parameters such as sample size.

- attempting to incorporate the findings into a simple, but readily applicable model which accurately predicts the peak shear strength by taking into account the physical mechanism involved.

- identifying the basic mechanisms of deformation   and the geotechnical behaviour of soil-rock interfaces.

9.2 Approach

The approach was to carry out a systematic laboratory based experimental programme consisting of direct shear tests at various constant normal stresses on sets of identical samples of interfaces. A synthetic rock was developed as a rock substitute and used in the experimental programme. For the investigation of rock-rock interfaces various types of natural rock surfaces were reproduced by casting a number of identical copies which were then tested at the appropriate normal stress. All samples were tested in the same relative shearing direction, under constant normal stress which varied from very low values up to a sufficiently high values to suppress dilation. A special programme comprising direct shear tests on joints of different sizes and rock strength was used to examine the effect of scale and rock strength on peak shear strength of rock discontinuities.

For the investigation of the shear behaviour of soil-rock interfaces the experimental programme consisted of direct shear tests, using the newly developed synthetic rock to form surfaces with various roughness, from very smooth to very rough planar and saw-toothed. Granular natural and artificial materials with spherical, round and subround particles of various sizes were used to investigate the effect of grain size as compared to the surface roughness.

9.3 Conclusions

The conclusions of each of the various aspects of the research have been summarised at the end of the relevant preceding chapters. The more important conclusions of the study are summarised below:

1. The use of casting materials to reproduce various rock surfaces is a convenient technique which has the advantage of making samples of nominally identical geometry and strength. However, care has to be taken when the frictional properties of the surface are of concern. Plaster or cement-based casting materials form on the reproduced surface a thin layer whose frictional properties have little relevance to those of the underlying material, especially at low normal stresses. Up to 10° difference in friction angle has been found due to this effect. In addition weak materials may form considerable surface debris which may induce mechanisms such as rolling friction, which are difficult to quantify.

2. The peak friction angle of modelled discontinuities, when the effect of dilation is removed, was found to be equal to the friction angle of the intact rock material as determined from the brittle-plastic transition state. This is valid for the whole spectrum of the dilatant behaviour of the rock discontinuity, which for the tests reported in this study was about 4 orders of magnitude This suggests that irrespective of normal stress, the state of stress at the contacts between the two rock walls of the discontinuity is the same as that of the brittle-plastic transition. For the synthetic rock used in this study, this value was found to be 46°. Such high values of friction angle at the brittle - plastic transition have been calculated for some fresh carbonate rocks, which this synthetic rock resembles. This value was 14° higher than that of a saw-cut surface from the same material. If this difference is independent of normal stress for natural joints as well, then the use of the friction angle of a saw-cut surface and an additional asperity failure component (which is difficult to determine independently) for modelling the shear behaviour of rock joints has no any obvious advantage.

3. The effect of scale was studied by conducting direct shear tests, using a weak plaster-based model material in addition to the newly developed synthetic rock. Considerable scatter was observed in the values of peak dilation angle especially for self weight tests. Again the peak friction angle was found to comprise one frictional and one geometrical component as described in (2) above. From both shear tests with dilation removed and triaxial tests in the brittle-ductile transition, the friction angle of the rock wall material was found to be 42°. The test results on the effect of scale, carried out on samples with length over one order of magnitude, suggest that the value of the non-dilational peak friction angle is independent of scale. The variation with sample length of the dilation rate is logarithmic and extrapolation to zero dilation will define the scale-free block size. For the joint type used this block size was found to be less than 2-3 m, and it can be estimated

from profiles of segments of various sizes from the rock surface. Blocks longer than this critical size will not dilate and therefore will exhibit purely frictional behviour. However, the limited number and scatter of the data, as well as the use of only one rock joint type do not permit generalisation of this conclusion.

4. The instantaneous rate of dilation at the instant of peak shear strength reduces logarithmically with normal stress, over four orders of magnitude. The critical normal stress at which the specimen ceases to dilate can be experimentally derived from a series of direct shear tests. It was found to be much lower than the unconfined compressive strength and about one order of magnitude lower than the brittle-plastic transition stress. It appears that it is independent of roughness and with the exception of discontinuities with large scale waviness, independent of scale. These findings indicate that the assumptions made by most models that the dilation is suppressed at a normal stress equal to the unconfined compressive strength of the material may not be always realistic.

5. The peak shear strength of a joint at a particular normal stress can be predicted by means of a new, simple, theoretical peak shear strength criterion which has been developed from the results of this study. The criterion suggests that the peak shear strength of a rock discontinuity arises from shearing of rock junctions under sufficiently high normal stress for the rock wall material to reach its brittle-plastic transition, and therefore the peak shear strength at any normal stress is the result of two components, one purely frictional, and one geometrical. This theory explains the origin and magnitude of the frictional component: the dilational component may be predicted from consideration of surface morphology and normal contact theory. The criterion is developed without reference to empirical parameters but all parameters used are physically meaningful. The maximum asperity slope which is used as the only parameter to describe surface roughness can be determined in-situ by routine methods and is a convenient parameter for use in constitutive laws concerning shear behaviour of rock joints. All the necessary parameters can be found from a series of carefully conducted direct shear tests on samples from the natural surface, without the need for any other index tests or specially prepared surfaces, etc. The form of the criterion and the nature of the parameters used make it quite convenient to incorporate into numerical models of rock mass .

6. For planar rough surfaces the peak shear strength of a single soil-rock interface is lower than that of the soil, provided that the roughness of the rock surface does not exceed two mean particle diameters. Several deformation mechanisms were identified: sliding, rolling and crushing of particles, indentation and ploughing.

7. The shear behaviour of double soil-rock interfaces depends on the nature and the thickness of the soil layer and the type and roughness of the rock wall surfaces. Evidence

is provided that in the case of granular soils the load is carried by grain bridges spanning the two rock walls. This explains the geometrical effect of the rock walls on the shear strength of a double interface where the thickness of the soil layer is greater than the amplitude of the rock walls surface. The critical thickness of a granular soil layer beyond which there is no effect of the rock walls on the shear strength of the interface, is a function of the mean particle diameter.

9.4 Practical recommendations

a) The newly developed criterion can be used directly in rock engineering practice for easy determination of the peak shear strength of unfilled rock discontinuities. The parameters needed are a) the friction angle of the rock wall material b) the maximum asperity slope of the surface and c) the critical normal stress which suppresses the dilation fully. All these parameters can be derived experimentally from a series of carefully conducted direct shear tests on samples of the discontinuity concerned. No other tests on prepared or other surfaces are needed nor are any other index tests or empirical correlations. The exclusive use of a set of samples from the natural surface emphasises the relevance of the acquired data to the problem in contrast to reliance on indirect determinations through empirical correlations.

b) The indications provided by this study that n-situ rock blocks longer than the critical scale-free size will not dilate, suggests that their behaviour will be purely frictional. Therefore, with the exception of surfaces dominated by large scale undulations, an estimation of in-situ shear strength can be made on the basis of the frictional component only. In the absence of any relevant data, the set of values for fresh rocks provided in this thesis can be used, at least for preliminary assessment of slope stability problems. Other parameters which may influence the overall shear behaviour such as water, infill, etc. must be considered independently. Analyses of rock slopes must be carried out on a c = 0 assumption. Laboratory and field tests should always be carried out following the ISRM recommendations and measuring the dilatancy of sample. Reports of test results without dilation measurement, as happens frequently in practice, are not adequate.

c) For coated or smooth surfaces, variable values of the frictional component which increases with normal stress are expected. In this case any direct shear tests on samples from the surface concerned must be carried out at the appropriate normal stress.

d) Assessment of shear strength of double soil-rock interface systems requires determination of the critical soil layer thickness beyond which the rock walls have no effect on the shear strength of the interface. This critical thickness can be estimated by a simple expression derived in this thesis.

9.5 Suggestions for further research

The newly developed criterion and the theory behind it proved to be valid for many published data sets. However, further validation is desirable. From testing of discontinuities of various types of rocks, various values of the required parameters (friction angle, dilation angle, critical normal stress) will be obtained, and used to update the values given in this work which can form the basis of a data-base. It should then be possible to estimate friction angles according to the rock origin and mineralogy

The appropriate step-size for the calculation of the instantaneous dilation angle needs to be investigated. Analysis of normal displacement - shear displacement behaviour from laboratory tests should be compared with analyses of data from surface profiles. Back-analyses of failed slopes where information on mineralogy and roughness characteristics of the failed rock are available would increase confidence in the use of the new criterion.

The variation of shear stress with shear displacement in terms of the asperity angle needs further study and evaluation for better understanding of the full shear-normal behaviour. Surface measurements at various shear displacements made on identical samples sheared under the same conditions will provide much information on the relation of the dilation angle and the shear displacement, which can be extended to the fully coupled hydromechanical behaviour.

The case of supersmooth and tightly interlocked surfaces needs to be studied, particularly where the controlling factor i.e. the dilation, is not free. Tests carried out under conditions of constant normal stiffness may provide an answer to this problem.

Single rock-soil interfaces with soils of particular interest, like rockfill, can be investigated by means of physical modelling. Double soil-rock interfaces are more complicated. Physical and numerical modelling could give some answers to various aspects of shear behaviour. Finite element methods used for different properties of the soil layer and the adjacent rock walls will give much information on the deformation of the interfaces, which if combined with physical modelling, will provide an adequate understanding of their shear behaviour.

REFERENCES

Acar Y.B., Durgunoglou H.T. & Tumay M.T. (1982). Interface Properties of Sand. *J. Geotech. Engng Div. Am. Soc. Civ. Engnrs* 108, 648-654.

Adachi T., Ogawa T. & Hayashi M. (1981). Mechanical Properties of Soft Rock and Rock Mass. *Proc. 10th Int. Conf. Soil Mech. Fdn Engng*, Stockholm, Vol. 1, pp. 527-530.

Al-Douri R.H. & Poulos H.G. (1991). Static and Cyclic Direct Shear Tests on Carbonate Sands. *Geotech. Testing J., GTJODJ* 15, 138-157.

Allen, K.W. (1963). Aspects of Adhesion. *Proc. Conf. on Adhesion*, Northampton, Vol. 1, pp. 11-21.

Amontons (1699). *Histoire de l'Academie Royale des Sciences avec les Memoires de Mathematique et de Physique.* 206 pp.

Andrle B. & Abrahams A.D. (1989). Fractal Techniques and the Surface Roughness of Talus Slopes. *Earth Surface Processes and Landforms* 14, 197-209.

Archard J.F. (1957). Elastic Deformation and the Laws of Friction. *Proc. R. Soc., London,* A243, 190-205.

Archard J.F. (1974). Surface Topography and Tribology. *Tribology Int.* 7, 213-220.

Arnold P. (1992). Joint Approach. Report of the BGS Meeting on Strength Characteristics of Rock Joints. *Ground Engng* 25, No 10, 20-23.

Aydan Ö., Ichikawa Y., Ebisu S., Komura S. & Watanabe A. (1990). Studies on Interfaces and Discontinuities and an Incremental Elasto-Plastic Constitutive Law. *Rock Joints; Proc. Int. Symp. on Rock Joints*, Loen, Norway (N. Barton & O. Stephansson, Eds), pp. 149-156. Balkema, Rotterdam.

Bailey, A.I. (1965). Surface Energy and Adhesion in Lamellar Solids. *Proc.Conf. on Adhesion,* Northampton 1965, pp. 32-39.

Baldovin G. (1970). The Shear Strength of some Rocks by Laboratory Tests. *Proc. 2nd Congr. ISRM,* V5, Belgrade, pp. 165-172.

Bandis S. (1980): *Experimental Studies of Scale Effects on Shear Strength and Deformation of Rock Joints.* PhD Thesis, Department of Earth Sciences, Univ. of Leeds, U.K.

Bandis S., Lumsden A.C. & Barton N. (1981). Experimental Studies of Scale Effects on the Shear Behaviour of Rock Joints. *Int. J. Rock Mech. Min. Sci. & Geomech. Abstr.* 18, 1-21.

Barton N.R. (1970). A Low Strength Model Material for Simulation of the Mechanical Properties of Intact Rock in Rock Mechanics Models. *Proc. 2nd Congr. ISRM*, Belgrade, Vol. 2, 99-110.

Barton N.R. (1971a): *A Model Study of the Behaviour of steep Excavated Rock Slopes.* Ph.D. Thesis, Univ. of London.

Barton N. (1971b). A Relationship Between Joint Roughness and Joint Shear Strength. *Proc. ISRM Symp. on Rock Fracture*, Nancy, France, Paper I-8.

Barton N.R. (1973). Review of a new shear strength criterion for rock joints. *Engng Geology*, 7, 287-332.

Barton N. (1976). The Shear Strength of Rock and Rock Joints. *Int. J. Rock Mech. Min. Sci. & Geomech. Abstr.* 13, 255-279.

Barton N. (1990). Scale Effects or Sampling Bias? *Scale Effects in Rock Masses 93; Proc. 1st Int. Workshop on Scale Effects in Rock Masses,* Loen, Norway (Pinto da Cunha, Ed.), pp. 31-55. Balkema, Rotterdam.

Barton N. & Bandis S. (1982). Effects of Block Size on the Shear Behaviour Jointed Rock. Proc. 23rd U.S. Symposium on Rock Mechanics, Berkeley, Ca. 739-760.

Barton N. & Bandis S. (1990). Review of Predictive Capabilities of JRC-JCS Model in Engineering Practice. *Rock Joints; Proc. Int. Symp. on Rock Joints*, Loen, Norway (Barton N. & Stephansson O., Eds), pp. 603-610. Balkema, Rotterdam.

Barton N.R. and Choubey V. (1977). The Shear Strength of Rock Joints in Theory and Practice. *Rock Mech.*, Vol. 10, pp. 1-54.

Barton N., Bandis S. & Bakhtar K. (1985). Strength, Deformation and Conductivity Coupling of Rock Joints. *Int. J. Rock Mech. Min. Sci. & Geomech. Abstr.* 22, 121-140.

Bergues J., Derlich S., Habib P., Massat H. & Vodar B. (1974). Étude de Quatre Roches Sous Très Hautes Pressions. *Advances in Rock Mechanics; Proc. 3rd Congr. Int. Soc. Rock Mech.*, Denver, Colorado, Vol. IIA, pp. 493-498. Nat. Acad. Sci., Washington D.C.

Bernaix J. (1967). New Laboratory Methods of Studying the Mechanical Properties of Rocks. *Int. J. Rock Mech. Min. Sci.* 6, 43-90.

Bieniawski Z.T. (1968). The Effect of Specimen Size on Compressive Strength of Coal. *Int. J. Rock Mech. Min. Sci.* 5, 325-335.

Bieniawski Z.T. (1974). Estimating the Strength of Rock Materials. *J. S. Afr. Inst. Min. Metal.* 74(8), 91-130.

Bilgin A. H. and Pasamehmetoglu G. A. (1990). Shear Behaviour of Shale Joints under Heat in Direct Shear. *Proc. Intnl. Symp. on Rock Joints, Loen,* Norway. Vol. 1, pp. 179-184.

Bishop A.W. (1972). Shear Strength Parameters for Undisturbed and Remoulded Soil Specimens. *Stress-Strain Behaviour of Soils* (R.H.G.Parry, Ed.) pp. 3-58. Foulis, London.

Blanton T.L. (1981). Effect of Strain Rates from 10^{-2} to 10 sec^{-1} in Triaxial Compression Tests on Three Rocks. *Int. J. Rock Mech. Min. Sci. & Geomech. Abstr.* 18, 47-62.

Boitnott G.N., Biegel R.L., Scholz C.H., Yioshioka N. & Wang W. (1992). Micromechanics of Rock Friction 2: Quantitative Modelling of Initial Friction with Contact Theory. *J. Geophys. Res.* 97, 8965-8978.

Bolton M.D. (1986). The Strength and Dilatancy of Sands. *Géotechnique* 36, 65-78.

Bosscher P.J. & Ortiz C.G. (1987). Frictional Properties Between Sand and Various Construction Materials. *J. Geotech. Engng. Div., ASCE* 113, 1035-1039.

Bowden F.P. and Tabor D. (1950). *The Friction and Lubrication of Solids.* Clarendon Press, Oxford, Pt I.

Bowden F.P. & Tabor D. (1964). *The Friction and Lubrication of Solids.* Vol. II. Clarendon Press, Oxford, Pt.II.

Bowden F.P. & Tabor D. (1973). *Friction.* DoubleDay, New York. 178 p.

Brace W.F. (1962). Behavior of Quartz during Indentation. *J. Geology* 71, 581-595.

Brace W.F. (1964). Brittle Fracture of Rocks. In *State of Stress in Earth's Crust* (W.R.Judd, Ed.), pp. 111-178. American Elsevier.

Bredthauer R.O. (1957). Strength Characteristics of Rock Samples under Hydrostatic Pressure. *Trans. Am. Soc. Mech. Engnrs.* 79, 695-706.

Bridgman, P.W. (1952). *Studies in Large Plastic Flow and Fracture.* McGraw-Hill, N. York.

Bridgewater J. (1980). On the Width of Failure Zones. *Geotechnique* 30, 533-536

Briggs G.A.D. & Briscoe B.J. (1976). Effect of Surface Roughness on Rolling Friction and Adhesion between Elastic Solids. *Nature* 260, 313-315.

British Standard Institution (1972). BS 915:Part 2. High Alumina Cement.

British Standard Institution (1978a). BS 4550: Methods of Testing Cement. Part 3: Physical tests.

British Standard Institution (1978b). BS 4550: Methods of Testing Cement. Part 5: Standard Sand for Testing Concrete Cubes.

British Standard Institution (1990). BS 1377: Soils for Civil Engineering Purposes. Part 7 : Shear Strength Tests (total stress).

Bromwell L.G. (1966). The Friction of Quartz in High Vacuum. *Massachusetts Institute of Technology, Dept. of Civ. Engng, Res. Report R66-18.*

Brook N. (1979). Estimating the Triaxial Strength of Rocks. *Int. J. Rock Mech. Min. Sci. & Geomech. Abstr.* 16, 261-264.

Brown E.T., Richards L.R. & Barr M.V. (1977). Shear Strength Characteristics of the Delabole Slates. *Proc. Conf. on Rock Engineering*, Newcastle upon Tyne, U.K., pp. 33-51.

Brown S.R. (1987). A Note on the Description of Surface Roughness Using Fractal Dimension. *Geophys. Res. Lett.* 14, 1095-1098.

Brown S.R. & Scholz C.H. (1985). Closure of Random Elastic Surfaces in Contact. *J. Geophys. Res.* 90, 5531-5545.

Brown S.R. & Scholz C.H. (1985b). Broad band width study of the topography of natural rock surfaces. *J. Geophys. Res.* 90, 12575-12582.

Brown S.R. & Scholz C.H. (1986). Closure of Rock Joints. *J. Geoph. Res.* 91, 4939-4948.

Brumund W.F. & Leonards G.A. (1973). Experimental Study of Static and Dynamic Friction Between Sand and Typical Construction Materials. *J. Test. Eval., JTEVA* 1, 162-165.

Byerlee J.D. (1967a). Frictional Characteristics of Granite under High Confining Pressure. *J. Geophys. Res.* 72, 3639-3648.

Byerlee J.D. (1967b). Theory of Friction Based on Brittle Fracture. *J. Appl. Phys.* 38, 2928-2934.

Byerlee J.D. (1968). Brittle-Ductile Transition in Rocks. *J. Geophys. Res.* 73, 4741-4750.

Byerlee J.D. (1970a). Static and Kinetic Friction of Granite at High Normal Stress. *Int. J. Rock Mech. Min. Sci.* 7, 577-582.

Byerlee J.D. (1972). The Mechanics of Stick-Slip. *Tectonophysics* 9, 475-486.

Byerlee J.D. (1978). Friction of Rocks. *Pure & Appl. Geophys.* 116, 615-626.

Campos de Orellana A.J. (1996). Pressure Solution Creep and Non-Associated Plasticity in the Mechanical Behavior of Potash Mine Openings. *Int. J. Rock Mech. Min. Sci. & Geomech. Abstr.* 33, No 4, 347-370.

Carr J.R. & Warriner J.B. (1989). Relation between the fractal dimension and joint roughness coefficient. *Bull. Assoc. Engng Geol.* XXV(2), 253-263.

Chappell B.A. (1975). Friction Characteristics of Graphite Coated Bedding Joints in Shale. *Int. J. Rock Mech. Min. Sci. & Geomech. Abstr.* 12, 33-39.

Chesters S., Wen H.Y. Lundin M. & Kasper G. (1989). Fractal Based Characterisation of Surface Texture. *Applied Surface Science* 40, 185-192.

Chitty D.E. & Blouin S.E. (1992). Strength, Deformation, and Fluid Flow Measurements on Joints in Porous Limestone. *Fractured and Jointed Rock; Pre-prints ISRM Conf.*, Lake Tahoe, California, pp. 349-357

Chiu H.K. & Dight P.M. (1983). Prediction of Performance of Rock-socketed Side - resistance-only Piles Using Profiles. *Int. J. Rock Mech. Min. Sci. & Geomech. Abstr.* 19, 21-31.

Ciment Fondu Lafarge (1990a). *Construction applications*. Circular CA1/790. Lafarge Special Cements, Essex.

Ciment Fondu Lafarge (1990b). *Guide for Use*. Circular CA4/890. Lafarge Special Cements, Essex.

Cottin B. & Reif P. (1980). Parametres Physiques Regissant Les Proprietes Mecaniques Des Pates Pures de Liants Alumineux. *Revue Des Materiaux De Construction* 661, 293-305.

Coulson J.H. (1970): *The Effects of Surface Roughness on the Shear Strength of Joints in Rock.* Ph.D. Thesis, Univ. of Illinois, U.S.A.

Coulson J.H. (1972). Shear Strength of Flat Surfaces. *Proc. 13th Symp. on Rock Mech.*, Urbana, Illinois, 1971 (Cording E.G., Ed.) pp. 77-105.

Cruden D.M (1983). Rockslope Movements in the Canadian Cordillera. *Can. Geotech. J.*, 22, 77-105.

Deere D.U. & Miller R.P. (1966). Engineering Classification and index properties for intact rock. Tech. Rept. No. AFWL-TR-65-116, Air Force Weapons Lab., Kirtland Air Force Base, New Mexico.

Denby B. & Scoble M.J. (1984). Quantification of Power Law Indices for Discontinuity Shear Strength Prediction. *Proc. 25th US Symp. on Rock Mech.*, Evanston, pp. 475-482.

Desai C.S. (1981). Behavior of Interfaces between Structural and Geological Media. Proc. *Int. Conf. on Recent Advances in Geotechnical Earthquake Engineering and Soil Dynamics,* Univ. of Rolla, Missouri, St. Louis, Mo, pp. 619-638.

Desai C.S. (1987). Static and Cyclic Response of Interfaces for Analysis and Design of Soil-Structure Interaction Problems. *Geotechnical Modelling and Applications,* Chap 4 (Sayed, S.M, Ed.). Gulf Publishing, Huston.

Desai C.S. & Fishman K.L. (1987). Constitutive Models for Rocks and Dscontinuities (Joints). *Proc. 28th U.S. Symp. on Rock Mechanics.* , Tuscon, pp. 609-619.

Dieterich J.H. (1972). Time-Dependent Friction in Rocks. *J. Geophys. Res.* 77, 3690-3697.

Dight P.M. & Chiu H.K. (1981). Prediction of Shear Behaviour of Joints Using Profiles. *Int. J. Rock Mech. Min. Sci. & Geomech. Abstr.* 18, 369-386.

Dyer M.R. (1985). *Observation of Stress Distribution in Crushed Glass with Aplication to Soil Reinforcement.* D. Phil Thesis, University of Oxford.

Edmond J.M. & Paterson M.S. (1972). Volume Changes During the Deformation of Rocks at high Pressures. *Int. J. Rock Mech. Min. Sci.* 9, 161-182.

Elliot G.M. (1982). *An Investigation of a Yield Criterion for Rock.* Ph. D. thesis, Univ. of London.

Elliot G.M. & Brown E.T. (1986). Further Development of a Plasticity Approach to Yield in Porous Rock. *Int. J. Rock Mech. Min. Sci. & Geomech. Abstr.* 23, pp. 151-156.

Engelder J.T. (1976). Effect of Scratch Hardness on Frictional Wear and Stick-Slip of Westerley Granite and Cheshire Quartzite. Proc. NATO Adv. Study Inst. on Petrophysics, J. Wiley, N.Y.

Engelder J.T. & Scholz C.H. (1976). The Role of Asperity Indentation and Ploughing in Rock Friction - II. Influence of Relative Hardness and Normal Load. *Int. J. Rock Mech. Min. Sci. & Geomech. Abstr.* 13, pp. 155-163.

Evans B., Fredrich J. T. & Wong T.-F. (1990). The Brittle-Ductile Transition in Rocks: Recent Experimental and Theoretical Progress. In *The Brittle-Ductile Transition in Rocks. The Heard Volume.* Geophysical Monograph 56, Duba et al (Eds), pp. 1-20, Am. Geophys. Union, Washington, D.C.

Fairhurst C. (1964). On the Validity of the "Brazilian" Test for Brittle Materials. *Int. J. Rock Mech. Min. Sci.* 1, 535-546.

Fecker E. (1970). *Geologische Kartierung des Gebietes nordwestlich von Neustadt/Weinstraße sowie Bau und Anwendung eines Profilographen*. Diplom-Thesis, Univ. of Karlsruhe.

Fecker E. & Rengers N. (1971). Measurement of large scale roughness of rock planes by means of profilograph and geological compass. *Proc. Symp. on Rock Fracture*, Nancy, France, Paper I-18.

Feder J. (1988). *Fractals*. Plenum Press, New York, 283 pp.

Franklin J.A. (1971). Triaxial Strength of Rock Masses. *Rock Mech.* 3, 86-98.

Franklin J.A. & Dusseault M.B.(1989). *Rock Engineering*. McGraw-Hill, NY., 601 pp.

Franklin J. A., Maertz N.H. & Bennet C.P. (1988). Rock Mass Characterization Using Photoanalysis. *Int. J. Min. Geol. Geol. Engng* 6, 99-112.

Fredrich J.T., Evans B. & Wong T.-F. (1990). Effect of Grain Size on Brittle and Semibrittle Strength: Implications for Micromechanics and Modelling of Failure in Compression. *J. Geophys. Res.* 95, 10907-10920.

Friedman M. & Logan J.M. (1973). Luders' Bands in Experimentally Deformed Sandstone and Limestone. *Geol. Soc. Am. Bull.* 84, 1465-1476.

Fuller K.N.G. and Tabor D. (1975). The Effect of Surface Roughness on the Adhesion of Elastic Solids. *Proc. R. Soc.* A345, 327-342.

Gaziev E.G. (1976). Morphology of Joints and Stability of Rock Masses. *Geology of Quaternary Period; Engng Geology; Problems of Hydrogeology of Arid Zones* (Nikiforova, K.V et al, Eds) Nauka, Moscow (in Russian).

Gaziev E.G. & Lapin L.V. (1984). Passive Anchor Reaction to Shearing Stress in a Rock Joint. *Proc. Int. Symp. on Rock Bolting*, Abisko, Sweden (O. Stephansson, Ed.), pp. 101-108.

Gerk A.P. & Tabor D. (1978). Indentation Hardnesss and Semiconductor-Metal Transition of Germanium and Silicon. *Nature* 271, 732-733.

Gerogiannopoulos N.G. & Brown E.T. (1978). The Critical State Concept Applied to Rock. *Int. J. Rock Mech. Min. Sci. & Geomech. Abstr.* 15, 1-10.

Gerrard C. (1986). Shear Failure of Rock Joints: Appropriate Constraints for Empirical Relations. *Int. J. Rock Mech. Min. Sci. & Geomech. Abstr.* 23, 421-429.

Giani G.P. (1992). *Rock Slope Stability Analysis*. Balkema, Rotterdam, 361 pp.

Giani, G.P., Ferrero A.M., Passarello, G. & Reinaudo, L. (1992). Scale Effect Evaluation on Natural Discontinuity Shear Strength. In Fractured and Jointed Rock Masses, Pre-prints, Lake Tahoe, California, V.2 , 456-462.

Goldstein M.A. , Goosev B., Pyrogovsky N., Tulinov R. & Turovskaya A. (1966). Investigation of Mechanical Properties of Cracked Rock. *Proc. 1st Congr. Rock Mech.,* Lisbon, Vol 1, pp. 521-524.

Goodman R.E. (1970). The Deformability of Joints. *Determination of the in situ modulus of deformation of rock, American Society for Testing and Materials Special Technical Publication,* No. 477, pp. 174-196.

Goodman R. (1974). The Mechanical Properties of Rock. *Advances in Rock Mechanics; Proc. 3rd Congr. Int. Soc. Rock Mech.,* Denver, Colorado, pp. 127-140.

Goodman R.E. (1976). *Methods of Geological Engineering in Discontinuous Rock.* West Publishing Co, N.York.

Goodman R. E. & Dubois J. (1972). Duplication of Dilatancy in Analysis of Jointed Rock. *J. Soil Mech. & Found. Div. , Proc. ASCE* 98, *SM4,* 399-422.

Greenwood J.A. (1967). The Area of Contact between Rough Surfaces and Flats. *J.Lubr. Technol., Trans. ASME* 1, 81-87.

Greenwood J.A. & Williamson J.B.P. (1966). Contact of Nominally Flat Surfaces. *Proc. Royal Society,* A 295, 300-319.

Griffith A.A. (1921). The Phenomena of Rupture and Flow in Solids. *Phil. Trans. R. Soc.* A221, 163-197.

Gyenge M. & Herget G. (1977). Mechanical Properties. *Pit Slope Manual,* Chap. 3, CANMET, CANMET Report 77-12, 87p.

Gyenge M., Jackson R., & Gorski B. (1991). Residual Strength Envelopes using the Confined Shear Test Method. *Proc. 32nd U.S. Symp. on Rock Mechanics,* Norman (Roegiers J.-C., Ed.), pp. 629-635. Balkema, Rotterdam.

Hadizadeh J. & Rutter E.H. (1983). The Low Temperature Brittle-Ductile Transition in a Quartzite and the Occurrence of Cataclastic Flow in Nature. *Geologische Rundschau* 72, 493-509.

Halling, J. (1978). Principles of Tribology. MacMillan, London, 401p.

Hamilton W.R., Woolley A.R. & Bishop A.C. (1987). *Minerals, Rocks and Fossils.* Country Life Books, London, 320 p.

Handanyan J.M., Danek E.R., D'Andrea R.A. & Sage J.D. (1990). The Role of Tension in Failure of Jointed Rocks. *Rock Joints; Proc. Int. Symp. on Rock*

Joints, Loen, Norway (Barton N. & Stephansson O., Eds), pp. 227-234. Balkema, Rotterdam.

Handin J. (1953). An Application of High Pressure in Geophysics: Experimental Rock Deformation. *Trans. Am. Soc. Mech. Engnrs*. 75, 315-324.

Handin J. (1966). Strength and Ductility. *Handbook of Physical Constants. Geol. Soc. Am. Memoir No 97*, Chap 11, pp. 223-289.

Handin J., & Hager R.V.Jr (1957). Experimental Deformation of Sedimentary rocks Under Confining Pressure: Tests at room Temperature on Dry Samples. *Bull. Amer. Ass. Petrol. Geologists* 41, 1-50.

Hardy W.B. and Hardy J.K. (1919). Note on Static Friction and on the Lubricating Properties of Certain Chemical Substances. *The Philos. Mag.* 38, 32-48.

Hassani F.P. & Scoble M.J. (1981). Properties of Weak Rocks, with Special Reference to the Shear Strength of their Discontinuities, as Encountered in British Surface Coal Mining. *Proc. Int. Symp. on Weak Rock*, Tokyo, pp. 355-363.

Hassani F.P. and Scoble M.J. (1985). Frictional Mechanism and Properties of Rock Discontinuities. *Proc. Int. Symp. on Fundamentals of Rock Joints*, Björkliden (Stephansson O., ed), pp. 185-196. Centek Publishers.

Heard H.C. (1960). Transition from Brittle Fracture to Ductile Flow in Solnhofen Limestone as a Function of Temperature, Confining Pressure, and Interstitial Fluid Pressure. *Geol. Soc. Am. Mem.* 79, 193-226.

Hencher S.R. (1976): A Simple Sliding Apparatus for the Measurement of Rock Joint Friction, Discussion. *Géotechnique* 26, 641-644.

Hencher S.R. (1977): *The Effect of Vibration on the Friction between Planar Rock Surfaces*. Ph.D. Thesis, Imperial College of Science & Technology, Univ. of London.

Hencher S.R. (1987). The Implications of Joints and Structures for Slope stability. *Slope Stability*, Chap. 5 (Anderson, G.M. & Richards, K.S., Eds).Wiley, New York, pp. 145-186.

Hencher S.R. (1995). Interpretation of Direct Shear Tests on Rock Joints. *Proc. 35th U.S. Symp. Rock Mech.*, Univ. of Nevada, Reno (Daemen J.J.K. & Schultz, R.A., Eds), pp. 99-106. Balkema, Rotterdam.

Hencher S.R. & Richards L.R. (1982). The Basic Frictional Resistance of Sheeting Joints in Hong Kong Granite. *Hong Kong Engineer* 11, 21-25.

Hencher S.R. & Richards L.R. (1989). Laboratory Direct Shear Testing of Rock Discontinuities. *Ground Engng* 22, 24-31.

Hencher S.R., Toy J.P. & Lumsden A.C. (1993). Scale Dependent Shear Strength of Rock Joints. *Scale Effects in Rock Masses 93; Proc. 2nd Int. Workshop on Scale Effects in Rock Masses* (Pinto da Cunha, Ed.), pp. 233-240.   Balkema, Rotterdam.

Heuze F.E. (1979). Dilatant Effects of Rock Joints. *Proc. 4th Congr. Int. Soc. Rock Mech., Montreux*, Vol. 1 pp. 169-173.

Hirth C. & Tullis J. (1986). Cataclastic Flow of Dry Non-Porous Quartzite. *Trans. Am. Geoph. Union* 67, 1186.

Hobbs B. E. (1993). The Significance of Structural Geology in Rock Mechanics. *Comprehensive Rock Engineering*, Vol. 1, Chap.1 (Hudson, J., Ed. in chief), pp. 25-62. Pergamon Press, Oxford.

Hobbs D.W. (1966). A Study of the Behaviour of Broken Rock under Triaxial Compression, and its Application to Mine Roadways. *Int. J. Rock Mech. Min. Sci.* 3, 11-43.

Hoek E. (1968). Brittle Failure of Rock. In *Rock mechanics in engineering practice.* Chap. 4 (K.G. Stagg & O.C. Zienkiewicz, Eds). John Wiley & Sons, London, pp. 99-124.

Hoek, E. (1983). Strength of Jointed Rock Masses. Twenty-third Rankine Lecture. *Géotechnique* 33, No 3, 185-244.

Hoek E. & Brown E.T. (1980a). *Underground Excavations in Rock.* Institution of Mining and Metallurgy, London.

Hoek E. & Brown E.T. (1980b). Empirical Strength Criterion for Rock Masses. *J. Geotech. Engng Div. Am. Soc. Civ. Engnrs* 106, 1013-1035.

Hoek E. & Brown E.T. (1988). The Hoek-Brown Failure Criterion - a 1988 Update. *Proc. 15th Canadian Rock Mech. Symp.*, pp. 31-38.

Hoek E. , Wood D. & Shah S. (1992). A Modified Hoek-Brown Failure Criterion for Jointed Rock Masses. *Proc. ISRM Symp: EUROCK'92*, Chester, U.K., pp. 209-213.

Hoek E. (1994). Strength of Rock and Rock Masses. *ISRM News Journal* 2, No 2, 4-16.

Horn H.M. & Deere D.U. (1962). Frictional Characteristics of Minerals. *Géotechnique* 12, 319-335.

Hoshino K., Koide H., Inami K., Iwamura S. & Mitsui S. (1972). Mechanical Properties of Japanese Tertiary Sedimentary Rocks under High Confining Pressures. Report No 244, Geol. Survey of Japan.

Hoskins E.R., Jaeger J.C. & Rosegreen K.J. (1968). A Medium-scale Direct Friction Experiment. *Int. J. Rock Mech. Min. Sci.* 5, 143-154.

Hsiung S.M., Ghosh A., Ahola M.P. & Chowdhury A.H. (1993). Assessment of Conventional Methodologies for Joint Roughness Coefficient Determination. *Int. J. Rock Mech. Min. Sci. & Geomech. Abstr.* 30, 825-829.

Hsiung S.M., Ghosh A. & Chowdhury A.H. (1995). On Natural Rock Joint Characterisation using Self-affine Fractal Approach. *Rock Mechanics. Proc. 35th U.S. Symp. Rock Mech.* (Daemen J.J.K. & Schultz, R.A., Eds), Univ. of Nevada, Reno, pp. 681-687. Balkema, Rotterdam.

Hsu-Sun K. (1979). Non-linear Analysis of the Mechanical Properties of Joints and Weak Intercalations in Rock. *Proc. 3rd Int. Conf. on Numerical Methods in Geomechanics*, Aachen, pp. 523-532.

Huang X., Haimson B.C., Plesha M.E. & Qiu X. (1993). An investigation of the mechanics of rock joints - Part I. Laboratory investigation. *Int. J. Rock Mech. Min. Sci. & Geomech. Abstr.* 30, 257-269.

Huang S.L., Oelfke S.M. & Speck R.C. (1992). Applicability of Fractal Characterisation and Modelling to Rock Joint Profiles. *Int. J. Rock Mech. Min. Sci. & Geomech. Abstr.* 29, 89-98.

Hudson J.A.(1992). *Rock Engineering Systems:Theory and Practice*. Ellis Horwood, Chichester, pp. 185.

Hutson R.W. & Dowding C.H. (1990). Joint Asperity Degradation During Cyclic Shear. *Int. J. Rock Mech. Min. Sci. & Geomech. Abstr.* 27, 109-119.

Hyett A.J. and Hudson J.A. (1990). A Photoelastic Investigation of the Stress State Close to Rock Joints. *Rock Joints; Proc. Int. Symp. on Rock Joints*, Loen, Norway (Barton N. & Stephansson O., Eds), pp. 227-234. Balkema, Rotterdam.

International. Society for Rock Mechanics (1981). *Rock Characterisation, Testing and Monitoring. ISRM Suggested Methods* (Brown E.T., Ed.). Pergamon, Oxford.

Jaeger J.C. (1971). Friction of Rocks and Stability of Rock Slopes. 11th Rankine Lecture. *Géotechnique* 21, 97-134.

Jewell R.A. (1980). *Some Effects of Reinforcement on Soils*. Ph.D. Thesis, University of Cambridge, U,K.

Jewell R.A. (1989). Direct Shear Tests on Sand. *Géotechnique* 39, 309-322.

Jewell R.A. (1996). *Soil Reinforcement with Geotextiles*. Special Publication 123, CIRIA, London, pp. 332.

Jing L., Nordlund E. & Stephansson O. (1992). An Experimental Study on the Anisotropy and Stress-dependency of the Strength and Deformability of Rock Joints. *Int. J. Rock Mech. Min. Sci. & Geomech. Abstr.* 29, 535-542.

Johnson, K.C., Kendall, K. and Roberts, A.D. (1971). Surface Energy and the Contact of Elastic Solids. *Proc. of the Royal Society,* Vol. A. 324, pp. 301-313.

Johnston I.W. (1985). The Strength of Intact Geomechanical Materials. *J. Geotech. Engng., ASCE* 3(6), 730-749.

Johnston I.W. & Choi S.K. (1986). A Synthetic Soft Rock for Laboratory Model Studies. *Géotechnique* 36, 251-263.

Johnston I.W. & Lam T.S.K. (1989a). Shear Behavior of Regular Triangular Concrete/Rock Joints - Analysis. *J. Geotech. Engng., ASCE* 115, 711-727.

Johnston I.W. & Lam T.S.K. (1989b). Shear Behavior of Regular Triangular Concrete/Rock Joints -Evaluation. *J. Geotech. Engng., ASCE* 115, 728-740.

Kane F.W. & Drumm E.C. (1987). A Modified 'cap' Model for Rock Joints. *Proc. 28th U.S. Sympos. on Rock Mech.*, Tuscon, pp. 699-705.

Kanji M.A. (1970). *Shear Strength of Soil-Rock Interfaces.* MSc thesis, Department of Geology, Univ. of Illinois, Urbana.

Kanji M.A. (1974). Unconventional Laboratory Tests for the Determination of the Shear Strength of Soil-Rock Contacts. *Advances in Rock Mechanics; Proc. 3rd Congr. Int. Soc. Rock Mech.*, Denver, Colorado, pp. 241-247

Kikuchi K., Saito K. & Kusunoki K. (1982). Geotechnically Integrated Evaluation on the Stability of Dam foundation Rocks. *Trans. 14th Int. Congr. Large Dams*, Rio de Janeiro, pp. 49-74

Kim M.K. & Lade P.V. (1984). Modelling Rock Strength in Three Dimensions. *Int. J. Rock Mech. Min. Sci. & Geomech. Abstr.* 21, 21-33.

Kishida H. & Uesugi M. (1987). Tests of the Interface Between Sand and Steel in the Simple Shear Apparatus. *Géotechnique* 37, 45-52.

Koerner R.M. (1970). Behavior of Single Mineral Soils in Triaxial Shear. *J. Soil Mech. & Found. Division, ASCE* 96, 1373-1390.

Koura M.M. & Omar M.A.(1981). The Effect of Surface Parameters on Friction. *Wear* 73, 235-246 .

Kraft L.M. (1971). Compaction of Concrete Slabs by Vibration. *Am. Concr. Inst. J.*, June, pp. 462-467.

Krahn J. and Morgenstern N.R. (1976). Mechanics of the Frank Slide. *Proc. Conf. on Rock Engineering for Foundations and Slopes.* Univ. of Colorado, Vol.1, pp. 309-332. ASCE, New York.

Krahn J. and Morgenstern N.R. (1979). The Ultimate Fictional Resistance of Rock Discontinuities. *Int. J. Rock Mech. Min. Sci. & Geomech. Abstr.* 16, 127-133.

Krsmanovic D. (1967). Initial and Residual Shear Strength of Hard Rocks. *Géotechnique* 17, 145-160.

Krsmanovic D. & Popovic M. (1966). Large Scale Field Tests of the Shear Strength of Limestone. *Proc. 1st Congr. Int. Soc. Rock Mech.*, Lisbon, V. 1, pp. 773-779.

Kulatilake P.H.S.W., Shou G., Morgan R.M.& Huang T.-H. (1994). A New Empirical Peak Shear Strength Criterion for Rock Joints. Rock Mechanics; Proc. 35th U.S. Symp. Rock Mech. (Nelson & Laubach, Eds), pp. 565-572. Balkema, Rotterdam.

Kulhawy F.H. & Peterson M.S. (1979). Behavior of Sand-Concrete Interfaces. *Proc. 6th Panamerican Conf. on Soil Mech. and Found. Engng*, Lima, Peru, pp. 225-236.

Kutter, H.K. (1974). Results of Laboratory Direct Shear Tests on Four Rock Types. Rock Mechanics Research Report Number 28, Imperial College, London.

Kutter H.K. & Rautenberg A. (1979). The Residual Shear Strength of Filled Joints in Rock. *Proc. 4th Congr. ISRM*, Montreaux, pp. 221-227.

Kutter H.K. & Otto F. (1990). Influence of Parallel and Cross Joints on Shear Behaviour of Rock Discontinuities. *Rock Joints; Proc. Int. Symp. on Rock Joints*, Loen, Norway (Barton N. & Stephansson O., Eds), pp. 243-250. Balkema, Rotterdam.

Ladanyi B. & Archambault G. (1970). Simulation of Shear Behaviour of Jointed Rock Masses. *Proc. 11th Symp. on Rock Mech.*, California, pp. 105-125.

Lade P.V. (1993). Rock Strength Criteria: The Theories and the Evidence. *Comprehensive Rock Engineering*, Vol. 1, Chap. 11 (Hudson, J. Ed. in chief), pp. 255-284. Pergamon Press, Oxford.

Lade P.V., Yamamuro J.A & Bopp P.A.(1996). Significance of Particle Crushing in Granular Materials. *J. Geotech. Engng., ASCE* 122, 309-316.

Lajtai E.Z. (1969a). Strength of Discontinuous Rocks in Direct Shear. *Géotechnique* 19, 218-233.

Lajtai E.Z. (1969b). Shear Strength of Weakness Planes in Rock. *Int. J. Rock Mech. Min. Sci.* 6, 499-515.

Lajtai E.J. & Gadi A.M. (1989). Friction on a Granite to Granite Interface. *Rock Mech. Rock Engng* 22, 25-49.

Lama, R.D. (1978). Influence of Clay Fillings on Shear Behaviour of Joints. *Proc. 3rd Intnl. Congress IAEG, Madrid,* Vol. **2**, pp 27-34.

Lambe T.W. & Whitman R.V. (1969). *Soil Mechanics*. J.Wiley & Sons, New York, p. 553.

Lee Y.-H., Carr J.R., Barr D.J. & Haas C.J. (1990). The Fractal Dimension as a Measure of the Roughness of Rock Discontinuity Profiles. *Int. J. Rock Mech. Min. Sci. & Geomech. Abstr.* 27, 453-464.

Leichnitz W. (1985). Mechanical Properties of Rock Joints. *Int. J. Rock Mech. Min. Sci. & Geomech. Abstr.* 22, 313-321.

Leichnitz W. & Natau O. (1979). The Influence of Peak Shear Strength Determination on the Analytical Rock Slope Stabilty. *Proc. 4th Congress ISRM*, Montreux. Vol. 2, pp.335-341.

Leong E.C. & Randolph M.F. (1992). A Model for Rock Interfacial Behaviour. *Rock Mech. Rock Engng.* 25, 187-206.

Lilly P.A. (1982). The Shear Behaviour of Bedding Planes in Mt McRae Shale with Implications for Rock Slope Design. . *Int. J. Rock Mech. Min. Sci. & Geomech. Abstr.* 19, 205-209.

Locher H.G. & Riedel U.G. (1970). Shear Tests on Layered Jurassic Limestone. *Proc. 2nd Congr. Rock Mech.,* Belgrade, Vol 2, Paper 3-I, 5 pp.

Logan J.M. (1987). Porosity and the Brittle-Ductile Transition in Sedimentary Rocks. *Physics and Chemistry of Porous Media II; AIP Conf. Proc. 154*, Ridgefield, CT, pp. 229-242.

Logan J.M. & Teufel L.W. (1986). The Effect of Normal Stress on the Real Area of Contact During Frictional Sliding of Rocks. *Pure & Appl. Geophys.* 124, 471-485.

Lundborg N. (1968). Strength of Rock-like Material. *Int. J. Rock Mech. Min. Sci.* 5, 427-454.

Lupini J.F., Skinner A.E. & Vaughan P.R. (1981). The Drained Residual Strength of cohesive Soils. *Géotechnique 31*, 181-213.

Maerz N.H., Franklin J.A. & Bennett C.P. (1990). Joint Roughness Measurements using Shadow Profilometry. *Int. J. Rock Mech. Min. Sci. & Geomech. Abstr.* 27, 329-343.

Maerz N.H. & Franklin J.A. (1990). Roughness Scale Effect and Fractal Dimension. *Scale Effects in Rock Masses; Proc. 1st Int. Workshop on Scale Effects in Rock Masses,* Loen, Norway (Pinto da Cunha, Ed.), pp. 121-126. Balkema, Rotterdam.

Mandelbrot B. (1983). *The Fractal Geometry of Nature.* W.Freeman, San Francisco, 468 pp.

Mandelbrot B. (1985). Self-affine Fractals and Fractal Dimensions. *Physica Scripta* 32, 257-260.

Manolopoulou S. (1994). The Effect of Soft Coatings on Shear Strength of Rock Joints. *Proc. 7th Int. IAEG Congress,* Lisbon, Vol. 2, pp. 913-917. Balkema, Rotterdam.

Martin C.D. & Chandler N.A. (1994). The Progressive Fracture of Lau du Bonnet Granite. *Int. J. Rock Mech. Min. Sci. & Geomech. Abstr.* 31, 643-659.

Martin G.R. & Millar P.J. (1974). Joint Strength Characteristics of a Weathered Rock. In Advances in Rock Mechanics, *Proc. 3rd Congr. Int. Soc. Rock Mech.,* Denver, Colorado, pp. 263-270.

Mason B. & Berry L.G. (1968). *Elements of Mineralogy.* W.H. Freeman, San Francisco, 550 pp.

Maurer W.C. (1965). Shear Failure of Rock Under Compression. *Soc. Petrol. Engnrs J.* 5, 167-176.

McClintock F.A. & Walsh J.B. (1962). Friction on Griffith Cracks in Rocks under Pressure. *Proc. 4th U.S. National Congr. of Applied Mechanics,* Berkley, pp. 1015-1021.

McMahon B.K. (1985). Some Practical Considerations for the Estimation of Shear Strength of Joints and other Discontinuities. *Proc. Int. Symp. on Fundamentals of Rock Joints,* Björkliden (Stephansson O., ed), pp. 475-485. Centek Publishers.

Michelis P. (1985). Polyaxial Yielding of Granular Rock. *J. Eng. Mech., ASCE* 111, 1049-1066.

Miller S.M., McWilliams P.C. & Kerkering J.C. (1989). Evaluation of Stereodigitizing for Measuring Rock Fracture Roughness. *Proc. 30th U.S. Symp. Rock Mech.,* W. Virginia Univ., pp. 201-208.

Miller S.M., McWilliams P.C. & Kerkering J.C. (1990). Ambiguities in Estimating Fractal Dimensions of Rock Facture Surfaces. *Proc. 31st U.S. Symp. Rock Mech.,* pp. 471-478.

Mogi K. (1965). Deformation and Fracture of Rocks under Confining Pressure. (2) Elasticity and Plasticity of Some Rocks. *Bull. Earthq. Res. Inst., Tokyo Univ.* 43, pp. 349-379.

Mogi K. (1966). Pressure Dependence of Rock Strength and Transition from Brittle Fracture to Ductile Flow. *Bull. Earthq. Res. Inst., Tokyo Univ.* 44, pp. 215-232.

Mogi K. (1967). Effect of the Intermediate Principal Stress on Rock Failure. *J. Geophys. Res.* 72, 5117-5131.

Mogi K. (1971). Effect of the Triaxial Stress System on the Failure of Dolomite and Limestone. *Tectonophysics* 11, 111-127.

Mogi K. (1972). Fracture and Flow of Rocks. *Tectonophysics* 13, 541-568.

Mogi K. (1974). On the Pressure Dependence of Strength of Rocks and the Coulomb Fracture Criterion. *Tectonophysics* 21, 273-285.

Muller P. & Siemes H. (1974). Festigkeit, Verformbarkeit und Gefugeregelung von Anhydrit- Experimentelle Stauchverformung unter Manteldrucken bis 5 kbar bei Temperaturen bis 300° C. *Tectonophysics 23*, 105-127.

Murphy D.J. (1971). High Pressure Experiments on Soil and Rock. *Proc. 13th symp. Rock Mech.* , pp.691-714.

Muralha J.A. & Cunha A. P. (1990). Analysis of Scale Effects in Joint Mechanical Behaviour. *Scale Effects in Rock Masses; Proc. 1st Int. Workshop on Scale Effects in Rock Masses,* Loen, Norway (Pinto da Cunha, Ed.), pp. 191-200. Balkema, Rotterdam.

Murrell S.A.F. (1965). The Effect of Triaxial Stress Systems on the Strength of Rocks at Atmospheric Temperatures. *Geophys. J. R. Astr. Soc.* 10, 231-281.

Murrell S.A.F. & Digby P.J. (1970). The Theory of Bittle Fracture Initiation under Triaxial Stress Conditions. I. *Geophys. J. R. Astr. Soc.* 19, 309-334; II, 499-512.

Murrell S.A.F. & Ismail I.A.H.(1976). The Effect of Decomposition of Hydrous Minerals on the Mechanical Properties of Rocks at High Pressures and Temperatures. *Tectonophysics* 31, 207-258.

Myers N.O. (1962). Characterisation of Surface Roughness. *Wear* 5, 182-189

Neville A.M. (1975). *High Alumina Cement Concrete.* The Construction Press, Lancaster.

Newland P.L. & Allely B.H. (1957). Volume Changes in Drained Triaxial Tests on Granular Materials. *Géotechnique* 8, No1, 17-34.

Nieble C., Midea N.F., Fujimura F. & Neto S.B. (1974). Shear Strength of Typical Features of Basaltic Rock Masses - Paran Basin - Brazil. In *Advances in Rock Mechanics, Proc. 3rd Congr. Int. Soc. Rock Mech.*, Denver, Colorado, pp. 294-301.

Nilsen B. (1985). Shear Strength of Rock Joints at Low Normal Stresses: A Key Parameter for Evaluating Rock Slope Stability. *Proc. Int. Symp. on Fundamentals of Rock Joints,* Björkliden (Stephansson O., ed), pp. 487-496. Centek Publishers.

Obert L., Brady B.T. & Schmechel F.W. (1976). The Effect of Normal Stiffness on the Shear Resistance of Rock. *Rock Mech.* 8, 57-72.

Odling N.E. (1994). Natural Fracture Profiles, Fractal Dimension and Joint Roughness Coefficients. *Rock Mech. Rock Engng.* 27(3), 135-153.

Ohnaka M. (1975). Frictional Characteristics of Typical Rocks. *J. Phys. Earth* 23, 87-112.

Ohnishi Y., Herda H. & Yoshinaka R. (1993). Shear Strength Scale Effect and the Geometry of Single and Repeated Rock Joints. *Scale Effects in Rock Masses 93; Proc. 2nd Int. Workshop on Scale Effects in Rock Masses (*Pinto da Cunha, Ed.), pp. 167-173. Balkema, Rotterdam.

Önalp A. (1993). Shearing Resistance of Fresh Joints: A Comparative Study of Portuguese Rocks. *Proc. ISRM Symp.: EUROCK'93*, Lisbon, pp. 651-654. Balkema, Rotterdham.

Orowan E. (1960). Mechanism of Seismic Faulting. In *Rock Deformation*, Criggs D.T. & Handin J. (Eds). *Geol. Soc. Amer. Memoirs* 79, 323-345.

Palmeira E.M. (1987). *The study of Soil-Reinforcement Interaction by Means of Large Scale Laboratory Tests*. D. Phil. Thesis, Univ. of Oxford.

Palmeira E.M. & Milligan G.W.E. (1989). Scale Effects in Direct Shear Tests on Sand. *Proc. 12th ICSMFE*, V.1 (Paper 8/17), Rio De Janeiro, pp. 739-742.

Pan X.D. & Hudson J.A. (1988). A Simplified Three Dimensional Hoek-Brown Yield Criterion. *Rock Mechanics and Power Plants. Proc. ISRM Symp. on Rock Mech. and Power Plants*, Madrid, Vol. 1, pp. 95-103.

Pande G.N. (1985). A Constitutive Model of Rock Joints. *Proc. Int. Symp. on Fundamentals of Rock Joints,* Björkliden (Stephansson O., ed), pp. 429-439 Centek Publishers.

Papaliangas T. (1986). *The Effect of Frictional Filling Material on Shear Behaviour of Rock Discontinuities*. MSc thesis, Department of Earth Sciences, Univ. of Leeds.

Papaliangas T., Hencher A.C. & Lumsden A.C. (1995). A Comprehensive Peak Shear Strength Criterion for Rock Joints. *Proc. 8th Int. Congress on Rock Mechanics*, Tokyo, Vol. 1, pp. 359-366.

Papaliangas T., Hencher S.R., Lumsden A.C. & Manolopoulou S. (1993). The Effect of Frictional Fill Thickness on the Shear Strength of Rock Discontinuities. *Int. J. Rock Mech. Min. Sci. & Geomech. Abstr.* 30, 81-91.

Papaliangas T. T., Hencher S.R. & Lumsden A.C. (1994). Scale Independent Shear Strength of Rock Joints. *Integral Approach to Applied Rock Mechanics* (M. Van Sint Jan, Ed. in chief), SOCHIGE, Santiago, Chile, Vol. 1, pp. 123-149.

Papaliangas T., Lumsden A.C., Manolopoulou S. and Hencher S.R. (1990). Shear Strength of Modelled Filled Rock Joints. *Rock Joints; Proc. Int. Symp. on Rock Joints*, Loen, Norway (Barton N. & Stephansson O., Eds), pp. 275-282. Balkema, Rotterdam.

Papaliangas T., Hencher S.R.. & Lumsden A.C. (1995). Laboratory Testing and Parameters Controlling the Shear Strength of Filled Rock Joints. Discussion. *Géotechnique* 45, No 1, 175-183.

Paterson M.S. (1978). *Experimental Rock Deformation - Brittle field*. Springer-Verlag, Berlin, p. 254.

Paterson M.S. (1958). Experimental Deformation and Faulting in Wombeyan Marble. *Bull. Geol. Soc. Am.*. 69, 465-476.

Patton F.D. (1966a). *Multiple Modes of Shear Failure in Rock and Related Materials*. Ph.D. Thesis, Univ. Illinois, 282 pp.

Patton F.D. (1966b). Multiple Modes of Shear Failure in Rock. *Proc. 1st Congr. Rock Mech.,* Lisbon, Vol 1, pp. 509-513.

Pease K.A. & Kulhawy F.H. (1984). Load Transfer Mechanisms in Rock Sockets and Anchors. Report EL-3777, Electric Power Research Institute, Palo Alto, California.

Pells P.N. (1993). Uniaxial Strength Testing. *Comprehensive Rock Engineering*, Vol 3, Chap. 3 (Hudson, J., Ed. in chief), pp. 67-85. Pergamon Press, Oxford.

Pereira P. J. and de Freitas M. H. (1993). Mechanisms of Shear Failure in Artificial Fractures of Sandstone and Their Implication for Models of Hydromechanical Coupling. *Rock Mech.* 26 (3), 195-214.

Plesha M.E. (1987). Constitutive Models for Rock Discontinuities with Dilatancy and Surface Degradation. *Int. J. Numer. Anal. Methods in Geomech.* 11, 345-322.

Potyondy J.G. (1961). Skin Friction Between Various Soils and Construction Materials. *Géotechnique* 11, 339-353.

Power W.L. & Tullis T.E. (1991). Euclidean and Fractal Models for the Description of Rock Surface Roughness. *J.Geophys. Res*. 96, 415-424.

Pratt H.R., Black A.D., Brown W.S. & Brace W.F. (1972). The Effect of Specimen Size on the Mechanical Properties of Unjointed Diorite. I*nt. J. Rock Mech. Min. Sci.* 9, 513-529.

Pratt H.R., Black A.D. & Brace W.C. (1974). Friction and Deformation of Jointed Quartz Diorite. *Proc. 3rd Int. Congr. on Rock Mech.*, Denver, Colorado, Vol IIA, pp. 306-310.

Price A.M. & Farmer I.W. (1979). Application of Yield Models to Rock. *Int. J. Rock Mech. Min. Sci. & Geomech. Abstr.* 16, 157-159.

Price A.M. & Farmer I.W. (1981). The Hvorslev Surface in Rock Deformation. *Int. J. Rock Mech. Min. Sci. & Geomech. Abstr.* 18, 229-234.

Procter D.C. & Barton P.R. (1974). Measurements of the Angle of Interparticle Friction. *Géotechnique* 24, 581-604.

Qiu X., Plesha M.E., Huang X. & Haimson B.C., (1993). An Investigation of the Mechanics of Rock Joints - Part II. Analytical Investigation. *Int. J. Rock Mech. Min. Sci. & Geomech. Abstr.* 30, 271-287.

Rabinowicz E. (1995). *Friction and Wear of Materials*. Second Edition. J. Wiley & Sons, N. York, pp. 315.

Raleigh C. B. & Paterson M.S. (1965). Experimental Deformation of Serpentinite and its Tectonic Implications. *J. of Geophys. Res*. 70, 3965-3985.

Reeves M.J. (1985). Rock Surface Roughness and Frictional Strength. *Int. J. Rock Mech. Min. Sci. & Geomech. Abstr.* 22, 429-442.

Rengers N. (1970). Influence of Surface Roughness on the Friction Properties of Rock Planes. *Proc. 2nd Congr. of the ISRM*, Belgrade, Vol. 1, paper 31, pp. 229-234.

Richards L.R. & Cowland J.W. (1982). The Effect of Surface Roughness on the Field Shear Strength of Sheeting Joints in Hong Kong Granite. *Hong Kong Engnr* 10, No10,39-43.

Ripley C.F. & Lee K.L. (1962). Sliding Friction Tests on Sedimentary Rock Specimens. *Trans. 7th Int. Congr. Large Dams*, Vol 4, Rome, 1961, pp. 657-671.

Roberds W.J. & Einstein H.H. (1978). Comprehensive Model for Rock Discontinuities. *J. Geotech. Engng., ASCE* 104, 553-569.

Robertson E.C. (1955). Experimental Study of the Strength of Rocks. *Bull. Geol. Soc. Amer.* 66, 1275-1314.

Roscoe K.H.(1970). The Influence of Strains in Soil Mechanics. *Géotechnique* 20, No 2, 129-170.

Ross-Brown D.M., Wickens E & Markland J. (1973). Terrestrial Photogrammetry in Open Pits - Part 2: An aid to Geological Mapping. *Trans. Sect. A, Inst. Min. Metal.* 82. pp. 115-130.

Ross-Brown D.M. & Walton G. (1975). A Portable Shear Box for Testing Rock Joints. *Rock Mech.* 7, 129-153.

Rowe P.W. (1962). The Stress-Dilatancy Relation for Static Equilibrium of an Assembly of Particles in Contact. *Proc. R. Soc.* A 269, 500-527.

Rowe P.W. (1969). The Relation Between the Shear Strength of Sands in the Triaxial Compression, Plane Strain and Direct Shear. *Géotechnique* 19, 75-86.

Rowe P.W. (1972). Theoretical Meaning and observed Values of Deformation Parameters for Soil. *Stress-Strain Behaviour of Soils* (R.H.G.Parry, Ed.), pp. 143-194.Foulis, London.

Rummel F. & Fairhurst C. (1970). Determination of the Post-failure Behaviour of Brittle Rock using a Servo-controlled Testing Mchine. *Rock Mech.* 2, 189-204.

Rummel F., Alheid H.J. & Frohn C. (1978). Dilatancy and Fracture Induced Velocity Changes in rock and their Relation to Frictional Sliding. *Pure & Applied Geophysics* 116, 743-764.

Rutter E.H. (1974). The Influence of Temperature, Strain Rate and Interstitial Water in the Experimental Deformation of Calcite Rocks. *Tectonophysics* 22, 311-334.

Rutter E.H. (1986). On the Nomenclature of Mode of Failure Transitions in Rocks. *Tectonophysics* 122, 381-387.

Ryabinin Yu. N., Beresnev B.I. & Martinov E.D. (1971). Mechanical Properties and Processes in Solids under High Pressure. *J. Geoph. Res.* 76, 1370-1375.

Sangha C.M. & Dhir R.K.(1975). Strength and Deformation of Rock Subject to Multiaxial Compressive Stresses. *Int. J. Rock Mech. Min. Sci.* 12, 277-282.

Sarra Pistone R. (1990). Scale Effect in the Shear strength of Rock Joints. *Scale Effects in Rock Masses; Proc. 1st Int. Workshop on Scale Effects in Rock Masses,* Loen, Norway (Pinto da Cunha, Ed.), pp. 201-206. Balkema, Rotterdam.

Schneider H.J. (1976). The Friction and Deformation Behaviour of Rock Joints. *Rock Mech.* 8, 169-184.

Scholz, C.H. & Engelder, J.T. (1976). The Role of Asperity Indentation and Ploughing in Rock Friction - I. Asperity Creep and Stick-Slip. *Int. J. Rock Mech. Min. Sci. & Geomech. Abstr.* 13, 149-154.

Scholz C.H. (1990). *The Mechanics of Earthquakes and Faulting*. Cambridge University Press, Cambridge.

Schwartz A.E. (1964). Failure of Rock in the Triaxial Shear Test. *Proc. 6th Symp. Rock Mech.*, Am. Inst. Min. Met. & Pet. Eng., Univ. of Missouri, Rolla, Ma, pp. 109-135.

Scott R.F. (1963). *Principles of Soil Mechanics*. Addison-Wesley, Reading, Massaschussets.

Scott T.E. & Nielsen K.C. (1991). The Effect of Porosity on the Brittle-Ductile Transition in Sandstones. *J. Geophys. Res.* 96, 405-414.

Seidel J.P. & Haberfield C.M.(1995). Towards an Understanding of Joint Roughness. *Rock Mech. & Rock Engng* 28, No 2, 69-92.

Selby M.J. (1987). Rock Slopes. *Slope Stability,* Chap. 15 (Anderson, G.M. & Richards, K.S., Eds). Wiley, New York, pp. 475-504.

Shimada M. (1981). The Method of Compression Test Under High Pressures in a Cubic Press and the Strength of Granite. *Tectonophysics* 72, 343-357.

Shimada M. (1986). Mechanism of Deformation in a Dry Porous Basalt at High Pressures. *Tectonophysics* 121, 153-173.

Shimada M. (1993). Two Types of Brittle Fracture of Silicate Rocks and scale Effect on Rock Strength: Their Implications in the Earth's Crust. *Scale Effects in Rock Masses 93; Proc. 2nd Int. Workshop on Scale Effects in Rock Masses (*Pinto da Cunha, Ed.), pp. 55-62. Balkema, Rotterdam.

Shimada M., Cho A. & Yukutake H. (1983). Fracture Strength of Dry Silicate Rocks at High Confining Pressures and Activity of Acoustic Emission. *Tectonophysics* 96, 159-172.

Shock R.N., Heard H.C. & Stephens D.R. (1973). Stress-Strain Behavior of a Granodiorite and two Graywackes on Compression to 20 kilobars. *J.Geophys. Res.* 78, 5922-5941

Siwak J.-M., Prevost J., Pecqueur G. & Mikolajczak A. (1993). Behaviour of Chalk. Geotechnical Engineering of Hard Soils-Soft Rocks. Anagnostopoulos et al. (Eds), pp.1657-1661. Balkema, Rotterdam.

Skinner A.E. (1969). A Note on the Influence of Interparticle Friction on the Shearing Strength of a Random Assembly of Spherical Particles. *Géotechnique* 19, 150-157.

Sowers G.B. & Sowers G.F. (1970). *Introduction to Soil Mechanics and Foundations*. MacMillan, ew York.

Stesky R.M. & Hannan S.S. (1987). Growth of Contact Area between Rough Surfaces under Normal Stress. *Geophys. Res. Lett.* 14, 550-553.

Stesky R.M. and Hannan S.S. (1989). A New Theory for the Static Contact Between Rough, Unmated Surfaces in Non-elastically Deforming Rock and its Implications for Rock Friction. *J. Struct. Geol.* 11, 787-798.

Stesky R.M., Brace W.F., Riley D.K., Robin P.-Y. F. (1974). Friction in Faulted Rock at High Temperature and Pressure. *Tectonophysics* 23, 177-203.

Stimpson B. (1970). Modelling Materials for Engineering Rock Mechanics. Int. J. Rock Mech. Min. Sci. 7, 77-121

Stimpson B. (1979). A New Approach to Simulating Rock Joints in Physical Models. *Int. J. Rock Mech. Min. Sci. & Geomech. Abstr.* 16, 215-216.

Stimpson B. (1982). A Rapid Field Method for Recording Joint Roughness Profiles. *Int. J. Rock Mech. Min. Sci. & Geomech. Abstr.* 19, 345-346.

Stroud M.A. (1971). *The Behaviour of Sand at Low Stress Levels in the Simple Shear Apparatus*. PhD Thesis, University of Cambridge.

Sun Z., Gerrard C. & Stephansson O. (1985). Rock Joint Compliance Tests for Compression and Shear Loads. *Int. J. Rock Mech. Min. Sci. & Geomech. Abstr.* 22, 197-213.

Swan G. (1981). Stiffness and Associated Joint Properties of Rock. *Proc. Conf. on Application of Rock Mechanics to Cut and Fill Mining* (Stephansson O. & Jones M.J., Eds), pp. 169-178. Inst. Min. Metall., London.

Swan G. (1983). Determination of Stiffness and Other Properties from Roughness Measurements. *Rock Mech. Rock Engng.* 16, 19-38.

Swan G. (1985). Methods of Roughness Analysis for Predicting Rock Joint Behaviour. *Proc. Int. Symp. on Fundamentals of Rock Joints,* Björkliden (Stephansson, O., ed), pp. 153-161. Centek Publishers.

Swan G. & Zonghi S. (1985). Prediction of Shear Behaviour of Joints Using Profiles. *Rock Mech. and Rock Engnr.* 18, 183-212.

Tabor D. (1975). A Simplified account of Surface Topography and the Contact between Solids. *Wear* 32, 269-271.

Tabor D. and Winterton R.H.S. (1969). The Direct Measurement of Normal and Retarded Van Der Waals Forces. *Proc. R. Soc.* A312, 435-450.

Tanimoto C. & Kishida K. (1994). Seismic Geotomography: Amplitude versus Velocity in Consideration of Joint Aperture and Spacing. *Proc. 1st North American Rock Mechanics Symp.* Univ. of Texas at Austin (Nelson, P.A. & Laubach S.E, Eds), pp.147-155. Balkema, Rotterdam.

Taylor D.W. (1948). *Fundamentals of Soil Mechanics.* John Wiley & Sons.

Terzaghi K. (1925). The Physical Causes of Proportionality between Pressure and Frictional Resistance, from *Erdbaumechanic*, transl. by A. Casagrande in, *From Theory to Practice in Soil Mechanics.* J. Wiley.

Timoshenko S. & Goodier J.N. (1951). *Theory of Elasticity.* McGraw-Hill , New York.

Toy, J. (1993). *An Appraisal of the Effects of Sample Size on the Shear Behaviour of Rock Discontinuities.* M.Sc. Thesis, Department of Earth Sciences, University of Leeds, U.K.

Tse R. & Cruden D. M. (1979). Estimating Joint Roughness Coefficients. *Int. J. Rock Mech, Min. Sci.* 16, 303-307.

Tsytovich N.A., Ukhov, S.B. & Burlakov V.N. (1970). Failure Mechanism of a Fissured Rock Base Upon Displacement of a Loading Plate. *Proc. 2nd Congr. ISRM*, Belgrade, Vol. 2, pp. 89-93.

Tullis I. & Yund R.A. (1977). Experimental Deformation of Dry Westerly Granite. *J. Geophys. Res.* 82, 5705-5718.

Turk N., Creig M.J., Dearman W.R. & Amin F.F. (1987). Characterisation of Rock Joint Surfaces by Fractal Dimension. *Proc. 28th U.S. Symp. on Rock Mech.*, Univ. of Arizona, pp. 1223-1236.

Von Karman, Th. (1911). Festigkeitsversuche unter Allseitigem Druck. *Zeit. des Verhandl. Deut. Ingr.* 55, 1749-1757.

Vereshchagin L.F., Yakovlev E.N., Vinogradov B.V., Sakun V.P. & Stepanov G.N. (1974). Transition of Diamond into the Metallic State. *High Temp. - High Press.* 6, 505-508.

Wakabayashi N. & Fukushige I. (1992). Experimental Study of the Relation between Fractal Dimension and Shear Strength. *Pre-prints Conf. on Fractured and Jointed Rock Masses*, Lake Tahoe, California, Vol. 1, pp. 126-131.

Wawersik W.R. & Fairhurst C. (1970). A Study of Brittle Rock Fracture in Laboratory Compression Experiments. *Int. J. Rock Mech. Min. Sci. & Geomech. Abstr.* 7, 561-575.

Weissbach G. (1978). A New Method for the Determination of the Roughness of Rock Joints in the Laboratory. *Int. J. Rock Mech. Min. Sci. & Geomech. Abstr.* 15, 131-133.

Welsh S.P. (1994). *The Effects of Infill on the Shear Strength of Rock Discontinuities.* Ph. D. Thesis, Dept. of Earth Sciences, Univ. of Leeds, U.K.

Wernick E. (1979). A True Direct Shear Apparatus to Measure Soil Parameters of Shear Bands. *Design Parameters in Geotechnical Engineering. Proc. 7th Europ. Conf. on Soil Mech. & Foundn. Engng.*, BGS, Vol. 2, pp. 175-182.

West L.J. (1992). *The Shear Behaviour of Heterogeneous Soils.* Ph. D. Thesis, Dept. of Earth Sciences, Univ. of Leeds, U.K.

Wong T.-F. (1990). Mechanical Compaction and the Brittle-Ductile Transition in Porous Sandstones. *Deformation Mechanisms, Rheology and Tectonics. Geological Society Special Publication No 54* (Knipe, R.J. & Rutter, E.H., Eds), London, Geological Society, pp. 111-122.

Wu, T.H. & Ali E.M. (1978). Statistical Representation of Joint Roughness. *Int. J. Rock Mech. Min. Sci. & Geomech. Abstr.* 15, 259-262.

Wyllie D.C. (1992). *Foundations on Rock.* Chapman & Hall, London, 333 pp.

Xie H. & Pariseau W.G. (1992). Fractal Estimation of Joint Roughness Coefficient. *Fractured and Jointed Rock Masses*, (Myer L.R., Cook N.G.W., Goodman R. & Tsang C.-F., Eds), pp. 125-131. Balkema, Rotterdam.

Yamada K., Takeda N., Kagami J. & Naoi T. (1978). Mechanisms of Elastic Contact and Friction Between Rough Surfaces. *Wear* 48, 15-34.

Yamaguchi U. & Shimotani T. (1986). A Case Study of Slope Failure in a Limestone Quarry. *Int. J. Rock Mech. Min. Sci. & Geomech. Abstr.* 23, 19-28.

Yoshinaka R. & Yamabe T. (1980). Strength Criterion of Rocks. *Soils & Foundations* 20(4), 113-126.

Yoshinaka R., Yoshida J., Arai H. & Arisaka S. (1993). Scale Effects on Shear Strength and Deformability of Rock Joints. *Scale Effects in Rock Masses 93; Proc. 2nd Int. Workshop on Scale Effects in Rock Masses* (Pinto da Cunha, Ed.), pp. 143-149. Balkema, Rotterdam.

Yudhbir, Lemanza W. & Prinzl F. (1983). An Empirical Failure Criterion for Rock Masses. *Proc. 5th Int. Congr. Rock Mech.*, Melbourne, Australia, Vol. B, pp. 1-8.

APPENDIX I

Table I.1 Chemical Analysis of CAC (according to the manufacturer)

Main constituents				
Al_2O_3	CaO	SiO_2	Fe_2O_3	FeO
39.0	38.5	4.5	12.0	4.0
Minor constituents						
TiO_2	MgO	K_2O	Na_2O	SO_3	S	Cl
2.5	0.6	0.15	0.10	0.15	0.02	0.01

Table I.2 Chemical Analysis of Andalusite

Al_2O_3	SiO_2	Fe_2O_3	MgO	TiO_2	MnO	CaO	Na2O	K2O	P2O5
58.61	37.92	1.35	0.79	0.25	0.02	0.25	0.20	0.29	0.25

Table I.3 Chemical analysis of synthetic rock (%)

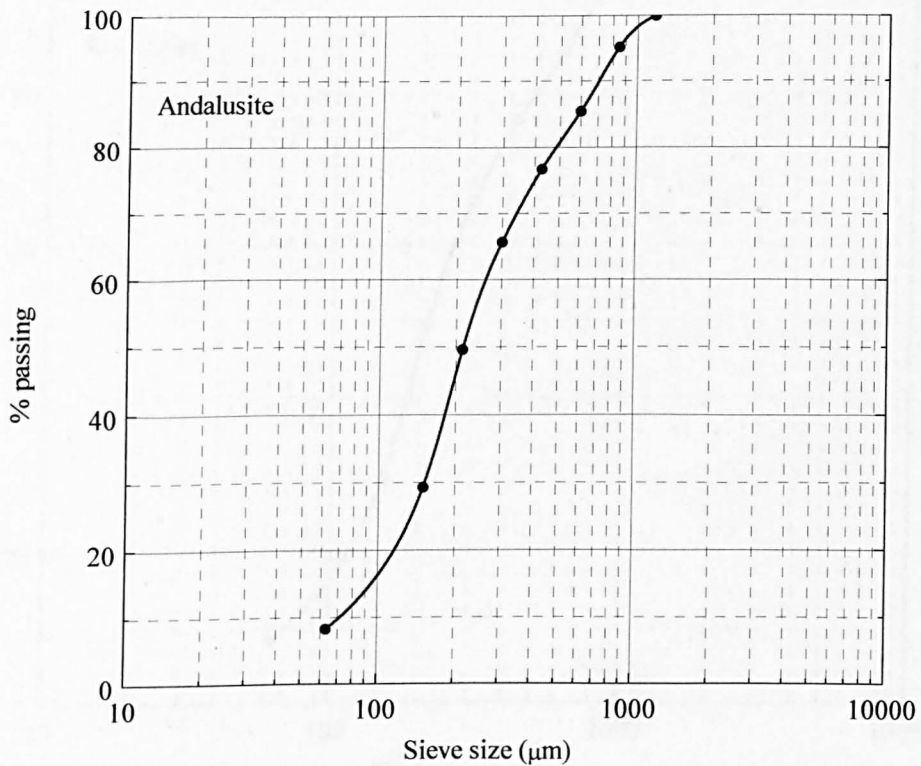| Al_2O_3	SiO_2	Fe_2O_3	MgO	TiO_2	MnO	CaO	Na2O	K2O	P2O5
47.51	19.35	9.22	0.59	1.10	0.05	21.58	0.02	0.16	0.02

Figure I.1: Grain size distribution of andalusite

APPENDIX I

Table I.1 Chemical Analysis of CAC (according to the manufacturer)

Main constituents				
Al_2O_3	CaO	SiO_2	Fe_2O_3	FeO
39.0	38.5	4.5	12.0	4.0
Minor constituents						
TiO_2	MgO	K_2O	Na_2O	SO_3	S	Cl
2.5	0.6	0.15	0.10	0.15	0.02	0.01

Table I.2 Chemical Analysis of Andalusite

Al_2O_3	SiO_2	Fe_2O_3	MgO	TiO_2	MnO	CaO	Na_2O	K_2O	P_2O_5
58.61	37.92	1.35	0.79	0.25	0.02	0.25	0.20	0.29	0.25

Table I.3 Chemical analysis of synthetic rock (%)

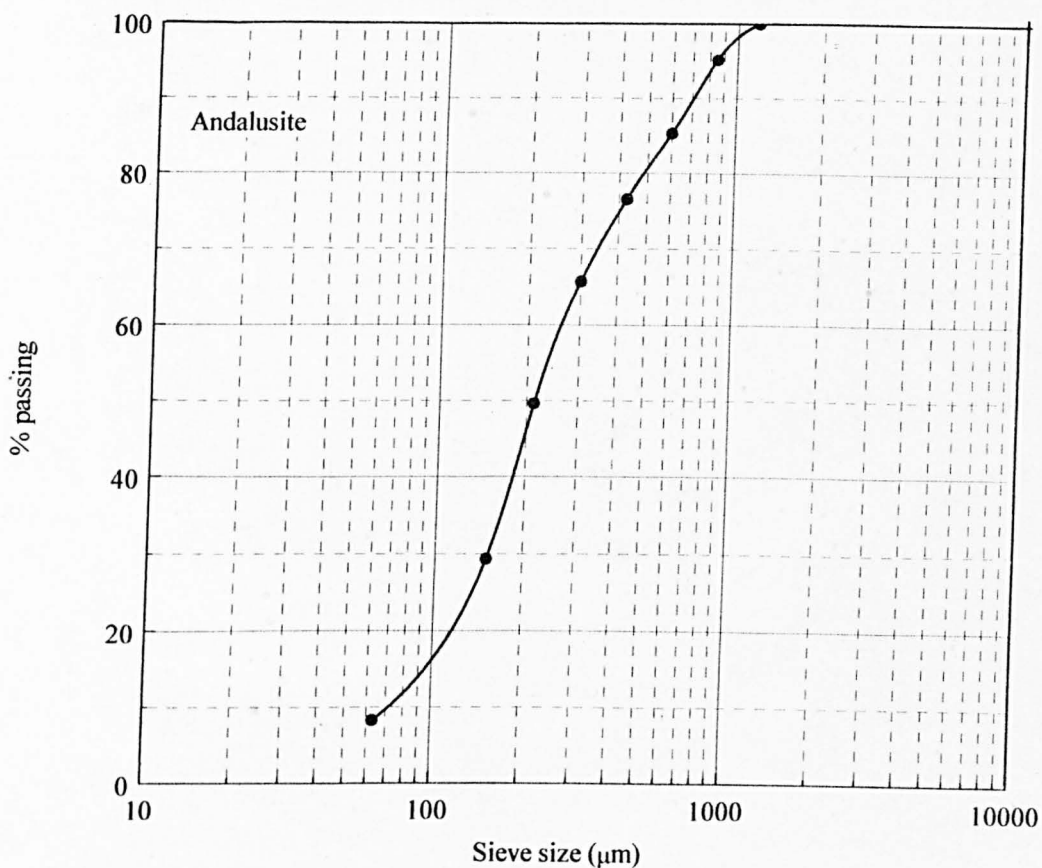| Al_2O_3	SiO_2	Fe_2O_3	MgO	TiO_2	MnO	CaO	Na_2O	K_2O	P_2O_5
47.51	19.35	9.22	0.59	1.10	0.05	21.58	0.02	0.16	0.02

Fig. I.1: Grain size distribution od andalusite